**UNIVERSIDAD COMPLUTENSE DE MADRID**
FACULTAD DE CIENCIAS QUÍMICAS


# TESIS DOCTORAL

## New optical biosensing strategies for the analysis of mycotoxins and toxigenic fungi in food

## Nuevas estrategias para el desarrollo de biosensores ópticos aplicados al análisis de micotoxinas y hongos toxigénicos en alimentos

MEMORIA PARA OPTAR AL GRADO DE DOCTOR

PRESENTADA POR

**Riikka Peltomaa**

Directoras

**María Cruz Moreno Bondi**
**Elena Benito Peña**

Madrid

UNIVERSIDAD COMPLUTENSE DE MADRID
FACULTAD DE CIENCIAS QUÍMICAS
Departamento de Química Analítica


# NEW OPTICAL BIOSENSING STRATEGIES FOR THE ANALYSIS OF MYCOTOXINS AND TOXIGENIC FUNGI IN FOOD

Nuevas estrategias para el desarrollo de biosensores ópticos aplicados al análisis de micotoxinas y hongos toxigénicos en alimentos

Directoras:

Dra. María Cruz Moreno Bondi
Catedrática de Universidad

Dra. Elena Benito Peña
Profesora Contratada Doctora

TESIS DOCTORAL QUE PRESENTA
Riikka Peltomaa

Madrid, 2019

UNIVERSIDAD COMPLUTENSE MADRID

# DECLARACIÓN DE AUTORÍA Y ORIGINALIDAD DE LA TESIS PRESENTADA PARA LA OBTENCIÓN DEL TÍTULO DE DOCTOR

D./Dña. Riikka Peltomaa

con número de DNI/NIE/Pasaporte Y3963258-G, estudiante en el Programa de Doctorado Química avanzada,

de la Facultad de Ciencias Químicas de la Universidad Complutense de Madrid, como autor/a de la tesis presentada para la obtención del título de Doctor y titulada:

New optical biosensing strategies for the analysis of mycotoxins and toxigenic fungi in food

(Nuevas estrategias para el desarrollo de biosensores ópticos aplicados al análisis de micotoxinas y hongos toxigénicos)

y dirigida por: Dra. María Cruz Moreno Bondi y Dra. Elena Benito Peña

**DECLARO QUE:**

La tesis es una obra original que no infringe los derechos de propiedad intelectual ni los derechos de propiedad industrial u otros, de acuerdo con el ordenamiento jurídico vigente, en particular, la Ley de Propiedad Intelectual (R.D. legislativo 1/1996, de 12 de abril, por el que se aprueba el texto refundido de la Ley de Propiedad Intelectual, modificado por la Ley 2/2019, de 1 de marzo, regularizando, aclarando y armonizando las disposiciones legales vigentes sobre la materia), en particular, las disposiciones referidas al derecho de cita.

Del mismo modo, asumo frente a la Universidad cualquier responsabilidad que pudiera derivarse de la autoría o falta de originalidad del contenido de la tesis presentada de conformidad con el ordenamiento jurídico vigente.

En Madrid, a 7 de mayo de 2019

Fdo.: 

Esta DECLARACIÓN DE AUTORÍA Y ORIGINALIDAD debe ser insertada en la primera página de la tesis presentada para la obtención del título de Doctor.

# Acknowledgments

This research was carried out during 2015–2019 in the Optical Chemosensors & Applied Photochemistry group (GSOLFA) at the Department of Analytical Chemistry of Complutense University of Madrid. Financial support was received from the European Union (SAMOSS; FP7-PEOPLE-2013-ITN; Contract 607590), the Spanish Ministry of Economy and Competitiveness and European Regional Development Fund (CTQ2015-69278-C2-1-R MINECO/FEDER, RTI2018-096410-B-C21), as well as Universidad Complutense de Madrid which are all gratefully acknowledged.

First of all, my supervisor professor María Cruz Moreno Bondi is greatly acknowledged for giving me the opportunity to work under guidance, for teaching me to be critical and determined every step of the way. Her inconceivable expertise related to analytical chemistry and biosensing is truly admirable, not to mention her commitment and passion for science. I also wish to thank her for giving me the opportunity to travel and carry out several research stages during these years. I am also grateful for welcoming me so warmly to a new country, the lab and GSOLFA, together with professor Guillermo Orellana.

I wish to express my sincerest gratitude to my second supervisor professor Elena Benito Peña for the opportunity to work with her and for her interest and positive attitude towards my work. Her scientific enthusiasm and dedication to her students have been indispensable for me during these years. I thank her especially for believing and placing her trust on me and for making me feel that my opinions even as a young student were valued.

I want to thank all my co-authors for their diligent work which helped to make the publications stronger and who are among the reasons that this thesis ever got finished. Especially, I want to thank Dr. Rodrigo Barderas for his guidance through the phage display and for his patience to answer all my questions countless times, professor Francisco Amaro-Torres for his phenomenal knowledge in his field and for being part of the non-chemist division of GSOLFA, Dr. Vicente Más for his expertise and advice related to the SPR experiments, and Silvia Vaghini for her efforts in the project as well as for her friendship during these years. I am also grateful for all the students who have contributed to the work in many ways.

I've been fortunate to be part of the great SAMOSS network, and I wish to thank all my fellows, Guido, Leena, Frank, Maria, Ola, Monica, Sandro, Laura, Koni, Sruj, and Heman, as well as the PIs and everyone else involved, for all the pleasant meetings we had during these years. I am also grateful for all the great the people I've had the privilege to work with during my

secondmends at the University of Miami, Micronit Microfluidics and Austrian Institute of Technology. Dr. Sandro Meucci is greatly acknowledged for his expertise in microfluidics and for his patience with the, what felt like, never-ending project of microfluidic genosensor. Dr. Ursula Sauer and all the great people at AIT are thanked for their help and company during my months in Tulln. I want to express my great appreciation also to professors Sylvia Daunert and Sapna Deo for giving me the opportunity to visit their lab in Miami and Dr. Trajen Head, Dr. Emre Dikici and Mindy Greene among others for all their help during my stay there.

My warmest thanks go to all my fine colleagues and friends at the GSOLFA group, my family in Madrid. Jose Ángel, Idoia, Lidia, JoseQ, Guido, Francesca, Luis, Mar, Miguel, Javi, Maxi, Paco, Alberto, Bettina, Álvaro, and everyone else who has been part of the group during these years are thanked for their company in the precious lunch and coffee breaks, providing good laughs, peer support and occasional Spanish lessons. I consider myself fortunate indeed to have had the opportunity to work with you! I want to thank my lab mates, Bettina, for all her help and support, and Álvaro, for his confidence in me and for the encouragement in the last steps to finish the thesis. My fellow SAMOSS member in Madrid, Guido is greatly acknowledged for his friendship and the peer support of living abroad. I wish to acknowledge Lidia for her friendship, for all the fun and also for the struggles we've shared, and JoseQ for always being so sympathetic and positive despite how long the day in the lab had been. I want to thank Idoia for her kindness and friendship, and Jose Ángel, for sharing the ups and downs of everyday life during two years.

I also wish to express my ingenuous appreciation to all my friends back in Finland. Leena, whose involvement in SAMOSS is among the reasons why I ended up in Madrid, is greatly acknowledged for her friendship during these years and especially during my summer in Vienna. I want to thank Milla and Anna, my biotech buddies, for their friendship which has lasted despite us all living in different countries. I am forever grateful to my oldest friends, Laura, Liina, Emmi, and Satu, for being part of my life for more than 20 years after which I am overwhelmed with wonderful memories that I will never forget.

Finally, I wish to express my sincerest gratitude to my family who has supported and encouraged me always, no matter where I go.

Madrid, May 2019

# Table of contents

# Figures and tables

# Abbreviations

| | |
|---|---|
| AChE | acetylcholinesterase |
| AF | aflatoxin |
| AP | alkaline phosphatase |
| AuNP | gold nanoparticle |
| bp | base pair |
| BSA | bovine serum albumin |
| CDR | complementary determining region |
| CIT | citrinin |
| $C_H$ | constant heavy domains of antibody |
| $C_L$ | constant light domain of antibody |
| CMOS | complementary metal–oxide–semiconductor |
| CV | coefficient of variation |
| DAb | domain antibody |
| DNA | deoxyribonucleic acid |
| DON | deoxynivalenol |
| DR | dynamic range |
| dsDNA | double-stranded DNA |
| ELISA | enzyme-linked immunosorbent assay |
| Fab | fragment antigen binding |
| $FB_1$ | fumonisin $B_1$ |
| Fc | antibody constant region, fragment crystallizable |
| FRET | Förster resonance energy transfer |
| GC | gas chromatography |
| GFP | green fluorescent protein |
| HPLC | high-performance liquid chromatography |
| HRP | horse-radish peroxidase |
| IAC | immuno affinity column |
| IARC | International Agency for Research on Cancer |
| $IC_{50}$ | half maximal inhibitory concentration |
| IgG | immunoglobulin G |
| IGS | internal spacer regions |
| IPTG | isopropyl β-D-1-thiogalactopyranoside |
| ITS | internal transcribed spacer regions |
| $K_d$ | dissociation constant |
| $k_{on}$ | association rate constant |
| $k_{off}$ | dissociation rate constant |
| LB | Luria broth |
| LOD | limit of detection |
| LSPR | localized surface plasmon resonance |

| | |
|---|---|
| MAb | monoclonal antibody |
| MBP | maltose-binding protein |
| MIP | molecularly imprinted polymer |
| MRL | maximum residue limit |
| MS | mass spectrometry |
| NTA | nitrilotriacetic acid |
| pIII | phage minor coat protein III |
| OD | optical density |
| OS-IA | open sandwich immunoassay |
| OTA | ochratoxin A |
| PAGE | polyacrylamide gel electrophoresis |
| PBS | phosphate buffered saline |
| PCR | polymerase chain reaction |
| QD | quantum dot |
| qPCR | quantitative or real-time PCR |
| RCA | rolling circle amplification |
| RNA | ribonucleic acid |
| RSD | relative standard deviation |
| SA | streptavidin |
| SAPE | streptavidin-coupled R-Phycoerythrin |
| S/B | signal-to-background ratio |
| scFv | single-chain fragment of antibody variable regions |
| SERS | surface-enhanced Raman spectroscopy |
| SPE | solid-phase extraction |
| SPR | surface plasmon resonance |
| ssDNA | single-stranded DNA |
| TEM | transmission electron microscopy |
| TLC | thin-layer chromatography |
| UCNP | upconverting nanoparticle |
| UV | ultraviolet |
| $V_H$ | variable heavy domain of antibody |
| $V_L$ | variable light domain of antibody |
| WHO | World Health Organization |
| ZEA | zearalenone |

# Abstract


## New optical biosensing strategies for the analysis of mycotoxins and toxigenic fungi in food

Mycotoxins are a diverse group of low molecular weight compounds produced as secondary metabolites by numerous species of filamentous fungi. This assemblage is chemically and toxigenically rather heterogeneous, but generally these toxins are known to cause disease and death in human and other vertebrates even at low concentrations. Mycotoxigenic fungi grow on a wide range of conditions and they can produce mycotoxins into the matrices on which they grow, often food intended for human consumption or animal feed. As a result of the ubiquitous nature of mycotoxigenic fungi, particularly in temperate and tropical regions of the world, mycotoxin contamination is often inevitable, and some calculations have estimated that approximately 25–50% of world crops are contaminated with these toxins. Although the awareness related to the hazards of mycotoxins as food and feed contaminants is growing, there are no absolute measures available for eliminating mycotoxins from agricultural products. While mycotoxin occurrence in the field can be decreased by good agronomic practices and planting resistant varieties, in the end, analytical methods capable of detecting mycotoxins and toxigenic fungi even at low concentration are of key importance for ensuring food safety.

Biosensors can provide rapid, sensitive, low cost, real-time, and on-site analysis with compact and low power devices, and owing to these appealing advantages they have emerged as one of most interesting approaches to overcome the limitations of many conventional methods, for example, for food safety applications. Biosensors and bioaffinity assays are based on the high specificity and sensitivity of biomolecular recognition which is subsequently transformed into an analytically useful signal by a transducer. Among the vast variety of different biosensors, major research efforts in the field together with advances in material sciences have enabled the development of sophisticated and miniaturized devices to answer to the increased need for novel analysis tools and biosensing strategies. The main objective of this thesis was to develop new methods for the analyses of mycotoxins and toxigenic fungi in food. To this aim, different assay concepts and formats were explored to assess the impact of the assay components on the performance of bioanalytical assays and biosensors. New recognition elements were designed or selected to guarantee sensitive and specific detection of these food contaminants with the objective of meeting the demands of simple, rapid and low-cost yet sensitive methods for food safety applications.

Among the most common and widely-spread fungi, genus *Fusarium* includes notorious producers of several mycotoxins and has been associated with plant diseases with virtually every plant family. In the first part of this thesis, species-specific DNA probes were designed on the basis of the intergenic spacer regions of the ribosomal DNA to enable the detection of highly similar fungal species, *Fusarium proliferatum* and *Fusarium verticillioides*. Based on species-specific capture and detection probes sandwich hybridization assays were implemented and optimized. With enzymatic detection, the developed genosensors were able to detect the synthetic target DNA in the low picomolar range with no significant cross-reactivity between the two species. The sensors were also used to analyze natural fungal contamination in maize samples after amplification of the genomic DNA using a common primer pair. The sample analyses were in accordance with previous results obtained with PCR, and no cross-reactivity between *F. verticillioides* and *F. proliferatum,* or other fungi species tested, was observed. The developed biosensors can provide a valuable tool to evaluate the potential for mycotoxin contamination in conditions where detection of mycotoxins directly is challenging, and ongoing work aims to integrate the method to a microfluidic platform for improved analysis.

The second and major part of the thesis focused on the development of various assay concepts for mycotoxin analysis. Epitope mimicking peptides, or mimotopes, which are capable of imitating the epitope of an antigen and thus bind to same antibody paratope, were selected from a phage-displayed peptide library for mycotoxins fumonisin $B_1$, T-2 toxin, and zearalenone. Such peptides present an intriguing alternative to overcome some of the limitations of competitive immunoassays conventionally established using toxin-conjugates. As mimotopes bind to the same antibody paratope as the target, they can be used as the competitor instead of the toxin-conjugate thus avoiding the cumbersome conjugation step. In this work, we have applied the selected mimotopes to various mimotope-based immunoassays to develop new and simple methods for mycotoxin detection. The developed methods include assays using the phage-displayed mimotopes, as well as the synthetic and recombinant counterparts of the peptides in heterogeneous and homogeneous assay formats. The development of microarray-based immunoassay and magnetic bead–based assay for fumonisin detection using the synthetic peptide with a biotin linker provided excellent detection limits and the necessary sensitivity to meet the regulatory limits set by the European Commission for fumonisins. On the other hand, the mimotopes were used to construct recombinant fusion proteins consisting of the mimotope with fluorescent or bioluminescent proteins Thus, the readily labeled mimotope-fusion could be directly applied to the immunoassays without the need for further labeling or secondary antibodies. Heterogeneous immunoassays using the mimotopes tagged with a yellow fluorescent protein (YFP) or *Gaussia* luciferase (GLuc) resulted in good analytical sensitivities in a rapid and simple assay concept. Moreover, the YFP-tagged fumonisin mimotope was used to develop a straightforward homogeneous fluorescence quenching immunoassay based on gold nanoparticles (AuNPs).

# Resumen

## Nuevas estrategias para el desarrollo de biosensores ópticos aplicados al análisis de micotoxinas y hongos toxigénicos en alimentos

Las micotoxinas son metabolitos secundarios tóxicos producidos por algunas cepas de hongos que contaminan alimentos, especialmente cereales y hortalizas. Estos compuestos de bajo peso molecular son químicamente y toxigénicamente heterogéneos; sin embargo, muchas de estas toxinas pueden originar enfermedades, y en ocasiones la muerte, tanto en humanos como en otros vertebrados. Los hongos toxigénicos crecen en muchas condiciones muy diversas, lo que puede dar lugar a la aparición de micotoxinas en los alimentos destinados tanto al consumo humano como al animal. Los hongos toxigénicos están ampliamente distribuidos por todo el mundo, particularmente en las regiones templadas y tropicales, por lo que la contaminación natural por micotoxinas es casi inevitable. De hecho, se estima que aproximadamente el 25–50% de los cultivos mundiales están contaminados por estas toxinas, y la preocupación sobre los peligros asociados a su presencia en alimentos es cada día mayor. Actualmente, no existen alternativas viables para su eliminación en los productos agrícolas; aunque el empleo de buenas prácticas agrícolas o la plantación de variedades resistentes a los hongos, pueden ayudar a mejorar este problema. En cualquier caso, se requieren métodos analíticos sensibles y selectivos para la detección de micotoxinas y hongos toxigénicos, a bajas concentraciones, a fin de garantizar la seguridad alimentaria.

Los biosensores son dispositivos que permiten la realización de análisis rápidos, sensibles, selectivos, en tiempo real, y en algunos casos "*in situ*", empleando instrumentos compactos y de bajo coste. Dadas sus indudables ventajas, estos dispositivos permiten evitar algunas de las limitaciones de los métodos analíticos convencionales, de forma que su empleo para el control de la seguridad alimentaria se ha incrementado notablemente en los últimos años. Los biosensores se basan en la alta especificidad y sensibilidad del reconocimiento biomolecular que, posteriormente, se transforma en una señal analíticamente útil empleando un transductor adecuado (óptico, eléctrico, de masa, *etc.)*. Los recientes avances en áreas como la ciencia de los materiales, el reconocimiento molecular, la biotecnología, la miniaturización o la microfluídica, entre otras, han favorecido el desarrollo de nuevos biosensores para la detección sensible y selectiva de micotoxinas y su aplicación el control de la seguridad alimentaria.

El objetivo principal de esta tesis doctoral ha sido el desarrollo de nuevos biosensores para el análisis de micotoxinas y hongos toxigénicos en alimentos. Con este fin, se han

explorado diferentes estrategias y formatos de ensayo evaluándose su impacto sobre los dispositivos desarrollados. En todos los casos, se han diseñado o seleccionado nuevos elementos de reconocimiento para llevar a cabo la detección sensible, selectiva, rápida y a bajo coste de estos contaminantes.

Entre los hongos toxigénicos, el género *Fusarium* es uno de los más comunes y ampliamente extendidos a nivel mundial. En la primera parte de esta tesis, se diseñaron sondas de ADN específicas para dos especies de *Fusarium* a partir de las regiones espaciadoras o intergénicas del ADN ribosómico. Esta aproximación permite distinguir entre especies hongos muy similares. Concretamente, se trabajó en la identificación de *Fusarium proliferatum* y *Fusarium verticillioide*s, ampliamente distribuidos en regiones templadas. Para el desarrollo del genosensor se diseñaron sondas de captura y detección, que permitieron su identificación inequívoca, a concentraciones picomolares, en muestras de maíz contaminadas naturalmente con dichos hongos, empleando ensayos de tipo sándwich y detección enzimática con un sustrato fluorescente. Para ello el ADN genómico se amplificó mediante PCR utilizando un par de cebadores comunes. Los resultados obtenidos demuestran la selectividad de los biosensores desarrollados para *F. verticillioides* y *F. proliferatum*, y constituyen una valiosa herramienta para evaluar la contaminación de alimentos con hongos toxigénicos. Actualmente, estamos trabajando en la integración de este genosensor en un dispositivo microfluídico.

En la segunda y principal parte de la tesis se han desarrollado inmunoensayos y plataformas biosensoras basados en medidas de luminiscencia para el análisis de micotoxinas. Concretamente, se han analizado fumonisina $B_1$, toxina T-2 y zearalenona utilizando péptidos miméticos o mimopéptidos. Dichos mimopéptidos imitan el epítopo característico de un antígeno, uniéndose al mismo parátopo que éstos en el correspondiente anticuerpo selectivo. Su empleo evita los problemas asociados a la fabricación y utilización de conjugados tóxicos de las micotoxinas de los inmunoensayos convencionales. Para seleccionar los mimopéptidos se ha aplicado la técnica de despliegue de proteínas o péptidos sobre la superficie de fagos ("*phage display*"). Los dispositivos desarrollados emplean, alternativamente, los fagos que despliegan el mimopéptido de interés o el mimopéptido obtenido sintéticamente. Los péptidos sintéticos se han utilizado para el desarrollo de "*microarrays*" e inmunoensayos basados en el empleo de partículas magnéticas para la determinación de micotoxinas. Se han alcanzado límites de detección muy inferiores a los límites máximos de residuos establecidos por la Unión Europea.

Por otra parte, se han diseñado y producido proteínas de fusión recombinantes compuestas por los mimopéptidos de las micotoxinas estudiadas y una proteína fluorescente (proteína fluorescente amarilla, YFP del inglés *yellow fluorescent protein*), o bioluminiscente (luciferasa *Gaussia,* GLuc del inglés *Gaussia luciferase*), que evita el empleo de anticuerpos secundarios, o de micotoxinas marcadas con una sonda luminiscente. Las proteínas recombinantes se han aplicado al desarrollo de dos tipos de ensayos. El primero se basa en un formato de tipo heterogéneo, empleando proteínas de fusión del péptido mimético y YFP, o GLuc, con el anticuerpo selectivo inmovilizado. En el segundo caso, la proteína recombinante se empleó en un ensayo de tipo homogéneo, utilizando nanopartículas de oro y medidas de desactivación de la fluorescencia. Este ensayo se realiza en una única etapa, sin la necesidad de lavados, reduciéndose el tiempo de análisis. La simplicidad y excelentes características analíticas de los métodos desarrollados son de gran utilidad para la determinación de micotoxinas en alimentos.

# 1 Introduction

## 1.1 Mycotoxigenic fungi

### 1.1.1 FUNGAL SECONDARY METABOLISM

Fungi are possibly the most diverse eukaryotic kingdom which has been estimated to comprise more than 1.5 million species including ubiquitous molds, yeasts, mushrooms, and polypores that are differentiated from plants and animals by their cell walls made of chitin and absorption as a mode of nutrition.[1] Although fungi are most abundant in tropical regions they can be found worldwide, partly because they are versatile by virtue of their high degree of adaptability to a variety of conditions.[2] Among the immense fungi kingdom there are several species which have served as important models for biomedical research, certain molds have become utterly renowned as producers of drugs, such as antibiotics, while others have been used in the production of cheese or in the fermentation of wine for centuries.[1] At the same time, many fungal species also present severe threats to human health. Fungal infections can have lethal consequences on human and animals, as well as in crops where fungal contamination causes more economic damage than any other group of microorganisms.[3] Fungi can also produce a range of toxic natural products which may pose severe health risks to humans and animals if they enter into the food chain.

Most fungi can grow in a wide variety of different habitats, including soil and water, frequently as symbionts or endophytes with other organisms, including bacteria, plants, algae, and animals, and become essential to their survival.[4,5] While some fungi obtain their nutrients from living hosts,[5] others have been forced to develop different lifestyles and modes of interaction with their hosts, such as killing the host and living off the dead organism, or growing fast on the plant surface preventing the survival of other competitors.[6,7] Fungi have also developed a number of strategies for protection and communication, one of which is the production of different types of secondary metabolites.[1]

Filamentous fungi, or molds, are multicellular organisms which grow by apical extension of their filaments.[6] These species are recognized as producers of many interesting secondary metabolites with a remarkable bioactive nature. In fact, more than half of such isolated compounds have been reported to display antibacterial, antifungal or antitumor activity.[8] Secondary metabolites are usually produced late in the growth of the fungi, often upon entering the stationary or resting phase,[9] and they are mainly synthesized by polymerization of primary metabolites by dedicated enzymes.[8] The transcriptional activation of the genes encoding for these enzymes depends on the developmental stage of the fungi and is often a consequence of environmental stimuli, such as temperature, light, and nutritional input. Unlike primary metabolites which are essential for normal growth, development, or reproduction, the role of secondary metabolites is less obvious. Although secondary metabolites are not directly involved in any fundamental metabolic processes, they exhibit a variety of biological activities which can contribute to the survival of the fungi in its environment, be crucial in fungal development, or actively shape the interactions with other organisms.[1]

The wide variety of bioactive secondary metabolites produced by filamentous fungi range from beneficial drugs and antibiotics to harmful toxins, and only a small fraction of them have been subjected to detailed analyses or have a commonly known biological function.[5] In fact, the total number of fungal secondary metabolites has been estimated to be from 2000 to as many as 3 million unique secondary metabolites.[10] Many of them have been found as the cause of intoxications, others are known for their antibacterial or pharmaceutically beneficial properties, whilst some remain simply as laboratory curiosities. Renowned secondary metabolites include, for example, natural pigment melanin which has been shown to have a protective role against ultraviolet (UV) damage and is required for the spore survival.[9] Other secondary metabolites function as weapons for the fungi defense, although at physiologically relevant concentrations, these metabolites have also been suggested to act as signaling molecules rather than as toxins.[8] Probably, the most prominent fungal secondary metabolites are antibiotics, such as penicillin, cephalosporin and other β-lactams, which have virtually revolutionized the treatment of infectious diseases. Other pharmaceutically important fungal secondary metabolites include immunosuppressive drugs, such as cyclosporin and mycophenolic acid which have an enormous clinical significance in organ transplantation.[11] Some secondary metabolites, such as the gibberellins, are infamous for their role as plant growth hormones, or for their insecticidal properties like in the case of peramine and lolines.[12] In fact, some toxic metabolites have been shown to protect the infected plants against insects suggesting their production as a possible manner for the fungi to limit competition for its food supply.[13] Certain toxins, known as mycotoxins, which are toxic to vertebrates in distinction from other metabolites, such as antibiotics, which affect only prokaryotes or other eukaryotes,[14] include a vast array of toxic and carcinogenic molecules which pose a severe threat to human and animal health.[3]

### 1.1.2 MYCOTOXIN PRODUCTION BY FILAMENTOUS FUNGI

Fungi that produce mycotoxins are referred to as mycotoxigenic fungi which include a wide variety of diverse fungal species which, in general, are not aggressive pathogens. The most important mycotoxins are produced primarily by three genera, *Aspergillus*, *Penicillium*, and *Fusarium*. Also, the genus *Alternaria* includes several mycotoxigenic species which play an important role in plant pathogenesis.[15] Many mycotoxins are produced by several species in one genus, but some toxins can be produced by species in phylogenetically different genera (**Table 1**). Whether the production of related mycotoxins in different genera is caused by horizontal gene transfer or by parallel evolution is not yet known.[16] Curiously, some strains are also known to produce different compounds or even produce the same compounds by different biosynthetic pathways.[17]

*Aspergillus* genus is the main producer of aflatoxins, and it commonly affects corn, cotton, peanuts, and certain tree nuts. Although the genus is not considered to be a major cause of plant diseases, it has a huge agricultural impact due to the high toxicity of the mycotoxins produced. Certain species in this genus produce not only harmful but also beneficial metabolites, such as drugs, and they are widely used in biotechnology, for example for the production of hydrolytic enzymes.[15,18] Species of the genus *Alternaria* are ubiquitous and abundant in the atmosphere as well as in soil, seed, and agricultural commodities. The genus is widely distributed in the environment and can infect more than 4000 host plants. These species are not only pathogenic to plants, causing spoilage and significant economic losses, but they also produce a wide variety of toxic secondary metabolites, mainly phytotoxins.[15,19] The genus *Penicillium* has its claim to fame as the producer of the first antibiotics discovered nearly a century ago, although some species of the genus are also renowned plant pathogens or mycotoxin producers. *Penicillium* fungi are typically associated with the storage of crops and the production of mycotoxins such as ochratoxin.[10] This complex genus, in terms of the number of species and range of habitats, is of great economic importance primarily as a cause of food and feed spoilage.[19]

Genus *Fusarium* is an extensively studied and widely-spread fungi. This genus has been associated as endophytes or with plant diseases with virtually every plant family, and thus *Fusarium* contamination can result in significant economic losses. Moreover, many *Fusarium* species are known to directly incite diseases in plants, humans, and domesticated animals, and they are notorious producers of several mycotoxins.[20] Variety of diseases caused by *Fusarium* in plants include root and stem rots, cankers, wilts, fruit or seed rots, and leaf diseases. In small grains, such as wheat and barley, *Fusarium* produces *Fusarium* head blight, a disease which is mainly associated with temperate regions and leads to serious reductions in the grain quality.[21] While some *Fusarium* strains have a wide host range and can colonize a variety of different crops, others are more restricted, such as *F. verticillioides* which is associated only with maize that can be infected with *Fusarium* ear rot.[17] Interestingly, *Fusarium* fungi can also grow as apparently symptomless endophytes under many conditions.[20] Thus, although fungal infections in the field are primarily transmitted by airborne spores, also infected but asymptomatic seeds can spread the infection.[22] Moreover, largely as a consequence of their ability to live without oxygen, species of *Fusarium* occur in almost every environment making them probably the most prevalent pathogen in maize and many other grains.[14,23]

Table 1. Examples of the most common mycotoxin-producing fungi and agricultural products commonly affected by these species.[14–16,20,24]

| Fungi species | Commodities affected | Major mycotoxins produced |
|---|---|---|
| ***Aspergillus*** | | |
| *A. flavus* | Ubiquitous in foods, mainly maize, peanut, and cottonseed | $AFB_1$ and $AFB_2$<br>Cyclopiazonic acid<br>Sterigmatocystin |
| *A. parasiticus* | Peanut, maize, cotton, spices, walnut | $AFB_1$ and $AFB_2$<br>$AFG_1$ and $AFG_2$ |
| *A. niger* | Grapes, maize, coffee, peanuts | OTA<br>$FB_2$, $FB_4$, $FB_6$ |
| *A. carbonarius* | Grapes, coffee, spices | OTA |
| *A. ochraceus* | Maize, peanuts, cottonseed, rice, cereal grains, coffee, spices | OTA, ochratoxins B and C<br>Penicillic acid |
| ***Penicillium*** | | |
| *P. citrinum* | Cereals, foods, feedstuffs | CIT |
| *P. verrucosum* | Cereals, stored grains, cured meat, cheese | OTA, CIT<br>Cyclopiazonic acid<br>Tenuazonic acid |
| *P. expansum* | Fruits, especially apples | Patulin<br>Tenuazonic acid<br>CIT |
| ***Fusarium*** | | |
| *F. graminearum* | Maize, wheat, barley | DON, nivalenol<br>ZEA, zearalanone, zearalanol |
| *F. culmorum* | Cereals | DON, nivalenol<br>HT-2 toxin<br>ZEA, zearalanone |
| *F. oxysporum* | Several crops, such as bean, cotton, potato, tomato, and banana | $FB_1$, $FB_2$, $FB_3$<br>Enniatins |
| *F. proliferatum* | Maize, wheat, sorghum, mango, asparagus | $FB_1$, $FB_2$, $FB_3$, $FB_4$<br>Moniliformin<br>Beauvericin |
| *F. verticillioides* | Maize | $FB_1$, $FB_2$, $FB_3$<br>DON<br>Zearalanone |
| *F. sporotrichioides* | Maize, small grains | T-2 toxin<br>HT-2 toxin<br>Beauvericin |
| ***Alternaria*** | | |
| *A. alternata* | Tomato, pear, apple, strawberry | Alternariols |
| *A. tenuissima* | Tomato, grapevine, strawberry | Alternariols<br>Tenuazonic acid |

*Abbreviations: aflatoxin $B_1/B_2$, $AFB_{1/2}$; aflatoxin $G_1/G_2$, $AFG_{1/2}$; citrinin, CIT; deozynivalenol, DON; fumonisin $B_{1-6}$, $FB_{1-6}$; ochratoxin A, OTA; zearalenone, ZEA.*

As a genus, *Fusarium* lacks certain morphological characters that can be used to easily differentiate the species, which has led to a somewhat confusing nomenclature among this family.[20] When the genus was first introduced in 1809, the primary character of *Fusarium* was the presence of a distinctive canoe- or banana-shaped conidia, but to date many *Fusarium* species have been poorly defined and characterized, and different biologies of morphologically similar strains have complicated the study of *Fusarium*.[20] Among the *Fusarium* genus, *F. verticillioides* and *F. proliferatum,* are among the most significant producers of toxic mycotoxins.[25] *F. proliferatum* is known to cause diseases worldwide in many crops, most important one being maize,[20] and it has been reported to produce a wide variety of mycotoxins often at high levels. The wide host range of this fungus has resulted in recovering these toxins from seemingly unlikely sources, such as asparagus or garlic.[20] The macroconidia of *F. proliferatum* is similar to other species in *Fusarium fujikuroi* species complex (formerly known as the *Gibberella fujikuroi* species complex), and in fact, *F. proliferatum* is easily confused with *F. fujikuroi, F. oxysporum, F. thapsinum,* and *F. verticillioides.* Another important mycotoxin producer, *F. verticillioides,* formerly known as *F. moniliforme,* is one of the most prevalent seed-borne fungi associated with maize worldwide,[26] and it is known not only as a mycotoxin producer but also for being allergenic to human and capable of infecting cancer.[20]

Due to the wide diversity of mycotoxin-producing fungi in a wide variety of crops both before and after the harvest, it is difficult to make general statements about the occurrence of the mycotoxigenic fungi. Some toxigenic species, mainly from *Fusarium* and *Alternaria* genera*,* are often classified to as "field fungi" because they require very high moisture content, whereas "storage fungi," such as *Aspergillus* and *Penicillium*, can also grow in low moisture environments.[19] More commonly these species occur in temperate regions, and climate change due to global warming has been estimated to alter the incidence of toxigenic fungi and even modify host resistance and host–pathogen interactions.[15] In addition to crops and plants, certain mycotoxigenic fungi, for example some species of *Fusarium* and *Aspergillus,* have been found in moisture-damaged buildings.[27]

Furthermore, the occurrence of mycotoxigenic fungi and subsequent mycotoxin contamination are affected by numerous external factors. Some are related to the susceptibility of crops, plant stress, harvesting practices, and storage of grains. First of all, fungal growth itself depends on favorable environmental conditions, and therefore, their occurrence varies among geographical areas and is strain-specific.[28] For example, infection and ear rot by *F. verticillioides* and *F. proliferatum,* along with subsequent mycotoxin contamination, are more common in warm and dry weather, and, although not conclusive in all crops, high temperatures seem to play a role for example in aflatoxin contamination.[10] Additionally, some microenvironmental factors are known to be a factor in mycotoxin production. For instance, the nitrogen and carbon sources that the fungi utilize as well as the pH of the environment are known to modulate mycotoxin production at the cellular level. Moreover, many epigenetic factors and environmentally activated genes have been identified to be relevant at the genomic level for certain mycotoxins. Production of mycotoxins also depends on when the infection occurs and on the host environment.[29,30] For example, insect damage is known to play a large role in mycotoxin contamination in several species.[15]

Although it is widely acknowledged that mycotoxins are usually produced to protect the fungi against other organisms, it still remains partly unanswered when and how fungi produce these toxins.[21] Proper harvesting practices and storage conditions are known to be a factor in

the initiation of fungal contamination and mycotoxin production.[29] Fungal contamination can be prevented by correct harvesting techniques, such as harvesting at the appropriate time after maturation of plants and inspecting of the harvesting equipment and storage facilities before the harvest.[29] Nevertheless, for the detection of a fungal infection and the potential for mycotoxin contamination, it is essential to develop methods to determine the presence of these mycotoxigenic species.

### 1.1.3 CONVENTIONAL METHODS FOR FUNGAL ANALYSIS

In order to detect mycotoxins or prevent their formation, it is essential to identify their producers. However, it has been a difficult task because the taxonomy of mycotoxigenic fungi is complicated and many taxonomical concepts have changed over the last centuries. Moreover, although the identification methods have rapidly evolved, many laboratories working with mycotoxins lack the required equipment for the most sophisticated analyses. As a result, there exists a number of misidentifications and incorrect connections between fungal species and mycotoxin production.[16]

Conventionally toxigenic fungi have been identified mainly based on morphological and cross-fertility criteria. However, recognition of the morphological characters is not always enough to accurately identify fungal isolates at the species level. In fact, these analyses are time-consuming and demand expertise in taxonomy and physiology of the fungi.[21] Accurate morphological characterization requires that the fungus is subcultured and handled with care, and moreover, growing fungus in a media that is appropriate for the morphological features to develop can take several weeks.[20] At the same time, the taxonomy of mycotoxigenic fungi is intricate, especially within the genera *Penicillium, Aspergillus, Alternaria,* and *Fusarium,* and the classification is still in a state of flux and new species continue to be described.[16] For these reasons, molecular diagnostics can offer interesting alternatives, although differentiation of some closely related species remains challenging.[20]

The availability of next-generation sequencing in the 21st century has significantly changed the concepts of fungal identification. As the genes responsible for the most important fungal contaminants have been identified, with alpha taxonomy and reliable sequence databases the presence of fungi in crops can be identified.[31] Thus, the development of methods for fungal detection based on polymerase chain reaction (PCR) has arisen as an alternative for culture-based methods. Since PCR-based methods are not dependent on the morphology and cultivability of the fungi, they can provide more reliable results and offer the possibility for multiplexing. PCR allows amplification of specific DNA fragments even from complex samples, and the amplified PCR products can be observed after gel electrophoresis and staining with DNA binding dyes.[21] More advanced technologies, such as real-time PCR, also known as quantitative PCR (qPCR),[32] have enabled monitoring DNA amplification in real time by using fluorescent reporter molecules. The fluorescence produced by the reporter increases as the reaction proceeds proportionally to the accumulation of the PCR product after each amplification cycle, which allows fast detection, identification, and quantification of the target. On the other hand, PCR has been combined with different technologies, such as restriction fragment length polymorphism, denaturing gradient gel electrophoresis, single-strand conformation

polymorphism, microsatellite length polymorphism, or enzyme-linked immunosorbent assays (ELISA).[16]

Some recommendations for identifying fungal species involve initial recognition of the fungal genus using morphological criteria and subsequent validation using molecular methods. Thus, in practice, fungal isolates are grown on a battery of indicative media and identified based on a combination of morphological, physiological, nutritional, and chemical data. For example, *Fusarium* isolates can be identified on Specifikke nutrient-arme agar (SNA), potato dextrose agar (PDA) and yeast extract sucrose (YES) agar.[20] Confirmatory analyses are often achieved by a BLAST (basic local alignment search tool) search of the DNA sequence of specific house-keeping genes, such as β-tubulin and calmodulin genes which usually provide good resolution at the species level.[16]

PCR can also target conserved functional genes or regions of taxonomical interest, or alternatively, focus on the genes involved in mycotoxin production.[16] For example, the biosynthetic pathway of fumonisins has been extensively studied and is known to be linked to 17 fumonisin biosynthetic (*FUM*) genes. The *FUM* gene cluster has been described in several fumonisin producers, and primer pairs designed for these sequences, mainly to *FUM1*, *FUM6,* and *FUM8*, have been used to detect fumonisin-producing *Fusarium* strains by PCR.[16] Real-time reverse-transcriptase (RT) PCR assays have been used to correlate the expression levels of *FUM1* and *FUM19* and fumonisin production in *F. verticillioides.* Moreover, specific primers designed on the *FUM1* and *FUM19* have enabled differentiation of closely related species, such as *F. verticillioides* and *F. proliferatum*.[33,34] On the other hand, the ribosomal genes include highly conserved parts, the 18S, 5.8S, and 28S units, which are separated from each other by two internal transcribed spacer regions (ITS1 and 2), and the repeated modules are linked by internal spacer regions (IGS). These spacer regions include high variability between different species and can be used to distinguish even closely related species. Furthermore, the multi-copy nature of ribosomal DNA is beneficial when quantifying small quantities of DNA. In comparison to assays using single-copy genes, the sensitivity can be more than 100 times better.[16,35]

Undoubtedly, novel molecular technologies have made significant contributions to the identification, characterization, and detection of fungal species. Moreover, the available databases of genomic DNA sequences and the increasing understanding of fungal epigenetics have simplified the design of new assays. Various methodologies and platforms reported in recent years for the detection of mycotoxin-producing fungi in food commodities have been established as an important tool for environmental and food safety. In this regard, the development of molecular technologies have also had a substantial influence on research in plant pathology, the management and control of plant disease.[16]

# 1.2 Mycotoxins

## 1.2.1 ORIGIN AND NATURE

The word mycotoxin, a combination of the Greek word for fungi or mold, *mykes,* and the Latin word *toxicum* meaning poison,[36] was originally established in 1962, after an unprecedented veterinary crisis in England, during which nearly 100 000 turkeys died of a mysterious "Turkey X" disease.[37] The incident was linked to the intake of moldy feed contaminated with toxic secondary metabolites from *Aspergillus flavus* and prompted the research on the toxicity and prevalence of these compounds identified as aflatoxins marking the beginning of what is often considered as modern mycotoxicology.[10,18] Despite the relatively short history of the word mycotoxin, the appearance of these toxins in food and feed has been suggested to origin back to the early stages of agricultural history for up to 10 000 years ago when cultivation and storage of crops began thus creating a new ecological niche for fungal growth.[31]

Mycotoxins are defined as low molecular weight products which are produced as secondary metabolites by filamentous fungi. This assemblage is chemically and toxigenically rather heterogeneous, but generally these toxins are known to cause disease and death in human and other vertebrates.[38] As secondary metabolites mycotoxins are not directly involved in fundamental metabolic processes, and they have no necessary function in the life cycle of the producer cells. Nonetheless, secondary metabolites usually have a role in a range of cellular processes such as transcription, development, and intercellular communication,[39] and although the complete function of mycotoxins is not understood, they are believed to display different biological activities which contribute to the survival of the fungi possibly by eliminating competing microorganisms from their growth environment.[1,14] Although all mycotoxins are of fungal origin, not all toxic compounds produced by fungi are classified as mycotoxins. Fungal products which are mainly toxic to bacteria, such as penicillin, are called antibiotics, whilst products toxic to plants are called phytotoxins.[38] On the other hand, mycotoxicoses, *i.e.,* diseases caused by mycotoxins, do not include mushroom poisonings which result from intentional consumption of mushrooms as food.[17]

Mycotoxins are usually very stable molecules which are produced by several genera, the most important ones being *Penicillium*, *Aspergillus*, and *Fusarium* species. Major crops commonly infected by these fungal species include cereals, cocoa, coffee, nuts, fruits, and beans.[1] Mycotoxins are heat-stable, and thus they are not destroyed by normal industrial processing or cooking and cannot be eliminated entirely without damaging the food.[14,23] Essentially, mycotoxin contamination is often inevitable due to the widespread of mycotoxigenic fungi, particularly in temperate and tropical regions of the world, and some calculations have estimated that approximately 25–50% of world crops are contaminated with mycotoxins,[40] making mycotoxins a major problem in food safety.

### 1.2.2 MYCOTOXINS AND FOOD SAFETY

More than 200 diseases, ranging from diarrhea to cancers, are related to food contaminated with natural toxins, harmful bacteria, viruses, parasites or other chemical substances, and the World Health Organization (WHO) has estimated that annually the death of 2 million people can be linked to unsafe food.[41] Food contamination can occur at any point during production, storage, distribution or preparation of foodstuffs, and thus it is essential that the entire production chain, from producer to consumer, is aware of the risks of unsafe food and the regulations set by the authorities to guarantee food safety.

A particular concern is related to low molecular weight food contaminants, such as mycotoxins, which are often hard to detect owing to their small size. The occurrence of mycotoxins in food can have major consequences, including fatal health effects and serious economic implications due to losses of food and feedstuff and diminished animal production.[16] Several severe incidents caused by mycotoxin contamination leading to intoxications in both human and animals are known throughout history.[1] The oldest recognized mycotoxicosis in humans occurred in the medieval times when an epidemic of ergotism, known as St. Anthony fire, arose as a consequence of fungal contamination in grains and was traced back to infection by the fungus *Claviceps purpurea*.[10] Several similar incidents have been reported, for example, cardiac beriberi in Japan during the 19$^{th}$ and 20$^{th}$ centuries which was connected to moldy rice contaminated with *Penicillium,* or the alimentary toxic aleukia, described in particular in the Soviet Union during World War II, which was associated with consuming grains contaminated with *Fusarium.*[31] Despite the increasing knowledge on mycotoxins as well as the actions for their detection and prevention, still in the 21$^{st}$ century some incidents of severe mycotoxicoses have been reported, such as aflatoxin poisoning in Kenya in 2004 leading to death of 125 people,[42] and aflatoxicosis in dogs after exposure to contaminated commercial dog food in the USA in 2005.[43]

Mycotoxins can be acutely or chronically toxic, or both at the same time, depending on the type of mycotoxin in question, the extent and duration of the exposure, the health and age of the exposed individual, as well as many other poorly understood synergistic effects involving genetics, dietary status, and interactions with other toxins.[14,38,40] Exposure to mycotoxins occurs mostly by ingestion of contaminated food, although it can also follow dermal contact or inhalation of toxicogenic molds containing mycotoxins.[14,40] Regardless of the way they get in contact with humans or animals, mycotoxins generally cause lowered performance, sickness, or even death already at very low concentrations.[31,38] Their range of actions include cytotoxic, nephrotoxic, hepatotoxic, teratogenic, mutagenic, carcinogenic, immunosuppressive, or estrogenic effects (Table 2).[1,40] Generally, the toxic effects of mycotoxins, are better understood in animals than in humans since the experimental studies appear more reliable.[14] While the health effects count for the most significant risk of mycotoxin contamination also the economic losses caused by mycotoxins and fungal contamination are worth mentioning. The economic consequences are diverse and can be associated with a reduction of food quality, reduction in animal production due to diseases or feed refusal, as well as increasing medical costs of mycotoxicosis treatments.[29,31]

Several national and international institutions and organizations, such as WHO, the European Commission (EC), the US Food and Drug Administration (FDA), and the Food and

Agriculture Organization (FAO) of the United Nations, have recognized the potential risks posed by mycotoxin contamination and addressed this problem by adopting laws and regulatory limits for major mycotoxin classes and selected individual mycotoxins.[44] For example, the European Food Safety Authority (EFSA) has been established to scientifically evaluate and communicate on the risks associated with the food chain with a central goal to protect consumer health by guaranteeing a high level of food safety. A key element of this is testing foodstuffs for the presence of various chemical and biological hazards and setting up regulatory limits to guarantee safe food for the consumer.[45] European Commission regulations and recommendations have established maximum residue limits (MRLs) for the major mycotoxins, including aflatoxins, ochratoxin A, patulin, deoxynivalenol, zearalenone, fumonisins, T-2 and HT-2 toxins, citrinin, and ergot alkaloids in food and feeds.[46–52]

Although the awareness related to the hazards of mycotoxins as food and feed contaminants is growing, there are no absolute measures available for eliminating mycotoxin contamination. While mycotoxin occurrence in the field can be decreased by good agronomic practices and planting resistant varieties, in the end, analytical methods capable of detecting mycotoxins even at low concentration are of key importance for ensuring food safety. Despite the efforts, as yet, many countries still lack appropriate guidelines to protect the consumers from the harmful effects of mycotoxins. Moreover, although the regulations in many countries are based on worldwide recommendations, there still remains a need for the regulations to be harmonized from country to country especially where trade contracts exist. Also, some concern has been raised about the regulatory levels becoming more strict as a response to the development of more sensitive detection methods rather than basing them on realistic health effects.[10,17]

### 1.2.3 OVERVIEW OF THE MOST ABUNDANT MYCOTOXINS

Following the discovery of aflatoxins in the 1960s, numerous other mycotoxins have been identified and nowadays far more than 400 compounds, produced by some 350 fungal species, have been described in the literature.[14] Currently, approximately 30 mycotoxins are considered a threat to human and animal health due to their toxic effects.[38] The major classes of mycotoxins are aflatoxins, ochratoxins, fumonisins, trichothecenes, zearalenone, and ergot alkaloids (Table 2). The classification of mycotoxins can be considered challenging due to their diverse chemical structures and biological effects. Whilst mycologists classify mycotoxins by the fungi that produce them, organic chemists have tried to classify them by structure, physicians and clinicians by the illness they cause or by the organ they affect, and biochemists according to their biosynthetic origin.[38]

Aflatoxins (AF), produced mainly by *Aspergillus flavus* and *Aspergillus parasiticus* in grains and legumes, are the most dangerous mycotoxins worldwide due to the widespread human exposure to high levels of aflatoxins and their carcinogenic properties. The naturally occurring aflatoxins are $AFB_1$, $AFB_2$, $AFG_1$, and $AFG_2$, for which “B” and “G” refer to the blue and green fluorescent colors produced by these compounds under UV light, among which $AFB_1$ is the most abundant and toxic.[1] In fact, $AFB_1$ is recognized as one of the most efficient inducers of liver cancer, and the International Agency for Research on Cancer (IARC) has included naturally occurring aflatoxins in group 1 carcinogens, considering the high degree of risk of this toxin to

human health.[53] In addition to the chronic effects, aflatoxin exposure may cause acute aflatoxicosis with vomiting, abdominal pain, hepatitis, and even death.[54]

Ochratoxins were the first group of mycotoxins identified after the discovery of aflatoxins.[14] Ochratoxin A (OTA), which is mainly produced by *Aspergillus ochraceus*, *Aspergillus carbonarius*, and *Penicillium verrucosum,* is a common mycotoxin because of the widespread of these fungal species which can grow in a wide range of conditions in both warm and cool climates.[1,29] Ochratoxins have been frequently isolated from cereal crops, meat products, and cheese varieties. The toxic mechanisms of OTA include inhibition of protein synthesis and disruption of hepatic microsomal calcium homeostasis.[14] OTA has been classified as a possible human carcinogen (group 2B) by IARC.[53]

Fumonisins, a group of polyketide mycotoxins produced mainly by *Fusarium verticillioide*s and *Fusarium proliferatum*, were discovered in 1988 as a result of many years of studying the moldy corn poisoning in horses, known as equine leukoencephalomalacia.[55,56] These toxins were recognized to be highly hepatotoxic and cardiotoxic in rats and were also linked to porcine pulmonary edema in pigs.[57] Later studies have identified fumonisins as the cause a variety of diseases in animals,[58] including both liver and kidney tumors in rodents,[25] and they have been linked to human carcinogenesis[59] and neural tube defects,[60] as well as plant diseases.[61] At least 15 different fumonisins have been identified,[26] among which fumonisin $B_1$ ($FB_1$) is the most prevalent and toxic. Based on animal studies and cases of human esophageal cancer, IARC has categorized $FB_1$ as possibly carcinogenic to humans (group 2B).[53] $FB_1$ bears a similar structure as cellular sphingolipids, and the toxicity of fumonisins appears to be a result of the interference in the metabolism of sphingolipids by inhibiting the enzyme ceramide synthase.[1,26] Fumonisins are common contaminants in maize but can also occur, for example, in wheat, sorghum, barley, soybean, and black tea. Because of the similar growth conditions of the toxigenic fungal species, fumonisins often co-occur with aflatoxins, especially in maize.[29] Fumonisins differ from most known mycotoxins by their hydrophilic nature which makes them difficult to study and potentially more harmful to human health, as they can remain undetectable most of the time. Moreover, it raises the specter that there might be many other mycotoxins yet to be discovered due to their hydrophilic nature.[38,40]

Trichothecenes are a large class of mycotoxins produced by several fungal genera, mainly *Fusarium*. They are nonvolatile low molecular weight compounds which share a common 12,13-epoxytrichothene skeleton that is responsible for their toxicological activity which is due to inhibition of protein or DNA synthesis or inhibition of the mitochondrial electron-transport system.[14,29]. Among the trichothecenes, deoxynivalenol (DON), produced mainly by *Fusarium graminearum* and *Fusarium culmorum*, is the most common and most widely studied, although also amongst the least toxic.[38] Type B trichothecene DON occurs mostly in grains such as wheat, barley, oats, rye, and maize throughout the world, and its capacity to provoke vomiting episodes in various species including humans clarifies its commonly used nickname “vomitoxin”.[1]

Highly similar T-2 and HT-2 toxins are type A trichothecene mycotoxins which are closely related epoxy-sesquiterpenoids produced by several *Fusarium* species. Both of these toxins have been found in grains, such as wheat, maize, oats, barley, rice, and beans.[25] HT-2 toxin and T-2 toxin, which is often rapidly metabolized to the former, are relatively stable withstanding grain processing, baking, and cooking, and in some cases, these toxins can even be enriched in cereal by-products.[62] The toxic effects of T-2 and HT-2 toxin include the inhibition of protein synthesis which also affects the synthesis of immunoglobulins and the humoral immunity.[25,62]

Zearalenone (ZEA) is produced by different species of *Fusarium* fungi which are pathogenic to cereal crops worldwide. Production of ZEA takes place mainly in temperate conditions before harvesting, but might also occur during or after harvest if the crops are not handled or dried properly.[1] The classification of zearalenone as mycotoxin is somewhat controversial; while it is biologically potent, the effects are hardly toxic, and in fact, it resembles 17β-estradiol and has thus been suggested to be classified rather as a nonsteroidal estrogen or mycoestrogen.[38]

Citrinin is a mycotoxin commonly found in maize, wheat, rye, barley, oats, and rice, and it is recognized mainly for its nephrotoxicity. Citrinin was first extracted from a culture of *Penicillium citrinum* but has been later found to be produced by species from *Penicillium, Aspergillus,* and *Monascus* genera. Interestingly, citrinin displays antibiotic activity against Gram-positive bacteria and has been described as a promising insecticide, although its application as a drug has been limited because of the high toxicity.[14]

Other well-known mycotoxins include for example ergot alkaloids which are the cause of ergotism, one of the oldest recognized mycotoxicoses, produced primarily by several species of plant pathogenic *Claviceps*, and patulin which is commonly found in apples and apple products, and occasionally in other fruits.[1] Additionally, the so-called "emerging mycotoxins" have raised concern in recent years. This group includes, for example, fusaproliferin, beauvericin, enniatins, and moniliformin. At the moment there is little available knowledge available on these toxins, but recent research efforts are focusing on determining their toxicity and occurrence.[29] Moreover, the presence of toxin precursors, metabolites, degradation products, or the so-called masked mycotoxins also represents a potential threat to consumer safety. The presence of these compounds may increase the toxicity of food commodities with an apparently low concentration of the parental toxin. Besides, their detection is in many cases still in its infancy. Such metabolites and masked mycotoxins have been reported at least for trichothecenes, fumonisins, ochratoxins and zearalenone.[25]

**Table 2.** Most abundant and toxic mycotoxins and their toxic effects.[1,14,38,53,63–66]

| Mycotoxin | Structure | Mechanisms of toxicity | Effects |
|---|---|---|---|
| Aflatoxins (AF)<br>$AFB_1$, $AFB_2$<br>$AFG_1$, $AFG_2$<br>$AFM_1$ | 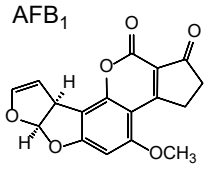 | DNA damage by the metabolized 8,9-epoxide form of $AFB_1$ | Acutely toxic, carcinogenic, immunosuppressive mutagenic, hepatotoxic, teratogenic |
| Citrinin (CIT) | 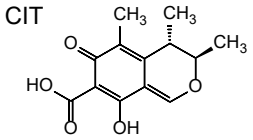 | Inhibition of RNA and DNA synthesis, induction of oxidative stress | Cytotoxic and nephrotoxic |
| Deoxynivalenol (DON) | 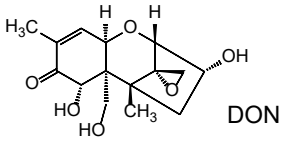 | Inhibition of protein synthesis by binding to ribosomes | Cytotoxic and genotoxic, causes nausea, vomiting, and diarrhea |
| Fumonisins<br>$FB_1$<br>$FB_2$ | 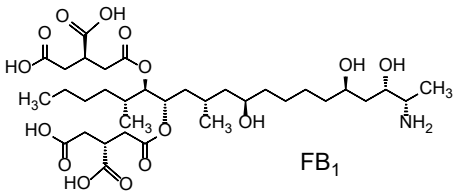 | Interferes with sphingolipid, phospholipid and fatty acid metabolism | Hepatotoxic, carcinogenic, teratogenic |
| Ochratoxin<br>OTA | 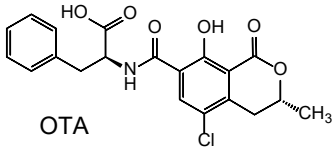 | Inhibition of protein synthesis and mitochondrial ATP production | Carcinogen, nephrotoxic, teratogenic, immunosuppressive |
| Patulin | 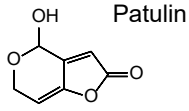 | DNA damage by formation of reactive oxygen species (ROS), induces apoptosis | Genotoxic, immunotoxic, neurotoxic, teratogenic |
| T-2 toxin<br>HT-2 toxin | 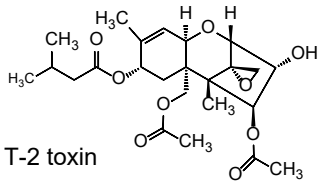 | Inhibition of protein and DNA synthesis | Cytotoxic, immunosuppressive |
| Zearalenone (ZEA) | 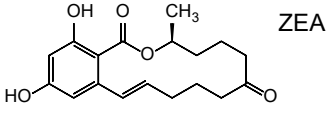 | Binding to oestrogenic receptors | Estrogenic |

### 1.2.4 CONVENTIONAL METHODS FOR MYCOTOXIN ANALYSIS

As the presence of mycotoxins is presently unavoidable, management strategies have been implemented to prevent the contaminated commodities from entering into the food chain. In 2003, the Council for Agricultural Science and Technology stated that the development of new technologies for mycotoxin analysis and improvement of detection (with specificity) of mycotoxins in prepared foods should be one important area of research that needs to be addressed in order to provide a safer food and feed supply in the 21st century.[10] Moreover, the requirement to meet the regulatory limits set by national and international authorities has prompted the development of a vast number of analytical methods for the identification and quantification of mycotoxins.[25]

Mycotoxins comprise a variety of different structures and occur in varying concentration ranges in a wide range of agricultural commodities, foodstuffs, and biological samples, and therefore, it is rather impossible to develop a single standard protocol for their analysis and detection. Thus, most methods target only individual mycotoxins, or at best a group of closely related mycotoxins. In principle, the detection methods can be divided into chromatographic methods, which are based on separation and detection of the toxins by different detectors, and bioanalytical assays or biosensors which rely on specific biorecognition elements capable of recognizing the target mycotoxin. The method chosen for each particular application should consider the sensitivity required, available instrumentation and expertise of the person performing the analysis, as well as the cost and analysis time.[25,67]

On the other hand, mycotoxin monitoring includes not only the analysis or quantification step but also the sampling and sample preparation.[16] Sampling refers to all the operations that are applied to a lot of an agricultural product and lead to a laboratory sample. This step specifies the size of the sample and how it is selected or taken from the lot, and it is often a major source of variability in mycotoxin analysis. Sample preparation includes grinding, homogenizing and sub-sampling in order to obtain an analytical portion for the actual analysis. This test portion is further solvent-extracted, most commonly with organic solvents, such as methanol, acetonitrile or acetone, depending on the physical properties of the analyte, and finally, the sample is analyzed to determine the mycotoxin concentration.[16,25]

Thin-layer chromatography (TLC) was the first chromatographic method to be applied to mycotoxin detection, and although nowadays it has been mainly replaced by more advanced techniques, TLC is still routinely used to some extent, for example, in developing countries. Additionally, TLC methods have been approved as AOAC International official methods for several mycotoxins, such as aflatoxins, OTA, DON, ZEA, and patulin. Improvements to the basic TLC include the use of high-performance TLC plates, two-dimensional and bi-directional TLC, quantification by fluorescence densitometry, or combined with surface-enhanced Raman spectroscopy.[16,68,69]

The predominant chromatographic method for mycotoxin detection is high-performance liquid chromatography (HPLC). The small size and polarity of most mycotoxins make them ideally suited for separation by reverse-phase HPLC using a variety of mobile phase compositions made up of water, methanol and acetonitrile or mixtures of these.[16] Most commonly HPLC separation is coupled with UV and fluorescence detectors which use either the natural UV absorption or fluorescence of the analyzed mycotoxins or suitable derivatization methods. For example, fumonisins and type A trichothecenes which naturally lack a UV absorption band require

derivatization before HPLC analysis.[16] Coupling of HPLC to mass spectrometry (MS) detection has enabled the development of analytical methods for the simultaneous quantification of mycotoxins, and it is considered as the reference method for unequivocal mycotoxin identification.[16,70] Recent developments in this field have provided interesting alternatives for the simultaneous detection of multiple mycotoxins, and moreover, MS-based detection has also contributed to the discovery unknown mycotoxins.[16,71,72] Also, some methods based on gas chromatography (GC) have been introduced, mainly for trichothecenes,[73,74] but the application of this technique for mycotoxin analysis is limited by the polarity of mycotoxins and often requires derivatization before injection into the GC column.[16] Chromatographic methods are useful for the separation and quantification of highly similar compounds, such as different analogs of aflatoxins or fumonisins. However, they usually require labor-intensive sample preparation, for example using immunoaffinity columns (IAC)[75,76] or solid-phase extraction sorbents (SPE).[77,78] Moreover, despite the high sensitivity and specificity that can be achieved with these methods, they require expensive and bulky instrumentation and skilled personnel to perform the analysis.[69]

Biosensors and bioanalytical assays are usually more appropriate for applications where fast and simple analysis are preferred, perhaps with the cost of slightly lower sensitivity. Immunochemical methods which rely on the high sensitivity and specificity achieved by mycotoxin-specific antibodies might not reach the accuracy and precision of chromatographic methods but have several advantages, such as simplicity, speed, and applicability to analyses in field conditions.[25] For example, widely used ELISAs, in contrast to chromatographic methods, do not usually require profound sample clean-up but can be combined with fast extraction step in aqueous methanol or acetonitrile followed by dilution of the extract to avoid the matrix effect.[16] Moreover, the speed and low cost usually make ELISA a superior option over HPLC when a large number of samples are screened for a single mycotoxin. In their simplest format, ELISAs can be based on visual detection or colorimetric readers, but higher sensitivity can be achieved with fluorescent or chemiluminescent detection, and the development of biosensors can also offer real-time readout and even perform the entire process automatically.[67,79]

# 1.3 Biosensors for mycotoxin monitoring

## 1.3.1 GENERAL CONCEPTS AND DEFINITIONS

The importance of monitoring and regulating various biologically significant molecules in many different disciplines, such as clinical chemistry, environmental protection, drug discovery, forensics, and food industry, has provoked the development of reliable analytical devices capable of accurate analysis.[80–85] Biosensors can provide rapid, sensitive, low cost, real-time, and on-site analysis with compact and low power devices, and owing to their appealing advantages they have emerged as one of most interesting approaches to overcome the limitations of many conventional methods, for example, for environmental monitoring and point-of-care medical applications.[86]

A chemical sensor, a device which is capable of transforming chemical information into an analytically useful signal, conventionally contains two components, a receptor which is responsible for the chemical or molecular recognition and a physicochemical transducer which subsequently transforms the recognition event to a measurable signal.[87] A chemical sensor becomes a biosensor when the recognition system is based on a biochemical mechanism.[88,89] The high specificity and sensitivity of biomolecular recognition, which is typically driven by a concert of many weak interactions, is the cornerstone of a wide range of diagnostic and synthetic technologies, such as biosensors.[90] Biosensors come in all shapes and sizes, so to say, and whilst several factors affect their performance, the receptor and the transducer account for the most crucial elements. The essence of the specific target recognition relies on the receptor which is capable of binding to the target analyte with sufficient specificity and sensitivity. Biosensors can be classified according to the type of the receptor or recognition element, for example as immunosensors or aptasensors when based on antibodies and aptamers, respectively. On the other hand, the transducer generates an output signal and thus provides a means to measure the biorecognition event. In terms of the transducer properties, biosensors can be classified as electrochemical, electrical, optical, mass sensitive, thermometric, micromechanical, or magnetic sensors.[89,91,92]

Within the scope of biosensors or bioaffinity assays, various concepts have been developed for analyte detection. Direct methods are capable of measuring direct binding of the target analyte to a usually immobilized recognition element. However, frequently the biorecognition is based on non-competitive or competitive assay formats. **Figure 1** represents a schematic of the most common assay formats used in immunoassays although the same concepts can be further applied to other biosensors or bioaffinity assays using different recognition elements. Non-competitive assays are most often based on two recognition elements which bind simultaneously to the target and are used in excess (**Figure 1A**). The competitive, or reagent-limited, assays in turn are based on the competition of the target analyte with a labeled analyte analog for a limited number of binding sites (**Figure 1B**). Thus, the labeled analyte, also referred to as the tracer, provides a means of assessing the amount of the free and bound analyte.[93] This competitive principle, where the signal intensity correlates inversely to the concentration of the analyte, formed the basis for the very first immunoassays described,[94] and since then it has been widely used in various applications, even though the

format shows some fundamental limitations. Firstly, competitive affinity assays are inherently less sensitive than non-competitive ones, partly because the sensitivity of a competitive assay is mainly governed by the equilibrium constant of the recognition element and alternative assay designs or label technologies are not able to provide as significant improvements as in non-competitive ones.[93] Moreover, labeling of the analyte can be challenging or result in randomly cross-linked or unstable molecules, which can affect the biorecognition. Nevertheless, small molecules which are not capable of binding more than one recognition element at a time conventionally must be detected using a competitive assay format.

On the other hand, bioaffinity assays can also be classified as heterogeneous or homogeneous, regardless of being competitive or non-competitive. Heterogeneous assays rely on a solid surface where one of the assay components is immobilized (**Figure 1A–B**) and washing steps are used to remove the unbound reagents. The separation step and high binding capacity of the solid surface can have significant effects on the assay performance. Most frequently used solid phases range from microparticles to microtiter plates where the immobilized compound, be it the recognition elements or the competitor, can be merely absorbed by non-specific interactions or immobilized by different covalent or site-specific coupling methods. Although the physical coupling of the recognition element often restricts its movement to some extent and affects the reaction kinetics, it should not disturb the target binding remarkably.[93] Commonly, multiplexing in heterogeneous systems can be achieved, for example, by printing separate spots for different analytes in an array.[95,96]

In homogeneous assays, a change or modulation of the signal is observed as a result of analyte binding, for example, based on energy transfer from one labeled molecule to another (**Figure 1C–D**). Such assays do not require a separation step of the unbound reagents, and therefore, they are usually simple mix-and-measure methods. Kinetics are usually fast in the homogeneous format making the entire assay protocol shorter and more straight-forward than in heterogeneous assays because the time-consuming incubation and washing steps can be avoided. However, at the same time the incorporation of washing steps have some advantages for improving the assay sensitivity, such as minimizing the effects of non-specific binding, and at least theoretically, the heterogeneous format is more sensitive than the homogeneous one.[97]

The repertoire of methods based on these basic concepts and other assay schemes is vast and impressive. Significant research efforts in the field, together with recent advances in the material sciences, have enabled the development of sophisticated and miniaturized devices to respond to the growing need for novel analysis tools and new methods for medical sciences as well as for environmental and food safety.[86] Simultaneously, the intentions to create easy-to-use systems have provoked the development of home tests and new point-of-care devices which fully take advantage of the idea of biosensors to be simple and accessible to conditions outside well-equipped laboratories. The following paragraphs introduce briefly the most commonly used reporter systems in optical biosensors and the available recognition elements. Particular focus will be given to different applications for mycotoxin detection. Selected examples of recently reported methods using different recognition elements and transducers are collected in **Table 3**. In this context, various bioaffinity assays are described in the same section, albeit biosensors in their strictest definition do not include assays which require additional processing steps, such as reagent addition, and are not capable of continuous and reversible measurements.[92,98]

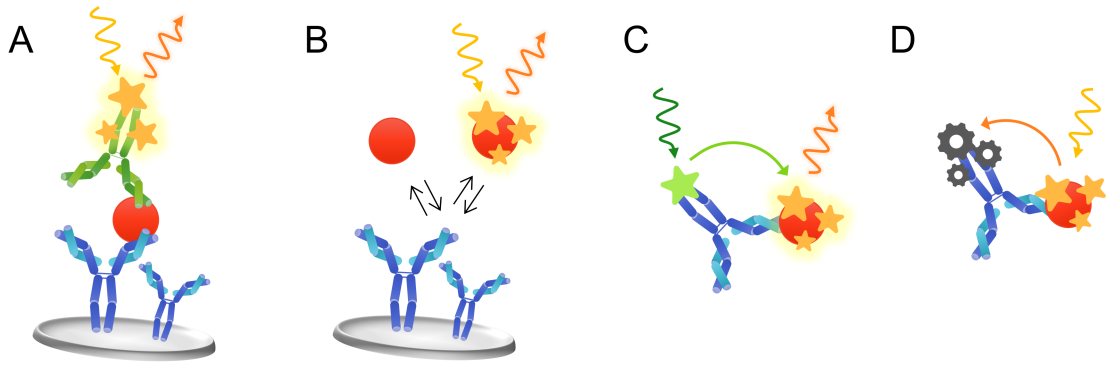


**Figure 1**. Examples of immunoassay concepts. (A) Heterogeneous two-site assay immunometric assay based on two antibodies which bind simultaneously to the target (red) forming a sandwich complex. The fluorescent label in the detection antibody allows quantification of the binding. (B) Heterogeneous competitive assay based on target binding antibody and a labeled competitor. The competition for a limited number of binding sites results in a signal intensity which correlates inversely to the concentration of the analyte. (C) Homogeneous competitive immunoassay based on energy transfer from labeled antibody to labeled competitor. In the presence of the target analyte, the distance between the two labels increases and no energy transfer is observed. (D) Homogeneous quenching assay based on competitor labeled with a fluorescent dye and antibody labeled with a quencher. In the presence of the target analyte, the fluorescence is recovered due to the larger distance between the label and the quencher.

## 1.3.2 OPTICAL DETECTION

Optical biosensors, which often bring together the fields of optics, fluidics, electronics, and biochemistry, have become a powerful detection and analysis tool during the last decades with vast applications in biomedical research, healthcare, food safety, pharmaceutical, and environmental analysis.[99] By definition, optical biosensors are based on measuring an optical phenomenon, such as light absorption, fluorescence, luminescence, total internal reflection, surface plasmon resonance (SPR), or other optical properties, upon the biorecognition event to detect and identify the target molecules. Optical detection is particularly attractive as it can be applied to multiplexed applications, and moreover, optics can be easily miniaturized at a relatively low cost, as cheap and sophisticated light sources and detection devices have become available in the last decades.[91]

### 1.3.2.1 Label-free and label-based methods

Generally, optical detection can be divided into label-based and label-free methods. Label-based methods rely on labels, such as fluorescent dyes or nanoparticles, which provide a measurable component for the biorecognition event. Label-free systems are capable of monitoring the recognition event directly having the biomolecules in their natural forms, *i.e.,* unlabeled and unmodified, with the significant advantage that no laborious labeling process is required. Therefore, this type of detection is, in a certain way, easy and cheap to perform, and it can provide information about the reaction kinetics and the thermodynamics of the molecular recognition events. Nevertheless, label-free methods require sophisticated and complex instrumentation, and they possess some intrinsic limitations especially for the analysis of small molecules.[100] The third review article (**publication VIII**) entitled "*Optical biosensors for label-free*

*detection of small molecules"*[100] included in Annex I of this thesis provides further insights and discussion on applications of label-free optical biosensors for small molecule detection.

Surface plasmon resonance (SPR) has been established as a landmark label-free biosensing platform in the last decades.[101] SPR measures the changes in the refractive index at the surface of a metal film where electromagnetic waves, known as surface plasmons, propagate upon illumination. Surface plasmons are highly dependent on environmental parameters and the geometry of the plasmonic structure, and thus, upon the target binding onto the surface, a change in the plasmon mode can be observed.[102] Prism couplers are most commonly used for the optical excitation, but also waveguide coupling, fiber optical coupling, and grating couplings have been employed.[99,103] Antibody-based SPR-platforms have been applied to mycotoxin detection in the competitive assay format by immobilizing a protein-conjugated mycotoxin onto the sensor surface, for example, for the detection of DON and nivalenol.[104,105] Alternatively, direct toxin detection has been established using aptamers and molecularly imprinted polymers as the recognition element for the detection of AFB, OTA, and citrinin.[106–108]

An interesting characteristic of some optical label-free platforms is their compatibility with label-based methods. Labels can be used to enhance or amplify the signal making them more versatile than other types of sensing platforms where only label-free detection can be implemented.[99] Numerous examples have demonstrated that metallic or magnetic nanoparticles, fluorophores, and quantum dots can be used to enhance SPR signals.[100,109] Although one could argue that after incorporating a label to the sensor configuration the method is no longer genuinely label-free, such approaches have shown significant improvements, especially for small molecule detection. For example, detection of OTA by SPR using a nanogold-enhanced assay was 10 times more sensitive than the non-enhanced one.[110] Other label-free mycotoxin detection methods include, for example, OTA detection using an optical fiber-based localized surface plasmon resonance (LSPR) aptasensor (**Figure 3B**),[111] or a planar waveguide operating on the polarization interferometry principle.[112]

Despite the increased number of label-free methods reported in the literature, which can largely be attributed to the availability of sophisticated commercial instruments, for example, SPR platforms such as BIAcore, label-based methods continue their reign in many disciplines. In comparison with label-free methods, label-based analyses inherently rely on the use of labels and thus require conjugation of the label of choice to one of the assay components, often the recognition element. Thus, high-quality recognition element and labels alone are not sufficient to guarantee reliable analysis, but the methods used for labeling or conjugation are of great importance. In some cases, the labeling reaction proves difficult as a consequence of a lack of appropriate reactive groups for the conjugation, low reaction yields, or the formation of heterogeneous mixtures of conjugated molecules. Occasionally, the conjugation can alter or even abolish the recognition event leading to inconclusive results.[113] A wide variety of different labeling strategies has been reported in the literature, including conventional covalent conjugation, for example, in the case of proteins using the primary amine groups of lysine residues, and novel biorthogonal or chemoselective conjugation methods, such as the so-called click-chemistry,[114] or various protein tags designed from modified enzymes and their synthetic ligands.[115,116]

Luminescent labels, including fluorescent, phosphorescent, as well as chemi- and bioluminescent molecules, are widely used reporters in optical sensing. The measurements can

be based on for example fluorescence intensity, decay time, anisotropy, quenching efficiency, or energy transfer using a variety of optical instruments ranging from smartphone cameras to highly sophisticated devices.[92] While classical spectroscopic instrumentation usually provides high sensitivity, the devices are often bulky, expensive, and require a powerful power supply unit. The tremendous progress in miniaturized and integrated sensor devices have introduced alternative light sources and detectors, for example, planar waveguides, optical fibers, and complementary metal-oxide-semiconductor (CMOS) imagers, which have been widely applied to develop portable and integrated instruments.[117,118]

### 1.3.2.2 Optical reporters

The main requirement of the reporter, or the label, is to provide a measurable signal using a detection system which allows detection of the label above the background noise.[93] In principle, the higher the signal from the label, the easier and more sensitive the detection will be.[118] The very first immunoassays were based on radioactive reporters, such as $^{125}$I, but they were later replaced with other systems due to the problems associated with safety and stability of the radiolabeled reagents. Commonly used reporters include enzymes, fluorescent dyes, luminescent proteins, and nanoparticles. Several factors can affect the choice of the label, including the molar absorptivity, quantum yield, optimal excitation and emission wavelengths, the Stokes' shift, fluorescence lifetime, and photostability.

Enzymes are one of the most used labels, in particular for immunoassays. Owing to their catalytic properties enzymes are capable of generating colored, fluorescent, or luminescent compounds from colorless or non-fluorescent substrates. Enzymes are usually measurable at very low concentrations because a single enzyme molecule can convert several substrate molecules, and the signal generating reaction progresses until the substrate of the enzyme runs out. However, enzymes might suffer from poor stability and short shelf-life which might affect their performance. Enzyme-based systems are also susceptible to interferences and variations in the assay conditions (pH, temperature, inhibitors, *etc.*) during the signal generation step, and in some cases, the reaction requires addition of specific cofactors.[93]

Nevertheless, enzymes are versatile labels which can be applied to different measuring schemes by simply changing the substrate. The simplest measurements rely on colorimetric substrates which can be observed visually in a qualitative manner or quantitatively using a spectrophotometer. The simplicity of colorimetric substrates comes with some cost in the sensitivity which is limited by the working range of the spectrophotometer.[93] Fluorescent substrates can usually provide sensitivities even several orders of magnitude higher than colorimetric ones, partly because fluorescent compounds can be repeatedly excited.[93] Alternatively, luminogenic substrates can be used for improved sensitivity. As chemiluminescent detection does not require an excitation light source, simple detectors can be used and provided that the incident light is efficiently isolated excellent sensitivities can be obtained.[97] Bioluminescence is a special type of chemiluminescence found in biological systems which has also been applied for detection to some extent.[119] Despite the high sensitivity, chemiluminescent and bioluminescent reactions are often complete within a few seconds, and the signal measurement must be rapid enough for quantification purposes. For this kind of fast reactions with flash-type kinetics, automatic reagent injectors may be required to obtain accurate and reproducible results.[97]

Horse-radish peroxidase (HRP), one of the most widely used enzymes for chemiluminescence measurements. It is a glycosylated hemoprotein which can function as an oxidoreductase with a wide variety of hydrogen donors to reduce hydrogen peroxide. HRP can be used in combination with different substrates to generate colored, fluorescent, or luminescent derivatives.[93] Various examples of HRP-based mycotoxin detection include mostly competitive assays using HRP-labeled secondary antibodies or HRP-conjugated toxins and colorimetric or chemiluminescent substrates.[120–123] Another common enzymatic label, alkaline phosphatase (AP), is a dimeric glycoprotein which can be easily conjugated to different molecules through its large number of free amino groups without loss of enzyme activity. AP catalyzes the hydrolysis of phosphate esters of alcohols, phenols, and amines.[97] This enzyme has been widely used to generate heterologous fusion proteins which consist of the recognition element, such as an antibody fragment, and the enzyme which can provide a way to measure the antibody binding. Production of such fusion proteins in *Escherichia coli* is rather straight-forward and results in readily conjugated recognition elements. For example, antibody fragments against OTA, $FB_1$, and HT-2 toxin have been expressed as AP-fusions and used for the toxin detection with colorimetric substrates.[124–126]

Fluorescence and phosphorescence, which refer to the emission of light from electronically excited states, are dominant methodologies in many disciplines, including biotechnology, medical diagnostics, forensics, and sensing.[127] Fluorescent reporters, which upon excitation, typically in the UV-range, emit light at a wavelength characteristic to the individual label, have been extensively used in optical sensors owing to many advantageous characteristics. These reporters, including directly fluorescent reporters as well as substrates which are converted to fluorescent products, exhibit high specific activity because one molecule can provide many photons of emitted light, since the cycle of excitation and fluorescence can be repeated many times for a single molecule during the measurement period.[97] Thus, high sensitivities down to a single molecule or a single photon detection can be achieved. Moreover, fluorescent assays are usually inexpensive, robust and many fluorophores have very long shelf lives. Conventional fluorescent reporters might suffer from high background signals because of light scattering which can arise from particulate matters in the sample or the solid phase and cause an increase in the background signal, but they continue to be routinely used in a variety of applications.[93,97] Organic dyes are widely used due to their availability and low price, and they offer tremendous diversity in terms of structures, spectroscopic properties, and chemical reactivities. Most widely used families of organic dyes include, for example, fluorescein, rhodamines, Alexa, BODIPY, and cyanine dyes, which can be used in a variety of measurement schemes.[118]

Fluorescence polarization, or anisotropy, is based on excitation of fluorophores by polarized light and can be used to measure the apparent size of a labeled complex.[127] Thus, fluorescence polarization measurements can provide information on the binding of small molecules, with fast Brownian rotation and low polarization, to larger molecules with slower rotation and higher polarization values. This principle has been used to detect small molecules by competitive immunoassays where the binding of a labeled competitor to the significantly larger antibody biomolecule is observed as changes in fluorescence anisotropy.[128] For example, fluorescein-labeled $FB_1$, ZEA, and T-2 toxin have been used in homogeneous fluorescence polarization assays for mycotoxin detection.[129–131] The use of dyes with distinguishable spectra

has been further applied to measure several toxins simultaneously in a universal multi-wavelength fluorescence polarization immunoassay.[132]

On the other hand, fluorescent proteins which have revolutionized cell biology by enabling visualization of intramolecular interactions and events also present an intriguing option for biosensors. The green fluorescent protein (GFP), a naturally fluorescent protein derived from jellyfish *Aequorea victoria,* contains a fluorophore structure which essentially resembles an organic dye and is formed within the folded protein structure. Mutations in GFP have given rise to new fluorescent proteins with different colors and nowadays these mutants cover nearly the entire visible range, starting from blue and extending into the near-infrared.[133] In addition, GFP-like fluorescent proteins have been obtained from different sources demonstrating the broad evolutionary and spectral diversity of this protein family.[118] For example, phycobiliproteins, intensely fluorescent proteins from blue-green and red algae, have been widely used because of their high quantum yields and excellent stability.[127] The possibility of co-expressing fluorescent proteins as heterologous fusions with other proteins of interest has served as a unique tool in molecular biology and cellular imaging. Applications of fluorescent proteins include biological labeling to track and quantify individual or multiple protein species inside the cell, the study of protein–protein interactions or intracellular events, as well as the detection of different target molecules.[118,134] Fluorescent proteins have also been used to develop biosensors both *in vivo* and *in vitro,* for example, to monitor the intracellular pH taking advantage of pH-sensitive GFP variants. Fluorescent proteins are remarkably stable, and they can be used and manipulated in multiple ways for different sensor applications.[134]

Organic fluorophores and fluorescent proteins almost always display short lifetimes, generally between 1 and 10 ns, which limits the dynamic information available. Long-lifetime probes can be used to overcome these limitations and avoid autofluorescence and scattering effects. Lanthanides are uniquely fluorescent metals which, when incorporated into chelating complexes, possess some exceptional features, such as long luminescence lifetime, narrow emission peaks, and large Stokes' shift.[118,127] Lanthanides have found widespread use in bioanalytical assays, including mycotoxin detection. For example, a structure-switching aptamer in combination with magnetic beads and $Tb^{3+}$ has been applied to the detection of OTA. In the absence of OTA, the aptamers were free to enhance the emission of $Tb^{3+}$ leading to a dramatic increase in the signal.[135]

Förster resonance energy transfer (FRET), which occurs when the emission spectrum of a donor fluorophore overlaps with the absorption spectrum of the acceptor molecule, is an extensively used phenomenon in sensing.[127] As the extent of energy transfer is determined not only by the extent of spectral overlap but also by the distance between the donor and acceptor, it can be used to measure binding events of two labeled molecules and has become a widely applied method in homogeneous assays using organic dyes, lanthanide chelates, or nanoparticles. For example, a time-resolved fluorescence resonance energy transfer (TR-FRET) assay for the detection of HT-2 toxin allowed detection of the toxin in a homogeneous format within only 10 min using europium and Alexa Fluor–labeled antibody fragments (**Figure 3A**).[136]

On the other hand, the development of new and better nanomaterials has favored the use of nanoparticles with unique size-dependent physical and chemical properties as optical reporters. Owing to their exceptional optical properties, nanomaterials, ranging from the original sphere-shaped nanoparticles to a broad variety of nanomaterials in diverse shapes and structures, such as nanotubes, nanowires, and quantum dots (QDs), have been considered

rather ideal for biosensor development.[137–139] Metal nanoparticles, particularly gold nanoparticles (AuNPs) have been used as labels for decades, and they continue to be one of the most widely used labels. AuNPs are relatively simple and rapid to synthesize, and their surface can be efficiently modified by thiols and other bioligands.[140] AuNP-labeled antibodies have been widely used in immunochromatographic tests using simple visual detection. The inherent physical characteristics of AuNPs also enable measuring these particles with surface-enhanced Raman spectroscopy (SERS) or LSPR.[140] AuNPs have also been used to amplify the signals obtained by SPR, for example for the detection of OTA and $AFB_1$.[109,110] Furthermore, AuNPs are exceptionally efficient fluorescence quenchers,[141,142] a phenomenon that has been attributed to various mechanisms, including FRET, nanometal surface energy transfer (NSET),[143,144] and dipole-to-metal particle energy transfer (DMPET).[145,146]

Dye nanoparticles or dye-doped nanoparticles, in which large quantities of dye molecules are trapped inside a polymer or silica matrix, can offer high optical intensity and excellent luminescent properties over conventional organic dyes.[138] For example, a rapid immunochromatographic assay for AF was developed based on time-resolved fluorescence measurements of europium nanospheres in which the lanthanide chelates were embedded inside polystyrene nanoparticles.[147] Moreover, inorganic lanthanide-doped nanoparticles, such as upconverting nanoparticles (UCNPs), have gained particular interest because of their extraordinary photochemical ability to convert infrared radiation to emission at visible wavelengths by sequential absorption of two or more photons. Despite their low quantum yields and quenching effects by water, UCNPs benefit from nearly complete elimination of autofluorescence and scattering effects. For example, homogeneous quenching assays based on luminescence resonance energy transfer (LRET) with UCNPs have shown excellent sensitivities for the detection of OTA.[148,149]

Semiconductor nanoparticles, commonly known as quantum dots (QD), exhibit many exceptional optical features, including high quantum yield, low photobleaching, high photochemical stability, size-tunable emission, and broad excitation spectra.[137] QDs have been widely used for biosensing, in particular as energy donors in combination with other dye acceptors in FRET-based detection schemes.[150] For instance, detection of OTA and fumonisins has been established with QDs and colloidal nanoparticles in different assay schemes.[151,152]

The variety of choices for optical reporters is extensive, and the aforementioned examples for mycotoxin detection represent only a fraction of the methods reported in the literature. Undoubtedly, the choice of the reporter has a direct effect on the sensitivity of the method, but yet, perhaps the most crucial element of all biosensors and bioaffinity assays is the recognition element which is responsible for the specific detection of the target analyte.

### 1.3.3 RECOGNITION ELEMENTS IN BIOSENSORS

The receptor, or the recognition element, is of key importance in biosensor development as its binding properties have a direct effect on the specificity and sensitivity of the method.[90,153] The recognition element of choice must be able to detect the target analyte even at low concentrations, and moreover it ought to differentiate it from other similar molecules which might be present in the sample simultaneously. Additionally, the availability, compatibility, stability, shelf-life, and cost can contribute to the choice of the receptor.[154]

The first developed biosensors were based on enzymes as recognition elements,[89] but later they have been accompanied and partly replaced with other alternatives, such as polyclonal and monoclonal antibodies, nucleic acids, and a variety of other protein binders. Generally speaking, biocatalytic sensors are based on a reaction catalyzed by macromolecules, mainly enzymes, whole cells, or tissues, whereas bioaffinity sensors are based on interactions of the analyte with the receptor. Although strictly speaking biosensors by definition[88] are based on recognition elements of biological origin, also synthetic and artificial materials have been widely used in their replacement in bioinspired or biomimetic sensors. These alternative receptors, including nanomaterials or membrane structures, molecularly imprinted polymers (MIPs), aptamers, various binding proteins, and phage-displayed or synthetic peptides, have been reported to overcome some of the limitations of natural biorecognition elements, mainly because these materials are usually robust, more stable and cheaper to produce than many natural receptors.[16]

### 1.3.3.1 Biorecognition elements

Glucose oxidase was the recognition element used in the very first biosensors, and since then enzyme-based biosensors have been used in various applications, perhaps most notably for glucose monitoring in blood.[89] These biosensors rely on the efficient biocatalytic properties of enzymes and their ability to specifically recognize their substrates. Such sensors for toxin detection are usually based on the inhibition of the enzyme immobilized on the sensor surface, and they often monitor the total toxicity of the sample but generally are not able to identify the toxin.[16] Development of modified enzyme receptors by genetic engineering for improved performance has been reported, but their analytical applications are still limited because the enzymes are usually not able to discriminate various toxic compounds from each other in the same sample.[155,156]

Acetylcholinesterase (AChE) obtained from electric eel is one of the most commonly used enzymes in biosensors for the detection of pesticides, heavy metals, and toxins.[155] AChE is a crucial enzyme for the transmission of nerve impulses to the cholinergic synapses, and its function is inhibited by nerve agents, organophosphorus, and certain toxins, such as $AFB_1$.[157,158] Based on the inhibition of AChE, various biosensors have been reported for the detection of $AFB_1$ with different measurement schemes.[159–162] Due to the reversible inhibition characterized by non-covalent interactions between $AFB_1$ and AChE, the degree of inhibition is not dependent on the incubation time or the amount of the enzyme, and the use of large quantities of the enzyme makes it possible to shorten reaction times even further.[159]

Whole-cell biosensors use living organisms, such as bacteria, yeast, algae, or tissue culture cells as the recognition elements by measuring their general metabolic status. Whole-cell biosensors often suffer from poor sensitivity compared to *in vitro* detection, but they can be suitable for initial screening and can be modified by simple genetic engineering methods for detecting a series of complex responses within a living cell.[163,164] Cell-based biosensors have been reported, for example, for evaluating the individual or combined toxicities of DON, ZEA, and aflatoxins.[165–167]

Antibodies are among the most widely used recognition elements in biosensors, not to mention their wide use in virtually all branches of biotechnology and biomedicine. Antibody-based biosensors, or immunosensors, and immunoassays rely on the exceptional ability of

antibodies to recognize their target analyte. Naturally, antibodies, or immunoglobulins (Ig), are produced by the immune system in the B-cell lymphocytes to bind and inactivate foreign or harmful pathogens. The vast recognition variety of antibodies is achieved by a high sequence variation on the amino acid level which is introduced during the transcription process of the B-cells by combinatorial assembly of the gene fragments, and further, by additional mutations after the primary recognition.[168] The conventional and most widely used IgG antibody (approximately 150 kDa, **Figure 2**) is composed of two identical heavy (50 kDa) and two light polypeptide chains (25 kDa) which are linked to each other by disulfide bonds. Both chains, the light and the heavy, have one variable domain ($V_L$ and $V_H$, respectively) and additionally, the light chain has a single constant domain ($C_L$), whereas the heavy chain contains three or four constant domains ($C_H$). The two antigen-binding fragments (Fabs) are responsible for binding to the target, whereas the highly conserved Fc-region (fragment crystallizable) interacts with effector molecules and cells.[168,169] From the analytical point of view, the most relevant region is the antigen-binding site, or paratope, which is rather small compared to the size of the whole antibody. The antigen-binding site is composed of six complementary determining regions (CDRs), or hypervariable regions, which are responsible for the target recognition.

Antibodies produced for biosensing and biotechnological applications are generally either polyclonal, monoclonal, or recombinant antibodies. Polyclonal antibodies can be purified from the sera of an immunized animal,[170] whereas monoclonal antibodies are produced by hybridoma cell lines.[171] The fact that polyclonal antibodies are a mixture of different antibody clones and susceptible to batch-to-batch variation limits their use in biosensing, although they often have better specificity than monoclonal antibodies and they are generally cheaper and faster to produce. Hybridoma technology allows producing large quantities of monoclonal antibodies with defined specificity and affinity, and they are usually the preferred option over polyclonal antibodies that are always a mixture of antibodies and suffer from poor reproducibility.[90,93]

First polyclonal antibodies against mycotoxins were described more than 40 years ago[172] and were soon after complemented with monoclonal antibodies.[173,174] Monoclonal antibodies continue to be the most widely used biorecognition element for mycotoxin detection, and during the last decades numerous immunoassays and immunosensors have been described with new intriguing characteristics in applications beyond the traditional ELISA, such as methods with improved separation steps using magnetic beads,[175–177] or novel detection schemes, including new label-based[132,178,179] and label-free approaches.[109,180–182] The availability of commercial antibodies has for its part facilitated the development of new methods, although some commercial antibodies have been demonstrated to have high cross-reactivity which limits their application to real samples where several toxins can be present simultaneously.[183,184]

Polyclonal and especially monoclonal antibodies have been the cornerstone of antibody-based detection methods during the past decades, but despite their wide use, they possess some intrinsic limitations mostly related to high cost and low stability, for example, at high temperatures or in stringent conditions.[185] The high specificity of antibodies can be partly attributed to their complex structure, but at the same time, it makes them susceptible to denaturation, degradation, or aggregation. Moreover, the large size of antibodies can cause steric hindrance, and the Fc-region often promotes non-specific binding.[153] Production of polyclonal and monoclonal antibodies is inherently dependent on animal immunization, and despite the uttermost significance of hybridoma technology, it is usually expensive and time-consuming.[93,185] In addition, small analytes, such as mycotoxins, are too small to be recognized

by the immune system and thus require conjugation to a carrier molecule for antibody production. The use of such conjugates complicates the process to some extent, and unfortunately, on occasion results in antibodies that recognize the target only in the context of the conjugate.[93]

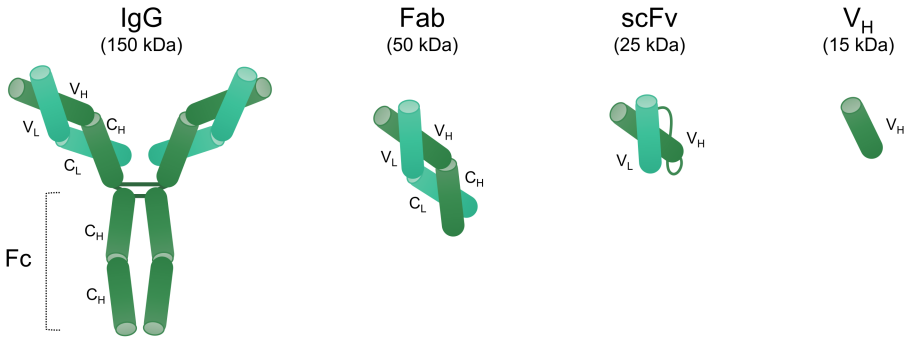


**Figure 2.** The antibody formats most commonly in biosensors include the conventional antibody (IgG), the recombinant antibody fragments Fab (fragment antigen binding), scFv (single-chain fragment variable), and $V_H$ single domain antibody.

On the other hand, nucleic acids, renowned as the carriers of genetic information and fundamental materials in all living organisms, including viruses and pathogens, present an exciting option for biosensing. Hybridization of nucleic acids by exceptionally strong base pairing with their complementary strand is the foundation of all types of DNA-based sensors, also known as genosensors.[90] DNA is particularly suitable as a molecular target, as it is a very stable molecule that can be isolated relatively simply even from complex biological samples.[90] Synthesis of short oligonucleotide probes is fairly straight-forward and can be used to include reactive groups or labels to allow probe immobilization or detection. The selected target DNA sequence should be unique in the organism in question and provide sufficient variability to other similar species. Ideally, the target should be present in the cell at a relatively high copy number, although PCR and other DNA amplification methods can provide powerful target amplification.[90] The conventional end-point PCR, which usually relies on agarose gel–based detection, is limited by the lack of specificity in the detection step which is susceptible to subjective band identification.[186] Real-time PCR (qPCR) combines PCR with fluorescently labeled probes allowing real-time monitoring of the amplification reaction. This robust, highly reproducible and sensitive method is widely used for pathogen identification, although it requires more complex instrumentation than the conventional PCR. Both end-point and qPCR methods have been reported for the detection of most common mycotoxigenic fungal species, such as *F. proliferatum*, *F. verticillioides,* and *F. oxysporum*.[187–191]

### 1.3.3.2 Bioinspired recognition elements

During the last two decades, various alternatives for natural recognition elements have arisen to complement the conventional bioreceptors. Such bioinspired or biomimetic recognition elements can be of synthetic or semi-natural origin, or be based on modified chemical structures

or materials which have the potential to overcome some of the limitations related to the conventional biorecognition elements.[192] Although it is unlikely, as well as unnecessary, that bioinspired recognition elements would completely replace the conventional biorecognition elements, they can be considered as a complementary option which might be more appropriate for some applications. For example, while antibodies and enzymes often suffer from poor stability, bioinspired recognition elements could be able to provide a means for developing robust, low-cost, or simple alternatives suitable for instance for high-throughput screening or low-resource settings.[193] Detailed discussion on bioinspired recognition elements for mycotoxin detection is presented in the second review article (**publication VII**) entitled "*Bioinspired recognition elements for mycotoxin sensors*"[193] included in Annex I of this thesis.

The advancements in recombinant DNA technology and protein engineering during the last few decades have made it possible to modify existing proteins or design new ones with selected properties. The rise of recombinant antibodies which possess several advantageous characteristics, such as smaller size and easy production, while preserving the target specificity of the intact antibody, is an excellent example of such progress. The best-known antibody fragments are the Fab fragment (50 kDa) and the even smaller scFv (single chain fragment variable; 25 kDa) which consists only of the $V_H$ and $V_L$ domains which are joined by a synthetic polypeptide linker (**Figure 2**).[194] The small size of recombinant antibody fragments has several advantages, including the decrease of nonspecific binding, often caused by the Fc-region of the intact IgG and the possibility to immobilize the antibodies at higher density.[194] Moreover, recombinant antibody technology has the potential to bypass the immune system and, at least theoretically, select new antibodies within a couple of weeks without animal immunization. Unlike full-length antibodies, recombinant antibody fragments can be propagated in bacteria, such as *E. coli,* which significantly lowers the cost of production as no specialized cell culture facilities for hybridoma cell lines are needed.[154,195]

Several recombinant antibodies have also been reported against mycotoxins. Recombinant antibodies which have been derived directly from monoclonal antibodies by cloning the gene fragments from the hybridoma cell lines and expressing them in *E. coli* have been described, for example, for DON,[196,197] $AFB_1$,[198] and $FB_1$.[199] However, the fragments isolated directly from hybridoma cell lines often demonstrate lower affinity than the parental monoclonal antibody, and thus, more frequently recombinant antibodies are selected from recombinant libraries (see **1.4.3 Phage-displayed libraries**) which moreover can avoid the initial production of monoclonal antibodies.[200]

For an even further reduced size of the recognition element, peptides present an interesting alternative since they still share the same fundamental chemical structure as proteins or antibodies. Small peptides are easy to synthesize and stable in a wide range of conditions.[201] Peptide binders can be derived from natural sources, for example from naturally occurring peptide hormones, or they can be selected from recombinant or chemical libraries. Both molecular biology and chemical techniques are available for identifying new peptide binders, and advances in bioinformatics and computational modeling have also made it possible to design peptide receptors *in silico*. As chemical synthesis has access to a wider diversity of the starting components, combinatorial peptide libraries can be constructed not only using natural compounds but also with unnatural amino acids or pseudo-peptide bonds.[202] Despite the appealing features, actually only a few peptides have been successfully used as recognition elements, and they often lack the required affinity for biosensor development. The limited

examples of peptide-based recognition of mycotoxins found in the literature include, for example, the development of an OTA binding peptide NFO4 which was based on a specific region of human oxidoreductase.[120,203] Peptides against OTA and aflatoxins have also been designed by computational modeling,[204] or by combinatorial synthesis.[205,206] On the other hand, peptides can be used as epitope mimics which can replace toxin-conjugates in competitive immunoassays (see **1.3.4 Particularities of small molecule detection**).

Alternatively, specially designed DNA or RNA molecules can be raised against virtually any target. Aptamers are relatively short (usually from 15 to 50 nucleotides) single-stranded RNA or DNA that can bind specifically various targets including ions, peptides, proteins, cells, antibodies, and organic molecules. Similarly, aptazymes (RNAzymes and DNAzymes) are engineered aptamers with allosteric properties which combine a target-binding strand and an enzyme strand. These bioinspired recognition elements can be obtained for specific targets by screening oligonucleotide libraries ($10^{14}$–$10^{15}$ variants) through the process of systematic evolution of ligands by exponential enrichment (SELEX).[207] Biosensors using aptamers as biorecognition elements, also referred to as aptasensors, were first described more than twenty years ago and have since then been used in various sensing applications. Aptamers can provide high stability and affinity, as well as simplicity, low cost, and excellent batch-to-batch reproducibility. For mycotoxin detection, application of various aptamers has been reported using different transduction schemes.[208] In particular, aptamers have been used in combination with metal and carbon nanostructures, such as AuNPs, graphene oxide (GO), single-walled carbon nanotubes (SWNTs), $MoS_2$ flakes or $TiO_2$ tubes, taking advantage of the strong quenching of fluorescent aptamer conjugates adsorbed on these surfaces.[209–211] For example, aptasensors for OTA and $AFB_1$ detection used single-walled carbon nanohorns (SWCNHs)[210] or nano-graphene oxides (**Figure 3C**),[212] respectively, to quench the fluorescence of labeled aptamers when unfolded. Improved sensitivity was obtained by a self-amplifying cycle where the target-bound aptamer was digested liberating the toxin for rebinding to a new aptamer. An alternative method for signal amplification in an electrochemical aptasensor was achieved using rolling circle amplification (RCA) to amplify the aptamer in the absence of target mycotoxin. Target binding to the aptamer inhibited the RCA, yielding a reduction of the redox signal.[213]

Moving even farther away from the natural biorecognition elements or the abovementioned approaches which rely on engineered or modified natural structures, MIPs are an example of an entirely synthetic approach. These bioinspired or biomimetic materials, also known as plastic antibodies, are prepared in the presence of the target analyte, or template, by polymerization of functional monomers and cross-linkers. Upon removal of the template, a three-dimensional network is retained with specific recognition cavities which are complementary in size, geometry, and arrangement of functional groups to the target.[214] MIPs have been described as artificial antibodies or artificial enzymes,[215] and in comparison with their biological counterparts, they show numerous advantages for sensor development including their low cost and ease of preparation, high physical and chemical stability, robustness, compatibility with organic solvents, and reusability.[216] However, in comparison with antibodies MIPs typically have lower affinity and specificity as well as slower binding kinetics than those of biological receptors. Several MIP-based sensors have been described for mycotoxins, for example, using MIPs functionalized with AuNPs in an electrochemical sensor,[217] or with QDs which were quenched in the presence of the target toxin.[218] In a different approach, citrinin was detected by

functionalizing disposable fiber optic sensors[219] or quartz crystal microbalance electrodes[220] with the MIPs.

### 1.3.4 PARTICULARITIES OF SMALL MOLECULE DETECTION

Small molecules, often defined as low molecular weight organic molecules typically less than 1000 Da in size, include of a wide variety of different chemical compounds, of either natural or pharmaceutical origin, many of which are biologically, pharmacologically, or environmentally relevant molecules. Myriad of different biosensors and bioanalytical assays have been reported for the diverse group of small molecule analytes, including mycotoxins, although owing to their small size they are often challenging analytes. To begin with, small molecules might be problematic targets for many recognition elements, in particular for antibodies.[93] While large analytes, such as proteins, can be detected with two-site or sandwich immunoassays, small molecules that inherently are not capable of binding two antibodies simultaneously must be conventionally analyzed using a competitive assay format. The important role of the recognition element is particularly eminent in such assay format because the recognition depends exclusively on the specificity of a single binder, and the sensitivity of the system is mainly defined by the equilibrium constant of the recognition element.[93,221] Moreover, the competitive assay format requires conjugation of the target to a carrier molecule or a label to enable immobilization or detection of this competitor. Synthesis of these conjugates can be challenging and time-consuming or result in randomly cross-linked or unstable molecules. Labeling of the analyte may also alter the epitope reducing or even abolishing the biorecognition event, which can compromise the assay sensitivity. Moreover, lot-to-lot variations of the conjugates, or even false positives caused by the release of the analyte moiety from the conjugate, are known to affect the assay reproducibility and accuracy.[93,222,223]

Instead of using the analyte-conjugate as the competitor, the so-called epitope mimics have been introduced as an intriguing alternative. The exceptional ability of these molecules to mimic the epitope of the analyte, and thus bind to the same antibody paratope, has been witnessed in several fields, including immunotherapy, epitope mapping, and allergy treatment.[224,225] For biosensor development, epitope mimics can provide significant advantages as they can replace the analyte-conjugate and thus overcome the limitations related to target conjugation.[193] Antibodies themselves, known as anti-idiotypic antibodies,[226] or short peptides, also called mimotopes, have been widely used for the detection of small molecules, mycotoxins in particular.[193,222]

Reported mimotopes, for example for the detection of DON,[227] $FB_1$,[228–230] OTA,[121,231–234] and ZEA,[235] vary in length and structure; use of linear 7-mer[121,231] and 12-mer[230] peptides, as well as cyclic mimotopes,[228] has been described. After the discovery of mimotopes from phage-displayed libraries, the phage-borne peptides have been used directly in ELISAs with colorimetric[231] and chemiluminescent[234] detection, as well as in dipstick[234] and dot-immunoassays.[236] Alternatively, the phage-borne peptides can be replaced with their synthetic or recombinant counterparts, thus avoiding the use of the phage in the assay. Short peptides, which are relatively simple and cheap to synthesize chemically, have been used in various immunoassays, for example for the detection OTA[121] and $FB_1$.[228,230] Interestingly, recombinant proteins, on the other hand, which can be produced in bacteria cost-effectively even in large

quantities, can be constructed of the mimotope in fusion with a protein ideal for coating, such maltose-binding protein (MBP),[229,233] or for detection, for example, fluorescent[237,238] or bioluminescent proteins.[239]

Nanobodies are the most widely used form of anti-idiotypic antibodies for mycotoxin detection. This special class of antibodies is derived from naturally occurring heavy chain antibodies in camelids and sharks and is renowned for the complete lack of the light chain. Hence, the antibody paratope is formed by a single $V_{HH}$ domain with three hypervariable loops, as opposed to six in the IgG.[169,240] The small size of nanobodies and their high stability to harsh conditions have gained significant attention in the field of biotechnology and biosensing.[169,241] Mostly because of their unsuitability for small molecule detection as a consequence of the special paratope, the majority of applications using nanobodies for mycotoxin detection employ them as epitope mimics. In fact, the exceptional convex-like structure of the paratope is known to bind well to clefts and cavities, making them highly suitable for molecular mimicry of haptens.[93,242] Detection of mycotoxins, including aflatoxin (**Figure 3D**),[243] citrinin,[244,245] DON,[246] $FB_1$,[124,242] and OTA,[247] using anti-idiotypic nanobodies has been reported to increase the sensitivity, at best 20-fold in comparison with the conventional assays using the toxin-conjugates.

On the other hand, since non-competitive immunoassays are usually considered superior to the competitive assays because of their higher sensitivity and specificity, novel methodologies have been implemented in order to benefit of these properties also in applications for small molecule detection. For such, non-conventional antibodies developed by recombinant antibody technology have been reported for small molecule detection. For example, the open sandwich immunoassay (OS-IA) is based on the association of separated $V_H$ and $V_L$ chains in the presence of the analyte and has been reported to outperform competitive assay in terms of sensitivity, working range, and assay time.[248] OS-IAs have been reported for the detection of ZEA using the $V_H$ and $V_L$ chains of a monoclonal anti-ZEA antibody. The non-competitive assays showed superior performance compared to the competitive assay,[249] although OS-IA in which the recognition still relies on only one antibody can suffer from cross-reactivity.[248,250] Alternatively, non-competitive immunoassays for small molecules have been reported using two antibodies, one of which, known as the anti-immune complex or anti-metatype antibody, binds to the primary antibody only when it is in complex with the target analyte. Such non-competitive immunoassays based on anti-immune complex antibodies have the added advantage of increased specificity due to the use of two antibodies instead of one. For example, anti-immune complex antibodies for the detection of HT-2 were selected from phage display libraries, and the developed immunoassays showed superior performance in comparison with the competitive ELISA (**Figure 3A**).[125,136]

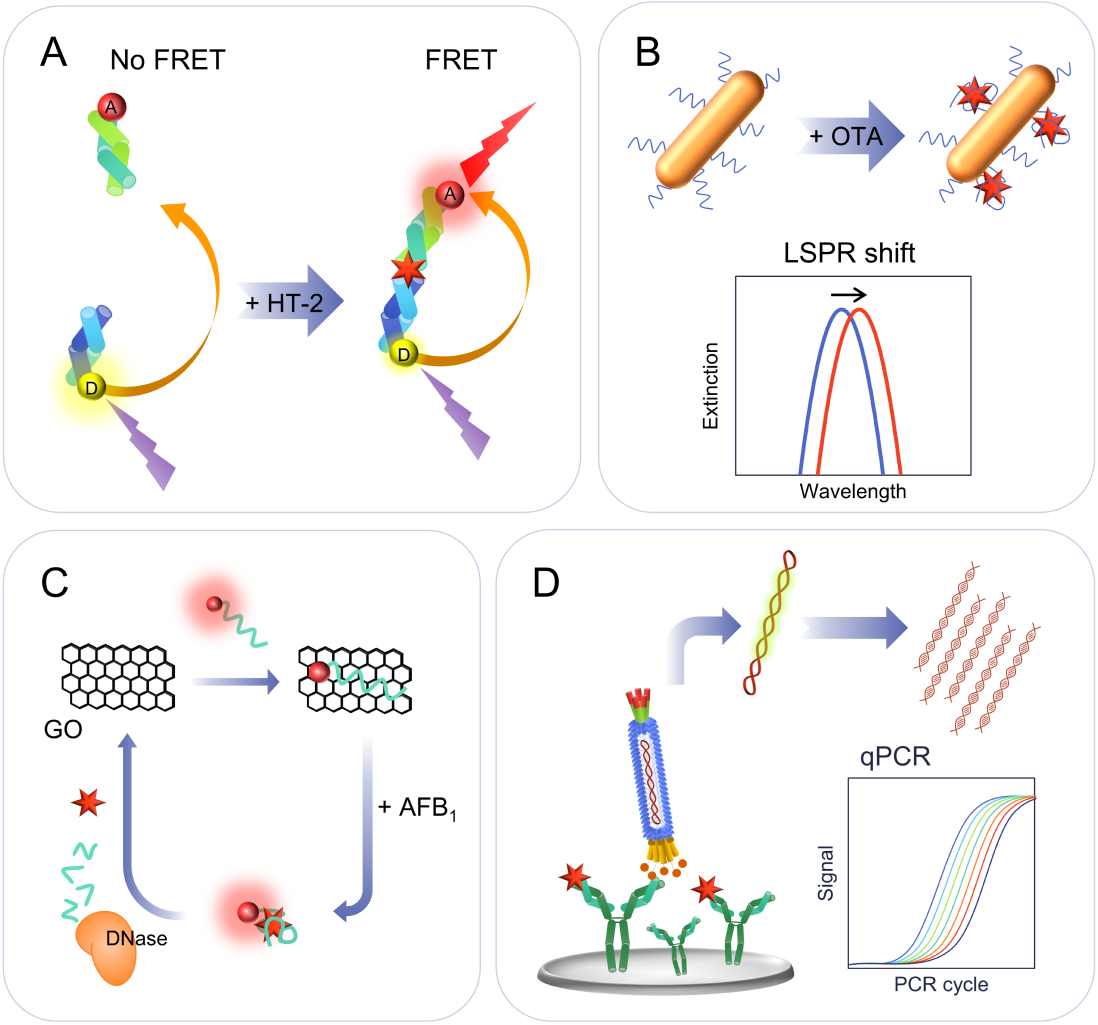


**Figure 3**. Examples of mycotoxin analysis based on different recognition elements and detection schemes. (A) Non-competitive HT-2 toxin assay based on the anti-immune complex Fab and HT-2 specific primary antibody. In the presence of the toxin, FRET (Förster resonance energy transfer) can occur due to the short distance between the two fluorophores. A, acceptor (Alexa Fluor); D, donor (europium dye). (B) Localized surface plasmon resonance (LSPR) sensor using aptamer-modified gold nanorods chemically attached to an optical fiber core. OTA binding to the aptamer induces an LSPR peak shift. (C) Detection of $AFB_1$ by DNA aptamer–based fluorescent assay using graphene oxide (GO) nanosheets to bind the labeled aptamer in the absence of the toxin and quench the fluorescence. Signal amplification was achieved using DNase I for regeneration. (D) Anti-idiotypic nanobody was used in a phage-based real-time immuno-PCR for the detection of aflatoxin. Figures adapted from A, Arola *et al.* (2016);[136] B, Lee *et al.* (2018);[111] C, Zhang *et al.* (2016);[212] and D, Lei *et al.* (2014).[243]

Table 3. Examples of biosensors and bioaffinity assays for mycotoxin detection.

| Target toxin | Recognition element | Assay | Solid phase | Label | Measurement | LOD | LR | Samples | Ref. |
|---|---|---|---|---|---|---|---|---|---|
| OTA | MAb | Competitive (mimotope) | Microtiter plate | HRP | CL | 0.005 ng $mL^{-1}$ | 0.006–0.245 ng $mL^{-1}$ | Coffee<br>Corn<br>Rice | 234 |
| AF | MAb | Competitive (AI-Nb) | Microtiter plate | TaqMan | PD-IPCR | 0.02 ng $mL^{-1}$ | *n.d.* | Corn<br>Rice<br>Peanut | 243 |
| HT-2 toxin | Fab | Non-competitive (IC) | – | Eu + AF647 | FRET | 0.38 ng $mL^{-1}$ | *n.d.* | Wheat | 136 |
| $AFB_1$ | Nb | Competitive ($AFB_1$–BSA) | Microtiter plate | HRP | A | *n.d.* | 0.117–5.676 ng $mL^{-1}$ | Corn<br>Rice<br>Peanut | 251 |
| OTA | Aptamer (RCA) | Direct | Gold electrode | MB | CV | 0.065 ppt | 0.1 ppt–5 ppb | Wine | 213 |
| $FB_1$ | Aptamer | Direct | Microcantilever | – | Cantilever deflection | 33 ng $mL^{-1}$ | 100–40000 ng $mL^{-1}$ | – | 252 |
| OTA | Aptamer | Direct | GNR on optical fiber | – | LSPR | 0.006 ng $mL^{-1}$ | 5.1–50718 ng $mL^{-1}$ | Grape juice | 111 |
| $AFB_1$ | AChE | Direct | SPE | – | A | 468 ng $mL^{-1}$ | 625–62500 ng $mL^{-1}$ | Olive oil | 162 |
| $AFB_1$ | MIP | Direct | Gold electrode | – | LSV | 0.3 fg $mL^{-1}$ | 1 fg $mL^{-1}$–1 µg $mL^{-1}$ | – | 217 |
| ZEA | MIP | Direct | – | QD | F | 0.64 ng $mL^{-1}$ | 9.55–99330 ng $mL^{-1}$ | Corn<br>Rice<br>Wheat flour | 253 |

*Abbreviations: A, amperometry; AChE, acetylcholinesterase; AF, AlexaFluor; AI-Nb, anti-idiotypic nanobody; BSA, bovine serum albumin; CL, chemiluminescence; CV, cyclic voltammetry; F, fluorescence; FRET, Förster resonance energy transfer; GNR, gold nanorod; HRP, horse-radish peroxidase; IC, immune complex; LOD, limit of detection determined the blank + 3 × standard deviation of the blank; LR, linear range; LSPR, localized surface plasmon resonance; LSV, linear sweep voltammetry; MAb, monoclonal antibody; MB, methylene blue; MIP, molecularly imprinted polymer; Nb, nanobody; n.d., not determined; QD, quantum dot; PD-IPCR, phage display mediated immuno polymerase chain reaction; RCA, rolling circle amplification; SPE, screen-printed electrode.*

# 1.4 Phage display for biosensor development

## 1.4.1 FILAMENTOUS BACTERIOPHAGES

Bacteriophages, or phages for short, are bacterial viruses which are ubiquitous in nature but harmless to humans. Their role as the main regulators of the microbial balance among the diverse variety of bacteria existing in the ecosystem makes them naturally eminent but owing to many interesting characteristics phages have also become an exceptional tool for many biotechnological applications.[90] The Greek origin of the name bacteriophage describes them as "bacteria-eaters,"[90] although perhaps more aptly they can be defined as parasites which are capable of infecting bacteria and multiplying within the bacterial host.[254] Upon infection, the phage takes over the biosynthetic machinery of the host cell to replicate its genetic material and subsequently produce over a thousand identical phage particles.[255]

Naturally, a myriad of different phages exist but generally, each phage particle, or virion, encloses its genome of DNA or RNA in a protein coat, or capsid.[256] Phages, while being abundant in nature and highly specific to bacteria, are extremely robust and can withstand even harsh conditions.[90] They can be classified based on their morphology, and further depending on their life cycle and propagation ways.[90] Lytic or productive phages, such as T4, T7, T3, and MS2 phages, are only capable of replicating their genome, assembling the phage virions, and releasing them by lysing and killing the host cell.[256,257] Lysogenic or temperate phages, such as λ phage, can multiply *via* lytic cycle or incorporate their genome into the host cell genome where it will produce a quiescent state.[257] Filamentous phages, distinct for their long rod-like shape, are lysogenic phages which do not lyse their host cell but secrete the newly assembled virions and continue the process. Filamentous phages can infect a wide variety of Gram-negative bacteria, for example, *E. coli*, and the most used phages include M13, fd, and f1 phages, all belonging to the Ff class, so named because they infect the bacterial host *via* the tip of the F conjugative pilus.[258]

M13, one of the most used phages, consists of a circular single-stranded DNA (ssDNA) genome packaged within the phage particle, a somewhat flexible protein cylinder of about 930 nm in length and 6.5 nm in diameter.[257] The filamentous capsid consists of the phage structural proteins, including the major coat protein (pVIII), which appears in approximately 2700 copies alongside the virion, and the minor coat proteins, capping both ends of the phage, pVII and pIX at one end and pIII and pVI in the other (**Figure 4A**).[257,259] The pIII is the largest and structurally most complex of the phage proteins, and it is essential for the infectivity, because of its role in the binding to the bacterial pilus, and necessary for the termination of viral assembly. The remaining six phage proteins are involved in viral replication and assembly.[258] As described previously, M13 can infect *E. coli* by attachment of the pIII to the pilus which is encoded by the bacterial genes carried on the F-factor. After phage binding, the pilus retracts until the phage reaches the bacterial surface and pIII can bind to the membrane proteins and transfer the phage genome into the host cell. The infecting phage disassembles, and the coat proteins are inserted into the bacterial membrane. Once inside the bacterial cell, the phage genome is converted to double-stranded DNA (dsDNA) by bacterial enzymes and the synthesis

of new phage proteins begins. Newly synthesized proteins finally assemble around the ssDNA genome and extrude from the bacterium. As a non-lytic phage, M13 does not kill the host cell, but the infected host can continue to grow and divide.[257,259]

The phage structure and its mode of replication have contributed to making phages a valuable tool for biological research.[257] Because of the natural assembly of phage virions they are simple and rapid to produce even in large quantities in bacteria, and they are relatively easy to purify in high yields.[258] Modifying the phage genome is relatively straight-forward as foreign DNA sequences can be easily inserted into the nonessential regions of the genome, making it a useful cloning vehicle in biotechnology.

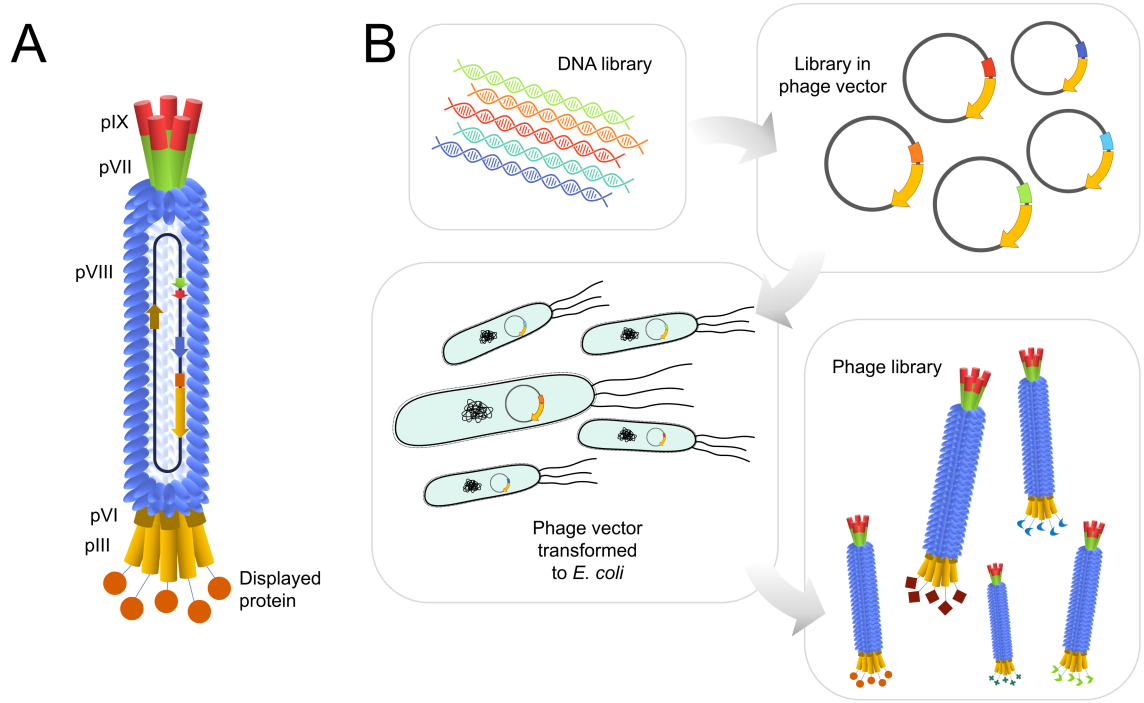


**Figure 4**. (A) The structure of filamentous phage M13 which consists of a protein coat made of the major coat protein (pVIII) and the minor coat proteins (pIII and pVI in one end and pVII and pIX in the other). The genomic DNA encoding for the coat proteins is enclosed within the protein coat. By introducing modified segments into the genomic DNA, the phage can be engineered to display foreign peptides or proteins as a fusion with one of the coat proteins, most commonly pIII. (B) Construction of phage-displayed libraries includes generation of the DNA library encoding for the different variants and introduction of the variable sequences in the phage DNA (typically phage vector or phagemid system). After transforming the DNA to bacteria, phages are amplified and will display individual protein or peptide variants outside the virion.

## 1.4.2 PRINCIPLES AND APPLICATIONS OF PHAGE DISPLAY

Phage display refers to the expression of peptide or protein variants on the surface of the phage virion by cloning the gene encoding for it as a fusion with one of the phage coat proteins.[257,260] This technique has been recognized as a powerful tool to screen and select binders on the basis of molecular recognition from phage-displayed libraries, assemblies of up to about 10 billion of phage clones each harboring a different variant of the displayed entity (**Figure 4B**).[258]

Filamentous phages are the most common ones used for phage display because they are rather ideal for inserting various-length DNA segments into the genome which is relatively small in size and accommodates well such modifications. Moreover, cloning and construction of fusions are facilitated by the possibility of isolating both ssDNA and dsDNA. Being non-lytic, filamentous phages do not kill the host cell but can be amplified in high quantities.[261] On the other hand, one of the drawbacks of using M13 for phage display is that, owing to the non-lytic propagation, all the compounds of the virion must be exported through the bacterial inner membrane before the phage assembly. On occasion, this has been a limitation for displaying large proteins whose size, sequence, or folding might prevent the translocation or disrupt the integrity of the capsid. In principle, this limitation can be obviated by using lytic phages, such as icosahedral T4 and especially T7, which assemble entirely in the cytoplasm.[262,263]

Nevertheless, based on filamentous phages, numerous display systems have been developed, using different coat proteins for the display together with phage or phagemid vectors. These phage display systems can be more specifically classified according to the arrangement of the coat protein genes which in the end affects the display valence, *i.e.,* whether the foreign peptide or protein is displayed on all or only part of the copies of the coat proteins.[254] The N-terminus of pIII was the first location used for the display of a foreign peptide,[264] and it is still the most commonly used, although all five capsid proteins have been employed for display.[258,261] The major coat protein, pVIII, can be used for both N- and C-terminal fusions, but only short peptides (6–8 residues) can be displayed without disturbing the phage's ability to replicate. Fusion with the major coat protein pVIII will normally lead to multivalent display with even thousands of copies whereas lower valencies, usually 1–5 copies per phage, are obtained with pIII fusions.

Commonly phage display is based on operating either on phage or phagemid vectors.[265] In the phage vector display, the foreign DNA sequence to be displayed is introduced to the phage genome fused with the gene of one of the coat proteins. As a result, the phage will express the foreign entity, peptide or protein, as a fusion with the coat protein. In some cases, for example, if the size of the target is too large, such display may interfere with phage assembly, and the phagemid system is preferred. Phagemids are phage-derived vectors which do not encode for all the structural and functional proteins of the phage but carry only the necessary replication origins and one kind of coat protein which is used for the display. Phagemid usually contains an antibiotic resistance gene and two origins of replication, a plasmid replication origin that allows them to replicate in high copy number in the host cell and a filamentous phage replication origin which is activated once the phagemid-bearing cell is superinfected with the helper phage. Thus, the phagemid by itself can replicate within a bacterial cell and maintain itself as a plasmid, but it is not able to finish the assembly of phage particles independently. Only when a helper phage vector containing also the genetic elements for phage packing is present, and thus, the host cell harbors both the phagemid and helper phage genome, phage particles can be produced. In fact, the superinfection results in two types of infective virions, particles carrying the helper phage DNA and particles with the phagemid DNA.[258,266]

Generally, the phagemid vectors are preferred especially when displaying entire proteins or antibody fragments. As the size of the phagemid is considerably smaller than the phage vector, they are easier to manipulate, maintain and propagate, and they usually allow higher transformation efficiencies and improved genetic stability. Moreover, the cloning is relatively simple in comparison with phage vectors which have a somewhat complex structure with

overlapping genes, promoters, and terminators.[261] In addition, the phagemid system is required if monovalent display is desired. Nevertheless, the phagemid system requires an additional infection with a helper phage to provide all the proteins needed to make ssDNA and new virion particles.[259] Helper phage usually has a modified packing signal to favor the packing of the phagemid,[267] and further modifications can allow, for example, multivalent display or inhibition of wild-type phage infection with trypsin-cleavable pIII display.[268,269] The tryptic helper phage (KM13) is sensitive to trypsin and loses its infectivity when incubated with this protease. Trypsin treatment after the selection can, therefore, eliminate the majority of the helper phages that do not display the foreign peptide of interest. In other words, only those phages carrying the fusion protein can maintain their infectivity and continue to propagate in the bacterial host.[257,258]

Wild-type or genetically modified phages, as well as individual phages displaying a particular protein or peptide of interest, are an interesting option to be used as recognition elements, and phage display has contributed to the widespread application of phages in a myriad of phage-based biosensors.[270] Advances and recent applications of phages to biosensor development have been reviewed in the first review article (**publication VI**) entitled "*Application of bacteriophages in sensor development*"[271] included in Annex I of this thesis. Nevertheless, by far the most renowned and intriguing application of phage display is the construction and use of phage-displayed libraries which can be used to select specific affinity binders against virtually any target. Such *in vitro* selection, also referred to as directed evolution, has established phage display as a valuable and remarkably versatile tool in many disciplines for selecting affinity binders and exploring interactions between proteins, peptides, and small-molecule ligands, making significant contributions to the study of molecular recognition.[257,258]

## 1.4.3 PHAGE-DISPLAYED LIBRARIES

### 1.4.3.1 Peptide libraries

Phage-displayed libraries are made of billions of phage clones, each one carrying a different foreign DNA insert and therefore displaying a unique peptide or protein sequence on its surface. Importantly, each unique phage can replicate upon bacterial infection.[254] The foreign DNA sequence coding for the displayed protein or peptide can derive from a natural source, or it can be deliberately designed and synthesized chemically.[258]

The use of peptide libraries is perhaps inferior to antibody libraries, but nevertheless, they have been widely used for various applications, for example, for diagnostics, epitope mapping, vaccine development, and protein–protein interaction studies. Moreover, peptides can provide information about interactional motifs, epitopes or binding sites of antibodies and other proteins. Phage-displayed peptides can also be useful intermediates in the development of small-molecule drugs.[272] Remarkably, peptides can be isolated against almost any protein target including, for example, antibodies, enzymes, receptors, transcription factors, and protein interaction domains.[258] Experience has shown that peptides identified by phage display commonly bind to protein functional sites rather than randomly or non-specifically to the surface. Such binding sites are often grooves or depressions in the protein surface with exposed hydrophobic groups making them suitable for specific target binding.[258] If the peptide binds to the functional site of the target protein, it will also most likely inhibit binding of others to the

same site. Taking advantage of this feature peptides have been used as surrogate ligands in a variety of competition-based assays for drug discovery.[258] Similarly, antibody binding peptides have been applied as epitope mimics in competitive immunoassays.

Many peptide libraries are made by joining the DNA sequences coding for the peptide directly into the phage genome at or near the N-terminus of gIII. As a result, potentially five copies of peptide–pIII fusions are displayed at one end of the phage particle. Fusion to the gVIII can result in more than 2000 copies of the peptide per phage. Thus, the multivalent nature of the display will have significant avidity effects, and potentially low-affinity binders might end up selected due to the high avidity.[272] The size of the peptide is limited in such systems but can be increased if a phagemid system is used. Moreover, the phagemid system allows reducing the avidity effects by a monovalent display. The size of peptide libraries in terms of the number of distinct peptide sequences is usually limited by bacterial transformation efficiency. Typically, peptide library sizes vary between $10^7$ and $10^9$ phages. Thus, the size of completely randomized peptides (*e.g.,* 20 different codons, at *n* different positions) is limited to $n = 6–8$. Despite these limitations also longer peptides, although incomplete in terms of nucleotide randomization, have been used to construct libraries with sufficient variety.[254,272]

Random peptide libraries can be derived by oligonucleotide-directed mutagenesis from ”degenerate” oligonucleotides which are synthesized chemically by adding mixtures of nucleotides to a growing nucleotide chain.[254,258] Random peptide libraries can be described as naïve in the sense that they are designed to be as unbiased as possible, and thus, they can provide specific binders for many different targets. However, selections from naïve libraries often result in binders with low or mediocre affinities, especially if the size of the library is not sufficient.[273] Randomness in the sequence can be introduced at nucleotide level varying all the nucleotides of the codons (”NNN”) resulting in highly biased diversity since some amino acids are represented by several codons and furthermore three codons are stop codons. Thus generally, degeneracy at the codon level is preferred as it gives a less biased representation of the amino acids. In fact, even less redundant diversity where only the third position of the codon is allowed to vary either as G/C or G/T (”NNK” or ”NNS”) is sufficient to cover all the 20 amino acids.[258]

In some cases, the randomization is restricted to certain regions thus creating a constrained library opposed to an unconstrained one. In general, constrained peptide libraries present less three-dimensional shapes than an unconstrained library, and therefore, the probability for target binding is reduced. However, those with appropriate conformations may possess far higher affinities than any unconstrained peptide because the loss in entropy on target binding is likely lower than for unconstrained peptides.[254,273] A common constraint on displayed peptides is a disulfide bond between two cysteine residues at fixed positions in an otherwise random sequence resulting in cyclic peptides. Similarly, coordination bonds between histidine residues and metal ions can constrain peptides.[254,273] Alternative, constrained peptides can be presented in the context of a protein scaffold, such as α-helices, β-sheets, or other secondary structure elements. In a sense, antibody libraries actually entail a protein scaffold where specific regions responsible for the antigen binding have been randomized.

### 1.4.3.2 Antibody libraries

Although the first use of phage display focused on peptides, antibody libraries have been arguably the most successful use of this technology and have led to the discovery of antibodies with affinities comparable to those obtained by hybridoma technology.[260,274] In fact, alongside with the development of monoclonal antibodies using hybridoma technology[171] and the isolation and cloning of antibody genes to enable expression of antibody fragments in bacteria,[275,276] the generation of antibody libraries by phage display can be considered as one of the groundbreaking methods for the antibody discovery.

Antibody libraries can be constructed from natural sources by isolating the B-cells of a source animal which has been immunized with the target antigen and using the isolated antibody genes to create the antibody library.[277] This kind of immunized libraries have a strong bias towards the antigen, and even a modest-sized library can be sufficient to isolate specific binders. However, construction of a separate immunized library is needed for each antigen, although immunization with several antigens simultaneously is also possible.[278] Most immunized libraries are produced from mouse,[279–283] but also other animals, such as rabbit,[278] chicken,[284] sheep,[285] monkey,[286] camel,[287] and shark,[288] have been used. Additionally, immunized human libraries have been made using blood from patients naturally infected with virus or parasites.[257,289]

On the other hand, naïve antibody libraries can be constructed completely *in vitro* resulting in non-immunized,[290] synthetic,[291] or semi-synthetic libraries.[292] The use of synthetic repertoires bypasses the need to isolate antibody genes and allows generating sequences with predefined properties or using optimal framework sequences.[293] Non-immunized libraries are a result of rearranged antibody genes isolated from B-cells of healthy individuals that have not been intentionally immunized. Semi-synthetic and combinatorial libraries combine natural and synthetic sequences. Such libraries are usually constructed by introducing synthetic diversity into a naïve library by PCR assembly of germline genes, or by recombination of *in vivo* formed CDRs.[260] Synthetic libraries are constructed entirely *in vitro,* using oligonucleotides to introduce diversity into the CDRs. While antibodies with mediocre affinities are readily screened from relatively small naïve or synthetic libraries, in general, for isolating high-affinity binders the diversity of the library becomes significant.[260] In fact, studies have shown a linear correlation between the library size and the highest affinity that has been isolated, meaning that, in particular in the case of naïve or synthetic libraries, the size of the library must be large enough to increase the probability of finding a given antibody and enhance the quality of the antibody.[294]

## 1.4.4 SELECTION OF BINDERS FROM PHAGE-DISPLAYED LIBRARIES

Individual clones from phage-displayed libraries theoretically can be directly screened for target binding, for example by immunoassays, in a manner resembling the screening of synthetic or chemical libraries which must be screened compound by compound. However, screening of libraries consisting of millions to billions of different clones is limited by the number of clones that can be examined.[260] In order to efficiently isolate specific binders the library needs to be coupled to a technology which provides a means to carry out selections from these repertoires. *In vitro* display technologies, which basically mimic the natural *in vivo* process of antibody

production, have enabled such proficient enrichment and selection of binders in a rapid and controllable manner. The essence of the display technologies resides in the physical linkage between the phenotype of the phage displaying the protein or peptide on the surface and the genotype encoding for that entity, packaged as the genetic information within the same phage particle. This link enables selection of phage-displayed libraries and powerful enrichment by selective propagation of the individual with the desired properties.[260] Thus, a single displayed entity, be it a peptide, protein or antibody fragment, of the desired trait, can be captured from a pool of billions of variants, its gene can be amplified and used for another selection round or whatever downstream purpose might be desired.[259]

Although phage display is the most renowned technique for screening libraries,[264,295] also other display methods, including cell surface display using bacteria,[296] yeast,[297] or mammalian cells,[298] as well as cell-free systems, such as ribosome display,[299] have been successfully applied to screening antibody libraries. Although less popular than phage display technology, these methods present some advantages, such as the ability of yeast cells to express complex proteins which require post-translational modifications, or the possibility to create larger libraries using cell-free methods which are not restricted by the bacterial transformation efficiency.[300]

The process of *in vitro* selections, whether it is based on phage or other display systems, commonly includes: (I) the generation of genotypic diversity by constructing protein or peptide libraries which consist of millions or billions of different variants, (II) the display method which creates a physical link between the expressed protein variant and the gene coding for it, (III) the application of selective pressure to screen for target-specific binders, and finally, (IV) amplification of the selected variants.[260] Remarkable features of *in vitro* selection technologies include the possibility of defining the selection conditions carefully, the potential for high throughput applications, and further improvement of selected binders by various protein engineering methods, for example, to achieve better affinity or stability, reduce unwanted cross-reactivities, or add tags for purification or immobilization.[93,169,301] These systems provide immediately the genes and corresponding DNA sequences of the clones selected against the specific target. Simple sub-cloning can allow presenting modifications or adding functionalities, such as purification tags or fusions to enzymes or fluorescent proteins.[301] Moreover, also conventionally challenging targets, including toxic or non-immunogenic molecules, have been successfully used.[302,303]

The screening process of phage-displayed libraries, commonly known as panning, includes introducing the phage-displayed library to the target captured to a solid surface, washing to remove the unbound and nonspecifically bound phages, elution of the bound phages, and amplification of the eluted phages through bacterial infection (**Figure 5A**). Ideally, only one round of selection is required, but as nonspecific binding limits the enrichment in one selection round, in most cases, 3–5 iterative rounds of selection and amplification are performed to select individual binders. A variety of modifications in the panning protocol and details for improved selections have been described for selecting high-affinity binders from phage-displayed libraries. Generally, the experiment can be designed to maximize either phage capture or affinity discrimination. While effective capture is best used for the first selection round, the conditions can be modified in the later rounds to produce better affinity discrimination.[257]

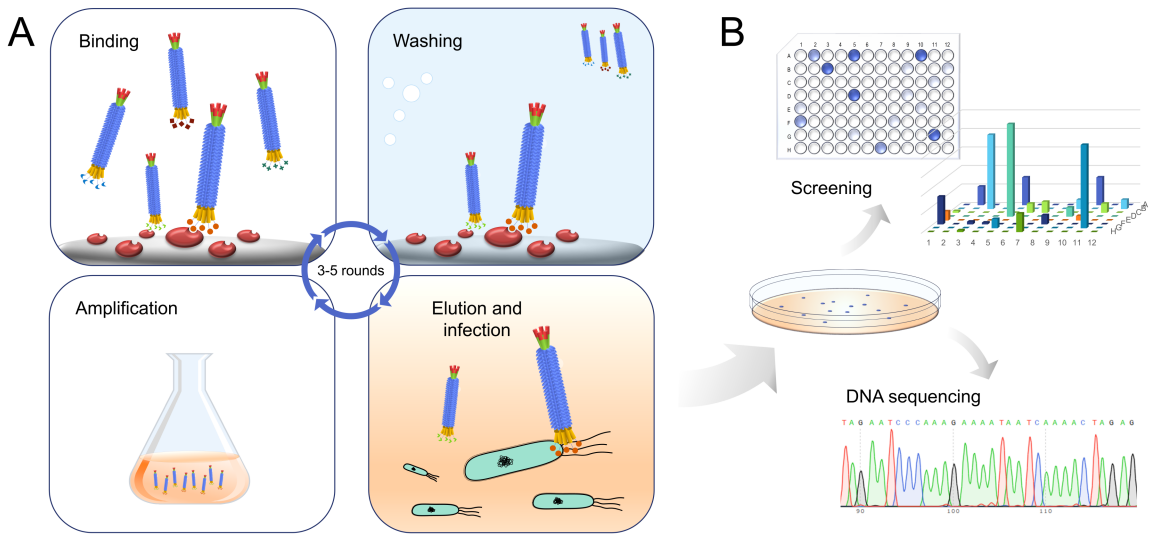


**Figure 5**. Selection of affinity binders from a phage-displayed library. (A) The selection process consists of binding, washing, elution, and amplification steps which are usually repeated to 3–5 times to enrich target-specific binders. (B) Target specificity of individual clones can then be determined by screening the monoclonal clones from single colonies in ELISA, and the positive clones can be identified by DNA sequencing.

The early rounds of selection are usually the most important ones. Any bias or loss of diversity during the first round will be amplified in the subsequent rounds. Moreover, since the number of potential binders is low among the highly diverse library, efforts should be made to maximize the capture of all interesting clones. When enrichment of selective clones is achieved, and the diversity is reduced in the later rounds, stringency can be increased by decreasing the target concentration or increasing the number or time of the washes.[258] The amount of background or nonspecific binders in the phage pool is significant, especially in the first round when the proportion of specific clones is still low. Certain additives, such as glycerol and surfactants, can be used to reduce the non-specific binding of the phage, but they can also reduce the specific binding. The probability of enriching unwanted binders against the solid phase, the blocking agents, or the carrier protein, can also be reduced by pre-selecting the library before the actual selection.

The selection is commonly carried out in solution or at solid phase. Most frequently the target is directly immobilized on a solid support, such as immunotube, beads or microtiter plate, which enables the separation of bound and unbound phages by simply washing the support.[258] Small molecules which cannot be directly immobilized are often conjugated to a carrier protein or chemically conjugated to a linker such as biotin. For binding in solution, a biotinylated target is incubated with the phages in solution, after which the target bound phages are captured by streptavidin, for example, using magnetic beads.[257] Because binding is an equilibrium reaction where the amount of the binder–target complex formed is determined by the affinity and the concentrations of the binder and the target, the amount of the target used for the selections is one of the critical factors in the process. Theoretical models suggest that high-affinity binders should be selected with the target concentration lower than the dissociation constant ($K_D$), but often a target excess is used in particular in the first rounds to allow capture of a higher fraction of the phage population and decrease the risk of losing the rare high-affinity binders.[304]

However, by using limited and decreasing amounts of the target in the later rounds, the selection favors high-affinity binders.[260] Additionally, if multivalent display is used, avidity will play a significant role in the binding and seemingly good binders with actually low affinity might be selected due to avidity effects. When selection of high-affinity binders is desired, monovalent display is thus preferred,[258] although the use of a controlled density of the target during the selections can reduce the avidity effects favoring one-to-one binding interactions, even with multivalent displays.[272]

On the other hand, also the washing steps are of great importance. Typically, affinity, in terms of the $K_D$ which is the ratio of the association ($k_{on}$) and dissociation rates ($k_{off}$), can be improved by removing phages with fast dissociation rates in the washing step. The number and length of the washings can be thus optimized to select high-affinity binders. Short incubation times, short washes, low target concentration, and decreased number of input phage might favor the selection of clones with fast binding.[260,305]

In the elution step, bound phages are typically eluted by addition of an acid or a base to break the binding interaction. If such elution step is not efficient enough, it will result in the loss of high-affinity binders. On the contrary, too harsh conditions might affect the infectivity of the phage and have consequences in the amplification step. Alternatively, elution can be done by competition, *i.e.,* by adding an excess of the free target to the selections, or by cleavage of phages which include a specific protease cleavage site between the phage and the displayed binder.[257] It should be also noted that the amplification step is susceptible to artifacts, such as biased production of clones which are capable of growing faster than an average clone.[258] Thus, clone enrichment is not only determined by the affinity of the binder but also the toxicity of the specific clones to the bacterial host, solubility, folding efficiency, and stability may contribute to the outcome of phage display.

In the end, the outcome of any selection process is a mixture of clones with different target-binding properties. Screening of individual clones, typically by phage-based ELISAs, is needed to evaluate their target-binging capabilities. Finally, DNA sequencing of selected clones can be used as a guideline to define at what stage to screen the library (**Figure 5B**).[260] Recent developments in automation of the selection process have enabled rapid screening, for example, for several targets simultaneously. Moreover, screening robots enable testing of thousands of different binders,[260] and protein microarrays can prove useful for high-throughput analysis of the specificity and affinity.[306]

In continuation of mimicking the natural selection process, similarly to affinity maturation *in vivo* in which the immune response is capable of producing antibodies with increased affinity,[168] a variety of *in vitro* techniques can be used to improve the affinity and specificity of the binders. The process, known as *in vitro* affinity maturation, comprises a variety of mutagenesis strategies which have been used to construct second-generation libraries based on desired characteristics of the parental peptide or antibody with some fixed or biased sequences. Diverse techniques used include random mutagenesis using DNA modifying enzymes or error-prone PCR, introduction of mutations to certain areas or residues of the antibody, usually in the variable region and the hypervariable loops, for example by oligonucleotide-directed mutagenesis. Also DNA recombination, including the use of natural evolution or recombination of the target gene, can be used to recombine homologous segments to emphasize the desired property, or to shuffle heterologous genes to create new diversity.[258,307]

## 1.4.5 PHAGE DISPLAY AND MYCOTOXINS

Small molecules, or haptens, are challenging targets for many binders because of their size. Because haptens are not immunogenic, for immunization, they need to be conjugated to a carrier protein. Alike, for phage display, small molecules are usually conjugated to a carrier protein, or chemically modified with biotin or reactive groups which enable their immobilization. As a result, the isolated antibodies from both natural and *in vitro* selections may also recognize part of the linker or carrier protein, and the soluble target is recognized less efficiently. Despite the inherent limitations of small molecules, many examples of applications of phage display for mycotoxin detection have been reported. In fact, the libraries can be designed taking into account specific prerequisites so as to find antibodies, for example, against haptens.[308] In addition, the selection conditions in phage display can be strictly controlled, and the library can be for example pre-selected against the carrier protein to avoid background binders, or to favor binding of the free target, the bound phages can be eluted in the presence of the soluble one.[309,310]

Various mycotoxin-specific antibodies have been selected from phage-displayed libraries and used for immunoassay or biosensor development. However, only a few examples of antibodies originating from naïve or synthetic libraries have been reported. For example, an $AFB_1$-specific scFv has been selected from a synthetic human scFv library (Tomlinson J) showing an excellent $K_D$ of $1.2 \times 10^{-12}$ M,[311] although other examples, such as $FB_1$-specific scFv selected from a naïve library showed only rather low affinity, with a $K_D$ of $4.08 \times 10^{-7}$ M.[312] In fact, immunized libraries which are already biased towards the target, have been more widely used, perhaps because they often, although not necessarily, result in binders with higher affinities. Phage-displayed scFv-libraries have been constructed from immunized mice, at least against $FB_1$,[279] OTA,[280] and ZEA.[281] Kinetic analysis by SPR showed excellent affinities in the nanomolar range for the anti-OTA and anti-ZEA antibody fragments demonstrating the advantage of using immunized libraries. Alternatively, so-called positive phage-display libraries have been constructed by randomly recombining the $V_H$ and $V_L$ gene fragments from hybridoma cell lines which secrete a specific monoclonal antibody. Such libraries have been reported at least against $AFB_1$[200] and $FB_1$,[313] both of which resulted in an scFv with improved affinity compared to the parental monoclonal antibody. Also, the use of nanobodies ($V_{HH}$) has been reported for example for the detection of OTA. Nanobody Nb28 was selected from an alpaca-derived $V_{HH}$-library and showed excellent performance in various assay schemes, including phage display-mediated immuno-polymerase chain reaction which provided one of the lowest detection limits reported so far for OTA,[314] direct competitive fluorescence enzyme immunoassay using a recombinant fusion of the same nanobody with alkaline phosphatase,[315] and ELISA with the soluble nanobody.[316]

Alternatively, phage display has been used to select epitope mimics which can replace toxin-conjugates in competitive assays, as discussed before (**1.3.4 Particularities of small molecule detection**). Both peptide and synthetic antibody libraries have been used to select binders against anti-toxin antibodies. The exceptional feature of phage display to search for binders, even without any prior knowledge about the antibody paratope, proves particularly useful in this application. Antibody–antigen interactions are usually a complex combination of

hydrogen bonds, electrostatic bonds, or Van der Waals forces, and unless the antibody paratope and antigen binding are extremely well characterized, rational design or computational modeling of epitope mimics would be challenging. Nonetheless, despite the lack of any of this information, phage display can be used to select binders for these antibodies. Moreover, whilst the selections for the primary binder, *i.e.,* the toxin-specific antibody, exquisitely look for high-affinity binders to provide excellent sensitivity in the final application, epitope mimics do not necessarily require such high affinity. In fact, a slightly lower affinity of the epitope mimic in comparison with the target toxin can be advantageous as weaker affinity indicates less amount of the analyte needed to participate in the competition leading to higher sensitivities.[242,247] Thus, naïve or synthetic libraries which might not have enough diversity to find high-affinity binders can be used to search for epitope mimics. For example, a naïve alpaca nanobody library, which was originally constructed for the screening of DON-specific nanobodies,[317] has been used to select anti-idiotypic nanobodies for the detection of several mycotoxins, including citrinin,[244,245] DON,[246] FB1,[124,242] and OTA.[247]

# 2 Aims of the study

The overall objective of this thesis was to develop new methods for the detection and quantification of mycotoxins and toxigenic fungi in food. To this aim, various assay concepts and formats were explored to assess the impact of different assay components on the performance of bioanalytical assays and biosensors. New recognition elements were designed or selected to achieve specific detection of these food contaminants with the objective of meeting the demands of simple, rapid and low-cost yet sensitive methods for the detection of mycotoxins or toxigenic fungi in agricultural products. The selected recognition elements were applied to the development of biosensors where the effect of the reporter and affinity binders were evaluated in both homogeneous and heterogeneous assay formats. More specifically, the aims of this Ph.D. thesis work were:

1) Development of species-specific DNA probes for the detection and differentiation of highly similar fungal species, *Fusarium proliferatum* and *Fusarium verticillioides,* and the development, optimization and application of the genosensors for the detection of these fungi in cereals.

2) Identification of mycotoxin mimicking peptides, or mimotopes, for mycotoxins fumonisin $B_1$, zearalenone and T-2 toxin from a phage-displayed peptide library.

3) Development of immunoassays for mycotoxin detection based on the use of the synthetic mimotopes in a microarray format and their application to the analysis of fumonisin $B_1$ in maize and wheat samples.

4) Construction and expression of recombinant fusion proteins consisting of the previously identified mimotopes and fluorescent or bioluminescent proteins.

5) Development of heterogeneous and homogeneous immunoassays based on the recombinant mimotope fusion proteins for mycotoxin detection in cereals.

6) Comparison of the different assay formats developed using the phage-borne, synthetic, and recombinant mimotopes.

# 3 Scientific publications

This thesis is based on the following publications, referred to in the text by their Roman numerals (**I–VIII**).

**I.** Peltomaa, R.; Vaghini, S.; Patiño, B.; Benito-Peña, E.; Moreno-Bondi, M. C. Species-specific optical genosensors for the detection of mycotoxigenic *Fusarium* fungi in food samples. *Anal. Chim. Acta*. **2016**. *935*, 231–238.

**II.** Peltomaa, R.; Benito-Peña, E.; Barderas, R.; Sauer, U.; González Andrade, M.; Moreno-Bondi, M. C. Microarray-based immunoassay with synthetic mimotopes for the detection of fumonisin $B_1$. *Anal. Chem*. **2017**. *89*, 6216–6223.

**III.** Peltomaa, R.; Amaro-Torres, F.; Carrasco, S.; Orellana, G.; Benito-Peña, E.; Moreno-Bondi, M. C. Homogeneous quenching immunoassay for fumonisin $B_1$ based on gold nanoparticles and an epitope-mimicking yellow fluorescent protein. *ACS Nano.* **2018**. *12*, 11333–11342.

**IV.** Peltomaa, R.; Agudo-Maestro, I.; Más, V.; Barderas, R.; Benito-Peña, E.; Moreno-Bondi, M. C. Development and comparison of mimotope-based immunoassays for the analysis of fumonisin $B_1$. *Submitted manuscript.*

**V.** Peltomaa, R.; Head, T.; Benito-Peña, E.; Deo, S.; Daunert, S.; Moreno-Bondi, M. C. *Gaussia* luciferase -based bioluminescent immunoassays for mycotoxin detection. *Manuscript in preparation.*

**VI.** Peltomaa, R.; López-Perolio, I.; Benito-Peña, E.; Barderas, R.; Moreno-Bondi, M. C. Application of bacteriophages in sensor development. *Anal. Bioanal. Chem.* **2016**. *408*, 1805–1828.

**VII.** Peltomaa, R.; Benito-Peña, E.; Moreno-Bondi, M. C. Bioinspired recognition elements for mycotoxin sensors. *Anal. Bioanal. Chem*. **2018**, *410*, 747–771.

**VIII.** Peltomaa, R.; Glahn-Martinez, B.; Benito-Peña, E.; Moreno-Bondi, M. C. Optical biosensors for label-free detection of small molecules. *Sensors.* **2018:** *18*,4126.

The original publications (**I–V**) and the review articles (**VI–VIII**; included in Annex I) have been reproduced with the permission from the copyright holders. In addition, some unpublished data is presented in the results and discussion section.

# 3.1 Detection of mycotoxigenic fungi

The genus *Fusarium* is one of the most common producers of mycotoxins and species within this genus are among the most abundant fungi found in agricultural products, such as maize, wheat, and barley. Although the presence of the fungi does not guarantee mycotoxin contamination, assessment of these fungi species is essential to prevent it and identify the mycotoxin producers in crops. *F. proliferatum* and *F. verticillioides* belong to the *Fusarium fujikuroi* species complex which causes a variety of devastating disease in plants and produce a range of menacing mycotoxins. A prerequisite for understanding the ecological behavior of the fungi in this species complex, or to evaluate the potential mycotoxin contamination, is the development of robust and reliable methods for their identification at the species level.

Conventional methods for fungal detection are based on culturing the fungi in specific media which inevitably takes several days and is challenging if the species have similar morphologies, as do *F. proliferatum* and *F. verticillioides*. This publication aimed to develop species-specific DNA probes, which would allow detection and discrimination of these closely related species, and to apply the developed of genosensors based on these probes to the detection of fungal contamination in maize samples. The work included targeting an intergenic spacer region of rDNA (IGS) which allowed differentiating both *Fusarium* spp., the design of capture and detection oligonucleotide probes for this specific region, optimization of the assay protocol using the designed DNA probes as the recognition elements, and finally, application of the develop method to fungi analysis in contaminated maize samples. The main advantages of the genosensors presented in this work over conventional culture-based methods include more sensitive and specific analysis, faster and less labor-intensive protocol resulting in a straightforward identification of the targets at the species level.

Analytica Chimica Acta 935 (2016) 231–238

Contents lists available at ScienceDirect

Analytica Chimica Acta

journal homepage: www.elsevier.com/locate/aca

# Species-specific optical genosensors for the detection of mycotoxigenic *Fusarium* fungi in food samples

Riikka Peltomaa [a], Silvia Vaghini [a], Belén Patiño [b], Elena Benito-Peña [a, **], María C. Moreno-Bondi [a, *]

[a] Department of Analytical Chemistry, Faculty of Chemistry, Complutense University, Ciudad Universitaria s/n, Madrid 28040, Spain
[b] Department of Microbiology III, Faculty of Biology, Complutense University, Ciudad Universitaria s/n, Madrid 28040, Spain



## Abstract

Plant-pathogenic *Fusarium* species, *Fusarium verticillioides* and *Fusarium proliferatum,* are the major producers of fumonisins which are one of the most common mycotoxins found in maize. Herein, we report the development of specific and sensitive genosensors for detecting these two closely related *Fusarium* species in food samples. The sensors are based on species-specific capture and detection probes, which bind to the intergenic spacer region of rDNA (IGS). Oligonucleotide functionalized magnetic microbeads are used to capture the target DNA which is then detected using biotinylated detection probes and a streptavidin-coupled label. The developed genosensors had detection limits of 1.8 pM and 3.0 pM for *F. proliferatum* and *F. verticillioides*, respectively, using synthetic DNA targets. Furthermore, the biosensors were used to analyze natural fungal contamination of commercial maize samples. After amplification of the genomic DNA, the sensors detected the presence of the fungi, in accordance with previous results obtained with PCR. No cross-reactivity between *F. verticillioides* and *F. proliferatum,* or other fungi species tested, was observed. The developed biosensors can provide a valuable tool to evaluate the potential for mycotoxin contamination in conditions where detection of mycotoxins directly is challenging.

## 3.1.1.1 Introduction

Fumonisins, a group of secondary metabolites produced primarily by *Fusarium* species, are one of the major food-borne toxins found in maize worldwide. Fumonisin $B_1$, the most abundant and toxic of fumonisins, has been reported to be neurotoxic, hepatotoxic, and nephrotoxic in animals, and it has been classified as a possible carcinogen to humans.[1–3] The European Union has set maximum residue limits (MRLs) for fumonisins and other mycotoxins, including aflatoxins, ochratoxin A, zearalenone, deoxynivalenol, T-2 and HT-2 toxin, patulin, and citrinin in food and feedstuff to ensure a high level of food safety.[4–6] In order to prevent food contamination it has also become important to identify the mycotoxin producers in food and feed, as it can elucidate

the mycotoxigenic potential of the analyzed samples.[7,8] Although the presence of the fungi does not guarantee mycotoxin contamination, several studies have shown a correlation between *Fusarium* and mycotoxin levels.[9–11] Thus, early detection of mycotoxigenic fungi can be a useful tool for food and feed quality control.

Mycotoxin-producing fungi species are frequently found in agricultural commodities, and they can grow on a wide range of substrates under a wide range of environmental conditions. The *Fusarium fujikuroi* species complex (formerly known as the *Gibberella fujikuroi* species complex) includes several closely related species in the genus *Fusarium* and is considered to be one of the main contaminants of crops. *Fusarium verticillioides* and *Fusarium proliferatum* are often found in this complex, and they have highly similar morphology and are phylogenetically close to each other.[12,13] These species are the major producers of fumonisins in maize, even in plants with no signs of infestation. While *F. proliferatum* is known to colonize a wide range of hosts, including maize, wheat, barley, pine trees, asparagus, and palm trees, *F. verticillioides* is mainly restricted to maize. For this reason, a remarkable effort has been made during the last two decades to distinguish unambiguously these toxigenic strains.[14–16]

Conventionally toxigenic *Fusarium* species have been identified with culture-based techniques and morphological classification using methods that are often laborious, time-consuming, and require taxonomical expertise in *Fusarium* species. More recently molecular diagnostic methods based on specific detection of fungal DNA have emerged to replace the cumbersome microbiological analysis.[17–21] Ribosomal DNA (rDNA) is the most commonly used target for the molecular identification of plant pathogenic fungi.[22] The nuclear rDNA consists of the internal transcribed spacer (ITS) and the intergenic spacer (IGS) regions. The ITS region is the most widely used and sequenced DNA region in molecular ecology of fungi, and it has been recommended as the universal fungal barcode sequence,[23] whereas the IGS region is less used. Nevertheless, the IGS region is known to have the highest variability between species, and it is considered to be the most rapidly evolving spacer region. This allows differentiating even genetically closely related species, such as *F. verticillioides* and *F. proliferatum*. Also, the multi-copy nature of the rDNA region can enhance the assay sensitivity compared to methods that are based on single-copy sequences.[10,24]

Direct detection of *Fusarium* species is challenging because the fungi often exist in species complexes, or at very low concentrations in clinical and natural environments. Different molecular genotypes or varieties can also exist within the species, and they may have different pathogenic profiles and virulence levels to the host.[25] PCR amplification of the target DNA offers a sensitive high-throughput method for identifying pathogens in complex mixtures even when they are no longer viable, and several PCR protocols have been developed for the detection of mycotoxigenic *Fusarium* species, such as *F. verticillioides*[11,26] and *F. proliferatum.*[10,27]

Nevertheless, conventional end-point PCR has several limitations. Lack of specificity of the agarose gel–based detection of the amplified target DNA can lead to false positive results. This may be due to the challenges in determining the exact amplicon size, subjectivity in band identification, and the potential occurrence of amplification artifacts with similar size as those of the real PCR product.[28,29] To overcome these problems, traditional PCR-based methods have evolved to quantitative approaches such as qPCR – also called real-time PCR – or, more recently, digital PCR,[30] and single molecule arrays (Simoa™).[31] Some *Fusarium* species as well have been detected with qPCR showing satisfactory results.[32,33] However, despite their inherent sensitivity, quantitative PCR techniques are not yet standard tools for the analysis of nucleic acids since

they require costly chemicals and consumables, complex instrumentation and qualified personnel. In addition, the simultaneous detection of several different pathogens with multiplex qPCR is difficult, as it requires complex primer design and careful optimization of the reaction conditions to allow specific and efficient target amplification. Furthermore, multiplexing based on the use of fluorescent dyes is limited by the availability of dyes with distinguishable spectra.[34,35]

PCR-enzyme-linked immunosorbent assays (PCR-ELISA) combine the high selectivity of the amplification-based DNA methods with the sensitivity of ELISA. Also, PCR-ELISA allows processing a large number of samples in a short time using only standard laboratory equipment, which demonstrates its suitability for the implementation of integrated screening methods for pathogen detection in food.[36] For example, a PCR-ELISA with a biotinylated capture probe has been used to detect the amplified PCR fragment of fumonisin-producing *Fusarium* species.[37] However, traditional ELISA-based methods have some limitations, such as large sample amounts required, recurrent non-specific adsorption of DNA, and reduced multiplexing capabilities.[38]

In response to these limitations, the combination of PCR and DNA biosensors – also called genosensors – is considered an attractive alternative for pathogen detection due to their simplicity, low cost, and the possibility of multiplexing, together with exquisite specificity attributable to the use of sequence-specific probes.[36] In particular, genosensors based on magnetic microbeads and PCR amplification, have been broadly used in clinical applications and food analysis because of their excellent sensitivity, reproducibility, reduced time of analysis, high sample throughput, and easy automation with minimum consumption of the sample and reagents.[39,40] To the best of our knowledge, only a few genosensors, mainly microarrays, have been developed for fungal pathogen screening and identification. One of the first was reported by Leinberger and coworkers who implemented a microarray platform which included capture probes of 16–24 bases for the fungal rRNA target genes. The method allowed the identification of 12 common pathogenic *Candida* and *Aspergillus* species in clinical isolates.[41]

Here we describe the development of new genosensors that combine the end-point PCR with magnetic microbead–based sensors for the simultaneous and accurate detection of both *F. proliferatum* and *F. verticillioides* for agro-food safety applications. This combination benefits from the advantages of the IGS region for designing one common primer pair for generating a PCR product for fumonisin producing *Fusarium* species, and two pairs of novel species-specific DNA probes that target either *F. proliferatum* or *F. verticillioides*. A bead-based sandwich hybridization assay is performed by incubating the sample, containing the common PCR amplicon, and magnetic microbeads coupled to capture probe and biotinylated detection probe. The assay protocols, including a selection of the optical reporter, are optimized to allow enhanced sensitivity and specificity. Finally, we demonstrate the suitability of the genosensors for the analysis of *Fusarium* contamination in natural maize samples, postulating this novel screening method as the basis of further implemented platforms with the multiplexing capabilities necessary to distinguish the wide range of fumonisins-producing fungi species.[42,43]

### 3.1.1.2 Materials and methods

#### Materials

LodeStars 2.7 Carboxyl paramagnetic beads with an average diameter of 2.7 µm were purchased from Agilent Technologies, Inc. (Santa Clara, CA, USA). Streptavidin R-phycoerythrin conjugate (SAPE), Pierce™ Streptavidin Poly-HRP (SA-poly-HRP), Qdot® 655 Streptavidin Conjugate, Dynabeads® Oligo(dT)25, Amplex UltraRed reagent together with bovine serum albumin (BSA), 1-ethyl-3-[3-dimethylaminopropyl] carbodiimide hydrochloride (EDC), BupH™ MES buffered saline and phosphate-buffered saline (PBS), Tris-EDTA (100× solution), and Blocker™ solution (casein in PBS) were purchased from Thermo Fisher Scientific (Waltham, MA, USA). Saline-sodium citrate buffer (SSC, 20× concentrate), sodium dodecyl sulfate solution (SDS, 20%), Tween-20, and betaine solution (5 M) were from Sigma-Aldrich (St. Louis, MO, USA). Black polypropylene 384-microplates were obtained from Eppendorf (Hamburg, Germany) and all oligonucleotides (**Table 4**) were from Integrated DNA Technologies, Inc. (San Diego, CA, USA). The NZY Plant/Fungi gDNA extraction kit was acquired from by NZYtech (Lisboa, Portugal) and Sabourad dextrose broth + chloramphenicol was from Conda (Madrid, Spain). For the PCR amplification, the KOD Xtreme Hot Start DNA Polymerase and dNTPs were purchased from Merck Millipore (Darmstadt, Germany). The assay incubations were performed in Digital shaking dry bath from Thermo Scientific (Waltham, MA, USA).

#### Design of species-specific oligonucleotide probes and primers

Species-specific capture and detection probes were designed to bind to the IGS region of *F. proliferatum* and *F. verticillioides.* Also, PCR primers were selected to bind to sequences that are common for both *Fusarium* species, which allowed amplification of both targets with the same primer pair in one reaction. The probes and primers were designed on the basis of sequence alignments of the IGS region of more than one hundred *Fusarium* strains (ten of those belonging to *F. verticillioides* and forty belonging to *F. proliferatum*) from different origins and other related species and genera obtained previously in our laboratory or retrieved from databases. Sequences were edited and aligned by ClustalW method using the MegAlign program of DNASTAR software (Lasergene, WI, USA). **Figure 11** in the supplementary material shows the partial alignment of the IGS sequence of representative strains of *Fusarium fujikuroi* species complex which includes *F. proliferatum* and *F. verticillioides,* and the primers and probes designed in this work. Schematic presentation of the primers and probes within the IGS region is presented in **Figure 6**.

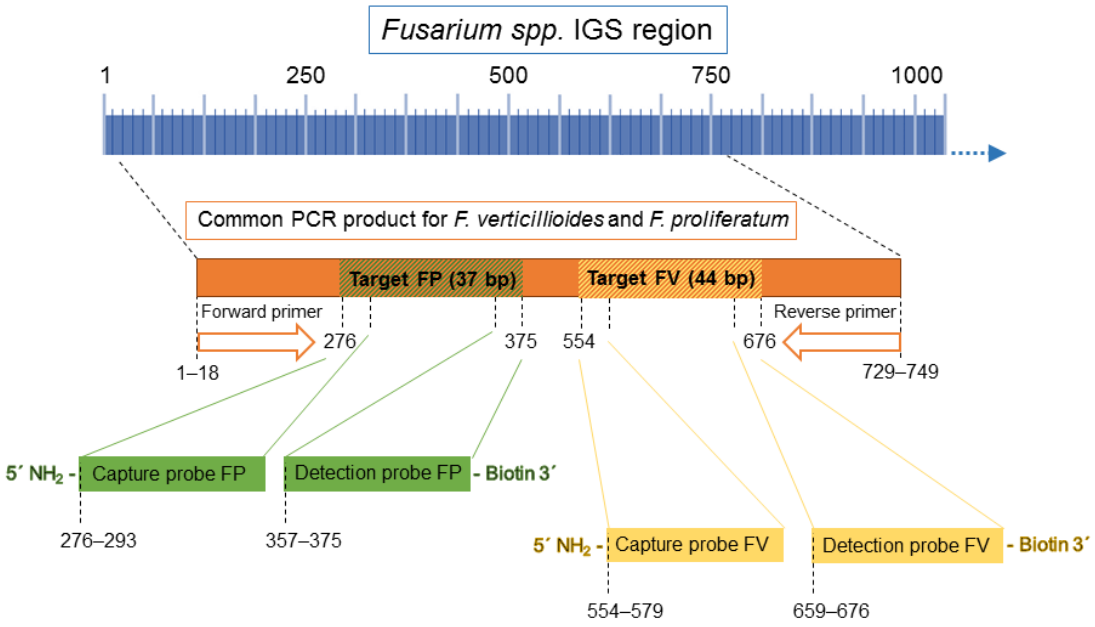


**Figure 6.** Schematic representation of partial *Fusarium* IGS region and location of the primers and probes designed in this work.

The oligonucleotide probe and PCR primer sequences are presented in **Table 4**. The capture probes included an amino modification in 5'-terminus for coupling, and the detection probes had a 3'-terminal biotin for labeling. The direct detection probe, that was used as a positive control hybridized, directly to the capture probe without the target sequence. The synthetic targets for both species included the complementary sequences of both the capture and detection probes.

**Table 4.** Oligonucleotide sequences of the species-specific probes for *F. proliferatum* and *F. verticillioides* (FP and FV, respectively) and PCR primers which amplify both of the species.

| Name | Sequence (5'→ 3') |
|---|---|
| Capture probe FP | 5' Amino modifier C12 – CGG CCA CCA GAG GAT GTG |
| Capture probe FV | 5' Amino modifier C12 – GAG TTT CCA GTC TCG CCG CTG ATG GA |
| Detection probe FP | GAC CAG AGC GAA CGT GGT C – 3' Biotin |
| Detection probe FV | TGT GGT CTG GTG GCC GCG – 3' Biotin |
| Direct detection probe FV | 5' Biotin – TCC ATC AGC GGC GAG ACT GGA AAC TC |
| Synthetic target FP | GAC CAC GTT CGC TCT GGT CCA CAT CCT CTG GTG GCC G |
| Synthetic target FV | CGC GGC CAC CAG ACC ACA TCC ATC AGC GGC GAG ACT GGA AAC TC |
| Forward primer | GTC CTG TAA GCA GTA GAG |
| Reverse primer | CTC GCG GGC CAC TTT TGA |

## Coupling of capture probes to magnetic particles

The capture probes FP and FV were conjugated from their terminal amino group to the carboxylated magnetic microbeads. First, the beads (1 mg) were washed twice with 0.01 M NaOH, followed by three washes with the coupling buffer (0.1 M MES, pH 5.7; 0.01% SDS) according to manufacturer's instructions. Next, the carboxyl surface was activated by adding

150 µL of 525 mM EDC in coupling buffer together with 5 nmol of amino-modified DNA to reach the total reaction volume of 500 µL. The reaction tube was incubated for 30 minutes at room temperature in slow shaking. Another 150 µL of 525 mM EDC solution was added, and the incubation was continued for 30 minutes as before. Finally, the beads were washed with 1x Tris-EDTA buffer three times and stored at +4 °C in the same buffer. The DNA coupling efficiency and the capture probe density on the bead surface was determined by measuring the amount of DNA remaining in the solution phase after immobilization, as previously reported.[44]

## Sample preparation

Five maize samples from commercial fields in Spain were kindly supplied by the Insect-plant Interaction Group from CIB-CSIC (Madrid, Spain). The samples were previously analyzed for fungal contamination by PCR assays. Briefly, the seeds (15–20 g) were ground with a grinder and sieved by a 0.1 mm screen to obtain a subsample of 0.08 g that was subsequently subjected to DNA extraction. Total DNA (120–200 ng) was used in PCR assays[10,18,26,45–49] to determine the presence of the fungi in the samples.

In parallel, the samples were tested with the genosensors. First, to extract the genomic DNA 3 g of ground maize sample was incubated in 50 mL Sabourad dextrose broth for 24 h at +28 °C, 120 rpm. The culture was filtered and homogenized in liquid nitrogen with mortar and pestle. Then, the genomic DNA was extracted from homogenized samples with NZY Plant/Fungi gDNA kit according to the manufacturer's instructions. The IGS region of the fungal DNA was amplified using PCR primers designed on the conserved regions of the *Fusarium* species. The PCR reaction contained 0.3 µM forward and reverse primers, 0.4 mM dNTPs, 0.7 M betaine, 0.02 U $\mu L^{-1}$ of KOD Xtreme Hot Start DNA Polymerase, and 1x Xtreme buffer. The total volume of the reaction was 50 µL. The thermal cycling of the PCR consisted of 2 min initial denaturation at +94 °C followed by 30 cycles of +98 °C for 10 s denaturation, +50 °C for 30 s annealing, and +68 °C for 1 min extension steps.

## Assay protocol

One-step sandwich hybridization assay was performed by mixing the capture probe coupled to the magnetic beads, the target DNA, and the biotinylated detection probe. First, to reduce the nonspecific binding the microcentrifuge tubes were blocked with Blocker™ for 1 h at +37 °C. Then, the target DNA (0–0.5 pmol of the synthetic target or 10 µL of sample in three replicates, except 6 replicates for the blank) was mixed with 0.5 pmol of detection probe and heated to +95 °C for 5 min to denature the DNA. After cooling the mixture on ice for 5 min, 6.5 µg of beads (approximately $5\times10^5$ beads), were added to reach the total reaction volume of 100 µL. All dilutions were made in hybridization buffer (5× PBS with 0.1 M betaine), and the reaction was incubated for 1.5 h at +60 °C with slow shaking (600 rpm). The beads were then washed three times with washing buffer A (2× SSC, 0.02% Tween-20) and 50 µL of SAPE (10 µg $mL^{-1}$), SA-QD (5 nM) or SA-poly-HRP (200 ng $mL^{-1}$) in hybridization buffer was added to each reaction tube. After 30 min incubation in shaking at room temperature, the beads were washed three times with washing buffer B (0.1% BSA, 0.02% Tween-20). Next, they were resuspended in 12 µL of hybridization buffer and transferred to the wells of a 384-microtiter plate. The SAPE and quantum dot reactions were directly measured with CLARIOstar microplate reader from BMG

Labtech (Ortenberg, Germany) after short shaking. For the enzymatic reaction, Amplex UltraRed reagent was mixed with hydrogen peroxide according to the manufacturer's instructions, and 50 µL of the substrate solution was added to each well to develop the fluorescent signal. The fluorescent signals were measured with the microplate reader using excitation/emission wavelengths of 490/578 nm for SAPE, 320/655 nm for quantum dots, and 510/590 nm for Amplex UltraRed.

### 3.1.1.3 Results and discussion

#### Probe design and assay optimization

The intergenic spacer region (IGS) of the ribosomal DNA is one of the most rapidly evolving sequences in the genome. The IGS region of *Fusarium* was chosen as the target DNA for developing species-specific genosensors since it has sufficient variability to discriminate closely related species, such as *F. verticillioides* and *F. proliferatum*. On the other hand, the use of IGS region to develop specific probes, instead of single-copy genes (either constitutive or toxin biosynthetic genes), enhances the sensitivity of the assay due to its multi-copy character.[24] The PCR primers were designed to hybridize to the conserved regions of the IGS so that the same primer pair will amplify both *F. proliferatum* and *F. verticillioides* DNA, as well as other *Fusarium* species, *F. saccharii*, *F. fujikuroi*, and *F. nygamai* within the *Fusarium fujikuroi* species complex (**Figure 11** in the supporting information). In this way, we could avoid the complex primer design and PCR reaction optimization that is required for developing multiplex PCR assays. Furthermore, the sequence variations within the PCR amplicon were exploited to identify and distinguish *F. proliferatum* and *F. verticillioides* by designing the species-specific capture and detection probes on these sequences.

**Figure 7** shows a schematic illustration of the target DNA detection by the genosensors. The sandwich complex is formed when the target DNA hybridizes with the species-specific detection and capture probes. The capture probes are coupled from their 5'-terminus to magnetic beads which allow efficient separation of the target even from complex mixtures. Biotin in the 3'-terminus of the detection probe allows detection of the hybridized complex in a flexible way using any streptavidin-coupled label.

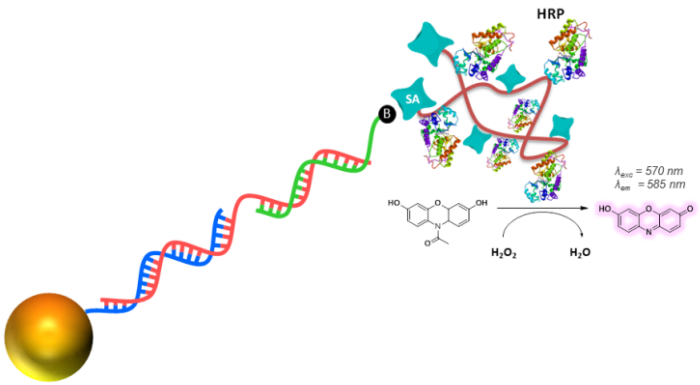


**Figure 7.** Schematic of the assay principle. Target DNA (red) is recognized by the capture probe (blue) coupled to magnetic microbeads and the biotinylated detection probe (green). Hybridized sandwich complex is then detected using SA-poly-HRP and Amplex UltraRed substrate.

After oligonucleotide coupling, the capture probe density on the bead surface was determined by measuring the amount of DNA remaining in the solution phase after immobilization. The optimized coupling protocol resulted in 268 pmol of oligonucleotides/mg of beads which is in accordance with the surface binding capacities reported for commercially available magnetic microbeads.[50] Due to the complexity of the genomic DNA the first experiments with the genosensors were done with synthetic target DNA that was complementary to the capture and the detection probes. The sandwich assay can be performed either in two steps, adding first the bead-coupled capture probes, washing and then adding the detection probe, or in one step where both probes and the target DNA are hybridized in one incubation step. We observed that both assay formats resulted in similar signal levels, but the 1-step format allowed higher reproducibility (RSD < 16% ) (**Figure 8A**), which is most likely due to the lower number of washing steps required in this setup. The optimal hybridization time was defined as 1.5 h, as it resulted in higher fluorescence signal intensities than shorter incubation times. However, longer incubation did not show further improvement in the assay (**Figure 8B**; **Figure 12** in the supporting information). As the GC-content of the IGS-region and the probes is rather high (55–75%), hybridization requires high temperatures for optimal binding. At +60 °C the signals obtained from the assay were best for both species, and this temperature was selected for assay development **(Figure 8C**). The effect of temperature was more evident for *F. verticillioides*, and it could be traced back to the higher GC-content, and higher $T_m$, of the probes.

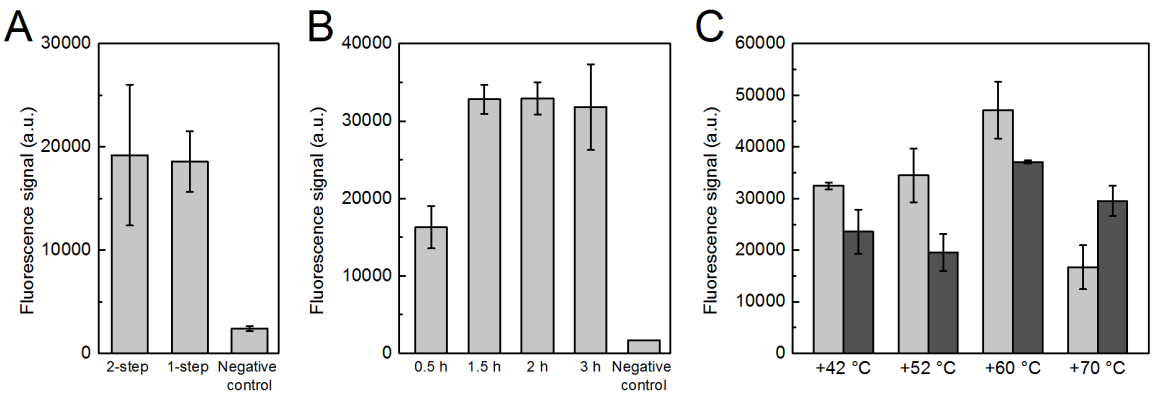


**Figure 8**. Optimization results: (A) one-step or two-step hybridization assay, (B) hybridization time, and (C) hybridization temperature, light grey *F. proliferatum* and dark grey *F. verticillioides* (*n* = 3).

## Selection of the most sensitive label

To increase the sensitivity of the assay, alternative labels were tested for fungi detection. Instead of streptavidin-coupled R-Phycoerythrin (SAPE), which is an intensely bright phycobiliprotein, streptavidin-coupled quantum dots and SA-poly-HRP were evaluated as well. Calibration curves with different labels are presented in **Figure 9**. Quantum dots showed increased sensitivity compared to SAPE, but the best sensitivity was achieved with the SA-poly-HRP as the label. The use of enzymatic detection allows signal amplification since each HRP molecule can catalyze many cycles of conversions of substrate molecules to the fluorescent product, leading to an increment of the analytical signal. Moreover, the use of SA-poly-HRP as label further increases the amount of fluorescent molecules produced per binding event further enhancing assay sensitivity, as described before.[51]

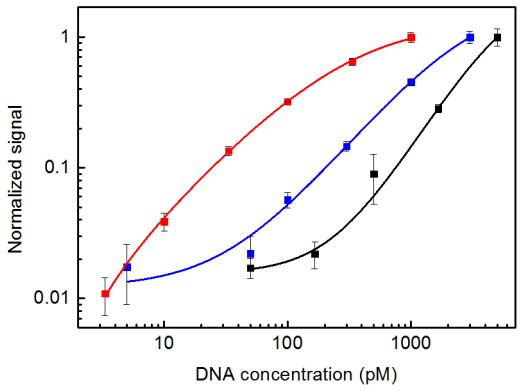


**Figure 9.** Comparison of different labels: Hybridized sandwich complex was detected using SA-poly-HRP (red), QD (blue) and SAPE (black) as a label. With four-parameter logistic fitting the $EC_{50}$ values were 0.3 nM, 2.8 nM, and 6.1 nM for SA-poly-HRP, QDs and SAPE, respectively (*n* = 3).

## Cross-reactivity and analytical sensitivity

After the determination of optimal assay conditions, we performed the cross-reactivity studies between *F. proliferatum* and *F. verticillioides* to confirm species-specific recognition of the genosensors. The sandwich hybridization assays were carried out with the synthetic target using *F. proliferatum* specific probes with *F. verticillioides* target, and *vice versa*. No significant cross-reactivity was observed since the signals from non-specific targets were at the level of the non-target background (**Figure 10**). Mirete *et al.* (2013)[43] have determined that the nucleotide sequence similarity of the IGS region between *F. proliferatum* and *F. verticillioides* is 85%, but the capture and detection probes of the genosensors were designed to bind to the regions with most variation. In this way, the high sequence variation of the IGS region was used to distinguish closely the related species, *F. proliferatum* and *F. verticillioides*. Using other targets, such as the genes involved in fumonisin biosynthesis, *FUM1,*[11] or even the ITS region,[37] this differentiation is not possible.

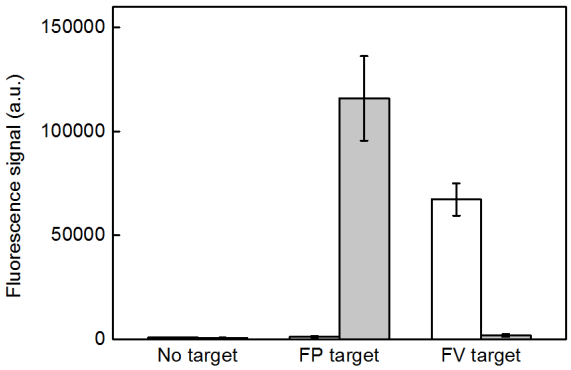


**Figure 10.** Cross-reactivity of the genosensors was studied by testing the *F. verticillioides* probes (white columns) and *F. proliferatum* probes (grey columns) with both *F. proliferatum* (FP) and *F. verticillioides* (FV) targets. SA-poly-HRP was used as the label ($n$ = 3).

Analytical performance of the genosensors was evaluated using the SA-poly-HRP as a label in the optimized assay conditions. The calibration graphs corresponding to the linear response range for both species are presented in the supplementary material (**Figure 13**). The fitting equations were $y = 2140.5[C]^{0.67}$ ($R^2$ = 0.9996) and $y = 2360.0[C]^{0.74}$ ($R^2$ = 0.996) for *F. proliferatum* and *F. verticillioides* respectively (6 points per calibration in three replicates, except six replicates for the blank). The lower limit of detection was defined as the signal of the blank plus three times the standard deviation above the background, in this case 1.8 pM (corresponding to 4.0 pg/sample and equivalent to $1.81 \times 10^8$ copies of target DNA) and 3.0 pM (corresponding to 2.0 pg/sample and equivalent to $1.08 \times 10^8$ copies of target DNA) for *F. proliferatum* and *F. verticillioides*, respectively. The slightly higher detection limit obtained in the case of *F. verticillioides* might be due to the higher GC-content of the probes which could cause less efficient binding to the target. The linear range of the assay was approximately 5–200 pM. Assay reproducibility was determined from fluorescence signals of three replicates

within the same day, or in three different days. The intra- and inter-assay relative standard deviations (RSD) using 30 pM synthetic target DNA were 6% and 14%, respectively, demonstrating the suitability of the genosensors for the qualitative detection of the fungi.

### Analysis of contaminated maize samples

Finally, to demonstrate the potential use of the genosensors for food analysis we tested five maize samples for fungal contamination. The samples were previously analyzed with PCR for the presence of fungi.[10,18,26,45–49] Two of the samples were not contaminated with *Fusarium*, sample 1 did not contain any fungi, and sample 2 was contaminated with *Aspergillus flavus*, another common fungus in maize. The other three samples were contaminated either with *F. proliferatum* or *F. verticillioides,* or both species as indicated in **Table 5**. The genomic DNA from these five maize samples was extracted using a commercial DNA extraction kit as described in Materials and methods. Since the genomic DNA is complex and difficult to use directly for hybridization assays the *Fusarium* IGS region was amplified by PCR with the primers that recognize both *F. proliferatum* and *F. verticillioides.*

After the amplification, the PCR reaction was directly analyzed with the two genosensors without any further purification. The samples were heated at +95 °C to denaturate the double-stranded PCR product and minimize secondary structures of the target DNA. The biotinylated detection probe was combined with 10 µL of the sample during heating to minimize the chance of rebinding of the complementary strands. To confirm the functionality of the assay and to assure that there was no significant interference from the PCR reaction we included a positive and negative control to the sample analysis. The negative control included magnetic microbeads with dT-oligo that does not bind to the target DNA, and the positive control was FV specific beads with a direct detection probe that binds to capture probe directly without the target DNA. The cut-off value was determined as previously reported for qualitative PCR-ELISA approaches[52, 53] as the mean signal of the negative controls plus three times the standard deviation of the negative controls. Samples that gave signals above this cut-off value were determined as positive. **Table 5** shows the excellent agreement between the previous analysis and the genosensors. No fungi were detected from the two samples without *Fusarium,* and sample 2 contaminated with *Aspergillus flavus* fungi showed no cross-reactivity neither with *F. proliferatum* nor *F. verticillioides* specific probes. Positive signals were obtained in the presence of either or both *F. proliferatum* and *F. verticillioides*, which confirmed the specificity and selectivity of the detection, as before observed with the synthetic target, as well as sufficient sensitivity for detecting the PCR amplicon.

**Table 5.** Results of the sample analysis. Five maize samples were analyzed with the genosensors for the presence of *F. proliferatum* or *F. verticillioides*. Positive and negative controls were included for each sample.

| Sample and fungal contamination according to previous PCR analysis | | Negative control | Positive control | *F. proliferatum* | *F. verticillioides* |
|---|---|---|---|---|---|
| 1 | – | – | + | – | – |
| 2 | *Aspergillus flavus* | – | + | – | – |
| 3 | *F. proliferatum* | – | + | + | – |
| 4 | *F. verticillioides* | – | + | – | + |
| 5 | *F. proliferatum, F. verticillioides* | – | + | + | + |

### 3.1.1.4 Conclusions

We have developed two optical genosensors for the selective detection of *F. proliferatum* and *F. verticillioides,* the major producers of fumonisins in maize. The system takes advantage of the IGS region of the fungal genomic DNA and two specific oligonucleotide probes, which allow highly specific detection of the two closely related species. The genosensors were able to detect the synthetic target DNA in the low picomolar range with no significant cross-reactivity between the two species, as well as identify the fungal contamination in maize samples using the amplified genomic DNA. A common primer pair was designed for the conserved sequences of the IGS region, which enabled amplification of both *Fusarium* species in one reaction. The same primer pair could also be used for other species in the *Fusarium fujikuroi* species complex, which will be a significant advantage when developing a multiplex sensor for several *Fusarium* species. In addition, the magnetic bead assay protocol implemented in this work could easily be automated providing a simple and robust method for the detection of mycotoxigenic *Fusarium* species in food samples.

### Acknowledgments

This study was supported by the EU (SAMOSS; FP7-PEOPLE-2013-ITN; Contract 607590) and the Ministry of Economy and Competitiveness (MINECO, CTQ2012-37573-C02).

## 3.1.1.5 Supporting information

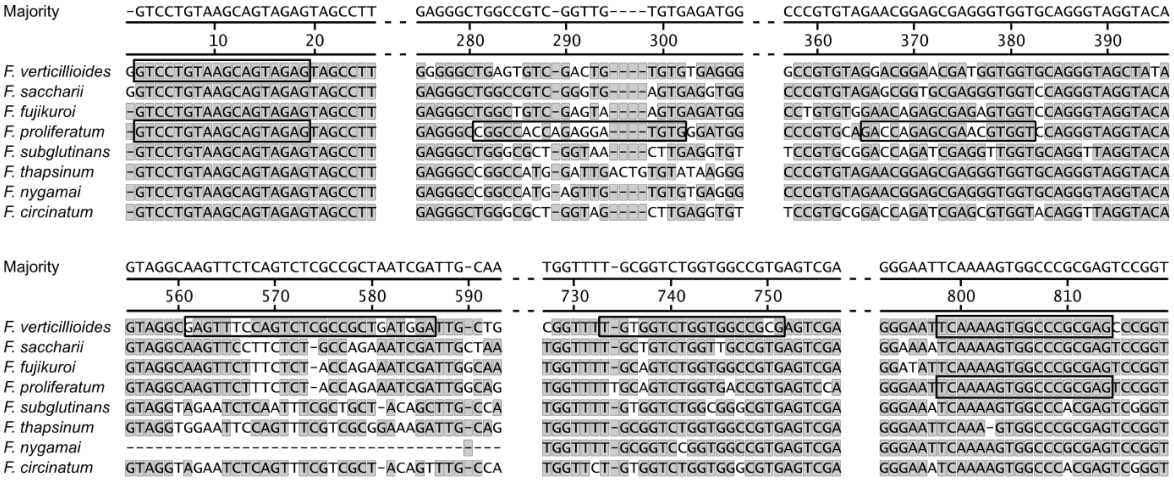


**Figure 11**. Partial alignment of the IGS sequence with representative strains of *Fusarium fujikuroi* species complex: *F. verticillioides* (accession number AJ880005.1); *F. saccharii* (AJ879944.1); *F. fujikuroi* (AJ879945.1); *F. proliferatum* (AJ879946.1); *F. subglutinans* (AJ879947.1); *F. thapsinum* (AJ879948.1); *F. nygamai* (AJ879949.1) and *F. circinatum* (AJ879950.1). The sequences corresponding the species-specific probes and PCR primers common for both *F. verticillioides* and *F. proliferatum* (as well as most of other *Fusarium* species) are marked with boxes in the alignment.

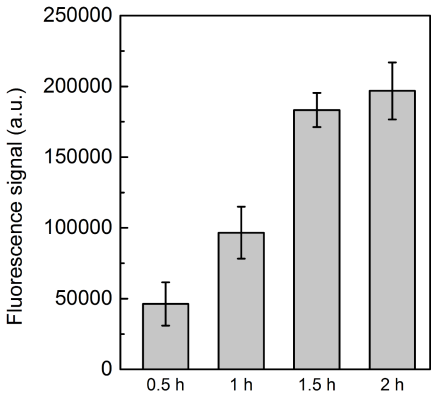


**Figure 12.** Optimization of the hybridization time using the synthetic target DNA and HRP detection.

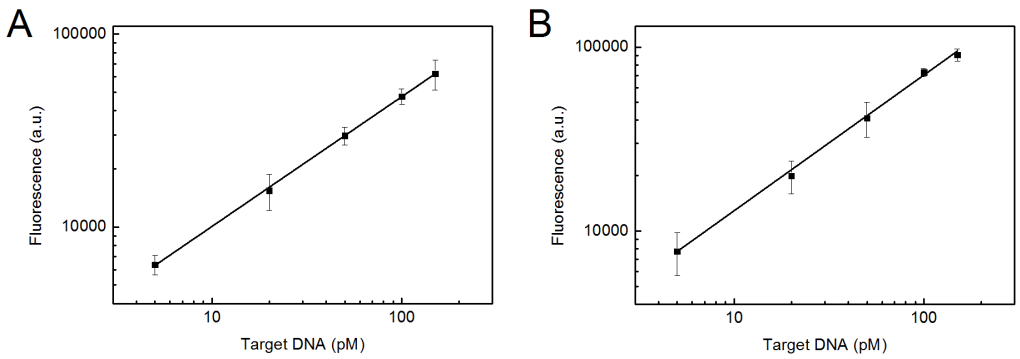


**Figure 13.** Calibration curves with enzymatic detection. The equations for allometric fittings for (A) *F. proliferatum* and (B) *F. verticillioides* were $y = 2140.5x^{0.67}$ ($R^2 = 0.9996$) and $y = 2360.0x^{0.74}$, ($R^2 = 0.996$), respectively ($n = 3$).

## 3.1.1.6 References


1. Gelderblom, W. C.; Jaskiewicz, K.; Marasas, W. F.; Thiel, P. G.; Horak, R. M.; Vleggaar, R.; Kriek, N. P., Fumonisins-novel mycotoxins with cancer-promoting activity produced by *Fusarium moniliforme*. *Appl. Environ. Microbiol*. **1988**, 54, 1806–1811.
2. Bryla, M.; Roszko, M.; Szymczyk, K.; Jedrzejczak, R.; Obiedzinski, M. W.; Sekul, J., Fumonisins in plant-origin food and fodder – A review. *Food Addit. Contam., Part A* **2013,** *30,* 1626–1640.
3. Stockmann-Juvala, H.; Savolainen, K., A review of the toxic effects and mechanisms of action of fumonisin B1. *Hum. Exp. Toxicol.* **2008**, *27*, 799–809.
4. European Commission. Commission regulation (EU) No 105/2010. *Off. J. Eur. Union* **2010**, *L35*, 7–8.
5. European Commission. Commission regulation (EC) No 1126/2007. *Off. J. Eur. Union* **2007**, *L255*, 14–17.
6. European Commission. Commission regulation (EC) No 1881/2006. *Off. J. Eur. Union*. **2006,** *L364*, 5–24.
7. Niessen, L., PCR-based diagnosis and quantification of mycotoxin-producing fungi. *Adv. Food Nutr. Res.* **2008,** *54*, 81–138.
8. De Saeger, S. (Editor) *Determining mycotoxins and mycotoxigenic fungi in food and feed*. Woodhead Publishing Limited: Oxford, **2011**.
9. Gil-Serna, J.; Mateo, E. M.; González-Jaén, M. T.; Jiménez, M.; Vázquez, C.; Patiño, B., Contamination of barley seeds with *Fusarium* species and their toxins in Spain: An integrated approach. *Food Addit. Contam., Part A* **2013,** *30*, 372–380.
10. Jurado, M.; Vazquez, C.; Marin, S.; Sanchis, V.; Teresa Gonzalez-Jaen, M., PCR-based strategy to detect contamination with mycotoxigenic *Fusarium* species in maize. *Syst. Appl. Microbiol.* **2006,** *29*, 681–689.
11. Sánchez-Rangel, D.; SanJuan-Badillo, A.; Plasencia, J., Fumonisin production by *Fusarium verticillioides* strains isolated from maize in Mexico and development of a polymerase chain reaction to detect potential toxigenic strains in grains. *J. Agric. Food Chem.* **2005,** *53*, 8565–8571.
12. Bennett, J. W.; Klich, M., Mycotoxins. *Clin. Microbiol. Rev.* **2003,** *16,* 497–516.
13. Creppy, E. E., Update of survey, regulation and toxic effects of mycotoxins in Europe. *Toxicol. Lett.* **2002,** *127*, 19–28.
14. Matny, O., Screening of mycotoxin produced by *Fusarium verticillioides* and *F. proliferatum* in culture media. *Asian. J. Agric. Rural Develop.* **2013,** *3*, 1001–1006.
15. Jurado, M.; Marín, P.; Callejas, C.; Moretti, A.; Vázquez, C.; González-Jaén, M. T., Genetic variability and Fumonisin production by *Fusarium proliferatum*. *Food Microbiol.* **2010,** *27*, 50–57.
16. Visentin, I.; Tamietti, G.; Valentino, D.; Portis, E.; Karlovsky, P.; Moretti, A.; Cardinale, F., The ITS region as a taxonomic discriminator between *Fusarium verticillioides* and *Fusarium proliferatum*. *Mycol. Res.* **2009,** *113*, 1137–1145.
17. Gong, L.; Jiang, Y.; Chen, F., Molecular strategies for detection and quantification of mycotoxin-producing *Fusarium* species: A review. *J. Sci. Food Agric.* **2015,** *95*, 1767–1776.

18. Jurado, M.; Vázquez, C.; Patiño, B.; González-Jaén, M. T., PCR detection assays for the trichothecene-producing species *Fusarium graminearum*, *Fusarium culmorum*, *Fusarium poae*, *Fusarium equiseti* and *Fusarium sporotrichioides*. *Syst. Appl. Microbiol.* **2005,** *28*, 562–568.
19. Mulè, G.; González-Jaén, M. T.; Hornok, L.; Nicholson, P.; Waalwijk, C., Advances in molecular diagnosis of toxigenic *Fusarium* species: A review. *Food Addit. Contam.* **2005,** *22*, 316–323.
20. Niessen, L., PCR-based diagnosis and quantification of mycotoxin producing fungi. *Int. J. Food Microbiol.* **2007,** *119*, 38–46.
21. Seifert, K. A.; Lévesque, C. A., Phylogeny and molecular diagnosis of mycotoxigenic fungi. *Eur. J. Plant Pathol.* **2004,** *110*, 449–471.
22. White, T. J.; Bruns, T. D.; Lee, S. B.; Taylor, J. W., Amplification and direct sequencing of fungal ribosomal RNA genes for phylogenetics. In *PCR Protocols: A guide to methods and applications*, Academic Press: New York, **1990**; pp 315–322.
23. Schoch, C. L.; Seifert, K. A.; Huhndorf, S.; Robert, V.; Spouge, J. L.; Levesque, C. A.; Chen, W.; Fungal Barcoding Consortium, Nuclear ribosomal internal transcribed spacer (ITS) region as a universal DNA barcode marker for fungi. *Proc. Natl. Acad. Sci. USA* **2012,** *109*, 6241–6246.
24. Suarez, M. B.; Walsh, K.; Boonham, N.; O'Neill, T.; Pearson, S.; Barker, I., Development of real-time PCR (TaqMan) assays for the detection and quantification of *Botrytis cinerea* in planta. *Plant. Physiol. Biochem* **2005,** *43*, 890–899.
25. Blackwell, M., The fungi: 1, 2, 3 ... 5.1 million species? *Am. J. Bot.* **2011,** *98*, 426–438.
26. Patiño, B.; Mirete, S.; González-Jaén, M. T.; Mulé, G.; Rodríguez, M. T.; Vázquez, C., PCR detection assay of fumonisin-producing *Fusarium verticillioides* strains. *J. Food Prot.* **2004,** *37*, 1278–1283.
27. Mulè, G.; Susca, A.; Stea, G.; Moretti, A., Specific detection of the toxigenic species *Fusarium proliferatum* and *F. oxysporum* from asparagus plants using primers based on calmodulin gene sequences. *FEMS Microbiol. Lett.* **2004,** *230*, 235–240.
28. Perelle, S.; Dilasser, F.; Malorny, B.; Grout, J.; Hoorfar, J.; Fach, P., Comparison of PCR-ELISA and LightCycler real-time PCR assays for detecting *Salmonella spp*. in milk and meat samples. *Mol. Cell Probes* **2004,** *18*, 409–420.
29. Smith, C. J.; Osborn, A. M., Advantages and limitations of quantitative PCR (Q-PCR)-based approaches in microbial ecology. *FEMS Microbiol. Ecol.* **2009,** *67*, 6–20.
30. Baker, M., Digital PCR hits its stride. *Nat. Methods* **2012,** *9*, 541–544.
31. http://www.quanterix.com/ [Cited May 25, 2016].
32. Lin, Z.; Xu, S.; Que, Y.; Wang, J.; Comstock, J. C.; Wei, J.; McCord, P. H.; Chen, B.; Chen, R.; Zhang, M., Species-specific detection and identification of *Fusarium* species complex, the causal agent of sugarcane pokkah boeng in China. *PLoS One* **2014,** *9*, e104195.
33. Nicolaisen, M.; Suproniene, S.; Nielsen, L. K.; Lazzaro, I.; Spliid, N. H.; Justesen, A. F., Real-time PCR for quantification of eleven individual *Fusarium* species in cereals. *J. Microbiol. Methods* **2009,** *76*, 234–240.
34. McCartney, H. A.; Foster, S. J.; Fraaije, B. A.; E., W., Molecular diagnostics for fungal plant pathogens. *Pest. Manag. Sci.* **2003,** *59*, 129–142.
35. Klein, D., Quantification using real-time PCR technology: applications and limitations. *Trends Mol. Med.* **2002,** *8*, 257–260.
36. Santiago-Felipe, S.; Tortajada-Genaro, L. A.; Puchades, R.; Maquieira, A., Recombinase polymerase and enzyme-linked immune-sorbent assay as a DNA amplification-detection strategy for food analysis. *Anal. Chim. Acta* **2014,** *811*, 81–87.
37. Grimm, C.; Geisen, R., A PCR-ELISA for the detection of potential fumonisin producing *Fusarium* species. *Lett Appl Microbiol* **1998,** *26*, 456–462.
38. http://info.luminexcorp.com/ [Cited May, 25 2016].
39. *Principles of bacterial detection: Biosensors, recognition receptors and microsystems*. Zourob, M.; Elwary, S.; Turner, A. (Editors) Springer: New York, **2008**.
40. Sotillo, A.; Pedrero, M.; de Pablos, M.; García, J. L.; García, E.; García, P.; Pingarrón, J. M.; Mingorance, J.; Campuzano, S., Clinical evaluation of a disposable amperometric magneto-genosensor for the detection and identification of *Streptococcus pneumoniae*. *J. Microbiol. Methods* **2014,** *103*, 25–28.
41. Leinberger, D. M.; Schumacher, U.; Autenrieth, I. B.; Bachmann, T. T., Development of a DNA microarray for detection and identification of fungal pathogens involved in invasive mycoses. *J. Clin. Microbiol.* **2005,** *43*, 4943–4953.

42. Carrasco, S.; Benito-Peña, E.; Walt, D. R.; Moreno-Bondi, M. C., Fiber-optic array using molecularly imprinted microspheres for antibiotic analysis. *Chem. Sci.* **2015,** *6*, 3139–3147.

43. Mirete, S.; Patino, B.; Jurado, M.; Vazquez, C.; Gonzalez-Jaen, M. T., Structural variation and dynamics of the nuclear ribosomal intergenic spacer region in key members of the *Gibberella fujikuroi* species complex. *Genome* **2013,** *56*, 205–213.

44. Walsh, M. K.; Wang, X.; Weimer, B. C., Optimizing the immobilization of single-stranded DNA onto glass beads. *J. Biochem. Biophys. Methods* **2001,** *47*, 221–231.

45. Gil-Serna, J.; Vázquez, C.; Sardiñas, N.; González-Jaén, M. T.; Patiño, B., Discrimination of the main Ochratoxin A-producing species in *Aspergillus* section *Circumdati* by specific PCR assays. *Int. J. Food Microbiol.* **2009,** *136*, 83–87.

46. González-Salgado, A.; González-Jaén, T.; Vazquez, C.; Patiño, B., Highly sensitive PCR-based detection method specific for *Aspergillus flavus* in wheat flour. *Food Addit. Contam., Part A* **2008,** *25*, 758–764.

47. González-Salgado, A.; Patiño, B.; Vázquez, C.; González-Jaén, M. T., Discrimination of *Aspergillus niger* and other *Aspergillus* species belonging to section *Nigri* by PCR assays. *FEMS Microbiol. Lett.* **2005,** *245*, 353–361.

48. Patiño, B.; González-Salgado, A.; González-Jaén, M.; Vázquez, C., PCR detection assays for the ochratoxin-producing *Aspergillus carbonarius* and *Aspergillus ochraceus* species. *Int. J. Food Microbiol.* **2005,** *104*, 207–214.

49. Sardiñas, N.; Vézquez, C.; Gil-Serna, J.; González-Jaén, M. T.; Patiño, B., Specific detection and quantification of *Aspergillus flavus* and *Aspergillus parasiticus* in wheat flour by SYBR(R) Green quantitative PCR. *Int. J. Food Microbiol.* **2011,** *145*, 121–125.

50. http://www.neb.com/products/s1420-streptavidin-magnetic-beads (Cited May, 25 2016); www.sigmaaldrich.com/catalog/product/roche/strepmagro (Cited May, 25 2016); www.gelifesciences.com/webapp/wcs/stores/servlet/catalog/en/GELifeSciences-fi/products/AlternativeProductStructure_24411/29103135 (Cited May, 25 2016); *Sample preparation techniques in analytical chemistry*, Mitra, S. (Editors) Wiley-Interscience, Hoboken, NJ, USA. **2003**.

51. Ojeda, I.; Moreno-Guzmán, M.; González-Cortés, A.; Yáñez-Sedeño, P.; Pingarrón, J. M., Electrochemical magnetoimmunosensor for the ultrasensitive determination of interleukin-6 in saliva and urine using poly-HRP streptavidin conjugates as labels for signal amplification. *Anal. Bioanal. Chem.* **2014,** *406*, 6363–6371.

52. Erhardt, A.; Schaefer, S.; Athanassiou, N.; Kann, M.; Gerlich, W. H., Quantitative assay of PCR-amplified hepatitis B virus DNA using a peroxidase-labelled DNA probe and enhanced chemiluminescence. *J. Clin. Microbiol.* **1996,** *34*, 1885–1891.

53. Musiani, M.; Venturoli, S.; Gallinella, G.; Zerbini, M., Qualitative PCR-ELISA protocol for the detection and typing of viral genomes. *Nat. Protoc.* **2007,** *2*, 2502–2510.

# 3.2 Mycotoxin detection

The second and major part of the thesis focused on the development of methods for the detection of mycotoxins fumonisin $B_1$ and zearalenone. Even though the presence of mycotoxigenic fungi has been shown to correlate with the mycotoxin levels, it is still crucial to detect the toxins themselves to guarantee food safety. The national and international regulations for the major mycotoxin classes have provoked the development of new methods for the detection and quantification of these compounds. Chromatographic methods continue their reign among the validated methods, but many biosensors and bioanalytical assays have been introduced as an alternative for fast screening or on-field applications.

The work aimed to develop new immunoassays for mycotoxin detection based on epitope mimicking peptides, or mimotopes. The exceptional ability of mimotopes to bind to the same antibody paratope as the target analyte makes them an intriguing alternative to replace the toxin-conjugates in competitive immunoassays. We have selected mimotopes from synthetic 12-mer peptide library by phage display using the mycotoxin-specific antibody as the target, anti-$FB_1$ in **publication II** and anti-ZEA in **publication V**. Later, the individual phages which showed the best performance in competitive phage-based immunoassays were identified by DNA sequencing. Thus, the identified mimotopes could be applied to the immunoassays without the phage which itself might not be an ideal component in the assay due to its immense size and biologically active nature.

As an alternative for the phage-borne mimotopes, two strategies were tested and compared. In **publications II** and **IV**, the synthetic counterpart of the $FB_1$-mimotope was used as a competitor in immunoassays in a microarray or magnetic bead format. The synthetic peptide was designed with a biotin-linker which enabled simple coupling of the mimotope to the solid surface, the array or magnetic beads, using neutravidin. In a different approach, recombinant fusion proteins were constructed of the same mimotopes together with fluorescent or bioluminescent proteins. The recombinant fusion proteins could be expressed in bacteria and used directly as the tracer in the immunoassays. Thus, no additional labeling steps or secondary antibodies were required, which simplified the assay protocol and shortened the time needed to perform the assay. **Publications III–V** report the development of such recombinant fusion proteins for $FB_1$ and ZEA detection using a yellow fluorescent protein and bioluminescent *Gaussia* luciferase as the fusion partner and tracer. The work includes optimization and comparison of different assay concepts, including plate-based and bead-based heterogeneous immunoassays, as well as a homogeneous quenching immunoassay based on the fluorescent fusion protein and gold nanoparticles.

**Publication IV** presents a comparison of the various assays based on different mimotope-formats, including the phage-borne, synthetic, and recombinant fusion proteins. As the immunoassay performance is dependent on many factors, including the used solid phase and label, a direct comparison of the different mimotope-formats was performed by surface plasmon resonance (SPR) in order to determine how the structural context of the mimotope affects the binding kinetics.

analytical chemistry

Article

pubs.acs.org/ac

# Microarray-Based Immunoassay with Synthetic Mimotopes for the Detection of Fumonisin $B_1$

Riikka Peltomaa,[†] Elena Benito-Peña,*[,†] Rodrigo Barderas,[‡] Ursula Sauer,[§] Martin González Andrade,[∥] and María C. Moreno-Bondi*[,†]

[†]Department of Analytical Chemistry, [‡]Biochemistry and Molecular Biology I Department, Faculty of Chemistry, Universidad Complutense de Madrid, Av. Complutense s/n, 28040 Madrid, Spain

[§]Center for Health and Bioresources, AIT Austrian Institute of Technology GmbH, Konrad-Lorenz-Straße 24, 3430 Tulln, Austria

[∥]Department of Biochemistry, Faculty of Medicine, Universidad Nacional Autónoma de México, Ciudad Universitaria, Coyoacán D.F., México City 04510, México

Reproduced from: *Analytical Chemistry* **2017**, *89*, 6216–6223.


## Abstract

Mimotopes, or epitope mimics, can be applied to competitive immunoassays, for the detection of low molecular weight natural toxicants, as an alternative to toxin-conjugates. In this work, we report the development of a microarray-based immunoassay for the detection of fumonisin $B_1$ using a novel mimotope selected by phage display technology. Fumonisin-specific antibody was used to isolate mimotopes from a 12-mer peptide library in successive selection rounds. Enrichment of antibody binding phages was observed after three panning rounds, and sequence analysis of randomly selected monoclonal phages revealed two conserved peptide sequences. Clone A2, with peptide sequence VTPNDDTFDPFR, showed the best response in enzyme-linked immunosorbent assay (ELISA) in terms of sensitivity and reproducibility and was selected for microarray development. A biotinylated synthetic derivative of this mimotope was immobilized onto epoxy-glass slides, and fumonisin $B_1$ was detected in a competitive binding inhibition assay using the anti-fumonisin antibody and a labeled secondary antibody. The array showed an $IC_{50}$ value of 37.1 ± 2.4 ng $mL^{-1}$ ($n$ = 9), a detection limit of 11.1 ng $mL^{-1}$, and a dynamic range from 17.3 to 79.6 ng $mL^{-1}$. Good specificity toward fumonisin $B_1$ and its structural analog, fumonisin $B_2$, was observed, together with negligible cross-reactivity for other mycotoxins produced by the same fungi species. The mimotope microarray was applied to the analysis of fumonisin $B_1$ in spiked maize and wheat samples. The method enabled quantification of the mycotoxin at the levels set by European legislation and holds promise for future adaptation to include other mycotoxins for multiplex detection.

## 3.2.1.1 Introduction

Fumonisins are a group of mycotoxins produced as secondary metabolites by *Fusarium* species. These fungal toxins are found worldwide, mainly in maize but have also been detected for example in wheat, rice, and soybean.[1,2] Among the 15 different naturally occurring fumonisins reported so far, the most abundant and toxic one is fumonisin $B_1$ ($FB_1$). This compound has been

shown to cause a variety of toxic effects in animals and was classified as possibly carcinogenic to humans.[3] The accumulation of fumonisins in food and feedstuff may pose severe consequences on animal and human health, and several international authorities, including the European Commission, have set maximum residue limits (MRLs) for these compounds in food.[4,5] The requirement to meet these regulations has motivated the development of novel analytical methods for the identification and quantification of fumonisins in various food commodities.

Currently, analytical methods for the determination of fumonisins are based on liquid chromatography (LC) with a diode array (DAD), fluorescence (FLD), or mass spectrometric (MS) detection preceded by a sample clean-up step using solid-phase extraction or, in some cases, immunoaffinity columns.[6–9] Though these methods provide excellent accuracy and reproducibility, they show some limitations, including high cost, long analysis times, and the requirement of highly skilled personnel and time-consuming sample preparation steps, which make them unsuitable for on-site analysis or high-throughput screening. The development of screening methods based on antibodies, or aptamers, in combination with novel detection techniques, has received much research attention lately.[6] In comparison to other analytical methods for mycotoxin detection, immunoassays are particularly attractive due to their high specificity, good sensitivity, ease of manipulation, fast response times, and low cost. Thereby, their use has expanded from specialized laboratory analysis to home testing.[10,11] Polyclonal[12] and monoclonal antibodies,[13] as well as recombinant antibody fragments,[14] have been applied to the development of immunoassays for fumonisins using different detection schemes, such as enzyme-linked immunosorbent assays (ELISAs), magnetic bead-based ELISAs,[15] along with some rapid and low-cost immunochromatographic tests[16,17] or fluorescence polarization assays.[18]

Nevertheless, these approaches require conjugation of the competing toxin molecule either to a carrier protein or to a label, which can be considered as one major drawback of the competitive immunoassay format generally applied to the detection of fumonisins. Synthesis of the toxin-conjugates can be time-consuming and challenging or result in randomly cross-linked and unstable molecules which might reduce immunoassay sensitivity.[19,20] Replacement of the toxin-conjugate for an epitope mimic, or mimotope, of the target mycotoxins as coating antigens has the potential to overcome such limitations. Mimotopes mimic the structure of the epitope and bind specifically to the same antibody paratope as the analyte eliciting a similar antibody response than the native epitope.[21,22] Moreover, they can be immobilized at high density while preserving their stability and specificity,[23] and their use avoids the risks associated with the manipulation of hazardous compounds.

Phage display offers a powerful alternative to search for mimotopes, even when previous knowledge of the antibody–antigen interaction mechanisms is scarce. Several groups have developed phage-displayed mimotopes, mostly peptides or anti-idiotypic antibodies, for example, for the detection of aflatoxin,[21] deoxynivalenol,[24] ochratoxin,[25] and zearalenone,[26] as well as for fumonisins.[27,28]

The majority of the mimotope assays described so far rely on the application of phage-borne peptides. Excellent sensitivities have been reported using this approach, and the phage-displayed mimotopes appear easy to produce. However, although biologically active phages are widely used in research, there exist some safety concerns and reluctance to use these bacterial viruses for diagnostic purposes.[29,30] As an alternative, other approaches have been reported

using genetically engineered peptide-fusion proteins; for example peptide–maltose binding protein (MBP) fusions were directly used as coating reagents in ELISA.[31,32] Nonetheless, genetic engineering required for the development of such fusion proteins, as well as expression and purification of the constructs, can be challenging due to problems associated with protein misfolding or degradation occasionally observed in the expression of heterologous fusion proteins.[33]

Chemical synthesis of small peptides is a well-established and widely used method[34] and could offer a simple alternative for using the phage-displayed mimotopes or the genetically engineered peptide-fusions. In fact, some studies have shown that the synthetic peptide alone is sufficient to act as the mimotope in competitive phage-free ELISAs.[35,36] Due to their small molecular weight, chemically synthesized peptides are stable in a wide range of conditions and less prone to lose their activity. Furthermore, during their synthesis, a variety of targeted modifications can be added, including biotinylation, the introduction of specific reactive groups, or fluorescent and affinity tags.[37]

Microarrays, also known as “microspot” assays, are renowned high-throughput tools mostly used for gene expression profiling, drug discovery, and protein–protein interaction studies due to their immense capabilities related to multiplexing, high sensitivity, enhanced reproducibility, reduced analysis time, and ease of automation, but the method is also an attractive alternative for immunoassay development.[38–40] A few microarray-based methods have been reported for the detection of mycotoxins,[41,42] some of them also for fumonisin analysis.[43,44] These approaches established simultaneous detection of several mycotoxins taking advantage of the multiplexing capacity of the microarray; however, in all cases, the toxin-conjugate was used in the competitive assay.

In this work, we describe the development of a novel mimotope-based microarray for the detection of fumonisin $B_1$ and its application to the analysis of the toxin in cereal samples. The mimotope was selected from a phage-displayed peptide library, and its epitope mimicking nature was confirmed by competitive ELISA. Following functionalization with a biotin linker, the peptide was spotted in an array format on a modified glass slide and binding of anti-fumonisin monoclonal antibodies was competitively inhibited by the target mycotoxin in the sample solution. The amount of antibody bound to the patterned mimotopes was revealed using a fluorescently labeled secondary antibody. Several parameters affecting immunoassay performance have been optimized, including the concentrations of the mimotope and the fumonisin-specific antibody, as well as the assay and spotting buffers. Finally, we have demonstrated the suitability of the microarray for fumonisin $B_1$ detection in spiked maize and wheat samples. The novel screening method shows promise as the basis of further development of multiplex mycotoxin detection to fully embrace the vast potential of microarray technology.

### 3.2.1.2 Experimental section

#### Materials

Ph.D.-12 Phage Display Peptide Library Kit was purchased from New England Biolabs (Ipswich, MA, USA) and the fumonisin antibody was from BioTez (Berlin, Germany). Nunc MaxiSorp 96-well plates, Amplex UltraRed reagent, *o*-phenylenediamine dihydrochloride (OPD), and NeutrAvidin Biotin Binding Protein were purchased from Thermo Fisher Scientific (Waltham, MA, USA). Mycotoxins fumonisin $B_1$ ($FB_1$), fumonisin $B_2$ ($FB_2$), T-2 toxin, and HT-2 toxin were from Fermentek Ltd. (Jerusalem, Israel), citrinin (CIT) from Thermo Fisher Scientific, alternariol (AOH) and tenuazonic acid (TeA) from Apollo Scientific (Bredbury, UK), deoxynivalenol (DON), cyclopiazonic acid (CPA), β-zearalenol (ZEL), zearalenone (ZEN), zearalanone (ZAN), and alternariol monomethyl ether (AME), as well as bovine serum albumin (BSA), CHAPS, and Tween-20 were from Sigma-Aldrich (St. Louis, MO, USA).

The biotinylated peptide A2 (VTPNDDTFDPFRGGGSK (Bio)–$NH_2$) and a non-related peptide F11 (GYGSILPFNPVFGGGSK (Bio)–$NH_2$) were synthesized at Peptide Synthetics (Fareham, UK). The HRP-conjugated anti-M13 antibody was obtained from GE Healthcare Inc. (Chicago, IL, USA) and the Alexa Fluor 647 AffiniPure Goat Anti-Mouse IgG (H+L) from Jackson ImmunoResearch Inc. (West Grove, PA, USA). For microarray development, the chip platform was proprietary ARChip Epoxy slide developed at AIT (EP 02799374; US 10/490543). The blank wheat quality control material was purchased from Romer laboratories (Getzersdorf, Austria), and the maize sample was from Saatbau (Linz, Austria).

#### Mimotope identification by biopanning

Fumonisin epitope mimics, or mimotopes, were selected from the commercial dodecapeptide library (Ph.D.-12) by consecutive rounds of phage display selection (**Figure 14**) according to manufacturer's instructions. Briefly, 96-well microtiter plate was coated, overnight at +4 °C, with the target monoclonal antibody (1 µg of antibody in 100 µL of PBS per well). The remaining protein-binding sites in the coated wells were then blocked with 5% (w/v) BSA in PBS (pH 7.2) for 1 h at +4 °C and washed six times with PBS-T [PBS (pH 7.2); 0.1% (v/v) Tween-20]. The phage library ($1 \times 10^{11}$ pfu) was added to the coated wells (two wells were used during rounds 1 and 2, and one well during rounds 3–5, with 100 µL per well) and incubated with slow shaking for 1 h at room temperature. The wells were then washed ten times with PBS-T, and finally, the bound phages were eluted with 100 µL of 0.2 M glycine-HCl (pH 2.2) for 10 min, after which, the supernatant was collected and neutralized immediately with 10 µL of 1 M Tris-HCl (pH 9.1). The eluate was amplified by infecting *E. coli* ER2738, and the amplified phage was used for the subsequent panning rounds. After each panning round, the number of eluted and amplified phages was determined by tittering, and the number of input phages was kept constant in all rounds. After the second panning round, the concentration of Tween-20 in the washing buffer was increased from 0.1% to 0.5% (v/v) for more stringent washes. After the third, fourth and fifth selection rounds, individual plaques were picked from the LB/IPTG/X-gal plates and tested in the phage-based ELISA to select the positive clones binding to the target antibody. The amino

acid sequence of the peptide displayed by these phages was identified by sequencing using the primer –96 gIII (CCC TCA TAG TTA GCG TAA CG).

## Phage-based ELISAs

To screen for the positive clones, the phage-displayed peptides were tested in direct phage-based ELISA and the best clones, further in a competitive assay (**Figure 15A**). To that aim, microtiter well plates were coated with the capture antibody (200 ng in 60 µL of PBS) by overnight incubation at +4 °C. The wells were then blocked with blocking buffer (PBS, pH 7.2; 2% (w/v) BSA) for 1 h at +4 °C and washed four times with PBS-T (PBS, pH 7.2; 0.1% (v/v) Tween-20). For the simple phage-based ELISA, the amplified phage stock was then added to the coated wells in 1:10- or 1:100-dilution, and for the competitive assay, the monoclonal phages ($10^8$ pfu $mL^{-1}$) were incubated together with different fumonisin $B_1$ concentrations (0–5000 ng $mL^{-1}$) for 1 h. For the cross-reactivity studies, fumonisin $B_1$ was replaced with other mycotoxins at the concentration of 500 ng $mL^{-1}$. After washing the plate four times, anti-M13-HRP (1/5000-dilution in blocking buffer) was added, and the incubation was continued for 1 h. All incubation steps were done in the total volume of 60 µL with slow shaking at room temperature. Finally, the plate was washed six times as described previously, and 60 µL of the substrate solution, either OPD or Amplex UltraRed, was added to each well according to the manufacturer's instructions. The absorbance (at 495 nm) or fluorescent signals (excitation at 510 nm and detection at 590 nm) were measured using a CLARIOstar microplate reader from BMG Labtech (Ortenberg, Germany).

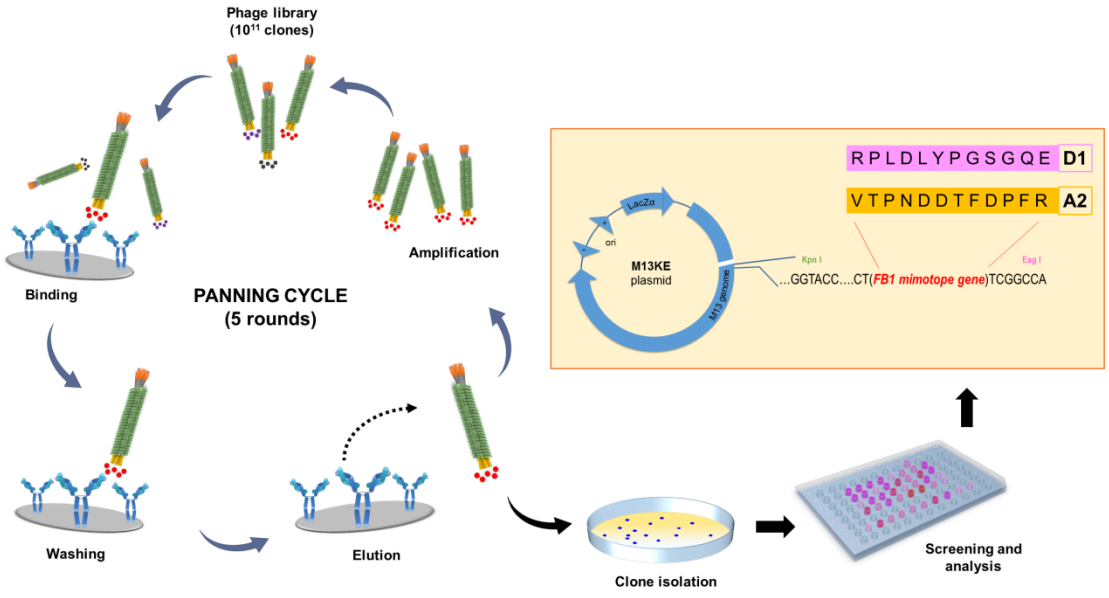


**Figure 14**. Workflow of the panning rounds carried out to isolate the antibody specific binder peptides A2 and D1.

## Microarray fabrication

The synthetic mimotope A2 was used for the development of a microarray for fumonisin $B_1$ detection. Biotinylated peptide (0.25 mg $mL^{-1}$ in printing buffer [PBS, pH 7.2; 0.005% (w/v) CHAPS; 0.01% (w/v) BSA]) was mixed with neutravidin in 1:4 molar ratio and arrayed onto ARChip Epoxy slides using Nanoprint Protein Microarrayer (Arrayit, Sunnyvale, CA, USA) equipped with SMP5 microspotting pin (Arrayit). Each probe was printed in triplicate in each array with 350 µm spot-to-spot distance, and 12 identical arrays were printed per slide. After printing, the slides were kept at +4 °C at least for 3 days to ensure complete probe immobilization, and they were blocked before use with PBS-T (PBS, pH 7.2; 0.1% (v/v) Tween-20) for 30 min in continuous stirring to remove any unbound probes. Then, the slides were washed twice in PBS and dried with compressed air.

## Mimotope assay

Mycotoxin detection was based on a competitive binding inhibition assay with the immobilized mimotope tagged with biotin (**Figure 3C**). The spiked samples, or the toxin standards in the range of 0 to 1500 ng $mL^{-1}$, were first pre-incubated with 100 ng $mL^{-1}$ fumonisin specific antibody in assay buffer (PBS, pH 7.2; 0.05% (v/v) Tween-20; 0.5% (w/v) BSA) for 30 min with slow shaking. To study the selectivity of the assay fumonisin $B_1$ was replaced with other mycotoxins produced by the same *Fusarium* species (fumonisin $B_2$, T-2 toxin, HT-2 toxin, deoxynivalenol, and zearalenone). Arrayit microarray hybridization cassette was used on the slides to form separated wells where 50 µL of the pre-incubated solution was applied in three replicates. The reaction was incubated with slow shaking for 2 h protected from light. After washing the wells twice with PBS-T, AF647-labeled anti-mouse IgG (1 µg $mL^{-1}$ in 50 µL of assay buffer) was added to each well and incubated for 1 h with slow shaking. Finally, the slides were washed three times, first with PBS-T, then PBS, and finally rinsed with MQ water, and dried with compressed air.

## Microarray imaging and data analysis

Fluorescence signals were measured with 633 nm excitation wavelength by an LS Reloaded microarray scanner from Tecan (Männedorf, Switzerland) and further analyzed with GenePix Pro 6.0 analysis software (Molecular Devices, Corp., Sunnyvale, CA, USA). The signals were background corrected, and non-valid spots, those given a flag "not found" by the image analysis software or excluded by an outlier test, were excluded. Mean values of remaining spots were used for down-stream data analysis.

For the calibrations, toxin standards at different concentrations were tested by the microarray, and the fluorescence signals were analyzed with Origin Pro 9.0 software (OriginLab Corp., Northampton, MA, USA) using a four-parameter logistic regression (4-PL) model (equation 1):

$$y = A_{min} + \frac{(A_{max} - A_{min})}{1 + \left(\frac{x}{IC_{50}}\right)^{b}} \qquad (1)$$

where $A_{max}$ is the asymptotic maximum (the signal in the absence of the analyte), $b$ and $IC_{50}$ are the slope of the curve and analyte concentration, respectively, at the inflection point, and $A_{min}$ is

the asymptotic minimum. The limit of detection (LOD) was determined as the fumonisin concentration where the antibody binding to the immobilized peptide was inhibited by 10% and the dynamic range of the method as the toxin concentration from 20% to 80% inhibition, as previously reported.[45] The cross-reactivity (CR) of the competitive assay was calculated based on the $IC_{50}$ values using the following formula (equation 2):

$$CR = \frac{IC_{50}(FB_1)}{IC_{50}(\text{other mycotoxin})} \times 100\% \qquad (2)$$

### Sample preparation

Blank maize and wheat samples were spiked with fumonisin $B_1$ and tested with the mimotope assay. The maize sample was ground with a mixer mill, and 5 g of the finely ground corn, or the blank wheat sample, was suspended in 10 mL of 60% (v/v) methanol in PBS and spiked with the toxin (200–4000 µg of $FB_1$ per kg of the maize or wheat sample). The mixtures were incubated in shaking for 30 min at room temperature, then centrifuged (4500 g, 10 min) and filtered with 0.22 µm filter to remove any insoluble material. For the assay, the extracts were diluted 1:10 in the assay buffer resulting in final methanol concentration of 6%.

## 3.2.1.3 Results and discussion

### Selection and characterization of phage-displayed mimotopes

A linear 12-mer phage display peptide library was subjected to successive rounds of selection to isolate antibody-specific binders (**Figure 14**). Efficient enrichment of antibody binding phages was observed after three rounds of panning as deduced from the increased phage titer during the panning rounds. Moreover, the signal-to-background ratios obtained with the entire phage pools in the phage-based ELISA increased after each panning round (**Figure 18A** in the supporting information). A total of 48 randomly selected phage plaques from the panning rounds 3–5 were tested to identify the individual specific binders. Altogether, 73% of the screened clones showed good signal-to-background ratios in the assays indicating specific binding to the fumonisin antibody. Sequencing of the positive clones revealed two conserved peptide sequences, VTPNDDTFDPFR and RPLDLYPGSGQE (named A2 and D1, respectively), both of which showed excellent signal-to-background ratios in the corresponding ELISAs (**Figure 18B** in the supporting information).

Three-dimensional structural models of these peptides were generated with different molecular modeling tools. Due to the lack of information on the structure of the commercial anti-fumonisin antibody paratope, we decided to simulate by molecular docking[46] the interaction of the selected mimotopes, A2 and D1, with the protein serine/threonine phosphatase-1 (PP-1c), which is known to be inhibited by fumonisin $B_1$[47] and compare the behavior of mimotopes and fumonisin $B_1$ in such interaction. The description of the molecular dynamics simulation, the three-dimensional structural models, and the protein-peptide/mycotoxin docking analysis are included in the supporting information. In good agreement with the experimental results of the phage-based ELISAs, the models suggested that A2 and D1 mimotopes are structurally and energetically similar, and moreover, their interaction with the protein is

comparable to that of fumonisin $B_1$ (**Figure 19**, **Figure 20** and **Figure 21** in the supporting information). Therefore, in principle, both A2 and D1 could be considered as excellent mycotoxin mimics for immunoassay development.

In order to confirm their functionality as fumonisin $B_1$ mimotopes, the phage-displayed peptides, A2 and D1, were further tested in competitive ELISAs (**Figure 15A**). Both clones showed inhibition by the mycotoxin with $IC_{50}$ values of 38.7 ± 5.4 ng $mL^{-1}$ and 85.8 ± 8.3 ng $mL^{-1}$ ($n$ = 3) for A2 and D1, respectively (**Figure 15B**). Furthermore, the monoclonal antibody was proven to be specific towards fumonisins $B_1$ and $B_2$ as no cross-reactivity was observed with other mycotoxins tested (T-2 toxin, HT-2 toxin, citrinin, alternariol, alternariol monomethyl ether, cyclopiazonic acid, β-zearalenol, zearalenone, zearalanone, and tenuazonic acid) (**Figure 22** in the supporting information). The clone A2 showed the best response in terms of sensitivity and reproducibility, and it was selected for microarray development.

## Assay optimization and array characterization

The phage-displayed mimotope was shown to compete against the toxin for the binding to the fumonisin-specific monoclonal antibody, but with a view to develop a robust method for fumonisin detection, we decided to replace the phage-borne peptide by its synthetic counterpart. The A2-mimotope was synthesized with C-terminal biotin which allows easy coupling of the peptide to, for example, a solid surface or a labeling molecule using the biotin–neutravidin binding interaction. The biotinylated peptide consisted of the mimotope sequence (VTPNDDTFDPFR) and a short linker (GGGS) connected to biotin that was coupled to the primary amine of the C-terminal lysine residue. The linker ensured sufficient space between the mimotope and biotin to avoid any steric hindrance for binding to the antibody. Furthermore, to mimic the structure of the phage-displayed peptide as closely as possible, the C-terminus of the synthetic peptide was amidated to avoid the free negatively charged carboxyl group that was not present in the phage during the panning selections.

The biotinylated peptides were immobilized *via* neutravidin on epoxy-slides. Preliminary experiments had shown high non-specific binding when streptavidin was selected for the coupling; however, the use of neutravidin is known to minimize non-specific adsorptions due to its neutral isoelectric point.[48, 49] Antibody binding to the immobilized biotin-mimotope was evaluated in direct binding assays at different antibody concentrations (25–2000 ng $mL^{-1}$). The binding curve (**Figure 16A**) confirmed that the synthetic peptide binds the monoclonal antibody, even in absence of the phage. Low non-specific binding of the antibody to the microarray surface was confirmed by spotting a nonrelated peptide as negative control.

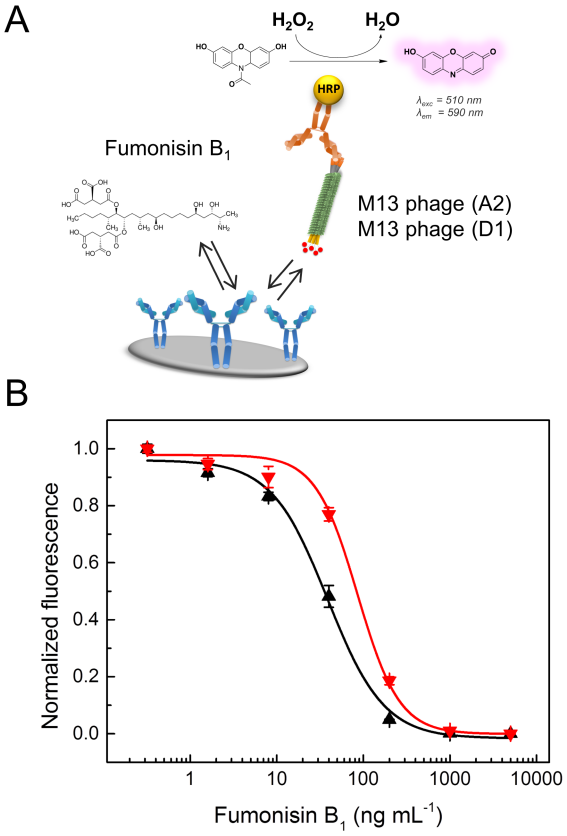


**Figure 15**. (A) Workflow of the competitive phage-based ELISA using anti-M13 conjugated to HRP with Amplex UltraRed substrate. (B) Comparison of the competitive binding curves of the phage-displayed mimotopes A2 (black) and D1 (red). The fluorescent signals were normalized to the mean maximum and minimum absolute signals and the results are shown as normalized means ± the standard error of the mean (*n* = 3). A four-parameter logistic fit (OriginPro 9.0) was used to calculate the $IC_{50}$ values.

Next, an on-chip binding inhibition assay was implemented for the detection of fumonisins $B_1$ (**Figure 16C**). After a checkerboard type of assay where different concentrations of the immobilized peptide (100–750 µg $mL^{-1}$) and neutravidin were exposed to increasing concentrations of the antibody (25–2000 ng $mL^{-1}$), 250 µg $mL^{-1}$ peptide, with a 1:4 molar ratio of neutravidin, and 100 ng $mL^{-1}$ antibody were selected as the working conditions (**Figure 23** in the supporting information). **Figure 16B** shows the competition inhibition curves obtained under the optimized conditions using fumonisin $B_1$ standard solutions in the range of 0–900 ng $mL^{-1}$. The $IC_{50}$ value and the LOD were 37.1 ± 2.4 ng $mL^{-1}$ (*n* = 9) and 11.1 ng $mL^{-1}$, respectively. The dynamic range calculated from 20–80% inhibition was between 17.3 and 79.6 ng $mL^{-1}$. Reproducibility of the microarray-based assay was demonstrated by low relative standard deviations (RSD) of 9.2% in average for intra-day (*n* = 9) and 7.6 and 10.9% for inter-day assays, on three different days, for toxin concentrations of 30 and 40 ng $mL^{1}$, respectively.

Compared to previously reported microarrays for fumonisin detection using a toxin-competitor (**Table 8** in the supporting information), the mimotope-based method showed similar[44] or superior[43] performance in terms of sensitivity and reproducibility. Although other mimotope-based assays for fumonisin $B_1$[27] have reported nearly 10-fold lower detection limits,

the microarray format benefits from the miniaturization capability of the array allowing lower reagent consumption with an automated and reproducible manner of manufacturing the array slides. For instance, the peptide ELISA based on synthetic peptide–BSA conjugate reported by Liu *et al.* (2013)[27] required almost 30 µg of the peptide-conjugate for coating just one microtiter well plate, whereas only with 5 µg of the peptide one can easily spot onto 200 slides with 12 arrays each.

The specificity of the assay was tested with different mycotoxins (**Table 6**) and, in accordance with the previous experiments with the phage-based ELISA, negligible cross-reactivity was observed with other mycotoxins produced by the same *Fusarium* species (T-2, HT-2, deoxynivalenol, and zearalenone). The monoclonal antibody was not able to distinguish fumonisin $B_1$ from its structural analog, fumonisin $B_2$, but similar $IC_{50}$ values were observed for both with no statistical difference (confidence level 95%).

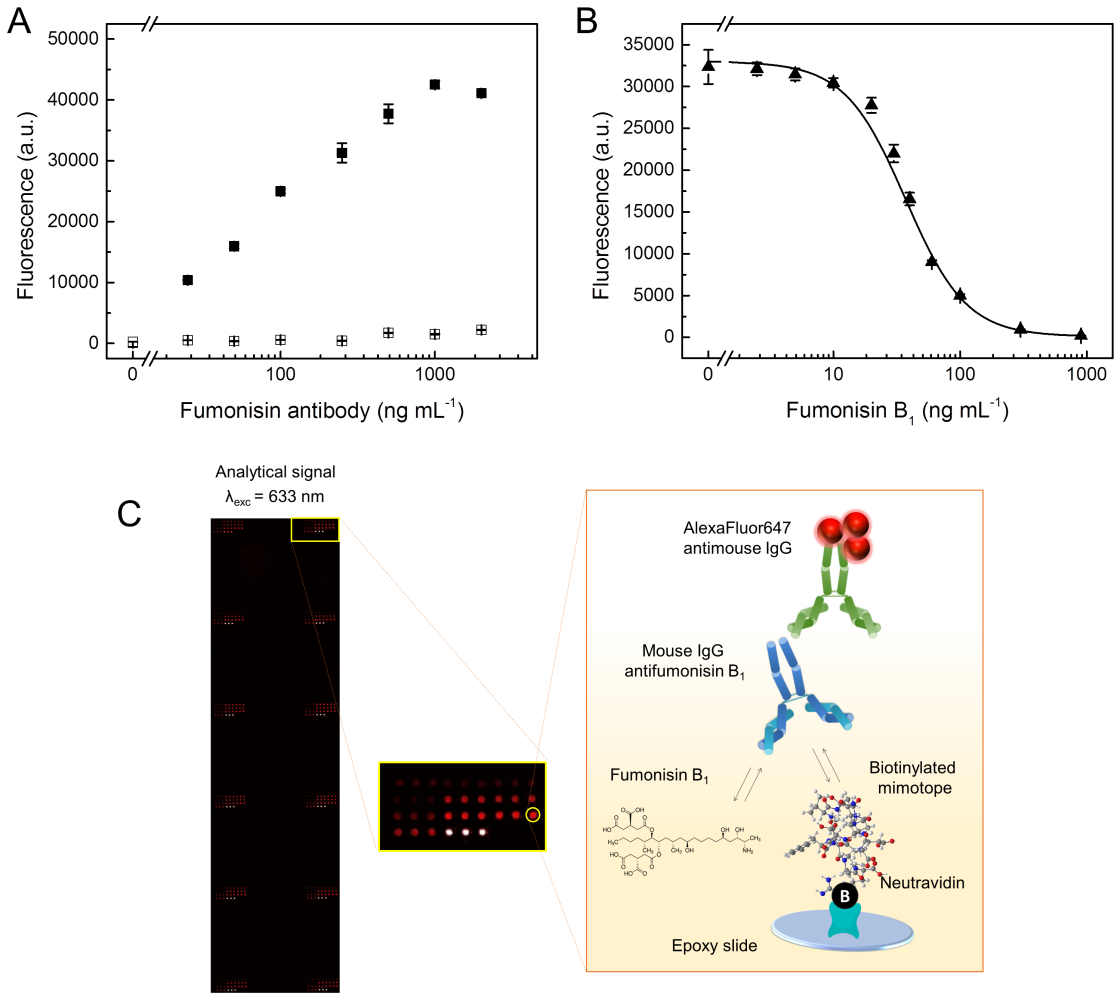


**Figure 16.** (A) Direct binding of the fumonisin antibody in different concentrations to the immobilized biotin-peptide A2 (closed symbols) and background binding to a non-related peptide F11 (open symbols). (B) Binding inhibition assay with the mimotope microarray. Results are shown as mean signals ± the standard error of the mean ($n$ = 9). A four-parameter logistic fit (OriginPro 9.0) was used to calculate the $IC_{50}$ values. (C) Schematic presentation of the microarray-based immunoassay for fumonisin detection with biotinylated mimotopes.

## Effect of methanol and sample matrix

Methanol is a commonly used solvent for mycotoxin extraction. However, high concentrations of this chemical are known to affect antibody–antigen binding, thus worsening the sensitivity of immunoassays.[50] The effect of methanol on the mimotope assay was studied by spiking the assay buffer with different methanol concentrations (**Figure 17A**). There was no significant difference between the $IC_{50}$ values obtained in the presence of 0–6% methanol; however, concentrations beyond 20% severely interfered with the assay. Moreover, antibody binding was decreased by more than half at values higher than 40%. Similar results of methanol effect on immunoassays have also been reported elsewhere.[19,31] A final concentration of 6% methanol was selected for sample analysis.

To evaluate the matrix effect, working standards for calibrations were prepared in maize or wheat blank matrix extracts, and the response was compared to that of the assay buffer. The comparison of the dose-response calibration curves obtained in these samples showed no statistically significant differences (confidence level 95%) (**Figure 17B**).

**Table 6**. Cross-reactivity with other *Fusarium* mycotoxins.

| Toxin | Chemical structure | $IC_{50}$ (ng $mL^{-1}$) | Cross-reactivity |
|---|---|---|---|
| Fumonisin $B_1$ | 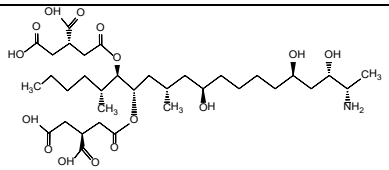 | 37.1 ± 2.4 | 100% |
| Fumonisin $B_2$ | 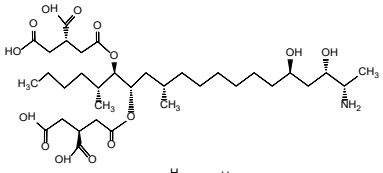 | 28.7 ± 6.4 | 120% |
| T-2 toxin | 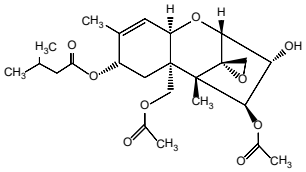 | > 1000 | < 4% |
| HT-2 toxin | 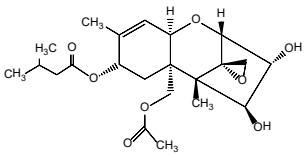 | > 1000 | < 4% |
| Deoxynivalenol | 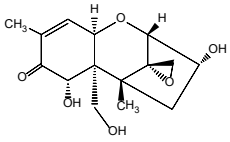 | > 1000 | < 4% |
| Zearalenone | 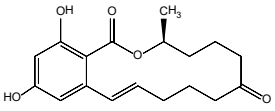 | > 1000 | < 4% |

### Sample analysis

Finally, the mimotope assay performance was evaluated with spiked samples using both maize and wheat matrices. Blank samples were spiked with the toxin standard in different concentrations, in the range of 200–2000 μg $kg^{-1}$ for maize and 600–4000 μg $kg^{-1}$ for wheat and measured using the developed microarray. The results (**Table 7**) showed mean recoveries of 73–122% in maize and 76–115% in wheat, with the corresponding coefficients of variations in the range of 5–12% and 3–10%. Thus, the method can be considered suitable for monitoring the total fumonisin concentration under the current regulatory limits of 4000 μg $kg^{-1}$ set for unprocessed maize products.[5] Wheat, which is not at the moment under the European Commission regulations, showed similar performance and could also be used as sample matrix to detect fumonisin in the selected concentration range. Further improvement of the sample analysis could possibly be achieved by optimizing the extraction procedure or using a preconcentration step to evaporate the methanol of the extract rather than diluting the sample.

**Table 7**. Analysis of spiked maize and wheat samples (*n* = 3 replicates, 3 spots/replicate).

| Matrix | Spiked $FB_1$ (μg $kg^{-1}$) | Measured $FB_1$ (μg $kg^{-1}$) | Recovery | CV |
|---|---|---|---|---|
| Maize | 200 | 244.7 | 122% | 5% |
| | 400 | 290.7 | 73% | 11% |
| | 600 | 551.3 | 92% | 9% |
| | 1000 | 814.8 | 81% | 12% |
| | 2000 | 1506.3 | 75% | 8% |
| Wheat | 600 | 548.4 | 91% | 10% |
| | 1000 | 1148.6 | 115% | 3% |
| | 2000 | 1513.7 | 76% | 10% |
| | 4000 | 3915.2 | 98% | 5% |

## 3.2.1.4 Conclusions

In this work, we reported the selection of a novel mimotope from a commercial peptide library using phage display technology, and furthermore, the development of mycotoxin microarray using the synthetic mimotope. By using the synthetic counterpart of the phage-displayed peptide, we could develop a robust method independent of the biologically active phage. The analytical characteristics, including sensitivity, specificity, and reproducibility, as well as the analysis of spiked maize and wheat samples demonstrated the suitability of the method as a tool to analyze fumonisins $B_1$ in food. The reported detection limit of the method is sufficient to meet the current regulatory limits set by the European legislation and could be further improved by optimizing the sample extraction method so as to minimize the matrix effect caused by real samples. Compared to previously reported microarrays for fumonisin detection using a toxin-competitor, the mimotope-based method showed similar or superior performance in terms of sensitivity and reproducibility. Moreover, the microarray format benefits from the miniaturization

capability of the array allowing lower reagent consumption with an automated and reproducible manner of manufacturing the array slides. Furthermore, the novel screening method presented here shows great promise as the first step for further development of multiplex mycotoxin detection tool that makes the most of the microarray technology.

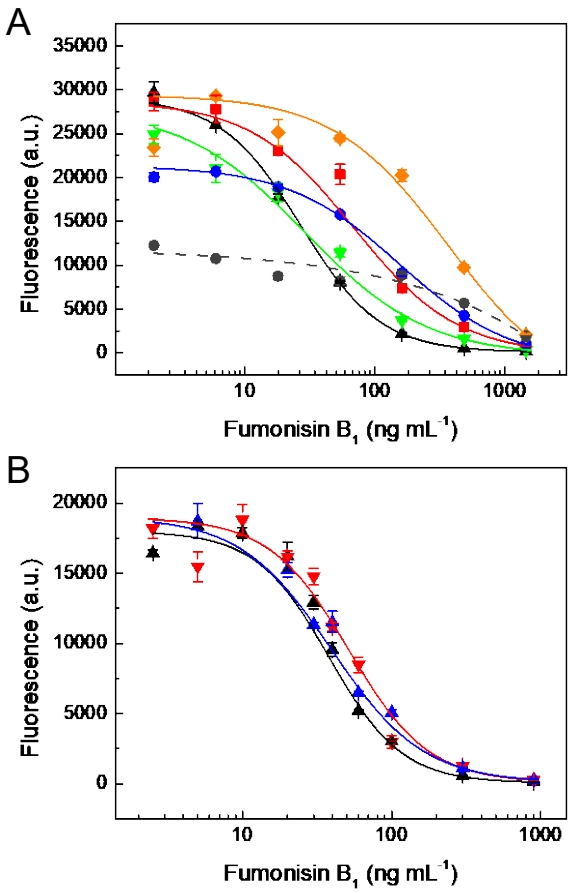


**Figure 17**. (A) Effect of methanol on the assay response. Calibration curves were repeated in 0% (black ▲); 5% (green ▼); 10% (red ■); 20% (blue ●); 30% (orange ◆); and 40% (dark grey ●) methanol concentration (v/v) in assay buffer. (B) Calibration curves in assay buffer (black ■), maize (red ▼), or wheat extract (blue ▲). Results are shown as mean signals ± the standard error of the mean (*n* = 9). A four-parameter logistic fit (OriginPro 9.0) was used to calculate the $IC_{50}$ values.

## Acknowledgments

This study was supported by the EU (SAMOSS; FP7-PEOPLE-2013-ITN; Contract 607590) and the Ministry of Economy and Competitiveness and European Regional Development Fund (CTQ2015-69278-C2-1-R MINECO/FEDER).

### 3.2.1.5 Supporting information

Supporting information includes the description of the molecular modeling tools used to create three-dimensional structural models of the peptides and fumonisin $B_1$, together with the results of the phage-based ELISA and microarray optimization. Comparison of the analytical characteristics of the developed microarray with other reported immunoassays for the detection of fumonisin $B_1$ is reported in **Table 8**.

#### Experimental part

**Molecular dynamics simulation.** Molecular dynamics (MD) simulations were performed to estimate the three-dimensional structure of both mimotopes, A2 (VTPNDDTFDPFRGGGS) and D1 (RPLDLYPGSGQEGGGS), together with a non-related peptide F11 (GYGSILPFNPVFGGGS). The MD simulations were built with the tLEaP module of AMBER14, starting from an extended conformation ($\varphi = \psi = \omega = 180°$). Subsequently, a simple structural refinement of full-atom was performed using "relax" application of Rosetta 3.2.[51,52] The coordinates of the peptides, resulting from the "relax" application, were processed with tLEaP in order to generate suitable topologies. Each peptide was subjected to the following protocol: hydrogens and other missing atoms were added using the LEaP module with the parm99 parameter set, $Na^+$ counterions were added to neutralize the system, then the structures were solvated in an octahedral box of explicit TIP3P model with water molecules localizing the box limits at a distance of 12 Å from the peptide surface. The total number of atoms in each simulated system ranged from 18196 to 25982, including the solvent molecules.

The simulations were performed at 1 atm and 298 K, maintained with the Berendsen barostat and thermostat, using periodic boundary conditions and particle mesh Ewald sums (grid spacing of 1 Å) for treating long-range electrostatic interactions with a 10 Å cutoff for computing direct interactions. The SHAKE algorithm was used to satisfy bond constraints, allowing employment of a 2 fs time step for the integration of Newton's equations as recommended in the AMBER package.[53,54] Amber ff99SB force field parameters[55,56] were used for all residues. The protocol consisted of performing an optimization of the initial structure, followed by 50 ps heating step at 298 K, 50 ps for equilibration at constant volume and 500 ps for equilibration at constant pressure. Three independent 20 ns MD simulations were performed. Frames were saved at 100 ps intervals for subsequent analysis. The analyses were conducted with cpptraj[57] on the trajectory time intervals where the convergence criteria were met. The total energy of the system (including solvation) was monitored during the simulations, and the pairwise mass-weighted root means square displacement (RMSD) on backbone CA, C and N atoms was used as a metric.

The structural model of fumonisin $B_1$ was constructed using HyperChem 8 software and subsequently minimized using Gaussian 09, revision A.02 (Gaussian Inc., Wallingford, CT) at DTF B3LYP/3-21G level of theory.

**Protein-peptide docking.** To compare the binding characteristics of fumonisin $B_1$ and the mimotopes A2 and D1 we predicted docking of these molecules to protein phosphatase-1,[58] an enzyme known to be inhibited by several toxins, including fumonisin $B_1$.[47] Docking of the toxin was constructed using the utilities implemented by AutoDockTools 1.5.4

(http://mgltools.scripps.edu/)[59,60] and docking of the peptides was performed using the CABS-dock web server which provides an interface for modeling protein-peptide interactions using a highly efficient protocol for the flexible docking of peptides to proteins.[61]

## Results and discussion

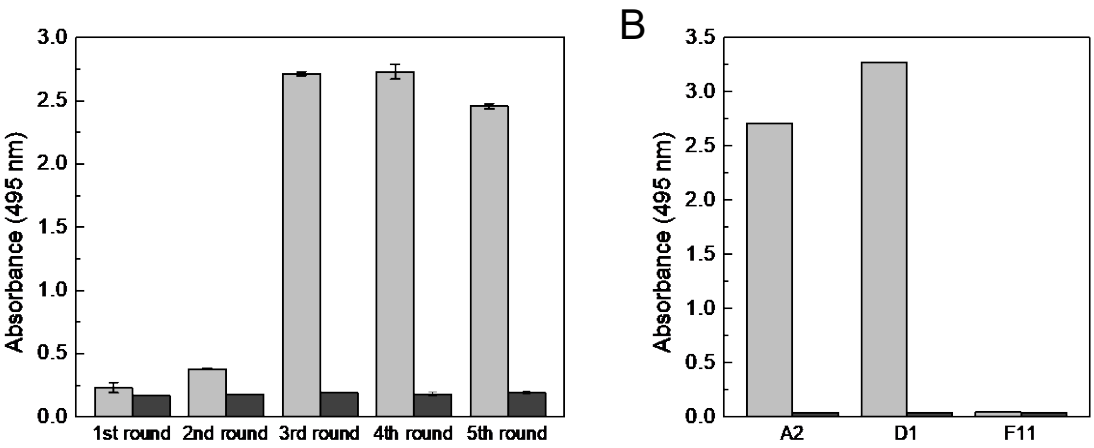


**Figure 18.** Selection of target binding phages. (A) Enrichment of target binding phage-peptides in the pannings was monitored by phage-based ELISA after five consecutive selection rounds. (B) Phage-based ELISA with monoclonal phage clones A2 and D1 showed specific binding to the target, whereas low background was observed with a non-related phage clone F11. Light grey bars present the specific binding to the target antibody and dark grey bars the background binding to the wells without the target coating.

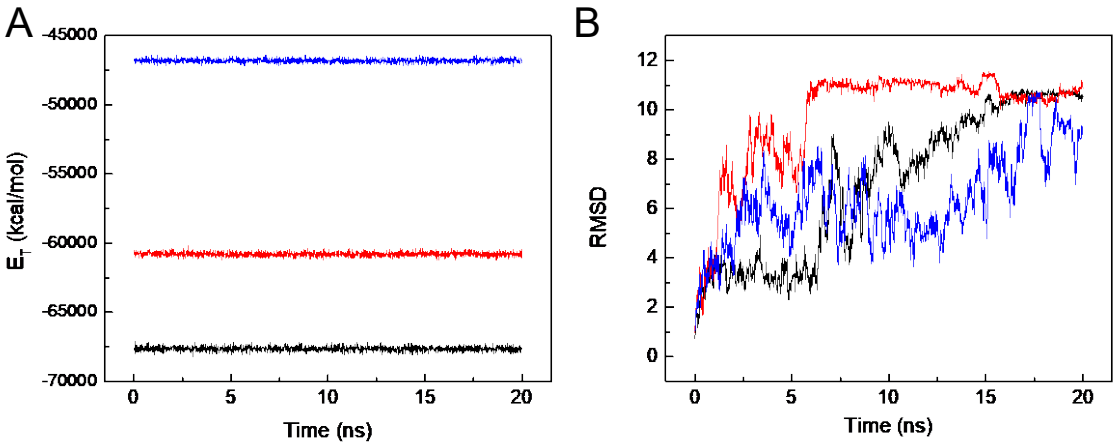


**Figure 19**. Molecular dynamics trajectory analysis. [A] Total energy ($E_T$) of the system as a function of the time of each peptide (black = A2; red = D1; blue = F11). The total energy remained stable throughout the dynamics which indicated that the prediction of the folding was stable for this time interval. Comparing the energies of the peptides we could observe the following order of structure stability: A2 > D1 > F11. [B] The root mean square displacement (RMSD) as a function of time for each peptide. This parameter indicated the convergence of peptide folding from the extended structure to its conformation adopted during the MD. Peptides D1 and A2 reached their stable conformation after 5 and 15 ns, respectively, whereas for the non-related peptide F11 it required a longer time.

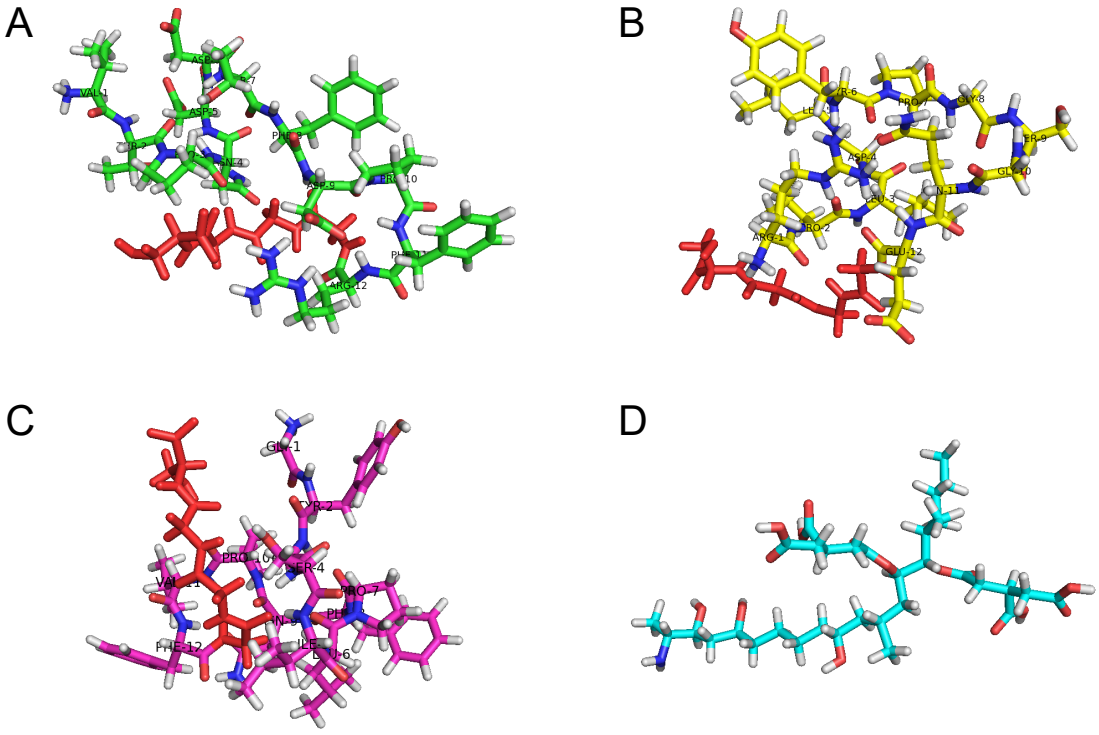


**Figure 20**. Models of mimotopes A2 (A) and D1 (B), as well as a non-related peptide F11 (C) and fumonisin $B_1$ (D). The peptides (A–C) consisted of 12 amino acids and a GGGS-linker, labelled in red in each structure. Molecular dynamics modelling indicated that peptides A2 and D1 have similar structural and energetic properties which may suggest that they also maintain similar binding or activity properties.

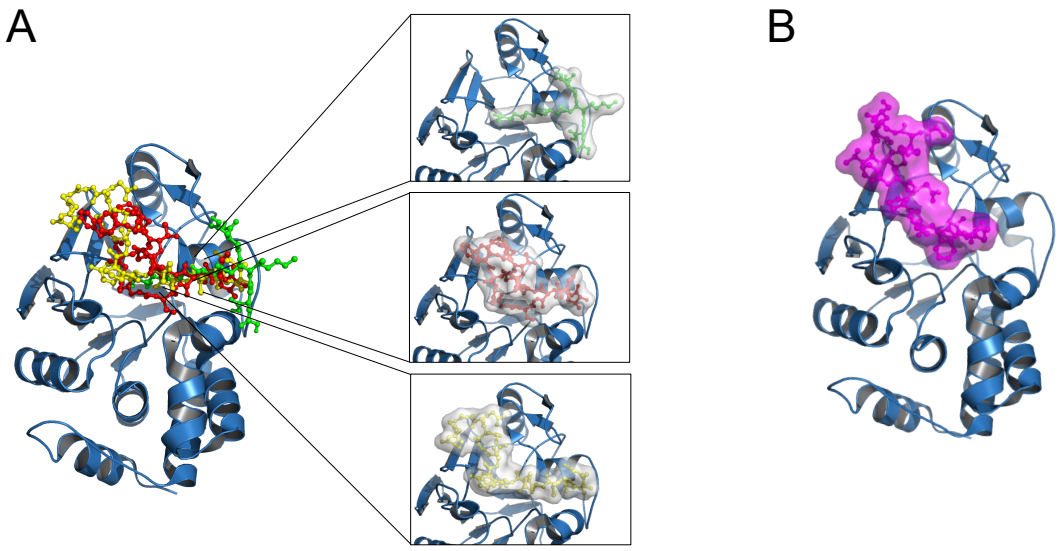


**Figure 21.** Comparison of the molecular docking of the peptides and fumonisin $B_1$ to protein phosphatase-1. (A) Docking of fumonisin $B_1$ (green sticks) to protein phosphatase-1 (PP-1c, skyblue cartoon), a well-known inhibitor of several toxins including fumonisin $B_1$.[47,58] The peptide-protein docking model predicts that the interaction of the peptides A2 (red sticks) and D1 (yellow sticks) with PP-1c takes place in the same region as for fumonisin $B_1$. (B) The non-related peptide F11 (magenta sticks) showed lower binding affinity to PP-1c as well as a different binding site.

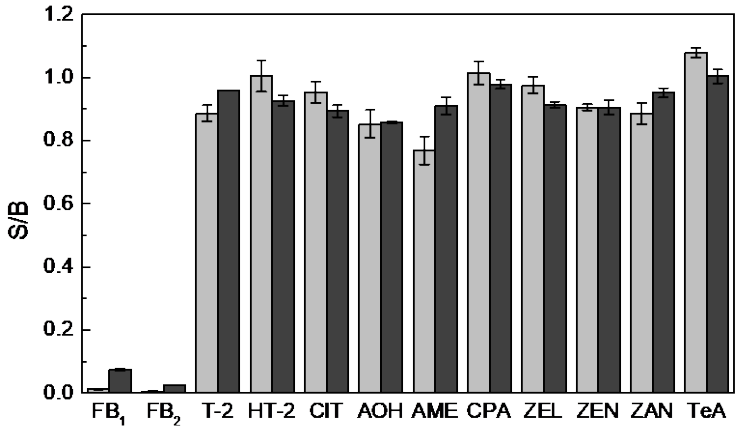


**Figure 22.** Cross-reactivity of the phage-based ELISA. Response in the competitive phage-based ELISA was studied with different mycotoxins, fumonisin $B_1$ ($FB_1$) and $B_2$ ($FB_2$), T-2 toxin, HT-2 toxin, citrinin (CIT), alternariol (AOH), alternariol monomethyl ether (AME), cyclopiazonic acid (CPA), β-zearalenol (ZEL), zearalenone (ZEN), zearalanone (ZAN), and tenuazonic acid (TeA). Only fumonisins $B_1$ and $B_2$ showed a response in the concentration of 500 ng $mL^{-1}$. Data present the signal-to-background ratios (background without any target) ± the standard error of the mean ($n$ = 3), light grey bars A2-phage and dark grey bars D1-phage.

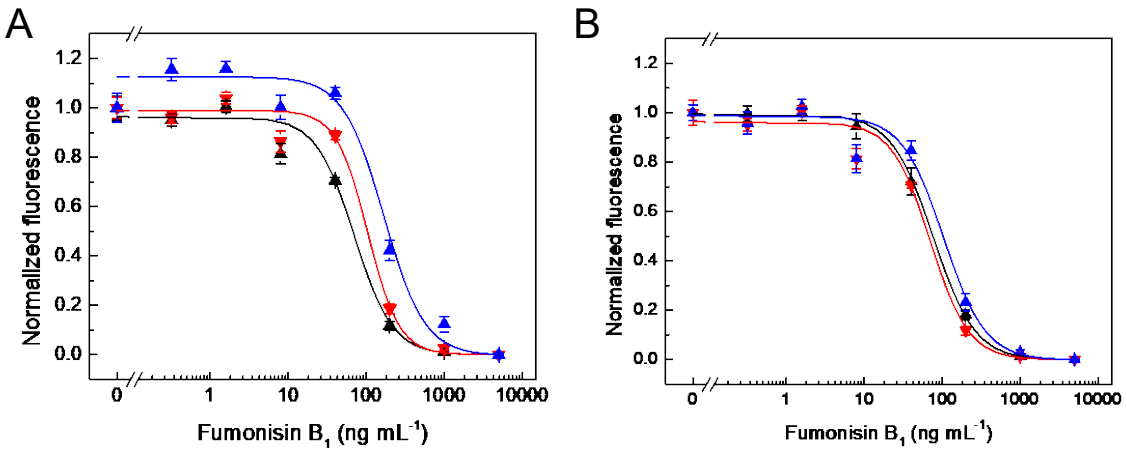


**Figure 23**. Microarray optimization. (A) Binding inhibition curves with the immobilized peptide in the concentration of 250 µg $mL^{-1}$ (black ▲), 500 µg $mL^{-1}$ (red ▼), or 750 µg $mL^{-1}$ (blue ▲). (B) Binding inhibition curves with 250 µg $mL^{-1}$ immobilized peptide with different neutravidin concentrations, 1:4-molar ratio (black ▲), 1:6-molar ratio (red ▼), or 1:8-molar ratio (blue ▲). Results are shown as normalized mean signals ± the standard error of the mean (*n* = 9). A four-parameter logistic fit (OriginPro 9.0) was used for the curve fitting.

.

Table 8. Comparison of the analytical characteristics of the developed microarray with other reported immunoassays for the detection of fumonisin $B_1$.

| Assay type | Label | Measurement | $IC_{50}$ and DR | LOD | Sample | Reference |
|---|---|---|---|---|---|---|
| ELISA with immobilized $FB_1$–OVA and recombinant scFv | HRP | Absorbance | 12.67 ng $mL^{-1}$<br>2.10–76.45 ng $mL^{-1}$ | 0.832 ng $mL^{-1}$<br>(8.32 µg $kg^{-1}$) | Spiked corn | [14] |
| Peptide-ELISA with immobilized mimotope–BSA and McAb | HRP | Absorbance | 6.06 ng $mL^{-1}$<br>1.77–20.73 ng $mL^{-1}$ | 1.18 ng $mL^{-1}$ | Maize, feedstuff, and wheat | [27] |
| ELISA on ICG-strip with immobilized $FB_1$–OVA and labelled PcAb | Golloidal gold | Visual | – | 5 ng $mL^{-1}$ | Maize, wheat, sorghum, and paddy | [16] |
| Microcantilever array with SAMs of $FB_1$-specific aptamer | – | Cantilever deflection | –<br>0.1–40 µg $mL^{-1}$ | 33 ng $mL^{-1}$ | – | [62] |
| Magnetoimmunosensor on CSPE with immobilized McAb and $FB_1$–HRP | HRP | Amperometry | 2.86 ng $mL^{-1}$<br>0.73–11.2 ng $mL^{-1}$ | 0.33 ng $mL^{-1}$ | Maize, beer | [63] |
| Multiplex suspension array immunoassay with immobilized McAb and $FB_1$–OVA–biotin | Phycoerythrin | Fluorescence | 41.5 ng $mL^{-1}$<br>11.6–110.3 ng $mL^{-1}$ | 6.0 ng $mL^{-1}$ | Spiked corn, wheat, and feedstuff | [21] |
| Multiplex homogeneous immunoassay with labelled $FB_1$ and McAb | AlexaFluor 647 | Fluorescence polarization | 1918 µg $kg^{-1}$<br>587.0–6265 µg $kg^{-1}$ | 66.3 ng $mL^{-1}$<br>(331.5 µg $kg^{-1}$) | Maize | [64] |
| Microarray-based ELISA with immobilized $FB_1$–BSA and PcAb | AP | Absorbance | –<br>– | 43 ng $mL^{-1}$ | – | [43] |
| Multiplex ELISA on reusable biochips with imobilized $FB_1$–BSA and McAb | HRP | Chemiluminescence | 644.8 µg $kg^{-1}$<br>10.5–138.5 ng $mL^{-1}$ | 9.9 ng $mL^{-1}$<br>(159.0 µg $kg^{-1}$) | Oat, wheat, rye, corn | [44] |
| Microarray-based immunoassay with covalently immobilized mimotope and McAb | AlexaFluor 647 | Fluorescence | 37.1 ng $mL^{-1}$<br>17.3–79.6 ng $mL^{-1}$ | 11.1 ng $mL^{-1}$ | Spiked maize and wheat | This work |

*Abbreviations: McAb = monoclonal antibody; scFv = single-chain fragment variable antibody; PcAb = polyclonal antibody; OVA = ovalbumin; HRP = horse-radish peroxidase; BSA = bovine serum albumin; SAM = self-assembled monolayer; CSPE = carbon screen-printed electrode; DR = dynamic range; AP = alkaline phosphatase; ICG = immunochromatographic.*

## 3.2.1.6 References


1. Bennett, J. W.; Klich, M., Mycotoxins. *Clin. Microbiol. Rev.* **2003,** *16*, 497–516.
2. Stockmann-Juvala, H.; Savolainen, K., A review of the toxic effects and mechanisms of action of fumonisin B1. *Hum. Exp. Toxicol.* **2008**, *27*, 799–809.
3. IARC, International Agency for Research on Cancer. Fumonisin $B_1$, in: *IARC monographs on the evaluation of the carcinogenic risks to humans: Some traditional herbal medicines, some mycotoxins, naphthalene and styrene*, **2002,** vol. 82. IARC, Lyon, France, pp 301–366.
4. European Commission. Commission regulation (EC) No 1881/2006. *Off. J. Eur. Union*. **2006**, *L364*: 5–24.
5. European Commission. Commission regulation (EC) No 1126/2007. *Off. J. Eur. Union*. **2007**, *L255*: 14–17.
6. Berthiller, F.; Brera, C.; Crews, C.; Iha, M. H.; Krska, R.; Lattanzio, V. M. T.; *et al.*, Developments in mycotoxin analysis: An update for 2014–2015. *World Mycotoxin J.* **2016,** *9*, 5–30.
7. Bryla, M.; Roszko, M.; Szymczyk, K.; Jedrzejczak, R.; Obiedzinski, M. W.; Sekul, J., Fumonisins in plant-origin food and fodder – A review. *Food Addit. Contam., Part A* **2013,** *30,* 1626–1640.
8. Senyuva, H. Z.; Gilbert, J.; Stroka, J., Determination of fumonisins $B_1$ and $B_2$ in corn by LC/MS with immunoaffinity column cleanup: Interlaboratory study. *J. AOAC Int.* **2010,** *93,* 611–621.
9. Solfrizzo, M. De Girolamo, A.; Gambacorta, L.; Visconti, A.; Stroka, J.; van Egmond, H. P., Determination of fumonisins $B_1$ and $B_2$ in corn-based foods for infants and young children by LC with immunoaffinity column cleanup: Interlaboratory validation study. *J. AOAC Int.* **2011,** *94*, 900–908.
10. Goryacheva, I. Y.; De Saeger, S.; Eremin, S. A.; Van Peteghem, C., Immunochemical methods for rapid mycotoxin detection: Evolution from single to multiple analyte screening: a review. *Food Addit. Contam.* **2007,** *24*, 1169–1183.
11. Köppen, R.; Koch, M.; Siegel, D.; Merkel, S.; Maul, R.; Nehls, I., Determination of mycotoxins in foods: Current state of analytical methods and limitations. *Appl. Microbiol. Biotechnol.* **2010,** *86*, 1595–1612.
12. Wang, S.; Quan, Y.; Lee, Y.; Kennedy, I. R., Rapid determination of fumonisin $B_1$ in food samples by enzyme-linked immunosorbent assay and colloidal gold immunoassay. *J. Agric. Food Chem.* **2006,** *54*, 2491–2495.
13. Yu, F.-Y.; Chu, F. S., Production and characterization of monoclonal antibodies against fumonisin $B_1$. *Food Agric. Immunol.***1999,** *11*, 297–306.
14. Zou, L.; Xu, Y.; Li, Y.; He, Q.; Chen, B.; Wang, D., Development of a single-chain variable fragment antibody-based enzyme-linked immunosorbent assay for determination of fumonisin $B_1$ in corn samples. *J. Sci. Food Agric.* **2014,** *94*, 1865–1871.
15. Wang, Y.-K.; Wang, Y.-C.; Wang, H.; Ji, W.; Sun, J; Yan, Y., An immunomagnetic-bead-based enzyme-linked immunosorbent assay for sensitive quantification of fumonisin $B_1$. *Food Control* **2014,** *40*, 41–45.
16. Venkataramana, M.; Navya, K.; Chandranayaka, S.; Priyanka, S. R.; Murali, H. S.; Batra, H. V., Development and validation of an immunochromatographic assay for rapid detection of fumonisin $B_1$ from cereal samples. *J. Food Sci. Technol.* **2014,** *51*, 1920–1928.
17. Wang, X. C.; Fan, H. X.; Fan, M. X.; Li, F. H.; Feng, S. B.; Li, J. C.; *et al.*, A sensitive immunochromatographic assay using colloidal gold-antibody probe for rapid detection of fumonisin $B_1$ in corn. *Food Addit. Contam., Part A* **2016,** *33*, 1435–1443.
18. Maragos, C. M.; Jolley, M. E.; Plattner, R. D.; Nasir, M. S., Fluorescence polarization as a means for determination of fumonisins in maize. *J. Agric. Food Chem.* **2001,** *49*, 596–602.
19. Shu, M.; Xu, Y.; Liu, X.; Li, Y.; He, Q.; Tu, Z.; Fu, J.; Gee, S. J.; Hammock, B. D., Anti-idiotypic nanobody-alkaline phosphatase fusion proteins: Development of a one-step competitive enzyme immunoassay for fumonisin $B_1$ detection in cereal. *Anal. Chim. Acta* **2016,** *924*, 53–59.
20. Xiao, H.; Clarke, J. R.; Marquardt, R. R.; Frohlich, A. A., Improved methods for conjugating selected mycotoxins to carrier proteins and dextran for immunoassays. *J. Agric. Food Chem.* **1995,** *43*, 2092–2097.

21. Wang, Y.; Li, P.; Majkova, Z.; Bever, C. R.; Kim, H. J.; Zhang, Q.; Dechant, J. E.; Gee, S. J.; Hammock, B. D., Isolation of alpaca anti-idiotypic heavy-chain single-domain antibody for the aflatoxin immunoassay. *Anal. Chem.* **2013,** *85*, 8298–8303.
22. Wu, C.-H.; Liu, I.-J.; Lu, R.-M.; Wu, H.-C., Advancement and applications of peptide phage display technology in biomedical science. *J. Biomed. Sci.* **2016,** *23*.
23. Frisk, M. L.; Tepp, W. H.; Johnson, E. A.; Beebe, D. J., Self-assembled peptide monolayers as a toxin sensing mechanism within arrayed microchannels. *Anal. Chem.* **2009,** *81*, 2760–2767.
24. Yuan, Q.; Pestka, J. J.; Hespenheide, B. M.; Kuhn, L. A.; Linz, J. E.; Hart, L. P., Identification of mimotope peptides which bind to the mycotoxin deoxynivalenol-specific monoclonal antibody. *Appl. Environ. Microbiol.* **1999,** *65*, 3279–3286.
25. He, Z. Y.; He, Q. H.; Xu, Y.; Li, Y. P.; Liu, X.; Chen, B.; Lei, D.; Sun, C. H., Ochratoxin A mimotope from second-generation peptide library and its application in immunoassay. *Anal. Chem.* **2013,** *85*, 10304–10311.
26. He, Q.-h.; Xu, Y.; Zhang, C.-z.; Li, Y.-p.; Huang, Z.-b., Phage-borne peptidomimetics as immunochemical reagent in dot-immunoassay for mycotoxin zearalenone. *Food Control* **2014,** *39*, 56–61.
27. Liu, X.; Xu, Y.; He, Q. H.; He, Z. Y.; Xiong, Z. P., Application of mimotope peptides of fumonisin $B_1$ in peptide ELISA. *J. Agric. Food Chem.* **2013,** *61,* 4765–4770.
28. Shu, M.; Xu, Y.; Wang, D.; Liu, X.; Li, Y.; He, Q.; Tu, Z.; Qiu, Y.; Ji, Y.; Wang, X., Anti-idiotypic nanobody: A strategy for development of sensitive and green immunoassay for fumonisin $B_1$. *Talanta* **2015,** *143*, 388–393.
29. Peltomaa, R.; López-Perolio, I.; Benito-Peña, E.; Barderas, R.; Moreno-Bondi, M. C., Application of bacteriophages in sensor development. *Anal. Bioanal. Chem.* **2016,** *408*, 1805–1828.
30. Smartt, A. E.; Ripp, S., Bacteriophage reporter technology for sensing and detecting microbial targets. *Anal. Bioanal. Chem.* **2011,** *400*, 991–1007.
31. Xu, Y.; Chen, B.; He, Q. H.; Qiu, Y. L.; Liu, X.; He, Z. Y.; Xiong, Z. P., New approach for development of sensitive and environmentally friendly immunoassay for mycotoxin fumonisin $B_1$ based on using peptide-MBP fusion protein as substitute for coating antigen. *Anal. Chem.* **2014,** *86*, 8433–8440.
32. Xu, Y.; He, Z.; He, Q.; Qiu, Y.; Chen, B.; Chen, J.; Liu, X., Use of cloneable peptide-MBP fusion protein as a mimetic coating antigen in the standardized immunoassay for mycotoxin ochratoxin A. *J. Agric. Food Chem.* **2014,** *62*, 8830–8836.
33. Baneyx, F.; Mujacic, M., Recombinant protein folding and misfolding in *Escherichia coli*. *Nat. Biotechnol.* **2004,** *22,* 1399–1408.
34. Stawikowski, M.; Fields, G. B. In *Current protocols in protein science*; Wiley: New York, **2012**; Chapter 18, Unit 18.11.
35. Liu, R.; Yu, Z.; He, Q.; Xu, Y., An immunoassay for ochratoxin A without the mycotoxin. *Food Control* **2007,** *18*, 872–877.
36. Zou, X.; Chen, C.; Huang, X.; Chen, X.; Wang, L.; Xiong, Y., Phage-free peptide ELISA for ochratoxin A detection based on biotinylated mimotope as a competing antigen. *Talanta* **2016,** *146*, 394–400.
37. Bazin, I.; Tria, S. A.; Hayat, A.; Marty, J. L., New biorecognition molecules in biosensors for the detection of toxins. *Biosens. Bioelectron.* **2017,** *87*, 285–298.
38. *The Immunoassay handbook: Theory and applications of ligand* binding ELISA and related techniques, 4th ed.; Wild, D., (Editor); Elsevier Science, Oxford, UK, **2013.**
39. Wilson, D. S.; Nock, S., Recent developments in protein microarray technology. *Angew. Chem. Int. Ed. Engl.* **2003,** *42*, 494-500.
40. Zhang, Z.; Li, P.; Hu, X.; Zhang, Q.; Ding, X.; Zhang, W., Microarray technology for major chemical contaminants analysis in food: Current status and prospects. *Sensors* **2012,** *12*, 9234–9252.
41. Hu, W.; Li, X.; He, G.; Zhang, Z.; Zheng, X.; Li, P.; Li, C. M., Sensitive competitive immunoassay of multiple mycotoxins with non-fouling antigen microarray. *Biosens. Bioelectron.* **2013,** *50*, 338–344.
42. Wang, Y.; Liu, N.; Ning, B.; Liu, M.; Lv, Z.; Sun, Z.; Peng, Y.; Chen, C.; Li, J.; Gao, Z., Simultaneous and rapid detection of six different mycotoxins using an immunochip. *Biosens. Bioelectron.* **2012,** *34*, 44–50.
43. Lamberti, I.; Tanzarella, C.; Solinas, I.; Padula, C.; Mosiello, L., An antibody-based microarray assay for the simultaneous detection of aflatoxin $B_1$ and fumonisin $B_1$. *Mycotoxin Res.* **2009,** *25*, 193–200.
44. Oswald, S.; Karsunke, X. Y.; Dietrich, R.; Martlbauer, E.; Niessner, R.; Knopp, D., Automated regenerable microarray-based immunoassay for rapid parallel quantification of mycotoxins in cereals. *Anal. Bioanal. Chem.* **2013,** *405*, 6405–6415.

45. Herranz, S.; Marazuela, M. D.; Moreno-Bondi, M. C., Automated portable array biosensor for multisample microcystin analysis in freshwater samples. *Biosens. Bioelectron.* **2012,** *33*, 50–55.
46. *Optimization in computational chemistry and molecular biology local and global approaches*. Floudas, C. A.; Pardalos, P.M. (Editors) Springer: New York, USA, **2000**.
47. Fukuda, H., Shima, H., Vesonder, R.F., Tokuda, H., Nishino, H., Katoh, S., Tamura, S., Sugimura, T., Nagao M., Inhibition of protein serine threonine phosphatases by fumonisin $B_1$, a mycotoxin. *Biochem. Biophys. Res. Comm.* **1996,** *220*, 160–165.
48. Cho, E. J.; Collett, J. R.; Szafranska, A. E.; Ellington, A. D., Optimization of aptamer microarray technology for multiple protein targets. *Anal. Chim. Acta* **2006,** *564*, 82–90.
49. Xu, Q.; Lam, K. S., Protein and Chemical Microarrays-Powerful Tools for Proteomics. *J. Biomed. Biotechnol.* **2003,** *2003*, 257–266.
50. Lippolis, V.; Pascale, M.; Valenzano, S.; Pluchinotta, V.; Baumgartner, S.; Krska, R.; Visconti, A., A rapid fluorescence polarization immunoassay for the determination of T-2 and HT-2 toxins in wheat. *Anal. Bioanal. Chem.* **2011,** *401*, 2561–2571.
51. Leaver-Fay, A.; Tyka, M.; Lewis, S.M.; Lange, O.F.; Thompson, J.; Jacak, R.; *et al.*, ROSETTA3: an object-oriented software suite for the simulation and design of macromolecules. *Methods Enzymol.* **2011.,** *487*, 545–574.
52. Rohl, C. A., Strauss, C.E., Misura, K.M., Baker, D., Protein structure prediction using Rosetta. *Methods Enzymol.* **2004,** *383*, 66–93.
53. Case, D.A.; Darden, T.A.; Cheatham, T.E. III; Simmerling, C.L.; Wang, J.; Duke, R.E.; *et al.*, **2012**. AMBER 12, University of California, San Francisco, USA.
54. Walker, R. C.; Crowley, M.F.; Case, D.A., The implementation of a fast and accurate QM/MM potential method in Amber. *J. Comput. Chem.* **2008,** *29*, 1019–1031.
55. Case, D. A.; Cheatham, T.E. III; Darden, T.; Gohlke, H.; Luo, R.; Merz, K.M. Jr.; Onufriev, A., Simmerling, C., Wang, B., Woods, R.J., The Amber biomolecular simulation programs. *J. Comput. Chem.* **2005.,** *26*, 1668–1688.
56. Lindorff-Larsen, K.; Piana, S.; Palmo, K.; Maragakis, P.; Klepeis, J.L.; Dror, R.O.; Shaw, D.E., Improved side-chain torsion potentials for the Amber ff99SB protein force field. *Proteins* **2010,** *78*, 1950–1958.
57. Roe, D. R. C., T. E., 3rd, PTRAJ and CPPTRAJ: Software for orocessing and analysis of molecular dynamics trajectory data. t *J. Chem. Theory Comput.* **2013,** *9*, 3084–3095.
58. Maynes, J. T.; Luu, H. A.; Cherney, M. M.; Andersen, R. J.; Williams, D.; Holmes, C. F.; James, M. N., Crystal structures of protein phosphatase-1 bound to motuporin and dihydromicrocystin-LA: Elucidation of the mechanism of enzyme inhibition by cyanobacterial toxins. *J. Mol. Biol.* **2006,** *356*, 111–120.
59. Huey, R.; Morris, G.M.; Olson, A.J., Goodsell, D.S., A semiempirical free energy force field with charge-based desolvation. *J. Comput. Chem.* **2007**, 1145–1152.
60. Morris, G. M.; Goodsell, D.S.; Halliday, R.S.; Huey, R.; Hart, W.E.; Belew, R.K.; Olson, A.J., Automated docking using a Lamarckian genetic algorithm and an empirical binding free energy function. *J. Comput. Chem.* **1998,** *19*, 1639–1662.
61. Kurcinski, M.; Jamroz, M.; Blaszczyk, M.; Kolinski, A.; Kmiecik, S., CABS-dock web server for the flexible docking of peptides to proteins without prior knowledge of the binding site. *Nucleic Acids Res.* **2015,** *43*, W419–W424.
62. Chen, X.; Bai, X.; Liac, H.; Zhang, B., Aptamer-based microcantilever array biosensor for detection of fumonisin $B_1$. *RSC Adv.* **2015,** *5*, 35448–35452.
63. Jodra, A.; López, M.A.; Escarpa, A., Disposable and reliable electrochemical magnetoimmunosensor for Fumonisins simplified determination in maize-based foodstuffs. *Biosens. Bioelectron.* **2015,** *64*, 633–638.
64. Li, C.; Wen, K.; Mi, T.; Zhang, X.; Zhang, H.; Zhang, S.; Shen, J.; Wang, Z., A universal multi-wavelength fluorescence polarization immunoassay for multiplexed detection of mycotoxins in maize. *Biosens. Bioelectron.* **2016,** *79*, 258–265.

ACS NANO Cite This: ACS Nano 2018, 12, 11333−11342 www.acsnano.org

ARTICLE

# Homogeneous Quenching Immunoassay for Fumonisin $B_1$ Based on Gold Nanoparticles and an Epitope-Mimicking Yellow Fluorescent Protein

Riikka Peltomaa,[†] Francisco Amaro-Torres,[‡] Sergio Carrasco,[†,⊥] Guillermo Orellana,[‡] Elena Benito-Peña,[*,†] and María C. Moreno-Bondi[*,†]

Reproduced from: *ACS Nano* **2018**, *12*, 11333−11342.


## Abstract

Homogeneous immunoassays represent an attractive alternative to traditional heterogeneous assays due to their simplicity, sensitivity, and speed. On the basis of a previously identified epitope-mimicking peptide, or mimotope, we developed a homogeneous fluorescence quenching immunoassay based on gold nanoparticles (AuNPs) and a recombinant epitope-mimicking fusion protein for the detection of mycotoxin fumonisin $B_1$ ($FB_1$). The fumonisin mimotope was cloned as a fusion protein with a yellow fluorescent protein that could be used directly as the tracer for $FB_1$ detection without the need of labeling or a secondary antibody. Furthermore, owing to the fluorescence quenching ability of AuNPs, a homogeneous immunoassay could be performed in a single step without washing steps to separate the unbound tracer. The homogeneous quenching assay showed negligible matrix effects in 5% wheat extract and high sensitivity for $FB_1$ detection, with a dynamic range from 7.3 to 22.6 ng $mL^{-1}$, a detection limit of 1.1 ng $mL^{-1}$, and $IC_{50}$ value of 12.9 ng $mL^{-1}$, which was significantly lower than the $IC_{50}$ value of the previously reported assay using the synthetic counterpart of the same mimotope in a microarray format. The homogeneous assay was demonstrated to be specific for fumonisins $B_1$ and $B_2$, as no significant cross-reactivity with other mycotoxins was observed, and acceptable recoveries (86% for $FB_1$ 2000 μg $kg^{-1}$ and 103% for $FB_1$ 4000 μg $kg^{-1}$), with relative standard deviation less than 6.5%, were reported from spiked wheat samples, proving that the method could provide a valuable tool for simple analysis of mycotoxin-contaminated food samples.

## 3.2.2.1 Introduction

Owing to their exceptional optical properties, nanomaterials are often considered ideal for biosensor development, and the vast progress in the field during the last decades has enabled development of ultrasensitive sensors.[1−4] Especially gold nanoparticles (AuNPs) have received particular attention due to their optical and electronic properties. Considering their

straightforward synthesis, high stability and biocompatibility, high electron density, and strong absorption in the visible region, AuNPs continue to be one of the most used materials for different sensing schemes.[5] The latter includes electrochemical,[6] surface-enhanced Raman scattering (SERS),[7] fluorescent,[8] and colorimetric assays, as well as other disciplines, such as material sciences, bioimaging, and electronics.[1,9,10] Furthermore, AuNPs are exceptionally efficient fluorescence quenchers,[11,12] a phenomenon that has been ascribed to various mechanisms, including Förster resonance energy transfer (FRET), nanometal surface energy transfer (NSET),[13,14] and dipole-to-metal particle energy transfer (DMPET).[15,16] Because of the high molar absorption coefficient of AuNPs compared to organic dyes and fluorescent proteins, broad energy bandwidth, as well as their tunable absorbance according to the nanoparticle size and geometry,[5] AuNPs have been applied as quenchers in fluorescent homogeneous assays[12] based on organic dyes,[17] polymers,[18] quantum dots,[16,19] as well as fluorescent proteins (FPs).[20]

FPs, which are widely used as markers for gene expression analysis or protein tracking within cells or organelles, and have revolutionized molecular biology in the last decades, are able to emit strong, stable fluorescence, and they can be expressed as fusion proteins in recombinant hosts.[21,22] Several FPs with enhanced fluorescence or different spectral characteristics have proven not only their excellence for studying biomolecular interactions but have also further expanded the scope of applications of these proteins, for example, for immunoassay development.[23–25] Particularly, FRET-based FP probes have been established as an important tool for studying various intracellular molecules and events,[23] demonstrating the tremendous potential of homogeneous sensing schemes for both *in vivo* and *in vitro* assays, where the bound and free tracers can be distinguished without the need of a separation step. Such homogeneous assay formats can result in significant cost and time savings by enabling simpler and faster protocols while, at least theoretically, being more sensitive than the heterogeneous assays.[12,26]

The exceptional ability of epitope-mimicking peptides, or mimotopes, to imitate the epitope of an antigen and thus bind to same antibody paratope, has been witnessed in several fields including immunotherapy, epitope mapping, and allergy treatment.[27,28] Furthermore, epitope-mimicking peptides and antibodies are an intriguing option to overcome some of the limitations of competitive immunoassays.[29,30] As they bind to the same antibody paratope as the antigen and elicit a similar antibody response, epitope mimics can be used as the competitor instead of the labeled antigen in applications where the conjugation of the target to a carrier molecule is challenging, or it can cause toxicity to the user. Several mimotopes have been selected from phage-displayed peptide libraries for the detection of low molecular weight targets such as pesticides,[31] neurotoxins,[32] cancer drugs,[33] mycotoxins,[34–36] and other chemicals.[37] Phage-borne peptides have shown great potential for the development of small-molecule immunoassays, but considering the large size and the biologically active nature of phages these methods are not always ideal for immunoassay development.[38,39] As an alternative, the synthetic counterparts of the phage-borne mimotopes[40–42] or recombinant peptide–protein fusions[43–45] have been suggested as phage-free options. Production of recombinant fusion proteins is an attractive alternative because of the low cost of producing recombinant proteins in bacteria and the variety of possibilities to design the protein tailored to the purpose, for example, including tags for purification or using an active enzyme as a fusion protein and later directly as the tracer.[46]

In this work, we present a simple and rapid immunoassay for fumonisin detection based on a recombinant fluorescent fusion protein and fluorescence quenching by AuNPs. Fumonisins are mycotoxins produced by *Fusarium* fungi as secondary metabolites[47] that can be found as natural contaminants commonly in maize but also in wheat, rice, sorghum, and beans.[48] Owing to the hepatotoxic and carcinogenic effects of fumonisins,[49] as well as the important economic consequences of mycotoxin contamination,[50] detection of these toxins is of great importance. Several international authorities, such as the European Commission[51,52] and the United States Food and Drug Administration,[53] have set regulatory limits to ensure food safety. Although maize is currently the only foodstuff that falls under international regulations, other cereals are also commonly affected by mycotoxin contamination. For instance, wheat may be an important contributor to the exposure to fumonisins in areas where this cereal is an important source of food, and less maize is consumed.[54,55] A recent study showed that the prevalence of fumonisins is very similar in stored wheat and stored maize,[56] underlining the importance of fumonisin analysis not only in maize-products but also in other foodstuffs. Chromatographic methods for mycotoxin detection, mostly high-performance liquid chromatography (HPLC) coupled with diode array, fluorescence, or mass spectrometry detection, can offer high sensitivity but are usually expensive and require highly skilled personnel and tedious sample cleanup. In contrast, biosensors and bioanalytical assays are considered convenient for the rapid determination of these toxins, as they are usually low cost while maintaining the required sensitivity and specificity.[57,58] In a previous paper, we reported the development of a microarray for the detection of fumonisin $B_1$ ($FB_1$), the most abundant and toxic of fumonisins, based on a synthetic mimotope.[40] Here, the $FB_1$-mimotope is produced recombinantly as a fusion with a yellow fluorescent protein (YFP), which, at the same time, functions as the tracer in the immunoassay. On the basis of a competitive immunoassay, the YFP-tagged $FB_1$-mimotope is used as the tracer in a heterogeneous reference assay with immobilized antibody and, furthermore, in a homogeneous quenching assay, where the binding event is observed as fluorescence quenching by AuNPs.

## 3.2.2.2 Results and discussion

Detection of low molecular weight analytes, such as mycotoxins, poses challenges for researchers, as direct detection of these molecules is difficult, and the conjugation or labeling needed for the competitive assay format is often challenging. Epitope mimics, which can replace the target conjugate and avoid the use of toxic compounds as assay[30] by creating a recombinant fusion protein of the same $FB_1$-mimotope and a YFP. Construction of such fluorescently tagged mimotope, which can be produced recombinantly in bacteria, allows developing simple immunoassays as neither labeling of the mimotope itself nor secondary antibodies are required. Furthermore, we report the application of the YFP-tagged mimotope to a homogeneous quenching immunoassay that employs AuNPs and enables detection and quantification of $FB_1$ in a simple, fast, one-step assay.

### Construction of the YFP-tagged mimotope

The YFP-tagged $FB_1$ mimopeptide was generated by cloning the $FB_1$-mimotope VTPNDDTFDPFR (named A2)[40] in fusion with *Zoanthus sp*. yellow fluorescent protein (YFP), *ZsYellow*,[59,60] using

standard molecular biology techniques.[61] In the mimotope-YFP fusion construct (**Figure 24**), the yellow fluorescent protein and A2-mimotope were separated by a glycine-serine (GS)-linker to ensure sufficient space for the mimotope binding, and a polyhistidine tag (His-tag) down-stream of YFP was used to purify the protein by affinity chromatography. To remove the His-tag after purification, a Tobacco Etch Virus (TEV) protease cleavage site was included between the YFP and the His-tag. Successful cleavage was confirmed because the fusion protein no longer bound to the nickel-nitrilotriacetic acid (Ni-NTA) matrix after the TEV-catalyzed reaction. The fluorescent excitation and emission spectra of the purified fluorescent fusion protein is shown in **Figure 30** in the supporting information.

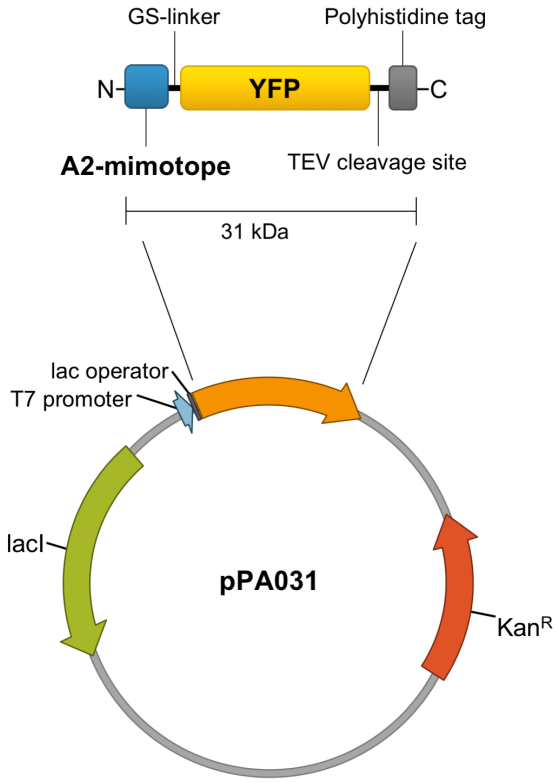


**Figure 24**. Scheme of the fusion protein construct and main features of the expression vector used for protein production in *E. coli.*

## Heterogeneous fluorescence immunoassay

The epitope-mimicking nature of the YFP fusion protein and its functionality as a tracer was studied in a heterogeneous fluorescence immunoassay, where an anti-$FB_1$ antibody is immobilized in microtiter wells, and competition between $FB_1$ and the mimotope-YFP is shown as low fluorescence readings in the presence of high $FB_1$ concentrations (**Figure 25A**). On the basis of the typical sigmoidal standard curve for a competitive heterogeneous assay[26] (**Figure 25B**) the half-maximal inhibitory concentration ($IC_{50}$) was 6.8 ± 0.3 ng $mL^{-1}$, and the lower limit of detection (LOD), determined as the average signal of the blank minus 3 times the standard deviation of the blank, turned out to be 3.5 ng $mL^{-1}$. The dynamic range of the assay, calculated from the $IC_{20}$ and $IC_{80}$ values (**Figure 25B**), was from 3.2 to 14.8 ng $mL^{-1}$. Although

the assay sensitivity was higher than those of the phage-based and synthetic peptide assays,[40] and the assay protocol was simplified because no secondary antibody was needed, the heterogeneous assay still required a few washing steps to remove the unbound reagents and overnight incubation to immobilize the capture antibody.

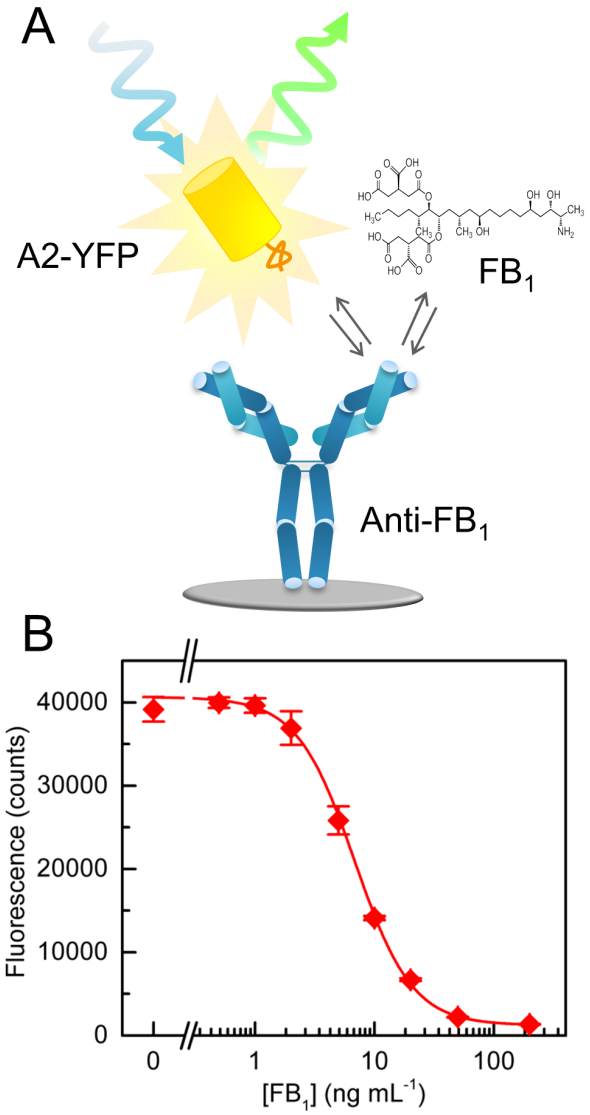


**Figure 25**. (A) Schematic representation of the heterogeneous fluorescence immunoassay using the mimotope-YFP construct and an immobilized anti-$FB_1$ antibody. (B) Dose–response curve of the competitive heterogeneous assay. Fluorescence readings (excitation at 500 nm, emission at 545 nm) are depicted as the average of the replicate samples ± the standard error of the mean ($n$ = 3). A four-parameter logistic fit (OriginPro 9.0) was used to calculate the IC values.

## Homogeneous quenching immunoassay

The recognition principle of the homogeneous assay is based on fluorescence quenching of the mimotope-YFP construct. As shown in **Figure 26**, the assay uses protein G -coated AuNPs that quench the emission of light upon antibody binding to mimotope-YFP. In the presence of the

target $FB_1$, competition between the latter and the mimotope prevents the fusion protein binding to the antibody, and fluorescence is recovered due to the larger distance from the AuNPs. Thus, the one-step assay allows distinguishing the antibody-bound tracer (mimotope-YFP) readily from the free tracer. In addition to the fast and straightforward protocol, which consist of only mixing the reagents and 20 min of incubation, the method benefits from the advantage of measuring a signal rise with increasing analyte concentrations in opposition to the heterogeneous reference assay. The low background signal in the absence of the target, due to the strongly quenched fluorescence, makes it easier to detect even small changes in the readout, as generally, it is considered better to measure a large signal against low background than to measure the difference between two large signals.[26]

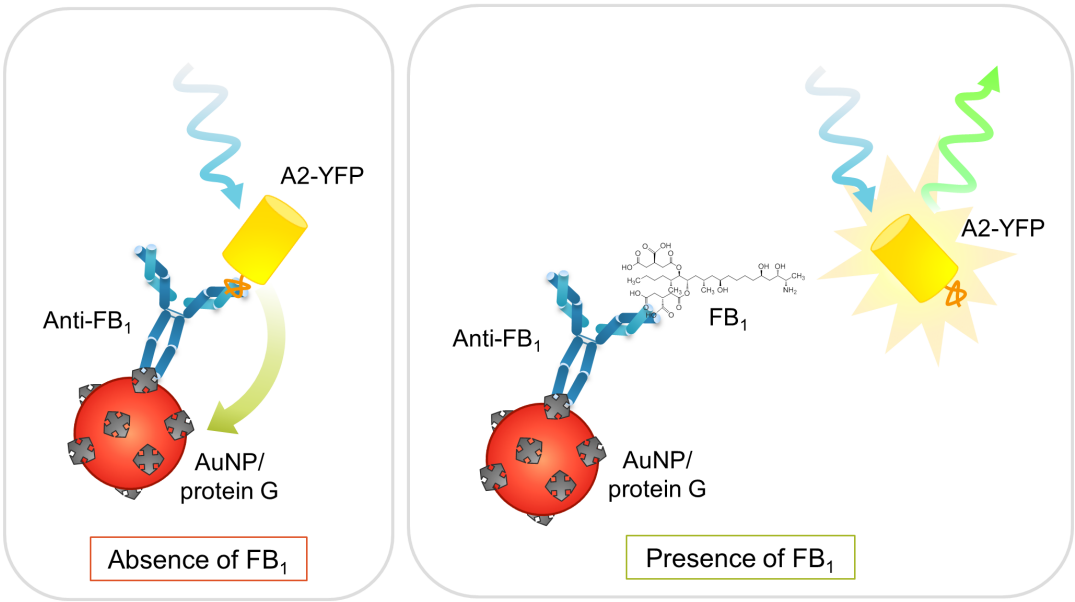


**Figure 26**. Schematic representation of the homogeneous quenching immunoassay based on the mimotope-YFP and an anti-$FB_1$ antibody immobilized on AuNP/protein G-conjugates. Upon mimotope-YFP binding to the antibody, the AuNP efficiently quenches the intrinsic fluorescence of YFP. In the presence of $FB_1$, the mimotope-YFP is not bound to the antibody, and its fluorescence is no longer turned off.

Since the efficiency of fluorescence quenching by the AuNP depends not only on the distance from the fluorophore but also on the nanoparticle size,[62] we tested the performance of different AuNPs in the homogeneous quenching immunoassay. Citrate-stabilized gold nanoparticles were prepared by a step-by-step growing procedure,[63] and their average diameters were determined to be 17.1 ± 2.0, 36.1 ± 3.3, and 72.4 ± 7.1 nm by transmission electron microscopy (TEM; **Figure 31** in the supporting information). The UV–vis absorption spectra of the AuNPs showed the typical plasmon band peaking at 519, 530, and 546 nm for the 17, 36, and 72 nm AuNPs, respectively (**Figure 27**). Furthermore, dynamic light scattering (DLS) was used to evaluate the average hydrodynamic diameter and polydispersity of the nanoparticles (**Figure 32** in the supporting information).

His-tag-mediated conjugation of recombinant protein G to the citrate-capped AuNPs allowed simple and flexible preparation of the protein-decorated AuNPs. First, a flocculation test was performed to determine the amount of protein required to stabilize the AuNPs. Aggregation

of bare AuNPs was observed upon addition of 10% (w/v) NaCl, whereas the protein-decorated AuNPs retained their typical plasmon band under the same conditions, confirming a successful protein coating (**Figure 33** in the supporting information). Moreover, the presence of a protein overlayer was observed by TEM (**Figure 34** in the supporting information), and the amount of immobilized protein was determined by hydrolysis and high-performance liquid chromatography (HPLC) analysis (**Figure 35** and **Table 9** in the supporting information). AuNPs might also have been directly coupled to antibodies by nonspecific absorption;[64,65] however, protein G -mediated linkage allows a more controlled coupling. Because the antibody is directly added to the assay reaction rather than to the coupling reaction, the exact amount of antibody in the final assay can be determined more precisely, and it is not subject to variations among the different batches prepared. Moreover, in this way, the antibodies would bind to the protein G -coated AuNPs in an oriented manner, ensuring that the antigen binding sites are available and not hindered, which might be (at least partially) the case for nonspecifically bound antibodies. Since AuNP-based surface energy transfer (SET) quenching is known to overcome the established distance limits of FRET,[14,66] the additional increase in the distance between AuNPs and the fluorescent protein produced by the protein G overlayer is not as critical as in energy-transfer assays based on organic dye acceptors that quench the donors' fluorescence.

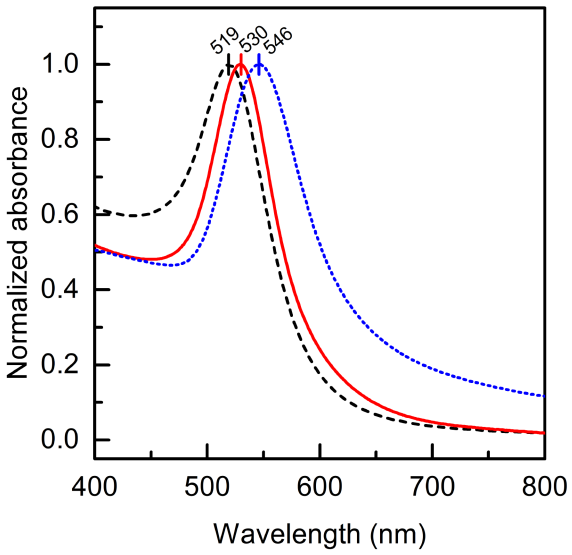


**Figure 27**. Normalized UV–vis absorption spectra of the 17 nm (black dashed line), 36 nm (red solid line), and 72 nm (blue dotted line) AuNPs prepared. Absorption maximums were 519, 530, and 546 nm, respectively.

The feasibility of the assay principle was evidenced by observing a strong fluorescence quenching upon the fusion protein binding to the antibody-conjugated AuNPs (Ab-AuNPs). **Figure 28** shows the variation of the mimotope-YFP fluorescence (0.5 μg $mL^{-1}$) with the concentration of AuNPs ranging from 0 to 4 nM for the 17, 36, and 72 nm sizes of the latter. Control experiments in the absence of the nanoparticle-bound antibody (**Figure 28**) confirmed that the fluorescence quenching was predominantly due to the specific binding of the mimotope-YFP to the anti-$FB_1$ Ab-AuNPs (1.5 μg $mL^{-1}$ of Ab) and not due to the (trivial) phenomena of light scattering, absorption of the excitation light (at 500 nm), and of the fluorescence (at 545 nm)

by the AuNPs themselves. Furthermore, in the presence of 100 ng mL$^{-1}$ $FB_1$, competition between $FB_1$ and epitope-mimicking mimotope-YFP resulted in fluorescence signals that were similar to the background levels without the antibody on the nanoparticles.

The higher SET efficiency of the smallest AuNPs of the three sizes tested has been rationalized previously in terms of quenching of the fluorophore occurring within the near field of the AuNP by formation of an image dipole of the former at the nanoparticle surface, once the size-dependent changes in the complex dielectric function and the absorptivity of the AuNPs are factored in.[67] The light scattering effect prevails for nanoparticles larger than 20 nm diameter, effectively decreasing the specific fluorescence quenching by SET. The maximum quenching efficiency (86%), determined from **Figure 28** data as $[1 - (I/I_0)] \times 100$, was obtained with 1 nM 17 nm antibody-decorated particles when 0.5 µg mL$^{-1}$ mimotope-YFP was used. Higher concentrations of AuNPs led to increased levels of quenching even in the absence of $FB_1$, indicating nonspecific binding of mimotope-YFP or rather the effect of the very strong absorption and scattering caused by the AuNPs, taking into account the minimal concentration of the fluorescent molecule. For the larger AuNPs, in particular, the nonspecific quenching was observed already at relatively low nanoparticle concentrations (2 pM).

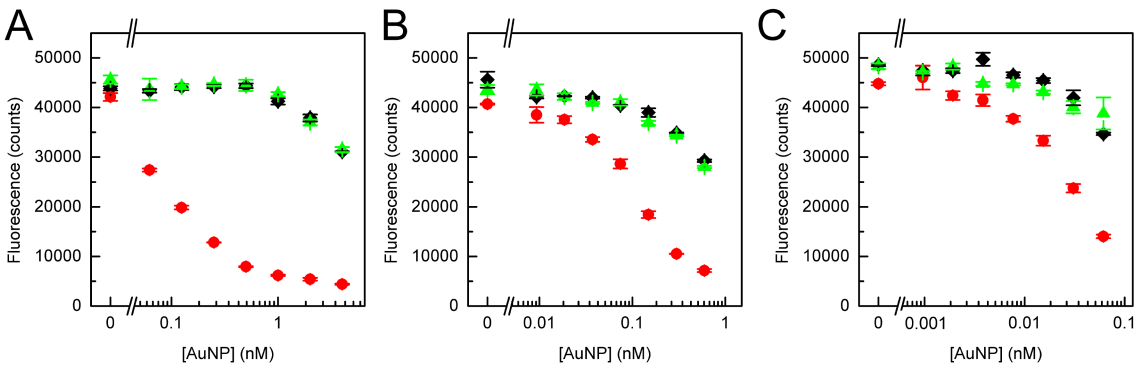


**Figure 28**. Fluorescence quenching produced by the 17 (A), 36 (B), and 72 nm (C) AuNPs in the presence of a constant mimotope-YFP concentration of 0.5 µg mL$^{-1}$. The effect of the AuNP concentration (0–4 nM) on the fluorescence signal was measured for the antibody-AuNP conjugates (1.5 µg mL$^{-1}$ of Ab) both in the absence (red circles) and in the presence (green triangles) of 100 ng mL$^{-1}$ of $FB_1$, or without the antibody (black diamonds). The fluorescence signals (excitation at 500 nm, emission at 545 nm) are shown as the average values of replicate samples ± the standard error of the mean ($n$ = 3).

To check the observed maximum efficiency of the nanoparticle SET on the 17 nm AuNPs against the predicted one,[67] we estimated the distance from the AuNP surface to the YFP chromophore. Taking into account the 3.2 nm protein G coating of the nanoparticle (from TEM, **Figure 34** in the supporting information) supporting the oriented antibody (9.5 nm from top to bottom)[66] and the 4 nm YFP with the chromophore buried approximately in the middle of the protein,[68,69] we can roughly estimate a fluorophore–surface distance of 15 nm. This value assumes that the mimotope has an insignificant effect. Theory predicts an 86% emission quenching efficiency at 18 nm from the surface of a 16.5 nm (diameter) AuNP,[67] a value that is very close to the estimated distance considering the approximations involved in our calculation. Furthermore, the efficient SET process between the fluorophore and the AuNP was shown to be of static nature:

single-photon timing fluorescence decay measurements are identical in the absence and in the presence of the antibody-decorated metal nanoparticles (a fluorescence lifetime of 3.60 ± 0.01 ns was determined for the free and AuNP-bound mimotope-YFP, **Figure 36** in the supporting information), yet the fluorescence intensity at the detector is *ca*. 6 times larger in the absence of the AuNPs.

For the further assay development, AuNP concentrations with best signal-to-background ratios calculated from maximal and minimal fluorescence signals without or with $FB_1$, respectively, were selected. To determine the optimum concentrations of mimotope-YFP and the antibody, a checker-board-type titration was performed with different dilutions. Increasing the mimotope-YFP concentrations obviously resulted in an increase in the fluorescence signals, but high concentrations exhibited also increased nonspecific binding in the presence of $FB_1$ (**Figure 37** in the supporting information). Therefore, 0.5 and 1.5 µg $mL^{-1}$ mimotope-YFP and antibody concentrations, respectively, were chosen for subsequent measurements.

In the homogeneous format, the assay kinetics are usually extremely fast, since slow diffusion does not limit the rate of the binding reaction to a surface as in heterogeneous assays.[26] In fact, already after 5 min of incubation, the specific fluorescence quenching could be observed in our assay (**Figure 38** in the supporting information). Somewhat further increase of the quenching was obtained after 45 min of incubation yielding an improved signal-to-background ratio (**Figure 38A** in the supporting information). However, after signal normalization, similar or better sensitivities (expressed as the $IC_{50}$ values) were found with shorter incubation times (**Figure 38B** in the supporting information). Therefore, a 20 min incubation was selected for further optimization, as it provided the required sensitivity but better reproducibility than still shorter incubation times. Then, the specificity of the immunoassay was evaluated by determining the cross-reactivity with other mycotoxins. The assay did not distinguish the structurally related $FB_1$ and $FB_2$ fumonisins, since the antibody is not specific to either of the isotopes. Nevertheless, negligible cross-reactivity toward other mycotoxins was observed (**Figure 39** in the supporting information).

On the basis of the optimized conditions, we applied the developed quenching assay to quantification of $FB_1$ using the various-sized AuNPs. Standard $FB_1$ solutions of different concentrations were mixed with fixed antibody, mimotope-YFP, and AuNP concentrations, and after 20 min of incubation, the fluorescence of the solutions was measured. **Figure 29A** shows the dose–response plots of the measured signal-to-background fluorescence ratios as a function of the $FB_1$ concentration. Typical sigmoidal calibration curves were obtained with all the AuNPs, but the larger the nanoparticle size, the lower the signal-to-background ratio resulted in agreement with the overall effects discussed above.

To investigate the effect of a real sample matrix, the analysis with 17 nm AuNPs was performed in either the assay buffer, that is, 10 mM phosphate buffer (pH 8.0) containing 0.1% (w/v) bovine serum albumin (BSA), or in wheat extracts diluted with the assay buffer. High concentrations of the sample extract interfered with the assay and resulted in lower maximum signals; however, 5% wheat extract in the final reaction volume showed negligible interference (**Figure 29B**). The calibration curve in this medium showed excellent reproducibility with an average intra-assay relative standard deviation (RSD) of 4.6% and an $IC_{50}$ value of 12.9 ± 1.0 ng $mL^{-1}$. The assay dynamic range ($IC_{20}$–$IC_{80}$) was from 7.3 to 22.6 ng $mL^{-1}$, and its limit of detection (LOD) was calculated to be 1.1 ng $mL^{-1}$, which was 10-fold better than previously reported with the synthetic peptide[40] and slightly lower than that of the heterogeneous reference

assay. The advantage of the homogeneous assay format with a low background signal in the absence of the target could be demonstrated by comparing its analytical performance to that of the heterogeneous assay: while the $IC_{50}$ of the heterogeneous assay (6.8 ± 0.3 ng $mL^{-1}$) was almost twofold better than that of the homogeneous assay, the LOD of the homogeneous assay was better than that of the heterogeneous one (LOD 3.5 ng $mL^{-1}$) due to the lower background signals and thus lower absolute and relative errors of the background. Compared to other bioanalytical assays reported in the literature (**Table 10** in the supporting information), similar and lower LODs for $FB_1$ detection have been described, but the homogeneous quenching assay benefits from significantly shorter assay time, and, due to the simple one-step protocol, the method would be ideally suited to multiplexing and automation.

Finally, two wheat samples spiked with $FB_1$ were analyzed with the homogeneous assay. Sample extracts were diluted in assay buffer, and recoveries of 86% (RSD 6.2%) and 103% (RSD 3.2%) were obtained for samples spiked with 2000 or 4000 µg $kg^{-1}$ $FB_1$, respectively. Current European regulation on fumonisins covers only maize-based products, and the maximum residue limit for unprocessed maize products is 4000 µg $kg^{-1}$. Therefore, the reported homogeneous quenching assay might be used as a reliable and accurate method even with real samples.

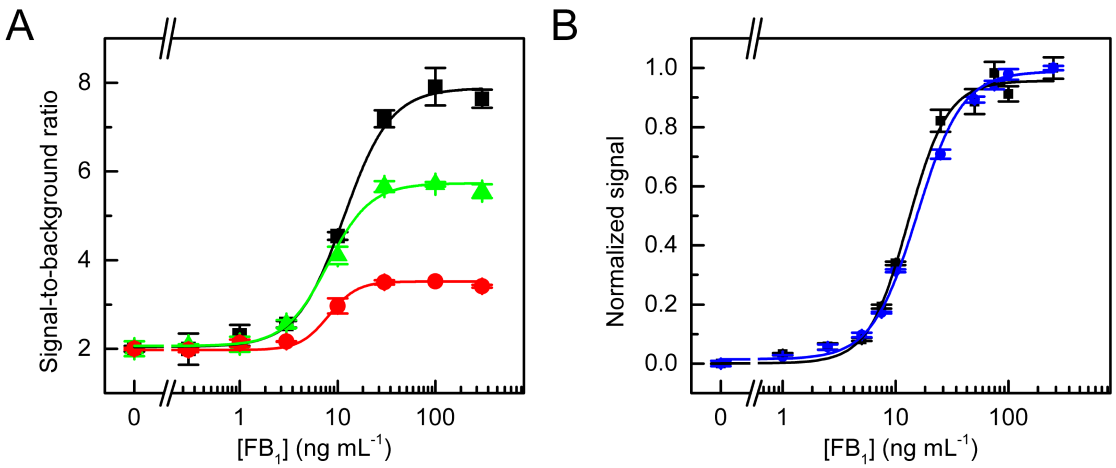


**Figure 29**. (A) Calibration curves for $FB_1$ obtained with AuNPs of different sizes: 17 nm (black squares), 36 nm (green triangles), and 72 nm (red circles). Signal-to-background ratios were calculated by dividing the fluorescence in the presence of $FB_1$ by the signal obtained in the absence of $FB_1$. (B) Comparison of the dose–response curves in assay buffer (black squares) and in 5% sample extract (blue circles) using 17 nm decorated AuNPs; fluorescence values were normalized to the mean maximum and minimum absolute signals, and the results are shown as normalized means ± the standard error of the mean ($n$ = 3). A four-parameter logistic fit (OriginPro 9.0) was used to calculate the IC values.

### 3.2.2.3 Conclusions

This work demonstrates the applicability of epitope mimics to sensitive immunoassays. The homogeneous quenching assay for the quantification of $FB_1$ mycotoxin based on gold NPs demonstrated superior analytical features, including lower detection limit and a more straightforward assay protocol than the heterogeneous reference assay. Notably, the

homogeneous assay based on fluorescent mimotope-YFP fusion protein we have developed is more sensitive than the previously reported immunoassay based on the synthetic mimotope. Because the fluorescent fusion protein was directly used as the tracer, there was no need for a further labeling reaction or secondary antibodies in contrast to other reported AuNP quenching immunoassays.[17,64] Recombinantly produced fusion proteins guarantee a fixed stoichiometry between the fusion partners and avoid issues related to batch-to-batch variations or heterogeneous conjugates that are often observed as the product of chemical conjugation reactions. The superb fluorescence quenching efficiency of AuNPs via nanoparticle surface energy transfer is an attractive feature for homogeneous assay development, and the use of His-tag-mediated AuNP coating provides a flexible and facile manner to create protein-conjugated AuNPs that can readily be used with different antibodies. Overall, the simplicity and analytical performance of the quenching assay provides an elaborated yet powerful tool for rapid analysis of mycotoxins in food samples.

## 3.2.2.4 Experimental section

### Materials

pZsYellow vector was obtained from Clontech Laboratories, while the expression vector pQE-T2−2 together with the Ni-NTA (nickel-nitrilotriacetic acid) magnetic agarose beads were from Qiagen. Chemically competent *Escherichia coli* One Shot BL21 Star (DE3) cells, Phusion HF DNA polymerase, restriction enzymes, and Pierce BCA protein assay kit were from Thermo Fisher Scientific. Oligonucleotides were obtained from Integrated DNA Technologies. HisTrap FF and PD-10 columns were from GE Healthcare. Bacterial cell lysis buffer and BSA were purchased from NZYTech. Amicon Ultra Centrifugal filters were from Merck Millipore, and Packard HTRF 96-well black plates were from Nunc. Protease inhibitor cocktail and TEV protease, together with sodium citrate (+99%) and tetrachloroauric(III) acid trihydrate ($HAuCl_4{\cdot}3H_2O$, +99.9%), were purchased from Sigma-Aldrich. Recombinant protein G with His-tag was obtained from Abcam.

The monoclonal antifumonisin antibody was purchased from BioTez. Mycotoxins fumonisin $B_1$ ($FB_1$), fumonisin $B_2$ ($FB_2$), T-2 toxin, and HT-2 toxin were from Fermentek; alternariol (AOH) was from Apollo Scientific, while deoxynivalenol (DON) and zearalenone (ZEA) were from Sigma-Aldrich. The blank wheat quality control material was purchased from Romer laboratories.

### Construction of fluorescent fusion proteins

For the expression of YPF-tagged mimotope A2, plasmid pPA031 was constructed. The *ZsYellow* gene was polymerase chain reaction (PCR)-amplified from vector pZsYellow by Phusion HF DNA polymerase with oligonucleotides RP08Fw and PA09Rv. The sense primer RP08Fw (5′-TTC GAG CTC ATG GTT ACT CCG AAT GAT GAT ACG TTT GAT CCT TTT CGG GGT GGA GGT TCG GCT CAT TCA AAG CAC GGT CTA-3′) contained a 5′-overhang composed of the DNA sequence encoding for the mimotope A2 (underlined) to generate the translational fusion A2-YFP. The antisense primer PA09Rv (5′-GCT GGT ACC TGG CCC TGA 474 AAA TAC AGG TTT TCG GCC AAG GCA GAA GGG AAT GC- 475 3′), hybridizing to the 3′-end of the *ZsYellow*, was used to add a TEV cleavage site between the 10xHis-tag and the C-terminus of YFP. The PCR product was subcloned at the SacI

and KpnI sites of pQE-T7-2 to generate pPA031. Successful cloning was confirmed by DNA sequence analysis.

### Fusion protein expression and purification

For the over-expression of the mimotope-YFP fusion protein, plasmid pPA031 was transformed into *E. coli* One Shot BL21 Star (DE3) cells and selected on LB agar plates with 50 µg/mL kanamycin. A single colony harboring the plasmid was used to inoculate 15 mL of preculture (LB medium supplemented with 50 µg/mL kanamycin), which was grown overnight at +30 °C. The cell growth was spectrophotometrically monitored, and, the following day, preculture in the exponential growth phase was used to inoculate a main culture of 250 mL (LB medium supplemented with 50 µg/mL kanamycin) to an optical density at 600 nm ($OD_{600}$) of 0.05. The main culture was grown at +37 °C with shaking until an $OD_{600}$ of 0.6 was reached, and isopropylβ-D-1-thiogalactopyranoside (IPTG) was added to a final concentration of 500 µM to induce fusion protein expression. The cultivation was then continued at +37 °C for 5 h. After that, the cells were collected by centrifugation (10 min at 5 000*g* at +4 °C) and resuspended in 10 mL of lysis buffer supplemented with protease inhibitor cocktail. The cells were lysed by sonication on ice for 3 min, after which the resultant cell debris was removed by centrifugation for 20 min at 15 000*g* at +4 °C. Successful expression of the fluorescent protein was confirmed by analyzing the fluorescence emission of the soluble and insoluble fractions as well as the culture media.

The fluorescent fusion protein was purified from the cell lysate by HisTrap column according to the manufacturer's instructions.[70] First, the clarified lysate was diluted (1:3 v/v) in binding buffer (20 mM phosphate buffer pH 7.2, 500 mM NaCl and 20 mM imidazole) to ensure optimal binding conditions for the purification. After the sample was loaded into the HisTrap column, the latter was washed with 30 mL of the binding buffer, and, finally, the His-tagged proteins were eluted by elution buffer (20 mM phosphate buffer pH 7.2, 500 mM NaCl, and 500 mM imidazole). Presence of the fluorescent protein in the elution fractions was followed spectrophotometrically, and the fluorescent fractions were pooled. The buffer was exchanged to 50 mM Tris buffer (pH 7.75) containing 150 mM NaCl with PD-10 according to manufacturer's instructions[70] and concentrated using Amicon Ultra 3K Centrifugal Filter Units.[71] The concentration of the stock was determined by BCA kit,[72] and to remove the C-terminal His-tag, 4 µg of TEV protease was added to 100 µg of the fusion protein (in 100 µL of 50 mM Tris buffer pH 7.75 containing 150 mM NaCl). After overnight incubation at +4 °C, the cleaved His-tag and the His-tagged TEV protease were removed by adding 50 µL of Ni-NTA magnetic agarose beads to the reaction. The beads were captured with an Nd magnet after 15 min, and the supernatant was collected. Successful His-tag cleavage was confirmed by observing the fluorescence emission in the fraction that did not bind to Ni-NTA beads. Finally, the protein concentration of the purified mimotope-YFP without His-tag was determined with a BCA assay kit, and its purity was verified by SDS polyacrylamide gel electrophoresis (PAGE). The fluorescent excitation and emission spectra of the purified fluorescent fusion protein are shown in **Figure 30** in the supporting information.

### Heterogeneous fluorescence immunoassay

The heterogeneous fluorescence immunoassay with mimotope-YFP (**Figure 25A**) was performed in 96-well black plates by coating the wells with capture antibody (100 ng in 60 µL of 0.2 M sodium carbonate/bicarbonate, pH 9.4) by overnight incubation at +4 °C. The wells were then blocked with blocking buffer (PBS pH 7.2; 3% (w/v) BSA) for 3 h at room temperature and washed twice with PBS-T (PBS pH 7.2; 0.05% (v/v) Tween-20). Toxin standards in the range from 0 to 250 ng $mL^{-1}$ (in three replicates) were added to the coated wells together with the 1 µg $mL^{-1}$ mimotope-YFP in assay buffer (PBS, pH 7.2; 0.05% (v/v) Tween-20; 0.1% (w/v) BSA) in a total reaction volume of 60 µL. After incubation of 1.5 h at slow shaking, the wells were washed four times with PBS-T. Finally, 60 µL of PBS was added to each well, and fluorescence signals (excitation at 500 nm; detection at 545 nm) were measured using a BMG Labtech CLARIOstar microplate reader.

### Gold nanoparticle (AuNP) synthesis and characterization

The effect of the gold nanoparticle size on the fluorescence quenching was evaluated by preparing the metal colloids following a step-by-step growing procedure described elsewhere,[63] with minor modifications. First, 97 mg (0.33 mmol) of trisodium citrate dihydrate was dissolved in 150 mL of Milli-Q water (used immediately after collection from the system, 18.2 MΩ cm at +25 °C, pH 7.33) in a 250 mL two-necked round-bottom flask attached to a condenser. A 25 mM $HAuCl_4$ stock solution was prepared by dissolving 246 mg of gold(III) chloride trihydrate in 25 mL of Milli-Q water. Once the solution containing sodium citrate boiled (+110 °C), 1 mL of the gold solution was rapidly injected under vigorous stirring, obtaining in this way citrate-capped AuNPs after *ca*. 10 min. The reaction mixture was cooled to +90 °C, and two consecutive injections of 1 mL of 560 $HAuCl_4$ solution were performed every 30 min. Then, 30 min after the second addition, 55 mL of the suspension was extracted, centrifuged (at 12 857*g* for 2 h) and resuspended into the same amount of Milli-Q water to yield the "generation 0" (Gen0) suspension. Then, 53 mL of Milli-Q water was added to the remaining mixture in the round-bottom flask and kept under stirring for 15 min, until the temperature reached +90 °C. Separately, a 60 mM sodium citrate stock solution was prepared (441 mg in 25 mL of Milli-Q water), and 2 mL of this stock solution was added to the reaction mixture to yield the seed solution for the following generation. In this case, three consecutive injections of 1 mL $HAuCl_4$ solution were incorporated at 30 min intervals. After 30 min of the third addition, 55 mL of the suspension was extracted and treated as described previously to obtain "generation 1" (Gen1). The procedure was repeated in an iterative fashion until "generation 6" (Gen6) was reached. For the assay optimization, samples of Gen0, Gen3, and Gen6, corresponding to 17, 36, and 72 nm nanoparticles, respectively, were used.

TEM images were acquired using a JEOL JEM-1400PLUS instrument operating at 120 kV, with a LaB6 electron source and a GATAN US1000 CCD camera (2k × 2k). The diameter of at least 150 particles was determined from these TEM images using ImageJ software (United States National Institutes of Health) to characterize the size distribution of the nanoparticles. The absorption spectra of the AuNPs were measured on a Varian Cary 3-Bio UV–vis spectrophotometer. Their concentration was determined from the UV–vis spectra using the reported absorption coefficients at 450 nm (ε450) for AuNPs of different sizes,[73] namely,

$3.24 \times 10^8$, $3.52 \times 10^9$, and $2.93 \times 10^{10}$ $M^{-1}$ $cm^{-1}$ for 17, 36, and 72 nm AuNPs, respectively. Hydrodynamic diameter and zeta potential measurements were conducted on a CGS-8 (ALV) instrument equipped with an Ar-ion laser (Coherent I300, 514.5 nm).

Recombinant protein G with His-tag was conjugated to citrate-stabilized AuNPs as previously described with minor modifications.[74] Initially, the protein concentration required to stabilize AuNPs was tested by flocculation tests with NaCl.[65] Briefly, 150 µL of AuNPs (2.5 nM) and different concentrations (0−7.8 µg $mL^{-1}$) of protein G in 10 mM phosphate buffer (pH 8.0) were mixed in an AuNP/protein mole ratio ranging from 1:0 to 1:120. After 15 min of incubation at room temperature, 50 µL of 10% NaCl solution was added to the above mixture, and the stability of the gold was monitored by its color and by the absorbance of the mixture. On the basis of the flocculation test, for the self-assembly of the AuNP-protein G conjugates, 6.5 µg $mL^{-1}$ (250 nM) protein G was added to a microcentrifuge tube containing a AuNP suspension (2.5 nM of 17 nm AuNPs, 0.4 nM of 36 nm AuNPs, or 0.04 nM of 72 nm AuNPs) in 10 mM phosphate buffer (pH 8.0). After incubation for 45 min at +4 °C, the suspension was washed twice by centrifugation at 12 000*g* for 20 min, and, finally, the AuNP-protein G conjugates were resuspended in 10 mM phosphate buffer (pH 8.0) with 0.1% (w/v) BSA, using 1/10 of the original reaction volume to achieve stocks of a higher concentration. Quantification of the protein G coverage was performed by hydrolysis of the protein immobilized onto the AuNPs and classical amino acid HPLC analysis of the hydrolysates, following the strategy described by Liu *et al.* (2017)[75] (see supporting information for method details).

## Homogeneous quenching immunoassay

The homogeneous quenching immunoassay with mimotope-YFP and protein G-coupled AuNPs (**Figure 4**) was performed in black 96-well plates in one step by mixing the assay components in 10 mM phosphate buffer (pH 8.0) containing 0.1% (w/v) BSA in a total reaction volume of 60 µL. After a checkerboard-type titration of the antibody and mimotope-YFP to determine their optimal concentrations, 1.5 µg $mL^{-1}$ anti-$FB_1$ antibody and 0.5 µg $mL^{-1}$ mimotope-YFP were used and mixed with the toxin standards in the range from 0 to 250 ng $mL^{-1}$ (in three replicates). For the optimization of AuNP-protein G conjugates, concentrations ranging from 0.001 to 4 nM were studied, but, for the calibration curves, 1 nM (17 nm AuNP), 0.6 nM (36 nm AuNPs), or 0.06 nM (72 nm AuNPs) concentrations were used. After 10−45 min of incubation at room temperature, fluorescence signals (excitation at 500 nm; detection at 545 nm) were measured using the CLARIOstar microplate reader.

## Sample preparation and analysis of spiked samples

A blank wheat reference material was used to confirm the functionality of the homogeneous assay with a real sample matrix. According to a previously described protocol for $FB_1$ extraction,[43] 5 g of the blank wheat sample was suspended in 25 mL of PBS or, for the spiked samples, 2 or 4 µg of $FB_1$ was added to 1 g of wheat suspended in 5 mL of PBS (2000 or 4000 µg $kg^{-1}$ of $FB_1$). Suspensions were ultrasonically extracted for 15 min and centrifuged at 15 000*g* for 15 min. The supernatant was filtered with a 0.22 µm nylon filter to remove any insoluble material and diluted in the assay buffer.

### Data analysis

For the toxin dose–response plots, the fluorescence signals were analyzed with OriginPro 9.0 software (OriginLab Corp.) using a four-parameter logistic regression (4-PL) function (**equation 1**):

$$y = A_{min} + \frac{(A_{max} - A_{min})}{1 + \left(\frac{x}{IC_{50}}\right)^{b}} \qquad (1)$$

where $A_{max}$ is the asymptotic maximum, $b$ and $IC_{50}$ are the slope of the curve and the analyte concentration, respectively, at the inflection point, and $A_{min}$ is the asymptotic minimum. The limit of detection (LOD) was determined using the average blank signal ± 3 × the standard deviation of the blank, while the dynamic range of the assay was defined as that corresponding to the 20% to 80% inhibition ($IC_{20}$–$IC_{80}$).

## 3.2.2.5 Supporting information

### Excitation and emission spectra of the purified fluorescent fusion protein

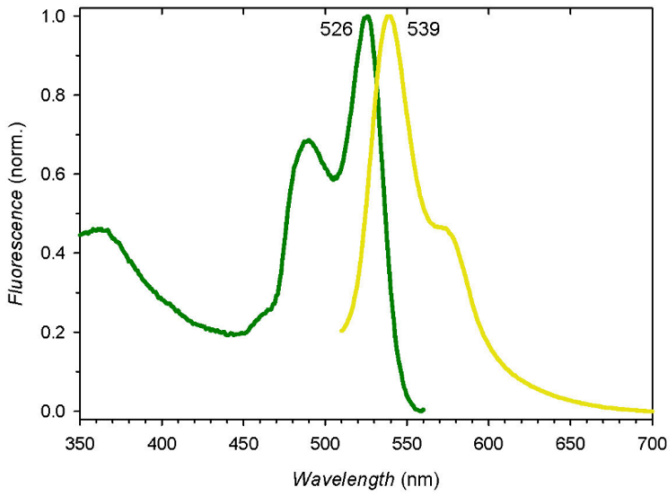


**Figure 30.** Excitation and emission spectra of the epitope-mimicking yellow fluorescent protein in 10 mM PBS (pH 8.0)/0.1% (w/v) BSA buffer.

### Characterization of gold nanoparticles

Citrate-stabilized gold nanoparticles (AuNPs) were prepared by a step-by-step growth procedure[62] as described in the Experimental section. Average diameters of the different generations were determined by transmission electron microscopy (TEM) to be 17.1 ± 2.0 nm, 36.1 ± 3.3 nm, and 72.4 ± 7.1 nm (**Figure 31**). Furthermore, dynamic light scattering (DLS) was used to evaluate the average hydrodynamic diameter and polydispersity of the particles (**Figure 32**).

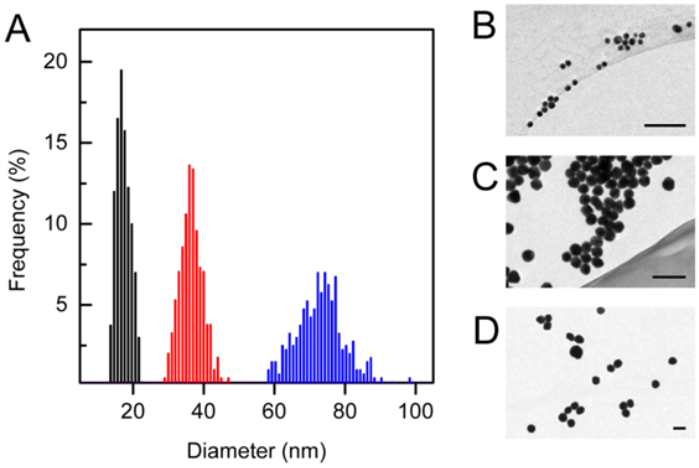


**Figure 31.** The diameter of at least 150 particles of each generation was determined from TEM images to characterize the size distribution of the particles (A). Average sizes of 17.1 ± 2.0 nm (black), 36.1 ± 3.3 nm (red), and 72.4 ± 7.1 nm (blue) were measured for generations 0, 3, and 6, respectively. Typical TEM images for AuNPs of different sizes are shown in figures B (17 nm AuNPs), C (36 nm AuNPs), and D (72 nm AuNPs). The scale bars correspond to 100 nm.

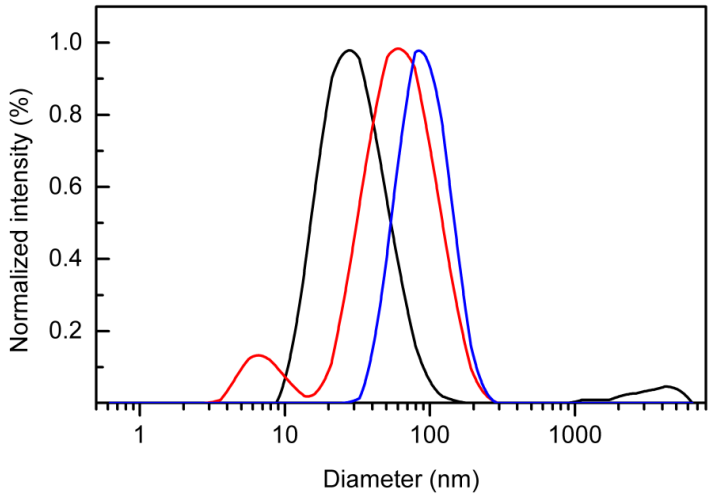


**Figure 32.** Plots of the normalized intensity distribution of the hydrodynamic diameters of 17 nm (black), 36 nm (red), and 72 nm AuNPs (black) measured by dynamic light scattering (DLS). Average mean hydrodynamic particle diameters (Z-average) of 26.8 nm, 45.0 nm, and 79.8 nm, and polydispersity indexes (PDI) of 0.251, 0.324, and 0.164 were measured for the 17 nm, 36 nm, and 72 nm AuNPs, respectively.

## Conjugation of protein G to AuNPs

Citrate-capped AuNPs were conjugated to recombinant protein G by His-tag-mediated self-assembly. Initially, a flocculation test was performed to determine the amount of protein required to stabilize AuNPs. Aggregation of bare AuNPs was observed upon addition of 10% (w/v) NaCl, whereas protein-coated AuNPs retained their typical plasmon band under these

conditions, confirming the successful protein coating (**Figure 33**). Furthermore, analysis of protein-conjugated AuNPs by TEM confirmed the presence of the protein coat (**Figure 33**).

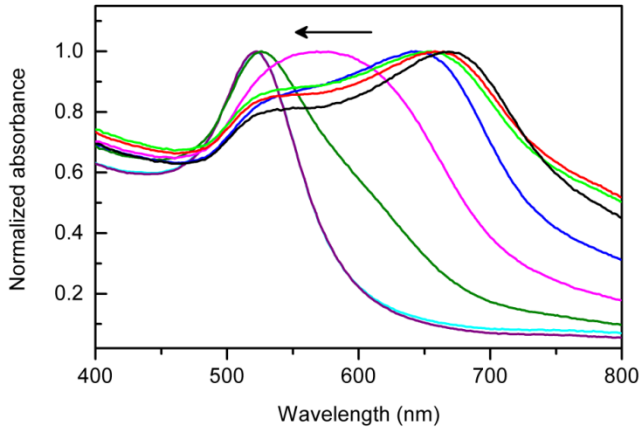


**Figure 33**. Evaluation of the minimum amount of protein required to stabilize the conjugates against salt-induced flocculation. Bare AuNPs (i.e., without added protein) aggregated upon addition of 10% (w/v) NaCl (black line) whereas high protein concentrations (AuNP/protein mole ratios above 1:100, cyan curve) remained colloidally stable, and no changes in the absorbance were observed. The arrow indicates the variation observed in the absorption spectra with increasing concentration of protein G (0–7.8 μg $mL^{-1}$, corresponding to mole AuNP/protein ratios from 1:0 to 1:120).

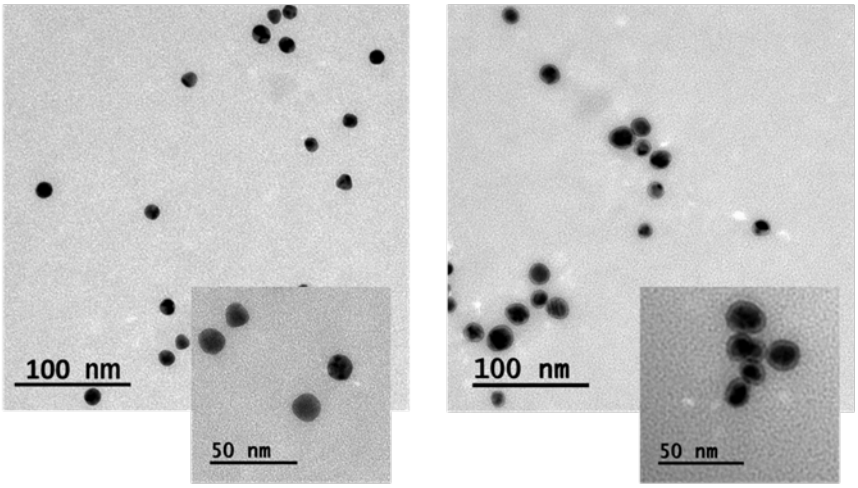


**Figure 34.** AuNPs (17 nm) with (right) and without (left) protein G coating were analyzed by TEM. Negative staining was performed using neutral phosphotungstic acid (3% solution buffered to pH 7 with sodium hydroxide). The size of the protein coat was measured to be 3.0 ± 0.2 nm from the TEM images, which was in agreement with theoretical calculations of the size of protein monolayer on the gold surface (assuming a globular protein, the diameter of the 26 kDa protein G was estimated to be 3.2 nm).

### Quantification of protein G on AuNPs

Quantification of protein coverage on gold nanoparticles was performed following the strategy described by Liu *et al*. (2017)[75] with some changes. The method is based on the hydrolysis of the protein immobilized onto gold nanoparticles and classical amino acid analysis of the hydrolysate.

Briefly, the AuNP-protein G conjugates were prepared following the protocol described in the Experimental Section, but the concentrated stocks were obtained using 10 mM phosphate buffer (pH 8.0), avoiding the presence of BSA. For the hydrolysis, an aliquot of 12.5 µL of the concentrated AuNP-protein G conjugate was diluted to 50 µL with phosphate buffer (10 mM, pH 8). Then, the dilute solution was mixed with 50 µL of 12 M hydrochloric acid and kept at +110 °C for 24 h. The digested sample was evaporated to dryness in order to remove the acid, and the solid residue was dissolved in 100 µL of borate buffer (0.2 M, pH 8.5). The obtained hydrolysis product was immediately diluted with 700 µL of borate buffer (0.2 M, pH 8.5) and 200 µL of 6-aminoquinolyl-*N*-hydroxysuccinimidyl carbamate (AQC) derivatization reagent (3 mg $mL^{-1}$ in anhydrous acetonitrile). The reaction mixture was kept in a shaker at 800 rpm and +55 °C for 10 min. Finally, the amino acids-AQC derivatives were analyzed in triplicate by HPLC-FLD (high-performance liquid chromatography with fluorescence detection).

Chromatographic separation of the amino acids-AQC derivatives was performed on a ZORBAX® SB-C18 (150 mm × 4.6 mm, 3.5 µm) HPLC column from Agilent (Torrance, CA). A gradient program was used with the mobile phase, combining solvent A (Milli-Q water supplemented with 0.1% trifluoroacetic acid (TFA)) and solvent B (acetonitrile supplemented with 0.1% TFA) as follows: 1–8% B (12 min), 8–11% B (13 min), 11% B (2 min), 11–20% B (2 min), 20% B (10 min), 20–100% B (8 min) and finally the initial condition, 1% B, was recovered in 8 min. Analyses were performed at a flow rate of 0.8 mL $min^{-1}$, and the column temperature was kept at +40 °C. The injection volume was 80 µL, and all the compounds eluted within 45 min. The excitation and emission wavelengths of the FLD detector were set at 254 nm and 395 nm, respectively. Calibration was carried out using protein G as the standard. Thus, protein G was hydrolyzed and derivatized following an identical protocol to that described above for the AuNPs-protein G conjugate samples.

Quantification was performed measuring the peak area at a retention time of 34 min that was previously identified as AQC-glycine derivative by comparing the retention time with a single glycine amino acid-AQC standard injection. The chromatograms of hydrolyzed protein G in amounts ranging from 0 to 100 ng are shown in **Figure 35**.

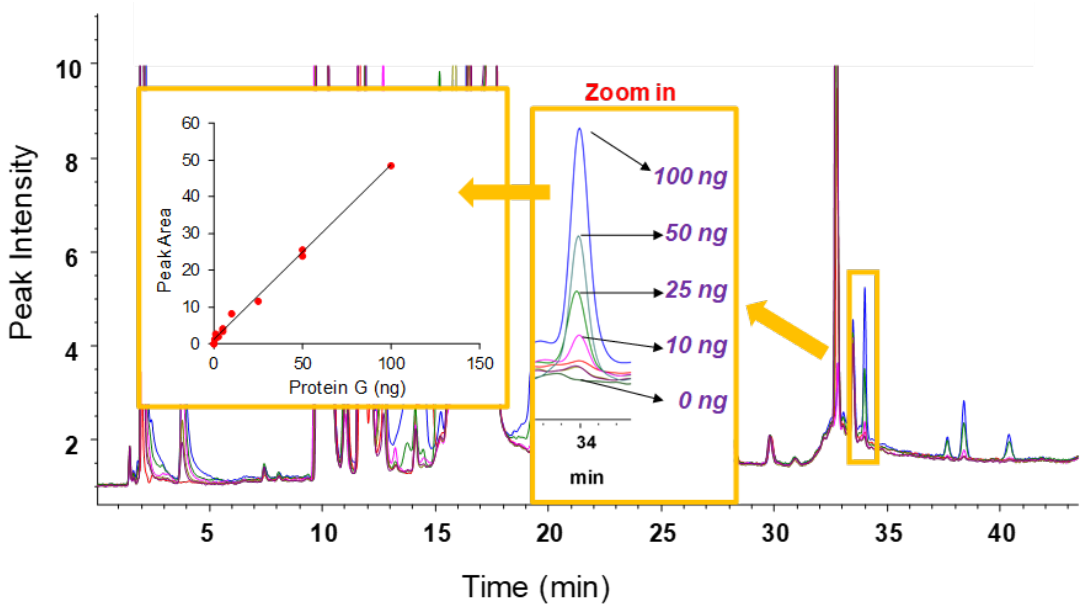


**Figure 35.** The chromatograms of protein G-based calibrants after hydrolysis and AQC derivatization.

The binding efficiency (B, %) was calculated according to (**eq 2**),

$$B(\%) = \left(\frac{Bound\ protein\ G}{Total\ protein\ G}\right) \times 100 \qquad (2)$$

where *Bound protein G* is the amount of protein immobilized on the AuNPs analyzed and the *Total protein G* is the amount of protein G in the reaction mixture. The results summarized in **Table 9** are in agreement with those obtained by other authors using a similar quantification methodology.[2]

**Table 9.** Summarized results of the protein G binding efficiency and surface coverage on AuNPs.

| Sample | Total protein G (µg) | Bound protein G (µg) | B (%) |
|---|---|---|---|
| 17 nm AuNPs | 3.25 | 1.57 ± 0.07* | 48 ± 2 |
| 26 nm AuNPs | 3.25 | 2.1 ± 0.1 | 64 ± 3 |
| 72 nm AuNPs | 3.25 | 2.1 ± 0.3 | 66 ± 8 |

**Confidence interval for n = 3 calculated as* $\pm t_{\alpha,\upsilon}\, {}^{s}/_{\sqrt{n}}$ *where α is the significance level set at 0.05 and ν, degrees of freedom.*

## Mimotope-YFP antibody emission decays

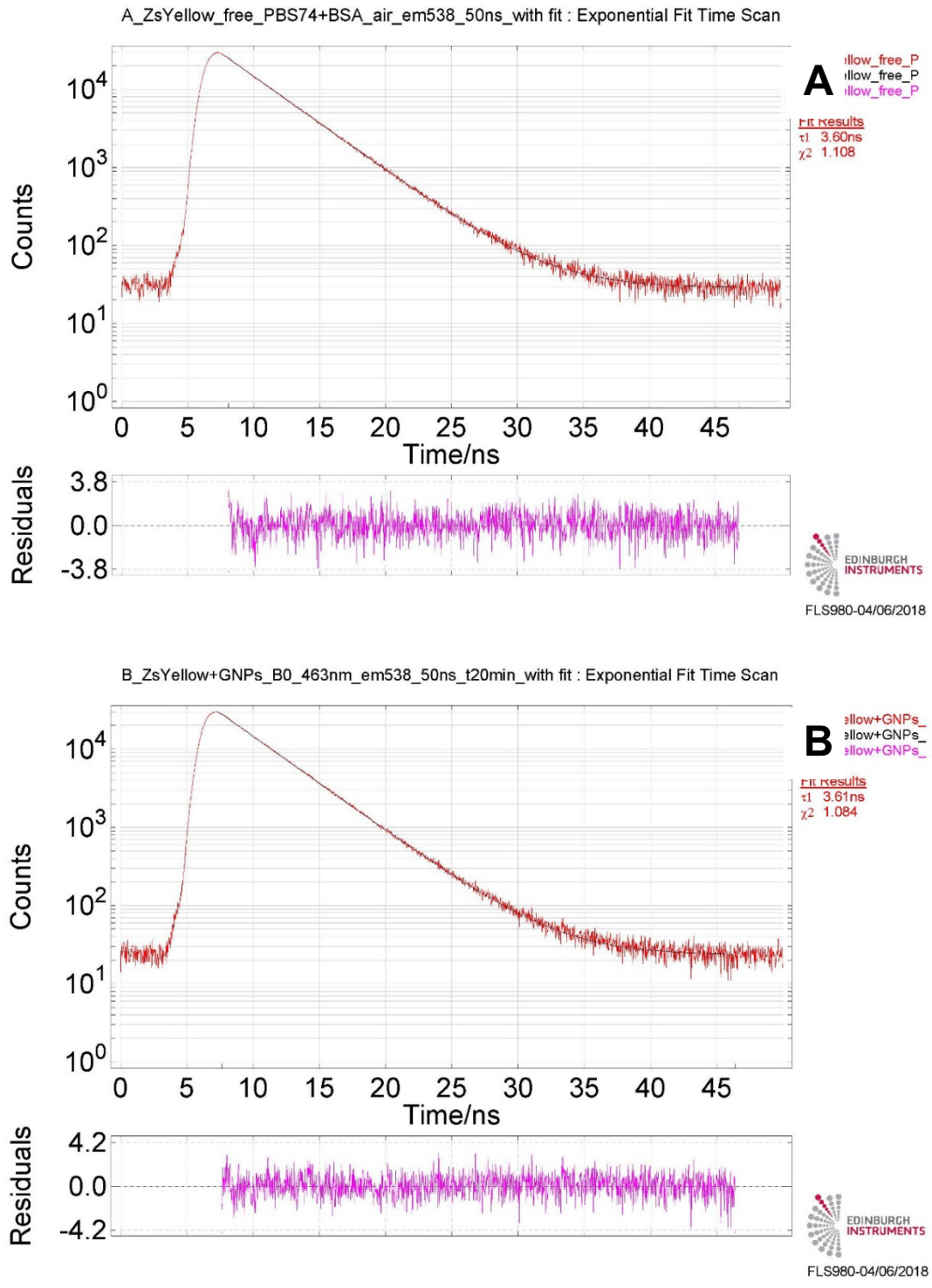


**Figure 36.** Mimotope-YFP antibody emission decay in 10 mM PBS (pH 8.0), 0.1% (w/v) BSA buffer in the absence (A) and in the presence (B) of 17 nm gold nanoparticles (Au-NPs) decorated with protein G and the oriented anti-$FB_1$ antibody in the same buffer after 20 min incubation. Excitation was performed with a 463-nm <1-ns laser diode pulsed at 900 KHz through a 465-nm band-pass interference filter; emission was monitored at 538 nm through a 500-nm blazed double monochromator, with a Hamamatsu R928P photomultiplier tube. In both cases, 30000 counts were collected at the peak channel, but (B) required 6 times as much time as (A).

## Assay optimization

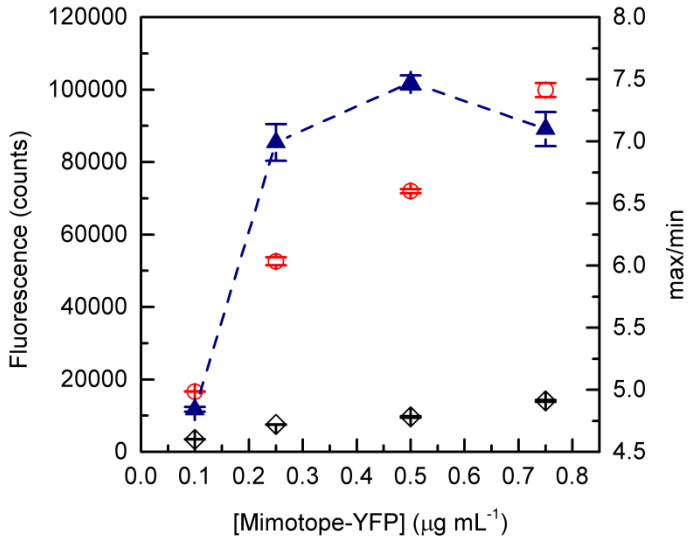


**Figure 37.** Optimization of the mimotope-YFP concentration in the homogeneous quenching immunoassay with 1 nM AuNP and 1.5 µg mL$^{-1}$ antibody. Maximal fluorescence signals without added $FB_1$ (red circles) and minimal signals with 100 ng mL$^{-1}$ $FB_1$ (black diamonds), and the ratio of the maximal to minimal signals (blue triangles, right *y*-axis) after 20 min incubation. Error bars indicate the standard error of the mean ($n$ = 3). A mimotope-YFP concentration of 0.5 µg mL$^{-1}$ with the best max/min ratio was selected for subsequent experiments.

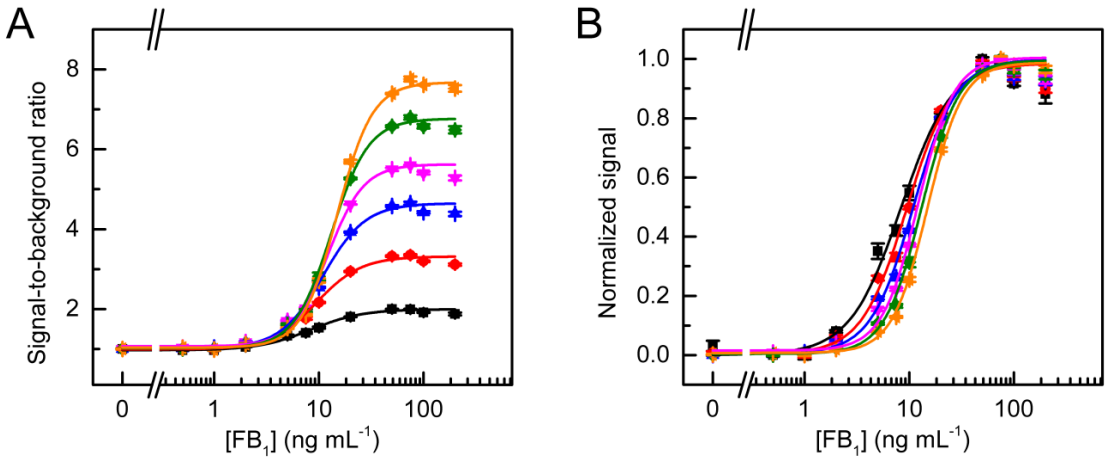


**Figure 38.** Assay kinetics with 17-nm AuNPs. Measurements were repeated after 5 min (black), 10 min (red), 15 min (blue), 20 min (magenta), 30 min (green), and 45 min (orange) incubation. Signal-to-background ratios (A) improved with longer incubation as fluorescence quenching increased. However, the shorter the incubation time the better sensitivity was observed, as can be seen in the normalized signals (B). An incubation time of 20 min was chosen for further experiments as it provided the required sensitivity but better reproducibility than shorter times. Error bars indicate the standard error of the mean ($n$ = 3). A four-parameter logistic fit (OriginPro 9.0) was used to calculate the $IC_{50}$ values.

**Table 10**. Comparison of the analytical characteristics of the novel homogeneous quenching immunoassay with other reported assays for the detection of $FB_1$. Preparation refers to preliminary steps required such as reagent immobilization, labeling, coating, etc. Assay time is the sum of assay incubation steps without taking into account the washing steps or measurement time. Washing steps refer to the total amount of washes during the entire assay protocol. The calculation method for the limit of detection (LOD) has been marked with † if the LOD was determined from 3SD of the blank, or with ‡ if 90% inhibition was used. Dynamic range (DR) is defined from the $IC_{20}$ and $IC_{80}$ values.

| Assay and measurement type | Recognition element | Label | $IC_{50}$ and DR | LOD | Preparative steps | Assay time | Washing steps | Sample | Ref. |
|---|---|---|---|---|---|---|---|---|---|
| ELISA (A) | Immobilized $FB_1$–OVA Recombinant scFv | HRP | 12.67 ng $mL^{-1}$ 2.10–76.45 ng $mL^{-1}$ | 0.832 ng $mL^{-1}$ (8.32 µg $kg^{-1}$) (†) | $FB_1$–OVA immobilization overnight | 2 h | 14x | Spiked corn | [76] |
| Peptide-ELISA (A) | Immobilized mimotope–BSA McAb | HRP | 6.06 ng $mL^{-1}$ 1.77–20.73 ng $mL^{-1}$ | 1.18 ng $mL^{-1}$ | Conjugate immobilization overnight | 2 h | 12x | Maize, feedstuff, and wheat | [77] |
| Magnetoimmuno-sensor on CSPE (Am) | Immobilized McAb $FB_1$–HRP | HRP | 2.86 ng $mL^{-1}$ 0.73–11.2 ng $mL^{-1}$ | 0.33 ng $mL^{-1}$ (‡) | – | 3 h | 13x | Maize, beer | [78] |
| Multiplexed homogeneous immunoassay (FP) | Labeled $FB_1$ McAb | AF 647 | 1918 µg $kg^{-1}$ 587.0–6265 µg $kg^{-1}$ | 331.5 µg $kg^{-1}$ (66.3 ng $mL^{-1}$) (†) | $FB_1$ labeling | 5 min | – | Maize | [79] |
| Microarray-based immunoassay (F) | Immobilized synthetic mimotope McAb | AF 647 | 37.1 ng $mL^{-1}$ 17.3–79.6 ng $mL^{-1}$ | 11.1 ng $mL^{-1}$ (‡) | Microarray printing | 3.5 h | 7x | Spiked maize and wheat | [40] |
| Homogeneous immunoassay (FQ) | McAb Mimotope-YFP | YFP AuNP | 12.9 ng $mL^{-1}$ 7.3–22.6 ng $mL^{-1}$ | 1.1 ng $mL^{-1}$ (†) | AuNP coating and washing 1 h 30 min | 20 min | – | Spiked wheat | This work |

*Abbreviations: A, absorbance; AF, AlexaFluor; Am, amperometry; AuNP, gold nanoparticle; BSA, bovine serum albumin; CSPE, carbon screen-printed electrode; DR, dynamic range; F, fluorescence; FP, fluorescence polarization; FQ, fluorescence quenching; HRP, horse-radish peroxidase; McAb, monoclonal antibody; OVA, ovalbumin; scFv, single-chain fragment variable antibody; YFP, yellow fluorescent protein.*

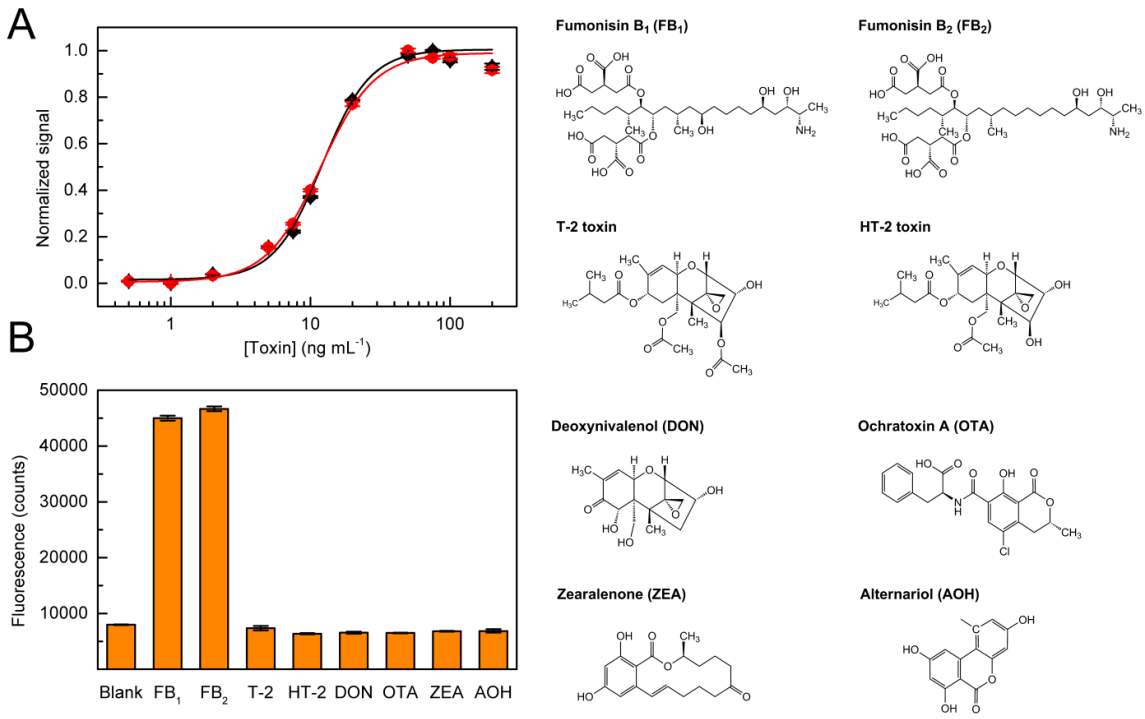


**Figure 39**. Specificity of the homogeneous assay assessed by testing different mycotoxins. Fumonisins $FB_1$ and $FB_2$ showed almost identical calibration curves (**A**; $FB_1$ black, $FB_2$ red), whereas other mycotoxins such as T-2 toxin, HT-2 toxin, deoxynivalenol (DON), ochratoxin A (OTA), zearalenone (ZEA), or alternariol (AOH), did not give any response in the assay when tested at 100 ng $mL^{-1}$ concentration as the fluorescence signals (**B**) were comparable to the background signal of the blank without any toxin. Error bars indicate the standard error of the mean (*n* =3). A four-parameter logistic fit (OriginPro 9.0) was used to calculate the $IC_{50}$ values. Structures of the tested mycotoxins are depicted on the right side.

## 3.2.2.6 References


1. Howes, P. D.; Chandrawati, R.; Stevens, M. M. Colloidal nanoparticles as advanced biological sensors. *Science* **2014**, *346*, 1247390.
2. Holzinger, M.; Le Goff, A.; Cosnier, S. Nanomaterials for biosensing applications: A review. *Front. Chem*. **2014**, *2*, 63.
3. De, M.; Ghosh, P. S.; Rotello, V. M. Applications of nanoparticles in biology. *Adv. Mater*. **2008**, *20*, 4225–4241.
4. Lei, J.; Ju, H. Signal amplification using functional nanomaterials for biosensing. *Chem. Soc. Rev*. **2012**, *41*, 2122–2134.
5. *Encyclopedia of metalloproteins*; Kretsinger, R. H., Uversky, V. N., Permyakov, E. A., (Editors); Springer: New York, USA, **2013**.
6. Guo, S.; Dong, S. Biomolecule-nanoparticle hybrids for electrochemical biosensors. *TrAC, Trends Anal. Chem*. **2009**, *28*, 96–109.
7. Porter, M. D.; Lipert, R. J.; Siperko, L. M.; Wang, G.; Narayanan, R. SERS as a bioassay platform: Fundamentals, design, and applications. *Chem. Soc. Rev*. **2008**, *37*, 1001–1011.
8. Deng, W.; Goldys, E. M. Plasmonic Approach to enhanced fluorescence for applications in biotechnology and the life sciences. *Langmuir* **2012**, *28*, 10152–10163.
9. Saha, K.; Agasti, S. S.; Kim, C.; Li, X.; Rotello, V. M. Gold nanoparticles in chemical and biological sensing. *Chem. Rev*. **2012**, *112*, 2739–2779.
10. Bazin, I.; Andreotti, N.; Hassine, A. I.; De Waard, M.; Sabatier, J. M.; Gonzalez, C. Peptide binding to ochratoxin A mycotoxin: A new approach in conception of biosensors. *Biosens. Bioelectron*. **2013**, *40*, 240–246.

11. *FRET–Förster resonance energy transfer*; Medintz, I. L., Hildebrandt, N., (Editors).; Wiley-VCH Verlag GmbH & Co: Weinheim, Germany, **2014**.
12. Sapsford, K. E.; Berti, L.; Medintz, I. L. Materials for fluorescence resonance energy transfer analysis: Beyond traditional donor-acceptor combinations. *Angew. Chem., Int. Ed*. **2006**, *45*, 4562–4589.
13. Jennings, T. L.; Singh, M. P.; Strouse, G. F. Fluorescent lifetime quenching near *d* = 1.5 nm gold nanoparticles: Probing NSET validity. *J. Am. Chem. Soc*. **2006**, *128*, 5462–5467.
14. Yun, C. S.; Javier, A.; Jennings, T.; Fisher, M.; Hira, S.; Peterson, S.; Hopkins, B.; Reich, N. O.; Strouse, G. F. Nanometal surface energy transfer in optical rulers, breaking the FRET barrier. *J. Am. Chem. Soc*. **2005**, *127*, 3115–3119.
15. Carminati, R.; Greffet, J. J.; Henkel, C.; Vigoureux, J. M. Radiative and non-radiative decay of a single molecule close to a metallic nanoparticle. *Opt. Commun*. **2006**, *261*, 368–375.
16. Pons, T.; Medintz, I. L.; Sapsford, K. E.; Higashiya, S.; Grimes, A. F.; English, D. S.; Mattoussi, H. On the quenching of semiconductor quantum dot photoluminescence by proximal gold nanoparticles. *Nano Lett*. **2007**, *7*, 3157–3164.
17. Mayilo, S.; Ehlers, B.; Wunderlich, M.; Klar, T. A.; Josel, H. P.; Heindl, D.; Nichtl, A.; Kürzinger, K.; Feldmann, J. Competitive homogeneous digoxigenin immunoassay based on fluorescence quenching by gold nanoparticles. *Anal. Chim. Acta* **2009**, *646*, 119–122.
18. You, C. C.; Miranda, O. R.; Gider, B.; Ghosh, P. S.; Kim, I. B.; Erdogan, B.; Krovi, S. A.; Bunz, U. H.; Rotello, V. M. Detection and identification of proteins using nanoparticle-fluorescent polymer 'chemical nose' sensors. *Nat. Nanotechnol.* **2007**, *2*, 318–232.
19. Qian, J.; Wang, C.; Pan, X.; Liu, S. A High-throughput homogeneous immunoassay based on Förster resonance energy transfer between quantum dots and gold nanoparticles. *Anal. Chim. Acta* **2013**, *763*, 43–49.
20. De, M.; Rana, S.; Akpinar, H.; Miranda, O. R.; Arvizo, R. R.; Bunz, U. H.; Rotello, V. M. Sensing of proteins in human serum using conjugates of nanoparticles and green fluorescent protein. N*at. Chem*. **2009**, *1*, 461–465.
21. Schmid, J. A.; Neumeier, H. Evolutions in science triggered by green fluorescent protein (GFP). *ChemBioChem* **2005**, *6*, 1149– 1156.
22. Tsien, R. Y. The green fluorescent protein. *Annu. Rev. Biochem.* **1998**, *67*, 509–544.
23. Tamura, T.; Hamachi, I. Recent progress in design of protein-based fluorescent biosensors and their cellular applications. *ACS Chem. Biol*. **2014**, 9, 2708–2717.
24. Chung, C.; Makino, R.; Ohmuro-Matsuyama, Y.; Ueda, H. Development of a fluorescent protein-antibody Förster resonance energy transfer probe for the detection and imaging of osteocalcin. *J. Biosci. Bioeng*. **2017**, *123*, 272–276.
25. Sakamoto, S.; Taura, F.; Pongkitwitoon, B.; Putalun, W.; Tsuchihashi, R.; Kinjo, J.; Tanaka, H.; Morimoto, S. Development of sensitivity-improved fluorescence-linked immunosorbent assay using a fluorescent single-domain antibody against the bioactive baphthoquinone, plumbagin. *Anal. Bioanal. Chem*. **2010**, *396*, 2955–2963.
26. *The Immunoassay handbook: Theory and applications of ligand* binding ELISA and related techniques, 4th ed.; Wild, D., (Editor); Elsevier Science, Oxford, UK, **2013.**
27. Luzar, J.; Štrukelj, B.; Lunder, M. Phage display peptide libraries in molecular allergology: From epitope mapping to mimotope-based immunotherapy. *Allergy* **2016**, *71,* 1526–1532.
28. Wai, C. Y. Y.; Leung, N. Y. H.; Leung, P. S. C.; Chu, K. H. Immunotherapy of food allergy: A comprehensive review. *Clin. Rev. Allergy Immunol*. **2017**.
29. Chauhan, R.; Singh, J.; Sachdev, T.; Basu, T.; Malhotra, B. D. Recent advances in mycotoxins detection. *Biosens. Bioelectron*. **2016**, *81*, 532–545.
30. Peltomaa, R.; Benito-Peña, E.; Moreno-Bondi, M. C. Bioinspired recognition elements for mycotoxin sensors. *Anal. Bioanal. Chem*. **2018**, *410*, 747–771.
31. Zhao, F.; Wang, H.; Han, X.; Yang, Z. Development and comparative study of chemosynthesized antigen and mimotope-based immunoassays for class-specific analysis of *O,O*-dimethyl organophosphorus pesticides. *Sci. Rep*. **2016**, *6*, 37640.
32. Gazarian, T.; Selisko, B.; Hérion, P.; Gazarian, K. Isolationand structure-functional characterization of phage display library-derived mimotopes of noxiustoxin, a neurotoxin of the scorpion *Centruroides noxius* Hoffmann. *Mol. Immunol*. **2000**, *37*, 755–766.

33. Liu, J.; Chisti, M. M.; Zeng, X. General signal amplification strategy for nonfaradic impedimetric sensing: trastuzumab detection employing a peptide immune-sensor. *Anal. Chem*. **2017**, *89*, 4013−4020.
34. Wang, Y.; Wang, H.; Li, P.; Zhang, Q.; Kim, H. J.; Gee, S. J.; Hammock, B. D. Phage-displayed peptide that mimics aflatoxins and its application in immunoassay. *J. Agric. Food Chem*. **2013**, *61*, 2426−2433.
35. He, Z. Y.; He, Q. H.; Xu, Y.; Li, Y. P.; Liu, X.; Chen, B.; Lei, D.; Sun, C. H. Ochratoxin A mimotope from second-generation peptide library and its application in immunoassay. *Anal. Chem*. **2013**, *85*, 10304−10311.
36. He, Q.-h.; Xu, Y.; Zhang, C.-z.; Li, Y.-p.; Huang, Z.-b. Phage-borne peptidomimetics as immunochemical reagent in dot-immunoassay for mycotoxin zearalenone. *Food Control* **2014**, *39*, 56−61.
37. Wang, J.; Liu, Z.; Li, G.; Li, J.; Kim, H. J.; Shelver, W. L.; Li, Q. X.; Xu, T. Simultaneous development of both competitive and noncompetitive immunoassays for 2,2′,4,4′-tetrabromodiphenyl ether using phage-displayed peptides. *Anal. Bioanal. Chem*. **2013**, *405*, 9579−9583.
38. Smartt, A. E.; Ripp, S. Bacteriophage reporter technology for sensing and detecting microbial targets. *Anal. Bioanal. Chem*. **2011**, *400*, 991−1007.
39. Peltomaa, R.; López-Perolio, I.; Benito-Peña, E.; Barderas, R.; Moreno-Bondi, M. C. Application of bacteriophages in sensor development. *Anal. Bioanal. Chem*. **2016**, *408*, 1805−1828.
40. Peltomaa, R.; Benito- Peña, E.; Barderas, R.; Sauer, U.; Gonzalez Andrade, M.; Moreno-Bondi, M. C. Microarray-based immunoassay with synthetic mimotopes for the detection of fumonisin $B_1$. *Anal. Chem*. **2017**, *89*, 6216−6223.
41. Zou, X.; Chen, C.; Huang, X.; Chen, X.; Wang, L.; Xiong, Y. Phage-free peptide ELISA for ochratoxin A detection based on biotinylated mimotope as a competing antigen. *Talanta* **2016**, *146*, 394−400.
42. Liu, R.; Yu, Z.; He, Q.; Xu, Y. An immunoassay for ochratoxin A without the mycotoxin. Food Control **2007**, *18*, 872−877.
43. Xu, Y.; Chen, B.; He, Q. H.; Qiu, Y. L.; Liu, X.; He, Z. Y.; Xiong, Z. P. New approach for development of sensitive and environmentally friendly immunoassay for mycotoxin fumonisin $B_1$ based on using peptide-MBP fusion protein as substitute for coating antigen. *Anal. Chem*. **2014**, *86*, 8433−8440.
44. Xu, Y.; He, Z.; He, Q.; Qiu, Y.; Chen, B.; Chen, J.; Liu, X. Use of cloneable peptide-MBP fusion protein as a mimetic coating antigen in the standardized immunoassay for mycotoxin ochratoxin A. *J. Agric. Food Chem.* **2014**, *62*, 8830−8836.
45. Carlomagno, M.; Lassabe, G.; Rossotti, M.; González-Techera, A.; Vanrell, L.; González-Sapienza, G. Recombinant streptavidin nanopeptamer anti-immunocomplex assay for noncompetitive detection of small analytes. *Anal. Chem*. **2014**, *86*, 10467−10473.
46. Ding, Y.; Hua, X.; Chen, H.; Liu, F.; González-Sapien, G.; Wang, M. Recombinant peptidomimetic-nano luciferase tracers for sensitive single-step immunodetection of small molecules. *Anal. Chem*. **2018**, *90*, 2230−2237.
47. Gelderblom, W. C.; Jaskiewicz, K.; Marasas, W. F.; Thiel, P. G.; Horak, R. M.; Vleggaar, R.; Kriek, N. P. Fumonisins – Novel mycotoxins with cancer-promoting activity produced by *Fusarium moniliforme*. *Appl. Environ. Microbiol*. **1988**, *54*, 1806−1811.
48. Scott, P. M. Recent research on rumonisins: A review. *Food Addit. Contam., Part A* **2012**, *29*, 242−248.
49. IARC, International Agency for Research on Cancer. Fumonisin $B_1$. In: *IARC monographs on the evaluation of the carcinogenic risks to humans: Some traditional herbal medicines, some mycotoxins, naphthalene and styrene*; IARC: Lyon, France, **2002**; Vol. 82, pp 301−366.
50. Bennett, J. W.; Klich, M. Mycotoxins. *Clin Microbiol Rev*. **2003**, *16*, 497−516.
51. European Commission. Commission regulation (EC) No 1881/2006. *Off. J. Eur. Union*. **2006**, *L364,* 5−24.
52. European Commission. Commission Regulation (EC) 1126/2007. *Off. J. Eur. Union*. **2007**, *L255*, 14−17.
53. U.S. Food and Drug Administration (FDA), Draft guidance for industry: Fumonisin levels in human food and animal feeds; Final guidance. (www.fda.gov/food/guidance regulation/). [Cited May 10, 2018].
54. World Health Organization, Department of Food Safety and Zoonoses (**2018**) Fumonisins, Ref. No.: WHO/NHM/ FOS/RAM/18.2 (http://origin.who.int/food safety/) [Cited Oct 8, 2018].

55. Evaluation of certain contaminants in food (Eighty-third Report of the Joint FAO/WHO Expert Committee on food additives). *WHO Technical Report Series*, No. 1002; WHO Technical Report Series, **2017**.
56. Udovicki, B.; Audenaert, K.; De Saeger, S.; Rajkovic, A. Overview on the mycotoxins incidence in Serbia in the period 2004–2016. *Toxins* **2018**, *10*, 279.
57. Köppen, R.; Koch, M.; Siegel, D.; Merkel, S.; Maul, R.; Nehls, I. Determination of mycotoxins in foods: Current state of analytical methods and limitations. *Appl. Microbiol. Biotechnol.* **2010**, *86*, 1595–1612.
58. Berthiller, F.; Brera, C.; Crews, C.; Iha, M. H.; Krska, R.; Lattanzio, V. M. T.; *et al.* Developments in mycotoxin analysis: An update for 2014–2015. *World Mycotoxin J.* **2016**, *9*, 5–30.
59. Matz, M. V.; Fradkov, A. F.; Labas, Y. A.; Savitsky, A. P.; Zaraisky, A. G.; Markelov, M. L.; Lukyanov, S. A. Fluorescent proteins from nonbioluminescent *Anthozoa* species. *Nat. Biotechnol*. **1999**, *17*, 969–973.
60. Clontech (**2002**) Living Colors User Manual, vol II. Red fluorescent protein, Protocol PT3404–1. www.clontech.com. [Cited May 10, 2018].
61. Sambrook, J.; Russell, D. W. *Molecular cloning: A laboratory manual,* 3rd ed.; Cold Spring Harbor Laboratory Press: Cold Spring Harbor, NY, USA, **2001**.
62. Li, M.; Cushing, S. K.; Wang, Q.; Shi, X.; Hornak, L. A.; Hong, Z.; Wu, N. Size-dependent energy transfer between CdSe/ZnS quantum dots and gold nanoparticles. *J. Phys. Chem. Lett*. **2011**, *2*, 2125–2129.
63. Bastus, N. G.; Comenge, J.; Puntes, V. Kinetically controlled seeded growth synthesis of citrate-stabilized gold nanoparticles of up to 200 nm: Size focusing *versus* ostwald ripening. *Langmuir* **2011**, *27*, 11098–11105.
64. Chen, J.; Huang, Y.; Zhao, S.; Lu, X.; Tian, J. Gold nanoparticles-based fluorescence resonance energy transfer for competitive immunoassay of biomolecules. *Analyst* **2012**, *137*, 5885–5890.
65. Hermanson, G. T. Preparation of colloidal gold-labeled proteins. In: *Bioconjugate techniques*, 2nd ed.; Elsevier Inc., **2008**; pp 924–935.
66. Guddat, L. W.; Herron, J. N.; Edmundson, A. B. Three-dimensional structure of a human immunoglobulin with a hinge deletion. *Proc. Natl. Acad. Sci. USA*. **1993**, *90*, 4271–4175.
67. Breshike, C. J.; Riskowski, R. A.; Strouse, G. F. Leaving Förster resonance energy transfer behind: Nanometal surface energy transfer predicts the size-enhanced energy coupling between a metal nanoparticle and an emitting dipole. *J. Phys. Chem. C* **2013**, *117*, 23942–23949.
68. Day, R. N.; Davidson, M. W. The fluorescent protein palette: Tools for cellular imaging. *Chem. Soc. Rev*. **2009**, *38*, 2887–2921.
69. Remington, S. J.; Wachter, R. M.; Yarbrough, D. K.; Branchaud, B.; Anderson, D. C.; Kallio, K.; Lukyanov, K. A. zFP538, a yellow-fluorescent protein from *Zoanthus*, contains a novel three-ring chromophore. *Biochemistry* **2005**, *44*, 202–212.
70. www.gelifesciences.com (Cited Oct 1, 2018).
71. www.merckmillipore.com (Cited Oct 1, 2018).
72. www.thermofisher.com (Cited Oct 1, 2018).
73. Haiss, W.; Thanh, N. T. K.; Aveyard, J.; Fernig, D. G. Determination of size and concentration of gold nanoparticles from UV–vis spectra. *Anal. Chem*. **2007**, *79,* 4215–4221.
74. Aldeek, F.; Safi, M.; Zhan, N.; Palui, G.; Mattoussi, H. Understanding the self-assembly of proteins onto gold nanoparticles and quantum dots driven by metal-histidine coordination. *ACS Nano* **2013**, *7*, 10197–10210.
75. Liu, S.; Horak, J.; Höldrich, M.; Lämmerhofer, M. Accurate and reliable quantification of the protein surface coverage on protein-functionalized nanoparticles. *Anal. Chim. Acta* **2017**, *989*, 29–37.
76. Zou, L.; Xu, Y.; Li, Y.; He, Q.; Chen, B.; Wang, D., Development of a single-chain variable fragment antibody-based enzyme-linked immunosorbent assay for determination of fumonisin $B_1$ in corn samples. *J. Sci. Food Agric*. **2014**, *94*, 1865–1871.
77. Liu, X.; Xu, Y.; He, Q. H.; He, Z. Y.; Xiong, Z. P., Application of mimotope peptides of fumonisin $B_1$ in peptide ELISA. *J. Agric. Food Chem*. **2013**, *61*, 4765–4770.
78. Jodra, A.; López, M. A.; Escarpa, A., Disposable and reliable electrochemical magnetoimmunosensor for fumonisins simplified determination in maize-based foodstuffs. *Biosens. Bioelectron*. **2015**, *64*, 633–638.
79. Li, C.; Wen, K.; Mi, T.; Zhang, X.; Zhang, H.; Zhang, S.; Shen, J.; Wang, Z., A Universal multi-wavelength fluorescence polarization immunoassay for multiplexed detection of mycotoxins in maize. *Biosens. Bioelectron*. *2016*, *79*, 258–265.

# DEVELOPMENT AND COMPARISON OF MIMOTOPE-BASED IMMUNOASSAYS FOR THE ANALYSIS OF FUMONISIN $B_1$

Riikka Peltomaa,[a] Irene Agudo-Maestro,[a] Vicente Más,[b] Rodrigo Barderas,[c] Elena Benito-Peña,[a,*] and María C. Moreno-Bondi[a,*]

[a] Department of Analytical Chemistry, Faculty of Chemistry, Complutense University, Ciudad Universitaria s/n, Madrid 28040, Spain.
[b] Centro Nacional de Microbiología - Instituto de Salud Carlos III, Ctra. Majadahonda-Pozuelo, 28220 Madrid, Spain.
[c] Chronic Disease Programme (UFIEC), Instituto de Salud Carlos III, Ctra. Majadahonda-Pozuelo Km 2.2, 28220 Madrid, Spain.

*Submitted manuscript*

## Abstract

Mycotoxins can be found as natural contaminants in many foods and feeds, and owing to their toxic effects, it is essential to detect them before they enter the food chain. An interesting approach for the analysis of mycotoxins by competitive immunoassays is the use of epitope mimicking peptides, or mimotopes, which can replace the toxin-conjugates traditionally used in such assays. Mimotopes can be selected from phage-displayed peptide libraries even without any prior knowledge of the antibody–antigen interaction, and after identifying the target specific clones, the individual clones can be efficiently amplified in bacteria and used directly in the immunoassay. Following such approach, we have previously selected and identified a dodecapeptide which functions as a mimotope for the mycotoxin fumonisin $B_1$. In this work, we present the development and comparison of various immunoassays based on this mimotope, named A2, which has been used in the phage-displayed format in which it was selected, but also as a fluorescent recombinant fusion protein or as a synthetic peptide. The best sensitivity was obtained with the magnetic bead–based assay using the synthetic peptide and enzymatic detection which provided a detection limit of 0.029 ng $mL^{-1}$. Analysis of the binding kinetics by surface plasmon resonance (SPR) further reinforced the suitability of the synthetic peptide for the competitive immunoassay as this mimotope showed a slightly lower affinity for the target antibody in comparison with the recombinant fusion protein.

## 3.2.3.1 Introduction

The small size of many diagnostically or environmentally relevant molecules presents particular challenges for the development of rapid methods for their detection. Immunoassays for low molecular weight analytes, or haptens, which contain only one epitope and thus are not able to bind more than one antibody at the same time, are usually performed in the competitive assay format. A major limitation of this approach is the requirement to conjugate the target molecule either to a carrier protein or to a label which allows the immobilization or detection of this

competitor for immunoassay development.[1] In some cases, the synthesis or chemical conjugation of these competitors can be problematic and time-consuming or result in a heterogeneous mixture of randomly cross-linked or unstable molecules which can reduce the immunoassay performance. Additionally, the analyte conjugation can unfavorably affect the antibody recognition, or the release of the analyte moiety from the conjugate might even cause false positive results.[2–4] Epitope mimics are an intriguing alternative to overcome such limitations related to the competitive immunoassay format.[2,5] Their exceptional ability to mimic the epitope of the analyte and thus bind to the same antibody paratope allows using epitope mimics as the competitor instead of the conjugated analyte itself. Several epitope mimicking antibodies, referred to as anti-idiotypic antibodies, as well as short peptides, known as mimotopes, have been described for various low molecular weight targets, including mycotoxins.[5,6]

Mycotoxins are low molecular weight compounds produced as secondary metabolites by filamentous fungi, and they can be found as natural contaminants in many vegetal foods and feeds, including cereal grains, nuts, fruits, spices, and beans.[7,8] Currently, approximately 400 compounds are recognized as mycotoxins, and about 30 of them are considered as a threat to human and animal health due to their cytotoxic, nephrotoxic, hepatotoxic, teratogenic, mutagenic, carcinogenic, immunosuppressive, or estrogenic effects.[7–9]. Due to the natural character of these toxins and the widespread distribution of mycotoxin-producing molds mycotoxin contamination is often inevitable,[9] and therefore, to guarantee food safety several national and international authorities, including the European Commission, have set maximum residue limits (MRLs) for the most common and toxic mycotoxins.[10–13] Whilst the conventional mycotoxin detection methods, based on liquid chromatography coupled with diode array (DAD), fluorescence (FLD) or mass spectrometry (MS) detection, offer high sensitivity and accuracy,[6,14,15] immunoassays and biosensors provide fast and low-cost alternatives. These simple features make them more suitable for multiplexed approaches as well as for field testing or low-resource settings, and can provide real-time readout and even fully automated processes.[16,17]

The concept of epitope mimics has been widely recognized in the field of mycotoxin research, and mimotopes have been reported for the most common mycotoxins, including aflatoxin,[18] deoxynivalenol (DON),[19] fumonisin $B_1$ ($FB_1$),[20–22] ochratoxin A (OTA),[23–27] and zearalenone.[28] Phage display[29–31] is a powerful technique that enables the selection of mimotopes from phage-displayed peptide libraries. Phage-borne peptides for mycotoxin detection have been applied to different immunoassays, for example using colorimetric[23] or chemiluminescent[25] detection, or developing rapid methods based on dipsticks[25] and dot-immunoassays.[28] Nevertheless, despite the wide use of phages in research, they might not be ideal components for immunoassay development due to their large size and biologically active nature.[32,33] Alternatively, after identifying the mimotope sequence from a phage-displayed library, the phage-borne peptides can be replaced by their synthetic or recombinant counterparts. Taking advantage of the rather well-established and straightforward chemical synthesis of short peptides, synthetic mimotopes have been demonstrated to be an attractive alternative to develop phage-free mimotope assays.[20,22,23,27] On the other hand, the vast possibilities of genetic engineering and the low cost of producing recombinant proteins in bacteria also make the use of recombinant mimotope-protein fusions an attractive option.[21,26,34] For example, for OTA and $FB_1$ recombinant mimotope-fusions with maltose binding protein

(MBP) have been used as coating agents in ELISA,[21,26] and recently, mimotopes tagged with bioluminescent[35] or fluorescent reporter proteins[36,37] enabled using the fusion protein directly as the tracer.

Despite the various applications of mimotopes particularly for mycotoxin detection,[5] the available information on comparing the alternative mimotope formats is still scarce. In this work, we have systematically compared the performance of seven different immunoassays using the phage-borne, synthetic, or recombinant mimotopes for the detection of $FB_1$. A previously identified mimotope[20] was produced in bacteria either by phage display or by expressing a recombinant fusion protein with a yellow fluorescent protein (YFP). The developed competitive immunoassays using these mimotopes were compared with the binding inhibition assay using the synthetic mimotope with a biotin linker. To further explore alternatives, to improve the assay sensitivity and working range, the immunoassays were transferred from the conventional microtiter plate–based format to magnetic beads with a large surface area available for the immobilization. Moreover, in order to study the differences in the binding kinetics of the interaction between the phage-borne, synthetic, or recombinant mimotopes with the anti-$FB_1$ antibody binding parameters, we performed kinetics analyses by surface plasmon resonance (SPR). This real-time and label-free analysis could provide a more accurate comparison of the mimotope binding to the target antibody independent of the used immobilization support, label, or secondary antibody.

## 3.2.3.2 Materials and methods

### Materials

The monoclonal anti-fumonisin antibody was purchased from BioTez (Berlin, Germany) and fumonisin B1 (FB1) was from Fermentek Ltd. (Jerusalem, Israel). Biotinylated peptide (A2-bio with the sequence VTPNDDTFDPFRGGGSK(Bio)−NH2) was synthesized at Peptide Synthetics (Fareham, UK). The HRP-conjugated anti-M13 antibody, together with the BIAcore sensor chips CM5 and CM3, the mouse antibody capture kit and amine coupling kit were obtained from GE Healthcare Inc. (Chicago, IL, USA). The peroxidase-conjugated AffiniPure Rabbit Anti-Mouse IgG (H+L) and monoclonal mouse anti-biotin were from Jackson ImmunoResearch Inc. (West Grove, PA, USA). The M13 major coat protein antibody was from Santa Cruz Biotechnology (Dallas, TX, USA). LodeStars 2.7 Carboxyl paramagnetic beads with an average diameter of 2.7 mm were purchased from Agilent Technologies, Inc. (Santa Clara, CA, USA) and Dynabeads Protein G, NeutrAvidin Biotin Binding Protein and Amplex UltraRed reagent together with 1-ethyl-3-[3-dimethylaminopropyl] carbodiimide hydrochloride (EDC), StartingBlock (TBS) Blocking Buffer and Blocker solution (casein in PBS) were from Thermo Fisher Scientific (Waltham, MA, USA). N-hydroxysulfosuccinimide (sulfo-NHS) was purchased from Fluorochem (Hadfield, UK). Black polypropylene 384-microplates were obtained from Eppendorf (Hamburg, Germany), black Packard HTRF 96-well plates from Nunc (Roskilde, Denmark) and clear Greiner polypropylene 96-well plates from Sigma-Aldrich (St. Louis, MO, USA). The pZsYellow vector was obtained from Clontech Laboratories (Mountain View, CA, US) and the expression vector pQE-T2-2 was from Qiagen (Hilden, Germany). Chemically competent Escherichia coli One Shot® TOP10 and BL21 Star (DE3) cells, the restriction enzymes, and Pierce™ bicinchoninic acid (BCA) protein assay kit

were from Thermo Fisher Scientific. PCR primers were obtained from Integrated DNA Technologies, Inc. (San Diego, CA, USA), and KOD Xtreme Hot Start DNA Polymerase was purchased from Merck Millipore (Darmstadt, Germany). HisTrap FF and PD-10 columns were from GE Healthcare. Bacterial cell lysis buffer and bovine serum albumin (BSA) were purchased from NZYTech (Lisbon, Portugal), and protease inhibitor cocktail from Sigma-Aldrich.

### Preparation of phage-displayed mimotopes and fusion proteins

Phage-displayed mimotopes (A2-phage) were prepared by infecting a 25-mL culture of E. coli ER2738 grown to the early-log phase (OD600 0.01–0.05) with the previously identified phage clone A2.[20] The culture was incubated at +37 °C with vigorous shaking (250 rpm) for 5 h. Next, the culture was centrifuged for 15 min (12 000 g, +4 °C), and the phage containing supernatant was mixed with 1/6 volume of PEG/NaCl (20% PEG 6000 in 2.5 M NaCl). After 3 h incubation on ice, the precipitated phages were collected by centrifugation for (15 min at 12 000 g, +4 °C). The phage precipitate was resuspended in 1 mL of PBS (pH 7.4), and the precipitation with PEG/NaCl was repeated. Finally, the phage stock was incubated at +65 °C for 15 min to kill any residual E. coli, and the phage titer was determined by plating serial dilutions of the phage suspension with E. coli.

### Construction and expression of the recombinant mimotope fusion protein

YFP-tagged FB1-mimotope (A2-YFP) was generated by cloning the $FB_1$-mimotope A2 with the peptide sequence VTPNDDTFDPFR[20] in fusion with *Zoanthus* sp. yellow fluorescent protein (YFP), ZsYellow,[38,39] using standard molecular biology techniques. Plasmid pA2-YFP was constructed by amplifying the ZsYellow gene from vector pZsYellow by PCR using KOD Xtreme Hot Start DNA polymerase. The sense primer (5'–TTC GAG CTC ATG GTT ACT CCG AAT GAT GAT ACG TTT GAT CCT TTT CGG GGT GGA GGT TCG GCT CAT TCA AAG CAC GGT CTA–3') hybridizing to the 5'-end of *ZsYellow* contained a 5'-overhang composed of the DNA sequence encoding for the mimotope A2 (underlined) to generate the translational fusion A2-YFP. The antisense primer (5'–GCT GGT ACC TCA GTG GTG GTG GTG GTG GTG GGC CAA GGC AGA AGG GAA TGC–3'), hybridizing to the 3'-end of the *ZsYellow*, was used to add a polyhistidine tag (His-tag) to the C-terminus of the fusion protein. The PCR product was subcloned at the SacI and KpnI sites of pQE-T7-2, and successful cloning was confirmed by DNA sequence analysis.

For the overexpression of the YFP-tagged A2, plasmid pA2-YFP was transformed into *E. coli* One Shot BL21 Star (DE3) cells and selected on LB agar plates with 50 µg/mL kanamycin. A single colony harboring the plasmid was used to inoculate 5-mL preculture (LB medium supplemented with 50 µg/mL kanamycin) which was grown overnight at +30 °C. The cell growth was followed spectrophotometrically, and the following day, the preculture was used to inoculate a main culture of 150 mL (LB medium supplemented with 50 µg/mL kanamycin) to an optical density at 600 nm ($OD_{600}$) of 0.05. The main culture was grown at +37 °C in shaking until an $OD_{600}$ of 0.7 was reached, and IPTG (isopropyl β-D-1-thiogalactopyranoside) was added to a final concentration of 500 µM to induce fusion protein expression. The cultivation was then continued at +37 °C for 5 h. Thereafter, the cells were collected by centrifugation (10 min at 5 000g at +4 °C) and resuspended in 10 mL of lysis buffer supplemented with protease inhibitor cocktail. The cells were lysed by sonicating on ice, after which the resultant cell debris was removed by

centrifugation for 15 min at 15 000g at +4 °C. Successful expression of the fluorescent proteins was confirmed by analyzing the fluorescence emission of the soluble and insoluble fractions as well as the culture media.

The fluorescent fusion protein was purified from the cell lysate by HisTrap column according to the manufacturer's instructions. First, the clarified lysate was diluted (1:3, v/v) in binding buffer (20 mM phosphate buffer; pH 7.2, 500 mM NaCl and 20 mM imidazole) to ensure optimal binding conditions for the purification. After loading the sample in the HisTrap column, the column was washed with 30 mL of the binding buffer and finally the His-tagged proteins were eluted by adding elution buffer (20 mM phosphate buffer; pH 7.2, 500 mM NaCl and 500 mM imidazole). The presence of the fluorescent protein in the elution fractions was followed spectrophotometrically, and the fluorescent fractions were pooled. The buffer was exchanged to 50 mM Tris buffer (pH 7.75) containing 150 mM NaCl and 0.02% (w/v) $NaN_3$ with PD-10 according to the manufacturer's instructions. Finally, the protein concentration of the purified A2-YFP was determined using the BCA assay kit.

### Protein coupling to magnetic beads

For the magnetic bead assays, the anti-$FB_1$ antibody or neutravidin were conjugated to carboxylated magnetic microbeads. First, the beads (1 mg for antibody coupling, 2 mg for neutravidin coupling) were washed twice with 0.01 M NaOH, followed by three washes with milli-Q water and a final wash with buffer A (100 mM MES, pH 5.7; 0.01% SDS). Beads were resuspended in buffer A, and 79 mM EDC and 113 mM sulfo-NHS were added to a final reaction volume of 200 µL (1 mg beads) or 1000 µL (2 mg beads). The reaction was incubated for 2 h at room temperature in shaking after which the beads were washed three times with buffer B (10 mM phosphate buffered saline, pH 7.4; 0.01% SDS), and 20 µg of antibody or 175 µg of neutravidin in buffer B were added to reach the total volume of 100 µL or 530 µL, respectively. Incubation was continued for 4 h, and after aspiration of the buffer, the antibody-coupled beads were blocked in StartingBlock (TBS) Blocking Buffer and the neutravidin-coupled beads in Blocker Casein for 1 h. Finally, the beads were washed with the blocking buffer three times and stored at +4 °C in the same buffer.

### MB-ELISA with phage-displayed mimotope

For the magnetic bead–based ELISA (MB-ELISA) using the phage-displayed peptide, antibody-coupled magnetic beads (0.05 mg $mL^{-1}$) were mixed with A2-phage ($2\times10^9$ pfu $mL^{-1}$) and the toxin standards in the range of 0–100 ng $mL^{-1}$ (in three replicates) in microcentrifuge tubes previously blocked with the Blocker Casein. The assay buffer was PBS, pH 7.4; 0.05% (v/v) Tween-20; 0.1% (w/v) BSA and the total reaction volume 100 µL. After 1 h incubation with shaking at room temperature, the beads were washed twice with PBS-T (PBS, pH 7.4; 0.05% (v/v) Tween-20). Then, HRP-labeled secondary antibody (anti-M13-HRP) was added to each tube (1:5000-dilution), and the incubation was continued for 30 min. Finally, the beads were washed as described previously, resuspended in 50 µL of assay buffer and transferred to the wells of a black 96-well plate. Amplex UltraRed reagent was mixed with hydrogen peroxidase according to the manufacturer's instructions, and 50 µL of the substrate solution was added to each well.

The fluorescence signals (excitation at 530 nm and detection at 590 nm) were measured using a CLARIOstar microplate reader from BMG Labtech (Ortenberg, Germany).

### MB-ELISA with the synthetic peptide

The MB-ELISA with the synthetic peptide was performed in the wells of a clear Greiner 96-well plate previously blocked with Blocker Casein during 1 h at room temperature. For the competitive pre-incubation step, the synthetic peptide A2-bio (1 µg $mL^{-1}$) together with the anti-$FB_1$ (100 ng $mL^{-1}$) were first mixed with the toxin standards in the range from 0 to 1000 ng $mL^{-1}$ (in three replicates) in a total reaction volume of 200 µL in PBS-T (PBS, pH 7.4; 0.05% (v/v) Tween-20). After 30 min incubation with shaking at room temperature, neutravidin-coupled magnetic beads (6.5 µg in 10 µL) were added to each well and incubation was continued for another 30 min. The beads were washed three times using a plate washer with magnetic support (HydroFlex, Tecan, Switzerland) with the same buffer, and the HRP-labeled anti-IgG secondary antibody (0.26 µg $mL^{-1}$ in a total volume of 200 µL per well) was added to each well followed by 30 min incubation at room temperature. Finally, the beads were washed three times as described previously, and the fluorescence signals were measured after addition of the Amplex UltraRed substrate as described before.

### Fluorescent protein immunoassay

For the fluorescent protein A2-YFP assay on magnetic beads, 100 ng of anti-$FB_1$ was mixed with 200 ng of A2-YFP together with the toxin standards in the range of 0–100 ng $mL^{-1}$ (in three replicates) in microcentrifuge tubes previously blocked with Casein in a total reaction volume of 60 µL using the same assay buffer as reported previously. After 1 h incubation with shaking at room temperature, protein G -beads (10 µg in 40 µL) were added to each tube, and the incubation was continued for another 15 min. The beads were then washed three times with PBS-T and finally resuspended in 20 µL of assay buffer and transferred to the wells of a black 384-well plate. Fluorescence signals (excitation at 500 nm; detection at 545 nm) from each well were measured with the microplate reader.

### Data analysis

For the mycotoxin calibrations, the fluorescence signals were normalized to the minimum and maximum signals and analyzed with Origin Pro 9.0 software (OriginLab Corp., Northampton, MA, USA) using the four-parameter logistic regression (4-PL) model (**equation 1**):

$$y = A_{min} + \frac{(A_{max} - A_{min})}{1 + \left(\frac{x}{IC_{50}}\right)^{b}} \qquad (1)$$

where $A_{max}$ is the asymptotic maximum, $A_{min}$ the asymptotic minimum, and $b$ and $IC_{50}$ are the slope of the curve and analyte concentration, respectively, at the inflection point. For comparing the different assays, the sensitivity defined as the lower limit of detection (LOD) was determined as the concentration for which the antibody binding to the mimotope was inhibited by 10%, and the dynamic range was defined as the toxin concentrations leading to inhibition between 20% and 80% ($IC_{20}$–$IC_{80}$).

### Affinity measurements by SPR

Surface plasmon resonance (SPR) analysis on BIAcore X100 (GE Healthcare) was performed to determine the affinity constant and binding kinetics of the interaction between the phage-borne, synthetic, or recombinant mimotopes (namely A2-phage, A2-bio, and A2-YFP, respectively) and the target antibody. For the analysis, each ligand was captured by a covalently coupled antibody (anti-mouse IgG, anti-biotin IgG, or anti-phage IgG) to the surface of a sensor chip CM5, or CM3 in case of the phage analysis. Covalent antibody immobilization of was carried out using the amine coupling kit by BIAcore following the manufacturer's instructions. Briefly, the carboxyl derivatized surface of the chip was first activated with EDC/NHS, afterwhich, the anti-mouse IgG (30 μg $mL^{-1}$ in 10 mM sodium acetate pH 5.0), the anti-biotin IgG (100 μg $mL^{-1}$ in 10 mM sodium acetate pH 5.0), or the anti-phage IgG (100 μg $mL^{-1}$ in 10 mM sodium acetate pH 5.5) were immobilized with approximately 5000, 9000, and 4000 response units (RUs), respectively. After capture antibody injection, the remaining active sites on the chip were blocked by injecting 1 M ethanolamine. Both the reference and sample channels were treated equally on all the chips.

For the A2-YFP analysis, the mouse anti-$FB_1$ antibody (5 μg $mL^{-1}$) diluted in the running buffer (20 mM phosphate buffer, pH 8.0; 200 mM NaCl; 0.1% Tween-20) was injected in the sample channel of the anti-mouse coupled CM5 chip, at a flow rate of 5 μL $min^{-1}$ for 150 s leading to a response of approximately 350 RU. A2-YFP was then injected in running buffer at concentrations ranging from 0 to 500 nM, in both the reference and sample channels at a flow rate of 30 μL $min^{-1}$ for 180 s. The chip surface was regenerated between cycles by injection of 10 mM glycine-HCl pH 1.7 at a flow rate of 5 μL $min^{-1}$ for 400 s.

For the A2-bio analysis, the synthetic A2-bio (20 ng $mL^{-1}$) was injected in the sample channel of the anti-biotin coupled CM5 chip in the same running buffer at a flow rate of 5 μL $min^{-1}$ for 180 s leading to a response of approximately 8 RU. Anti-$FB_1$ was then injected in the running buffer at concentrations ranging from 0 to 500 nM, in both the reference and sample channels at a flow rate of 30 μL $min^{-1}$ for 180 s. Between cycles, the surface was regenerated by injection of 10 mM glycine-HCl (pH 3.0) at a flow rate of 5 μL $min^{-1}$ for 400 s.

For the phage analysis, the A2-phage ($10^{13}$ pfu $mL^{-1}$) was coupled to the sample channel of the anti-phage functionalized CM3 chip in the running buffer, at a flow rate of 5 μL $min^{-1}$ for 180 s leading to a response of approximately 40 RU. The anti-$FB_1$ antibody, at 1000 nM concentration in the running buffer, was then injected in both the reference and sample channels at a flow rate of 30 μL $min^{-1}$ for 180 s. As no binding was seen, an anti-phage-HRP was injected as a control to confirm the successful capture of the phage. The binding data with A2-YFP and A2-bio were fit to a 1:1 Langmuir binding model for calculation of the kinetic parameters using the BIAcore evaluation software. The affinity constant ($K_D$) values were derived from the kinetic constants by the quotient between the association rate ($k_{on}$) and the dissociation rate ($k_{off}$).

## 3.2.3.3 Results and discussion

### Phage-based immunoassays

Phage display is a robust technique to search for epitope mimics even without prior knowledge of the antibody–antigen interactions. After identifying a novel epitope mimicking peptide, or

mimotope, using phage display, the most straightforward approach is probably the use of the peptide linked to the phage for the assay development. We have previously identified $FB_1$-mimotope, named A2, from the Ph.D.-12 commercial dodecapeptide library (New England Biolabs).[20] After pannings, the epitope mimicking nature of A2 was demonstrated in a competitive immunoassay using the phage-displayed mimotope and the anti-$FB_1$ antibody immobilized onto a microtiter plate. The lower detection limit (LOD) defined as the $FB_1$ for which the antibody binding to the peptide was inhibited by 10%, was 7.47 ng $mL^{-1}$ and the $IC_{50}$ value 38.7 ng $mL^{-1}$, as previously reported.[20]

The antibody immobilization procedure is evidently one of the crucial factors affecting the assay performance in all heterogeneous immunoassays which inherently rely on immobilizing one of the assay components.[1] To further improve the detection limit we transferred the phage-based $FB_1$ ELISA to a magnetic bead–based assay format (MB-ELISA, **Figure 40A**) where the anti-$FB_1$ was immobilized on magnetic beads rather than non-specifically on the surface of a microtiter plate. The MB-ELISA showed significantly improved sensitivity in comparison with the assay on the 96-well plate, which could be attributed to the increased surface area of the beads compared to the plate. The sensitivity in terms of the LOD and $IC_{50}$ value was 0.87 ng $mL^{-1}$ and 2.70 ng $mL^{-1}$, respectively (**Figure 41**).

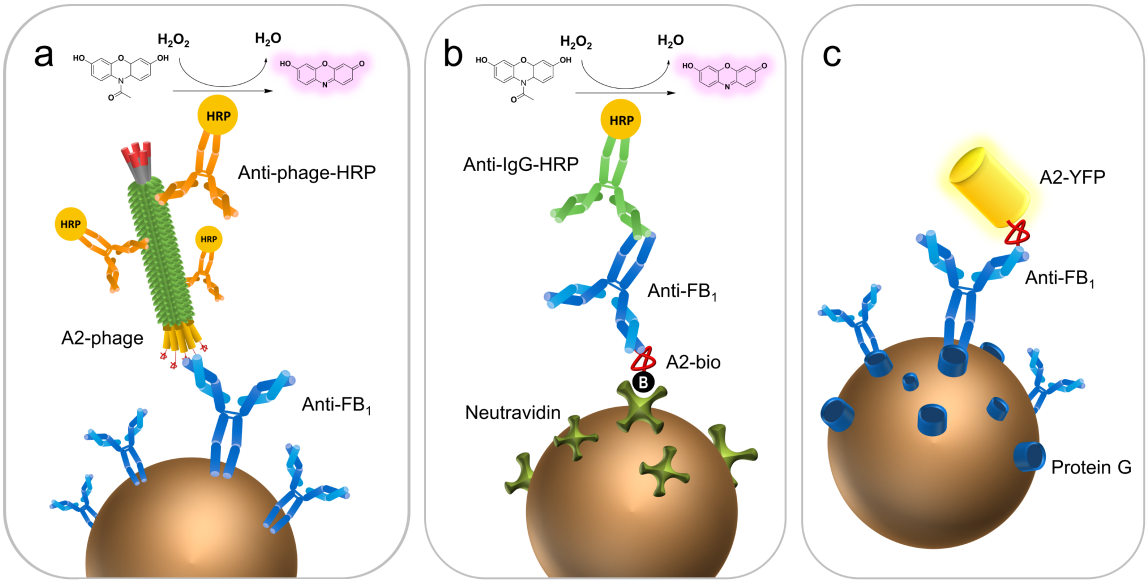


**Figure 40**. Principles of the competitive immunoassays based on magnetic beads and mimotopes either in (a) phage-displayed (A2-phage), (b) synthetic (A2-bio), or (c) recombinant fusion protein (A2-YFP), optimized in this work. *Abbreviations: bio, biotin; $FB_1$, fumonisin $B_1$; HRP, horse-radish peroxidase; YFP, yellow fluorescent protein.*

## Use of the synthetic mimotopes

Despite their wide use in research, there exist some safety concerns to use phages, bacterial viruses, for diagnostic purposes.[32] We recently showed how the phage-displayed mimotope for $FB_1$ could be replaced by its synthetic counterpart for $FB_1$ detection. The peptide-based immunoassay in a microarray format showed an LOD of 11.1 ng $mL^{-1}$ and held promise for adaptation to a multiplexed immunoassay by including other mycotoxins in the same

microarray.[20] The microarray-based immunoassay relied on the use of a fluorescently labeled secondary antibody, and in order to improve the sensitivity, this label was replaced by an enzyme, horse-radish peroxidase (HRP), and applied in a magnetic bead assay format (MB-ELISA) (**Figure 40B**). The use of an enzymatic label could improve the detection limits obtained in immunoassays because of the signal amplification achieved since each enzyme can catalyze many cycles of conversions of substrate molecules to the fluorescent product, leading to an increase in the analytical signal. In fact, the $IC_{50}$ value (1.85 ng $mL^{-1}$) obtained with the MB-ELISA was 20-fold lower than with the microarray (37.1 ng $mL^{-1}$). Moreover, since the magnetic beads allowed immobilization of a higher amount of peptide on their surface compared to the spots in the array, the dynamic range (0.13–25.6 ng $mL^{-1}$) was also substrantially wider than for the microarray (17.3–79.6 ng $mL^{-1}$). Unlike in the microarray where the peptide was spotted on the surface of the chip prior to the assay, the MB-ELISA format included a competitive pre-incubation step where the peptide and $FB_1$ were mixed together with the antibody and incubated in solution. Subsequently, the peptide-bound antibodies were captured by the neutravidin-coupled MBs *via* the biotin-linker on the peptide (A2-bio). The solution-based competitive binding to the antibody provided faster kinetics and resulted in a lower sensitivity, with an LOD of 0.029 ng $mL^{-1}$ (**Figure 41**).

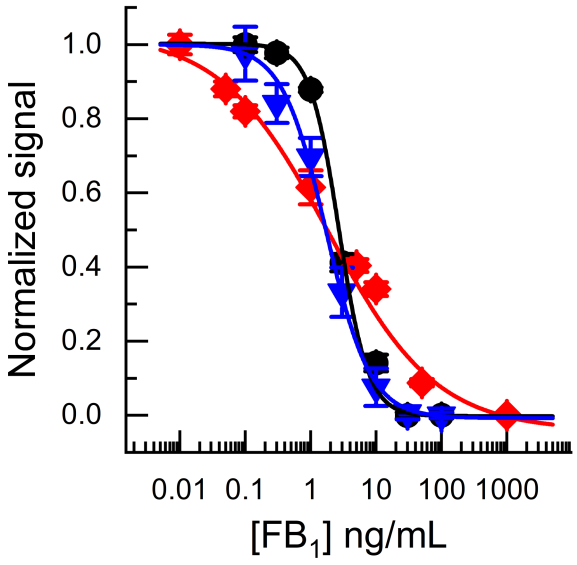


**Figure 41**. Mimotope-based assays on magnetic beads using the A2-phage (black circles), synthetic A2-bio (red diamonds), or recombinant A2-YFP (blue triangles). The signals (normalized to the maximum and minimum values) are depicted as the average of three replicates ± standard error of the mean ($n$ = 3). The response was fitted to a four-parameter logistic curve fit (Origin 9.0).

### Assays with the recombinant fusion mimotope

The synthetic peptide–based assays showed improved analytical characteristics compared with the phage-based assay, but nevertheless, the use of synthetic peptides relied on chemical synthesis which is susceptible to batch-to-batch variations and can be costly if dependent on

commercial providers. To overcome such limitations, we further studied the possibility of using the mimotope as a fusion partner with a fluorescent protein. Such recombinant fusion proteins can be produced cost-effectively in bacteria even in large quantities, and the fusion protein can be designed by genetic engineering to include, for example, specific tags which will enable simple purification or immobilization. Moreover, by using a fluorescent protein as the second part of the fusion protein, the mimotope can be readily produced with a label and could be directly used as the tracer. Thus, neither separate labeling reactions with additional purification steps, nor secondary antibodies are required for the immunoassay. With these considerations in mind, we described previously the construction of a fusion protein of the mimotope A2 and the yellow fluorescent protein (YFP), ZsYellow. The fusion protein was expressed in *E. coli*, and after affinity purification using the C-terminal polyhistidine tag, the fusion protein was used directly in the immunoassay, either in a heterogeneous or a homogeneous assay format where the antibody was immobilized on a microtiter well plate or gold nanoparticles, respectively.[37]

The main advantage of using YFP-tagged mimotope (A2-YFP) was the simplified assay protocol which consisted of only one incubation step, since no secondary antibody was needed. The LOD and $IC_{50}$ values of the plate-based heterogeneous assay were 2.01 ng $mL^{-1}$ and 6.83 ng $mL^{-1}$, respectively, which demonstrated not only that the novel YFP-tagged mimotope could function as the competitor in the assay but also that the assay format and the YFP as a label could provide good sensitivity. The homogeneous assay using gold nanoparticles and fluorescence quenching as the sensing mechanism resulted in a somewhat higher $IC_{50}$ value (12.9 ng $mL^{-1}$), the approach but could benefit from a more straightforward and faster assay protocol.[37]

Considering the tendency of improving the assay sensitivity significantly bu using magnetic beads, also the heterogeneous A2-YFP assay was transferred to the MB format (**Figure 40C**). By using protein G–coupled beads to capture the antibody, the competition step between the mimotope and the mycotoxin for the antibody binding sites was performed in solution subsequently capturing the immunocomplex with protein G–beads. As anticipated, the MB-assay provided improved sensitivity with an LOD of 0.31 ng $mL^{-1}$ and an $IC_{50}$ value of 1.72 ng $mL^{-1}$ (**Figure 41**), which could be the result of not only the large surface area of magnetic beads but also the pre-incubation step in solution and the use of protein G for oriented antibody immobilization. Nevertheless, partly due to lower absolute signals in comparison with the plate-based assay, the measurement of the fluorescence of the YFP on the MB surface was not as reproducible as the measurements from the bottom of the well plate, which resulted in higher within assay relative standard deviation (RSD) values from the MB-assay (9.4%) than from the plate assay (6.4%). However, by automating the magnetic bead handling or by exploring alternative measurement schemes for the beads instead of the microplate reader, we believe that the detection and reproducibility of the bead-based assay could be improved in the future.

### Analysis of binding kinetics

In order to examine the mimotope binding to the target antibody more accurately, and above all, independently of the other assay components, SPR analyses were performed with a BIAcore instrument. Since the response in SPR is roughly proportional to the size of the analyte and due to the vast differences in the sizes of the different mimotopes (~14 MDa A2-phage; 29 kDa

A2-YFP; 2035 Da A2-bio), it was not feasible to measure all the interactions using in the same assay format.

Despite the wide use of phage display for mimotope discovery, there are only a few studies reporting the binding kinetics of phage-displayed mimotopes.[40] More often such analyses involve the expression of the displayed protein or peptide as a fusion in the absence of the phage itself. As in this case we were particularly interested in the kinetics of the mimotope binding in the context of the phage, the A2-phage was immobilized on the sensor surface with a covalently coupled anti-phage capture antibody. The anti-$FB_1$ antibody was passed through the chip surface as the analyte. However, no binding was seen at the antibody concentrations tested (1000 nM) under the ligand capture conditions achieved, which suggests a poor accessibility of phage-displayed the mimotope for the selective binding sites. Successful immobilization of the phage was anyhow observed as the anti-phage-HRP was shown to bind specifically to the sample channel after the A2-phage immobilization (**Figure 42A**).

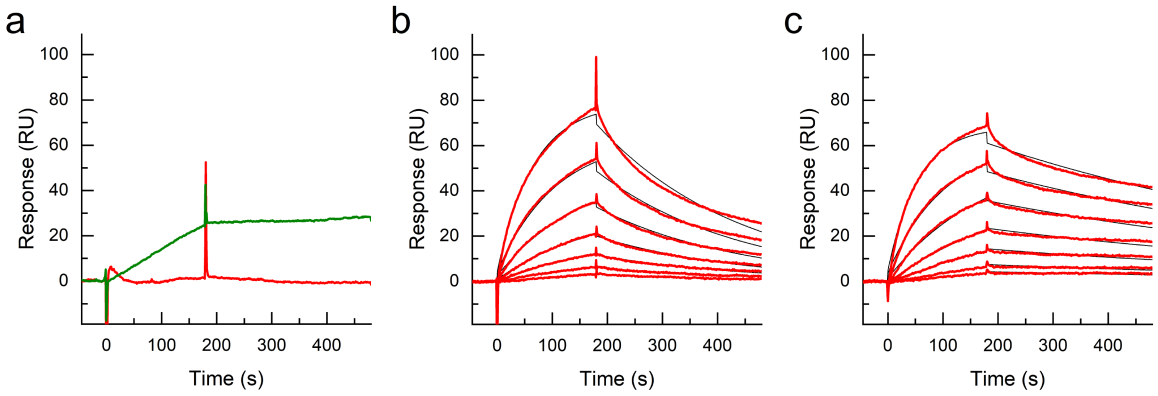


**Figure 42**. Kinetic analyses by surface plasmon resonance (SPR). (A) Analysis with the A2-phage did not show a measurable signal with the anti-$FB_1$ (red) although successful immobilization of the phage could be confirmed with the anti-phage antibody (green). (B) Binding of the anti-$FB_1$ antibody (0–500 nM) to the immobilized synthetic mimotope A2-bio, and (C) the recombinant A2-YFP (0–500 nM) to the immobilized anti-$FB_1$. Sensorgrams obtained for seven different concentrations (red) are shown in for each mimotope together with the data fitted (black) to a 1:1 binding model.

Owing to the small size of the synthetic A2-bio, the peptide was bound to the sample channel *via* its biotin-linker using a sensor chip with a covalently coupled anti-biotin capture antibody. Different concentrations of the anti-$FB_1$ antibody (0–500 nM) were then passed through the sensor surface as the analyte (**Figure 42B**). The binding association ($k_{on}$) and dissociation ($k_{off}$) rates could be measured leading to a $K_D$ of 170nM. Interestingly, the analysis of A2-YFP with the immobilized anti-$FB_1$ antibody provided the best affinity values ($K_D$ 38 nM), as the measured $k_{on}$ was faster and the $k_{off}$ slower than than for the synthetic peptide (**Figure 42C**). A comparison of the binding parameters determined by SPR analyses is shown in **Table 11**.

**Table 11**. Calculated binding parameters from the SPR analyses (**Figure 42**) including the association ($k_{on}$), dissociation ($k_{off}$) and equilibrium dissociation ($K_D$) constants.

| Mimotope | $K_D$ | $k_{on}$ ($M^{-1}$ $s^{-1}$) | $k_{off}$ ($s^{-1}$) |
|---|---|---|---|
| A2-phage | *n.d.* | *n.d.* | *n.d.* |
| A2-bio | 170 nM | $2.27 \times 10^4$ | $3.85 \times 10^{-3}$ |
| A2-YFP | 38 nM | $3.49 \times 10^4$ | $1.33 \times 10^{-3}$ |

## Comparison of the $FB_1$ immunoassay formats

New technologies have spurred the development of novel methods for mycotoxin detection, and notably, the use of mimotopes has become an exciting alternative for mycotoxin immunoassays. Several research groups have reported various immunoassays using mimotopes, most commonly with the phage-borne peptide but more recently also with the synthetic counterpart of this peptide, or a recombinant fusion protein. We have previously selected a mimotope for mycotoxin $FB_1$, and in this work, the mimotope was applied to various immunoassays using either the phage-borne, synthetic, or recombinant fusion mimotope. The assay with the synthetic peptide in a magnetic bead–based ELISA (MB-ELISA) provided the best sensitivity which could be attributed to a pre-incubation step in solution prior to the magnetic bead capture, the high surface area provided by the magnetic beads and the signal amplification by the enzymatic reaction. The effect of the bead-based format on the assay sensitivity was also observed using the phage-borne peptide and the recombinant YFP-tagged mimotope. Although the use of the YFP-tagged mimotope did not improve the the sensitivity of the assay in comparison with the synthetic peptide assay, its application can be regarded as a highly attractive alternative as no secondary antibodies or separate labeling reactions are required.

A systematic comparison of the analytical characteristics of the immunoassays optimized using the different mimotopes and assay formats is presented in **Table 12**. Whilst the microarray-based method could be an advantageous tool for multiplexed mycotoxin analysis, in comparison with the other methods, it shows the highest detection limit for $FB_1$, although the value is well belowe the EU regulatory levels.[20] Moreover, microarray development requires the most complex instrumentation since a microarray printer and fluorescent scanner are needed. Nonetheless, the same assay format as in the microarray using the synthetic peptide shows great promise in the MB-ELISA. In particular, the wide dynamic range and low detection limit obtained with this approach demonstrate the advantages of using magnetic beads for the analysis. The major improvement in the sensitivity compared to the microarray is most likely due to, not only the use of magnetic beads, but also the enzymatic detection. As the MB-ELISA is based on the use of a secondary antibody labeled with an enzyme, instead of the AF647-label as in the microarray, signal amplification evidently leads to an increment of the analytical signal. Similarly, the use of the HRP-labelled secondary antibody in combination with the phage-based assays could be seen as a signal amplification method and possibly has great effect on the assay sensitivity. Moreover, since the HRP-labelled anti-phage antibody targets the phage major coat protein pVIII which is present in usually more than 2000 times in one phage, significant signal amplification can be achieved. Finally, perhaps a bit surprisingly, the YFP-tagged mimotope assays were able to compete with the enzyme-based methods in terms of sensitivity.

As discussed previously, the immunoassay sensitivity, which is inherently highly dependent on the affinity of the target-specific antibody,[1] can be affected by the choice of the label and the immobilization support, among other factors. Moreover, the performance of a competitive immunoassay depends not only on the affinity of the target analyte but also on the affinity of the competitor. Often a slightly lower affinity of the competitor can be advantageous since a smaller amount of the analyte is needed for the competition, leading to higher sensitivities.[27,41,42] With many factors changing among the immunoassays tested, the abovementioned assays with the phage-displayed, synthetic, or recombinant mimotopes do not actually provide sufficient information to draw conclusions about the affinity of the mimotopes. Therefore, we decided to perform kinetic analysis of the different mimotope formats by SPR in order to conclude if the differences in the sensitivities of the various immunoassays tested could arise from the variation of the binding affinities. Although the peptide sequence was the same in all cases, it is noteworthy that the presence of the fluorescent protein or the phage can affect the binding kinetics. The results of the SPR were not conclusive in all the aspects as the experiments with the phage-displayed peptide could not provide any numerical values of the affinity. Nevertheless, it could be concluded that the phage binds poorly to the antibody, perhaps due to the large size of the phage which might lead to the slow association. The phage-displayed peptide is expressed outside the phage virion as a fusion with the minor coat protein pIII which is present in the phage in five copies clustered at one end of the mature phage leading to pentavalent display of the peptides.[43] Thus, in the immunoassay, the avidity also might have a significant effect in comparison to the synthetic peptide or fluorescently-tagged mimotope. As mentioned earlier, the substantial signal amplification of the HRP-labelled antibody in the phage-based immunoassays could explain why the A2-phage with a seemingly poor binding is still performing mediocrely in the assay.

In the case of the synthetic A2-bio and recombinant A2-YFP, the measured $K_D$ values were in the nanomolar range. Significant differences could be seen in both the association and dissociation phases; the synthetic peptide showed a slower association rate and a faster dissociation rate than A2-YFP leading also to a higher $K_D$. These differences observed in the kinetic analyses suggest a more appropriate folding of the antibody epitope in the context of the recombinant fusion protein mimotope than for the synthetic peptide. When comparing the MB-based immunoassays, both of these peptides showed a very similar sensitivity in terms of the $IC_{50}$ value. However, the synthetic peptide provides a much wider dynamic range and lower detection limits, which we have previously attributed to the use of a pre-incubation step prior to the capture with the magnetic beads. Based on the kinetic analysis, we can also conclude that the lower affinity of the synthetic peptide to the antibody might also be an important feature for the improved sensitivity as a smaller amount of the toxin is required to compete with the mimotope.

**Table 12**. Comparison of the immunoassays using the $FB_1$ mimotope A2 as phage-displayed (A2-phage), synthetic with a biotin linker (A2-bio) or recombinant format (A2-YFP).

| Mimotope | Immobilization support | $IC_{50}$ (ng/mL) | LOD* (ng/mL) | Dynamic range** (ng/mL) | Average RSD | Ref. |
|---|---|---|---|---|---|---|
| A2-phage | 96-well plate | 38.7 | 7.47 | 13.7–109 | 4.7 % | [20] |
| A2-phage | MB | 2.70 | 0.87 | 1.32–5.51 | 12.6 % | This work |
| A2-bio | Microarray | 37.1 | 11.1 | 17.3–79.6 | 9.2 % | [20] |
| A2-bio | MB | 1.85 | 0.029 | 0.13–25.6 | 9.5% | This work |
| A2-YFP | 96-well plate | 6.83 | 2.01 | 3.16–14.8 | 6.4% | [37] |
| A2-YFP | – *homogeneous* | 12.9 | 5.29 | 7.34–22.6 | 4.6% | [37] |
| A2-YFP | MB | 1.72 | 0.31 | 0.59–5.04 | 9.4% | This work |

*Abbreviations: MB, magnetic beads; RSD, relative standard deviation; YFP, yellow fluorescent protein.*
** LOD defined as the concentration in which the antibody binding to the mimotope was inhibited by 10%*
***Dynamic range defined between 20 and 80% inhibition, i.e., $IC_{20}$–$IC_{80}$*

### 3.2.3.4 Conclusions

In this work, we have developed immunoassays for FB1 detection based on mimotopes originally selected by phage display. A systematic comparison of various immunoassays based on the $FB_1$-mimotope, named A2, was conducted using the phage-displayed mimotope as well as a fluorescent recombinant fusion protein and a synthetic peptide with a biotin-linker. Furthermore, in order to improve the assay sensitivity and working range, immunoassays based on magnetic beads and enzymatic detection were established. Comparison of the assay performance showed the best sensitivity using the synthetic mimotope together with enzymatic detection and magnetic beads as the immobilization support which could be traced back to the large surface of the beads area available for the immobilization as well as the signal amplification by the enzyme and a solution-based competitive binding between the antibody its target. Moreover, analysis of the binding kinetics by SPR further reinforced the suitability of the synthetic peptide for the competitive immunoassay as this mimotope showed a slightly lower affinity for the target antibody in comparison with the recombinant fusion protein. Together these comparative results of the immunoassays and SPR can provide important insights for the development of novel mimotope-based immunoassays for various low molecular weight targets in the future.

#### Acknowledgments

This research was funded by the Spanish Ministry of Economy and Competitiveness grant number CTQ2015-69278-C2-1-R/AIE and RTI2018-096410-B-C21. R.P. acknowledges UCM for a predoctoral grant and R.B. the PI17CIII/00045 grant from the AES-ISCIII program.

## 3.2.3.5 References


1. The Immunoassay handbook*: Theory and applications of ligand* binding ELISA and related techniques, 4th ed.; Wild, D., (Editor); Elsevier Science, Oxford, UK, **2013.**
2. Chauhan, R.; Singh, J.; Sachdev, T.; Basu, T.; Malhotra, B. D. Recent advances in mycotoxins detection. *Biosens. Bioelectron.* **2016**, *81*, 532–545.
3. Qiu, Y.-L.; He, Q.-H.; Xu, Y.; Bhunia, A. K.; Tu, Z.; Chen, B.; Liu, Y.-Y. Deoxynivalenol-mimic nanobody isolated from a naïve phage display nanobody library and its application in immunoassay. *Anal. Chim. Acta* **2015**, *887*, 201–208.
4. Xiao, H.; Clarke, J. R.; Marquardt, R. R.; Frohlich, A. A. Improved methods for conjugating selected mycotoxins to carrier proteins and dextran for immunoassays. *J. Agric. Food Chem.* **1995**, *43*, 2092–2097.
5. Peltomaa, R.; Benito-Peña, E.; Moreno-Bondi, M. C. Bioinspired recognition elements for mycotoxin sensors. *Anal. Bioanal. Chem.* **2018**, *410*, 747–771.
6. Berthiller, F.; Brera, C.; Crews, C.; Iha, M. H.; Krska, R.; Lattanzio, V. M. T.; *et al.* Developments in mycotoxin analysis: An update for 2014-2015. *World Mycotoxin J.* **2016**, *9*, 5–30.
7. Freire, F. D. C. O.; da Rocha, M. E. B. Impact of mycotoxins on human health. In *Fungal Metabolites*; Mérillon, J.-M., Ramawat, K. G., Eds.; Springer International Publishing: Cham, Switzerland. **2016**; pp 1–23.
8. Goyal, S.; Ramawat, K. G.; Mérillon, J. M. Different shades of fungal metabolites: an overview. In *Fungal Metabolites*; Merillon, J.-M., Ramawat, K. G., Eds.; Springer International Publishing: Cham, Switzerland. **2016**; pp 1–29.
9. Bennett, J. W.; Klich, M. Mycotoxins. Clinical Microbiol. Reviews 2003, 16, 497–516.
10. European Commission. Commission regulation (EC) No 1881/2006. *Off. J. Eur. Union* 2006, L364, 5–24.
11. European Commission. Commission regulation (EC) No 1126/2007. *Off. J. Eur. Union* **2007**, *L255*, 14–17.
12. European Commission. Commission regulation (EC) No 105/2010. *Off. J. Eur. Union* **2010**, *L37*, 7–8.
13. European Commission. Commission regulation (EC) No 165/2010. *Off. J. Eur. Union* **2010**, *L50*, 8–12.
14. Senyuva, H. Z.; Gilbert, J.; Stroka, J., Determination of fumonisins $B_1$ and $B_2$ in corn by LC/MS with immunoaffinity column cleanup: Interlaboratory study. *J. AOAC Int.* **2010,** *93*, 611–621.
15. Solfrizzo, M. De. Girolamo, A.; Gambacorta, L.; Visconti, A.; Stroka, J.; van Egmond, H. P., Determination of fumonisins $B_1$ and $B_2$ in corn-based foods for infants and young children by lc with immunoaffinity column cleanup: Interlaboratory validation study. *J. AOAC Int.* **2011,** *94*, 900–908.
16. Goryacheva, I. Y.; Saeger, S. D.; Eremin, S. A.; Peteghem, C. V. Immunochemical methods for rapid mycotoxin detection: evolution from single to multiple analyte screening: A review. *Food Additives and Contaminants* **2007**, *24*, 1169–1183.
17. Köppen, R.; Koch, M.; Siegel, D.; Merkel, S.; Maul, R.; Nehls, I. Determination of mycotoxins in foods: current state of analytical methods and limitations. *Appl. Microbiol. Biotechnol.* **2010**, *86*, 1595–1612.
18. Wang, Y.; Wang, H.; Li, P.; Zhang, Q.; Kim, H. J.; Gee, S. J.; Hammock, B. D. Phage-displayed peptide that mimics aflatoxins and its application in immunoassay. *J. Agric. Food Chem.* **2013**, *61*, 2426–2433.
19. Yuan, Q.; Pestka, J. J.; Hespenheide, B. M.; Kuhn, L. A.; Linz, J. E.; Hart, L. P. Identification of mimotope peptides which bind to the mycotoxin deoxynivalenol-specific monoclonal antibody. *Appl. Environ. Microbiol.* **1999**, *65*, 8.
20. Peltomaa, R.; Benito-Peña, E.; Barderas, R.; Sauer, U.; González Andrade, M.; Moreno-Bondi, M. C. Microarray-based immunoassay with synthetic mimotopes for the detection of fumonisin$B_1$. *Anal. Chem.* **2017**, *89*, 6216–6223.
21. Xu, Y.; Chen, B.; He, Q.; Qiu, Y.-L.; Liu, X.; He, Z.; Xiong, Z. New approach for development of sensitive and environmentally friendly immunoassay for mycotoxin fumonisin $B_1$ based on using peptide-MBP fusion protein as substitute for coating antigen. *Anal. Chem.* **2014**, *86*, 8433–8440.
22. Liu, X.; Xu, Y.; He, Q.; He, Z.; Xiong, Z. Application of mimotope peptides of fumonisin $B_1$ in peptide ELISA. *J. Agric. Food Chem.* **2013**, *61*, 4765–4770.
23. Liu, R.; Yu, Z.; He, Q.; Xu, Y. An immunoassay for ochratoxin a without the mycotoxin. *Food Control* **2007**, *18*, 872–877.

24. Lai, W.; Fung, D. Y. C.; Yang, X.; Renrong, L.; Xiong, Y. Development of a colloidal gold strip for rapid detection of ochratoxin a with mimotope peptide. *Food Control* **2009**, *20*, 791–795.
25. He, Z.; He, Q.; Xu, Y.; Li, Y.; Liu, X.; Chen, B.; Lei, D.; Sun, C. Ochratoxin A mimotope from second-generation peptide library and its application in immunoassay. *Anal. Chem.* **2013**, *85*, 10304–10311.
26. Xu, Y.; He, Z.; He, Q.; Qiu, Y.; Chen, B.; Chen, J.; Liu, X. Use of cloneable peptide–MBP fusion protein as a mimetic coating antigen in the standardized immunoassay for mycotoxin ochratoxin A. *J. Agric. Food Chem.* **2014**, *62*, 8830–8836.
27. Zou, X.; Chen, C.; Huang, X.; Chen, X.; Wang, L.; Xiong, Y. Phage-free peptide ELISA for ochratoxin A detection based on biotinylated mimotope as a competing antigen. *Talanta* **2016**, *146*, 394–400.
28. He, Q.-H.; Xu, Y.; Huang, Y.-H.; Liu, R.-R.; Huang, Z.-B.; Li, Y.-P. Phage-displayed peptides that mimic zearalenone and its application in immunoassay. *Food Chem.* **2011**, *126*, 1312–1315.
29. Barbas, C.F.; Burton, D.R.; Silverman, G.J. *Phage Display: A Laboratory Manual*; Cold Spring Harbor: New York, **2001**.
30. Smith, G.P. Filamentous fusion phage: Novel expression vectors that display cloned antigens on the virion surface. *Science* **1985**, 228, 1315–1317
31. McCafferty, J.; Griffiths, A.D.; Winter, G.; Chiswell, D.J. Phage antibodies: Filamentous phage displaying antibody variable domains. *Nature* **1990**, *348*, 552–554.
32. Peltomaa, R.; López-Perolio, I.; Benito-Peña, E.; Barderas, R.; Moreno-Bondi, M. C. Application of bacteriophages in sensor development. *Anal. Bioanal. Chem.* **2016**, *408*, 1805–1828.
33. Smartt, A. E.; Ripp, S. Bacteriophage reporter technology for sensing and detecting microbial targets. *Anal. Bioanal.* Chem. **2011**, *400*, 991–1007.
34. Carlomagno, M.; Lassabe, G.; Rossotti, M.; González-Techera, A.; Vanrell, L.; González-Sapienza, G. Recombinant streptavidin nanopeptamer anti-immunocomplex assay for noncompetitive detection of small analytes. *Anal. Chem.* **2014**, *86*, 10467–10473.
35. Ding, Y.; Hua, X.; Chen, H.; Liu, F.; González-Sapien, G.; Wang, M. Recombinant peptidomimetic-nano luciferase tracers for sensitive single-step immunodetection of small molecules. *Anal. Chem.* **2018**, *90*, 2230–2237.
36. Ding, Y.; Hua, X.; Du, M.; Yang, Q.; Hou, L.; Wang, L.; Liu, F. Gonzalez-Sapienza G, Wang M (2018) Recombinant, fluorescent, peptidomimetic tracer for immunodetection of imidaclothiz. *Anal Chem*. **2018**, *90*, 13996–14002.
37. Peltomaa, R.; Amaro-Torres, F.; Carrasco, S.; Orellana, G.; Benito-Peña, E.; Moreno-Bondi, M. C. Homogeneous quenching immunoassay for fumonisin $B_1$ based on gold nanoparticles and an epitope-mimicking yellow fluorescent protein. *ACS Nano* **2018**, *12*, 11333–11342.
38. Matz, M. V.; Fradkov, A. F.; Labas, Y. A.; Savitsky, A. P.; Zaraisky, A. G.; Markelov, M. L.; Lukyanov, S. A. Fluorescent proteins from nonbioluminescent *Anthozoa* species. *Nature Biotechnol.* **1999**, *17*, 969–973.
39. Clontech (2002) Living Colors User Manual, vol II. Red Fluorescent Protein, Protocol PT3404−1. www.clontech.com. [Cited May 10, 2018].
40. He, Q.; Xu, Y.; Zhang, C.; Li, Y.; Huang, Z. Phage-borne peptidomimetics as immunochemical reagent in dot-immunoassay for mycotoxin zearalenone. *Food Control* **2014**, *39*, 56–61.
41. Ji, Y.; He, Q.; Xu, Y.; Tu, Z.; Yang, H.; Qiu, Y.; Wang, X.; Liu, Y. Phage displayed anti-idiotypic nanobody mediated immuno-pcr for sensitive and environmentally friendly detection of mycotoxin ochratoxin A. *Anal. Methods* **2016**, *8*, 7824–7831.
42. Shu, M.; Xu, Y.; Wang, D.; Liu, X.; Li, Y.; He, Q.; Tu, Z.; Qiu, Y.; Ji, Y.; Wang, X. Anti-idiotypic nanobody: a strategy for development of sensitive and green immunoassay for fumonisin $B_1$. *Talanta* **2015**, *143*, 388–393.
43. New England Biolabs (NEB) Ph.D. Phage Display Libraries - Instruction Manual. www.neb.com. [Cited January 31, 2019].

# *GAUSSIA* LUCIFERASE -BASED BIOLUMINESCENT IMMUNOASSAYS FOR MYCOTOXIN DETECTION

Riikka Peltomaa,[a] Trajen Head,[b] Elena Benito-Peña,[a] Sapna Deo,[b] Sylvia Daunert,[b,*] and María C. Moreno-Bondi[a,*]

[a] Department of Analytical Chemistry, Faculty of Chemistry, Complutense University, Ciudad Universitaria s/n, Madrid 28040, Spain.

[b] Department of Biochemistry and Molecular Biology, University of Miami Miller School of Medicine, Miami, FL 33136, USA.

* Corresponding authors

*Manuscript in preparation*

## Abstract

Mimotopes, or epitope mimicking peptides, have been introduced as an interesting alternative to the analyte-conjugates for competitive immunoassays for the detection of low molecular weight molecules, such as mycotoxins. In this work, we report the development of recombinant fusion proteins based on bioluminescent *Gaussia* luciferase (GLuc), the smallest known luciferase, and mimotopes for mycotoxins zearalenone (ZEA) and fumonisin $B_1$ ($FB_1$). The newly identified mimotope for ZEA and a previously reported mimotope for $FB_1$ were cloned as a fusion protein with GLuc that could be then used directly as the tracer for the toxin detection without the need of labeling or a secondary antibody. The bioluminescent immunoassays based on an immobilized antibody and the mimotope-GLuc fusions showed $IC_{50}$ values of 0.35 and 1.3 ng $mL^{-1}$, detection limits of 0.091 and 0.21 ng $mL^{-1}$, for ZEA and $FB_1$, respectively. Both assays demonstrated superior sensitivity that is significantly better than, for example, a previously reported assay using the fumonisins mimotope cloned as a fusion protein with a yellow fluorescent protein.

## 3.2.4.1 Introduction

Mycotoxins are low molecular weight natural contaminants produced as secondary metabolites by filamentous fungi.[1] The genus *Fusarium*, mainly *F. proliferatum, F. verticillioides, F: graminearum,* and *F. oxysporum*, is a renowned mycotoxin producer and one of the most abundant fungal species commonly found in agricultural products, especially in maize.[2,3] As a results of global warming, the geographic distribution of mycotoxigenic fungi can change as hot and dry conditions often favors the fungal infection and this can contribute to give rise to increased levels of mycotoxins in agricultural products.[4,5] Among the wide variety of mycotoxins produced by *Fusarium*, fumonisins, trichothecenes, and zearalenone account for the most important ones.[6] Fumonisins are common contaminants in maize but can also occur for example in wheat, sorghum, barley, soybean, and black tea. Among at least 15 different fumonisins identified,[7] fumonisin $B_1$ ($FB_1$) is the most prevalent and toxic. Based on animal studies and

cases of human esophageal cancer, the International Agency for Research on Cancer (IARC) has categorized $FB_1$ as possibly carcinogenic to humans (group 2B).[8] $FB_1$ bears a similar structure as cellular sphingolipids, and the toxicity of fumonisins appears to be a result of interference in the metabolism of sphingolipids by inhibiting the enzyme ceramide synthase.[7,9] Zearalenone (ZEA) is produced mainly in temperate regions where *Fusarium* contamination is frequent, most commonly at the field before harvesting, but might also occur during or post-harvest if the crops are not handled or dried properly.[9] ZEA is biologically potent and as its structure resembles sufficiently 17β-estradiol it is known for its estrogenic properties.[1]

Owing to the toxic effects, as well as the significant economic consequences of mycotoxin contamination, several international authorities, such as the European Commission[10,11] and the United States Food and Drug Administration,[12] have set regulatory limits for the major mycotoxins in food and feed. Currently, many analytical methods for mycotoxin analysis combine liquid or gas chromatographic separation (LC or GC) with a diode array (DAD), fluorescence (FLD) or mass spectrometric (MS) detection. Though these methods can provide excellent accuracy and reproducibility, they are usually expensive and require highly skilled personnel and tedious sample cleanup. In contrast, biosensors and bioanalytical assays are considered convenient for the rapid determination of these toxins, as they are usually low cost while maintaining the required sensitivity and specificity.[13,14]

Development of bioaffinity assays for small molecules, such as mycotoxins, poses some particular challenges mainly because they consist of only one epitope and thus usually must be detected in the competitive assay format.[15,16] A major limitation of this format is the requirement to conjugate the target molecule to a carrier protein or a label which allows the immobilization or detection of this competitor.[17] In some cases, synthesis or chemical conjugation of these competitors can be challenging and time-consuming or result in a heterogeneous mixture of randomly cross-linked or unstable molecules which in the worst case are not recognized by the antibody any longer. The exceptional ability of epitope-mimicking peptides, or mimotopes, to imitate the epitope of the analyte and thus bind to same antibody paratope, has been presented as an intriguing option to overcome these limitations in the competitive immunoassays.[15]

Several mimotopes have been selected from phage-displayed peptide libraries for the detection of low molecular weight targets such as pesticides,[18] neurotoxins,[19] cancer drugs,[20] and mycotoxins.[21–23] Phage display provides an elegant method to identify mimotopes from phage-displayed peptide libraries even without prior knowledge about the paratope of the antibody.[24] Phage-borne mimotopes have shown great potential for mycotoxin detection, but considering the large size and the biologically active nature of phages, these methods are not always ideal for immunoassay development.[25,26] Alternatively, the synthetic counterparts of the phage-borne mimotopes[27–29] or recombinant peptide–protein fusions[30–34] have been suggested as phage-free options. In particular, recombinant fusions either with fluorescent[30,33] or bioluminescent[34] proteins have shown great potential as the fusion can be used directly as the tracer without the need for secondary antibodies or further labeling.

In previous work, we have reported the development of a microarray-based immunoassay for the detection of $FB_1$ using a synthetic mimotope,[27] and a homogeneous quenching assay using a recombinant mimotope tagged with a yellow fluorescent protein (YFP).[30] The YFP-tagged mimotope provided improved sensitivity and a faster and simpler protocol compared to the assays based on the phage-displayed or synthetic mimotopes. With this in mind, we aimed to develop alternative recombinant fusions which could be used for mycotoxin detection in

mimotope-based immunoassays but with improved sensitivity as a result of the luciferase-catalized light-emitting reaction. In this work, we describe the selection of ZEA mimotopes from a random dodecapeptide library and the use of the selected epitope mimics in a competitive phage-based ELISA. In continuation, the ZEA-mimotope and the previously identified $FB_1$-mimotope are used to construct recombinant fusion proteins with the bioluminescent *Gaussia* luciferase (GLuc). GLuc, isolated originally from copepod, *Gaussia princeps*, exhibits high luminescent emission and has emerged as a prominent reporter protein for bioluminescent detection applications.[35,36]

## 3.2.4.2 Experimental section

### Materials

Ph.D.-12 Phage Display Peptide Library Kit, pMAL-c5X vector, NEB Express Competent *E. coli*, amylose resin, and Factor Xa were purchased from New England Biolabs (Ipswich, MA, USA). The monoclonal anti-zearalenone antibody was from Soft Flow Hungary Ltd (Pécs, Hungary) and the anti-fumonisin antibody from BioTez (Berlin, Germany). Clear and black MaxiSorp 96-well plates together with Pierce Centrifuge Columns and 1-Step Ultra TMB-ELISA Substrate Solution were purchased from Thermo Fisher Scientific (Waltham, MA, USA). Fumonisin $B_1$ ($FB_1$) and zearalenone (ZEA) were obtained from SantaCruz Biotechnology (Dallas, TX, USA), and the HRP-conjugated anti-M13 antibody was obtained from GE Healthcare Inc. (Chicago, IL, USA). KOD Xtreme Hot Start Master Mix was from Millipore (Billerica, MA, USA) and Ni-NTA agarose from Qiagen (Valencia, CA, USA). ProBlock Gold Bacterial Protease Inhibitor Cocktail was purchased from Gold Biotechnology Inc. (St. Louis, MO, USA) and native coelenterazine was from NanoLight Technology (Pinetop, AZ, USA).

### Identification of mimotopes by phage display

$FB_1$ and ZEA mimotopes were selected from the commercial dodecapeptide library (Ph.D.-12) by three consecutive rounds of selections according to manufacturer's instructions with minor modifications. Similarly to the previously described $FB_1$ mimotope (named A2),[27] ZEA mimics were identified from the phage-displayed library by consecutive selection rounds using the anti-toxin antibody as the target. For each selection round, wells of a 96-well microtiter plate were coated with the target monoclonal antibody by an overnight incubation at +4 °C. For the first round, three wells were coated with 1 µg of antibody in 100 µL of 0.1 M sodium bicarbonate per well, whereas for the subsequent rounds the amount of antibody was reduced to 0.5 µg and 0.25 µg per well, and the number of wells to two and one in the second and third rounds, respectively. Similarly, pre-selection wells were coated with 5 mg $mL^{-1}$ bovine serum albumin (BSA). The following day, the remaining protein-binding sites in the coated wells were blocked with 3% (w/v) BSA in PBS (pH 7.2) for 2 h at room temperature in slow shaking and washed three times with PBS-T [PBS (pH 7.2); 0.1% (v/v) Tween-20]. For the first round, 100-fold representation of the library ($2 \times 10^{11}$ pfu) diluted in PBS with 0.05% Tween-20 and 0.1% BSA was added to the pre-selection wells and incubated with slow shaking for 1.5 h at room temperature. The solution was then transferred to the wells coated with the target antibody, and

the incubation was continued for another 1.5 h. The wells were then washed six times with PBS-T, and finally, the bound phages were eluted with 100 µL of 0.2 M glycine-HCl (pH 2.2) with 0.01% BSA for 10 min, after which, the supernatant was collected and neutralized immediately with 40 µL of 1 M Tris-HCl (pH 9.1). The eluate was amplified by infecting *E. coli* ER2738, and the amplified phage was used for the subsequent panning rounds. After each panning round, the number of eluted and amplified phages was determined by titering, and the number of input phages ($2 \times 10^{11}$ pfu) was kept constant in all rounds. The incubation time in the pre-selection and target wells was reduced to 1 h in the second and third rounds while the number of washes was increased to ten and the concentration of Tween-20 in the washing buffer was increased from 0.1% to 0.5% (v/v) for more stringent washes. Moreover, in order to favor the elution of good ZEA mimics, a competitive elution step was used instead of glycine. After the washes, 100 ng $mL^{-1}$ of ZEA in the second round and 10 ng $mL^{-1}$ of ZEA in the third round, was added to each well and incubated for 1 h after which the solution was collected and used to the infect the bacteria. After the three selection rounds, individual plaques were picked from the LB/IPTG/X-gal plates and tested in the phage-based ELISA to select the positive clones binding to the target antibody. Finally, to identify the peptide sequences, the selected clones were sequenced using the primer -96 gIII (5'–CCC TCA TAG TTA GCG TAA CG–3').

### Phage-based ELISA

The success of the pannings was evaluated in a phage-based ELISA using the immobilized anti-ZEA antibody and HRP-labeled anti-HRP secondary antibody (**Figure 44C**). For the ELISA, microtiter well plates were coated with the anti-ZEA capture antibody (200 ng in 60 µL of 0.2 M sodium carbonate/bicarbonate, pH 9.4) by overnight incubation at +4 °C. The wells were then blocked with blocking buffer (PBS, pH 7.2; 3% (w/v) BSA) for 2 h at +4 °C and washed two times with PBS-T (PBS, pH 7.2; 0.1% (v/v) Tween-20). Next, the amplified phage stock was added to the coated wells in 1:30- or 1:100-dilution and incubated for 1 h. For the competitive assay, additionally different concentrations of ZEA (0–1000 ng $mL^{-1}$) were added to the wells. After washing the plate four times, anti-M13-HRP (1/5000-dilution in blocking buffer) was added and the incubation was continued for 1 h. All incubation steps were done in the total volume of 60 µL with slow shaking at room temperature. Finally, the plate was washed four times as described previously, and 60 µL of TMB substrate solution was added to each well. After 1–5 min incubation, the reaction was stopped by adding 60 µL of 2 M sulfuric acid to each well, and the absorbance (at 450 nm) was measured using a CLARIOstar microplate reader from BMG Labtech (Ortenberg, Germany).

### Construction of bioluminescent fusion proteins

For the expression of GLuc-tagged mimotopes, plasmids pRP006 and pRP010 were constructed. The *GLuc* gene was PCR-amplified from vector pCoIdI-GLuc using KOD Xtreme Hot Start Master Mix. The DNA sequence encoding for the mimotope (A2, VTPNDDTFDPFR; or SF, SFDYFLWDSTET) together with the GS-linker were added to the 5'-end and a polyhistidine tag to the 3'-end of GLuc in three sequential PCR-reactions using the primers listed in **Table 13** (PCR I: Forward Primer 1 and Reverse Primer 1; PCR II: Forward Primer 2 and Reverse Primer 2; PCR III:

Forward Primer 3 and Reverse Primer 2). The PCR product from the third PCR-reaction was then subcloned at the NdeI and BamHI sites to pMAL-c5X expression vector (**Figure 43A**).

**Table 13**. PCR primers used to create the mimotope-GLuc fusions. Forward primers 1–3 (A2/ZF2) were used to add the DNA sequence encoding for the mimotope (in bold) to the 5' of the GLuc (underlined) by three sequential PCR reactions. Two universal reverse primers were used for both fusions to introduce a polyhistidine tag to the 3' of GLuc. Restriction enzyme NdeI and BamHI (in cursive) were used to subclone the translational fusion to the pMAL-c5X expression vector.

| Primer name | DNA sequence (5'→3') |
|---|---|
| Forward Primer A2-1 | **GAT CCT TTT CGG** GGT GGA GGT TCG ATG AAA CCG ACC |
| Forward Primer A2-2 | **GTT ACT CCG AAT GAT GAT ACG TTT GAT CCT TTT CGG** |
| Forward Primer A2-3 | GGT GGA GGT TCG *CAT ATG* **GTT ACT CCG AAT** |
| Forward Primer ZF2-1 | **TCT ACT GAG ACG** GGT GGA GGT TCG ATG AAA CCG ACC |
| Forward Primer ZF2-2 | **AGT TTT GAT TAT TTT CTT TGG GAT TCT ACT GAG ACG** |
| Forward Primer ZF2-3 | GGT GGA GGT TCG *CAT ATG* **AGT TTT GAT TAT** |
| Universal Reverse Primer-1 | CTA ATG ATG ATG ATG ATG ATG ATC ACC ACC TGC |
| Universal Reverse Primer-2 | CGA ACC TCC ACC *GGA TCC* CTA ATG ATG ATG |

## Fusion protein expression and purification

For the overexpression of the mimotope-GLuc fusion proteins, plasmids pRP006 and pRP010 were transformed into *E. coli* NEB Express cells and selected on LB agar plates with 100 µg $mL^{-1}$ ampicillin. A single colony harboring the plasmid was used to inoculate 5-mL preculture (LB medium supplemented with 100 µg $mL^{-1}$ ampicillin), which was grown overnight at +37 °C, 250 rpm. The following day, overnight preculture was expanded into a main culture of 300 mL (LB medium supplemented with 100 µg $mL^{-1}$ ampicillin) and the growth was continued at +37 °C until the optical density at 600 nm ($OD_{600}$) of 0.6 was reached. The protein expression was then induced by IPTG (isopropyl β-D-1-thiogalactopyranoside) at a final concentration of 1 mM followed by growth for 4 h at +16 °C. The cells were collected by centrifugation (10 min at 5000g at +4 °C) and resuspended in 10 mL of lysis buffer (50 mM Tris-HCl, pH 8.7; 150 mM NaCl) supplemented with protease inhibitor cocktail. Then, the cells were lysed by sonication on ice for 10 min, after which the resultant cell debris was removed by centrifugation for 20 min at 12,000g at +4 °C, and the supernatant was filtered by a syringe through a 0.45 µm filter.

The clarified lysate was then incubated with amylose resin for 30 minutes, collected on a Pierce Centrifuge Column by gravity flow and washed with 10 column volumes of the lysis buffer. The protein was then eluted in 1 mL fractions with the lysis buffer supplemented with 10 mM maltose. The MBP-tag was cleaved by Factor Xa (2.5% (w/w)) during 6 h at room temperature. The cleaved product was then purified using Ni-NTA resin. After capturing the cleaved mimotope-GLuc with C-terminal polyhistidine tag, the resin was washed with 10 column volumnes of the lysis buffer supplemented with 20 mM imidazole, and finally, the product was eluted with the lysis buffer supplemented with 250 mM imidazole in 1 mL fractions. The purifications were

followed by by SDS-PAGE analysis (**Figure 43B**), and the concentration of the purified protein stock was determined by BCA kit.

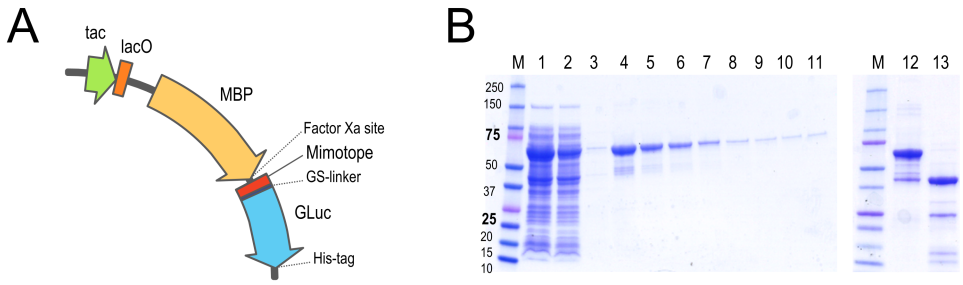


**Figure 43**. (A) Main features of the expression vectors (pRP006 and pRP010) used for mimotope-GLuc fusion protein production in *E. coli*. (B) SDS-PAGE analysis of A2-GLuc purification: lane 1, cell lysate before purification; 2–3, flow-through and wash fractions of the amylose purification; 4–12, eluted MPB-mimotope-GLuc fusion (64 kDa); 13, actor Xa cleavage reaction with MBP (43 kDa) and mimotope-GLuc (21 kDa; red arrow) which was further purified by Ni-NTA; M, molecular marker (Precision Plus Protein Dual Color Standard).

## Bioluminescent immunoassays

The immunoassays with bioluminescent mimotope-GLuc fusions were performed in black 96-well plates by coating the wells with capture antibody (50 ng in 60 µL of 0.2 M sodium carbonate/bicarbonate, pH 9.4) by overnight incubation at +4 °C. The wells were then blocked with blocking buffer (PBS pH 7.2; 3% (w/v) BSA) for 4 h at room temperature and washed twice with PBS-T (PBS pH 7.2; 0.1% (v/v) Tween-20). Toxin standards ranging from 0 to 250 ng $mL^{-1}$ (in three replicates) were added to the coated wells together with 1 µg $mL^{-1}$ A2-GLuc (for $FB_1$), or 40 ng $mL^{-1}$ SF-GLuc (for ZEA) in assay buffer (PBS, pH 7.2; 0.05% (v/v) Tween-20; 0.1% (w/v) BSA) in a total reaction volume of 60 µL. After incubation of 1.5 h at slow shaking, the wells were washed four times with PBS-T. Finally, the bioluminescence intensity of each well was measured in the CLARIOstar by injecting 60 µL of native coelenterazine at a final concentration of 2.0 µg $mL^{-1}$ (in PBS).

## Data analysis

The immunoassay data with different toxin concentrations were normalized to the minimum and maximum signals, and the normalized signals were analyzed with Origin Pro 9.0 software (OriginLab Corp., Northampton, MA, USA) using a four-parameter logistic regression (4-PL) model (equation 1):

$$y = A_{min} + \frac{(A_{max} - A_{min})}{1 + \left(\frac{x}{IC_{50}}\right)^{b}} \qquad (1)$$

where $A_{max}$ is the asymptotic maximum (the signal in the absence of the analyte), $A_{min}$ is the asymptotic minimum, and $b$ and $IC_{50}$ are the slope of the curve and the analyte concentration at the inflection point, respectively. The limit of detection (LOD) was determined as the toxin

concentration where the antibody binding to the peptide was inhibited by 10% and the dynamic range of the method as the toxin concentration from 20% to 80% inhibition.

### 3.2.4.3 Results and discussion

#### Selection and characterization of phage-displayed zearalenone mimotopes

Zearalenone (ZEA) mimotopes were selected from the linear 12-mer phage display peptide library (Ph.D.-12) in three successive rounds of panning. The first round was performed with high concentrations of the target antibody and gentle washes to maximize the capture of all interesting clones, whereas during the subsequent rounds the amount of the antibody was reduced, and the stringency of the washes was increased. Moreover, the elution step was performed by competition with the decreasing amounts of the free toxin instead of the nonspecific acid elution used in the first round. The use of these strategies for the mimotope selections allowed an efficient enrichment of antibody binding phages was observed after three rounds of panning. This observation was evidenced by the increased phage titers during the panning rounds and from the excellent signal-to-background ratios obtained in the ELISA using the entire phage pools after each panning round (**Figure 44A**). A total of 15 individual phage clones were randomly selected from the third panning round, amplified, and tested similarly in the phage-based ELISA. Altogether, 14 out of 15 clones showed good signal-to-background ratios in the assay indicating specific binding to the anti-ZEA antibody. Moreover, competition with the free ZEA (1000 ng $mL^{-1}$) was seen with all the clones demonstrating successful selection of ZEA mimicking peptides (**Figure 44B**).

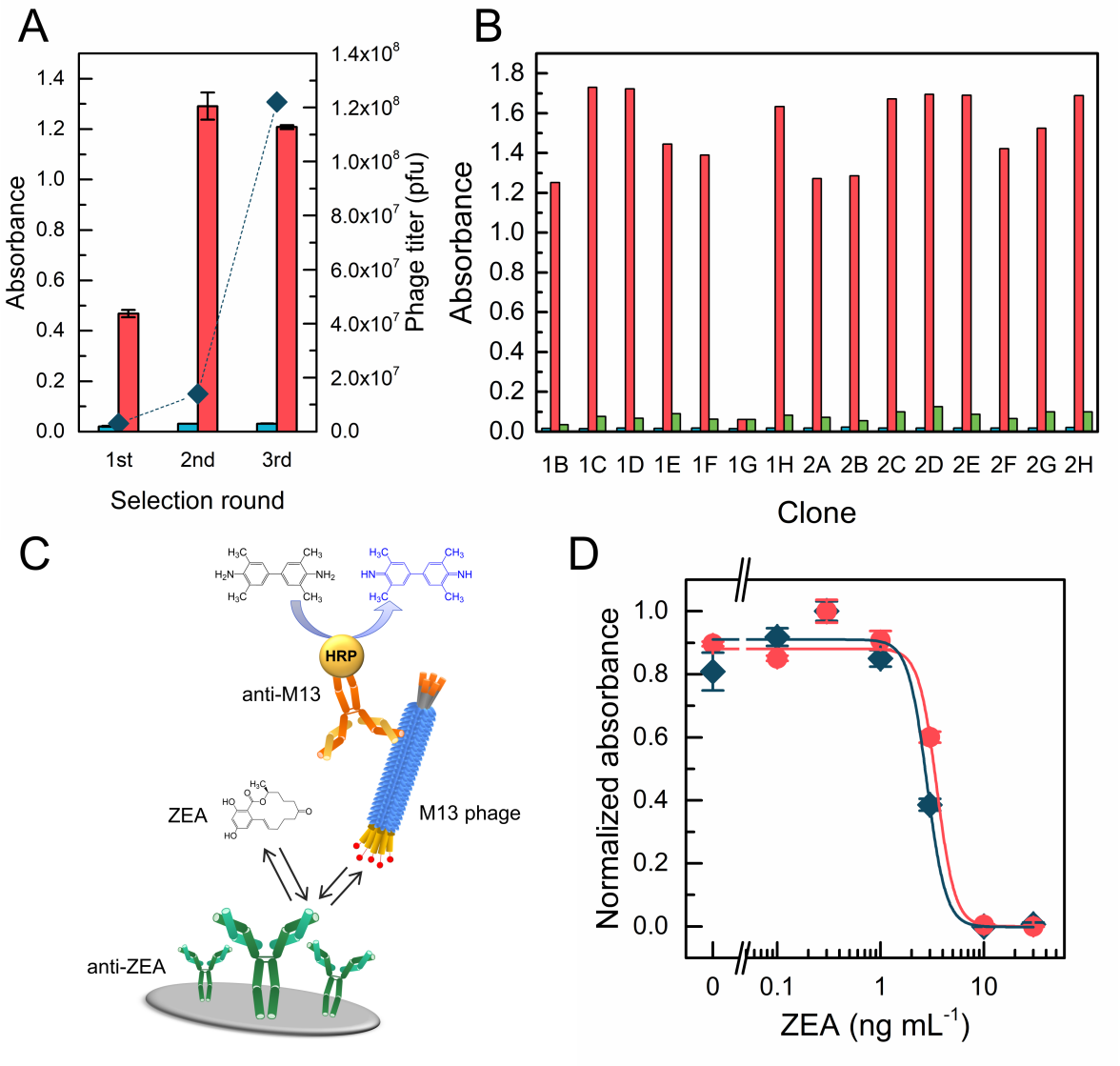


**Figure 44**. Selection of zearalenone mimotopes and tests with phage-based ELISAs. (A) Polyclonal phage-based ELISA after each selection rounds showed specific binding to the target antibody (red) and low non-specific binding to background wells coated with BSA (blue). Likewise, enrichment of the phages was seen in the phage titers after each selection round (blue diamonds; right y-axis). (B) Monoclonal phage-based ELISA with 15 individual clones. High specific binding to the target antibody (red) was seen with all except one clone, and low signals were measured in the background wells (blue) and in the presence of free zearalenone (green). (C) Schematic of the competitive phage-based ELISA using the phage (M13) -displayed mimotopes and anti-M13 conjugated to HRP. (D) Comparison of the competitive binding curves of the phage-displayed mimotopes GW (gray) and SF (red). The results are shown as normalized means ± the standard error of the mean ($n$ = 3). A four-parameter logistic fit (OriginPro 9.0) was used to calculate the $IC_{50}$ values.

The DNA sequencing results showed two conserved peptide sequences, GWWGPYGEIELL and SFDYFLWDSTET (named GW and SF, respectively), which were further tested in the competitive ELISA with different toxin concentrations (**Figure 44C**). The ELISA with the representative phage clones GW and SF showed good sensitivities with $IC_{50}$ values of 2.8 ± 0.2 ng $mL^{-1}$ and 3.5 ± 0.2 ng $mL^{-1}$ for GW and SF, respectively (**Figure 44D**). Clone SF gave a better response in terms of reproducibility and was selected for further applications.

### Bioluminescent immunoassay based on GLuc fusion protein

Recombinant mimotope-fusions were constructed based on bioluminescent GLuc in fusion with the newly identified ZEA-mimotope SF and a previously studied $FB_1$-mimotope A2.[27] The epitope-mimicking nature of the recombinant fusion proteins and their functionality as the tracer was confirmed in a competitive immunoassay, where the capture antibody was immobilized in microtiter wells, and competition between target toxin, $FB_1$ or ZEA, and the mimotope-GLuc was shown as low luminescence readings in the presence of high toxin concentrations. On the basis of the typical sigmoidal standard curve for a competitive heterogeneous assay,[3] (**Figure 45**) the half maximal inhibitory concentrations ($IC_{50}$) were 0.35 ± 0.06 ng $mL^{-1}$ and 1.3 ± 0.1 ng $mL^{-1}$ for ZEA and $FB_1$, respectively. Comparison of the analytical characteristics of the bioluminescent immunoassay with other methods developed using the same mimotopes is presented in **Table 14**.

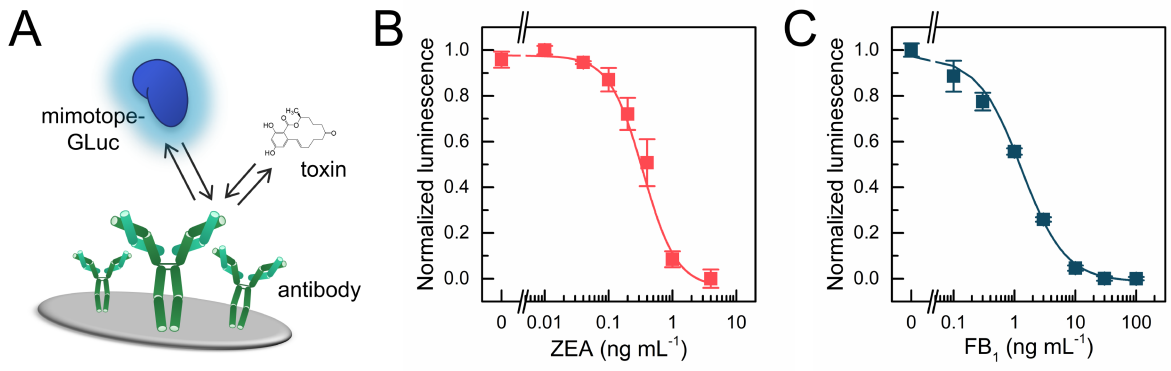


**Figure 45.** GLuc-based immunoassays. (A) Schematic of the competitive bioluminescent immunoassay using the GLuc-tagged mimotopes. (B) ZEA calibration with SF-GLuc and (C) $FB_1$ calibration with A2-GLuc. The results are shown as normalized means ± the standard error of the mean ($n$ = 3). A four-parameter logistic fit (OriginPro 9.0) was used to calculate the $IC_{50}$ values.

## 3.2.4.4 Conclusions

In this work, we reported the selection of a zearalenone mimotope from a commercial peptide library using phage display technology, and furthermore, the development of bioluminescent immunoassays using recombinant GLuc-fusion proteins based on zearalenone and fumonisins $B_1$ mimotopes. The bioluminescent immunoassays offered simpler methodology compared to the phage-based assay as the GLuc-tagged mimotope could be directly used as the tracer, and no further labeling or secondary antibodies were required. Compared to the previously reported methods for fumonisin detection using the same mimotope and the phage-based zearalenone assay, the bioluminescent based assay offered higher or comparable sensitivity.

**Table 14**. Comparison of the immunoassays using the ZEA- and $FB_1$ mimotopes as phage-displayed or recombinant fusion proteins.

| Mimotope | Target | $IC_{50}$ (ng/mL) | LOD* (ng/mL) | Dynamic range** (ng/mL) | Average RSD | Ref. |
|---|---|---|---|---|---|---|
| A2-phage | $FB_1$ | 38.7 | 7.5 | 13.7–109 | 4.7 % | [27] |
| A2-YFP | $FB_1$ | 6.8 | 2.0 | 3.2–14.8 | 6.4% | [30] |
| A2-GLuc | $FB_1$ | 1.3 | 0.21 | 0.41–4.1 | 6.1% | This work |
| SF-phage | ZEA | 3.5 | 2.3 | 2.7–4.6 | 12.0% | This work |
| SF-GLuc | ZEA | 0.35 | 0.09 | 0.15–0.80 | 9.0% | This work |

*Abbreviations: GLuc, Gaussia luciferase; $FB_1$, fumonisin $B_1$; RSD, relative standard deviation; YFP, yellow fluorescent protein; ZEA, zearalenone.*
**LOD defined as the concentration in which the antibody binding to the peptide is inhibited by 10%*
***Dynamic range defined between 20 and 80% inhibition, i.e., $IC_{20}$–$IC_{80}$*

## Acknowledgments

This research was funded by the Spanish Ministry of Economy and Competitiveness grant number CTQ2015-69278-C2-1-R/AIE and RTI2018-096410-B-C21. RP acknowledges Complutense University for a predoctoral contract.

### 3.2.4.5 References


1. Bennett, J. W.; Klich, M. Mycotoxins. *Clin. Microbiol. Rev.* **2003**, *16*, 497–516.
2. DeVries, J. W.; Trucksess, M. W.; Jackson, L. S. *Mycotoxins and Food Safety*; Springer, New York, NY, USA, **2002**.
3. Leslie, J. F.; Summerell, B. A. *The Fusarium Laboratory Manual*, 1st ed.; Blackwell Pub: Ames, Iowa, **2006**.
4. Medina, Á.; González-Jartín, J. M.; Sainz, M. J. Impact of global warming on mycotoxins. *Curr. Opin. Food Sci.* **2017**, *18*, 76–81
5. Braun, M. S.; Wink, M. Exposure, occurrence, and chemistry of fumonisins and their cryptic derivatives. *Compr. Rev. Food Sci. Food Saf.* **2018**, *17*, 769–791.
6. Bräse, S.; Encinas, A.; Keck, J.; Nising, C. F. Chemistry and biology of mycotoxins and related fungal metabolites. *Chem. Rev.* **2009**, *109*, 3903–3990.
7. Stockmann-Juvala, H.; Savolainen, K. A review of the toxic effects and mechanisms of action of fumonisin $B_1$. *Hum. Exp. Toxicol.* **2008**, *27*, 799–809.
8. International Agency for Research on Cancer (IARC). Monographs on the Evaluation of Carcinogenic Risks to Humans, Some Naturally Occurring Substances: Food Items and Constituents, Heterocyclic Aromatic Amines and Mycotoxins.; International Agency for Research on Cancer: Lyon, France, **1993**; Vol. 56.
9. Goyal, S.; Ramawat, K. G.; Mérillon, J. M. Different shades of fungal metabolites: an overview. In *Fungal Metabolites*; Merillon, J.-M., Ramawat, K. G., Eds.; Springer International Publishing: Cham, Switzerland, **2016**; pp 1–29.
10. European Commission. Commission regulation (EC) No 1881/2006. *Off. J. Eur. Union* **2006**, *L364*, 5–24.
11. European Commission. Commission regulation (EC) No 1126/2007. *Off. J. Eur. Union* **2007**, *L255*, 14–17.
12. U.S. Food and Drug Administration (FDA). www.fda.gov/food/guidanceregulation (Cited Jan 30, 2019).
13. Köppen, R.; Koch, M.; Siegel, D.; Merkel, S.; Maul, R.; Nehls, I. Determination of mycotoxins in foods: current state of analytical methods and limitations. *Appl. Microbiol. Biotechnol.* **2010**, *86*, 1595–1612.
14. Berthiller, F.; Brera, C.; Crews, C.; Iha, M. H.; Krska, R.; Lattanzio, V. M. T.; *et al.* Developments in mycotoxin analysis: An update for 2014-2015. *World Mycotoxin J.* **2016**, *9*, 5–30.
15. Peltomaa, R.; Benito-Peña, E.; Moreno-Bondi, M. C. Bioinspired recognition elements for mycotoxin sensors. *Anal. Bioanal. Chem.* **2018**, *410*, 747–771.
16. Chauhan, R.; Singh, J.; Sachdev, T.; Basu, T.; Malhotra, B. D. Recent advances in mycotoxins detection. *Biosens. Bioelectron.* **2016**, *81*, 532–545.
17. *The Immunoassay handbook: Theory and applications of ligand* binding ELISA and related techniques, 4th ed.; Wild, D., (Editor); Elsevier Science, Oxford, UK, **2013.**
18. Zhao, F.; Wang, H.; Han, X.; Yang, Z. Development and comparative study of chemosynthesized antigen and mimotope-based immunoassays for class-specific analysis of *o,o*-dimethyl organophosphorus pesticides. *Sci. Rep.* **2016**, *6,* 37640.
19. Gazarian, T.; Selisko, B.; Hérion, P.; Gazarian, K. Isolation and structure–functional characterization of phage display library-derived mimotopes of noxiustoxin, a neurotoxin of the scorpion *Centruroides noxius* Hoffmann. *Mol. Immunol.* **2000**, *37*, 755–766.
20. Liu, J.; Chisti, M. M.; Zeng, X. General signal amplification strategy for nonfaradic impedimetric sensing: trastuzumab detection employing a peptide immunosensor. *Anal. Chem.* **2017**, *89*, 4013–4020.
21. Wang, Y.; Wang, H.; Li, P.; Zhang, Q.; Kim, H. J.; Gee, S. J.; Hammock, B. D. Phage-displayed peptide that mimics aflatoxins and its application in immunoassay. *J. Agric. Food Chem.* **2013**, *61*, 2426–2433.
22. He, Z.; He, Q.; Xu, Y.; Li, Y.; Liu, X.; Chen, B.; Lei, D.; Sun, C. Ochratoxin A mimotope from second-generation peptide library and its application in immunoassay. *Anal. Chem.* **2013**, *85*, 10304–10311.
23. He, Q.; Xu, Y.; Zhang, C.; Li, Y.; Huang, Z. Phage-borne peptidomimetics as immunochemical reagent in dot-immunoassay for mycotoxin zearalenone. *Food Control* **2014**, *39*, 56–61.

24. Barbas, C. F. I.; Burton, D. R.; Scott, J. K.; Silverman, G. J. *Phage Display: A Laboratory Manual*; Cold Spring Harbor Laboratory Press: Cold Spring Harbor, NY, USA, **2001.**
25. Smartt, A. E.; Ripp, S. Bacteriophage reporter technology for sensing and detecting microbial targets. *Anal. Bioanal. Chem.* **2011**, *400*, 991–1007.
26. Peltomaa, R.; López-Perolio, I.; Benito-Peña, E.; Barderas, R.; Moreno-Bondi, M. C. Application of bacteriophages in sensor development. *Anal. Bioanal. Chem.* **2016**, *408*, 1805–1828.
27. Peltomaa, R.; Benito-Peña, E.; Barderas, R.; Sauer, U.; González Andrade, M.; Moreno-Bondi, M. C. Microarray-based immunoassay with synthetic mimotopes for the detection of fumonisin $B_1$. *Anal. Chem.* **2017**, *89*, 6216–6223.
28. Zou, X.; Chen, C.; Huang, X.; Chen, X.; Wang, L.; Xiong, Y. Phage-free peptide ELISA for ochratoxin A detection based on biotinylated mimotope as a competing antigen. *Talanta* **2016**, *146*, 394–400.
29. Liu, R.; Yu, Z.; He, Q.; Xu, Y. An immunoassay for ochratoxin A without the mycotoxin. *Food Control* **2007**, *18*, 872–877.
30. Peltomaa, R.; Amaro-Torres, F.; Carrasco, S.; Orellana, G.; Benito-Peña, E.; Moreno-Bondi, M. C. Homogeneous quenching immunoassay for fumonisin $B_1$ based on gold nanoparticles and an epitope-mimicking yellow fluorescent protein. *ACS Nano* **2018**, *12*, 11333–11342.
31. Xu, Y.; Chen, B.; He, Q.; Qiu, Y.-L.; Liu, X.; He, Z.; Xiong, Z. New approach for development of sensitive and environmentally friendly immunoassay for mycotoxin fumonisin $B_1$ based on using peptide-MBP fusion protein as substitute for coating antigen. *Anal. Chem.* **2014**, *86*, 8433–8440.
32. Xu, Y.; He, Z.; He, Q.; Qiu, Y.; Chen, B.; Chen, J.; Liu, X. Use of cloneable peptide–MBP fusion protein as a mimetic coating antigen in the standardized immunoassay for mycotoxin ochratoxin a. *J. Agric. Food Chem.* **2014**, *62*, 8830–8836.
33. Ding, Y.; Hua, X.; Du, M.; Yang, Q.; Hou, L.; Wang, L.; Liu, F.; Gonzalez-Sapienza, G.; Wang, M. Recombinant, fluorescent, peptidomimetic tracer for immunodetection of imidaclothiz. *Anal. Chem.* **2018,** *90*, 2230−2237.
34. Ding, Y.; Hua, X.; Chen, H.; Liu, F.; González-Sapien, G.; Wang, M. Recombinant peptidomimetic-nano luciferase tracers for sensitive single-step immunodetection of small molecules. *Anal. Chem.* **2018**, *90*, 2230–2237.
35. Tannous, B. A. Gaussia luciferase reporter assay for monitoring biological processes in culture and *in vivo*. *Nat. Protoc.* **2009**, *4*, 582–591.
36. Moutsiopoulou, A.; Hunt, E.; Broyles, D.; Pereira, C. A.; Woodward, K.; Dikici, E.; Kaifer, A.; Daunert, S.; Deo, S. K. Bioorthogonal protein conjugation: application to the development of a highly sensitive bioluminescent immunoassay for the detection of interferon-γ. *Bioconjug. Chem.* **2017**, *28*, 1749–1757.

# 4 Results and discussion

## 4.1 Fungal genosensors

Fungal contamination is a common and widely spread problem which can lead to global health issues, environmental challenges, and important economic losses. Certain fungi species are renowned pathogens while others are harmful solely for their capacity to produce toxic secondary metabolites, mycotoxins. Among mycotoxigenic fungi, genus *Fusarium* is one of most the prevalent producers of common mycotoxins in the northern temperate regions, and species of this family are commonly found in cereal crops in America, Europe, and Asia making them a major agricultural problem.[21] Some *Fusarium* species, such as *F. verticillioides*, have a very narrow host range, infecting predominantly certain cereals, whereas other species, such as *F. proliferatum*, are rather ubiquitous in grains and other plants. In **publication I**, we have developed species-specific genosensors for the detection of these two *Fusarium* species. Their distinction using conventional methods is challenging due to their highly similar morphologies, but the development of molecular methods has enabled specific and sensitive detection of these fungi. The following section discusses further the background and some additional aspects of the work presented in **publication I**.

### 4.1.1 SELECTION OF SPECIFIC DNA PROBES FOR *FUSARIUM*

In essence, biosensors, which have become the fastest growing technology for pathogen detection in recent years,[90] are dependent on specific recognition elements capable of recognizing the target analyte and distinguishing it from other similar molecules. Biosensors, based on oligonucleotide probes, DNA or RNA, also known as genosensors, rely on the

exceptional specificity of base pairing and the immense sequence variety of nucleic acids. By designing specific probes, complementary to the chosen target nucleic acid, genosensors can be applied to the analysis of virtually any target ranging from infectious diseases to foodborne pathogens. The specificity of the interaction relies on selecting unique target sequences which differ sufficiently from other potential cross-reactive sequences, making the probe selection one of the most critical steps in the development of these devices. Ideally, a candidate target sequence should be present in the cell at a relatively high copy number, while being adequately heterologous at the sequence level to allow the distinction of the target at both genus and species level.[90]

For fungal detection, various DNA sequences have been used as targets for characterizing the genetic variability among fungi families, or for detecting and quantifying specific species. Commonly used target genes include both nuclear and mitochondrial DNA regions. Widely used genes comprise translation elongation factors (*tef-1α*), calmodulin, and *β*-tubulin.[21] On the other hand, in the case of mycotoxigenic fungi, some prefer to use the genes involved in the biosynthesis of mycotoxins as they have been presumed to relate with the amount of the toxin present in the sample. For example, *FUM6* and *FUM8* genes within the fumonisins biosynthetic cluster have been widely used to identify fumonisin-producers. However, although correlation between mycotoxin concentration and their biosynthetic genes has been found,[318] other studies with different *Fusarium* species and different mycotoxins have shown distinct results.[21,319] Moreover, biosynthetic gene targets are usually not capable of providing the required selectivity for identifying fungi at the species level.

On the other hand, ribosomal DNA (rDNA) is one of the most used target sequences for *Fusarium* detection and identification. The eukaryotic ribosome is composed of small and large subunits which are encoded by the genes 5.8S, 18S, and 28S. These three genes are generally found together, separated by internal transcribed spacers (ITS1 and ITS2), in a repetitive manner and separated by the intergenic spacer (IGS) (**Figure 46A**).[320] A high degree of sequence homogeneity is seen among rDNA within different species even though variation among rDNA copies within species and even within individuals has been observed. This is due to the fact that while the core regions of rDNA are usually highly conserved, the spacer sequences, especially the IGS, tend to show a high level of variation even among closely related species.[320,321] Moreover, owing to the repetitive nature of rDNA, it can provide higher sensitivity as a target in comparison with single-copy genes.

*Fusarium* fungi are widespread worldwide, and this large family of fungi has been found in a variety of agricultural products. The *Fusarium fujikuroi* species complex (formerly known as the *Gibberella fujikuroi* species complex) includes several closely related species in the genus *Fusarium*, most important ones being *F. proliferatum, F. verticillioides, F. fujikuroi,* and *F. sacchari.* The species within this complex are highly similar in terms of both morphology and phylogenetics, which makes distinguishing the individual species difficult. Above all, conventional methods based on morphological and cross-fertility criteria undergo difficulties in identifying fungal isolates at the species level. In the past decades, development of PCR and molecular biology methods for *Fusarium* detection, among others, have spurred the identification and detection of fungal species with the advantage of being independent of the fungal morphology and cultivability.[21]

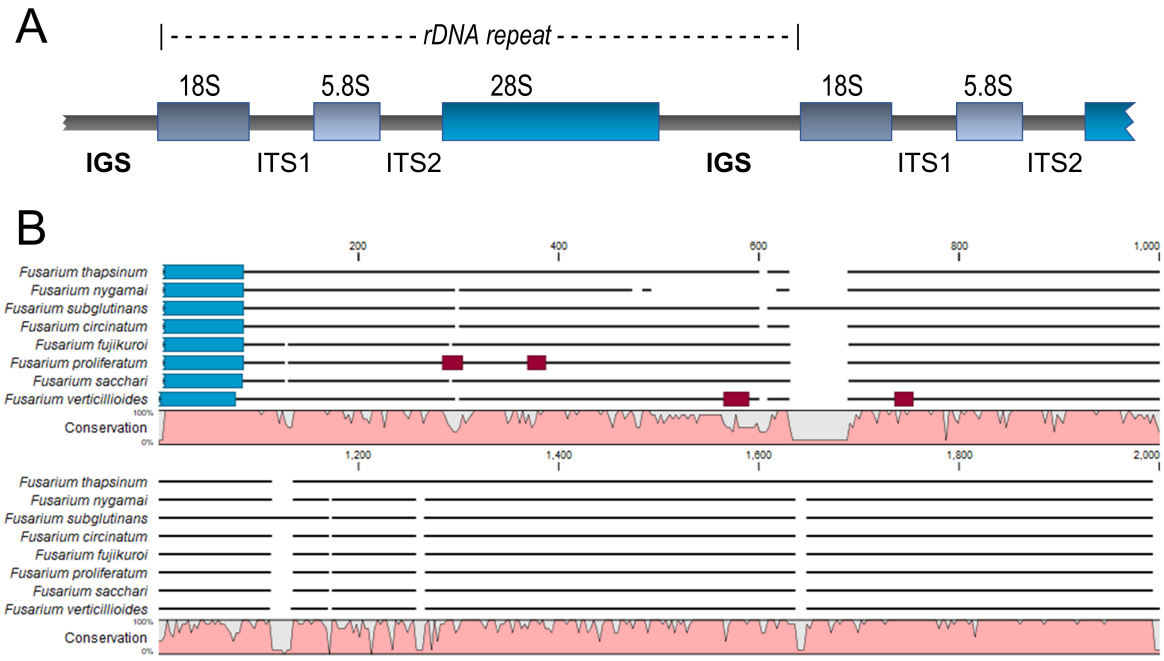


**Figure 46**. (A) Regions of fungi ribosomal DNA (rDNA) which consists of repeated sequences encoding for the ribosome subunits. The genes are flanked by the internal transcribed spacers (ITS1 and ITS2) and the intergenic spacer (IGS). Figure modified from Weider *et al.*[320] (B) Sequence alignment of the IGS sequence of representative strains of *Fusarium fujikuroi* species complex. Partial 28S gene is shown in blue, the location of the species-specific detection and capture probes for *F. proliferatum* and *F. verticillioides* are shown in dark red. DNA sequences on the partial 28S rRNA gene and the IGS region were collected from GenBank and aligned and visualized using CLC Sequence Viewer (http://www.clcbio.com/).

Having recognized the pre-requisites for designing the recognition elements for the identification of *F. proliferatum* and *F. verticillioides* at the species level, in **publication I**, species-specific probes for these species were designed on the IGS region. Sequence alignment of the IGS region of more than one hundred *Fusarium* strains showed that it bears enough variability between the species within the *Fusarium fujikuroi* species complex to allow their differentiation (**Figure 46B**). Since such variability was observed in the sequences of such highly similar species, we assumed that also other species would provide at least similar differences. Species-specific capture and detection probes (marked in dark red in **Figure 46B**) for each species, *F. proliferatum* and *F. verticillioides,* were designed on the IGS region on those sections which showed enough variability.

On the other hand, although previous studies have reported the development of specific primers for each fungal species using the IGS regions,[187,188] in this work, we decided to use a single primer pair which could amplify all *Fusarium* species, and the species-specific identification would happen subsequently using the species-specific capture and detection probes.

## 4.1.2 SIGNAL AMPLIFICATION STRATEGIES

### 4.1.2.1 Choice of the label and detection method

A magnetic bead–based sandwich hybridization assay (**Figure 7**) for *F. proliferatum* and *F. verticillioide*s was established using two species-specific probes which together could provide a high level of specificity. The capture probe was immobilized onto magnetic microbeads which functioned as the solid support, while the detection probe was functionalized with biotin. The biotin-linker allowed flexibility when choosing a label for the system, because practically anything labeled with streptavidin (SA) or other biotin-binding protein could be used to generate a measurable signal. After the initial experiments using streptavidin-coupled R-Phycoerythrin (SAPE), an intensely bright phycobiliprotein, as the label, other options were studied in order to increase the sensitivity of the assay. Experiments with SA-coupled quantum dots and SA-poly-HRP showed increased sensitivity. In particular, it was noted that the enzymatic detection using SA-poly-HRP led to a 20-fold higher sensitivity compared to SAPE (**Figure 9**).

The use of an enzymatic label enabled not only enhanced sensitivity but also provided further flexibility in the measurement scheme. The wide use of HRP has spurred the development of different substrates for the same enzyme. In their simplest format, measurements of HRP are based on chromogenic substrates which yield in a color change in the presence of enzyme. Often higher sensitivity can be achieved by using fluorescent or chemiluminescent substrates. The latter enables the use of simple luminometers or other readers capable of measuring total luminescence without the need for an excitation light source. Such approaches might be desired for low-resource settings or devices with a limited size. To compare the performance of the fluorescent substrate Amplex UltraRed used in **publication I** to a chemiluminescent substrate LumiPhos-HRP (PS-atto), we performed the calibration curve with *F. proliferatum* in similar manner but using as the substrate either Amplex UltraRed or LumiPhos-HRP, together with fluorescent (excitation at 510 nm / detection at 590 nm) or chemiluminescent detection (detection at 405–465 nm), respectively. Chemiluminescent detection showed a slightly lower detection limit (1.3 pM of synthetic target DNA) than fluorescent detection (1.8 pM) (**Figure 47**). However, the latter showed better signal-to-background ratios and thus could be considered to result in more reliable results.

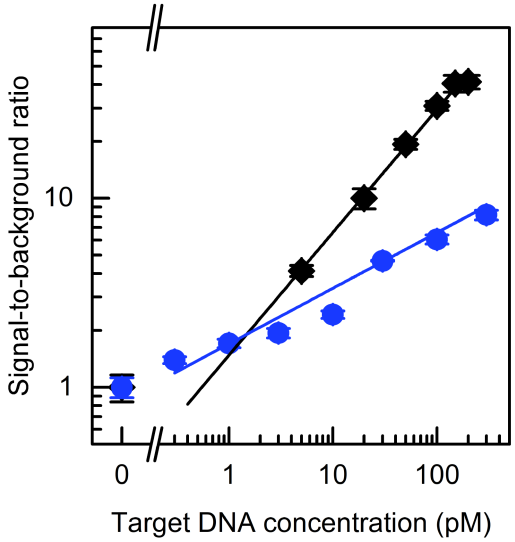


**Figure 47**. Detection of *F. proliferatum* using SA-HRP as a label and fluorescent (black) or chemiluminescent (blue) substrates. Normalized signals are depicted as the average of the analysis of replicate samples ± the standard error of the mean ($n$ = 3). Allometric fits (OriginPro 9.0) were used to calculate the lower detection limits (blank + 3 × SD of blank).

### 4.1.2.2 Second detection probe

To further improve the sensitivity of the method we explored the possibility of introducing a second detection probe to the system. For example, a hybridization assay in the Simoa system has been reported to use up to three biotinylated detection probes, which resulted in dramatic improvements in the sensitivity.[322] With a similar idea (**Figure 48B**), we designed a second biotinylated detection probe for *F. proliferatum* which could hybridize to the target DNA simultaneously with the original detection probe and the capture probe. As a result, one target DNA strand would be labeled with two biotins and, subsequently, two SA-HRPs instead of one. As expected, this approach led to further signal amplification, and higher signals were measured with two detection probes than with one (**Figure 48A**). However, no significant improvement in the sensitivity (in terms of lower detection limits) were observed, since the normalized signals with one or two detection probes resulted in similar responses (inset of **Figure 48A**).

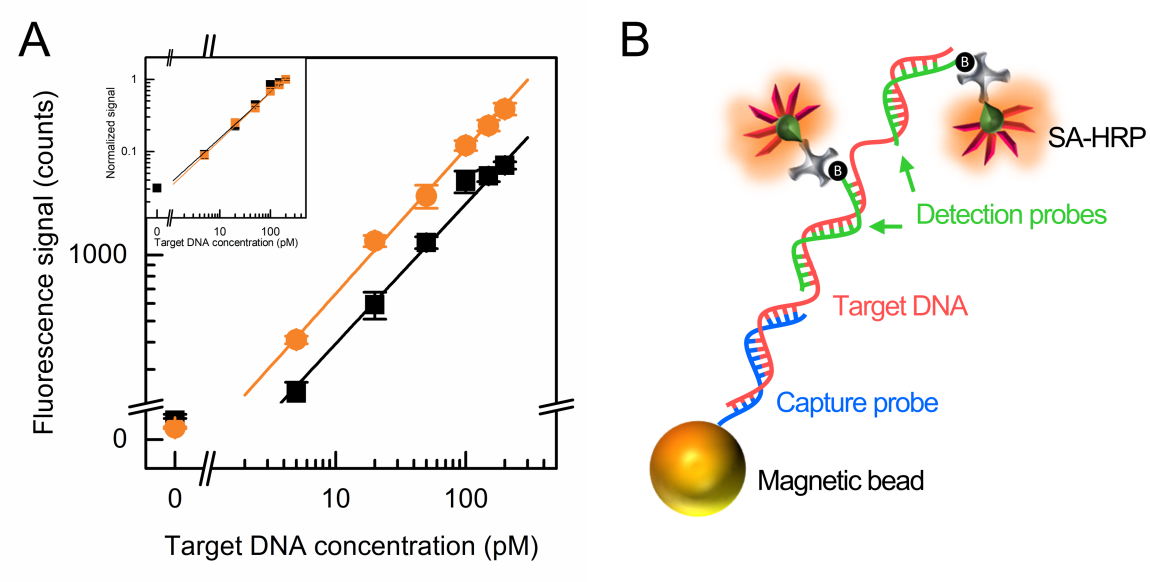


**Figure 48.** Detection of *F. proliferatum* synthetic target using one (black) or two (orange) detection probes and SA-HRP with the fluorescent substrate for the detection. (A) More intense fluorescence signals were measured with two detection probes, but normalized signals (inset) did not show any improvement compared to a single detection probe. Signals are depicted as the average of the replicate samples ± the standard error of the mean ($n$ = 3) and fitted with an allometric fit (OriginPro 9.0). (B) Scheme of the assay using two detection probes (green) instead of just one to bind to the target DNA (red) simultaneously with the capture probe (blue).

### 4.1.2.3 Fragmentation of genomic DNA

Regardless of the sensitivity of the assay using the synthetic target DNA, analysis of the genomic DNA inevitably poses further challenges. First of all, in real samples, the amount of the target DNA is usually very small, and moreover, genomic DNA is a considerably large and highly structured molecule compared to the synthetic target, and therefore it is possible to obtain very different signals.[323] Genomic double-stranded DNA, often folded in complex tertiary or quaternary structures resembling fairly a large polymer, might be difficult to open enough to allow binding of the detection probes. Moreover, steric hindrance can complicate the probe binding. Denaturation at high temperatures will unwind and separate the double-stranded DNA, but rehybridization might favor the reorganization of the double-stranded DNA rather than binding of the short oligonucleotide probes.

A few attempts to apply the genosensors to analyze directly the genomic DNA extracted from contaminated maize samples showed that despite the excellent sensitivity achieved with the synthetic target DNA, poor responses were obtained with the crude genomic DNA. To alleviate the complexity of the genomic DNA a handful of strategies have been reported in the literature including, for example, specific enzymatic digestion of double-stranded DNA and RNA–DNA heteroduplexes resulting in a sample with merely ssDNA and double-stranded RNA,[324] as well as fragmentation of the DNA. Some have reported fragmentation of genomic DNA by sonication,[325,326] but such harsh method will lead to physical shearing and non-specific fragmentation of the DNA and might be a problem if the target DNA is cut from the sequence between the locations where the capture and detection probes hybridize. More specific

fragmentation can be achieved by enzymatic digestion using specific restriction enzymes.[322] To explore this strategy (**Figure 49A**) we attempted to digest the crude extracted genomic DNA using the restriction enzyme EcoRI. Analysis of the fragmented DNA in comparison with the crude extract showed slightly better results; however, a high variation between replicate samples and inconsistent results between days were observed, which were a limitation for real sample analysis (**Figure 49B–C**).

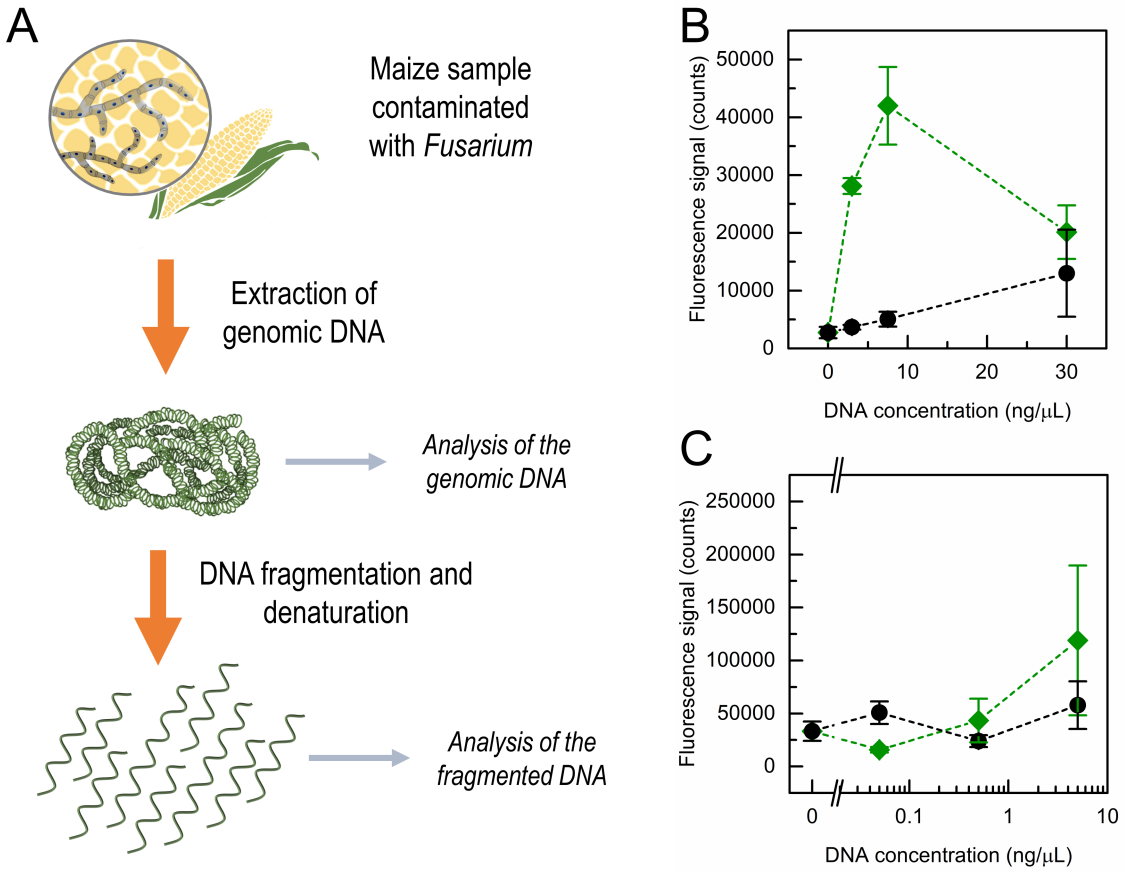


**Figure 49**. Analysis of fragmented genomic DNA. (A) Genomic DNA was extracted from a maize sample contaminated with *Fusarium* fungi after which the crude genomic DNA was analyzed with the genosensor, directly or after enzymatic digestion. (B–C) Genosensor response for different concentrations of the genomic DNA with (green diamonds) and without (black circles) fragmentation. Significant variations were observed between replicates and analyses done on different days (B–C). The fluorescence signals are shown as the average of the replicate analysis of the samples ($n$ = 3) ± the standard error of the mean.

### 4.1.2.4 Amplification of the IGS region by PCR

Finally, despite the previous attempts to detect the fungal genomic DNA directly without amplification, the final application of the genosensors for sample analysis was completed after DNA amplification. The complexity of the genomic DNA and the presence of fungi at low concentrations in clinical and natural environments could explain the challenges in direct detection of *Fusarium,* despite the aforementioned attempted amplification strategies. In fact, the poor sensitivity is a common failing in hybridization-based genosensors, and even the most

sensitive systems require target amounts in the order of $10^9$–$10^{10}$ molecules for detection.[90] Although the reported detection limits in **publication I** were lower than this range ($1.81 \times 10^8$ and $1.08 \times 10^8$ copies of *F. proliferatum* and *F. verticillioides* synthetic target DNA, respectively), after several fruitless attempts it became evident that DNA amplification was entailed before the analysis.

Since the development of PCR more than 30 years ago, the application of DNA amplification methods has expanded enormously in the fields of clinical, veterinary, food, and environmental diagnostics. PCR continues to be the most widely applied amplification method, although years of research have introduced several exciting improvements to the technology, including optimized DNA polymerases and real-time PCR. Besides, isothermal amplification methods, such as loop-mediated isothermal amplification (LAMP) or helicase-dependent amplification, have gained remarkable attention as an exciting alternative for PCR because the amplification does not require thermal cycling but can be performed at a constant temperature. Several reports in the literature have shown the applicability of such methods for identifying foodborne bacteria and fungal pathogens.[327] For the detection of some *Fusarium* species, LAMP primers have been designed, for example, based on *tri5* and *tri6* genes which are involved in the trichothecene biosynthesis,[328] or using the 28S ribosomal DNA sequences as the target. Unfortunately, the high GC-content of the IGS regions makes this highly variable region a rather impossible target to develop such isothermal methods.[329]

Nevertheless, standard thermal cyclers for PCR are these days rather common laboratory equipment, and the additional step of PCR in this work did not increase the analysis time extensively, as no further purification was required, and the PCR reaction could be directly used for the analysis. To avoid having a complex mixture of several PCR primers and having to handle with cross-reactivity issues in the amplification, or complicated PCR reaction optimization, we designed a common primer pair which could be used to amplify the IGS region of most of the *Fusarium* species within the *F. fujikuroi* species complex (**Figure 50A**). The complexity of the genomic DNA as a target was also noted in the PCR reaction which required optimization and a specific PCR polymerase optimized for the amplification of long or GC-rich DNA templates. Amplification with the KOD Xtreme Hot Start DNA Polymerase kit, using betaine as an enhancer, enabled amplification of the IGS region using contaminated maize as the sample matrix (**Figure 50B**). Analysis of samples contaminated with *Fusarium* or other fungal species demonstrated the applicability of the developed genosensors to real samples and proved that these devices could provide a simple and robust method for the detection of mycotoxigenic *Fusarium* species in food samples.

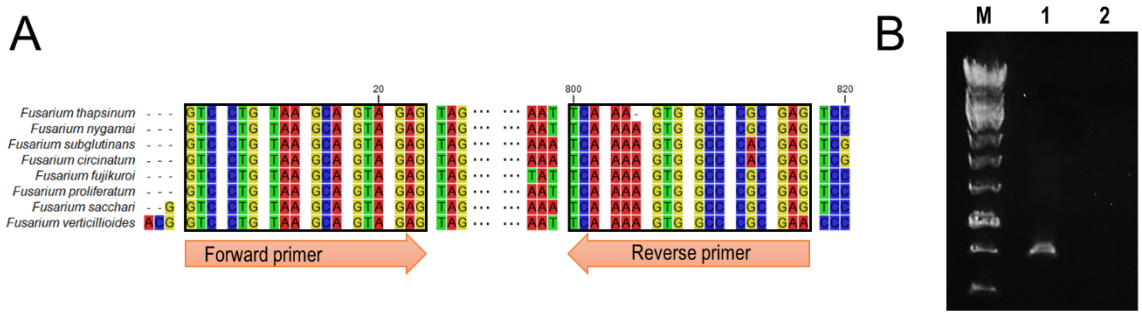


**Figure 50**. (A) Schematic of the IGS region with the common primer pair (orange arrows) used to amplify the genomic rDNA of most of the species in the *Fusarium fujikuroi* species complex. (B) Analytical gel electrophoresis was used to confirm successful PCR amplification using as a template a maize sample contaminated with *F. proliferatum.* PCR product (746 bp) was seen when using KOD Xtreme Hot Start DNA Polymerase (lane 1) although KAPA HiFi HotStart DNA Polymerase (lane 2) could not amplify the target from the same sample. Lane M shows the molecular marker, GeneRuler 1kb.

### 4.1.3 INTEGRATION OF THE OPTICAL GENOSENSOR ON A MICROFLUIDIC PLATFORM

Recently, considerable efforts have been devoted to developing integrated test platforms using microfluidic lab-on-a-chip technologies. In fact, microfluidics has been even described as a powerful tool with the potential to significantly change the way modern biology is performed.[330] These platforms can enable measuring or quantifying the target analyte in a fully automated fashion, and the most advanced systems include the integration of various processes, from raw sample pretreatment to specific biomolecular detection.[331] Microfluidic chip–based approaches for DNA analysis have been reported to overcome some of the limitations seen in other applications, such as long reaction times and various manual operations which are required in traditional approaches.[332] The advantages of using microfluidic systems with small dimensions for bioanalytical assays include the possibility of using only minute quantities of the reagents and short reaction times, because the molecular diffusion lengths are of the order of the microchannel dimension.[331] Therefore, for example, the drawbacks of slow DNA hybridization can be avoided by flowing the assay components through microfluidic channels.

A myriad of miniaturized fluidic systems has been designed with various geometrical microchannel designs based on different microfluidic flow patterns. In particular, microparticles have been combined with microfluidics systems which can be modified to generate controlled hydrodynamic forces acting on the particles.[331] The movement of magnetic particles is often controlled by external magnets or electromagnets, and for optical detection the particles can be concentrated at a designated detection site. As the surface chemistry of the microchannels themselves is often irreproducible, the use of microparticles as the solid surface can circumvent such drawbacks because the particle surface chemistry can be controlled off-chip.[331] In continuation with the work described in **publication I**, we aimed to develop an integrated platform for *Fusarium* detection using the same assay concepts reported previously but performing the reaction in a microfluidic chip.

Glass is a widely used material for microfluidics but also plastic polymers have many interesting properties and have the advantage of lower cost and ease of chemical modification.[331,333] The integrated microdevice (**Figure 51**) for fungi detection, designed in collaboration with Micronit Microtechnologies (Enschede, The Netherlands), was fabricated by micro-milling using an optically highly transparent polymer (cyclic olefin copolymer). The Micronit clamping system was used to provide the connections to the syringe pump, the integrated heater, and the complementary metal–oxide–semiconductor (CMOS) detector.

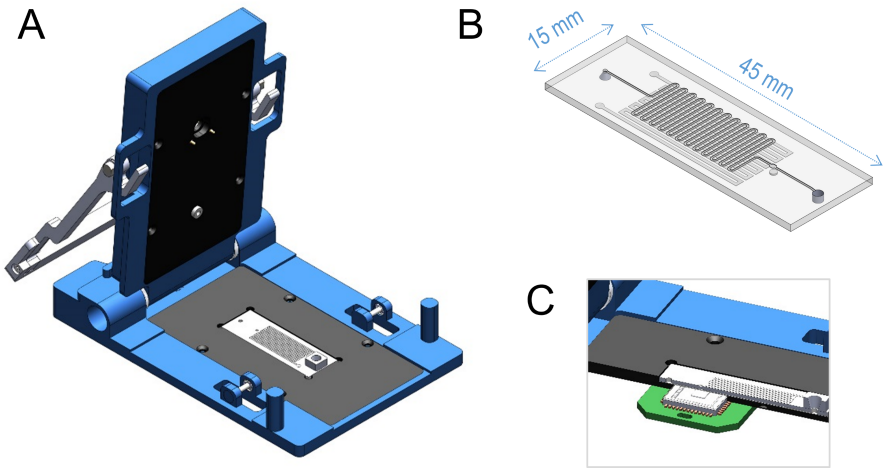


**Figure 51.** Chip design for the integrated genosensor. (A) Chip in the Micronit clamping system which provides the connections for the fluidic (syringe pump), electric (integrated heater), and optical (CMOS detector) structures of the system. (B) Microfluidic chip (dimensions 15 × 45 mm) designed for fungi detection. (C) CMOS detector (on the green support) placed under the capture chamber to measure the luminescence signals. Figure copyright: Sandro Meucci/Micronit Microtechnologies.

More specifically, the microfluidic chip consisted of a serpentine channel for the DNA hybridization, a chamber for the capture of the beads, and an integrated heater (**Figure 52**). The heating element was required to achieve the temperature of +60°C for optimal DNA hybridization (**Figure 8C**). For this purpose, conductive silver paste was dispensed on top of the chip (at 1.1 mm distance above the channel), and a temperature sensor was placed at the bottom of the chip (at 0.1 mm distance below the channel). Electrical connections to the heater and the temperature sensor were used for the feedback-controlled temperature system. The detection chamber downstream of the serpentine channel was designed and optimized for the capture of the magnetic microparticles using an external magnet which was positioned above the detection chamber. After the magnetic capture, the beads were washed, followed by the generation of a fluorescent or chemiluminescent signal by addition of the substrate. Fluorescent detection using a fluorescent microscope was used in the preliminary experiments, however it was later replaced by a chemiluminescent detector using a simple and low-cost configuration without an external light source. The chemiluminescent signal was generated using luminol and hydrogen peroxide (PS-atto) as substrate for the enzyme HRP. As confirmed previously (**Figure 47**) the use of chemiluminescent detection could provide the required assay sensitivity.

The measurements in the integrated system were carried out using a small yet sensitive CMOS detector from Anitoa (Menlo Park, CA, USA). The CMOS sensor is ultra-sensitive, highly integratable and a low power detector,[334] which makes it compatible with the generation of low-cost and portable microfluidic systems platforms.

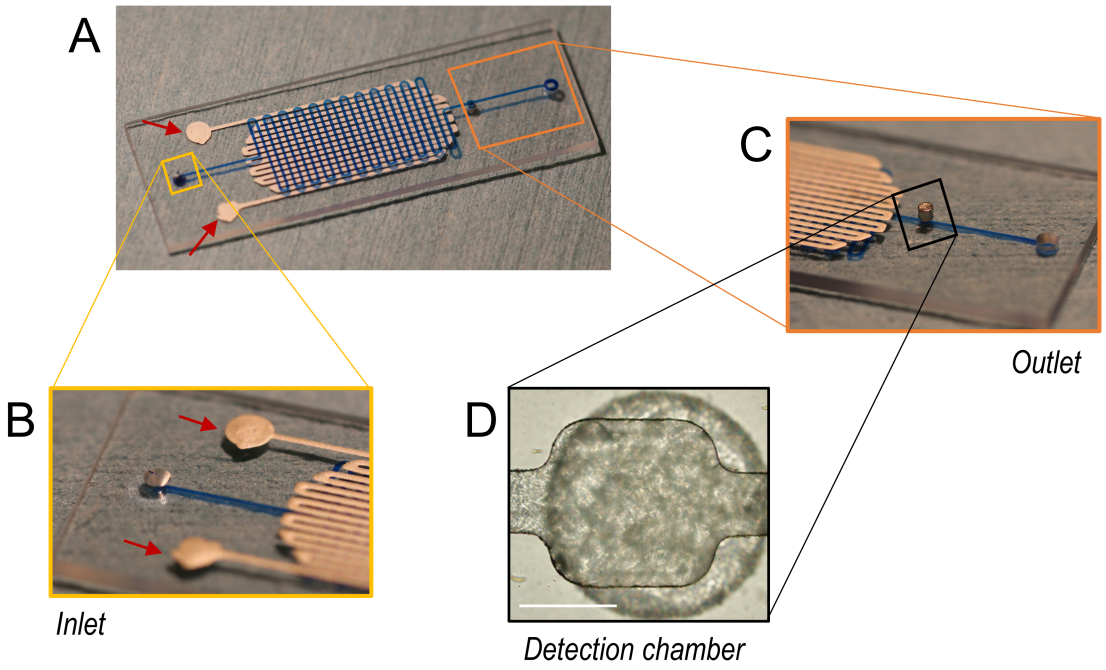


**Figure 52.** Microfluidic approach for *Fusarium* detection. (A) Chip with the hybridization channel (blue dye solution indicates the fluidic path) with a total volume of 6 µL (300 µm × 100 µm). (B) Open reservoir as the inlet allowed to add each reagent manually. (C) The outlet was connected to a syringe pump and was preceded with the (D) detection chamber (600 µm × 600 µm) where an external magnet was used to capture the microbeads. An integrated heater (indicated with red arrows in A–B) made of conductive silver paste was used as the heating element to reach the required hybridization temperature. Figure copyright: Sandro Meucci/Micronit Microtechnologies.

Preliminary experiments with fluorescent detection showed highly intense emission signals from the detection chamber after adding the fluorogenic substrate Amplex UltraRed (**Figure 53**). It is known that microfluidic systems benefit from the large surface-to-volume ratio of the microchannels, but, at the same time, often also the non-specific binding of reagents to surfaces increases with the surface-to-volume ratio.[335] Such behavior was vastly observed in the integrated genosensor, and high non-specific binding of the SA-HRP was seen to the uncoated polymer surface. Several ways to prevent the non-specific adsorption of proteins have been reported, for example, covering the surfaces with PEG or copolymers, such as Pluronic.[335] Preliminary results to block the channels with casein or BSA did not have the expected effect, but a significant improvement in the background was observed with Pluronic-127 coating (**Figure 53**, right). The microchannels covered with the copolymer showed reduced background signals in the absence of the target ssDNA, and the irreproducibility was decreased in comparison with the uncoated chip indicating that the coating could also help to standardize the surface properties of the channel.

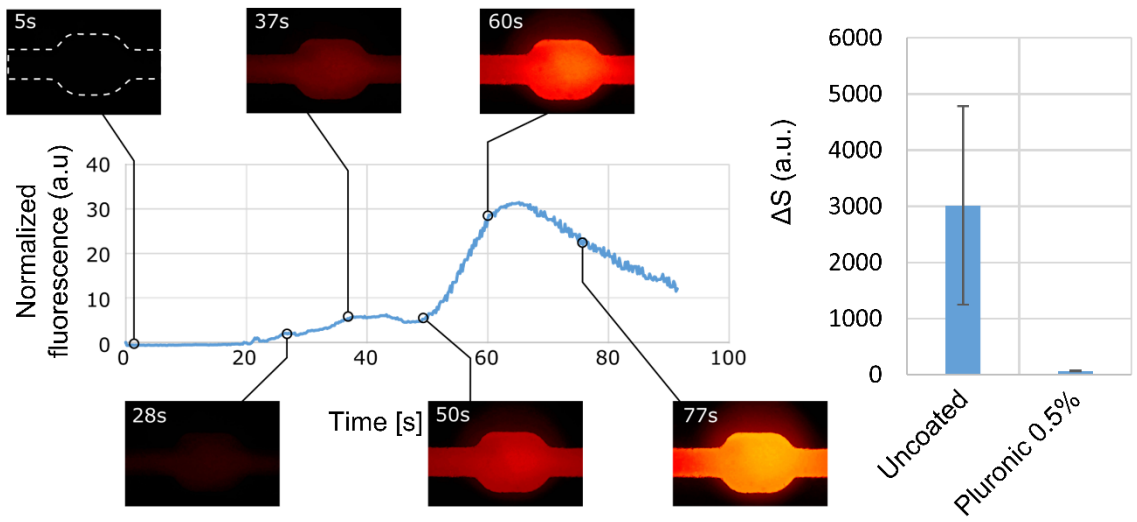


**Figure 53.** Fluorescent detection on the integrated genosensor showed intense emission from the detection chamber after addition of the substrate (Amplex UltraRed). High non-specific binding of SA-HRP to the uncoated surface was seen in the absence of the target (right graph) but coating the microchannels with Pluronic-127 (0.5%, w/v) was seen to improve the background and decrease the irreproducibility observed with the uncoated chip.

In the preliminary experiments, the efficiency of on-chip hybridization was evaluated by flowing the assay components through the heated microchannel but removing the beads after the reaction and performing the magnetic capture and fluorescence detection outside the chip. The comparison was then made with a reaction done in a microcentrifuge tube in the conventional way (1.5 h incubation at +60 °C). The on-chip hybridization produced similar results as the off-chip protocol (**Figure 54A**) but notably required significantly shorter reaction times (< 20 min).

In parallel, the chemiluminescent detection with the CMOS detector was studied by performing the hybridization off-chip but afterward flowing the beads onto the chip and capturing them in the detection chamber using a permanent magnet. The CMOS detector was then used to monitor the luminescence signals from the chamber upon adding the substrate (PS-atto). While the response from the negative control (no target ssDNA) resulted in low background signals, luminescence produced by the enzymatic reaction was seen in the presence of the target ssDNA (**Figure 54**). We are currently testing the fully integrated system, in collaboration with Dr. Meucci from Micronit Microtechnologies, to optimize the on-chip hybridization platform with integrated detection for *Fusarium* detection.

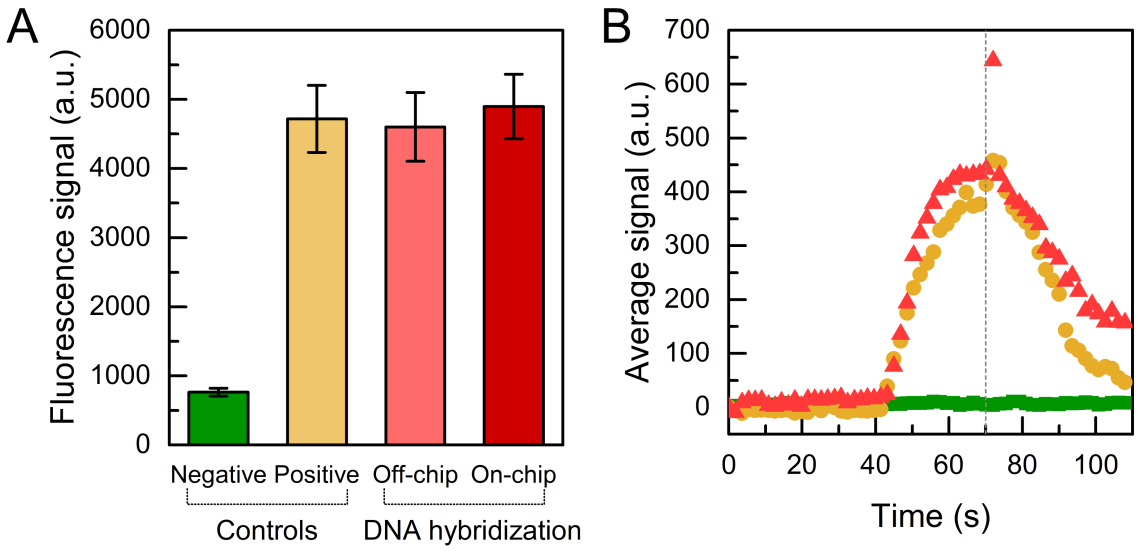


**Figure 54.** Preliminary results with the integrated approach for *Fusarium* detection. (A) On-chip DNA hybridization was tested using a direct *F. proliferatum* detection probe which was flowed through the microfluidic channel with the capture probe functionalized beads using the integrated heater set to +60 °C. Afterward, the beads were collected from the chip, and the fluorescence signals were measured after adding the fluorescent substrate (Amplex UltraRed). The response of the on-chip hybridization was then compared to the off-chip hybridization doing the assay in microcentrifuge tube at +60 °C. (B) Chemiluminescent measurement using the integrated CMOS detector. The hybridized sandwich complex was captured on the chip using an external magnet, and the CMOS detector was used to measure the luminescence signals from the beads in the detection chamber after adding the chemiluminescent substrate. Response from a control reaction without the target (green) was compared to the signals obtained when using 1 nM ssDNA target in the reaction (in two replicates; red triangles and yellow circles). The dashed line at 70 s indicates the time point where the flow of the substrate was stopped, and a decrease in the signals is seen.

# 4.2 Selection of mimotopes

The use of mimotopes has been introduced as an interesting alternative for the detection of small molecule analytes in competitive immunoassays. These short peptides are capable of mimicking the analyte and binding to the same antibody paratope, and thus, they can replace the hapten-conjugates conventionally used in competitive immunoassays. In this work, we have used a commercial peptide library to select mimotopes for mycotoxins with the final aim of developing detection methods for these toxins. Remarkably, mimotopes can be selected from phage-displayed libraries using the analyte-specific antibody as the target, even without any prior knowledge about the antibody–analyte binding. The following section discusses further the background and selection of mimotopes for $FB_1$ (**publication II**) and ZEA (**publication V**) together with unpublished results with T-2 toxin.

## 4.2.1 Ph.D.-12 PEPTIDE LIBRARY

The Ph.D. (for *Ph*age *D*isplay) system is based on simple M13 phage vector for display of peptides in the N-terminus of the phage minor coat protein pIII.[336] Commercially available libraries by New England Biolabs (Ipswich, MA, USA) based on this system are available in linear heptapeptide (Ph.D.-7 Library) and dodecapeptide (Ph.D.-12 Library), as well as a disulfide-constrained heptapeptide (Ph.D.-C7C Library) formats.[337] These combinatorial libraries consist of approximately $10^9$ unique and random peptides fused to the N-terminus of the minor coat protein (pIII) of M13 phage. The library insert is preceded by the pIII signal sequence (pIII leader) which is essential for the secretion, and a short spacer (GGGS) is included between the randomized segment and the pIII to improve accessibility to the displayed peptide. The phage vector M13KE (**Figure 55**), a derivative of M13mp19, can be simply and rapidly propagated without the need for antibiotic selection or helper phage superinfection.[336] On the other hand, the use of M13KE rather than the phagemid system results in a multivalent display where all five copies of pIII of each virion will be fused to the displayed peptide. Moreover, the vector contains the *lacZα* gene which allows identification of the phages from blue plaques on Xgal-containing media when using an appropriate *lacZα*-complementing strain (for example ER2738).[336]

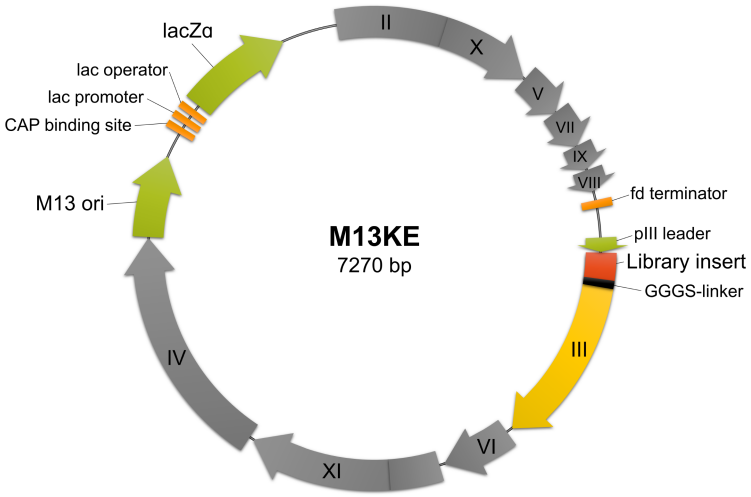


**Figure 55.** Map of the Ph.D. (M13KE) vector. The library insert (red; 12 amino acids in the case of Ph.D.-12) has been introduced as N-terminal fusion to pIII (yellow). A short spacer (GGGS-linker) is included between the randomized segment and the pIII. The *lacZα* in the vicinity of the (+)-origin of replication (M13 ori) permits blue–white screening to detect contamination with wild-type phages.

Various applications using these random peptide libraries have been reported, including epitope mapping, vaccine development, protein–protein interaction studies, and epitope mimicking.[224,225,336,338] Epitope mimics, also sometimes called antigenic mimics or immugenic mimics when used to elicit new antibodies, have an exceptional ability to mimic an epitope and bind to the paratope of an antibody that has been raised against another antigen. Epitope mimics are not necessarily true structural mimics but might bind in an entirely different way *via* different interactions than the original epitope.[254] The advantages of epitope mimics over the natural antigen as diagnostic reagents include an easier and cheaper manufacture, and they can be used even when the natural antigen is unknown or undefined.[254,272] For immunoassay development, epitope mimics are an intriguing alternative to be used as the competitor instead of the antigen-conjugate. In this work, epitope mimicking peptides, or mimotopes, have been selected for mycotoxins from phage-displayed peptide libraries. The identified mimotopes have then been used in competitive immunoassays to replace the use of toxin-conjugates. This approach not only avoids the cumbersome conjugation step but also allows developing toxin-free assays which are easier and cheaper to manufacture and safer to the user than the conventional methods.

### 4.2.2 PANNING SELECTIONS

A multitude of factors can have a significant effect on the outcome of the pannings. Although many theoretical aspects have been described in the literature and a variety of strategies have been reported with excellent outcomes, often with a new target the best selection conditions have to be investigated by trial and error. One successful strategy for finding good binders by phage display has in fact been described as “try everything you can think of.”[339] The

methodology, affinity, and avidity can be affected by selecting a library with a suitable display format and peptide structure. Moreover, the selection conditions including the target immobilization methods and a variety of elution methods also play an essential role in the quest for optimal binders.

In this work, a total of five selections for mimotopes for $FB_1$, ZEA, and T2-toxin were completed with minor modifications to the protocols recommended by the manufacturer.[337] **Table 15** summarizes the conditions used in each of the rounds. The first screenings from the Ph.D.-12 library, for $FB_1$ and T-2 toxin, were performed without major modifications. The target antibody for $FB_1$ or T-2 toxin was immobilized by non-specific absorption to the plastic surface of the microtiter plate, and after incubation and stringent washes, the bound phages were eluted in acidic conditions with glycine-HCl (pH 2.2). While such an approach resulted in an excellent mimotope for $FB_1$ (**publication II**), the selections for T-2 toxin were somewhat inconclusive. Thus, later experiments with ZEA and T-2 toxin were performed in modified conditions, by evaluating the antibody immobilization strategy, the use of alternative elutions, and the effect of the pre-selection.

**Table 15**. Summary of the selection condition used in this thesis for the identification of mycotoxin mimotopes using the Ph.D.-12 library. Various strategies employed included introducing a pre-selection step prior to the target selection, a competitive elution step with the free toxin, and a bead-based panning with oriented antibody immobilization. Key changes to the original protocol by the manufacturer in each protocol are indicated in bold.

| | | **$FB_1$** | **Zearalenone (i)** | **Zearalenone (ii)** | **T-2 toxin (i)** | **T-2 toxin (ii)** |
|---|---|---|---|---|---|---|
| **1st** | Negative selection | BSA | – | **BSA** | BSA | – |
| | Target selection | 10 µg/ml anti-$FB_1$ | **10 µg/ml** anti-ZEA | **10 µg/ml** anti-ZEA | 10 µg/ml anti-T2 | 300 ng anti-T2 (**protein G** –MBs) |
| | Washing | 5x PBS-T(0.1%) | 6x PBS-T(0.1%) | 6x PBS-T(0.1%) | 5x PBS-T(0.1%) | 5x PBS-T(0.1%) |
| | Elution | Glyc-HCl | Glyc-HCl | Glyc-HCl | Glyc-HCl | Glyc-HCl |
| **2nd** | Negative selection | BSA | – | **BSA** | BSA | MBs and anti-DON (“cross-reactant”) |
| | Target selection | 10 µg/ml anti-$FB_1$ | **5 µg/ml** anti-ZEA | **5 µg/ml** anti-ZEA | 10 µg/ml anti-T2 | 300 ng anti-T2 (**protein A** –MBs) |
| | Washing | 10x PBS-T(0.1%) | 10x PBS-T(0.5%) | 10x PBS-T(0.5%) | 10x PBS-T(0.1%) | 10x PBS-T(0.1%) |
| | Elution | Glyc-HCl | **100 ng/ml ZEA** | **100 ng/ml ZEA** | Glyc-HCl | Glyc-HCl |
| **3rd** | Negative selection | – | – | **BSA** | BSA | MBs and anti-DON (“cross-reactant”) |
| | Target selection | 10 µg/ml anti-$FB_1$ | **2.5 µg/ml** anti-ZEA | **2.5 µg/ml** anti-ZEA | 10 µg/ml anti-T2 | 300 ng anti-T2 (**protein G** –MBs) |
| | Washing | 10x PBS-T(0.5%) | 10x PBS-T(0.5%) | 10x PBS-T(0.5%) | 10x PBS-T(0.1%) | 10x PBS-T(0.1%) |
| | Elution | Glyc-HCl | **10 ng/ml ZEA** | **10 ng/ml ZEA** | Glyc-HCl | **50 µg/mL T-2 toxin** |
| **4th** | Negative selection | – | | | BSA | MBs and anti-DON (“cross-reactant”) |
| | Target selection | 10 µg/ml anti-$FB_1$ | | | 10 µg/ml anti-T2 | 300 ng anti-T2 (**protein G** –MBs) |
| | Washing | 10x PBS-T(0.5%) | | | 10x PBS-T(0.1%) | 10x PBS-T(0.1%) |
| | Elution | Glyc-HCl | | | Glyc-HCl | **50 µg/mL T-2 toxin** |
| **5th** | Negative selection | – | | | BSA | |
| | Target selection | 10 µg/ml anti-$FB_1$ | | | 10 µg/ml anti-T2 | |
| | Washing | 10x PBS-T(0.5%) | | | 10x PBS-T(0.1%) | |
| | Elution | Glyc-HCl | | | Glyc-HCl | |

*Abbreviations: BSA, bovine serum albumin; Glyc-HCl (0.2 M glycine-HCl, pH 2.2); MBs, magnetic beads; PBS-T, PBS with Tween-20 (percentage in parenthesis)*

### 4.2.2.1 Selection of zearalenone mimotopes

The selections of zearalenone (ZEA) mimotopes were conducted using a similar protocol applied for $FB_1$.[230] In the first selection round, a high concentration of the antibody was immobilized to guarantee the capture of the all the selective clones from the library. In the subsequent second and third rounds, when a preliminary enrichment had already been achieved, decreasing amounts of the immobilized antibody were used. Thus, the avidity effects of the multivalent phage display could be diminished, and peptides with better affinity could be selected. Moreover, in order to favor the selection of binders which are capable of competing with the free toxin, the elution step in the second and third rounds was performed by competition with ZEA, instead of the acidic elution that was used in the first round. Also, the toxin concentration was reduced in the third round (100 ng $mL^{-1}$ and 10 ng $mL^{-1}$ of ZEA in the second and third rounds, respectively) to favor the elution of the peptides providing the highest assay sensitivities, rather than those with highest affinities. Altogether, the more restricted selection conditions should favor enrichment of the best mimotopes. In parallel, the effect of the pre-selection step was studied by comparing selections where the phage pools were introduced directly to the target (i) with those that included a pre-selection step with the blocked plate (ii). The idea of the pre-selection step was to remove non-specific binders which recognize the components of the solid surface, or the blocking agents used, from the pool before the actual selection. The risk of such selection is the coincidental elimination of a fraction of interesting binders. In this case, no significant differences were observed between the two approaches, neither in the output titers nor in the response in the ELISAs (**Figure 56**). Enrichment of specific binders was seen in both cases, and it was concluded that, in this case, the pre-selection step did not have any significant contribution on the background signal. Probably, the competitive elution step in the second and third rounds had an important effect in this matter, as it could provide high specificity in the elution step regardless of the specificity of the binding in the first place.

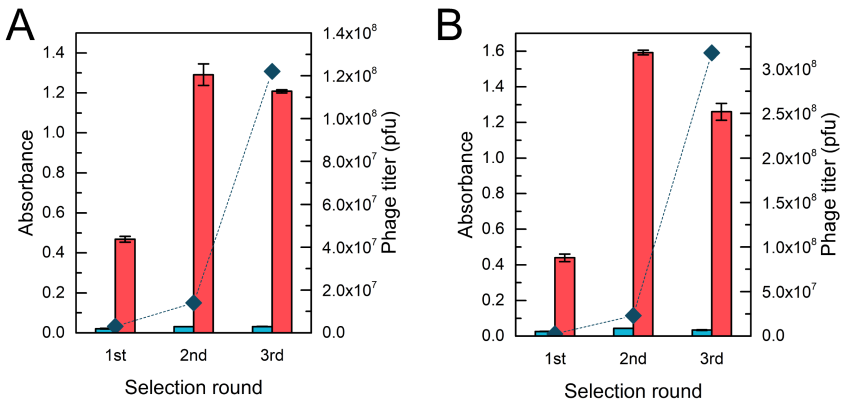


**Figure 56**. Results of the ELISA with the polyclonal phage pools after each selection round for zearalenone (ZEA) mimotopes with (A) and without (B) a pre-selection step. Binding of the phages was tested to the background (blue) and the immobilized target anti-ZEA antibody (red). Likewise, enrichment of the phages could be depicted as increasing phage titers after each selection round (blue diamonds; right y-axis).

### 4.2.2.2 Selection of T-2 toxin mimotopes

T-2 toxin was one of the mycotoxin targets which was included in the objectives of this work because it is produced by the same *Fusarium* genus as fumonisins. However, working with this hydrophobic toxin proved to be challenging on several occasions, and the results were not as promising or straightforward as with $FB_1$ and ZEA. Mimotope selections for T-2 toxin were conducted with different strategies, but in the end, none of them could provide us with a robust mimotope. The first selections were done in a similar way as for $FB_1$ in **publication II**,[230] and enrichment and specific binding was seen in the ELISA with the polyclonal phage pools after each round (**Figure 57A**).

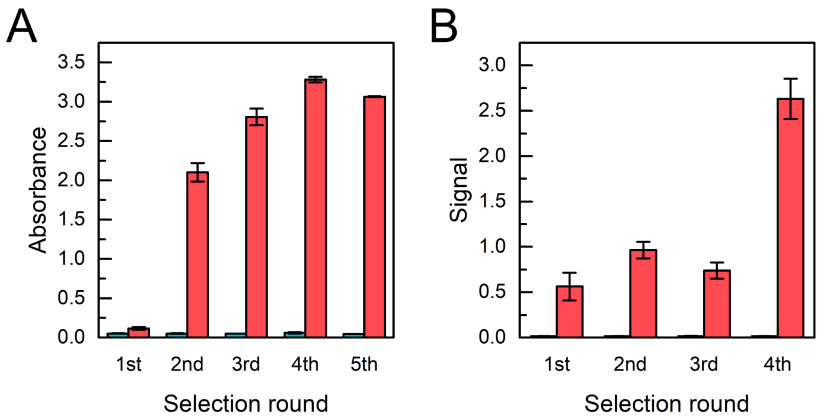


**Figure 57**. Results of the ELISA with the polyclonal phage pools after each selection round of T-2 toxin mimotopes (A) selection on the plate (i), and (B) selection on magnetic beads (ii). Binding of the phages was tested to the background (blue) and the immobilized target anti-T2 antibody (red).

Amplification and analysis of individual monoclonal phages revealed a number of clones capable of binding specifically to the T-2 toxin antibody (**Figure 58A**). However, sequencing of the positive clones did not reveal clearly conserved sequences or consensus motifs, and thus, six different monoclonal clones were tested in the competitive assay with the free toxin to confirm their functionality as epitope mimics. All tested clones showed competition, but the provided sensitivities and reproducibility varied significantly. **Figure 59** shows the assays performed on three different days with six of the clones. Based on the competitive ELISA results, clones F11 and H11 showed the best performance in the competitive assay, both in terms of sensitivity and reproducibility, and were selected for the subsequent experiments.

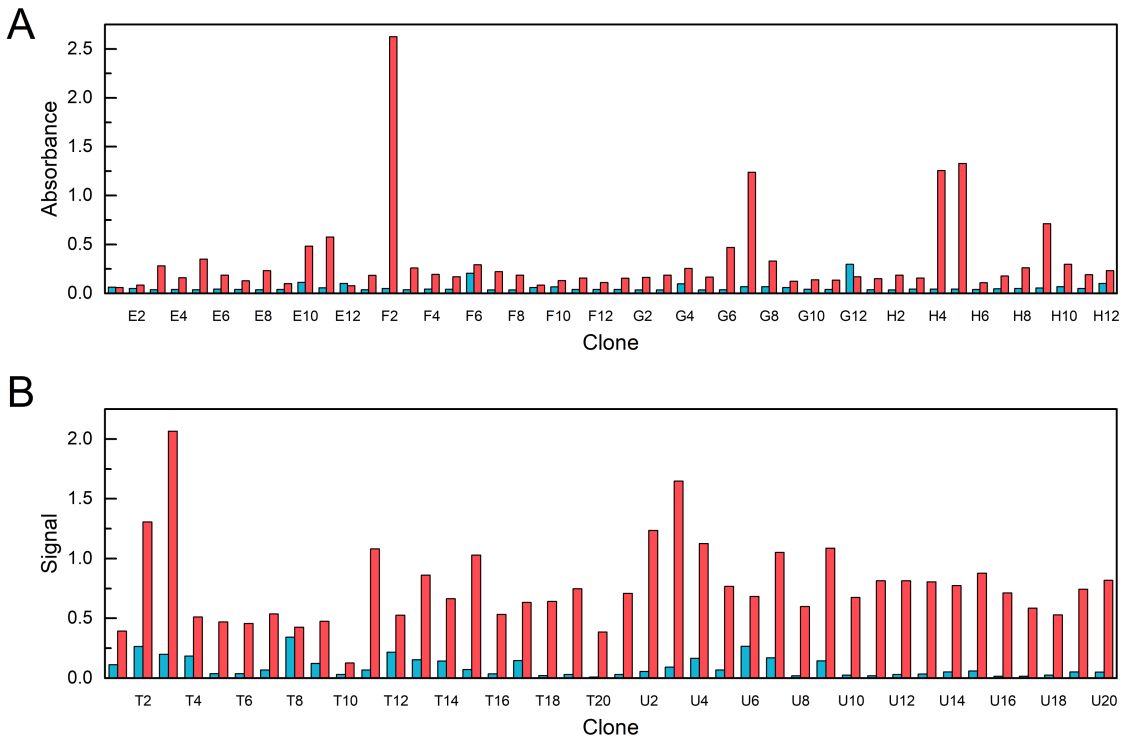


**Figure 58**. Results of the ELISA with the monoclonal T-2 toxin mimotopes from the selection on (A) plate (i), and (B) magnetic beads (ii). Binding to the background (blue) and the anti-T2 antibody (red) was tested, and the clones with the best signal-to-background ratios were identified by DNA sequencing.

Later, the selections for T-2 toxin mimics were repeated from scratch using magnetic beads functionalized with protein A or protein G as the solid surface. This strategy was thought to result in the selection of better mimotopes as the binding step could be performed in solution followed by antibody capture in an oriented manner. Moreover, a competitive elution step with the free toxin was used in the third and fourth rounds, instead of the treatment at low pH to release the bound phages. Enrichment and high specific binding to the antibody was observed already after one round, and the second and third rounds did not result in further enrichment, as confirmed in the ELISA (**Figure 57B**). This could probably be explained with the more stringent conditions used in the elution step in the third round. The fourth round showed significant further enrichment, and the majority of the monoclonal clones selected from the third and fourth rounds showed specific binding to the target (**Figure 58B**).

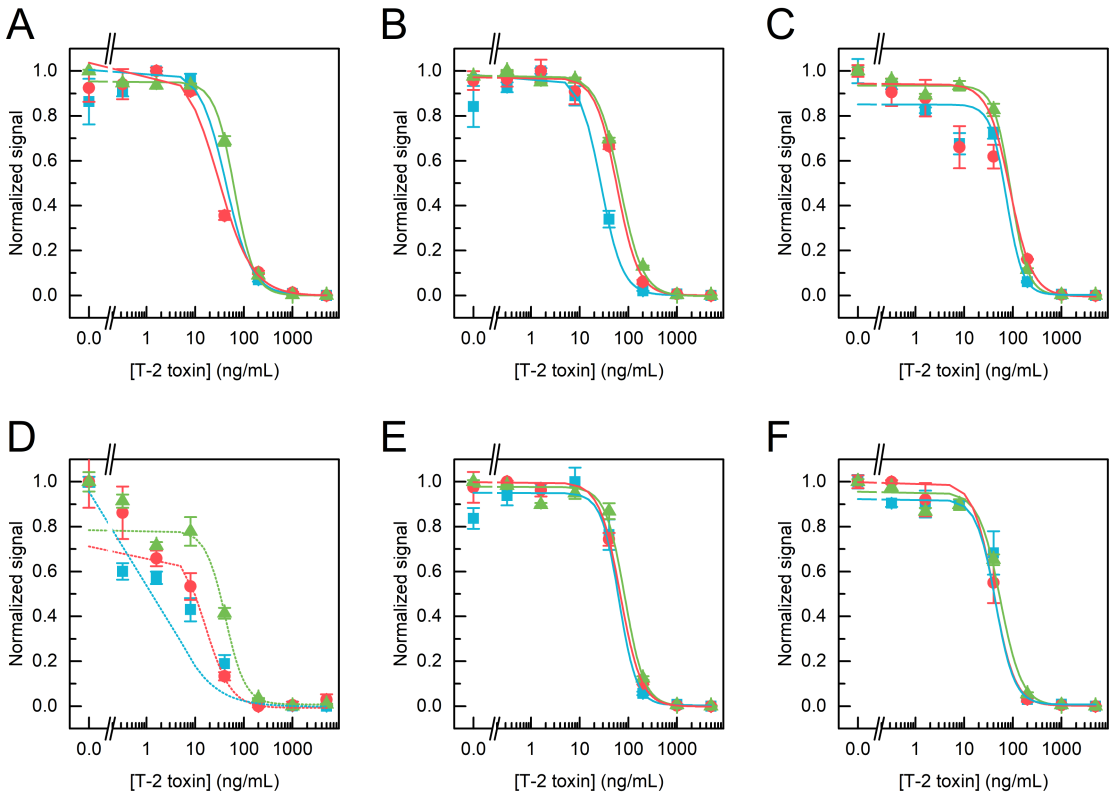


**Figure 59**. Competitive phage-based ELISA with T-2 toxin mimotopes (A) F5, (B) F11, (C) G5, (D) H5, (E) H9, and (F) H11 from the first (i) selections. Normalized signals are depicted as the average of the replicate measurements ± the standard error of the mean ($n$ = 3) and fitted with the four-parameter logistic fit (OriginPro 9.0). Each assay was repeated three times on different days (blue, green, red) to test the inter-day variation.

Sequencing of the T-2 monoclones from the second selections (ii) revealed only one new peptide sequence (namely T13) which was further tested in the competitive ELISA. In comparison with the previously selected mimotopes (F11 and H11), T13 showed better sensitivity which perhaps could be attributed to the competitive elution step. The binding kinetics was not studied directly but based on the results of the ELISA and the cross-reactivity studies, T13 was suspected of having lower affinity to the antibody than F11 and H11. Lower affinity could provide better sensitivity as lower concentrations of the free toxin could induce competition, but at the same time the binding was less specific, and some non-specific binding and cross-reactivity with other antibodies were observed (**Figure 60**).

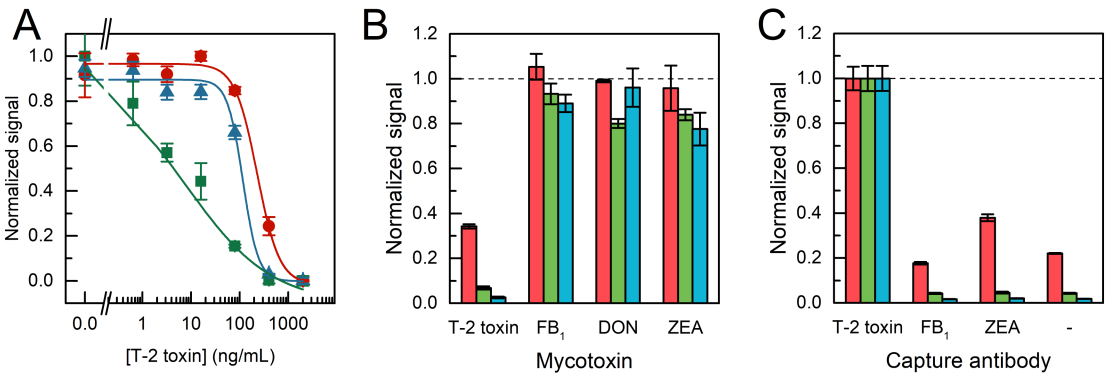


**Figure 60.** (A) Competitive phage-based ELISA with the monoclonal T-2 toxin mimotopes F11 (red), H11 (blue), and T13 (green). Normalized signals are depicted as the average of the replicate measurements ± the standard error of the mean ($n$ = 3) and fitted with a four-parameter logistic fit (OriginPro 9.0). (B) Cross-reactivity with different mycotoxins (1 µg $mL^{-1}$) and (C) binding to the background or other anti-toxin antibodies. Signals are normalized to the signal obtained in the absence of the toxin with the anti-T2 antibody.

### 4.2.2.3 Identification of mycotoxin mimicking peptides

Following the pannings and the phage-based ELISAs, selected positive clones which showed specific binding to their target antibody were identified by DNA sequencing. **Table 16** presents all the identified sequences from the pannings against $FB_1$, ZEA, and T-2 toxin antibodies. Clear enrichment of certain peptide sequences was seen in the case of $FB_1$ and ZEA, and among the ten sequenced clones, only four different sequences were observed. In both cases, two conserved sequences (A2 and D1 for $FB_1$, and SF and GW for ZEA) were present in 80% of all the phages. Based on the sensitivity and reproducibility of the competitive assays using these clones, mimotopes A2 (**publication II; Figure 15**) and SF (**publication V; Figure 44**) were selected as the best candidates for $FB_1$ and ZEA, respectively.

For T-2 toxin two separate selections were conducted, but the identified sequences did not clearly show enriched or conserved peptides. A total of twenty clones were sequenced, among which 12 different sequences were observed. Some similarities were seen between these peptides, and short conserved motifs could be observed (**Table 16**). Based on the competitive assays clones F11 and T13 were selected for further assay development.

**Table 16**. Identified peptide sequences from the fumonisin $B_1$ ($FB_1$), T-2 toxin, and zearalenone (ZEA) mimotope pannings. The best candidates selected for the subsequent experiments are indicated with an asterisk after the mimotope name. The frequency (%) refers to the occurrence of the same sequence found among the sequenced clones (10 clones for $FB_1$ and ZEA, 20 clones for T-2 toxin). Conserved amino acids or motifs are indicated in bold, and X refers to an unknown amino acid.

| Target toxin | Mimotope name | Sequence | Frequency |
|---|---|---|---|
| $FB_1$ | D1 | -----RPL**D**LYPGSGQE--- | 60% |
| $FB_1$ | A2(*) | VTPNDDTF**D**PFR-------- | 20% |
| $FB_1$ | C9 | VXGIXNGW**E**SYE-------- | 10% |
| $FB_1$ | D8 | --------**D**MVPTFWLTEFT | 10% |
| ZEA | SF [B1](*) | SFDYFL**W**DSTET----- | 50% |
| ZEA | GW [F2] | ----GW**W**GPYGEIELL- | 30% |
| ZEA | B2 | --SMTP**W**HILAPRA--- | 10% |
| ZEA | H2 | -----T**W**GPYGEAPLWP | 10% |
| T-2 toxin | F11(*) | NVAGHSPF**DY**VF---------- | 15% |
| T-2 toxin | H5 | ----TPQP**DY**LHLLMK------- | 15% |
| T-2 toxin | F5 | ----ETAM**DY**LFRKPS------- | 10% |
| T-2 toxin | G5 | --------SSSLES**WQ**HFLR--- | 10% |
| T-2 toxin | H9 | ----------YNP**WQ**D**FW**SSQP | 10% |
| T-2 toxin | H11 | ---SS**DPFSY**LFRNA-------- | 10% |
| T-2 toxin | H6 | ---YV**DPFS**MVFSK**W**-------- | 5% |
| T-2 toxin | T13(*) | -----SGVYKVAY**DWQ**H------ | 5% |
| T-2 toxin | E7 | --------SLVND**DWQ**Q**FW**T--- | 5% |
| T-2 toxin | G3 | --------VTPNS**DW**EA**FW**A--- | 5% |
| T-2 toxin | G11 | --------YRHPSS**W**ET**FW**S--- | 5% |
| T-2 toxin | H2 | ITRQADMLSQVF---------- | 5% |

Comparison of all the peptide sequences identified as mimotopes revealed some common characteristics, although the targets were different. The reported frequency of each amino acid within the original Ph.D.-12 library[338] was compared to the frequency of the amino acids among the clones sequenced for $FB_1$, ZEA, and T-2 toxin (**Figure 61**) to determine if certain amino acids were favored in the selections. Most remarkably, for all the targets the fraction of aromatic and negatively charged amino acids was incremented in comparison with their original frequency in the library. Enrichment of these amino acids suggests their essential role in the binding interactions to the antibody paratope. Some rational can also be seen when comparing the amino acids content of the mimotopes for different targets, in particular in the case of $FB_1$ which is more hydrophilic (log $K_{OW}$ = 1.84[340]) than the other mycotoxins (log $K_{OW}$ (ZEA) = 3.580;[341] log $K_{OW}$ (T-2 toxin) = 2.27, est.[342]). Whereas the percentage of the hydrophobic amino acids (A, I, L, M, V, F, W, Y) amongst the mimotopes sequenced for T-2 toxin and ZEA was 43–45%, the sequenced $FB_1$ mimotopes contained only 29% of the hydrophobic amino acids. The observed trend of an augmented fraction of aromatic and negatively charged residues, as seen in **Figure 61**, is also consistent with previous reports stating that mycotoxin mimotopes usually contain several charged and aromatic amino acids.[193]

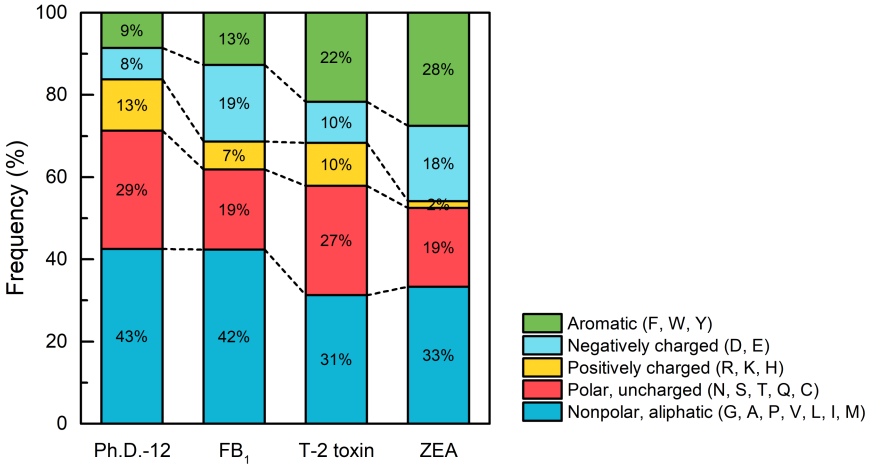


**Figure 61**. The frequency of amino acids observed in the original Ph.D.-12 library[338] and among the sequenced clones (**Table 16**) after 3–5 selection rounds for fumonisin $B_1$ ($FB_1$), T-2 toxin, and zearalenone (ZEA) mimotopes.

### 4.2.2.4 Anti-immune complex peptides

Given that theoretically the sensitivity, kinetics, and linear range of the non-competitive or sandwich-type immunoassays are superior to the competitive ones,[93,343] one of our aims was to develop non-competitive assays for mycotoxin detection. The anti-immune, or anti-metatype, concept refers to antibodies which are capable of binding to the primary antibody only when it is bound to the antigen (**Figure 62**). Antibodies with such extraordinary characteristics were originally monoclonal antibodies developed by immunization,[344] but later on phage-displayed libraries with antibodies[136,345,346] and peptides[347–351] have been used as well. Although the exact nature of the anti-immune complex interaction is controversial,[344] non-competitive immunoassays based on such two-site format have been shown to improve the sensitivity and specificity in comparison with competitive assays.[136,347]

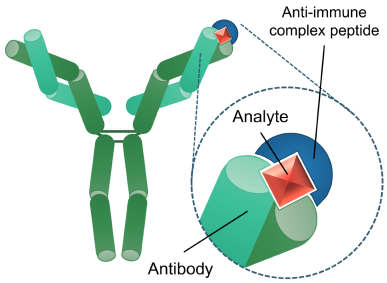


**Figure 62**. Scheme of the non-competitive immunoassays with the anti-immune complex peptide. Such antibody–analyte–peptide trivalent interaction allows the development of noncompetitive sandwich-type assays for small molecule detection.

With these aspects in mind, we screened the same Ph.D.-12 peptide library for anti-immune complex binders for mycotoxin detection. Selections against $FB_1$, T-2 toxin, and ZEA antibodies in the presence of the corresponding toxin were performed. In this case, a pre-selection with the antibody alone was conducted to favor the selection of those clones interacting with the antibody–analyte complex. In the case of $FB_1$ and T-2 toxin, a total of five selection rounds were completed. The phage-based ELISAs with the polyclonal phages after each round showed enrichment of antibody binding clones after the second or third rounds, and similar signals were observed in the presence and absence of the target toxin (**Figure 63A–B**). Thus, the selections did not seem successful as genuine anti-immune complex peptides should bind only to the antibody when bound to the toxin analyte. Similarly, the selection of peptides binding to the ZEA anti-immune complex was unsuccessful, and no enrichment was observed after three rounds neither in the phage-based ELISA nor in the phage titers after each round (**Figure 63C**). For ZEA, also a total of 80 monoclones from the third round were amplified and tested individually by ELISA, but none of them showed the expected response as an anti-immune complex peptide.

It remains to be uncovered whether and how anti-immune peptides can be selected from the peptide library in question. The only conclusion that can be drawn from these experiments, and in agreement with previous reports,[347] is that anti-immune complex binders are difficult to obtain. This could be partially explained considering that, when bound to the antibody, many small molecules are in fact buried rather deep in the antibody paratope. Actually, it has been reported that up to 85% of the accessible surface of a small molecule analyte can be buried when bound to the antibody,[352,353] and therefore, only a small fraction of the analyte remains available for contributing to the formation of the immune complex.[347] Moreover, nearly all the previously reported anti-immune complex peptides have been selected from peptide libraries with constrained peptides loops.[347,349–351,354] In the work of Wang *et al.* (2013), all New England Biolabs libraries, Ph.D.-7, Ph.D.-12, and Ph.D.-C7C, were used to select anti-immune complex peptides for 2,2′,4,4′-tetrabromodiphenyl ether. The Ph.D.-C7C with cyclic heptapeptides showed a larger increase in titer during the selection rounds in comparison with the Ph.D.-7 and Ph.D.-12 libraries.[355] Moreover, the best anti-immune complex peptide was found from this constrained library, suggesting that since cyclic peptides may have a higher affinity to the target than linear ones, they might present a more appropriate alternative for the selection of anti-immune complex peptides.

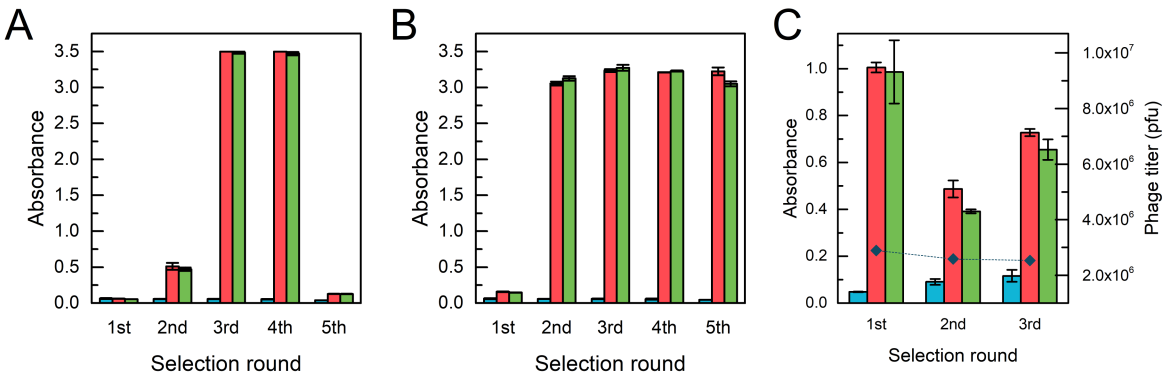


**Figure 63**. Selection of anti-immune complex peptides for (A) $FB_1$, (B) T-2 toxin, and (C) ZEA. Binding of the polyclonal phage pools to the background (blue), the anti-toxin antibody (red), and the anti-immune complex (green; antibody together with the corresponding toxin, 300 ng $mL^{-1}$ $FB_1$ or T-2 toxin, or 1000 ng $mL^{-1}$ ZEA) were determined after each round. For ZEA, the phage titers after each round are indicated with blue diamonds in the right y-axis.

# 4.3 Phage-displayed antibody libraries

All the work described in the publications and with the mimotopes was carried out using commercial monoclonal antibodies. These antibodies, at least in the case of $FB_1$ and ZEA, provided excellent sensitivity and specificity for the detection of their target toxin. However, the use of commercial antibodies is subject to certain limitations. One obvious drawback is the price and the dependency on the commercial provider. Moreover, in some cases, the manufacturer provides only limited details about the product, and some commercial antibodies for mycotoxins have been demonstrated to have high cross-reactivity with other similar toxins.[183,184] Thus, this work also aimed to select recombinant antibodies from a phage-displayed antibody library. Successful selection of mycotoxin-specific antibodies could potentially replace commercial monoclonal antibodies, and after identifying a good recombinant binder, it could be produced in bacteria in a cost-effective manner and with the desired modifications.

## 4.3.1 THE DOMAIN ANTIBODY LIBRARY

The commercial domain antibody (DAb) library used in this work is based on a single human $V_H$ framework (V3-23/D47) where diversity has been introduced in the antigen-binding site, *i.e.*, CDRs, by PCR mutagenesis. The DAb library, with a size of $3 \times 10^9$, has been constructed in the phagemid format which leads to mostly monovalent display (**Figure 64**).[356,357] Thus, the library has the potential for selecting high-affinity binders, as it has been reported, for example, for the multiple sclerosis antigenic peptide CSF114(Glc)[358] and for *Mycobacterium tuberculosis* heat shock protein,[359] using the same library.

In this work, the selection of $FB_1$ and T-2 toxin binders was conducted using immobilized $FB_1$–BSA or T2–HSA -conjugates, as the target, according to the manufacturer's protocols.[356,357] Briefly, a 1000-fold excess of the DAb-library ($3 \times 10^{12}$ phages) was pre-selected against BSA/HSA-coated wells and then incubated with the toxin-conjugate immobilized to a microtiter plate by non-specific absorption. After stringent washes, the phages were eluted by incubation with trypsin, which cuts the c-Myc tag between the $V_H$ fragment and the phage pIII thus releasing the bound phages. Also, during the elution step the trypsin-sensitive helper phages (KM13) are removed, and the background binders originating from the helper are decreased. In the case of $FB_1$, alternatively competitive elution with the free toxin was used to release those bound phages which are capable of binding the free toxin with high affinity. The eluted phages were amplified in TG1 bacteria and precipitated with polyethylene glycol (PEG). The amplified phages were then used for the subsequent panning rounds and tested in the phage-based ELISA with the immobilized target and an HRP-labeled secondary antibody.

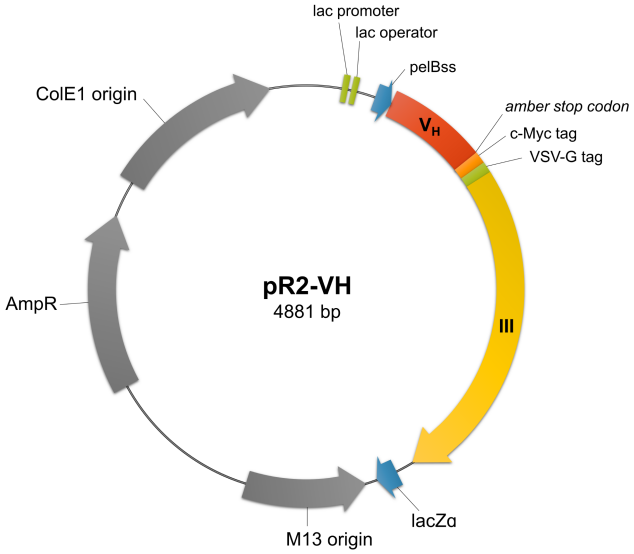


**Figure 64.** Map of the DAb phagemid vector (pR2-VH) with the most important features. The $V_H$ sequence (DAb, 12 kDa) has been introduced as N-terminal fusion to pIII. The amber stop codon located between the $V_H$ and pIII is suppressed by the strain used for phage amplification (TG1) and is introduced as a glutamine.

## 4.3.2 SELECTION OF ANTIBODY FRAGMENTS FOR MYCOTOXINS

Despite its wide use, phage display is susceptible to certain risks which can make it a complicated, demanding, and time-consuming technology.[360,361] Although the selection of antibodies have been reported, for example, against mycophenolic acid, OTA,[280] $ABF_1$,[311] and ZEA[281] with excellent affinities in the nanomolar range or higher, phage display may result in the selection of moderate affinity binders which are not able to compete with the affinities of monoclonal antibodies for biosensor development. Moreover, phage display selections are notorious for also identifying false positive hits, and at times, instead of specific binders, panning selections yield phages with no actual affinity toward the target but to other components of the screening system, such as contaminants in the target sample, the solid phase, or blocking agents. For example, plastic binders with high abundance of aromatic amino acid residues and those against albumin are frequently selected from peptide libraries.[362] Variety of strategies have been employed to avoid, or at least minimize, the enrichment of such binders.[363] On the other hand, certain clones might enrich during the selections rounds, not because they exhibit affinity to the target but because they propagate faster than an average clone. Each replication step enables them to prevail in the phage pool creating bias regarding the actual target-binding capabilities.

Unfortunately, the ventures with the DAb library in this work made us aware of many of these challenges. T-2 toxin which already proved itself a difficult toxin to mimic (**4.2.2.2 Selection of T-2 toxin mimotopes**) was not any more successful target for antibody selections. The three panning rounds against the T2–HSA-conjugate showed enrichment in the phages eluted after each round. A comparison to a control panning, without the target, in the second and third rounds suggested that the enrichment was specific to T2–HSA (**Figure 65A**). In

fact, binding of the polyclonal phage pools after each round showed a similar trend in the ELISAs (**Figure 65B**). However, although enrichment of the phages was seen, the extent of the background binding was substantial. Binding to blocked wells, and in particular to HSA-coated wells, showed significant non-specific binding among the phages and could not be tolerated. Analysis of 36 individual clones showed a similar trend in the ELISAs (**Figure 65C**), and the selections wound up fruitless.

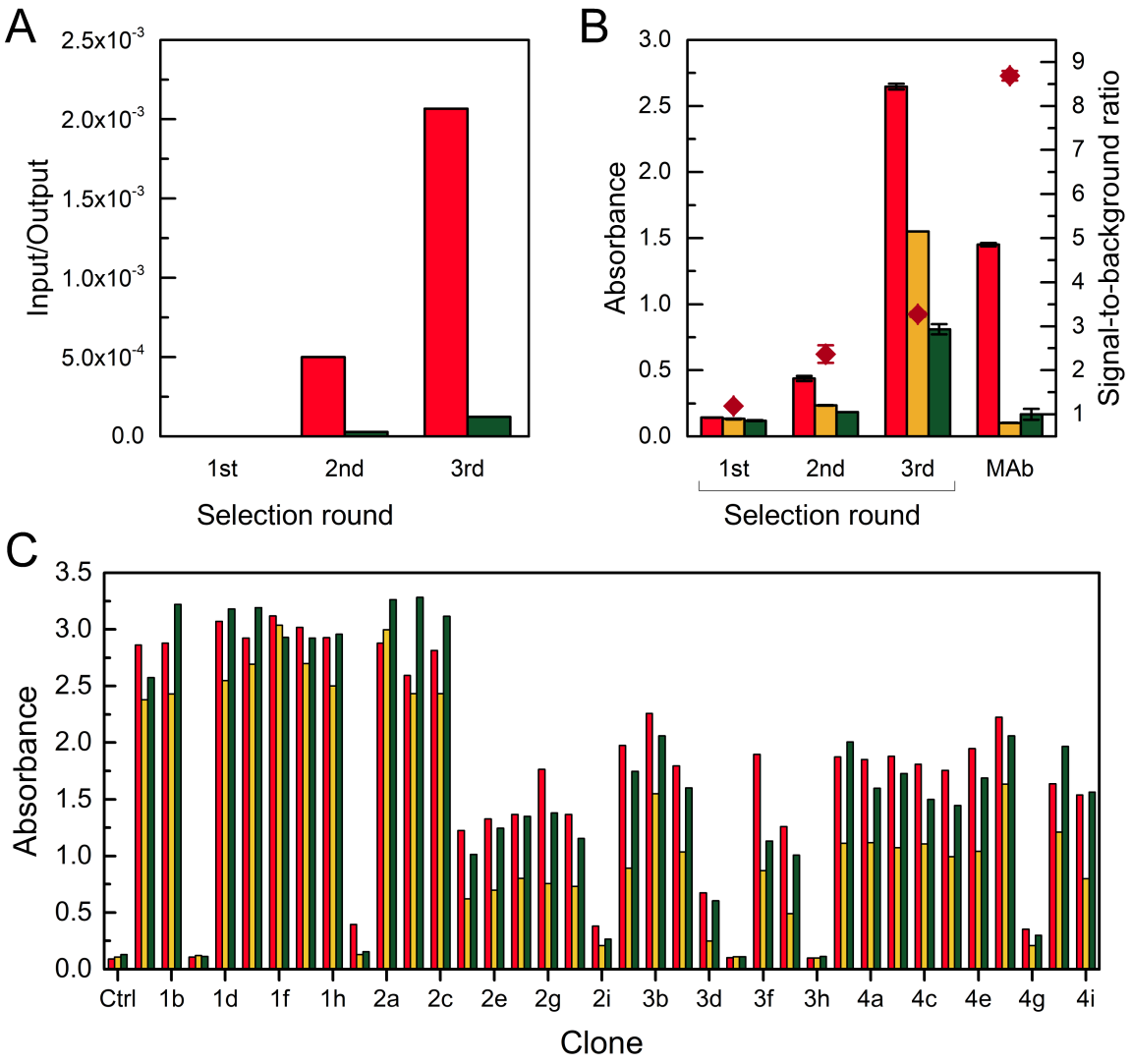


**Figure 65**. Selection of domain antibodies for T-2 toxin. (A) The ratio between the input phages (pfu) and output phages (pfu) after each selection round. Pannings against T2–HSA (red) showed enrichment after three selection rounds (the bar of the first round is not visible in the scale used). A control panning (green) against the wells without the target in the second and third round showed some enrichment in the background binders as well. (B) ELISAs with the polyclonal phage pools after each round. Binding was tested to the target T2–HSA (red), HSA (yellow), and wells blocked with 5% milk (green). The commercial anti-T2 monoclonal antibody (MAb) was used as a positive control. The signal-to-background ratios (red diamonds, right y-axis) were calculated from the signal from T2–HSA coating divided with the background signals from the non-coated wells. (C) ELISAs with monoclonal phages. Binding was tested similarly to the target T2–HSA (red), HSA (yellow), and wells blocked with 5% milk (green).

Later, for $FB_1$ pannings an additional second pre-selection step was included in order to eliminate the background binders that were a problem for T-2 toxin, and thus the phage pools were passed through two background wells prior to the target selection. Whether this had the wanted effect, or the less hydrophobic nature of the target resulted in lower background, was not studied in further detail, but in this case, the extent of the background binders was lower than before. A total of three panning rounds were conducted with immobilized $FB_1$–BSA and trypsin elution. In addition, another parallel third round was done with competitive elution using the free toxin. Comparison of the phages eluted from each round, *i.e.* the output phage, from the target selection ($FB_1$–BSA-coating) and a control selection (BSA-coating) showed enrichment of specific binders. The competitive elution with the toxin showed a decrease in the background binders as expected (**Figure 66A**). The results from the ELISA were consistent with the output phage and showed enrichment of specific binders towards $FB_1$–BSA. Thus, individual phages were amplified from the second and third rounds, and the binding was tested similarly in the phage-based ELISAs. Again, BSA-coated wells were used as a control and target binding was tested with $FB_1$–BSA-coated wells in the absence and presence of free $FB_1$ (**Figure 67A**). All of the 48 clones tested showed specific binding to the target $FB_1$–BSA in comparison with the background binding to BSA. However, addition of the free toxin (2 µg $mL^{-1}$ of $FB_1$) did not have the expected effect, and no competition was observed even with such high toxin concentration.

Further tests with increased toxin concentrations and varied assay conditions showed similar negative results. A final experiment, with an overnight incubation step of the phage-displayed DAb with the toxin, resulted to some extent of competition, and slightly lower signals were observed in the presence of high concentration of $FB_1$ (**Figure 67B**). Nevertheless, it was clear that the selected binders had a significantly higher affinity towards the $FB_1$–BSA than to the free $FB_1$. This could be a result of so-called bridge-effect wherein the antibody recognizes the hapten only in the context of the protein-conjugate and some parts of the conjugate or the linker have a significant contribution to the binding. Thus, the antibody does not recognize, or recognizes with low affinity, the free hapten which in fact would be the wanted target. Therefore, such binders are useless for the intended application, and thus far, also the selections for $FB_1$-binding antibodies were inconclusive.

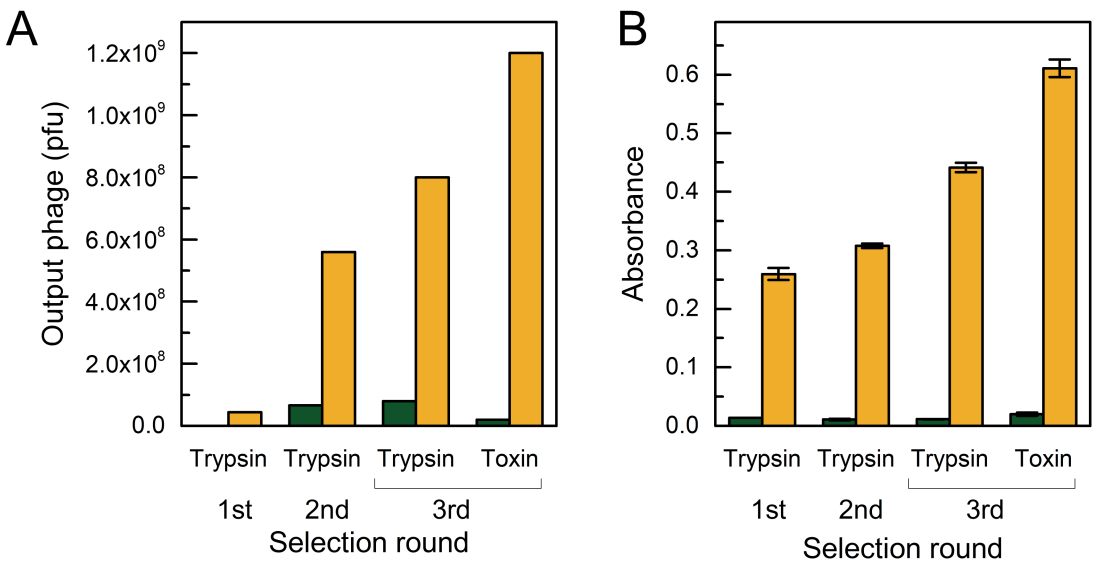


**Figure 66**. Selection of domain antibodies for $FB_1$. (A) Output phage (pfu) after each round for the target ($FB_1$–BSA, yellow) and control pannings (BSA, green). (B) ELISA with the polyclonal phage pools after each round. Binding was tested to the target $FB_1$–BSA (yellow), and BSA (green). In the first and second rounds the elution was done with trypsin, and in the third round the elution with trypsin and free $FB_1$ (toxin) was compared.

The failure to isolate target binding phages recognizing $FB_1$ or T-2 toxin with high affinity could be due to the absence of such phages in the library that was used, or to the selective loss of suitable phages during the selection procedure. Alternative libraries could provide better antibodies for small targets, such as $FB_1$ and T-2 toxin. In the literature, many of the mycotoxin-specific antibodies discovered by phage display have been selected from immunized libraries which are already strongly biased towards the target.[136,200,279–281] It should be also noted that the DAb library used in this work might not include appropriate antibodies for small molecules. As has been reported in the case of nanobodies,[193,364] the paratope of single-domain antibodies consists of only three hypervariable loops, rather than six as in the intact IgG or the scFv and Fab fragments.[93] Thus, the structure or the complexity of the antigen binding site, with a limited number of conformational structures, might not be suitable for small molecule recognition.[365]

On the other hand, the target is evidently a crucial element of the selections, and it is possible that the toxin-conjugates used in this work were not optimal for the purpose. The protein context, as well as the used linker and degree of purity, can have significant effects on the antibody binding, exactly as in the case of raising hapten-specific antibodies by immunizations.[93] If the structure of the conjugate hinders binding to the toxin itself or due to steric hindrance the antibody is not capable of interacting with the target, the results could be similar to those seen in this work. As discussed already in the case of the mimotopes, the stringency of the selection conditions also has dramatical effects on the outcome, and even small stringency differences during the selection might result in the selection of a completely different phage population.[361]

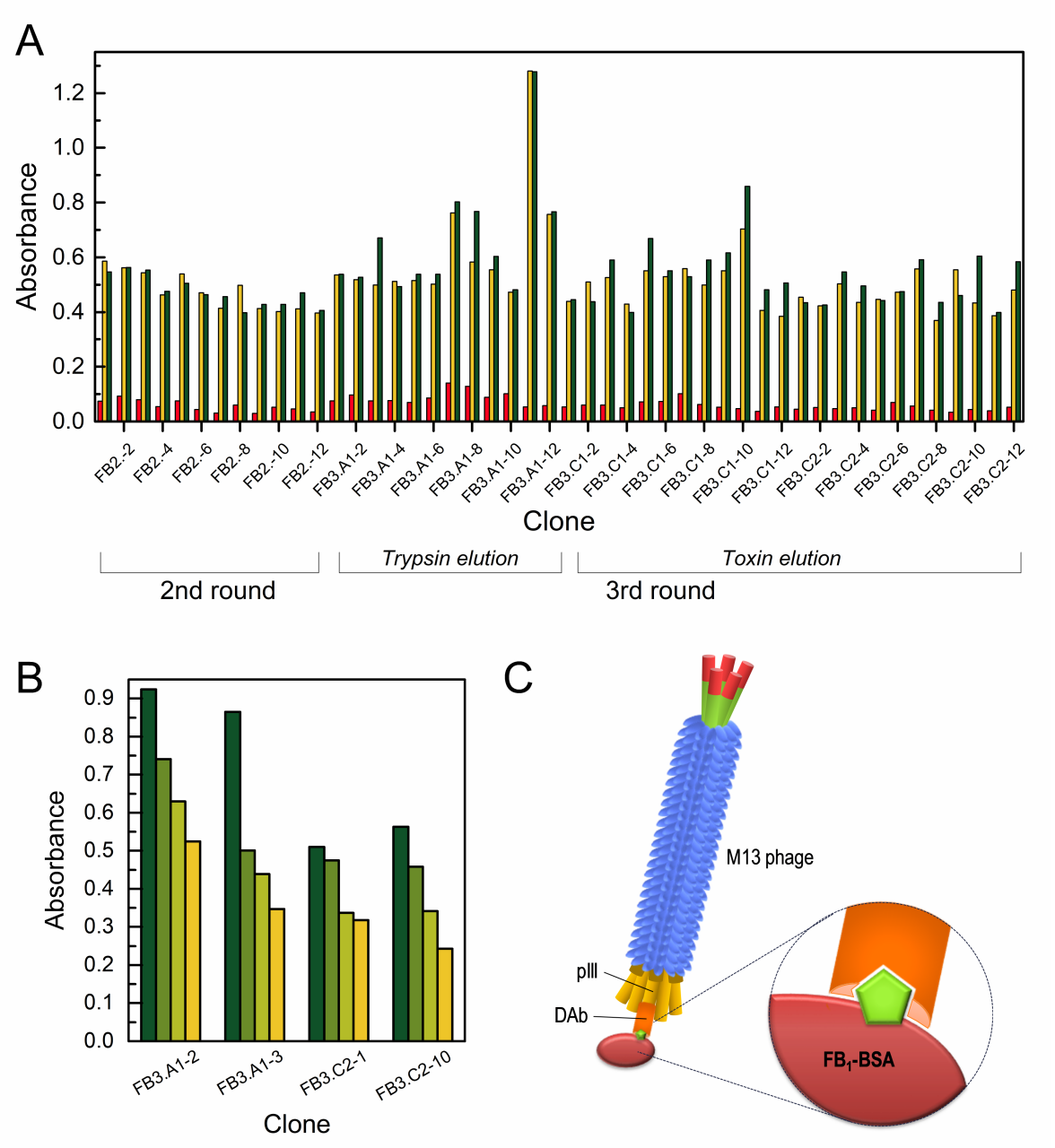


**Figure 67**. Selection of domain antibodies for $FB_1$. (A) ELISA with monoclonal phages from the second and third rounds. Binding was tested to BSA (red) and the target $FB_1$–BSA in the absence (yellow) and presence of 2 μg $mL^{-1}$ $FB_1$ (green). (B) Competitive assay with selected monoclones with an overnight pre-incubation step with the toxin. As a control (dark green) no $FB_1$ was used, or 5 μg $mL^{-1}$ (green), 10 μg $mL^{-1}$ (light green), or 25 μg $mL^{-1}$ $FB_1$ (yellow). (C) Schematic of the hypothesized binding of the phage-displayed DAb which recognized the $FB_1$–BSA only in the context of the protein-conjugate.

# 4.4 Mimotope-based immunoassays

Despite the unsuccessful selection of mycotoxin-specific recombinant antibodies, we have developed various novel methods for mycotoxin detection based on the commercial antibodies and the newly identified mimotopes. After identifying the mimotopes for $FB_1$, ZEA, and T-2 toxin from the phage-displayed peptide library, as described in the previous sections, three alternative strategies for immunoassay development were followed. Firstly, and perhaps most straightforwardly, the phage-borne peptides were directly used in the immunoassay after identifying the best individual clones. As it was already seen in the phage-based ELISA, which was used to evaluate the success of the pannings, the phage-displayed mimotopes were used in competitive assays, based on immobilized antibodies, and subsequent detection with an HRP-labeled anti-phage secondary antibody. This approach was the least complicated method to evaluate and compare the performance of the individual clones and could be used as a means to select the best mimotope candidates. However, as discussed in **publication IV**, the phage-borne mimotopes did not provide the best sensitivity in comparison with the alternative assay formats. The SPR analysis revealed that the phage-displayed mimotope possessed very slow binding kinetics, which was attributed to the enormous size of the phage virion. Nevertheless, signal amplification could be achieved using the anti-phage-HRP secondary antibody which binds to the major coat protein of the phage, and further improvement in the assay sensitivity was attained using magnetic beads as the solid phase.

On the other hand, after identifying the mimotopes in terms of the amino acid sequence, they could be synthesized or produced without the phage. In our second approach, the mimotopes were chemically synthesized with a biotin-linker and could be used in different approaches. **Publication II** presented the microarray-based immunoassay using the synthetic peptide, which was immobilized on the array surface using neutravidin. Similarly, the synthetic peptide was later (**publication IV**) applied to a bead-based immunoassay that provided lower detection limits. The synthetic peptide proved itself as an outstanding recognition element not only for the excellent sensitivity that could be achieved but also owing to the versatility of the approach. The biotin-linker which was included to the peptide during the synthesis could be used to immobilize it to various solid surfaces, such as the microarray or magnetic beads which were used in this work, or likewise for conjugation to practically any label or other molecule modified with a biotin-binding protein, such as neutravidin or streptavidin.

The third approach to use the mimotopes relied on genetically constructed recombinant fusion proteins for which the peptides were cloned as translational fusions with fluorescent or bioluminescent proteins. In this manner, the recombinant fusion protein was produced directly with a label and could be applied to the immunoassays without further labeling or secondary antibodies. Although the construction of the recombinant proteins by genetic engineering might be considered more laborious than peptide synthesis, the bacterial expression provided an exhaustive source of the protein once the translational fusion was constructed. However, at times, expression of heterologous proteins might turn out challenging due to problems associated with protein misfolding or degradation occasionally observed in their expression of heterologous fusion proteins.[366] **Publications III–V** present the development of fluorescent and

bioluminescent fusion proteins for the detection of $FB_1$ and ZEA. These assays provide excellent sensitivities and, in particular, simplified analytical methods using the mimotope-fusions as the tracer. The following sections discuss the background and further unpublished results obtained with the different mimotopes and assay formats for the detection of $FB_1$, ZEA, and T-2 toxin.

### 4.4.1 DETECTION OF ZEARALENONE ON MAGNETIC BEADS

As discussed above, the phage-borne peptides can be directly used to develop competitive immunoassays to detect the target toxin. In the case of ZEA, originally two conserved peptide sequences were identified in the panning among which SF provided better reproducibility, although the sensitivity obtained with both peptides, SF and GW, seemed to be very similar (**Figure 44D**). Even though the sensitivity of the assay was excellent, the very narrow dynamic range obtained in the competitive phage-based assay was a matter of concern. Based on the thorough investigation of different assay formats in the case of $FB_1$, the ZEA assay was also implemented in a bead-based format with the aim to improve the dynamic range. Similarly as for $FB_1$ (**publication V**), the assay was based on the covalent immobilization of the anti-ZEA antibody on carboxylated magnetic microbeads. Competition between the toxin and the phage-displayed mimotope (SF) was later revealed using the HRP-labeled anti-phage antibody. After optimizing the amount of the SF-phage in the assay (**Figure 68A**), calibration with ZEA was performed. A significant improvement in the assay sensitivity and dynamic range was observed using the beads in comparison with the plate-based approach (**Figure 68B**). The $IC_{50}$ values for ZEA assays on magnetic microbeads and microtiter plate were 0.31 ± 0.02 ng $mL^{-1}$ and 2.43 ± 0.08 ng $mL^{-1}$, respectively. The dynamic range (from $IC_{80}$ to $IC_{20}$) for the bead-assay was from 0.16 to 0.61 ng $mL^{-1}$ while for the plate assay the range ranged between 1.96 and 3.01 ng $mL^{-1}$. The detection limits, defined as the $IC_{90}$ value, were 0.11 and 1.72 ng $mL^{-1}$ for the bead and plate-based assays, respectively.

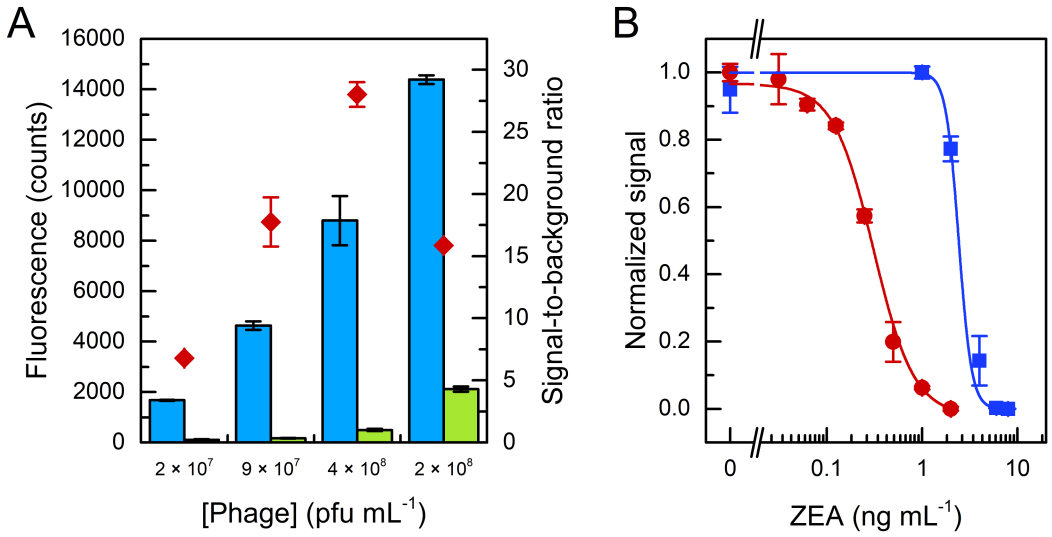


**Figure 68**. Competitive phage-based immunoassays for ZEA. (A) Optimization of the amount of the phage in the bead-based immunoassay in the absence of free ZEA (blue) and in the presence of 3 ng $mL^{-1}$ ZEA (green). Best signal-to-background ratio (red diamonds, right y-axis) was obtained with $4 \times 10^8$ pfu $mL^{-1}$, and it was used for the toxin calibration. (B) ZEA calibration using as the solid phase a microtiter plate (blue) or magnetic microbeads (red). Normalized signals are depicted as the average of the replicate samples ± the standard error of the mean ($n$ = 3) and fitted with a four-parameter logistic fit (OriginPro 9.0).

## 4.4.2 DUPLEX MICROARRAY ASSAYS FOR $FB_1$ AND T-2 TOXIN DETECTION

In parallel with the work reported in **publication II**, we aimed to develop a microarray-based immunoassay for T-2 toxin analysis with the final objective of developing a duplex method for the simultaneous detection of $FB_1$ and T-2 toxin.

### 4.4.2.1 Optimization of the microarray spotting

For the duplex microarray development, immobilization of the $FB_1$ and T-2 toxin mimotopes to the array was optimized in terms of the spotting buffer as well as the peptide and neutravidin concentrations. Moreover, direct immobilization of the peptides without neutravidin was tested in parallel. Tested spotting buffers were: (a) 1× PBS (pH 7.2) with 0.01% sodium-deoxycholate, (b) 1× PBS (pH 7.2) with 0.005% CHAPS and 0.01% BSA, and (c) 1× PBS (pH 7.2). Spotting buffer (b) with CHAPS and BSA provided the best spot quality (**Figure 69A**) and was selected for the subsequent experiments. Biotinylated peptides A2-bio ($FB_1$-mimotope) and F11-bio (T2-mimotope) were spotted in the same array at different concentrations (0.10 mg $mL^{-1}$; 0,25 mg $mL^{-1}$; or 0.75 mg $mL^{-1}$) with or without neutravidin (1:8 molar ratio). Binding of the $FB_1$ and T-2 toxin-specific antibodies at different concentrations was then measured to both peptides spotted at different concentrations (**Figure 69**). Although some binding was observed at high antibody concentrations, it was clearly seen that the direct spotting of the peptides to

the epoxy-surface did not provide good binding. This could be due to the absence of appropriate reacting groups for the binding, unfavorable folding of the peptide or steric hindrance after the spotting which prevents antibody binding. Nevertheless, the spotting with neutravidin resulted in excellent signals. High concentrations of the spotted peptide resulted in some non-specific binding (**Figure 69C–D**) but could provide the required signal-to-background ratios. The concentration of neutravidin and both peptides were later optimized more specifically to provide competitive assays with the highest sensitivity for toxin detection (**Figure 23**, **Figure 70**).

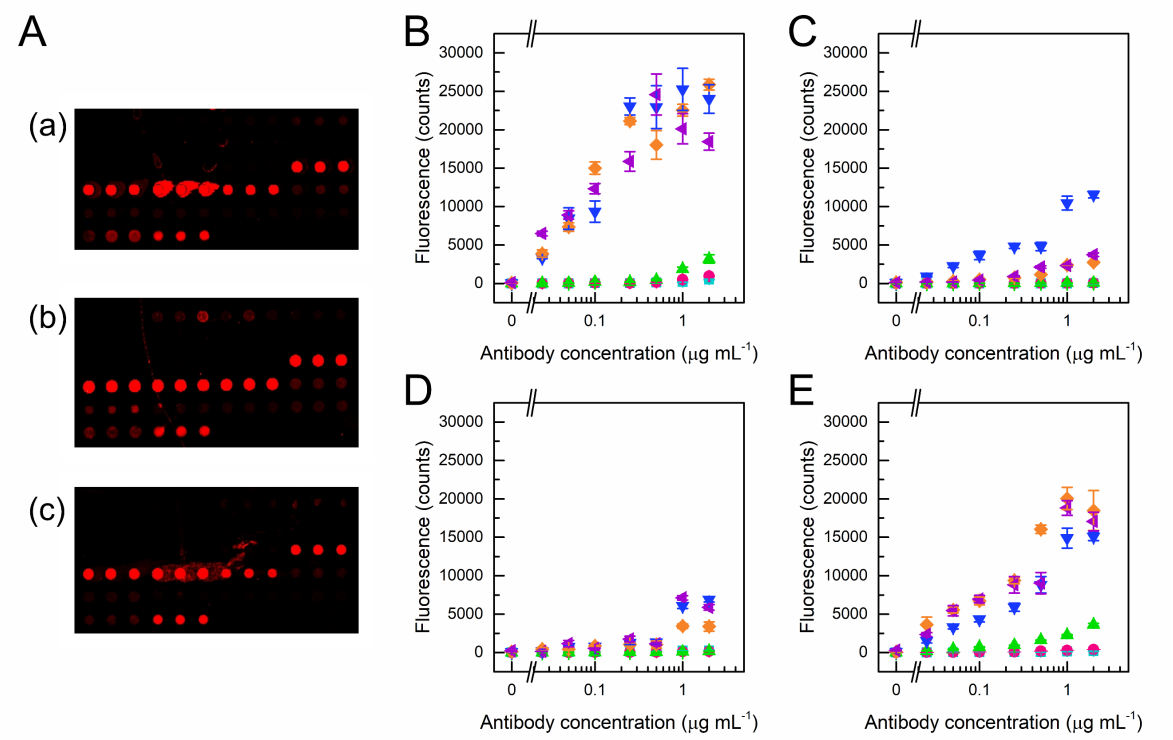


**Figure 69**. Optimization of the peptide (A2-bio and F11-bio) spotting. (A) The array was spotted with: (a) 1× PBS (pH 7.2), 0.01% sodium-deoxycholate; (b) 1× PBS (pH 7.2), 0.005% CHAPS, 0.01% BSA; or (c) 1× PBS (pH 7.2). Then, binding of different antibody concentrations to the peptides spotted with spotting buffer was tested (b). (B) Specific binding of anti-$FB_1$ to A2-bio; and (C) non-specific binding to F11-bio. (D) Non-specific binding of anti-T2 to A2-bio; and (E) specific binding to F11-bio. Both peptides were spotted with (orange, purple, blue) neutravidin and without (green, red, light blue) in three different concentrations, 0.10 mg $mL^{-1}$ (purple, green); 0,25 mg $mL^{-1}$ (orange, red); or 0.75 mg $mL^{-1}$ (blue, light blue). The fluorescence signals are depicted as the average of three replicate spots in three replicate arrays ± standard error of the mean (*n* = 9).

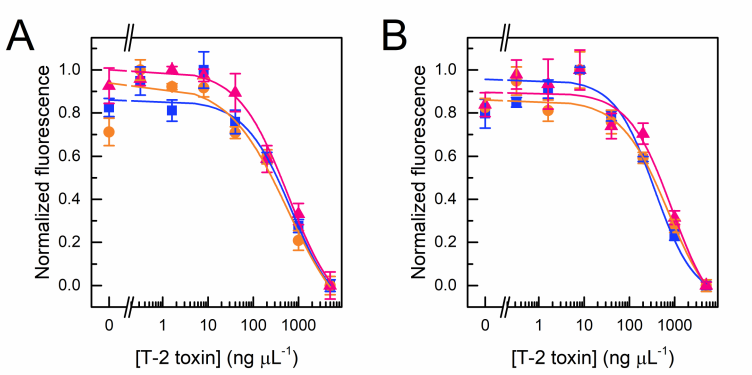


**Figure 70**. Optimization of the F11-bio spotting. (A) Binding inhibition curves with the peptide immobilized at a concentration of 0.25 mg mL$^{-1}$, (blue) 0.50 mg mL$^{-1}$ (orange), or 0.75 mg mL$^{-1}$ (red). (B) Binding inhibition curves with 0.25 mg mL$^{-1}$ immobilized peptide F11 at different neutravidin concentrations, 1:4-molar ratio (blue), 1:6-molar ratio (orange) or 1:8-molar ratio (red). Results are shown as normalized mean signals ± the standard error of the mean (*n* = 9). A four-parameter logistic fit (OriginPro 9.0) was used for the curve fitting.

### 4.4.2.2 T-2 toxin assay based on biotinylated F11-mimotope

Similarly as described for $FB_1$ in **publication II**, the competitive binding inhibition assay for T-2 toxin was optimized in terms of the antibody concentration. **Figure 71A** shows the toxin calibration performed with 10–250 ng mL$^{-1}$ anti-T2 antibody where it can be observed that lower antibody concentrations led to lower absolute signals but could provide slightly better sensitivities. The assay with 10 ng mL$^{-1}$ antibody exhibited an $IC_{50}$ value of 287 ng mL$^{-1}$ and a limit of detection ($IC_{90}$) 7.7 ng mL$^{-1}$.

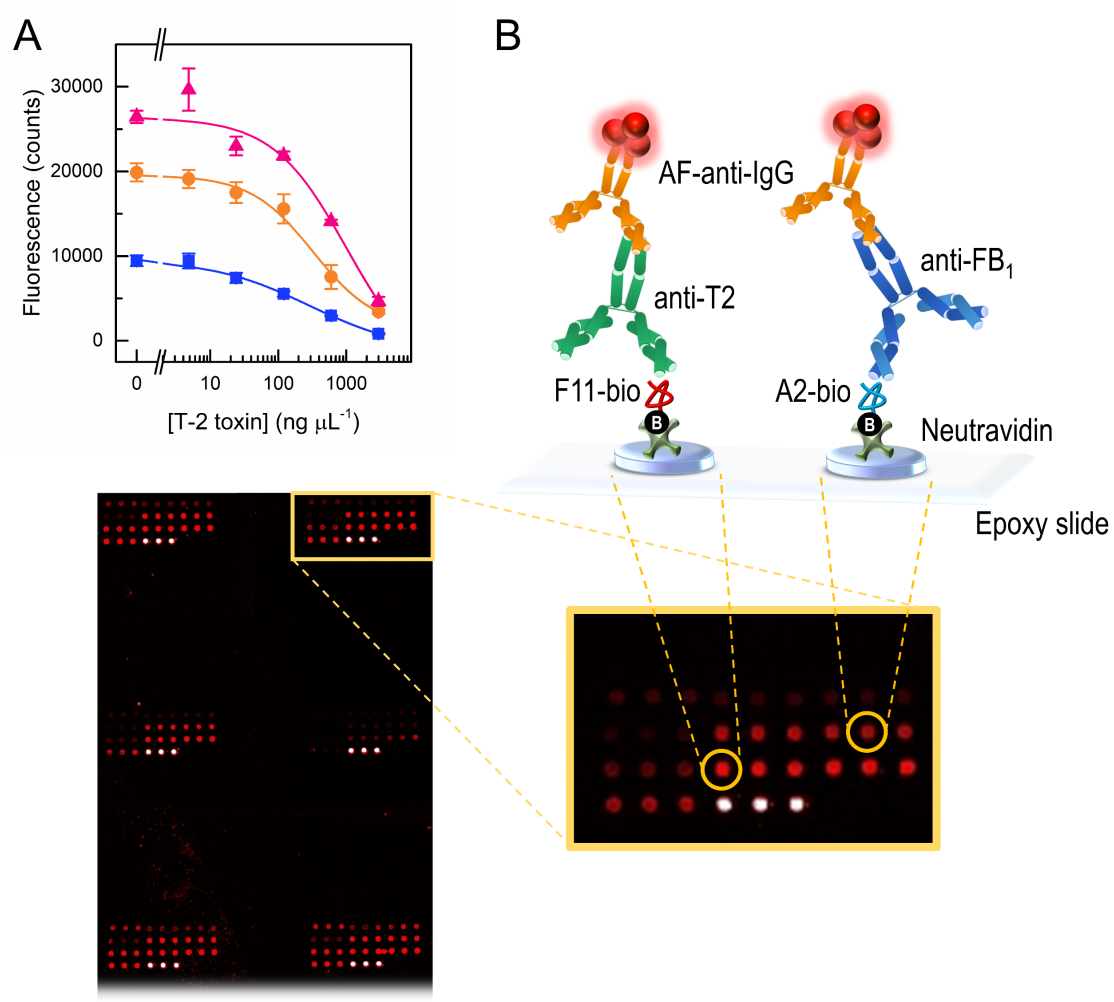


**Figure 71.** (A) Optimization of T-2 toxin antibody concentration in the microarray. Anti-T2 toxin was used at 250 ng $mL^{-1}$ (red), 40 ng $mL^{-1}$ (orange), and 10 ng $mL^{-1}$ (blue). Results are shown as mean fluorescence signals ± the standard error of the mean ($n$ = 9). A four-parameter logistic fit (OriginPro 9.0) was used for the curve fitting. (B) Scheme of the duplex microarray where A2-bio and F11-bio are spotted on the same array and $FB_1$ and T-2 toxin can be detected simultaneously using an anti-IgG secondary antibody labeled with AlexaFluor (AF).

### 4.4.2.3 Duplex microarray assays of $FB_1$ and T-2 toxin

For the duplex mycotoxin assay both peptides were spotted to the same microarray (in triplicate spots) and the binding of one or both antibodies together with varying concentrations of one or both toxins, $FB_1$ and T-2 toxin, was tested. The $FB_1$-assay (**Figure 72C**; blue squares) with anti-$FB_1$ and $FB_1$ as a unique target showed excellent performance in terms of sensitivity and reproducibility (as described in **publication II**). Non-specific binding to the immobilized T-2 toxin mimotope F11-bio was not observed (**Figure 72D**; blue squares). Similarly, the T-2 toxin assay, although significantly less sensitive and less reproducible, showed specific response in the presence of the anti-T2 and T-2 toxin alone (**Figure 72A–B**; purple squares). The simultaneous addition of both antibodies to the reaction increased the complexity of the assay most likely due to the appearance of secondary signals caused by non-specific binding and cross-reaction between the two antibodies. The results showed some irregular behavior and non-specific

binding to the non-target peptide. For example, in the presence of both antibodies, high concentrations of T-2 toxin and no $FB_1$, we could also observe a change in the signals originating from the $FB_1$-mimotope A2-bio spot (**Figure 72B**; green squares). This might originate from non-specific binding of the anti-T2 antibody to the A2-bio to some extent, or from non-specific binding of the high concentrations of T-2 toxin to the anti-$FB_1$ antibody. In either case, possibly due to this unwanted response, also the specific signals from the T2-mimotope F11-bio with the T-2 toxin were somewhat unusual (**Figure 72A**; green squares). Similarly, in the case of $FB_1$, some irregularities were seen in the non-specific signals (**Figure 72D**; red circles). In the duplex assay with both antibodies and both toxins simultaneously, the competitive response was observed for both toxins (**Figure 72D**; orange diamonds), but as the response differed from the singleplex assay sufficiently, we could not conclude that the duplex assay would provide reliable results. Further work is required, to optimize the duplex assay for the simultaneous detection of both mycotoxins. To begin with, the low-dose hook effect that is seen for both toxins when both antibodies are present (for example **Figure 72A**, green squares, and **Figure 72C**, red circles) might be an indication that the antibody concentration is not optimal. In fact, the antibody concentrations were optimized separately and might require further testing for the duplex assay. Also, alternative buffer compositions might improve the observed non-specific binding.

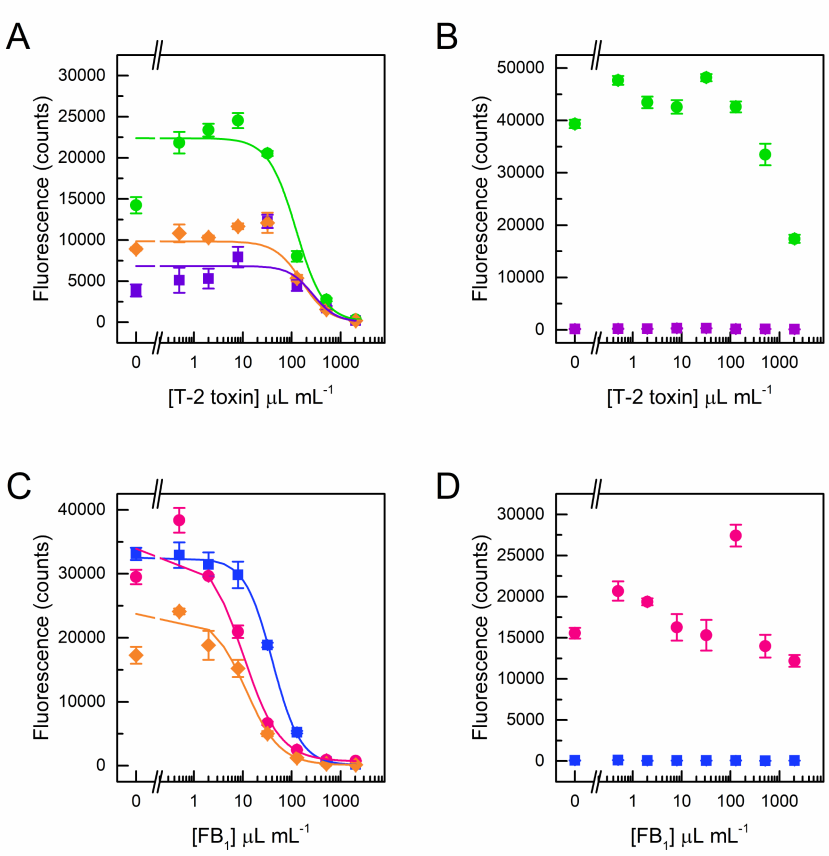


**Figure 72.** Duplex microarray assay for the detection of $FB_1$ and T-2 toxin. A2-bio and F11-bio were spotted onto the same array, and the signals were measured from both spots (A and C, A2-bio 250 µg $mL^{-1}$; B and D, F11-bio 250 µg $mL^{-1}$) in the presence of anti-$FB_1$ (blue), anti-T2 (purple), or both antibodies (orange, red, and green). Different concentrations of one or both toxins were tested (blue and red, only $FB_1$; green and purple, only T-2 toxin; orange both toxins simultaneously). Results are shown as the mean fluorescence signals ± the standard error of the mean (*n* = 9). A four-parameter logistic fit (OriginPro 9.0) was used for the curve fitting.

### 4.4.3 FLUORESCENT FUSION PROTEINS

As an alternative for the use of phage-borne or synthetic mimotopes, recombinant peptide–protein fusions have been suggested as a fascinating option for biosensor development. They can be produced in bacteria cost-effectively even in large quantities. Moreover, the countless possibilities offered by genetic engineering enable the design of different fusions tailored for the purpose. The fusion can be designed to consist of a protein such as MBP, which can be used as an affinity tag for further purification and immobilization, or alternatively fluorescent or luminescent proteins can be used to provide an optical signal for the assay. Fluorescent proteins (FPs) which are able to emit a strong and stable fluorescence signal present one attractive alternative for such an approach. The use of FPs as markers for gene expression analysis or protein tracking within cells or organelles, is often seen to have revolutionized molecular biology in the last decades, and simultaneously, FPs with enhanced fluorescence or different spectral characteristics have become an exciting alternative for biosensing in both *in vivo* and *in vitro* assays.

### 4.4.3.1 Construction of fluorescent fusion proteins for $FB_1$ and T-2 toxin

The mimotopes for $FB_1$ and T-2 toxin identified in the first round of selections, namely A2 and F11, respectively, were used as the basis to construct fluorescently tagged mimotopes. Three different fluorescent proteins (FPs) with a distinguishable spectrum were chosen to prepare the fluorescently-tagged mimotopes. ZsYellow and mOrange were both used in combination with the $FB_1$-mimotope A2 whereas EmGFP was fused with the T2-mimotope F11. To construct the translational mimotope-FP fusion by PCR amplification, a long 5'-overhang was used in the forward primer to amplify the gene encoding for the FP, resulting in an N-terminal fusion with the mimotope. The same linker (GGGS) between the pIII and the mimotope that was present in the pannings was included in the fusion protein design, to ensure sufficient space between the mimotope and the FP. Additionally, a polyhistidine tag was added to the C-terminus of the FP for purification, likewise, with a 5'-overhang in the reverse primer. **Table 17** summarizes the primers used to create the mimotope-FP fusions which were subsequently subcloned into the pQE-T7-2 expression vector using KpnI and SacI restriction enzyme sites (**Figure 73A**). Successful cloning was confirmed by DNA sequencing, and moreover, bright fluorescence emission after inducing the protein expression was a clear indicative of successfull clonage.

**Table 17**. Primers used to create the fluorescently-tagged mimotopes. The mimotope sequences (A2 or F11) are shown in bold, restriction enzyme sites in cursive, and the sequence hybridizing to the fluorescent protein is underlined.

| Primer name | Sequence (5'→3') |
|---|---|
| FP-SacI-V5-ZsYellow | TTC*GAGCTC*ATG**GTTACTCCGAATGATGATACGTTTGATCCTTTTCGG**GGTGGAG GTTCGGCTCATTCAAAGCACGGTCTA |
| RP-KpnI-6H-ZsYellow | GCTG*GTACC*TCAGTGGTGGTGGTGGTGGTGGGCCAAGGCAGAAGGGAATGC |
| FP-SacI-V5-mOrange | TTC*GAGCTC*ATG**GTTACTCCGAATGATGATACGTTTGATCCTTTTCGG**GGTGGAG GTTCGGTGAGCAAGGGCGAGGAGAAT |
| RP-KpnI-6H-mOrange | GCTG*GTACC*TCAGTGGTGGTGGTGGTGGTGCTTGTACAGCTCGTCCATGCC |
| FP-SacI-F11-EmGFP | TTC*GAGCTC*ATG**GGGTATGGGTCTATTCTTCCTTTTAATCCGGTGTTT**GGTGGAG GTTCGGTGAGCAAGGGCGAGGAGCTG |
| RP-KpnI-6H-EmGFP-v2 | GCTG*GTACC*TCAGTGGTGGTGGTGGTGGTGCTTGTACAGCTCGTCCAT |

The FP-tagged mimotopes were then purified from the crude cell extracts by affinity chromatography using the C-terminal polyhistidine tag (**Figure 73C**). The emission spectra of the purified fusions proteins (**Figure 73B**) were very similar to those reported in the literature for the intact FPs. The measured emission maxima were 511 nm, 541 nm, and 566 nm for F11-EmGFP, A2-ZsYellow, and A2-mOrange, respectively, also similar to those reported in the literature for EmGFP, ZsYellow, and mOrange (511 nm, 540 nm, and 564 nm, respectively).

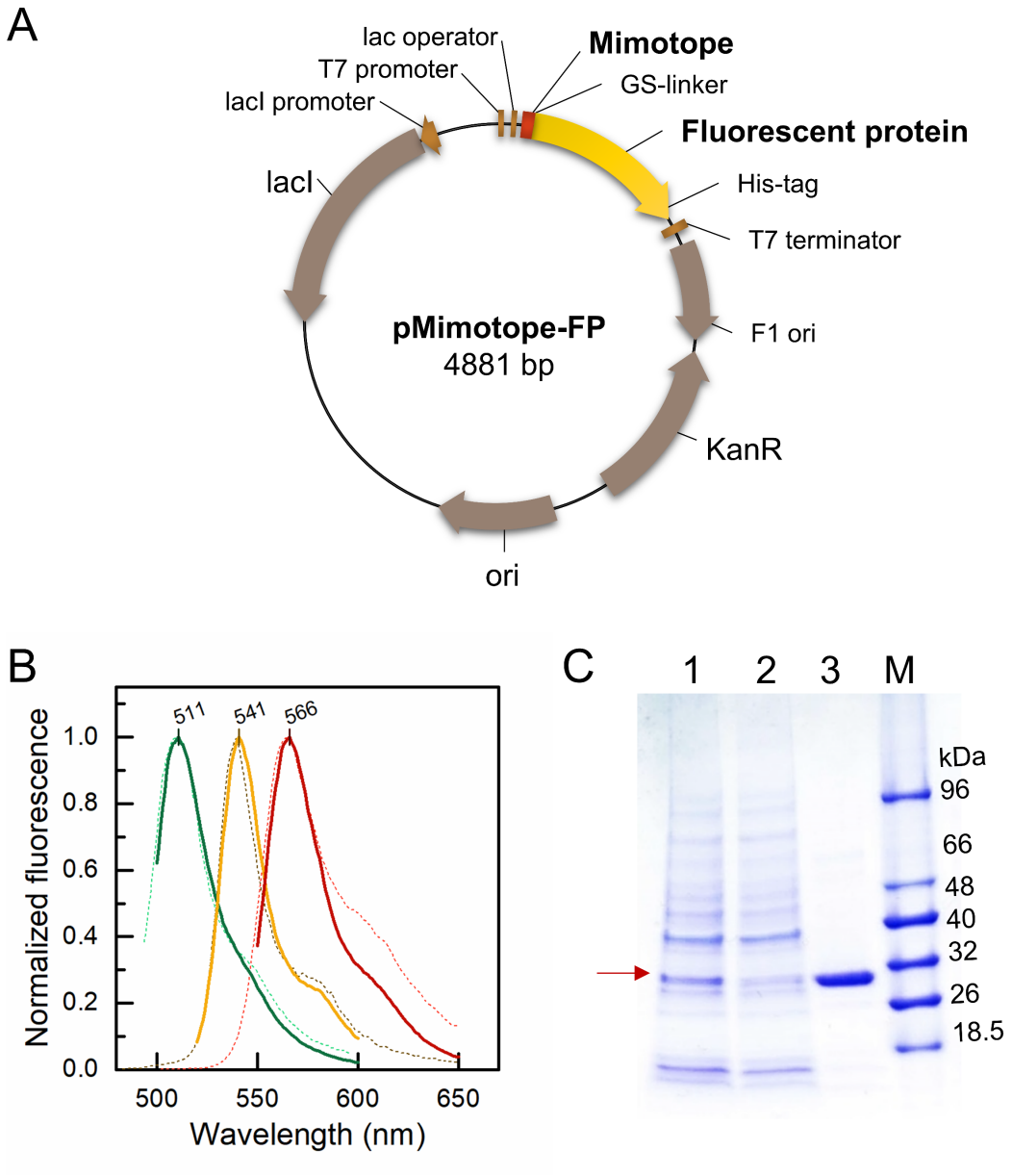


**Figure 73.** (A) Main features of the expression vector for fusion proteins consisting of the mimotope (A2 or F11) and fluorescent protein ZsYellow, mOrange, or EmGFP. (B) Fluorescence emission spectra and emission maxima of the purified fusion proteins, A2-ZsYellow (yellow), A2-mOrange (red), and F11-EmGFP (green). The dashed lines represent the emission spectra reported in the literature. Excitation wavelengths were 472 nm, 490 nm, and 520 nm for EmGFP, ZsYellow, and mOrange, respectively. (C) Purification of the F11-EmGFP by HisTrap was monitored by SDS-PAGE analysis. Lane 1 unpurified lysate; 2, HisTrap flow-through; 3, Elution; M, molecular marker.

Binding of the purified fusion proteins was tested using the mycotoxin specific antibody, anti-$FB_1$ or anti-T2, immobilized to the microtiter well plate. Low non-specific binding to the plate without the antibody was seen, and in the case of A2-ZsYellow and F11-EmGFP high specific binding was observed to the anti-$FB_1$ and anti-T2 antibodies, respectively (**Figure 74**). Curiously, A2-mOrange did no bind to its target antibody, but similar signals were observed in both target and control wells. The measured emission showed that the FP expression was successfll, but it was evident that the mimotope was not capable of binding its target. It is possible that despite

of the linker that was used, the FP might cause steric hindrance preventing the binding, or that protein folding in the context of this FP in particular had an unwanted effect on the mimotope recognition. Regardless of the negative outcome of the experiments with A2-mOrange, the concept of FP-tagged mimotopes was further studied using the F11-EmGFP and in particular, A2-ZsYellow which showed excellent performance in the immunoassays. Later, in **publication III**, a new ZsYellow-fusion, A2-YFP (PA031) was constructed, and a TEV-cleavage site was included before the polyhistidine tag in order to remove the tag after the purification. This fusion protein was used to develop heterogeneous and homogeneous immunoassays for $FB_1$ detection, as discussed in **publications III–IV.**

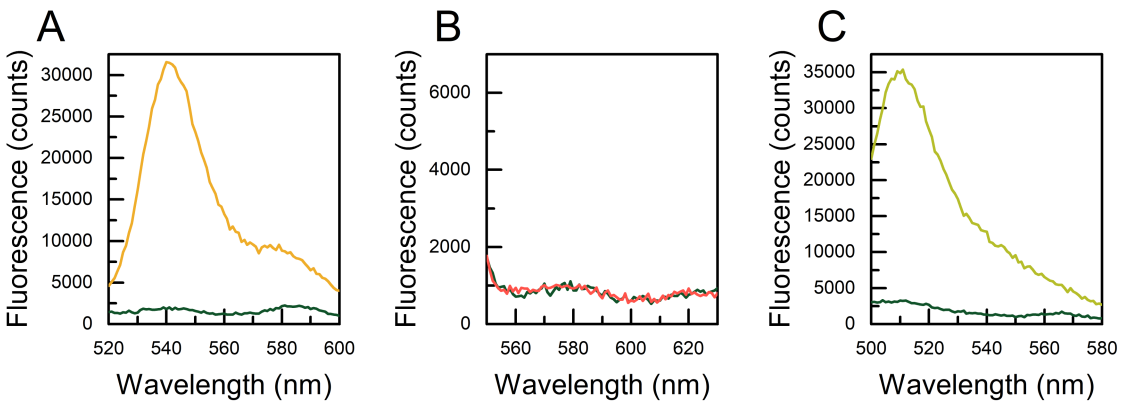


**Figure 74.** Binding of the fluorescent fusion proteins to their target antibody (200 ng of anti-$FB_1$ or anti-T2 per well) and background binding (dark green) to the plate in the absence of the antibody. (A) A2-ZsYellow (anti-$FB_1$-coating yellow; excitation at 490 nm), (B) A2-mOrange (anti-$FB_1$-coating orange; excitation at 520 nm), (C) F11-EmGFP (anti-T2 coating green; excitation at 475 nm).

### 4.4.3.2 Fluorescent protein microarray

The FP-tagged mimotopes were also applied in a microarray-based immunoassay format. This work was carried out collaboration with Dr. Ursula Sauer from Austrian Institute of Technology (AIT). In this case, the toxin-specific antibodies were spotted on the array and binding of the FP-tagged mimotopes in the presence of different concentrations of the target toxins was studied. In comparison with the previously described microarray with the synthetic peptides, the FP-array could have the potential to provide shorter and simpler assay protocols since no secondary antibodies are required. In the preliminary experiments, the direct binding of FP-tagged mimotopes, A2-ZsYellow and F11-EmGFP, to the spotted anti-$FB_1$ and anti-T2 antibodies was studied to confirm the functionality of the mimotopes and the specificity of the binding. Both mimotopes showed binding to their target antibody, although some non-specific binding was observed as well (**Figure 75**). The highest antibody concentration (500 µg $mL^{-1}$) tested provided the best signal-to-background ratio and was chosen for the subsequent experiments.

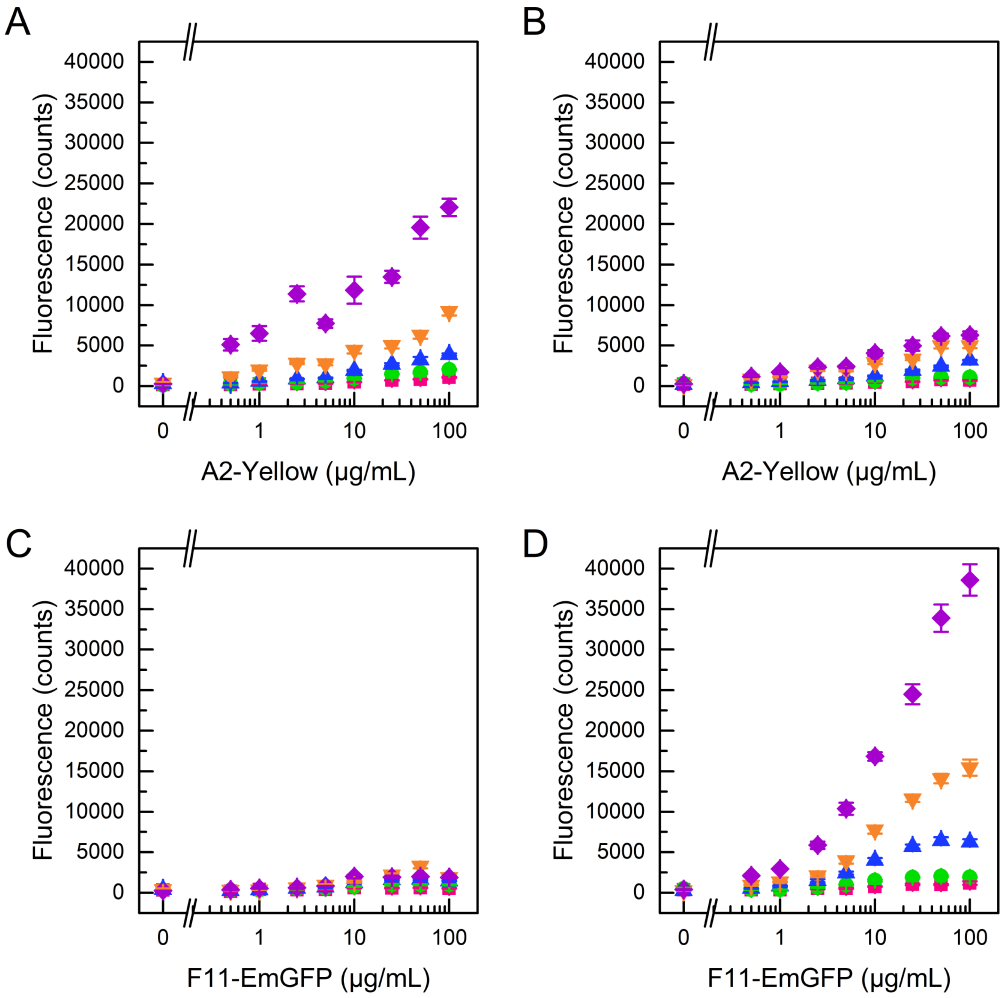


**Figure 75.** Binding of the fluorescent fusion proteins to their target antibody in the microarray. Binding of different concentrations of A2-ZsYellow to (A) the target anti-$FB_1$ antibody and (B) the non-target anti-T2 antibody. Binding of different concentrations of F11-EmGFP to (C) the non-target anti-$FB_1$ antibody and (D) the target anti-T2 antibody. Different concentrations of the antibodies were spotted onto the microarray, 500 µg $mL^{-1}$ (purple), 250 µg $mL^{-1}$ (orange), 100 µg $mL^{-1}$ (blue), 50 µg $mL^{-1}$ (green), and 20 µg $mL^{-1}$ (red). The signals are depicted as the average of three replicate spots in three replicate arrays ± standard error of the mean ($n$ = 9).

Next, the competitive assay was tested with both toxins and mimotope-fusions separately. Competitive inhibition was observed in the presence of the toxins, but the assay sensitivity and reproducibility were rather poor (**Figure 76**). For both toxins, the use of 5 µg $mL^{-1}$ FP-tagged mimotope showed the best response, but the results were not promising, and thus the duplex assay was not implemented. However, the A2-YFP was successfully applied to $FB_1$ detection in heterogeneous plate- and bead-based assays as well as in homogeneous quenching immunoassay (**publications III** and **IV**). Ongoing work with the F11-EmGFP intends to find out if the fusion could provide a robust means for T-2 toxin detection.

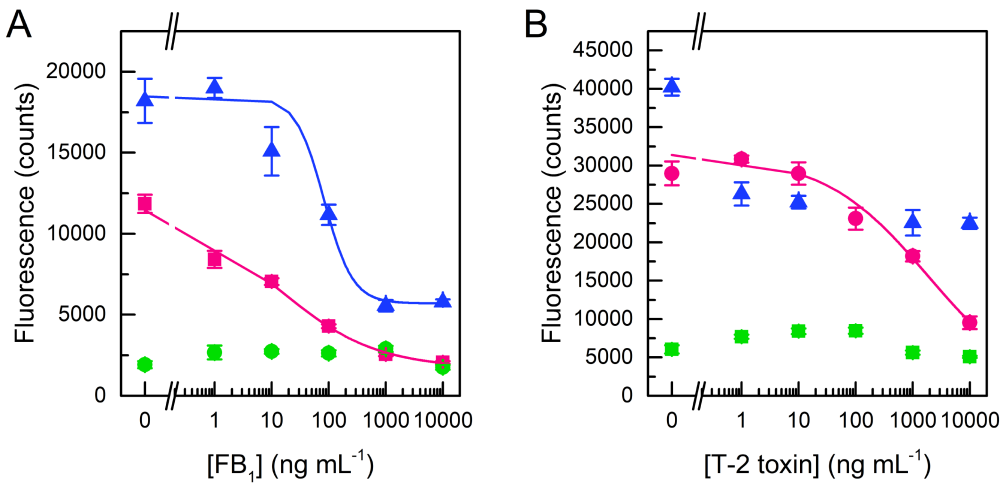


**Figure 76.** Microarray-based competitive immunoassays using fluorescent proteins (A) A2-ZsYellow and (B) F11-EmGFP for the detection of $FB_1$ and T-2 toxin, respectively. Binding of the fluorescent fusion proteins to their target antibody in the microarray in the presence of the target mycotoxin. The anti-toxin antibodies (500 ng $mL^{-1}$) were spotted onto the same microarray and binding of the mimotope-tagged fluorescent protein (green 2.5 µg $mL^{-1}$, red 5 µg $mL^{-1}$, or blue 10 µg $mL^{-1}$) was tested with different toxin concentrations. The signals are depicted as the average of three replicate spots in three replicate arrays ± standard error of the mean ($n$ = 9) and fitted with a four-parameter logistic fit (OriginPro 9.0).

### 4.4.3.3 Optimization of the homogeneous quenching immunoassay

The homogeneous quenching immunoassay presented in **publication III** was based on the use of the fluorescent YFP-tagged mimotope A2 and AuNPs. The simple homogeneous one-step assay provided good sensitivity in only 20 min without the need for washing steps. Various parameters of the homogeneous assay were optimized, including the reaction volume, temperature, plate blocking, buffer, and AuNP blocking (**Figure 77**). The total reaction volume (60–100 µL) did not have significant effects on the assay sensitivity or reproducibility (**Figure 77A**). The lowest volume used provided a slightly better response, and moreover, would result in lower reagent consumption and was thus selected for the subsequent experiments. It was also concluded that neither a prior blocking of the wells nor a pre-incubation step with the A2-YFP and anti-$FB_1$ before adding the AuNPs improved the results (**Figure 77B**). The incubation temperature (between +26 °C and +37 °C) did not have any significant effects on the sensitivity either (**Figure 77C**), whereas the assay buffer was seen to change the response considerably (**Figure 77D**). The presence of the surfactant Tween-20 in the assay buffer resulted in significantly lower absolute signals, as well as worse signal-to-background ratios. The best response was obtained 10 mM phosphate buffer (pH 8.0) supplemented with 0.1% BSA. As the low total reaction volume was concluded to provide the best results, the assay was also performed in a 384-well plate instead of the 96-well plate. However, the 96-well plate provided better reproducibility and signal-to-background ratios (**Figure 77E**). Finally, blocking of the AuNPs after protein G coupling was optimized. Blocking with PEG instead of BSA was tested and resulted in lower background signals, although at the same time, also lower maximum signals were observed (**Figure 77F**). Thus, the experiments were continued with the BSA blocking which was also used in the assay buffer to prevent the non-specific binding.

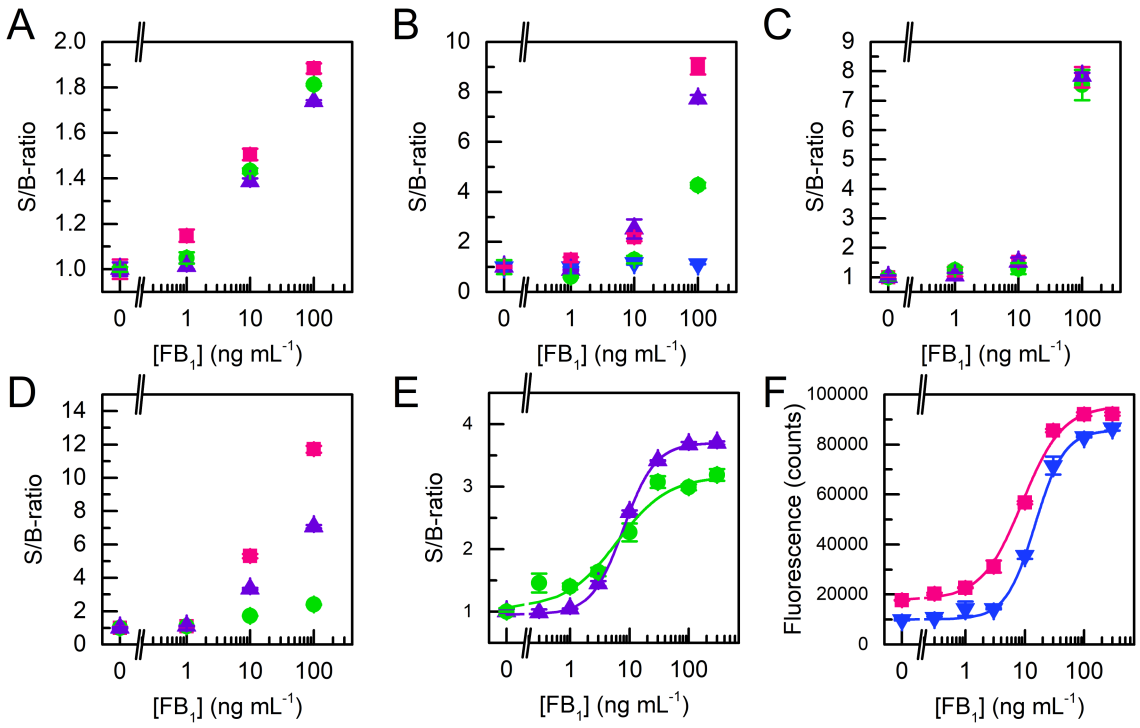


**Figure 77**. Optimization of the homogeneous quenching immunoassay with A2-YFP. Experiments were completed with (A) different reaction volumes, 60 µL (red), 80 µL (green), or 100 µL (violet), (B) with a prior blocking of the plate with Starting block (blue) or Protein free blocking buffer (green), in comparison with wells without blocking (red and violet, with and without pre-incubation before adding the gold, respectively), (C) at different temperatures, +26 °C (red), +30 °C (green), or +37 °C (violet), (D) using different assay buffers, 10 mM phosphate buffer, pH 8, with 0.1% BSA (red), 0.5% BSA (violet), or 0.1% BSA and 0.05% Tween-20 (green), (E) in a 96-well plate (violet) or 384-plate (green) at a total reaction volume of 60 µL in both cases, and (F) alternative blockings of the AuNP:protGs either with 0.1% BSA (red), or 0.1% PEG-6000 (blue).

The AuNPs used in **publication III** were prepared a step-by-step growing procedure, and the process resulted in seven generations of AuNPs with increasing sizes. Based on the plasmon peak, the sizes of different generations varied between 17 and 72 nm. In parallel with the experiments reported in **publication III** with generations 0, 3, and 6 (17 nm, 36 nm, and 72 nm AuNPs, respectively), also the in-between generations (1–4) were tested in the quenching assay. First, different concentration of the AuNPs coated with protein G were evaluated to confirm their quenching ability and determine the concentration providing the best response (**Figure 78**). Comparison of the fluorescence emission measured in the presence and absence of $FB_1$ was used to calculate the signal-to-background ratios and determine the AuNP concentration of each generation resulting in the best sensitivity. Fluorescence quenching, as well as competition with the free $FB_1$, was observed with all generations, although the best results were obtained with the smallest AuNPs (generation 0, 17 nm). Similar results were seen in the competitive assay with different $FB_1$ concentrations (**Figure 79**), and it was evident that the larger the AuNP, the lower were the signal-to-background ratios obtained. **Publication III** reports the application of the optimized assay with the generation 0 AuNPs to the analysis of spiked wheat samples.

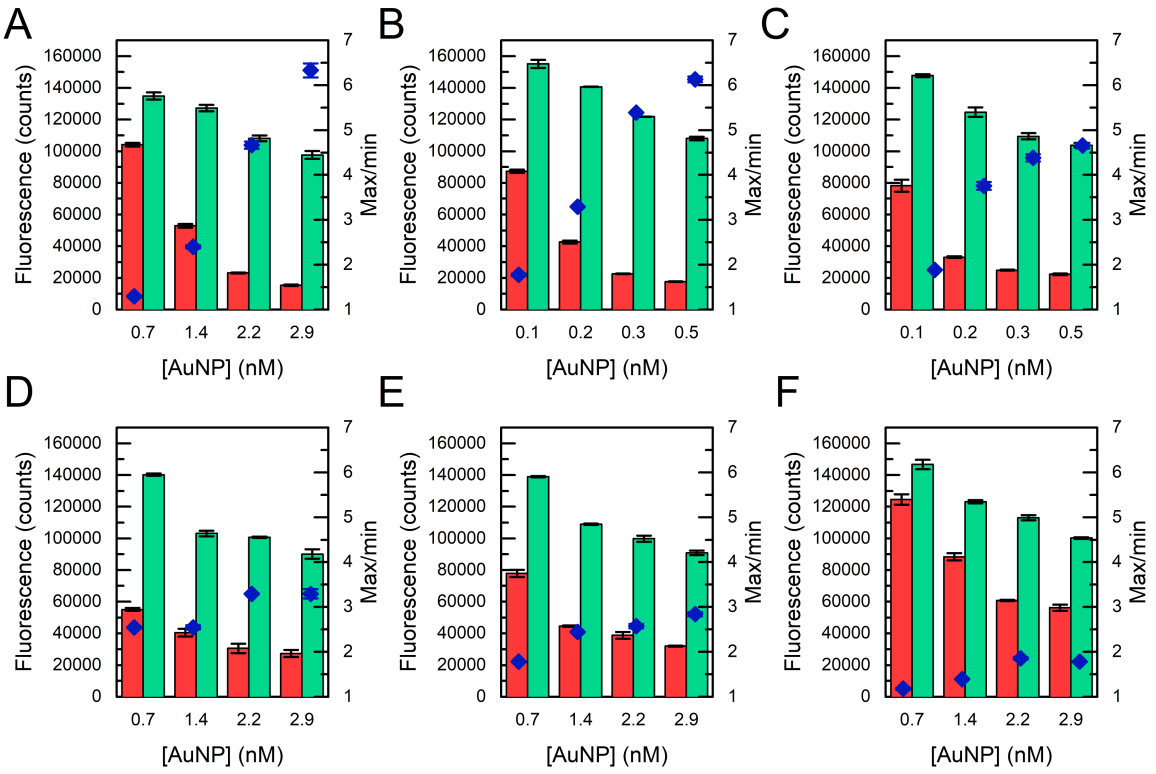


**Figure 78**. Fluorescence quenching with different sizes of AuNPs (A) Generation 0; 17 nm, (B) Generation 1; 27 nm, (C) Generation 2; 30 nm, (D) Generation 3; 36 nm, (E) Generation 4; 54 nm, (F) Generation 6; 74 nm. Signals measured in the absence of $FB_1$ (red) and in the presence 40 µg $mL^{-1}$ $FB_1$. The ratio (Max/min) between these two signals is shown in the right y-axis (blue diamonds). The fluorescence signals are depicted as the average of replicate samples ± the standard error of the mean ($n$ = 3).

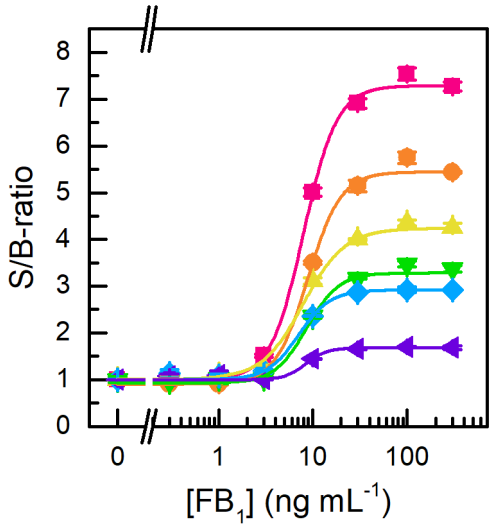


**Figure 79**. Calibration curves with all AuNP generations, 0 (red), 1 (orange), 2 (yellow), 3 (green), 4 (blue), and 6 (violet). The fluorescence signals are depicted as the average signal-to-background ratio ± standard error of the mean ($n$ = 3) and fitted with a four-parameter logistic fit (OriginPro 9.0).

### 4.4.4 BIOLUMINESCENT FUSION PROTEINS

In an alternative, yet similar, approach to the FP-tagged mimotopes, the mimotopes for $FB_1$ (A2), ZEA (SF and GW), and T-2 toxin (F11 and T13) were used to construct fusion proteins with a bioluminescent protein *Gaussia* luciferase (GLuc). This work was carried out in collaboration with the group of prof. Sylvia Daunert from University of Miami. In a similar manner to the FP, the bioluminescent GLuc could provide a measurable feature for the mimotope and could be used as the tracer in the immunoassay. Moreover, owing to the intrinsic nature of bioluminescence, the measurement could be accomplished without the need for an excitation light source and the enzymatic activity of the luciferase was thought to improve the assay sensitivity. In parallel with GLuc-tagged mimotopes (A2-GLuc and SF-GLuc) described in **publication V**, we constructed GLuc-fusions also of the mimotopes F11, T13, and GW to compare which fusion could provide the best response for the detection of ZEA and T-2 toxin. After expression and purification of the GLuc-tagged mimotopes, direct binding of the proteins to their target antibody was tested to confirm the specific binding to the antibody. Good signal-to-background ratios were observed with different concentrations of A2-GLuc, SF-GLuc, and GW-GLuc (**Figure 80A–C**), which exhibited significantly higher luminescent signals from the wells coated with anti-$FB_1$, or anti-ZEA antibodies, in comparison with the background wells without the antibody. The persistently challenging T2-mimotopes showed some specific binding to the anti-T2 antibody, but the non-specific binding to the background wells was substantial for both F11-GLuc and T13-GLuc fusion proteins (**Figure 80D–E**).

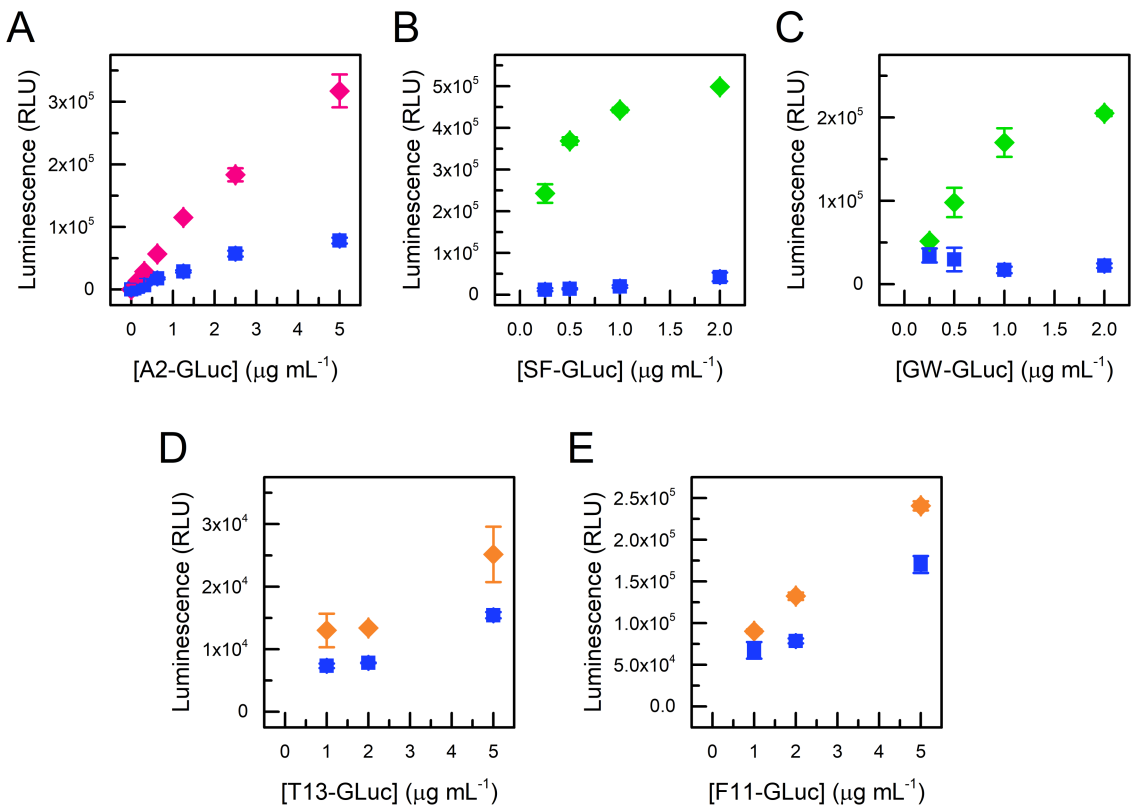


**Figure 80**. Binding of the GLuc-fusion protein to their target antibody and background binding to BSA-coated wells (blue squares). (A) A2-GLuc binding to immobilized anti-$FB_1$ (red), (B) SF-GLuc and (C) GW-GLuc binding to anti-ZEA (green), (D) T13-GLuc and (E) F11-GLuc binding to anti-T2 (orange).

A checkerboard-type titration was performed with all the mimotope fusions in order to determine the optimal concentrations of the immobilized antibody and the GLuc-tagged mimotope for the competitive assay. For the $FB_1$ assay, different concentrations of A2-GLuc (0.125–1 µg $mL^{-1}$) were combined with varying concentrations of the immobilized anti-$FB_1$ (50–400 ng per well). The highest concentration of A2-GLuc together with the highest amount of the antibody resulted in most intense bioluminescent signals, but a similar trend was also seen in the presence of free $FB_1$ in the reaction (**Figure 81**). To obtain the best sensitivity in the competitive assay, those concentrations of A2-GLuc and anti-$FB_1$ that provided the best signal-to-background ratio, in the absence and presence of $FB_1$ (0.25 µg $mL^{-1}$ A2-GLuc with 50 ng of anti-$FB_1$), were selected for the subsequent experiments. Similarly, the concentrations of SF-GLuc and GW-GLuc were optimized together with the amount of anti-ZEA (**Figure 82**), in the presence and absence of free ZEA in the reaction. A further experiment with SF-GLuc, and different amounts of anti-ZEA (10–1000 ng per well), was carried out in order to determine if the dynamic range of the assay could be improved with higher amounts of the immobilized antibody. The results showed that low amounts of the antibody (10–20 ng) could not provide sufficient signals in the absence of the toxin, but higher amounts showed increasing signals (**Figure 83A**). Although all antibody concentrations showed the competition with high concentrations of ZEA, the best sensitivity was seen with 50 ng of anti-ZEA per well.

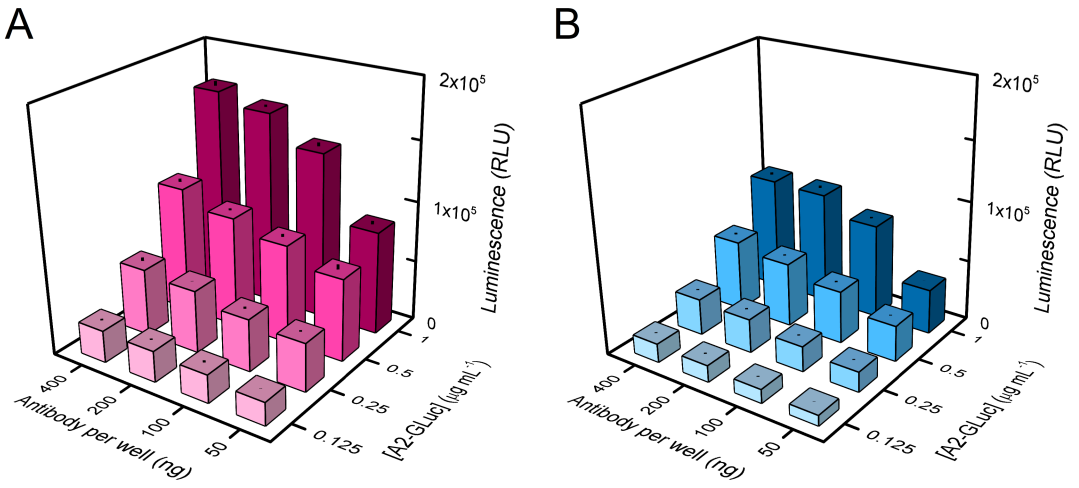


**Figure 81.** Checkerboard titration with A2-GLuc (A) without (red) and (B) with 5 ng mL$^{-1}$ $FB_1$ (blue). Various concentrations of the immobilized antibody (50–400 ng/well) and A2-GLuc (0.125–1 µg mL$^{-1}$) were tested in both conditions and those resulting in the highest signal-to-background ratios were selected for the subsequent experiments.

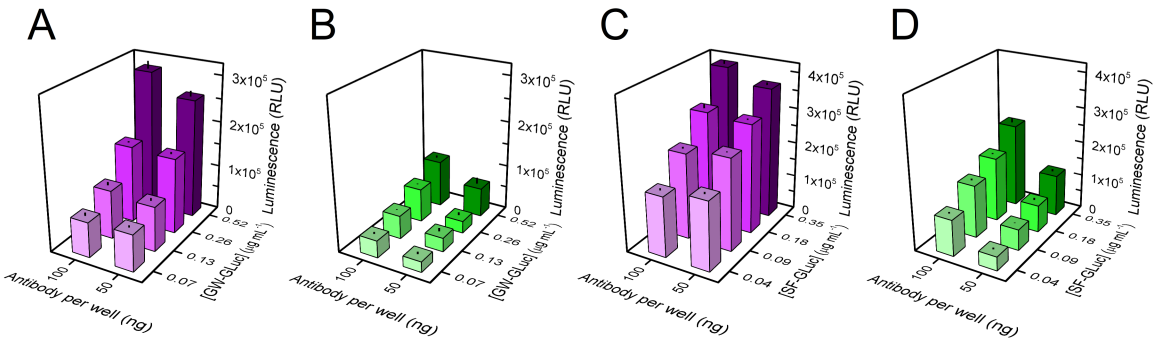


**Figure 82.** Checkerboard titration with (A–B) GW-GLuc and (C–D) SF-GLuc without (violet) and with 1 ng mL$^{-1}$ ZEA (green). Various concentrations of the immobilized antibody (50–100 ng/well) and mimotope-GLucs (0.04–0.52 µg mL$^{-1}$) were tested in both conditions, and those resulting in the highest signal-to-background ratios were selected for the subsequent experiments.

Next, a calibration curve with 0–30 ng mL$^{-1}$ of ZEA was performed using the optimized concentrations of the immobilized anti-ZEA and SF-GLuc, or GW-GLuc. Both assays showed good sensitivity for ZEA detection with similar $IC_{50}$ values (0.45 ± 0.05 ng mL$^{-1}$ and 0.60 ± 0.03 ng mL$^{-1}$ for GW-GLuc and SF-GLuc, respectively). Although GW-GLuc provided a slightly better sensitivity, the assay with SF-GLuc proved to be more reproducible in terms of intra- and interday variations and was thus designated as the best mimotope for ZEA detection.

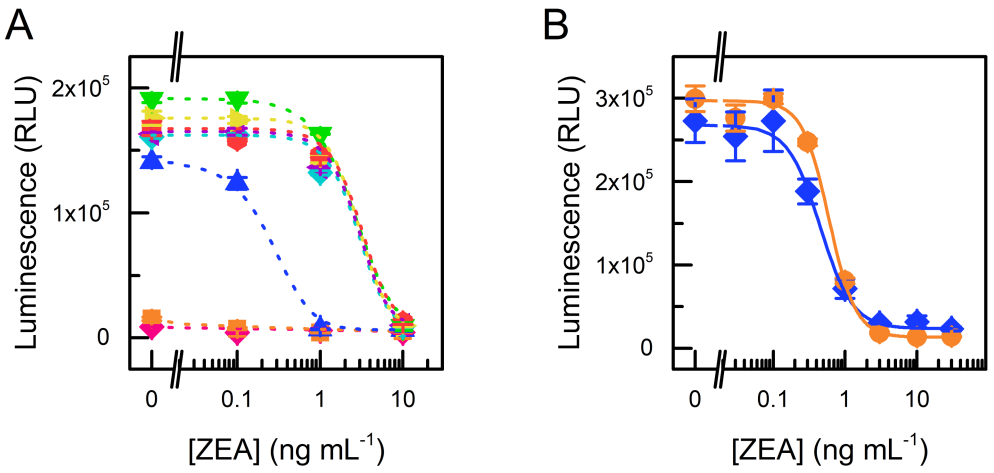


**Figure 83**. Optimization of the ZEA assay. (A) Various antibody concentrations were tested in the assay (10–1000 ng/well) but the lowest concentrations (10–20 ng; red and orange) did not result in good signals. Best sensitivity was seen with 50 ng (blue) whereas higher concentrations resulted in higher absolute signals but lower sensitivity. (B) Comparison of the optimized assay with GW-GLuc (blue) and SF-GLuc (orange). The signals are depicted as the average of three replicate spots in three replicate arrays ± standard error of the mean ($n$ = 9). A four-parameter logistic fit (OriginPro 9.0) was used to estimate the assay sensitivity.

Also for the detection of T-2 toxin, the bioluminescent immunoassay was further optimized with F11-GLuc despite the high background signals observed. In the checkerboard titration, competition with a high concentration of T-2 toxin (1000 ng mL$^{-1}$) was observed to some extent, and the antibody and F11-GLuc concentrations providing the best signal-to-background ratio (100 ng per well and 1 µg mL$^{-1}$, respectively) were used in the further attempts to improve the assay performance.

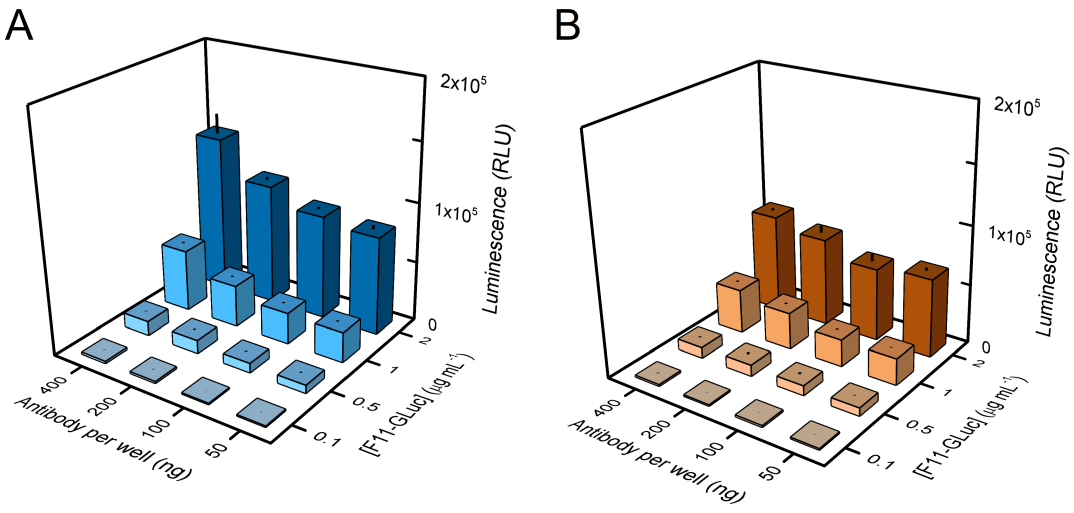


**Figure 84**. Checkerboard titration with F11-Gluc (A) without (blue) and (B) with 1000 ng mL$^{-1}$ T-2 toxin (brown). Various concentrations of the immobilized antibody (50–400 ng/well) and F11-GLuc (0.1–2 µg mL$^{-1}$) were tested in both conditions and those resulting in the highest signal-to-background ratios were selected for the subsequent experiments.

Different blocking buffers (3% BSA, 10% BSA, Protein-free blocking buffer, StartingBlock, Casein, and SuperBlock) were tested to determine if the extent of the non-specific binding to the plate could be reduced (**Figure 85A**). Some differences were observed in the signal levels, but none of the buffers tested provided significant improvements to the non-specific binding. The competitive assay was further tested with different concentrations of T-2 toxin (0–1000 ng $mL^{-1}$) using alternative buffers (**Figure 85B**). The best results were obtained adding 0.1% or 1% BSA in the assay buffer, but the assay did not provide enough sensitivity for the detection of T-2 toxin in food samples. Further optimization of the assay protocol might present some improvements in the response, but, unfortunately, so far, the experiments with bioluminescent T-2 toxin assay have been somewhat unsuccessful.

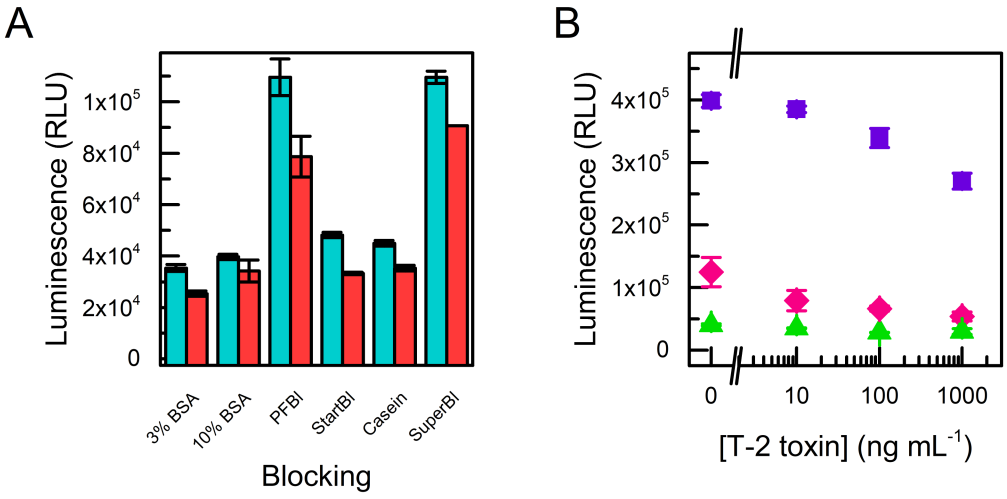


**Figure 85.** (A) Optimization of T-2 toxin assay with the immobilized anti-T2 and F11-GLuc without (blue) and with 2000 ng $mL^{-1}$ T-2 toxin (red) using different blocking buffers. PFBl, Protein-free blocking buffer, StartBl, Starting block; SuperBl, SuperBlock (all from ThermoScientific) (B) Competitive T-2 toxin assay with F11-GLuc in StartingBlock (green triangles), 1% BSA (red diamonds), or in 0.1% BSA (violet squares).

# 4.5 Discussion

*Fusarium* genus includes more than 70 described species, many of which are common plant pathogens worldwide. Moreover, many species in this family are notorious producers of mycotoxins and owing to the natural origin of these toxins, mycotoxin contamination in both food and feed is often inevitable. The toxicity of these compounds even at low concentrations has necessitated the need for sensitive and reliable methods for their detection.[222] At the same time, in order to detect mycotoxins or prevent mycotoxin formation, it is considered essential to identify the producers of these toxins. While conventional culture-based methods for fungal detection are time-consuming and challenging, especially if the species have similar morphologies, molecular methods based on highly specific DNA primers or probes are capable of distinguishing even closely related species. The genosensors developed in this work for the detection of *F. proliferatum* and *F. verticillioide*s enabled detection of the synthetic target DNA at low pM levels and could be applied to analyze *Fusarium* contamination in maize after PCR amplification of the genomic DNA. The developed sensors could provide a valuable tool to evaluate the potential for mycotoxin contamination in conditions where direct detection of mycotoxins is challenging. Moreover, the suggested microfluidic approach, which yet remains in its preliminary stage, presents an interesting alternative for the development of an integrated method which might be able to achieve better sensitivities, faster analysis times, and lower reagent consumption than conventional methods.

Another interesting approach in the future would be to combine the genosensors with the immunoassays described in this work, in order to investigate the simultaneous occurrence of mycotoxin-producing *Fusarium* species and fumonisins. Although some studies have reported this kind of correlation between the mycotoxin concentrations and the presence of the fungi,[318] it remains essential to detect also the mycotoxins themselves to determine what kind of threat they might pose to the consumer. The establishment of national and international regulations has been an important incentive for the development of new analytical methods with high sensitivities. However, some experts have also expressed their concern about the fact that the regulatory limits are set according to the toxin concentrations detected with the most sophisticated methodology, rather than being consistent with the toxic levels.[10]

Regulations exist, not only for the presence of mycotoxins in different food commodities, but also for the sampling protocols, and in fact, regulatory agencies have even set improvements in sampling of food and feed products as one of their priorities.[16,25] The wide variety of food matrices and the often heterogeneous distribution of the toxins within the sample makes this step one of the most crucial parts of the analysis and is often also associated with the largest source of variability.[16] Sample preparation has also been reported to affect the analysis of toxigenic fungi in addition to the analysis of mycotoxins.[367] Matrix-dependent recoveries have been reported, for example, for fumonisins which tend to exhibit a strong interaction with matrix macroconstituents.[368] Another challenge for the development of new methods of analysis is the lack of certified reference materials for certain toxins and different food matrices.[25]

In general, the small size of mycotoxins, or equally other small molecular weight contaminants, has hindered the development of analytical methods for routine use. Conventional methods, typically based on chromatography, can provide accurate and precise detection but are often time-consuming, or require complex and expensive instrumentation. Such methods, mostly based on HPLC coupled with MS-detection, have been advocated by international organizations as reference methods for the analysis of these compounds,[369] and recent research efforts have focused particularly on the development of multi-analyte methods.[370] However, these analyses require extremely careful sample preparation to avoid any analyte losses during this step due to the chemical differences between the target molecules. For example, fumonisins have proven to be a challenging target in such approaches.[371]

Biosensors and bioanalytical assays have the potential to overcome some of the limitations of chromatographic methods, mainly related to the cost and high throughput potential, and they can be regarded as valuable complements for food safety applications due to their merits in simplicity, rapidity and low cost while maintaining the required sensitivity and specificity. Evidently, molecular recognition plays a key role in biosensors, and the recognition element lies at the heart of all biosensing applications. One of the aims of this thesis has been to study alternative recognition elements which could improve mycotoxin analysis. Various natural and bioinspired recognition elements have been described in the literature for mycotoxin sensors, and although monoclonal and polyclonal antibodies still at large continue their reign as the recognition element of choice in many applications, alternative methods have the potential to overcome some of their limitations.[193] At the same time, a myriad of different label technologies and transduction schemes have been described for mycotoxin detection, many of them with excellent sensitivity and performance. Moreover, owing to their unique physicochemical characteristics, various nanomaterials have also gained increasing attention for biosensor development.[372,373]

Biosensors can be implemented in integrated systems which are capable of fully automated processes. Miniaturization enables the use of samples, or sample extracts, down to nanoliter volumes and often leads to an increased speed of analysis using small footprint devices. However, despite the technical advances of integrated systems, the challenge of integrating the sampling and processing of solid samples, in particular in miniaturized analytical systems, remains yet to be tackled.[370,374] Although a variety of emerging technologies have been reported for rapid mycotoxin measurements, so far, they have not been implemented for commercial usage, and ELISA and lateral flow assays continue to be among the most popular methods for simple mycotoxin analysis.[374] **Table 18** presents examples of commercially available test kits for fumonisin, ZEA, and T-2 toxin detection.

**Table 18.** Examples of commercially available test kits for the detection of fumonisins, zearalenone, or T-2/ HT-2 toxin.

| Test (company) | Test type | Target toxin | Detection range | Test time | Ref. |
|---|---|---|---|---|---|
| Veratox (Neogen) | ELISA | FB<br>T-2/HT-2<br>ZEA | 50–600 ppb<br>25–250 ppb<br>25–500 ppb | 10–15 min | [375] |
| Reveal Q+ (Neogen) | LF | FB<br>T-2/HT-2<br>ZEA | 0.3–6 ppm<br>50–600 ppb<br>50–1200 ppb | 6 min | [375] |
| Rosa Fast (Charm) | LF | FB<br>T-2/HT-2<br>ZEA | 0.5–1.5 ppm<br>25–200 ppb<br>100–350 ppb | 5–10 min | [376] |
| QuickTox Kit (Envirologix) | LF | FB<br>T-2/HT-2<br>ZEA | 0.2–20 ppm<br>25–2500 ppb<br>50–520 ppb | 5 min | [377] |
| AgraQuant (Romer Labs) | ELISA | FB<br>T-2<br>ZEA | 200–5000 ppb<br>10–500 ppb<br>20–1000 ppb | 15 min | [378] |
| AgraStrip (Romer Labs) | LF | FB<br>ZEA | 150–30000 ppb<br>30–1000 ppb | 3 min | [378] |
| EuroProxima | ELISA | FB<br>T-2 toxin | LOD 1–2 ppb<br>LOD 20–50 ppb | 1h 30min | [379] |

*Abbreviations: FB, fumonisins; ELISA, enzyme-linked immunosorbent assay; LF, lateral flow; ZEA, zearalenone.*

One of the aims of this thesis was the development of methods of the detection of mycotoxins in food samples. The main part of this work focused on the development of mimotope-based immunoassays for the detection of $FB_1$, ZEA, and T-2 toxin. Mimotopes for each toxin were selected by phage display from the same commercial peptide library using the toxin-specific antibody as the target. The degree of success in the selections varied for different toxins, ranging from the excellent mimotopes found for $FB_1$ and ZEA to the mediocre or rather poor mimotopes identified for T-2 toxin, which could be considered as an indicator of the delicate nature of phage display. Despite being a robust and widely used, or even a revolutionary technology, it is susceptible to particular risks. The complicated and demanding side of phage display was uncovered in the quests of mimotopes for the T-2 toxin, as well as with the fruitless attempts to select anti-immune complex peptides and anti-toxin antibody fragments. At its best, the immense potential of phage display for different applications is undeniable, but the technology can also prove itself time-consuming and inconclusive.

Nonetheless, the successful selection of mimotopes for $FB_1$ and ZEA was followed by the application of these peptides to various methods developed for the detection of these toxins. The use of mimotopes could circumvent the conjugation of the toxins themselves to a label or a carrier protein, and the immunoassay could be performed using the mimotope as the competitor. Thus, one cumbersome and time-consuming, not to mention often expensive, step to prepare the mycotoxin-conjugate could be avoided, and at the same time, the mimotope

assay could be described to be more user-friendly, as it did not require toxic compounds except as the calibrants.

Among the various immunoassays developed in this work, a comparison revealed that the synthetic peptide assay with magnetic microbeads provided the best sensitivity. This outcome could be traced back to the slightly lower affinity of the synthetic peptide in comparison with the recombinant fusion protein. Thus, the synthetic peptide could provide better sensitivity since lower amounts of the target was required to observe the competition. On the other, magnetic microbeads as the solid support could provide efficient capture of the biotinylated mimotope after a homogeneous pre-incubation step in solution with the target toxin and the antibody, and the enzymatic detection with HRP-labeled secondary antibody led to signal amplification. It will be curious to see if a similar behavior will be observed in the case of ZEA as future work aims to develop a similar assay based on the synthetic ZEA-mimotope and magnetic beads for ZEA detection and compare the performance to the assays described in this work using the phage-displayed mimotope and bioluminescent fusion protein.

The recombinant fusion proteins, consisting of the mimotope tagged with a fluorescent or bioluminescent protein, provided an exciting alternative for the synthetic mimotopes. After constructing the heterologous fusions by genetic engineering, the recombinant proteins could be produced cost-effectively in bacteria even in high amounts. Moreover, the recombinantly produced fusion proteins guaranteed a fixed stoichiometry between the fusion partners and could avoid issues related to batch-to-batch variations or heterogeneous conjugates that are often observed as the product of chemical conjugation reactions. Notably, the recombinant fusion proteins could then be directly used in the assays without the need for further labeling or secondary antibodies. Thus, the assay protocol could be simplified and shortened. Further simplification was achieved by implementing a homogeneous assay based on the fluorescently tagged mimotope and gold nanoparticles. The excellent fluorescence quenching efficiency of AuNPs *via* nanoparticle surface energy transfer was demonstrated to be an attractive feature for homogeneous assay development, and the use of His-tag-mediated AuNP coating provided a flexible and facile manner to create protein-conjugated AuNPs. Overall, the simplicity and analytical performance of the quenching assay provided an elaborated yet powerful tool for rapid analysis of mycotoxins in food samples.

Finally, it should be noted that the aim of the work described in this thesis has been to develop new methods for mycotoxin analysis, and it is important to underline that, at this point, the majority of the analysis has been done in buffer and only a few spiked samples were tested. Although these preliminary experiments have shown promise as the first step towards the development of new analytical methods and such sample analysis can be considered as sufficient test for proof-of-concept analysis, in the future it must be broadened to analyze real samples. Moreover, within the scope of this thesis, sample extraction protocols did not receive particular, and perhaps sufficient, attention although undoubtedly sampling and sample treatment are possibly one of the most critical issues to be considered for mycotoxin analysis. For optimal mycotoxin extraction, appropriate extraction conditions should be optimized to achieve high yields and minimal interference with the detection method. Despite how sensitive the analytical method is, should the sample not represent correctly the real situation, everything else is vain.

# 5 Summary and conclusions

Nature produces a variety of different species, among which fungi play an important yet somewhat unexplored role. The widespread occurrence of pathogenic or mycotoxigenic fungi has spurred the development of new analytical methods to detect and identify these species. Moreover, the toxic nature of many fungal secondary metabolites, mycotoxins, has been reported as a major threat to public health not to mention the massive economic losses caused every year due to fungal and mycotoxin contaminations. Years of research have made it evident that early detection of both, fungi and mycotoxin contamination, could improve the living conditions around the world. Moreover, an important motivation for the development of new methods has been the establishment of national and international regulatory limits designed to guarantee food safety for the consumers.

Nowadays, biosensing methods are able to compete with traditional culture-based or chromatographic techniques for the detection of mycotoxigenic fungi and mycotoxins. These methods are often able to provide rapid, sensitive, selective, robust, and cost-effective analysis of these targets in food samples. Optical biosensors, in particular, can be considered ideal for conditions where expensive or bulky instrumentation cannot be used, or trained personnel is not available to perform the analysis. Biosensor technologies have been a rapidly evolving field during the past decades, but for environmental and food safety applications they still have been partly described to be in their infancy, especially for real sample analysis. The challenging sample matrices are complex in nature and can often interfere with the detection of the target analytes in biosensors.

A wide variety of different biosensor concepts have been reported in the literature based on various recognition elements and transduction schemes, and it is hardly possible, nor necessary, to design one optimal platform for every situation. In this work, we have aimed to develop new biosensors for mycotoxin analysis, which could offer comparable or better

sensitivities, along with simplified methodologies and concepts in comparison with currently available devices, and that could be integrated into simple systems and transferred to low-resource settings or conditions in the field. Saying this, it is clear that the novel methods presented here are far from complete as they still require laboratory expertise and equipment, or rely on bulky and expensive instrumentation, such as a microplate reader or a microarray scanner. However, notably, these biosensors show potential for further implementation into integrated systems.

The main conclusions based on the publications presented in this thesis are summarized in the following section:

In the first part of this thesis (**publication I**), we developed novel genosensors for the detection of two fungal species which are among the most common ones found in maize and are responsible for producing several mycotoxins. *Fusarium proliferatum* and *Fusarium verticillioides* are closely related fungi with highly similar morphologies, which makes their identification challenging. Based on the species-specific capture and detection probes designed on the intergenic spacer (IGS) region sandwich hybridization assays for both species were implemented. The optimized assay protocol with enzymatic detection had detection limits of 1.8 pM and 3.0 pM for *F. proliferatum* and *F. verticillioides*, respectively, using synthetic DNA targets. In addition, a common primer pair was designed to amplify both *Fusarium* species simultaneously, and thus, after PCR amplification of the IGS region, the genosensors could be applied to the analysis of naturally contaminated maize sample. The sensors could detect the presence of both fungi species separately and simultaneously in contaminated maize samples, in consistency with previous results obtained by PCR. No cross-reactivity between *F. verticillioides* and *F. proliferatum*, or other fungi species tested, was observed. The developed sensors can provide a valuable tool to evaluate the potential for mycotoxin contamination in conditions where detection of mycotoxins directly is challenging. Furthermore, ongoing efforts aim to integrate this assay into a microfluidic platform to develop a simple, robust, and potentially an even fully automated method for the detection of mycotoxigenic *Fusarium* species in food samples.

The second and major part of the thesis focused on the development of bioanalytical methods for the detection of mycotoxins. The first publication on fumonisin detection (**publication II**) described the discovery of the fumonisin mimotope and laid the foundation of its application in different biosensing schemes (**publications III–V**). Selection of the mimotopes for fumonisin (**publication II**), and later for zearalenone (**publication V**) and T-2 toxin (unpublished), from the commercial phage display peptide library, gives an idea about the versatility of these libraries and the enormous potential of phage display in the quest for new recognition elements.

**Publication II** presented a novel immunoassay for fumonisin detection based on a microarray format. This approach based on the synthetic mimotope allowed detection of fumonisin $B_1$ in ng $mL^{-1}$ range and could be applied to the analysis of spiked wheat and maize samples at the levels set by European legislation. Perhaps the most interesting outlook of this approach would be to include other mycotoxins in the same array to embrace the full potential of microarrays for multiplexed detection. Preliminary efforts envisioned the introduction of T-2 toxin as a second target for duplex detection with the microarray; however, the approach requires still further work and optimization.

In **publications III** and **V**, the mimotopes for fumonisin and zearalenone were produced recombinantly as fusion proteins with fluorescent and bioluminescent proteins. These approaches allowed us, not only to have our own, in principle, unlimited source of the fusion protein from a bacterial expression system, but also the mimotopes were readily produced with a label and could be directly used in the assay, without the need for further labeling or a secondary antibody. The immunoassay for $FB_1$ with the fluorescent fusion protein, A2-YFP, provided a limit of detection and $IC_{50}$ value of 0.3 ng $mL^{-1}$ and 1.7 ng $mL^{-1}$, respectively, in the magnetic bead–based heterogeneous assay, which demonstrated not only that the YFP-tagged mimotope could function as the competitor in the assay but also that the assay format and the YFP as a label could provide good sensitivity. The bioluminescent immunoassays based the mimotope-GLuc fusions enabled even higher sensitivities than the fluorescence-based ones with limits of detection and $IC_{50}$ values of 0.2 ng $mL^{-1}$ and 1.3 ng $mL^{-1}$, respectively, for $FB_1$, and 0.09 ng $mL^{-1}$ and 0.35 ng $mL^{-1}$ for ZEA. On the other hand, **publication IV** aimed to develop a rapid one-step immunoassay based on the fluorescent fusion protein using functionalized gold nanoparticles as fluorescence quenchers. Although the sensitivity in terms of the $IC_{50}$ value, 12.9 ng $mL^{-1}$, was slightly worse than for the heterogeneous formats, the simple one-step protocol showed excellent performance for sample analysis with a significant decrease in the assay time.

Altogether these results (**publications II–V**) demonstrate the versatility of mimotopes for biosensing. Once a good mimotope had been identified it can be used directly in the phage-displayed format, or as the synthetic peptide or as a recombinant fusion protein. Each mimotope format has its advantages, and the most appropriate option can be selected depending on the application. Whilst the phage-displayed format is perhaps the simplest one after selecting the mimotopes from a phage library, and in principle can be used even without actually identifying the peptide sequence, the phage is inherently large in size and its biologically active nature might be disadvantageous for analytical purposes. The well-established synthesis of short peptides makes them also an attractive alternative. In **publications II** and **IV**, the synthetic fumonisin mimotope with a biotin-linker was immobilized to the microarray or on the magnetic beads surface *via* neutravidin and was used in the immunoassay. Studies in **publication IV** demonstrated that the best sensitivity among the different mimotope assays tested could be in fact achieved using the synthetic mimotope. The construction of recombinant fusions is perhaps more cumbersome than ordering the synthetic peptide, but once constructed it can provide an exhaustive source of the fusion protein which can be produced readily with a label.

**Publication IV** could be considered as a summary of the work done in this thesis, although it did not cover the later work with the bioluminescent proteins. The aim of this publication was to compare the different mimotope and assay formats. For a fair comparison of the mimotopes, we performed analysis of the binding kinetics by surface plasmon resonance (SPR). This label-free technique enabled determination of the kinetics and direct comparison the mimotope binding independently of the solid phase or label used in the assay. Interestingly, the phage-displayed peptide, which in fact can be described as the original mimotope, showed the worst performance in SPR. The slightly lower affinity value in terms of the $K_D$ of the synthetic peptide to the antibody in comparison with the recombinant fusion might be among the reasons why this mimotope could provide the best sensitivity in the bead-based assays.

# 6 References


1. Goyal, S.; Ramawat, K. G.; Mérillon, J. M. Different shades of fungal metabolites: an overview. In *Fungal metabolites*; Merillon, J.-M., Ramawat, K. G. (Editors); Springer International Publishing: Cham, Switzerland, 2016.
2. Dube, H. C. *An Introduction to fungi*, 4th edition; Scientific Publishers: India, 2013.
3. Birren, B.; Lander, E.; Fink, G. *Fungal genome initiative: White paper developed by the fungal research community*; Whitehead Institute Center for Genome Research: Cambridge, MA, USA, 2003.
4. Blackwell, M. The fungi: 1, 2, 3 ... 5.1 million species? *Am. J. Bot.* 2011, *98*, 426–438.
5. Horbach, R.; Navarro-Quesada, A. R.; Knogge, W.; Deising, H. B. When and how to kill a plant cell: Infection strategies of plant pathogenic fungi. *J. Plant Physiol.* 2011, *168*, 51–62.
6. Powers-Fletcher, M. V.; Kendall, B. A.; Griffin, A. T.; Hanson, K. E. Filamentous fungi. *Microbiol. Spectr.* 2016, *4*.
7. Dube, H. C. *An Introduction to fungi*, 4th edition; Scientific Publishers: India, 2013.
8. Keller, N. P. Fungal secondary metabolism: Regulation, function and drug discovery. *Nat. Rev. Microbiol.* 2018, *17*, 167–180.
9. Calvo, A. M.; Wilson, R. A.; Bok, J. W.; Keller, N. P. Relationship between secondary metabolism and fungal development. *Microbiol. Mol. Biol. Rev.* 2002, *66*, 447–459.
10. *Mycotoxins: Risks in plant, animal, and human systems*; Council for Agricultural Science and Technology; Task force report; Council for Agricultural Science and Technology: Ames, IA, USA, 2003.
11. Demain, A. L.; Fang, A. The natural functions of secondary metabolites. *Adv. Biochem. Eng. Biotechnol.* 2000, *69*, 1–39.
12. Hoffmeister, D.; Keller, N. P. Natural products of filamentous fungi: Enzymes, genes, and their regulation. *Nat. Prod. Rep.* 2007, *24*, 393–416.

13. Drott, M. T.; Lazzaro, B. P.; Brown, D. L.; Carbone, I.; Milgroom, M. G. Balancing selection for aflatoxin in *Aspergillus flavus* is maintained through interference competition with, and fungivory by insects. *Proc. Biol. Sci.* **2017**, *284,* 20172408.

14. Bräse, S.; Encinas, A.; Keck, J.; Nising, C. F. Chemistry and biology of mycotoxins and related fungal metabolites. *Chem. Rev.* **2009**, *109*, 3903–3990.

15. *Mycotoxigenic fungi: Methods and protocols*; Moretti, A., Susca, A. (Editors); Methods in molecular biology; Humana Press; Springer: New York, NY, USA, **2016**.

16. *Determining mycotoxins and mycotoxigenic fungi in food and feed*; De Saeger, S. (Editor); Woodhead Publishing: Cambridge, UK, 2011.

17. DeVries, J. W.; Trucksess, M. W.; Jackson, L. S. *Mycotoxins and food safety*; Springer: New York, NY, USA, **2002**.

18. *The Aspergilli: Genomics, medical aspects, biotechnology, and research methods*; Goldman, G., Osmani, S. (Editors); CRC Press: Boca Raton, FL, USA, **2007**.

19. Logrieco, A.; Bottalico, A.; Mulé, G.; Moretti, A.; Perrone, G. Epidemiology of toxigenic fungi and their associated mycotoxins for some mediterranean crops. *Eur. J. Plant Pathol.* **2003**, *109*, 645–667.

20. Leslie, J. F.; Summerell, B. A. *The Fusarium laboratory manual*, 1st edition; Blackwell Pub: Ames, IA, USA, **2006**.

21. Gong, L.; Jiang, Y.; Chen, F. Molecular strategies for detection and quantification of mycotoxin-producing *Fusarium* species: A review. *J. Sci. Food Agric.* **2015**, *95*, 1767–1776.

22. Desjardins, A. E.; Busman, M.; Muhitch, M.; Proctor, R. H. Complementary host–pathogen genetic analyses of the role of fumonisins in the *Zea mays–Gibberella moniliformis* interaction. *Physiol. Mol. Plant Pathol.* **2007**, *70*, 149–160.

23. Creppy, E. E. Update of survey, regulation and toxic effects of mycotoxins in Europe. *Toxicol. Lett.* **2002**, *127*, 19–28.

24. Amaike, S.; Keller, N. P. *Aspergillus flavus*. *Annu. Rev. Phytopathol.* **2011**, *49*, 107–133.

25. Berthiller, F.; Brera, C.; Crews, C.; Iha, M. H.; Krska, R.; Lattanzio, V. M. T.; MacDonald, S.; Malone, R. J.; Maragos, C.; Solfrizzo, M.; *et al*. Developments in mycotoxin analysis: An update for 2014–2015. *World Mycotoxin J.* **2016**, *9*, 5–30.

26. Stockmann-Juvala, H.; Savolainen, K. A review of the toxic effects and mechanisms of action of fumonisin $B_1$. *Hum. Exp. Toxicol.* **2008**, *27*, 799–809.

27. Tuomi, T.; Reijula, K.; Johnsson, T.; Hemminki, K.; Hintikka, E.-L.; Lindroos, O.; Kalso, S.; Koukila-Kähkölä, P.; Mussalo-Rauhamaa, H.; Haahtela, T. Mycotoxins in crude building materials from water-damaged buildings. *Appl. Environ. Microbiol.* **2000**, *66*, 1899–1904.

28. Anfossi, L.; Giovannoli, C.; Baggiani, C. Mycotoxin detection. *Curr. Opin. Biotechnol.* **2016**, *37*, 120–126.

29. Marroquín-Cardona, A. G.; Johnson, N. M.; Phillips, T. D.; Hayes, A. W. Mycotoxins in a changing global environment – A review. *Food Chem. Toxicol.* **2014**, *69*, 220–230.

30. Woloshuk, C. P.; Shim, W.-B. Aflatoxins, fumonisins, and trichothecenes: A convergence of knowledge. *FEMS Microbiol. Rev.* **2013**, *37*, 94–109.

31. Pitt, J. I.; Miller, J. D. A concise history of mycotoxin research. *J. Agric. Food Chem.* **2017**, *65*, 7021–7033.

32. Navarro, E.; Serrano-Heras, G.; Castaño, M. J.; Solera, J. Real-time PCR detection chemistry. *Clin. Chim. Acta* **2015**, *439*, 231–250.

33. López-Errasquín, E.; Vázquez, C.; Jiménez, M.; González-Jaén, M. T. Real-time RT-PCR assay to quantify the expression of *FUM1* and *FUM19* genes from the fumonisin-producing *Fusarium verticillioides*. *J. Microbiol. Methods* **2007**, *68*, 312–317.

34. Jurado, M.; Marín, P.; Callejas, C.; Moretti, A.; Vázquez, C.; González-Jaén, M. T. Genetic variability and fumonisin production by *Fusarium proliferatum*. *Food Microbiol.* **2010**, *27*, 50–57.

35. Edwards, S. G.; Callaghan, J.; Dobson, A. D. W. PCR-based detection and quantification of mycotoxigenic fungi. *Mycological Research* **2002**, *106*, 1005–1025.

36. Turner, N. W.; Subrahmanyam, S.; Piletsky, S. A. Analytical methods for determination of mycotoxins: A review. *Anal. Chim. Acta* **2009**, *632*, 168–180.

37. Blount, W. P. Turkey "X" disease. *Turkeys* **1961**, *9*, 55–58.

38. Bennett, J. W.; Klich, M. Mycotoxins. *Clin. Microbiol. Rev.* **2003**, *16*, 497–516.

39. Brakhage, A. A. Regulation of fungal secondary metabolism. *Nat. Rev. Microbiol.* **2013**, *11*, 21–32.

40. Freire, F. D. C. O.; da Rocha, M. E. B. Impact of mycotoxins on human health. In *Fungal metabolites*; Mérillon, J.-M., Ramawat, K. G. (Editors); Springer International Publishing: Cham, Switzerland, **2016**.

41. World Health Organization (WHO). Food safety and zoonoses. www.who.int/foodsafety (Cited Jan 31, 2019).

42. Muture, B. N.; Ogana, G. Aflatoxin levels in maize and maize products during the 2004 food poisoning outbreak in Eastern Province of Kenya. *East Afr. Med. J.* **2005**, *82*, 275–279.

43. Newman, S. J.; Smith, J. R.; Stenske, K. A.; Newman, L. B.; Dunlap, J. R.; Imerman, P. M.; Kirk, C. A. Aflatoxicosis in nine dogs after exposure to contaminated commercial dog food. *J. Vet. Diagn. Invest.* **2007**, *19*, 168–175.

44. Krska, R.; Schubert-Ullrich, P.; Molinelli, A.; Sulyok, M.; MacDonald, S.; Crews, C. Mycotoxin analysis: An update. *Food Addit. Contam., Part A* **2008**, *25*, 152–163.

45. European Food Safety Authority (EFSA). Mycotoxins. www.efsa.europa.eu/topics/topic/mycotoxins (Cited Jan 31, 2019).

46. European Commission. Commission regulation (EC) No 1881/2006. *Off. J. Eur. Union* **2006**, *L364*, 5–24.

47. European Commission. Commission regulation (EC) No 1126/2007. *Off. J. Eur. Union* **2007**, *L255*, 14–17.

48. European Commission. Commission recommendation (EC) No 165/2013. *Off. J. Eur. Union* **2013**, *L91*, 12–15.

49. European Commission. Commission regulation (EC) No 105/2010. *Off. J. Eur. Union* **2010**, *L35*, 7–8.

50. European Commission. Commission regulation (EC) No 165/2010. *Off. J. Eur. Union* **2010**, *L50*, 8–12.

51. European Commission. Commission directive (EC) No 32/2002. **2002**.

52. European Commission. Commission recommendation (EC) No 576/2006. *Off. J. Eur. Union* **2006**, *L229*, 7–10.

53. International Agency for Research on Cancer (IARC). *Monographs on the evaluation of carcinogenic risks to humans, some naturally occurring substances: Food items and constituents, heterocyclic aromatic amines and mycotoxins.* International Agency for Research on Cancer: Lyon, France, **1993**; Vol. 56.

54. Etzel, R. A. Mycotoxins. *JAMA* **2002**, *287*, 425–427.

55. Gelderblom, W. C. A.; Vleggaar, R.; Kriek, N. P. J. Fumonisins – Novel mycotoxins with cancer-promoting activity produced by *Fusarium moniliforme*. *Appl. Environ. Microbiol.* **1988**, *54*, 6.

56. Marasas, W. F. Discovery and occurrence of the fumonisins: A historical perspective. *Environ. Health Perspect.* **2001**, *109*, 239–243.

57. Ross, P. F.; Nelson, P. E.; Richard, J. L.; Osweiler, G. D.; Rice, L. G.; Plattner, R. D.; Wilson, T. M. Production of fumonisins by *Fusarium moniliforme* and *Fusarium proliferatum* isolates associated with equine leukoencephalomalacia and a pulmonary edema syndrome in swine. *Appl. Environ. Microbiol* **1990**, *56*, 3225–3226.

58. *Fumonisin $B_1$*; Marasas, W. F. O., Miller, J. D., Riley, R. T., Visconti, A. (Editors); Environmental Health Criteria; World Health Organization: Geneva, Switzerland, **2000**.

59. International Agency for Research on Cancer (IARC). *Monographs on the evaluation of carcinogenic risk to humans. some traditional herbal medicines, some mycotoxins, naphthalene and styrene*.; IARC Press: Lyon, France, **2002**; Vol. 82.

60. Marasas, W. F. O.; Riley, R. T.; Hendricks, K. A.; Stevens, V. L.; Sadler, T. W.; Gelineau-van Waes, J.; Missmer, S. A.; Cabrera, J.; Torres, O.; Gelderblom, W. C. A.; *et al*. Fumonisins disrupt sphingolipid metabolism, folate transport, and neural tube development in embryo culture and *in vivo*: A potential risk factor for human neural tube defects among populations consuming fumonisin-contaminated maize. *J. Nutr.* **2004**, *134*, 711–716.

61. Williams, L. D.; Glenn, A. E.; Zimeri, A. M.; Bacon, C. W.; Smith, M. A.; Riley, R. T. Fumonisin disruption of ceramide biosynthesis in maize roots and the effects on plant development and *Fusarium verticillioides*–induced seedling disease. *J. Agric. Food Chem.* **2007**, *55*, 2937–2946.

62. Scientific opinion on the risks for animal and public health related to the presence of T-2 and HT-2 toxin in food and feed. *EFSA Journal* **2011**, *9*, 2481.

63. Peraica, M.; Radić, B.; Lucić, A.; Pavlović, M. Toxic effects of mycotoxins in humans. *Bull. World Health Organ.* **1999**, *77*, 754–766.

64. European Food Safety Authority (EFSA). Scientific opinion on the risks for public and animal health related to the presence of citrinin in food and feed. *EFSA Journal* **2012**, *10*, 2605.

65. European Food Safety Authority (EFSA). Risks to human and animal health related to the presence of deoxynivalenol and its acetylated and modified forms in food and feed. *EFSA Journal* **2017**, *15*.

66. European Food Safety Authority (EFSA). Risks for animal health related to the presence of zearalenone and its modified forms in feed. *EFSA Journal* **2017**, *15*.

67. Köppen, R.; Koch, M.; Siegel, D.; Merkel, S.; Maul, R.; Nehls, I. Determination of mycotoxins in foods: Current state of analytical methods and limitations. *Appl. Microbiol. Biotechnol.* **2010**, *86*, 1595–1612.

68. Qu, L.-L.; Jia, Q.; Liu, C.; Wang, W.; Duan, L.; Yang, G.; Han, C.-Q.; Li, H. Thin layer chromatography combined with surface-enhanced Raman spectroscopy for rapid sensing aflatoxins. *J. Chromatogr. A* **2018**, *1579*, 115–120.

69. Sydenham, E. W.; Shephard, G. S. Chromatographic and allied methods of analysis for selected mycotoxins. In *Progress in food contaminant analysis*; Gilbert, J. (Editor); Springer US: Boston, MA, USA, **1996**.

70. Streit, E.; Schwab, C.; Sulyok, M.; Naehrer, K.; Krska, R.; Schatzmayr, G. Multi-mycotoxin screening reveals the occurrence of 139 different secondary metabolites in feed and feed ingredients. *Toxins* **2013**, *5*, 504–523.

71. O'Mahony, J.; Clarke, L.; Whelan, M.; O'Kennedy, R.; Lehotay, S. J.; Danaher, M. The use of ultra-high pressure liquid chromatography with tandem mass spectrometric detection in the analysis of agrochemical residues and mycotoxins in food – Challenges and applications. *J. Chromatogr. A* **2013**, *1292*, 83–95.

72. Varga, E.; Glauner, T.; Berthiller, F.; Krska, R.; Schuhmacher, R.; Sulyok, M. Development and validation of a (semi-)quantitative UHPLC-MS/MSmethod for the determination of 191 mycotoxins and other fungal metabolites in almonds, hazelnuts, peanuts and pistachios. *Anal. Bioanal. Chem.* **2013**, *405*, 5087–5104.

73. Rodríguez-Carrasco, Y.; Berrada, H.; Font, G.; Mañes, J. Multi-mycotoxin analysis in wheat semolina using an acetonitrile-based extraction procedure and gas chromatography-tandem mass spectrometry. *J. Chromatogr. A.* **2012**, *1270*, 28–40.

74. Rodríguez-Carrasco, Y.; Font, G.; Moltó, J. C.; Berrada, H. Quantitative determination of trichothecenes in breadsticks by gas chromatography-triple quadrupole tandem mass spectrometry. *Food Addit. Contam. Part A* **2014**, *31*, 1422–1430.

75. Hu, X.; Hu, R.; Zhang, Z.; Li, P.; Zhang, Q.; Wang, M. Development of a multiple immunoaffinity column for simultaneous determination of multiple mycotoxins in feeds using UPLC-MS/MS. *Anal. Bioanal. Chem.* **2016**, *408*, 6027–6036.

76. Marley, E.; Brown, P.; Mackie, J.; Donnelly, C.; Wilcox, J.; Pietri, A.; Macdonald, S. Analysis of sterigmatocystin in cereals, animal feed, seeds, beer and cheese by immunoaffinity column clean-up and HPLC and LC-MS/MS quantification. *Food Addit. Contam. Part A* **2015**, *32*, 2131–2137.

77. Zhao, Y.; Wan, L.-H.; Bai, X.-L.; Liu, Y.-M.; Zhang, F.-P.; Liu, Y.-M.; Liao, X. Quantification of mycotoxins in vegetable oil by UPLC-MS/MS after magnetic solid-phase extraction. *Food Addit. Contam. Part A* **2017**, *34*, 1201–1210.

78. Drzymala, S. S.; Weiz, S.; Heinze, J.; Marten, S.; Prinz, C.; Zimathies, A.; Garbe, L.-A.; Koch, M. Automated solid-phase extraction coupled online with HPLC-FLD for the quantification of zearalenone in edible oil. *Anal. Bioanal. Chem.* **2015**, *407*, 3489–3497.

79. Goryacheva, I. Y.; Saeger, S. D.; Eremin, S. A.; Peteghem, C. V. Immunochemical methods for rapid mycotoxin detection: Evolution from single to multiple analyte screening: A review. *Food Addit. Contam.* **2007**, *24*, 1169–1183.

80. D'Orazio, P. Biosensors in clinical chemistry. *Clin. Chim. Acta* **2003**, *334*, 41–69.

81. D'Orazio, P. Biosensors in clinical chemistry – 2011 update. *Clin. Chim. Acta* **2011**, *412*, 1749–1761.

82. Bahadır, E. B.; Sezgintürk, M. K. Applications of commercial biosensors in clinical, food, environmental, and biothreat/biowarfare analyses. *Anal. Biochem.* **2015**, *478*, 107–120.

83. Sharma, H.; Mutharasan, R. Review of biosensors for foodborne pathogens and toxins. *Sens. Actuators Chem. B* **2013**, *183*, 535–549.

84. Van Dorst, B.; Mehta, J.; Bekaert, K.; Rouah-Martin, E.; De Coen, W.; Dubruel, P.; Blust, R.; Robbens, J. Recent advances in recognition elements of food and environmental biosensors: a review. *Biosens. Bioelectron.* **2010**, *26*, 1178–1194.

85. Justino, C. I. L.; Duarte, A. C.; Rocha-Santos, T. A. P. Recent progress in biosensors for environmental monitoring: A review. *Sensors* **2017**, *17*.

86. Sadana, A.; Sadana, N. *Handbook of biosensors and biosensor kinetics*; Elsevier: Amsterdam, The Netherlands, **2011**.

87. Hulanicki, A.; Glab, S.; Ingman, F. Chemical sensors: Definitions and classification. *Pure Appl. Chem.* **1991**, *63*, 1247–1250.

88. Nagel, B.; Dellweg, H.; Gierasch, L. M. Glossary for chemists of terms used in biotechnology (IUPAC recommendations 1992). *Pure Appl. Chem.* **1992**, *64*, 143–168.

89. Turner, A.; Karube, I.; Wilson, G. S. *Biosensors : Fundamentals and applications*; Oxford University Press, Oxford, NY, USA, **1987**.

90. *Recognition receptors in biosensors*; Zourob, M. (Editor); Springer: New York, NY, USA, **2010**.

91. *Biosensing for the 21st century*; Renneberg, R., Andresen, D., Eds.; Advances in biochemical engineering, biotechnology; Springer: Berlin, Germany, **2008**.

92. Borisov, S. M.; Wolfbeis, O. S. Optical biosensors. *Chem. Rev.* **2008**, *108*, 423–461.

93. *The Immunoassay handbook: Theory and applications of ligand binding, ELISA, and related techniques*, 4th ed.; Wild, D., Ed.; Elsevier Science, Oxford, United Kingdom, **2013**.

94. Yalow, R. S.; Berson, S. A. Assay of plasma insulin in human subjects by immunological methods. *Nature* **1959**, *184*, 1648–1649.

95. Janotta, M.; Krska, R. Technology and applications of protein microarrays. *Anal. Bioanal. Chem.* **2004**, *379*, 338–340.

96. Cretich, M.; Damin, F.; Pirri, G.; Chiari, M. Protein and peptide arrays: Recent trends and new directions. *Biomol. Eng.* **2006**, *23*, 77–88.

97. *Principles and practice of immunoassay*; Price, C. P., Newman, D. J., Eds.; Palgrave Macmillan, United Kingdom, 1991.

98. Thévenot, D. R.; Toth, K.; Durst, R. A.; Wilson, G. S. Electrochemical biosensors: Recommended definitions and classification. *Biosens. Bioelectron.* **2001**, *16*, 121–131.

99. Fan, X.; White, I. M.; Shopova, S. I.; Zhu, H.; Suter, J. D.; Sun, Y. Sensitive optical biosensors for unlabeled targets: A review. *Anal. Chim. Acta* **2008**, *620*, 8–26.

100. Peltomaa, R.; Glahn-Martínez, B.; Benito-Peña, E.; Moreno-Bondi, M. C. Optical biosensors for label-free detection of small molecules. *Sensors* **2018**, *18*, 4126.

101. Homola, J. Surface plasmon resonance sensors for detection of chemical and biological species. *Chem. Rev.* **2008**, *108*, 462–493.

102. Hunt, H. K.; Armani, A. M. Label-free biological and chemical sensors. *Nanoscale* **2010**, *2*, 1544.

103. Abbas, A.; Linman, M. J.; Cheng, Q. New trends in instrumental design for surface plasmon resonance–based biosensors. *Biosens. Bioelectron.* **2011**, *26*, 1815–1824.

104. Kadota, T.; Takezawa, Y.; Hirano, S.; Tajima, O.; Maragos, C. M.; Nakajima, T.; Tanaka, T.; Kamata, Y.; Sugita-Konishi, Y. Rapid detection of nivalenol and deoxynivalenol in wheat using surface plasmon resonance immunoassay. *Anal. Chim. Acta* **2010**, *673*, 173–178.

105. Meneely, J.; Fodey, T.; Armstrong, L.; Sulyok, M.; Krska, R.; Elliott, C. Rapid surface plasmon resonance immunoassay for the determination of deoxynivalenol in wheat, wheat products, and maize-based baby food. *J. Agric. Food Chem.* **2010**, *58*, 8936–8941.

106. Wu, W.; Zhu, Z.; Li, B.; Liu, Z.; Jia, L.; Zuo, L.; Chen, L.; Zhu, Z.; Shan, G.; Luo, S.-Z. A direct determination of AFBs in vinegar by aptamer-based surface plasmon resonance biosensor. *Toxicon.* **2018**, *146*, 24–30.

107. Atar, N.; Eren, T.; Yola, M. L. A molecular imprinted SPR biosensor for sensitive determination of citrinin in red yeast rice. *Food Chem.* **2015**, *184*, 7–11.

108. Zhu, Z.; Feng, M.; Zuo, L.; Zhu, Z.; Wang, F.; Chen, L.; Li, J.; Shan, G.; Luo, S.-Z. An aptamer based surface plasmon resonance biosensor for the detection of ochratoxin A in wine and peanut oil. *Biosens. Bioelectron.* **2015**, *65*, 320–326.

109. Karczmarczyk, A.; Dubiak-Szepietowska, M.; Vorobii, M.; Rodriguez-Emmenegger, C.; Dostálek, J.; Feller, K.-H. Sensitive and rapid detection of aflatoxin $M_1$ in milk utilizing enhanced SPR and p(HEMA) brushes. *Biosens. Bioelectron.* **2016**, *81*, 159–165.

110. Karczmarczyk, A.; Reiner-Rozman, C.; Hageneder, S.; Dubiak-Szepietowska, M.; Dostálek, J.; Feller, K.-H. Fast and sensitive detection of ochratoxin A in red wine by nanoparticle-enhanced SPR. *Anal. Chim. Acta* **2016**, *937*, 143–150.

111. Lee, B.; Park, J.-H.; Byun, J.-Y.; Kim, J. H.; Kim, M.-G. An optical fiber-based LSPR aptasensor for simple and rapid *in-situ* detection of ochratoxin A. *Biosens. Bioelectron.* **2018**, *102*, 504–509.

112. Al-Jawdah, A.; Nabok, A.; Jarrah, R.; Holloway, A.; Tsargorodska, A.; Takacs, E.; Szekacs, A. Mycotoxin biosensor based on optical planar waveguide. *Toxins* **2018**, *10*, 272.

113. Kalia, J.; Raines, R. T. Advances in bioconjugation. *Curr. Org. Chem.* **2010**, *14*, 138–147.

114. Kolb, H. C.; Finn, M. G.; Sharpless, K. B. Click chemistry: Diverse chemical function from a few good reactions. *Angew. Chem. Int. Ed. Engl.* **2001**, *40*, 2004–2021.

115. Los, G. V.; Encell, L. P.; McDougall, M. G.; Hartzell, D. D.; Karassina, N.; Zimprich, C.; Wood, M. G.; Learish, R.; Ohana, R. F.; Urh, M.; *et al*. HaloTag: A novel protein labeling technology for cell imaging and protein analysis. *ACS Chem. Biol.* **2008**, *3*, 373–382.

116. Gautier, A.; Juillerat, A.; Heinis, C.; Corrêa, I. R.; Kindermann, M.; Beaufils, F.; Johnsson, K. An engineered protein tag for multiprotein labeling in living cells. *Chem. Biol.* **2008**, *15*, 128–136.

117. Monat, C.; Grillet, C.; Domachuk, P.; Smith, C.; Magi, E.; Moss, D. J.; Nguyen, H. C.; Tomljenovic-Hanic, S.; Cronin-Golomb, M.; Eggleton, B. J.; *et al*. Frontiers in microphotonics: Tunability and all-optical control. *Laser Phys. Lett.* **2006**, *4*, 177.

118. Demchenko, A. P. *Introduction to fluorescence sensing*, 2nd edition; Springer International Publishing: Switzerland, **2015**.

119. Scott, D.; Dikici, E.; Ensor, M.; Daunert, S. Bioluminescence and its impact on bioanalysis. *Annu. Rev. Anal. Chem.* **2011**, *4*, 297–319.

120. Soleri, R.; Demey, H.; Tria, S. A.; Guiseppi-Elie, A.; IBN Had Hassine, A.; Gonzalez, C.; Bazin, I. Peptide conjugated chitosan foam as a novel approach for capture-purification and rapid detection of hapten – Example of ochratoxin A. *Biosens. Bioelectron.* **2015**, *67*, 634–641.

121. Zou, X.; Chen, C.; Huang, X.; Chen, X.; Wang, L.; Xiong, Y. Phage-free peptide ELISA for ochratoxin A detection based on biotinylated mimotope as a competing antigen. *Talanta* **2016**, *146*, 394–400.

122. Sun, L.; Zhao, Q. Competitive horseradish peroxidase–linked aptamer assay for sensitive detection of aflatoxin $B_1$. *Talanta* **2018**, *179*, 344–349.

123. Jie, M.; Yu, S.; Yu, F.; Liu, L.; He, L.; Li, Y.; Zhang, H.; Qu, L.; Harrington, P. de B.; Wu, Y. An ultrasensitive chemiluminescence immunoassay for fumonisin $B_1$ detection in cereals based on gold-coated magnetic nanoparticles. *J. Sci. Food Agric.* **2018**, *98*, 3384–3390.

124. Shu, M.; Xu, Y.; Liu, X.; Li, Y.; He, Q.; Tu, Z.; Fu, J.; Gee, S. J.; Hammock, B. D. Anti-idiotypic nanobody-alkaline phosphatase fusion proteins: Development of a one-step competitive enzyme immunoassay for fumonisin $B_1$ detection in cereal. *Anal. Chim. Acta* **2016**, *924*, 53–59.

125. Arola, H.; Tullila, A.; Nathanail, A.; Nevanen, T. A simple and specific noncompetitive ELISA method for HT-2 toxin detection. *Toxins* **2017**, *9*, 145.

126. Sun, Z.; Wang, X.; Chen, Q.; Yun, Y.; Tang, Z.; Liu, X. Nanobody-alkaline phosphatase fusion protein-based enzyme-linked immunosorbent assay for one-step detection of ochratoxin A in rice. *Sensors* **2018**, *18*, 4044.

127. Lakowicz, J. R.; Masters, B. R. *Principles of fluorescence spectroscopy*, 3rd ed.; Springer, New York, NY, USA, **2008**.

128. Smith, D. S.; Eremin, S. A. Fluorescence polarization immunoassays and related methods for simple, high-throughput screening of small molecules. *Anal. Bioanal. Chem.* **2008**, *391*, 1499–1507.

129. Zhang, X.; Eremin, S. A.; Wen, K.; Yu, X.; Li, C.; Ke, Y.; Jiang, H.; Shen, J.; Wang, Z. Fluorescence polarization immunoassay based on a new monoclonal antibody for the detection of the zearalenone class of mycotoxins in maize. *J. Agric. Food Chem.* **2017**, *65*, 2240–2247.

130. Li, C.; Mi, T.; Oliveri Conti, G.; Yu, Q.; Wen, K.; Shen, J.; Ferrante, M.; Wang, Z. Development of a screening fluorescence polarization immunoassay for the simultaneous detection of fumonisins $B_1$ and $B_2$ in maize. *J. Agric. Food Chem.* **2015**, *63*, 4940–4946.

131. Lippolis, V.; Pascale, M.; Valenzano, S.; Pluchinotta, V.; Baumgartner, S.; Krska, R.; Visconti, A. A rapid fluorescence polarization immunoassay for the determination of T-2 and HT-2 toxins in wheat. *Anal. Bioanal. Chem.* **2011**, *401*, 2561–2571.

132. Li, C.; Wen, K.; Mi, T.; Zhang, X.; Zhang, H.; Zhang, S.; Shen, J.; Wang, Z. A universal multi-wavelength fluorescence polarization immunoassay for multiplexed detection of mycotoxins in maize. *Biosens. Bioelectron.* **2016**, *79*, 258–265.

133. Tsien, R. Y. The green fluorescent protein. *Annu. Rev. Biochem.* **1998**, *67*, 509–544.

134. Crone, D. E.; Huang, Y.-M.; Pitman, D.; Schenkelberg, C.; Fraser, K.; Macari, S.; Bystroff, C. GFP-based biosensors. In *State of the art in biosensors - General aspects*; Rinken, T., (Editor); InTech, **2013**.

135. Zhang, J.; Zhang, X.; Yang, G.; Chen, J.; Wang, S. A signal-on fluorescent aptasensor based on $Tb^{3+}$ and structure-switching aptamer for label-free detection of ochratoxin A in wheat. *Biosens. Bioelectron.* **2013**, *41*, 704–709.

136. Arola, H. O.; Tullila, A.; Kiljunen, H.; Campbell, K.; Siitari, H.; Nevanen, T. K. Specific noncompetitive immunoassay for HT-2 mycotoxin detection. *Anal. Chem.* **2016**, *88*, 2246–2452.

137. Tang, D.; Cui, Y.; Chen, G. Nanoparticle-based immunoassays in the biomedical field. *Analyst* **2013**, *138*, 981.

138. Kang, H.; Wang, L.; O'Donoghue, M.; Cao, Y. C.; Tan, W. Nanoparticles for biosensors. In *Optical biosensors* (2nd edition); Ligler, F. S., Taitt, C. R., (Editors); Elsevier: Amsterdam, The Netherlands, **2008**.

139. Howes, P. D.; Chandrawati, R.; Stevens, M. M. Colloidal nanoparticles as advanced biological sensors. *Science* **2014**, *346*, 1247390–1247390.

140. Cao, X.; Ye, Y.; Liu, S. Gold nanoparticle-based signal amplification for biosensing. *Anal. Biochem.* **2011**, *417*, 1–16.

141. *FRET – Förster resonance energy transfer*; Medintz, I. L., Hildebrandt, N. (Editors); Wiley-VCH Verlag GmbH & Co: Weinheim, Germany, **2014**.

142. Sapsford, K. E.; Berti, L.; Medintz, I. L. Materials for fluorescence resonance energy transfer analysis: beyond traditional donor–acceptor combinations. *Angew. Chem. Int. Ed. Engl.* **2006**, *45*, 4562–4589.

143. Jennings, T. L.; Singh, M. P.; Strouse, G. F. Fluorescent lifetime quenching near *d* = 1.5 nm gold nanoparticles: Probing NSET validity. *J. Am. Chem. Soc.* **2006**, *128*, 5462–5467.

144. Yun, C. S.; Javier, A.; Jennings, T.; Fisher, M.; Hira, S.; Peterson, S.; Hopkins, B.; Reich, N. O.; Strouse, G. F. Nanometal surface energy transfer in optical rulers, breaking the fret barrier. *J. Am. Chem. Soc.* **2005**, *127*, 3115–3119.

145. Carminati, R.; Greffet, J.-J.; Henkel, C.; Vigoureux, J. M. Radiative and non-radiative decay of a single molecule close to a metallic nanoparticle. *Opt. Commun.* **2006**, *261*, 368–375.

146. Pons, T.; Medintz, I. L.; Sapsford, K. E.; Higashiya, S.; Grimes, A. F.; English, D. S.; Mattoussi, H. On the quenching of semiconductor quantum dot photoluminescence by proximal gold nanoparticles. *Nano Lett.* **2007**, *7*, 8.

147. Wang, D.; Zhang, Z.; Li, P.; Zhang, Q.; Ding, X.; Zhang, W. Europium nanospheres-based time-resolved fluorescence for rapid and ultrasensitive determination of total aflatoxin in feed. *J. Agric. Food Chem.* **2015**, *63*, 10313–10318.

148. Dai, S.; Wu, S.; Duan, N.; Chen, J.; Zheng, Z.; Wang, Z. An ultrasensitive aptasensor for ochratoxin A using hexagonal core/shell upconversion nanoparticles as luminophores. *Biosens. Bioelectron.* **2017**, *91*, 538–544.

149. Jo, E.-J.; Byun, J.-Y.; Mun, H.; Bang, D.; Son, J. H.; Lee, J. Y.; Lee, L. P.; Kim, M.-G. Single-step LRET aptasensor for rapid mycotoxin detection. *Anal. Chem.* **2018**, *90*, 716–722.

150. Geißler, D.; Hildebrandt, N. Recent developments in förster resonance energy transfer (FRET) diagnostics using quantum dots. *Anal. Bioanal. Chem.* **2016**, *408*, 4475–4483.

151. Anfossi, L.; Di Nardo, F.; Cavalera, S.; Giovannoli, C.; Spano, G.; Speranskaya, E. S.; Goryacheva, I. Y.; Baggiani, C. A lateral flow immunoassay for straightforward determination of fumonisin mycotoxins based on the quenching of the fluorescence of CdSe/ZnS quantum dots by gold and silver nanoparticles. *Mikrochim. Acta* **2018**, *185*, 94.

152. Tian, J.; Wei, W.; Wang, J.; Ji, S.; Chen, G.; Lu, J. Fluorescence resonance energy transfer aptasensor between nanoceria and graphene quantum dots for the determination of ochratoxin A. *Anal. Chim. Acta* **2018**, *1000*, 265–272.

153. Skottrup, P. D. Small biomolecular scaffolds for improved biosensor performance. *Anal. Biochem.* **2010**, *406*, 1–7.

154. Byrne, B.; Stack, E.; Gilmartin, N.; O'Kennedy, R. Antibody-based sensors: Principles, problems and potential for detection of pathogens and associated toxins. *Sensors* **2009**, *9*, 4407–4445.

155. Amine, A.; Mohammadi, H.; Bourais, I.; Palleschi, G. Enzyme inhibition-based biosensors for food safety and environmental monitoring. *Biosens. Bioelectron.* **2006**, *21*, 1405–1423.

156. Vidal, J. C.; Bonel, L.; Ezquerra, A.; Hernández, S.; Bertolín, J. R.; Cubel, C.; Castillo, J. R. Electrochemical affinity biosensors for detection of mycotoxins: A review. *Biosens. Bioelectron.* **2013**, *49*, 146–158.

157. Arduini, F.; Amine, A.; Moscone, D.; Palleschi, G. Biosensors based on cholinesterase inhibition for insecticides, nerve agents and aflatoxin $B_1$ detection (review). *Mikrochim. Acta* **2010**, *170*, 193–214.

158. Andreescu, S.; Marty, J.-L. Twenty years research in cholinesterase biosensors: From basic research to practical applications. *Biomol. Eng.* **2006**, *23*, 1–15.

159. Arduini, F.; Errico, I.; Amine, A.; Micheli, L.; Palleschi, G.; Moscone, D. Enzymatic spectrophotometric method for aflatoxin B detection based on acetylcholinesterase inhibition. *Anal. Chem.* **2007**, *79*, 3409–3415.

160. Arduini, F.; Neagu, D.; Pagliarini, V.; Scognamiglio, V.; Leonardis, M. A.; Gatto, E.; Amine, A.; Palleschi, G.; Moscone, D. Rapid and label-free detection of ochratoxin A and aflatoxin $B_1$ using an optical portable instrument. *Talanta* **2016**, *150*, 440–448.

161. Puiu, M.; Istrate, O.; Rotariu, L.; Bala, C. Kinetic approach of aflatoxin $B_1$–acetylcholinesterase interaction: A tool for developing surface plasmon resonance biosensors. *Anal. Biochem.* **2012**, *421*, 587–594.

162. Ben Rejeb, I.; Arduini, F.; Arvinte, A.; Amine, A.; Gargouri, M.; Micheli, L.; Bala, C.; Moscone, D.; Palleschi, G. Development of a bio-electrochemical assay for $AFB_1$ detection in olive oil. *Biosens. Bioelectron.* **2009**, *24*, 1962–1968.

163. Gui, Q.; Lawson, T.; Shan, S.; Yan, L.; Liu, Y. The application of whole cell-based biosensors for use in environmental analysis and in medical diagnostics. *Sensors* **2017**, *17*, 1623.

164. Ye, Y.; Guo, H.; Sun, X. Recent progress on cell-based biosensors for analysis of food safety and quality control. *Biosens. Bioelectron.* **2019**, *126*, 389–404.

165. Xia, S.; Zhu, P.; Pi, F.; Zhang, Y.; Li, Y.; Wang, J.; Sun, X. Development of a simple and convenient cell-based electrochemical biosensor for evaluating the individual and combined toxicity of DON, ZEN, and $AFB_1$. *Biosens. Bioelectron.* **2017**, *97*, 345–351.

166. Gu, W.; Zhu, P.; Jiang, D.; He, X.; Li, Y.; Ji, J.; Zhang, L.; Sun, Y.; Sun, X. A novel and simple cell-based electrochemical impedance biosensor for evaluating the combined toxicity of DON and ZEN. *Biosens. Bioelectron.* **2015**, *70*, 447–454.

167. Larou, E.; Yiakoumettis, I.; Kaltsas, G.; Petropoulos, A.; Skandamis, P.; Kintzios, S. High throughput cellular biosensor for the ultra-sensitive, ultra-rapid detection of aflatoxin $M_1$. *Food Control* **2013**, *29*, 208–212.

168. Janeway, C. A.; Travers, P.; Walport, M.; Shlomchik, M. J. *Immunobiology: The immune system in health and disease*, ($5^{th}$ edition); Garland Science: New York, NY, USA, **2001**.

169. Vincke, C.; Muyldermans, S. Introduction to heavy chain antibodies and derived nanobodies. In *Single domain antibodies*; Saerens, D., Muyldermans, S. (Editors); Humana Press: Totowa, NJ, USA, **2012**.

170. Cooper, H. M.; Paterson, Y. Production of polyclonal antisera. *Curr. Protoc. Neurosci.* **2009**, *Chapter 5*, Unit 5.5.

171. Köhler, G.; Milstein, C. Continuous cultures of fused cells secreting antibody of predefined specificity. *Nature* **1975**, *256*, 495–497.

172. Langone, J. J.; Van Vunakis, H. Aflatoxin B specific antibodies and their use in radioimmunoassay. *J. Natl. Cancer Inst.* **1976**, *56*, 591–595.

173. Sun, Z. T. Monoclonal antibody against aflatoxin $B_1$ and its potential application. *Zhonghua Zhong Liu Za Zhi* **1983**, *5*, 401–405.

174. Groopman, J. D.; Trudel, L. J.; Donahue, P. R.; Marshak-Rothstein, A.; Wogan, G. N. High-affinity monoclonal antibodies for aflatoxins and their application to solid-phase immunoassays. *Proc. Natl. Acad. Sci. USA.* **1984**, *81*, 7728–7731.

175. Vidal, J. C.; Bertolín, J. R.; Ezquerra, A.; Hernández, S.; Castillo, J. R. Rapid simultaneous extraction and magnetic particle-based enzyme immunoassay for the parallel determination of ochratoxin a, fumonisin $B_1$ and deoxynivalenol mycotoxins in cereal samples. *Anal. Methods* **2017**, *9*, 3602–3611.

176. Kong, W.; Xiao, C.; Ying, G.; Liu, X.; Zhao, X.; Wang, R.; Wan, L.; Yang, M. Magnetic microspheres–based cytometric bead array assay for highly sensitive detection of ochratoxin A. *Biosens. Bioelectron.* **2017**, *94*, 420–428.

177. Urusov, A.; Petrakova, A.; Vozniak, M.; Zherdev, A.; Dzantiev, B. Rapid immunoenzyme assay of aflatoxin $B_1$ using magnetic nanoparticles. *Sensors* **2014**, *14*, 21843–21857.

178. Beloglazova, N. V.; Speranskaya, E. S.; Wu, A.; Wang, Z.; Sanders, M.; Goftman, V. V.; Zhang, D.; Goryacheva, I. Y.; De Saeger, S. Novel multiplex fluorescent immunoassays based on quantum dot nanolabels for mycotoxins determination. *Biosens. Bioelectron.* **2014**, *62*, 59–65.

179. Wu, S.; Duan, N.; Zhu, C.; Ma, X.; Wang, M.; Wang, Z. Magnetic nanobead-based immunoassay for the simultaneous detection of aflatoxin $B_1$ and ochratoxin A using upconversion nanoparticles as multicolor labels. *Biosens. Bioelectron.* **2011**, *30*, 35–42.

180. Joshi, S.; Segarra-Fas, A.; Peters, J.; Zuilhof, H.; van Beek, T. A.; Nielen, M. W. F. Multiplex surface plasmon resonance biosensing and its transferability towards imaging nanoplasmonics for detection of mycotoxins in barley. *Analyst* **2016**, *141*, 1307–1318.

181. Ricciardi, C.; Castagna, R.; Ferrante, I.; Frascella, F.; Luigi Marasso, S.; Ricci, A.; Canavese, G.; Lorè, A.; Prelle, A.; Lodovica Gullino, M.; *et al*. Development of a microcantilever-based immunosensing method for mycotoxin detection. *Biosens. Bioelectron.* **2013**, *40*, 233–239.

182. Ma, H.; Sun, J.; Zhang, Y.; Bian, C.; Xia, S.; Zhen, T. Label-free immunosensor based on one-step electrodeposition of chitosan-gold nanoparticles biocompatible film on Au microelectrode for determination of aflatoxin $B_1$ in maize. *Biosens Bioelectron* **2016**, *80*, 222–229.

183. Zachariasova, M.; Hajslova, J.; Kostelanska, M.; Poustka, J.; Krplova, A.; Cuhra, P.; Hochel, I. Deoxynivalenol and its conjugates in beer: A critical assessment of data obtained by enzyme-linked immunosorbent assay and liquid chromatography coupled to tandem mass spectrometry. *Anal. Chim. Acta* **2008**, *625*, 77–86.

184. Tangni, E. K.; Motte, J.-C.; Callebaut, A.; Pussemier, L. Cross-reactivity of antibodies in some commercial deoxynivalenol test kits against some fusariotoxins. *J. Agric. Food Chem.* **2010**, *58*, 12625–12633.

185. Bazin, I.; Tria, S. A.; Hayat, A.; Marty, J.-L. New biorecognition molecules in biosensors for the detection of toxins. *Biosens. Bioelectron.* **2017**, *87*, 285–298.

186. Smith, C. J.; Osborn, A. M. Advantages and limitations of quantitative PCR (Q-PCR)-based approaches in microbial ecology: Application of Q-PCR in microbial ecology. *FEMS Microbiol. Ecol.* **2009**, *67*, 6–20.

187. Patiño, B.; Mirete, S.; González-Jaén, M. T.; Mulé, G.; Rodríguez, M. T.; Vázquez, C. PCR detection assay of fumonisin-producing *Fusarium verticillioides* strains. *J. Food Prot.* **2004**, *67*, 1278–1283.

188. Jurado, M.; Vázquez, C.; Marín, S.; Sanchis, V.; Teresa González-Jaén, M. PCR-based strategy to detect contamination with mycotoxigenic *Fusarium* species in maize. *Syst. Appl. Microbiol.* **2006**, *29*, 681–689.

189. Sánchez-Rangel, D.; SanJuan-Badillo, A.; Plasencia, J. Fumonisin production by *Fusarium verticillioides* strains isolated from maize in Mexico and development of a polymerase chain reaction to detect potential toxigenic strains in grains. *J. Agric. Food Chem.* **2005**, *53*, 8565–8571.

190. Mulè, G.; Susca, A.; Stea, G.; Moretti, A. Specific detection of the toxigenic species *Fusarium proliferatum* and *F. oxysporum* from asparagus plants using primers based on calmodulin gene sequences. *FEMS Microbiol. Lett.* **2004**, *230*, 235–240.

191. Scauflaire, J.; Godet, M.; Gourgue, M.; Liénard, C.; Munaut, F. A multiplex real-time PCR method using hybridization probes for the detection and the quantification of *Fusarium proliferatum*, *F. subglutinans*, *F. temperatum*, and *F. verticillioides*. *Fungal Biol.* **2012**, *116*, 1073–1080.

192. Moreno-Bondi, M. C.; Benito-Peña, E. Analytical applications of biomimetic recognition elements. *Anal. Bioanal. Chem.* **2016**, *408*, 1725–1726.

193. Peltomaa, R.; Benito-Peña, E.; Moreno-Bondi, M. C. Bioinspired recognition elements for mycotoxin sensors. *Anal. Bioanal. Chem.* **2018**, *410*, 747–771.

194. Holliger, P.; Hudson, P. J. Engineered antibody fragments and the rise of single domains. *Nat. Biotechnol.* **2005**, *23*, 1126–1136.

195. Charlton, K. A. Expression and isolation of recombinant antibody fragments in *E. coli*. In *Antibody engineering: methods and protocols*; Lo, B. K. C. (Editor); Methods in molecular biology; Humana Press: Totowa, NJ, USA, **2004**.

196. Romanazzo, D.; Ricci, F.; Volpe, G.; Elliott, C. T.; Vesco, S.; Kroeger, K.; Moscone, D.; Stroka, J.; Van Egmond, H.; Vehniäinen, M.; *et al*. Development of a recombinant Fab-fragment based electrochemical immunosensor for deoxynivalenol detection in food samples. *Biosens. Bioelectron.* **2010**, *25*, 2615–2621.

197. Maragos, C. M.; Li, L.; Chen, D. Production and characterization of a single chain variable fragment (scFv) against the mycotoxin deoxynivalenol. *Food Agric. Immunol.* **2012**, *23*, 51–67.

198. Min, W.-K.; Kweon, D.-H.; Park, K.; Park, Y.-C.; Seo, J.-H. Characterisation of monoclonal antibody against aflatoxin $B_1$ produced in hybridoma 2C12 and its single-chain variable fragment expressed in recombinant *Escherichia coli*. *Food Chem.* **2011**, *126*, 1316–1323.

199. Min, W.-K.; Cho, Y.-J.; Park, J.-B.; Bae, Y.-H.; Kim, E.-J.; Park, K.; Park, Y.-C.; Seo, J.-H. Production and characterization of monoclonal antibody and its recombinant single chain variable fragment specific for a food-born mycotoxin, fumonisin $B_1$. *Bioprocess Biosyst. Eng.* **2010**, *33*, 109–115.

200. Li, X.; Li, P.; Lei, J.; Zhang, Q.; Zhang, W.; Li, C. A simple strategy to obtain ultra-sensitive single-chain fragment variable antibodies for aflatoxin detection. *RSC Advances* **2013**, *3*, 22367.

201. Liu, Q.; Wang, J.; Boyd, B. J. Peptide-based biosensors. *Talanta* **2015**, *136*, 114–127.

202. Tothill, I. E. Peptides as molecular receptors. In *Recognition receptors in biosensors*; Zourob, M. (Editor); Springer: New York, NY, USA, **2010**.

203. Bazin, I.; Andreotti, N.; Hassine, A. I. H.; De Waard, M.; Sabatier, J. M.; Gonzalez, C. Peptide binding to ochratoxin A mycotoxin: A new approach in conception of biosensors. *Biosens. Bioelectron.* **2013**, *40*, 240–246.

204. Heurich, M.; Altintas, Z.; Tothill, I. Computational design of peptide ligands for ochratoxin A. *Toxins* **2013**, *5*, 1202–1218.

205. Giraudi, G.; Anfossi, L.; Baggiani, C.; Giovannoli, C.; Tozzi, C. Solid-phase extraction of ochratoxin a from wine based on a binding hexapeptide prepared by combinatorial synthesis. *J. Chromatogr. A.* **2007**, *1175*, 174–180.

206. Tozzi, C.; Anfossi, L.; Baggiani, C.; Giovannoli, C.; Giraudi, G. A combinatorial approach to obtain affinity media with binding properties towards the aflatoxins. *Anal. Bioanal. Chem.* **2003**, *375*, 994–999.

207. Pfeiffer, F.; Mayer, G. Selection and biosensor application of aptamers for small molecules. *Front. Chem.* **2016**, *4,* 25.

208. Cho, E. J.; Lee, J.-W.; Ellington, A. D. Applications of aptamers as sensors. *Annu. Rev. Anal. Chem.* **2009**, *2*, 241–264.

209. Lv, X.; Zhang, Y.; Liu, G.; Du, L.; Wang, S. Aptamer-based fluorescent detection of ochratoxin A by quenching of gold nanoparticles. *RSC Adv.* **2017**, *7*, 16290–16294.

210. Lv, L.; Li, D.; Cui, C.; Zhao, Y.; Guo, Z. Nuclease-aided target recycling signal amplification strategy for ochratoxin A monitoring. *Biosens. Bioelectron.* **2017**, *87*, 136–141.

211. Sharma, A.; Hayat, A.; Mishra, R.; Catanante, G.; Bhand, S.; Marty, J.; Sharma, A.; Hayat, A.; Mishra, R. K.; Catanante, G.; *et al*. Titanium dioxide nanoparticles ($TiO_2$) quenching based aptasensing platform: Application to ochratoxin A detection. *Toxins* **2015**, *7*, 3771–3784.

212. Zhang, J.; Li, Z.; Zhao, S.; Lu, Y. Size-dependent modulation of graphene oxide–aptamer interactions for an amplified fluorescence-based detection of aflatoxin $B_1$ with a tunable dynamic range. *Analyst* **2016**, *141*, 4029–4034.

213. Huang, L.; Wu, J.; Zheng, L.; Qian, H.; Xue, F.; Wu, Y.; Pan, D.; Adeloju, S. B.; Chen, W. Rolling chain amplification based signal-enhanced electrochemical aptasensor for ultrasensitive detection of ochratoxin A. *Anal. Chem.* **2013**, *85*, 10842–10849.

214. Moreno-Bondi, M. C.; Urraca, J.; Navarro, F.; Carrasco, S. Preparation of molecularly imprinted polymers. In *Molecularly imprinted polymers: A handbook for academia and industry.*; Alvarez-Lorenzo, C., Concheiro, A., Eds.; Smithers Rapra, Shawbury, United Kingdom, **2013**.

215. Haupt, K. Biomaterials: plastic antibodies. *Nat. Mater.* **2010**, *9*, 612–614.

216. Moreno-Bondi, M. C.; Navarro-Villoslada, F.; Urraca, J. L.; Benito-Peña, E. Molecularly imprinted polymers as selective recognition elements in optical sensing. *Curr. Anal. Chem.* **2008**, *4*, 316–340.

217. Jiang, M.; Braiek, M.; Florea, A.; Chrouda, A.; Farre, C.; Bonhomme, A.; Bessueille, F.; Vocanson, F.; Zhang, A.; Jaffrezic-Renault, N. Aflatoxin $B_1$ detection using a highly-sensitive molecularly-imprinted electrochemical sensor based on an electropolymerized metal organic framework. *Toxins* **2015**, *7*, 3540–3553.

218. Zhang, W.; Han, Y.; Chen, X.; Luo, X.; Wang, J.; Yue, T.; Li, Z. Surface molecularly imprinted polymer capped Mn-doped ZnS quantum dots as a phosphorescent nanosensor for detecting patulin in apple juice. *Food Chem.* **2017**, *232*, 145–154.

219. Ton, X.-A.; Acha, V.; Bonomi, P.; Tse Sum Bui, B.; Haupt, K. A disposable evanescent wave fiber optic sensor coated with a molecularly imprinted polymer as a selective fluorescence probe. *Biosens. Bioelectron.* **2015**, *64*, 359–366.

220. Fang, G.; Liu, G.; Yang, Y.; Wang, S. Quartz crystal microbalance sensor based on molecularly imprinted polymer membrane and three-dimensional Au nanoparticles@mesoporous carbon CMK-3 functional composite for ultrasensitive and specific determination of citrinin. *Sens. Actuators Chem.* **2016**, *230*, 272–280.

221. Jackson, T. M.; Ekins, R. P. Theoretical limitations on immunoassay sensitivity. current practice and potential advantages of fluorescent $Eu^{3+}$ chelates as non-radioisotopic tracers. *J. Immunol. Methods* **1986**, *87*, 13–20.

222. Chauhan, R.; Singh, J.; Sachdev, T.; Basu, T.; Malhotra, B. D. Recent advances in mycotoxins detection. *Biosens. Bioelectron.* **2016**, *81*, 532–545.

223. Xiao, H.; Clarke, J. R.; Marquardt, R. R.; Frohlich, A. A. Improved methods for conjugating selected mycotoxins to carrier proteins and dextran for immunoassays. *J. Agric. Food Chem.* **1995**, *43*, 2092–2097.

224. Luzar, J.; Štrukelj, B.; Lunder, M. Phage display peptide libraries in molecular allergology: From epitope mapping to mimotope-based immunotherapy. *Allergy* **2016**, *71*, 1526–1532.

225. Wai, C. Y. Y.; Leung, N. Y. H.; Leung, P. S. C.; Chu, K. H. Immunotherapy of food allergy: A comprehensive review. *Clin. Rev. Allergy Immunol.* **2017**.

226. Uner, A.; Gavalchin, J. Idiotypes. In *Encyclopedia of life sciences*; John Wiley & Sons, Ltd: Chichester, United Kingdom, **2006**.

227. Yuan, Q.; Pestka, J. J.; Hespenheide, B. M.; Kuhn, L. A.; Linz, J. E.; Hart, L. P. Identification of mimotope peptides which bind to the mycotoxin deoxynivalenol-specific monoclonal antibody. *Appl. Environ. Microbiol.* **1999**, *65*, 8.

228. Liu, X.; Xu, Y.; He, Q.; He, Z.; Xiong, Z. Application of mimotope peptides of fumonisin $B_1$ in peptide ELISA. *J. Agric. Food Chem.* **2013**, *61*, 4765–4770.

229. Xu, Y.; Chen, B.; He, Q.; Qiu, Y.-L.; Liu, X.; He, Z.; Xiong, Z. New approach for development of sensitive and environmentally friendly immunoassay for mycotoxin fumonisin $B_1$ based on using peptide-MBP fusion protein as substitute for coating antigen. *Anal. Chem.* **2014**, *86*, 8433–8440.

230. Peltomaa, R.; Benito-Peña, E.; Barderas, R.; Sauer, U.; González Andrade, M.; Moreno-Bondi, M. C. Microarray-based immunoassay with synthetic mimotopes for the detection of fumonisin $F_1$. *Anal. Chem.* **2017**, *89*, 6216–6223.

231. Liu, R.; Yu, Z.; He, Q.; Xu, Y. An immunoassay for ochratoxin A without the mycotoxin. *Food Control* **2007**, *18*, 872–877.

232. Lai, W.; Fung, D. Y. C.; Yang, X.; Renrong, L.; Xiong, Y. Development of a colloidal gold strip for rapid detection of ochratoxin A with mimotope peptide. *Food Control* **2009**, *20*, 791–795.

233. Xu, Y.; He, Z.; He, Q.; Qiu, Y.; Chen, B.; Chen, J.; Liu, X. Use of cloneable peptide–MBP fusion protein as a mimetic coating antigen in the standardized immunoassay for mycotoxin ochratoxin A. *J. Agric. Food Chem.* **2014**, *62*, 8830–8836.

234. He, Z.; He, Q.; Xu, Y.; Li, Y.; Liu, X.; Chen, B.; Lei, D.; Sun, C. Ochratoxin A mimotope from second-generation peptide library and its application in immunoassay. *Anal. Chem.* **2013**, *85*, 10304–10311.

235. He, Q.-H.; Xu, Y.; Huang, Y.-H.; Liu, R.-R.; Huang, Z.-B.; Li, Y.-P. Phage-displayed peptides that mimic zearalenone and its application in immunoassay. *Food Chem.* **2011**, *126*, 1312–1315.

236. He, Q.; Xu, Y.; Zhang, C.; Li, Y.; Huang, Z. Phage-borne peptidomimetics as immunochemical reagent in dot-immunoassay for mycotoxin zearalenone. *Food Control* **2014**, *39*, 56–61.

237. Peltomaa, R.; Amaro-Torres, F.; Carrasco, S.; Orellana, G.; Benito-Peña, E.; Moreno-Bondi, M. C. Homogeneous quenching immunoassay for fumonisin $B_1$ based on gold nanoparticles and an epitope-mimicking yellow fluorescent protein. *ACS Nano* **2018**, *12*, 11333–11342.

238. Ding, Y.; Hua, X.; Du, M.; Yang, Q.; Hou, L.; Wang, L.; Liu, F.; Gonzalez-Sapienza, G.; Wang, M. Recombinant, fluorescent, peptidomimetic tracer for immunodetection of imidaclothiz. *Anal. Chem.* **2018**.

239. Ding, Y.; Hua, X.; Chen, H.; Liu, F.; González-Sapien, G.; Wang, M. Recombinant peptidomimetic-nano luciferase tracers for sensitive single-step immunodetection of small molecules. *Analytical Chemistry* **2018**, *90*, 2230–2237.

240. Hamers-Casterman, C.; Atarhouch, T.; Muyldermans, S.; Robinson, G.; Hamers, C.; Songa, E. B.; Bendahman, N.; Hamers, R. Naturally occurring antibodies devoid of light chains. *Nature* **1993**, *363*, 446–448.

241. Dumoulin, M.; Conrath, K.; Van Meirhaeghe, A.; Meersman, F.; Heremans, K.; Frenken, L. G. J.; Muyldermans, S.; Wyns, L.; Matagne, A. Single-domain antibody fragments with high conformational stability. *Protein Sci.* **2009**, *11*, 500–515.

242. Shu, M.; Xu, Y.; Wang, D.; Liu, X.; Li, Y.; He, Q.; Tu, Z.; Qiu, Y.; Ji, Y.; Wang, X. Anti-idiotypic nanobody: a strategy for development of sensitive and green immunoassay for fumonisin $B_1$. *Talanta* **2015**, *143*, 388–393.

243. Lei, J.; Li, P.; Zhang, Q.; Wang, Y.; Zhang, Z.; Ding, X.; Zang, W. Anti-idiotypic nanobody-phage based real-time immuno-PCR for detection of hepatocarcinogen aflatoxin in grains and feedstuffs. *Anal. Chem.* **2014**, *86*, 10841–10846.

244. Xu, Y.; Xiong, L.; Li, Y.; Xiong, Y.; Tu, Z.; Fu, J.; Tang, X. Citrinin detection using phage-displayed anti-idiotypic single-domain antibody for antigen mimicry. *Food Chem.* **2015**, *177*, 97–101.

245. Xu, Y.; Xiong, L.; Li, Y.; Xiong, Y.; Tu, Z.; Fu, J.; Chen, B. Anti-idiotypic nanobody as citrinin mimotope from a naïve alpaca heavy chain single domain antibody library. *Anal. Bioanal. Chem.* **2015**, *407*, 5333–5341.

246. Qiu, Y.-L.; He, Q.-H.; Xu, Y.; Bhunia, A. K.; Tu, Z.; Chen, B.; Liu, Y.-Y. Deoxynivalenol-mimic nanobody isolated from a naïve phage display nanobody library and its application in immunoassay. *Anal. Chim. Acta* **2015**, *887*, 201–208.

247. Ji, Y.; He, Q.; Xu, Y.; Tu, Z.; Yang, H.; Qiu, Y.; Wang, X.; Liu, Y. Phage displayed anti-idiotypic nanobody mediated immuno-pcr for sensitive and environmentally friendly detection of mycotoxin ochratoxin A. *Anal. Methods* **2016**, *8*, 7824–7831.

248. Fan, M.; He, J. Recent progress in noncompetitive hapten immunoassays: A review. In *Trends in immunolabelled and related techniques*, Abuelzein, E. (Editor); Rijeka: InTech, **2012**.

249. Suzuki, T.; Munakata, Y.; Morita, K.; Shinoda, T.; Ueda, H. Sensitive detection of estrogenic mycotoxin zearalenone by open sandwich immunoassay. *Anal. Sci.* **2007**, *23*, 65–70.

250. Li, P.; Deng, S. Mimetic peptide and special antibody: promising agents for optimizing hapten-analyzing systems. *Anal. Methods* **2016**, *8*, 2554–2560.

251. He, T.; Wang, Y.; Li, P.; Zhang, Q.; Lei, J.; Zhang, Z.; Ding, X.; Zhou, H.; Zhang, W. Nanobody-based enzyme immunoassay for aflatoxin in agro-products with high tolerance to cosolvent methanol. *Anal. Chem.* **2014**, *86*, 8873–8880.

252. Chen, X.; Bai, X.; Li, H.; Zhang, B. Aptamer based microcantilever array biosensor for detection of fumonisin $B_1$. *RSC Advances* **2015**, *45*, 35448-35452.

253. Fang, G.; Fan, C.; Liu, H.; Pan, M.; Zhu, H.; Wang, S. A novel molecularly imprinted polymer on CdSe/ZnS quantum dots for highly selective optosensing of mycotoxin zearalenone in cereal samples. *RSC Adv.* **2014**, *4*, 2764–2771.

254. Smith, G. P.; Petrenko, V. A. Phage display. *Chem. Rev.* **1997**, *97*, 391–410.

255. Yau, K. Emerging trends in the synthesis and improvement of hapten-specific recombinant antibodies. *Biotechnol. Adv.* **2003**, *21*, 599–637.

256. *Bacteriophages: Biology and applications*; Kutter, E., Sulakvelidze, A. (Editors); CRC Press: Boca Raton, FL, USA, **2005**.

257. Barbas, C. F. I.; Burton, D. R.; Scott, J. K.; Silverman, G. J. *Phage display: A laboratory manual*; Cold Spring Harbor Laboratory Press: Cold Spring Harbor, NY, USA, **2001**.

258. *Phage display in biotechnology and drug discovery*, 2nd edition; Sidhu, S. S., Geyer, C. R. (Editors); CRC Press: Boca Raton, FL, USA, **2015**.

259. Kehoe, J. W.; Kay, B. K. Filamentous phage display in the new millennium. *Chem. Rev.* **2005**, *105*, 4056–4072.

260. Hoogenboom, H. R. Selecting and screening recombinant antibody libraries. *Nat. Biotechnol.* **2005**, *23*, 1105–1116.

261. Clackson, T.; Lowman, H. B. *Phage display: A practical approach*; Oxford University Press, New York, NY, USA, **2004**.

262. Danner, S.; Belasco, J. G. T7 phage display: A novel genetic selection system for cloning RNA-binding proteins from cDNA libraries. *Proc. Natl. Acad. Sci. USA* **2001**, *98*, 12954–12959.

263. Krumpe, L. R. H.; Mori, T. T7 lytic phage-displayed peptide libraries: Construction and diversity characterization. In *Therapeutic peptides: Methods and protocols*; Nixon, A. E., (Editor); Methods in molecular biology; Humana Press: Totowa, NJ, USA, **2014**.

264. Smith, G. P. Filamentous fusion phage: Novel expression vectors that display cloned antigens on the virion surface. *Science* **1985**, *228*, 1315–1317.

265. O'Connell, D.; Becerril, B.; Roy-Burman, A.; Daws, M.; Marks, J. D. Phage versus phagemid libraries for generation of human monoclonal antibodies. *J. Mol. Biol.* **2002**, *321*, 49–56.

266. Lowman, H. B.; Bass, S. H.; Simpson, N.; Wells, J. A. Selecting high-affinity binding proteins by monovalent phage display. *Biochemistry* **1991**, *30*, 10832–10838.

267. Russel, M.; Kidd, S.; Kelley, M. R. An improved filamentous helper phage for generating single-stranded plasmid DNA. *Gene* **1986**, *45*, 333–338.

268. Rondot, S.; Koch, J.; Breitling, F.; Dübel, S. A helper phage to improve single-chain antibody presentation in phage display. *Nat. Biotechnol.* **2001**, *19*, 75–78.

269. Kristensen, P.; Winter, G. Proteolytic selection for protein folding using filamentous bacteriophages. *Fold Des.* **1998**, *3*, 321–328.

270. Mao, C.; Liu, A.; Cao, B. Virus-Based chemical and biological sensing. *Angew. Chem. Int. Ed. Engl.* **2009**, *48*, 6790–6810.

271. Peltomaa, R.; López-Perolio, I.; Benito-Peña, E.; Barderas, R.; Moreno-Bondi, M. C. Application of bacteriophages in sensor development. *Anal. Bioanal. Chem.* **2016**, *408*, 1805–1828.

272. Lowman, H. B. Bacteriophage display and discovery of peptide leads for drug development. *Annu. Rev. Biophys. Biomol. Struct.* **1997**, *26*, 401–424.

273. Sidhu, S. S.; Lowman, H. B.; Cunningham, B. C.; Wells, J. A. Phage display for selection of novel binding peptides. *Meth. Enzymol.* **2000**, *328*, 333–363.

274. Bradbury, A. R. M.; Marks, J. D. Antibodies from phage antibody libraries. *J. Immunol. Methods* **2004**, *290*, 29–49.

275. Ward, E. S.; Güssow, D.; Griffiths, A. D.; Jones, P. T.; Winter, G. Binding activities of a repertoire of single immunoglobulin variable domains secreted from *Escherichia coli*. *Nature* **1989**, *341*, 544–546.

276. Plückthun, A.; Skerra, A. Expression of functional antibody Fv and Fab fragments in *Escherichia coli*. *Meth. Enzymol.* **1989**, *178*, 497–515.

277. Huse, W. D.; Sastry, L.; Iverson, S. A.; Kang, A. S.; Alting-Mees, M.; Burton, D. R.; Benkovic, S. J.; Lerner, R. A. Generation of a large combinatorial library of the immunoglobulin repertoire in phage lambda. *Science* **1989**, *246*, 1275–1281.

278. Li, Y.; Cockburn, W.; Kilpatrick, J. B.; Whitelam, G. C. High affinity scFvs from a single rabbit immunized with multiple haptens. *Biochem. Biophys. Res. Commun.* **2000**, *268*, 398–404.

279. Hu, Z.-Q.; Li, H.-P.; Liu, J.-L.; Xue, S.; Gong, A.-D.; Zhang, J.-B.; Liao, Y.-C. Production of a phage-displayed mouse scFv antibody against fumonisin $B_1$ and molecular docking analysis of their interactions. *Biotechnol. Bioprocess Eng.* **2016**, *21*, 134–143.

280. Tullila, A.; Nevanen, T. Utilization of multi-immunization and multiple selection strategies for isolation of hapten-specific antibodies from recombinant antibody phage display libraries. *Int. J. Mol. Sci.* **2017**, *18*, 1169.

281. Edupuganti, S. R.; Edupuganti, O. P.; O'Kennedy, R. Generation of anti-zearalenone scFv and its incorporation into surface plasmon resonance–based assay for the detection of zearalenone in sorghum. *Food Control* **2013**, *34*, 668–674.

282. Clackson, T.; Hoogenboom, H. R.; Griffiths, A. D.; Winter, G. Making antibody fragments using phage display libraries. *Nature* **1991**, *352*, 624.

283. Shen, Y.; Yang, X.; Dong, N.; Xie, X.; Bai, X.; Shi, Y. Generation and selection of immunized Fab phage display library against human B cell lymphoma. *Cell Res.* **2007**, *17*, 650–660.

284. Yamanaka, H. I.; Inoue, T.; Ikeda-Tanaka, O. Chicken monoclonal antibody isolated by a phage display system. *J. Immunol.* **1996**, *157*, 1156–1162.

285. White, G. P.; Meeusen, E. N.; Newton, S. E. A single-chain variable region immunoglobulin library from the abomasal lymph node of sheep infected with the gastrointestinal nematode parasite haemonchus contortus. *Vet. Immunol. Immunopathol.* **2001**, *78*, 117–129.

286. Men, R.; Yamashiro, T.; Goncalvez, A. P.; Wernly, C.; Schofield, D. J.; Emerson, S. U.; Purcell, R. H.; Lai, C.-J. Identification of chimpanzee Fab fragments by repertoire cloning and production of a full-length humanized immunoglobulin G1 antibody that is highly efficient for neutralization of dengue type 4 virus. *J. Virol.* **2004**, *78*, 4665–4674.

287. Arbabi Ghahroudi, M.; Desmyter, A.; Wyns, L.; Hamers, R.; Muyldermans, S. Selection and identification of single domain antibody fragments from camel heavy-chain antibodies. *FEBS Lett.* **1997**, *414*, 521–526.

288. Dooley, H.; Flajnik, M. F.; Porter, A. J. Selection and characterization of naturally occurring single-domain (IgNAR) antibody fragments from immunized sharks by phage display. *Mol. Immunol.* **2003**, *40*, 25–33.

289. Cheng, X.-J.; Hayasaka, H.; Watanabe, K.; Tao, Y.-L.; Liu, J.-Y.; Tsukamoto, H.; Horii, T.; Tanabe, K.; Tachibana, H. Production of high-affinity human monoclonal antibody fab fragments to the 19-kilodalton C-terminal merozoite surface protein 1 of *Plasmodium falciparum*. *Infect Immun* **2007**, *75*, 3614–3620.

290. Vaughan, T. J.; Williams, A. J.; Pritchard, K.; Osbourn, J. K.; Pope, A. R.; Earnshaw, J. C.; McCafferty, J.; Hodits, R. A.; Wilton, J.; Johnson, K. S. Human antibodies with sub-nanomolar affinities isolated from a large non-immunized phage display library. *Nat. Biotechnol.* **1996**, *14*, 309–314.

291. Griffiths, G. W.; Williams, S. C.; Hartley, O.; Tomlinson, I. M.; Waterhouse, P.; Crosby, W. L.; Kontermann, R. E.; Jones, P. T.; Low, N. M.; Allison, T. J. Isolation of high affinity human antibodies directly from large synthetic repertoires. *EMBO J.* **1994**, *13*, 3245–3260.

292. Barbas, C. F.; Bain, J. D.; Hoekstra, D. M.; Lerner, R. A. Semisynthetic combinatorial antibody libraries: A chemical solution to the diversity problem. *Proc. Natl. Acad. Sci. USA* **1992**, *89*, 4457–4461.

293. Knappik, A.; Ge, L.; Honegger, A.; Pack, P.; Fischer, M.; Wellnhofer, G.; Hoess, A.; Wölle, J.; Plückthun, A.; Virnekäs, B. Fully synthetic human combinatorial antibody libraries (HuCAL) based on modular consensus frameworks and CDRs randomized with trinucleotides. *J. Mol. Biol.* **2000**, *296*, 57–86.

294. Ling, M. M. Large antibody display libraries for isolation of high-affinity antibodies. *Comb. Chem. High Throughput Screen.* **2003**, *6*, 421–432.

295. McCafferty, J.; Griffiths, A. D.; Winter, G.; Chiswell, D. J. Phage antibodies: Filamentous phage displaying antibody variable domains. *Nature* **1990**, *348*, 552–554.

296. Charbit, A.; Boulain, J. C.; Ryter, A.; Hofnung, M. Probing the topology of a bacterial membrane protein by genetic insertion of a foreign epitope; expression at the cell surface. *EMBO J.* **1986**, *5*, 3029–3037.

297. Boder, E. T.; Wittrup, K. D. Yeast surface display for screening combinatorial polypeptide libraries. *Nat. Biotechnol.* **1997**, *15*, 553–557.

298. Zhou, C.; Jacobsen, F. W.; Cai, L.; Chen, Q.; Shen, W. D. Development of a novel mammalian cell surface antibody display platform. *MAbs* **2010**, *2*, 508–518.

299. Hanes, J.; Plückthun, A. In vitro selection and evolution of functional proteins by using ribosome display. *Proc. Natl. Acad. Sci. USA* **1997**, *94*, 4937–4942.

300. Levin, A. M.; Weiss, G. A. Optimizing the affinity and specificity of proteins with molecular display. *Mol. BioSyst.* **2006**, *2*, 49–57.

301. Bradbury, A. R. M.; Sidhu, S.; Dübel, S.; McCafferty, J. Beyond natural antibodies: The power of *in vitro* display technologies. *Nat. Biotechnol.* **2011**, *29*, 245–254.

302. Kehoe, J. W.; Velappan, N.; Walbolt, M.; Rasmussen, J.; King, D.; Lou, J.; Knopp, K.; Pavlik, P.; Marks, J. D.; Bertozzi, C. R.; *et al*. Using phage display to select antibodies recognizing post-translational modifications independently of sequence context. *Mol. Cell. Proteomics.* **2006**, *5*, 2350–2363.

303. Nissim, A.; Hoogenboom, H. R.; Tomlinson, I. M.; Flynn, G.; Midgley, C.; Lane, D.; Winter, G. Antibody fragments from a "single pot" phage display library as immunochemical reagents. *EMBO J* **1994**, *13*, 692–698.

304. Hawkins, R. E.; Russell, S. J.; Winter, G. Selection of phage antibodies by binding affinity. mimicking affinity maturation. *J. Mol. Biol.* **1992**, *226*, 889–896.

305. Katakura, Y.; Zhuang, G.; Nakatani, T.; Furuta, T.; Omasa, T.; Kishimoto, M.; Suga, K.; Shioya, S. A practical kinetic model for efficient isolation of useful antibodies from phage display libraries. *J. Mol. Catal. B Enzym.* **2004**, *28*, 191–200.

306. Poetz, O.; Ostendorp, R.; Brocks, B.; Schwenk, J. M.; Stoll, D.; Joos, T. O.; Templin, M. F. Protein microarrays for antibody profiling: specificity and affinity determination on a chip. *Proteomics* **2005**, *5*, 2402–2411.

307. Barderas, R.; Desmet, J.; Alard, P.; Casal, J. I. Affinity maturation by semi-rational approaches. *Methods Mol. Biol.* **2012**, *907*, 436–486.

308. Persson, H.; Lantto, J.; Ohlin, M. A focused antibody library for improved hapten recognition. *J. Mol. Biol.* **2006**, *357*, 607–620.

309. Moghaddam, A.; Løbersli, I.; Gebhardt, K.; Braunagel, M.; Marvik, O. J. Selection and characterisation of recombinant single-chain antibodies to the hapten aflatoxin $B_1$ from naïve recombinant antibody libraries. *J. Immunol. Methods* **2001**, *254*, 169–181.

310. Charlton, K.; Harris, W. J.; Porter, A. J. The isolation of super-sensitive anti-hapten antibodies from combinatorial antibody libraries derived from sheep. *Biosens. Bioelectron.* **2001**, *16*, 639–646.

311. Yang, L.; Ding, H.; Gu, Z.; Zhao, J.; Chen, H.; Tian, F.; Chen, Y. Q.; Zhang, H.; Chen, W. Selection of single chain fragment variables with direct coating of aflatoxin $B_1$ to enzyme-linked immunosorbent assay plates. *J. Agric. Food Chem.* **2009**, *57*, 8927–8932.

312. Lauer, B.; Ottleben, I.; Jacobsen, H.-J.; Reinard, T. Production of a single-chain variable fragment antibody against fumonisin $B_1$. *J. Agric. Food Chem.* **2005**, *53*, 899–904.

313. Hu, Z.-Q.; Li, H.-P.; Wu, P.; Li, Y.-B.; Zhou, Z.-Q.; Zhang, J.-B.; Liu, J.-L.; Liao, Y.-C. An affinity improved single-chain antibody from phage display of a library derived from monoclonal antibodies detects fumonisins by immunoassay. *Anal. Chim. Acta* **2015**, *867*, 74–82.

314. Liu, X.; Xu, Y.; Xiong, Y.; Tu, Z.; Li, Y.; He, Z.; Qiu, Y.; Fu, J.; Gee, S. J.; Hammock, B. D. $V_{HH}$ phage-based competitive real-time immuno-polymerase chain reaction for ultrasensitive detection of ochratoxin A in cereal. *Anal. Chem.* **2014**, *86*, 7471–7477.

315. Liu, X.; Xu, Y.; Wan, D.; Xiong, Y.; He, Z.; Wang, X.; Gee, S. J.; Ryu, D.; Hammock, B. D. Development of a nanobody–alkaline phosphatase fusion protein and its application in a highly sensitive direct competitive fluorescence enzyme immunoassay for detection of ochratoxin A in cereal. *Anal. Chem.* **2015**, *87*, 1387–1394.

316. Liu, X.; Tang, Z.; Duan, Z.; He, Z.; Shu, M.; Wang, X.; Gee, S. J.; Hammock, B. D.; Xu, Y. Nanobody-based enzyme immunoassay for ochratoxin A in cereal with high resistance to matrix interference. *Talanta* **2017**, *164*, 154–158.

317. Tu, Z.; Xu, Y.; He, Q.; Fu, J.; Liu, X.; Tao, Y. Isolation and characterisation of deoxynivalenol affinity binders from a phage display library based on single-domain camelid heavy chain antibodies ($V_{HH}$s). *Food Agric. Immunol.* **2012**, *23*, 123–131.

318. Nicolaisen, M.; Supronienė, S.; Nielsen, L. K.; Lazzaro, I.; Spliid, N. H.; Justesen, A. F. Real-time PCR for quantification of eleven individual *Fusarium* species in cereals. *J. Microbiol. Methods* **2009**, *76*, 234–240.

319. Sarlin, T.; Yli-Mattila, T.; Jestoi, M.; Rizzo, A.; Paavanen-Huhtala, S.; Haikara, A. Real-time PCR for quantification of toxigenic *Fusarium* species in barley and malt. *Eur. J. Plant Pathol.* **2006**, *114*, 371–380.

320. Weider, L. J.; Elser, J. J.; Crease, T. J.; Mateos, M.; Cotner, J. B.; Markow, T. A. The functional significance of ribosomal (r)DNA variation: Impacts on the evolutionary ecology of organisms. *Annu. Rev. Ecol. Evol. Syst.* **2005**, *36*, 219–242.

321. Schoch, C. L.; Seifert, K. A.; Huhndorf, S.; Robert, V.; Spouge, J. L.; Levesque, C. A.; Chen, W.; Fungal barcoding consortium; *et al*. Nuclear ribosomal internal transcribed spacer (ITS) region as a universal DNA barcode marker for fungi. *Proc. Natl. Acad. Sci. USA* **2012**, *109*, 6241–6246.

322. Song, L.; Shan, D.; Zhao, M.; Pink, B. A.; Minnehan, K. A.; York, L.; Gardel, M.; Sullivan, S.; Phillips, A. F.; Hayman, R. B.; *et al*. Direct detection of bacterial genomic DNA at sub-femtomolar concentrations using single molecule arrays. *Anal. Chem.* **2013**, *85*, 1932–1939.

323. *Detection of non-amplified genomic DNA*; Spoto, G., Corradini, R. (Editors); Soft and biological matter; Springer Netherlands, **2012.**

324. Goodrich, T. T.; Lee, H. J.; Corn, R. M. Direct detection of genomic DNA by enzymatically amplified SPR imaging measurements of RNA microarrays. *J. Am. Chem. Soc.* **2004**, *126*, 4086–4087.

325. Storhoff, J. J.; Lucas, A. D.; Garimella, V.; Bao, Y. P.; Müller, U. R. Homogeneous detection of unamplified genomic DNA sequences based on colorimetric scatter of gold nanoparticle probes. *Nat. Biotechnol.* **2004**, *22*, 883–887.

326. D'Agata, R.; Corradini, R.; Ferretti, C.; Zanoli, L.; Gatti, M.; Marchelli, R.; Spoto, G. Ultrasensitive detection of non-amplified genomic DNA by nanoparticle-enhanced surface plasmon resonance imaging. *Biosens. Bioelectron.* **2010**, *25*, 2095–2100.

327. Niessen, L.; Luo, J.; Denschlag, C.; Vogel, R. F. The application of loop-mediated isothermal amplification (LAMP) in food testing for bacterial pathogens and fungal contaminants. *Food Microbiol.* **2013**, *36*, 191–206.

328. Denschlag, C.; Rieder, J.; Vogel, R. F.; Niessen, L. Real-time loop-mediated isothermal amplification (LAMP) assay for group specific detection of important trichothecene producing *Fusarium* species in wheat. *Int. J. Food Microbiol.* **2014**, *177*, 117–127.

329. Shan, L.; Abdul Haseeb, H.; Zhang, J.; Zhang, D.; Jeffers, D. P.; Dai, X.; Guo, W. A loop-mediated isothermal amplification (LAMP) assay for the rapid detection of toxigenic *Fusarium temperatum* in maize stalks and kernels. *Int. J. Food Microbiol.* **2019**, *291*, 72–78.

330. Beebe, D. J.; Mensing, G. A.; Walker, G. M. Physics and applications of microfluidics in biology. *Annu Rev Biomed Eng* **2002**, *4*, 261–286.

331. Gijs, M. A. M.; Lacharme, F.; Lehmann, U. Microfluidic applications of magnetic particles for biological analysis and catalysis. *Chem. Rev.* **2010**, *110*, 1518–1563.

332. Vojtísek, M.; Iles, A.; Pamme, N. Rapid, multistep on-chip DNA hybridisation in continuous flow on magnetic particles. *Biosens Bioelectron* **2010**, *25*, 2172–2176.

333. Clayton, J. Go with the microflow. *Nature Methods* **2005**, *2*, 621–627.

334. Anitoa. www.anitoa.com (Cited Feb 15, 2019).

335. Tegenfeldt, J. O.; Prinz, C.; Cao, H.; Huang, R. L.; Austin, R. H.; Chou, S. Y.; Cox, E. C.; Sturm, J. C. Micro- and nanofluidics for DNA analysis. *Anal. Bioanal. Chem.* **2004**, *378*, 1678–1692.

336. Noren, K. A.; Noren, C. J. Construction of high-complexity combinatorial phage display peptide libraries. *Methods* **2001**, *23*, 169–178.

337. New England Biolabs (NEB). Ph.D. Phage display libraries - Instruction manual. www.neb.com (Cited Jan 31, 2019).

338. New England Biolabs, www.neb.com (Cited Jan 15, 2019).

339. Wells, J. A. Hormone mimicry. *Science* **1996**, *273*, 449–450.

340. Norred, W. P.; Plattner, R. D.; Dombrink-Kurtzman, M. A.; Meredith, F. I.; Riley, R. T. Mycotoxin-induced elevation of free sphingoid bases in precision-cut rat liver slices: specificity of the response and structure–activity relationships. *Toxicol. Appl. Pharmacol.* **1997**, *147*, 63–70.

341. ChemIDplus - A ToxNet Database: Zearalenone https://chem.nlm.nih.gov/chemidplus/rn/17924-92-4 (Cited Mar 21, 2019).

342. US EPA. Estimation Program Interface (EPI Suite. Ver. 4.1 Nov 2012) https://www.epa.gov/tsca-screening-tools/epi-suitetm-estimation-program-interface (Cited Mar 21, 2019).

343. Jackson, T. M.; Ekins, R. P. Theoretical limitations on immunoassay sensitivity. *J. Immunol. Methods* **1986**, *87*, 13–20.

344. Ullman, E. F.; Milburn, G.; Jelesko, J.; Radika, K.; Pirio, M.; Kempe, T.; Skold, C. Anti-immune complex antibodies enhance affinity and specificity of primary antibodies. *Proc. Natl. Acad. Sci. USA* **1993**, *90*, 1184–1189.

345. Pulli, T.; Höyhtyä, M.; Söderlund, H.; Takkinen, K. One-step homogeneous immunoassay for small analytes. *Anal. Chem.* **2005**, *77*, 2637–2642.

346. Akter, S.; Vehniäinen, M.; Spoof, L.; Nybom, S.; Meriluoto, J.; Lamminmäki, U. Broad-spectrum noncompetitive immunocomplex immunoassay for cyanobacterial peptide hepatotoxins (microcystins and nodularins). *Anal. Chem.* **2016**, *88*, 10080–10087.

347. González-Techera, A.; Vanrell, L.; Last, J. A.; Hammock, B. D.; González-Sapienza, G. Phage anti-immune complex assay: general strategy for noncompetitive immunodetection of small molecules. *Anal. Chem.* **2007**, *79*, 7799–7806.

348. Kim, H.-J.; McCoy, M.; Gee, S. J.; González-Sapienza, G. G.; Hammock, B. D. Noncompetitive phage anti-immunocomplex real-time polymerase chain reaction for sensitive detection of small molecules. *Anal. Chem.* **2011**, *83*, 246–253.

349. Dong, J.-X.; Xu, C.; Wang, H.; Xiao, Z.-L.; Gee, S. J.; Li, Z.-F.; Wang, F.; Wu, W.-J.; Shen, Y.-D.; Yang, J.-Y.; et al. Enhanced sensitive immunoassay: noncompetitive phage anti-immune complex assay for the determination of malachite green and leucomalachite green. *J. Agric. Food Chem.* **2014**, *62*, 8752–8758.

350. Hua, X.; Zhou, L.; Feng, L.; Ding, Y.; Shi, H.; Wang, L.; Gee, S. J.; Hammock, B. D.; Wang, M. Competitive and noncompetitive phage immunoassays for the determination of benzothiostrobin. *Anal. Chim. Acta* **2015**, *890*, 150–156.

351. Kim, H.-J.; Rossotti, M. A.; Ahn, K. C.; González-Sapienza, G. G.; Gee, S. J.; Musker, R.; Hammock, B. D. Development of a noncompetitive phage anti-immunocomplex assay for brominated diphenyl ether 47. *Anal. Biochem.* **2010**, *401*, 38–46.

352. Monnet, C.; Bettsworth, F.; Stura, E. A.; Du, M.-H. L.; Ménez, R.; Derrien, L.; Zinn-Justin, S.; Gilquin, B.; Sibaï, G.; Battail-Poirot, N.; *et al*. Highly specific anti-estradiol antibodies: Structural characterisation and binding diversity. *J. Mol. Biol.* **2002**, *315*, 699–712.

353. Lamminmäki, U.; Kankare, J. A. Crystal structure of a recombinant anti-estradiol Fab fragment in complex with 17β-estradiol. *J. Biol. Chem.* **2001**, *276*, 36687–36694.

354. Rossotti, M. A.; Carlomagno, M.; González-Techera, A.; Hammock, B. D.; Last, J.; González-Sapienza, G. Phage anti-immunocomplex assay (PHAIA) for clomazone: Two-site recognition increases assay specificity and facilitates adaptation into a rapid on-site format. *Anal. Chem.* **2010**, *82,* 8838–8843.

355. Wang, J.; Liu, Z.; Li, G.; Li, J.; Kim, H.-J.; Shelver, W. L.; Li, Q. X.; Xu, T. Simultaneous development of both competitive and noncompetitive immunoassays for 2,2′,4,4′-tetrabromodiphenyl ether using phage-displayed peptides. *Anal. Bioanal. Chem.* **2013**, *405*, 9579–9583.

356. Lee, C. M. Y.; Iorno, N.; Sierro, F.; Christ, D. Selection of human antibody fragments by phage display. *Nat. Protoc.* **2007**, *2*, 3001–3008.

357. Christ, D. Selection of human antibody fragments by phage display www.sourcebioscience.com (Cited Feb 8, 2018).

358. Niccheri, F.; Real-Fernàndez, F.; Ramazzotti, M.; Lolli, F.; Rossi, G.; Rovero, P.; Degl'Innocenti, D. Human recombinant domain antibodies against multiple sclerosis antigenic peptide CSF114(Glc). *J. Molec. Recognit.* **2014**, *27*, 618–626.

359. Dass, S. A.; Norazmi, M. N.; Dominguez, A. A.; Miguel, M. E. S. G. S.; Tye, G. J. Generation of a T cell receptor (TCR)-like single domain antibody (sDAb) against a *Mycobacterium tuberculosis* (*Mtb*) heat shock protein (HSP) 16kDa antigen presented by human leukocyte antigen (HLA)-A*02. *Mol. Immunol.* **2018**, *101*, 189–196.

360. Hammers, C. M.; Stanley, J. R. Antibody phage display: technique and applications. *J. Invest. Dermatol.* **2014**, *134*, e17.

361. Bruin, R. de; Spelt, K.; Mol, J.; Koes, R.; Quattrocchio, F. Selection of high-affinity phage antibodies from phage display libraries. *Nat. Biotechnol.* **1999**, *17*, 397–399.

362. Bakhshinejad, B.; Zade, H. M.; Shekarabi, H. S. Z.; Neman, S. Phage display biopanning and isolation of target-unrelated peptides: in search of nonspecific binders hidden in a combinatorial library. *Amino Acids* **2016**, *48*, 2699–2716.

363. Vodnik, M.; Zager, U.; Strukelj, B.; Lunder, M. Phage display: selecting straws instead of a needle from a haystack. *Molecules* **2011**, *16*, 790–817.

364. Bever, C. S.; Dong, J.-X.; Vasylieva, N.; Barnych, B.; Cui, Y.; Xu, Z.-L.; Hammock, B. D.; Gee, S. J. $V_{HH}$ antibodies: emerging reagents for the analysis of environmental chemicals. *Anal. Bioanal. Chem.* **2016**, *408*, 5985–6002.

365. de Marco, A. Biotechnological applications of recombinant single-domain antibody fragments. *Microb. Cell Fact.* **2011**, *10*, 44.

366. Baneyx, F.; Mujacic, M. Recombinant protein folding and misfolding in *Escherichia coli*. *Nat. Biotechnol.* **2004**, *22*, 1399–1408.

367. Yli-Mattila, T.; Rämö, S.; Hussien, T.; Rauvola, M.; Hietaniemi, V.; Kaitaranta, J. Different grain grinding methods affect detection of *Fusarium graminearum* DNA and mycotoxins. *Phytopathol. Mediterr.* **2017**, *56*, 167-174–174.

368. EFSA Panel on Contaminants in the Food Chain (CONTAM); Knutsen, H.-K.; Alexander, J.; Barregård, L.; Bignami, M.; Brüschweiler, B.; Ceccatelli, S.; Cottrill, B.; Dinovi, M.; Edler, L.; *et al*. Risks for animal health related to the presence of fumonisins, their modified forms and hidden forms in feed. *EFSA Journal* **2018**, *16*, e05242.

369. European Commission (EC). *Guidance Document on Identification of Mycotoxins in Food and Feed (SANTE/12089/2016).* https://ec.europa.eu/food/sites/food/files/safety/docs/cs_contaminants_sampling_guid-doc-ident-mycotoxins.pdf (Cited Apr, 9, 2019).

370. Tittlemier, S. a.; Cramer, B.; Dall'Asta, C.; Iha, M. h.; Lattanzio, V. m. t.; Malone, R. j.; Maragos, C.; Solfrizzo, M.; Stranska-Zachariasova, M.; Stroka, J. Developments in mycotoxin analysis: An update for 2017–2018. *World Mycotoxin J.* **2019**, *12*, 3–29.

371. Cladière, M.; Delaporte, G.; Le Roux, E.; Camel, V. Multi-class analysis for simultaneous determination of pesticides, mycotoxins, process-induced toxicants and packaging contaminants in tea. *Food Chem.* **2018**, *242*, 113–121.

372. Rhouati, A.; Bulbul, G.; Latif, U.; Hayat, A.; Li, Z.-H.; Marty, J. L. Nano-aptasensing in mycotoxin analysis: Recent updates and progress. *Toxins* **2017**, *9*, 349.

373. Goud, K. Y.; Kailasa, S. K.; Kumar, V.; Tsang, Y. F.; Lee, S. E.; Gobi, K. V.; Kim, K.-H. Progress on nanostructured electrochemical sensors and their recognition elements for detection of mycotoxins: A review. *Biosens. Bioelectron.* **2018**, *121*, 205–222.

374. Soares, R. R. G.; Ricelli, A.; Fanelli, C.; Caputo, D.; Cesare, G. de; Chu, V.; Aires-Barros, M. R.; Conde, J. P. Advances, challenges and opportunities for point-of-need screening of mycotoxins in foods and feeds. *Analyst* **2018**, *143*, 1015–1035.

375. Neogen Food Safety. https://foodsafety.neogen.com (Cited Feb 28, 2019).

376. ROSA Lateral Flow. http://www.charm.com/products/test-and-kits/mycotoxin-tests/rosa-lateral-flow/ (Cited Feb 28, 2019).

377. Mycotoxin Test Kits. www.envirologix.com/mycotoxin-testing/mycotoxin-test-kits/ (Cited Feb 28, 2019).

378. Mycotoxin Test Kits. www.romerlabs.com/en/products/test-kits/mycotoxin-test-kits/ (Cited Feb 28, 2019).

379. Mycotoxins ELISA. http://europroxima.com/products/contaminants-and-residues/mycotoxins-elisa/ (Cited Feb 28, 2019).

# Annex I: Review articles

Anal Bioanal Chem (2016) 408:1805–1828
DOI 10.1007/s00216-015-9087-2

REVIEW

# Application of bacteriophages in sensor development

Riikka Peltomaa[1] · Irene López-Perolio[1] · Elena Benito-Peña[1] · Rodrigo Barderas[2] · María Cruz Moreno-Bondi[1]

Reproduced from: *Analytical and Bioanalytical Chemistry* **2016**, *408*, 1805–1825.


## Abstract

Bacteriophage-based bioassays are a promising alternative to traditional antibody-based immunoassays. Bacteriophages, shortened to phages, can be easily conjugated or genetically engineered. Phages are robust, ubiquitous in nature, and harmless to humans. Notably, phages do not usually require inoculation and killing of animals; and thus, the production of phages is simple and economical. In recent years, phage-based biosensors have been developed featuring excellent robustness, sensitivity, and selectivity in combination with the ease of integration into transduction devices. This review provides a critical overview of phage-based bioassays and biosensors developed in the last few years using different interrogation methods such as colorimetric, enzymatic, fluorescent, surface plasmon resonance, quartz crystal microbalance, magnetoelastic, Raman, or electrochemical techniques.

### Keywords

Bacteriophage, phage display technology, biosensing, biosensor, biorecognition element

## Introduction

Bacteriophages, as well as plants and some animal viruses, have proven to be useful tools in biotechnology, agricultural, and clinical medicine.[1,2] Although antibodies, enzymes, or nucleic acids have been traditionally used for the development of sensitive and selective analytical methods based on different transduction mechanisms, recently, bacteriophages have recently become of great interest for analytical chemistry to be used as probes for biosensing and imaging.

Bacteriophages or phages are viruses ubiquitous in nature but harmless to humans. Since in some cases phages destroy bacterial cells, they were used in the early 1900s as a medical therapy against some bacterial infections.[3,4] However, they were later displaced by antibiotics in the 1940s.[3,4] Phages are extremely robust and stable virus particles, which use bacterial cells as hosts to replicate. Phages are composed of a protein coat that encapsulates its RNA or DNA genome comprising four to hundreds of genes.[5] Proteins of the phage coat can be easily conjugated or genetically engineered to display peptides, proteins, or antibodies targeting a wide variety of molecules, including biopolymers, toxins, proteins, or even specific contaminant

Anal Bioanal Chem (2018) 410:747–771
https://doi.org/10.1007/s00216-017-0701-3

REVIEW

# Bioinspired recognition elements for mycotoxin sensors

Riikka Peltomaa[1] · Elena Benito-Peña[1] · María C. Moreno-Bondi[1]

Reproduced from: *Analytical and Bioanalytical Chemistry* 2018, *410*, 747–771.


## Abstract

Mycotoxins are low molecular weight molecules produced as secondary metabolites by filamentous fungi that can be found as natural contaminants in many foods and feeds. These toxins have been shown to have adverse effects on both human and animal health, and are the cause of significant economic losses worldwide. Sensors for mycotoxin analysis have traditionally applied elements of biological origin for the selective recognition purposes. However, since the 1970s there has been an exponential growth in the use of genetically engineered or synthetic biomimetic recognition elements that allow some of the limitations associated with the use of natural receptors for the analyses of these toxins to be circumvented. This review provides an overview on recent advances in the application of bioinspired recognition elements, including recombinant antibodies, peptides, aptamers, and molecularly imprinted polymers, to the development of sensors for mycotoxins based on different transduction elements.

## Introduction

Mycotoxins are low molecular weight (approximately 700) natural products produced as secondary metabolites by filamentous fungi mainly, although not exclusively, when they reach maturity [1]. Unlike primary metabolites, these compounds are believed to have no function in the life cycle of the producer cell.[2] They can be found as natural contaminants in many vegetal foods or feeds, including nuts (almonds and walnuts), cereals (rice, wheat, and maize), oilseeds (soybean, peanuts), fruits, dried fruits, spices, beans, forage, wines and grape juices, or in foods of animal origin, such as milk, eggs, or meat.[1, 2] Alternatively, exposure to these toxins can be produced by inhalation of dust containing mycotoxigenic fungal spores.[1] Regardless of the way they come in contact with humans, or domestic animals, including birds, they may cause lowered performance, sickness, or even death even at very low concentrations.[3, 4] Their range of actions includes cytotoxic, nephrotoxic, hepatotoxic, teratogenic, mutagenic, carcinogenic, immunosuppressive, and estrogenic effects.[1, 2] In any case, their effect on health depends on factors such as the concentration in the contaminated food and the exposure time, the synergistic effect of other mycotoxins, and environmental factors associated especially with the storage conditions of foodstuff.[1]

sensors

MDPI

*Review*

# Optical Biosensors for Label-Free Detection of Small Molecules

**Riikka Peltomaa, Bettina Glahn-Martínez, Elena Benito-Peña and María C. Moreno-Bondi ***

Departamento de Química Analítica, Facultad de Ciencias Químicas, Universidad Complutense de Madrid, E-28040 Madrid, Spain; rpeltoma@ucm.es (R.P.); ab.glahn@ucm.es (B.G.-M.); elenabp@ucm.es (E.B.-P.)
* Correspondence: mcmbondi@ucm.es; Tel.: +34-913-945-147

Reproduced from: *Sensors* **2018**, *18*, 4126


## Abstract

Label-free optical biosensors are an intriguing option for the analyses of many analytes, as they offer several advantages such as high sensitivity, direct and real-time measurement in addition to multiplexing capabilities. However, development of label-free optical biosensors for small molecules can be challenging as most of them are not naturally chromogenic or fluorescent, and in some cases, the sensor response is related to the size of the analyte. To overcome some of the limitations associated with the analysis of biologically, pharmacologically, or environmentally relevant compounds of low molecular weight, recent advances in the field have improved the detection of these analytes using outstanding methodology, instrumentation, recognition elements, or immobilization strategies. In this review, we aim to introduce some of the latest developments in the field of label-free optical biosensors with the focus on applications with novel innovations to overcome the challenges related to small molecule detection. Optical label-free methods with different transduction schemes, including evanescent wave and optical fiber sensors, surface plasmon resonance, surface-enhanced Raman spectroscopy, and interferometry, using various biorecognition elements, such as antibodies, aptamers, enzymes, and bioinspired molecularly imprinted polymers, are reviewed.

## Origin and occurrence of small molecules

Small molecules can be defined as low molecular weight organic molecules which are typically less than 1000 Da in size. This category includes a wide variety of different chemical compounds, of either natural or pharmaceutical origin, many of which are biological, pharmacologically, or environmentally relevant, which makes detection and quantification of these molecules important in many disciplines. Naturally, nearly every cell contains a collection of 100 to 200 different low molecular weight organic molecules, including the common amino acids, nucleotides, sugars, and their phosphorylated derivatives. Additionally, there exists a wide variety of small biomolecules which are specific to certain types of cells or organisms, for example, many plants contain so-called secondary metabolites which include compounds that

give plants their characteristic scents, and compounds such as morphine, nicotine, and caffeine that are valued for their physiological effects on humans.[1] On the other hand, small synthetic molecules, man-made or produced by synthetic biology,[2] have been extensively applied in a broad variety of fields including pharmaceutical, clinical, environmental, or food analysis, to name a few.

Many small molecules are well-known contaminants in food, feed, and other agricultural products. For example, mycotoxins, which are produced as secondary metabolites by filamentous fungi, include more than 500 different small molecules with different physicochemical properties and various effects ranging from cancer to acute toxicity and developmental defects. Agriculturally, the most critical mycotoxins are aflatoxins, fumonisins, trichothecenes, ochratoxins, and zearalenone family which are common contaminants in crops worldwide.[3, 4] Algal toxins, phycotoxins, and cyanotoxins, in turn, are produced by toxicogenic microalgae and cyanobacteria, and they can enter the marine food chain via phytoplankton and subsequently to humans by contaminated seafood. Several small molecule toxins originating from seafood are known to cause severe illnesses, such as paralytic shellfish poisoning, puffer fish poisoning, and neurotoxic shellfish poisoning, and it has been reported that seafood poisonings are increasing in frequency and new intoxications are emerging.[5, 6] All the aforementioned toxins are known to cause, besides a threat to human and animal health, but also substantial economic losses in aqua- and agriculture, and many of them fall under national and international regulations.

Along with the naturally produced contaminants, many synthetic low molecular weight compounds are environmentally and pharmacologically significant. For example, biological and chemical warfare agents which can be lethal even at low levels are some of the most feared weapons of mass destruction. Nerve agents, which are usually organophosphates, have rapid and severe effects on human and animal health due to their ability to block acetylcholinesterase (AChE) that is essential for the normal functioning of the nervous systems. Also, many pesticides and insecticides belong to the same chemical class of organophosphates, and they possess the same mode of action as nerve agents but are less hazardous.[7] For example, chlorpyrifos, a broad spectrum pesticide which belongs to the group of organophosphates and is used worldwide in a wide range of crops, presents a major concern for potential environmental contamination and overuse, improper storage or disposal of these molecules.[8, 9]

Pharmaceuticals, either of natural or synthetic origin, are ubiquitous substances of interest not only in clinical medicine but also in drug screening and environmental safety. Small molecules, in particular, are of great interest in pharmaceutical research, for example, because they can cross the blood-brain barrier. Detection of many drugs is diagnostically and clinically relevant but is also of interest in pharmaceutical sciences for drug screening and development of new biotherapeutics, as well as for studying the activity, kinetics, and stability of pharmaceuticals.[10] Therapeutic drug monitoring, which aims to optimize the pharmacological response of a drug while avoiding adverse effects, measures the drug concentrations in a biological matrix and with appropriate interpretation affects the prescribing procedures.[11] On the other hand, after administration, many drugs are excreted by the patients into wastewater, and in fact, rather often many pharmaceutical products and residues have been found in wastewaters, surface waters and even drinking water.[12] Pharmaceuticals vary from antibiotics to non-steroidal anti-inflammatory drugs, such as ibuprofen, or anti-cancer drugs which are of particular concern not only for human health but also for the environment due to their unique

properties in combination with poor biodegradability.[13, 14] On the other hand, many small molecules can behave as endocrine disrupting chemicals (EDCs), *i.e.*, they interfere with the body's endocrine system and produce adverse developmental, reproductive, neurological, and immune effects in both humans and wildlife.[15] According to the World Health Organization (WHO), EDCs and potential EDCs consist mainly of man-made compounds found in various materials, such as pesticides, metals, additives, or contaminants in food and personal care products, and they are a public health issue worldwide.[16]

Conventionally, many small molecules are detected by chromatographic methods which usually provide high sensitivity and specificity.[9] However, due to the high cost, bulky instrumentation, and required expertise, these methods are not suitable for every purpose; whereas, biosensors can offer a cheaper and faster alternative. Myriad of different biosensors and bioanalytical assays have been reported for the diverse group of small molecule analytes, ranging from traditional enzyme-linked immunosorbent assays (ELISAs)[17, 18] and lateral flow tests[19] to microarrays[20] and fluorescent[21] or electrochemical sensors,[22] just to mention a few examples. Some of the advantages of biosensors over classical methods for small molecule detection include real-time monitoring, high specificity, fast response times, reduced consumption of organic solvents and sample manipulation, portability, compactness, and easy operation avoiding the need of skilled personnel.[23]

## Biosensors for small molecule detection

Generally, biosensors consist of a bioreceptor, the recognition element responsible for capturing the target analyte, and a transducer, whose properties are altered upon analyte binding.[24] In the context of this review, the majority of the methods can be defined as affinity biosensors since they are based on a specific biorecognition element which is capable of binding to the analyte. Antibodies continue to be one of the most used bioreceptors due to their exceptional specificity and sensitivity, but also nucleic acids, aptamers, peptides, and molecularly imprinted polymers (MIPs) are widely used. On the other hand, catalytic biosensors are based on a bioreceptor, such as an enzyme or whole cell, which is capable of recognizing the analyte and transforming them into a product through a chemical reaction.[25] Usually, the bioreceptor is immobilized on the surface of a transducer where the biorecognition event can be monitored by different transduction schemes which measure the binding event. The binding event can produce, for example, an increase in mass, or a change in the electrical resistivity or refractive index of the surface, which can be monitored by various detection methods, such as mechanical, electrical, or optical signals.

Optical transducers are based on measuring a change in the optical properties in the presence of the analyte, such as absorption, reflectance, emission, or interferometric pattern, which can be recorded by a photodetector. Many optical biosensors require the use of labels, for example, fluorescent dyes, enzymes, or nanoparticles, which are used as a means to measure the biorecognition event. Although such label-based methods are widely used and usually very sensitive, they inevitably require the involvement of a label and a chemical conjugation step to link the label to the biorecognition event. The necessity of labeling makes these methods limited by the success and efficiency of the conjugation step, which furthermore in some cases might even alter the biorecognition event. Thus, label-free biosensors can offer some significant advantages and better accuracy over label-based methods since label-free

biosensors do not require the use of a label to monitor the binding event. Advantages of label-free methods include simplicity and speed of the measurement procedure; these methods enable real-time monitoring of the binding reaction, thus giving access to the kinetic and thermodynamic parameters of the molecular recognition process.[26, 27]

Development of biosensors for small molecule detection represents particular challenges which might not be an issue with larger analytes. Firstly, small molecules are challenging targets for many recognition elements, in particular for antibodies since haptens alone fail to stimulate the immune system responsible for antibody production.[28] Consequently, hapten-specific antibodies are usually selected using the hapten conjugated to a larger carrier molecule, which at times results in antibodies specific for the conjugate rather than for the free hapten. Furthermore, small molecules which are components of physiological pathways, such as amino acid, are not immunogenic. Recombinant antibodies have been presented as an interesting alternative for monoclonal and polyclonal antibodies, and several recombinant antibody-based immunoassays and sensors have been reported during the last two decades.[29, 30] Potentially, recombinant antibodies can overcome some of the limitations of their conventional counterparts; they can be selected from naïve repertoires avoiding animal immunization and modified by genetic engineering to improve their binding or include reactive groups or tags intended for conjugation or protein purification. Because of their small size, recombinant antibody fragments can contribute to decreased non-specific binding and lower steric hindrance compared to the intact antibody. However, despite some interesting properties, recombinant antibodies rarely show better or even similar affinities than conventional antibodies,[31] which limits their use for the detection of small molecules which are present at low concentrations and thus require recognition elements with high affinity.

Alternatively, biosensors can be based on several other bioreceptors or bioinspired recognition elements. Aptamers are short synthetic DNA or RNA molecules which form a three-dimensional structure which allows them to bind target molecules with high specificity and sensitivity.[32] Aptamers are readily synthesized and modified for immobilization or labeling purposes, and owing to their small size, high chemical and thermal stability, and low price, aptamers can be an intriguing alternative for antibodies. Nonetheless, once again, it can be particularly challenging to find good aptamer binders for analytes with small size.[33] Thus, aptamer-based label-free methods often rely on different signal amplification methods to compensate for the shortcomings of the recognition element.[33] Enzymes which were among the first recognition elements used in biosensors are a rather obvious choice as a recognition element for targets which are known enzyme inhibitors, for example, organophosphates;[9,34] however, their use can be limited by poor stability or loss of activity as a result of the immobilization. Molecularly imprinted polymers (MIPs), also known as plastic antibodies, are artificial materials, and although strictly speaking, they do not match the description of a biosensor which by definition relies on biological recognition element, MIPs are an exciting option for biosensor development due to their high physical and chemical stability, robustness, low cost, and ease of preparation.[35] Molecular imprinting allows the design and preparation of custom-made polymeric materials that contain binding sites with selective affinity to the analyte, similar to some biological receptors, such as antibodies, enzymes, or other protein receptors. For MIP synthesis, the selected print molecule, which may be the analyte or a substitute molecule, interacts via covalent or non-covalent bonds with functional monomers that polymerize in the presence of a crosslinker. Once the template molecule is removed, the

resulting three-dimensional supramolecular structure contains specific recognition sites that are complementary to the template molecule or/and target molecule.

In their simplest format, label-free biosensors are based on direct detection of the target which binds to the recognition element immobilized on the sensor surface (**Figure 1A**). Compared to small molecules, binding of large molecules usually produces a larger response which is often roughly in proportion to the mass of the molecule. Thus, for direct detection, the requirement is that the analyte of interest produces a sufficient response in a required concentration range, which in practice means that the molecular weight of the target must be large enough to generate a measurable signal change. Generally speaking, the sandwich assay format can be used to improve the response and the assay sensitivity; however, small molecules which are composed of only one epitope are not suitable for this approach.[36] Alternatively, small molecules can be measured indirectly using either a competitive or an inhibition detection format (**Figures 1B–C**).

In the competitive format, the sensing surface is coated with the recognition element while the analyte and its conjugated analog compete for a limited number of binding sites on the surface. In the inhibition detection format, reversely, the analyte-conjugate is immobilized on the surface, and the recognition element is added together with the analyte in solution.[25] Regardless of the assay format, or the recognition element of choice, the immobilization step to the sensor surface is critically important to all biosensor configurations. The functionalized biosensor surface should provide high specific binding of the target analyte while maintaining low non-specific binding or cross-reactivity towards interfering molecules present in the same samples.

The repertoire of methods based on optical label-free detection is vast and impressive. In this review, we aim to revise the latest developments in the field with particular attention to solutions that improve the methods for small molecule detection, or present innovative alternatives to overcome some of the limitations mentioned above. Significant research efforts in the field of evanescent wave and fiber optic biosensors, surface plasmon resonance (SPR) and localized surface plasmon resonance (LSPR) biosensors, as well as surface-enhanced Raman spectroscopy (SERS), and interferometry are described.

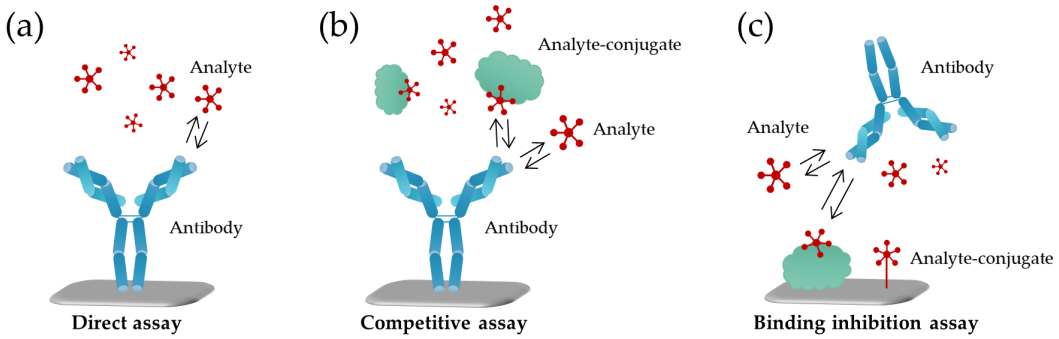


**Figure 1**. Schematic presentation of assay formats generally used for small-molecule detection. (A) In a direct assay, target analyte binds to the recognition element, *e.g.*, the antibody which is immobilized on the sensor surface; (B) In a competitive assay, the analyte competes with its conjugate for the binding to the immobilized recognition element; (C) In a binding inhibition assay, similarly the analyte and analyte-conjugate compete for the binding, but the analyte-conjugate is the one immobilized on the sensor surface either directly via a linker or as a protein-conjugate. Also, other recognition elements besides antibodies are applied to biosensor development using the same assay formats.

## Fiber optic and evanescent wave biosensors

Evanescent wave systems have found broad applicability and flexibility for biosensor design as they confine the interactions between light input/output and fluidics inflow/outflow to a single interface.[37] Evanescent wave biosensors can be based on the use of cylindrical or planar waveguides. Several fiber optic configurations, including tapered optical fibers, photonic crystal fibers, hollow-core fibers, or long-period fiber gratings have been proposed to improve the interaction between the evanescent field and the sensing layer. In most cases, the cladding of the fiber is modified by a sensing layer and any change in the optical or structural properties of the material, such as the refractive index, thickness or absorption will change the transmission properties of the fiber.[38] In absorption sensors, light absorption of the evanescent wave by a sensing layer will result in a decrease of the guided light in the fiber core. In luminescent sensors, the evanescent light will excite the luminescent molecules located near the waveguide surface, and the emitted light will be captured and guided by the waveguide. Therefore, the background signal from the bulk sample can be minimized, and these methods are usually very sensitive and selective for the detection of small molecules in comparison with label-free techniques.[37, 39, 40] However, only a few molecules can be detected directly using this approach without the use of labels.

Optical waveguide light mode spectroscopy (OWLS) is an optosensing technique that applies the evanescent field for the in situ and label-free study of surface processes at the molecular level.[41] In this approach, polarized laser light is diffracted by a grating and incoupled into a thin waveguide. The incoupling resonance takes place at precise angles, depending on the characteristic optical parameters of the sensor chips and the refractive index of the external medium. Photodiodes detect the intensity of the incoupled light. The effective refractive index is determined from the resonance incoupling angle which is detected with high accuracy and allows the evaluation of the layer thickness and coverage (or mass) of the adsorbed or bound material with excellent sensitivity. OWLS has been applied for example to the analysis of mycotoxins ochratoxin A (OTA) and aflatoxin $B_1$ ($AFB_1$) in grain samples using direct and indirect

assay formats. Higher sensitivities were obtained using the inhibition assay with an immobilized antigen, and the response range was between 0.5 and 10 ng/mL for both mycotoxins. The same conclusion was obtained for the analysis of trifluralin and zearalenone, two environmental endocrine disrupters, vitellogenin, an endocrine marker[42] in environmental samples and deoxynivalenol (DON), a mycotoxin in wheat.[43] The competitive immunosensor was shown to be more sensitive for the target compounds than the noncompetitive ones. This behavior can be explained considering that the OWLS signal is sensitive to relative masses bound to the waveguide surface. Binding of an antibody to an immobilized antigen conjugate produces a higher signal than binding of small analytes, as in the case of the mycotoxins or the herbicide, to an immobilized antibody. The same group applied the OWLS immunosensor to the analysis of $AFB_1$ in 60 spice paprika samples from different countries, finding that 16 samples were contaminated with $AFB_1$, and 9 samples contained $AFB_1$ above the official maximum residue level (5 µg/kg) set by the European Commission. Excellent correlation was observed with the results obtained by ELISA and high-performance liquid chromatography (HPLC) with fluorescent detection.[44]

In a completely different approach, the Haupt group[45] reported the development of disposable evanescent wave fiber optic sensors by coating 4-cm long injection-molded tapered polystyrene waveguides with 2,4-dichlorophenoxyacetic acid (2,4-D) (**Figure 2**) or citrinin selective MIPs containing a fluorescent signaling monomer, *N*-(2-(6-4-methylpiperazin-1-yl)-1,3-dioxo-1*H*-benzo[*de*]isoquinolin-2(3*H*)-yl-ethyl)acrylamide, which can be excited by the evanescent wave. Polymer coating on the cylindrical waveguide was carried out either by in situ photopolymerization of the MIP on the fiber using the evanescent wave, or by dip coating with the MIP particles. An increase in fluorescence intensity proportional to the analyte concentration was observed in the presence of the target compound with a limit of quantification of 1 nM for 2,4-D and good selectivity to the herbicide. The biomimetic sensors obtained by in situ polymerization of the MIP were less sensitive than those obtained using the MIP particles.

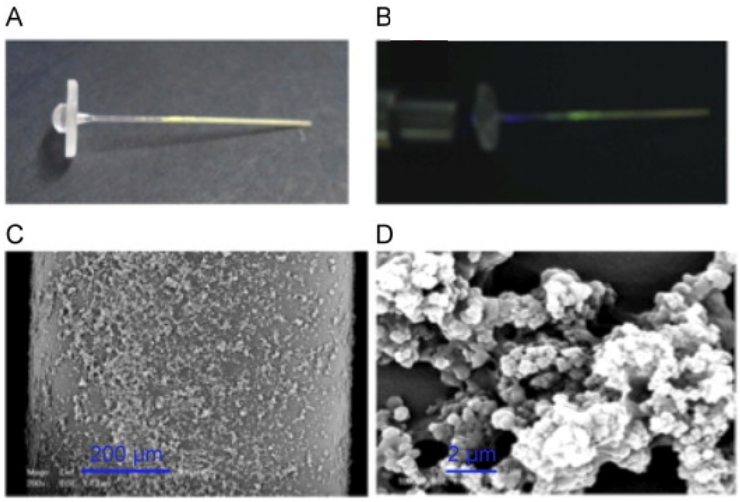


**Figure 2.** (A) Photograph of the polystyrene evanescent wave fiber optic waveguide coated with fluorescent 2,4-D MIP particles using polyvinyl alcohol as glue. (B) Injection of the light with a fiber optic bundle and collection through the lens ($\lambda_{exc}$ = 410 nm; $\lambda_{em}$ = 515 nm). (C–D) SEM micrographs of the surface of the 2,4-D-MIP-coated optical fiber (reprinted from [46] with permission from Elsevier).

Barrios *et al.*[47] demonstrated the applicability of aluminum nanohole arrays (NHAs), deposited onto a microscope coverslip, for sensing applications. The pre-polymerization mixture was deposited onto the NHAs, and the light was efficiently confined inside favoring the photopolymerization of submicron-sized MIP patterns selective to rhodamine 123 (R123), as a model template molecule. The final size could be tuned by changing the dose of green radiation applied during the polymerization step. Evaluation of the selective recognition of R123 by the imprinted polymer was carried out by fluorescence lifetime imaging microscopy with single photon timing measurements. A similar approach has been applied to the development of biosensors for the detection of biotin as a model analyte, in combination with glass, polycarbonate compact discs (PC CDs) or transferable aluminum NHAs onto flexible pressure-sensitive adhesive tapes using label-free SPR measurements.[47, 48]

Margheri *et al.*[49] described the detection of heavy metal ions by self-assembling a monolayer of a fluorescent indicator which was quenched in the presence of Hg(II) ions on the external surface of an optical fiber waveguide formed by a metal (Au)-dielectric (SiO2) bilayer known as metal–clad optical waveguide (MCOW). The thin Au metal layer (~20 nm) guided the zero-order TE and TM modes with the lowest possible losses, and the thickness of the dielectric layer was selected to propagate the same modes. On the other hand, the fluorescent layer and the metal were separated by the SiO2 layer, thus avoiding the metal-induced fluorescence quenching. The authors estimated a limit of detection of 150 nM and response time of approximately 2 min which were in the same order of magnitude as the best ones reported in the literature for this metal ion. Further improvements were proposed by the substitution of Au with an Ag layer and increasing the number of sensing sites by enriching a hydrogel volumetric matrix.

Genetically modified organisms have also been coupled to optical fibers for the development of label-free biosensors for the sensitive and selective detection of a wide range of compounds of interest in different fields such as food analysis, environmental monitoring, and clinical diagnostics, among others.[50–54] Sensor performance depends on the introduction of a reporter gene into the host cell, whose expression is modulated by the interaction of the analyte with the molecular recognition element, and promoter sequences.[55] Widely used reporter genes include *lux* (bacterial luciferase), *Luc* (firefly luciferase), *GFP* (green fluorescent protein), and *lacZ* (β-galactosidase). The activity of the reporter protein can be monitored upon the addition of the corresponding (*e.g.*, bioluminescent, fluorescent) substrate or directly as in the case of the GFP.[56]

In a different approach, non-genetically modified microorganisms, such as green microalgae based on mutant algae clones which are the result of evolutionary strategies, have also been applied to the development of biosensors for the analysis of pesticides or heavy metals. Two different approaches have been used for this purpose. The first was based on monitoring the variation in the algal chlorophyll fluorescence at 682 nm, as a result of the inhibition of the algal photosystem II by the pollutant.[57, 58] Alternatively, herbicide concentration was evaluated by monitoring the inhibition of the photosynthetic $O_2$ production by the target compound using an oxygen optode.[59]

In addition, several fiber optic sensors are based on SPR which requires the use of a metal-dielectric interface. Different optical structures have been reported for SPR-based fiber optic biosensors, including D-shaped, de-cladded, end mirror or tapered fiber structures.[38] Some

relevant examples of fiber optic SPR sensors and the basis of SPR sensing are described in the following section.

## Surface plasmon resonance

Surface plasmon resonance (SPR) is one of the most advanced and most used label-free detection techniques because of the high sensitivity and versatility of the method, as well as the possibility for a real-time read-out and direct measurement of binding kinetics. As a result of tremendous research on SPR during the last decades and the availability of advanced commercial instruments, SPR-based biosensors can be considered as a landmark label-free biosensing platform for characterizing and quantifying biomolecular interactions.[36, 60] SPR sensors measure changes in the refractive index which occur at the surface of a metal film where electromagnetic waves, called surface plasmons, propagate upon illumination. Since surface plasmons are highly dependent on the geometry of the plasmonic structure and the environmental parameters, changes such as biomolecule binding to the surface will change the plasmon mode.[61] Prism couplers are most commonly used, but alternatively, optical excitation can be based on waveguide couplers, diffraction gratings, or integrated optical fibers.[62] Prism-based coupling requires bulky instrumentation and thus is not compatible with portable platforms or point-of-care devices. Instead, optical fibers are low cost and ideal for miniaturization, which has made them as the subject of intense research.[63, 64] A major contribution to SPR-based biosensors is the use of metal nanostructures which are smaller than the incident wavelength and when interacting with light waves generate a resonance phenomenon known as localized surface plasmon resonance (LSPR). One of the most interesting features of LSPR is the possibility of tuning the SPR intensity by varying the size, shape, composition, and environment of the nanostructures which can be for example metal nanoparticles, carbon nanotubes or nanowires.[62]

Direct detection of small molecules by SPR is challenging due to their small size and subsequently the small change in the refractive index produced by analyte binding, which generally leads to measurements with too low signal-to-noise ratios.[65] Nevertheless, direct detection is more straightforward and has several advantages over indirect methods, such as shorter assay times, lower sample volumes, no need for the conjugated analyte competitor, and the possibility for direct kinetic measurements.[66] Advances in SPR instrumentation, such as detection systems with lower noise and improved fluidics as well as advanced immobilization methods and new sensor chips, have simultaneously decreased the total noise and improved the signal intensities and reproducibility.[65] The most advanced commercial SPR instruments, such as Biacore, claim the detection of analytes down to 100 Da[67] and although the early immunosensors for small molecule detection relied almost inevitably on the competitive assay formats, during the last decade several examples of direct small molecule detection have been reported.

The performance of SPR sensors is highly dependent on the chemical interface and bio-functionalization, as well as the optical, electrical and structural features of the instrument.[62] The choice of a recognition element indisputably has a direct effect on the assay sensitivity and specificity, but moreover, the immobilization of the interacting molecule, either the recognition element or the analyte-conjugate, is crucial. A robust biomolecule coating on the sensor surface should be stable and, in many cases, preferably regenerable. It is critical to ensure that the

surface coating and the immobilization do not degrade the biological activity of the recognition element or result in steric hindrance, and a sufficient number of molecules must be immobilized to ensure reliable signals simultaneously minimizing the non-specific binding to the surface.[68] The following sections discuss SPR-based methods reported for small molecule detection using different recognition elements, and **Table 1** summarizes some of the most interesting approaches from recent years.

## Antibody-based SPR sensors

Owing to their unique properties and an immense variety of possible specificities antibodies continue to be the most used recognition element in SPR sensors, although alternative options for small molecule detection, mostly aptamers or molecularly imprinted polymers (MIPs), have also been reported.[36] Despite the extensive use of both SPR and antibodies, only a few examples of direct SPR-based immunosensors have been described, and direct SPR methods for small molecule detection still might suffer from poor sensitivity. For example, Tomassetti *et al*.[69] compared a direct-flow SPR immunosensor for ampicillin detection with a competitive amperometric immunosensor which showed better sensitivity and wider dynamic range than direct detection by SPR. SPR sensor was more selective, as well as faster and simpler in the analysis, compared to the amperometric method in the concentration range from $10^{-6}$ M to $10^{-2}$ M. In comparison, an LSPR sensor composed of core-shell nanosensors for the detection of atrazine was prepared using polystyrene nanospheres, as the "core" of the nanochip, and a gold layer which was thermally deposited onto the core as the "shell". After studying the response of three types of nanosensors with different Au film and shell dimensions, the authors biofunctionalized one of the nanosensors with an atrazine specific antibody and proved direct detection of atrazine at 10 ng/mL.[70]

The importance of the recognition element immobilization procedure has been established in several applications. For example, direct detection of tetrodotoxin was performed with Biacore T200 instrument using CM5 and CM7 sensor chips for antibody immobilization. Introduction of higher conjugation substrate, CM7, provided significantly greater response compared to CM5 substrate with a lower number of antibody binding sites, although analysis with CM5 gave better sensitivity than CM7 ($EC_{50}$-values 2.98 ng/mL and 12.45 ng/mL, respectively) (**Figure 3A**). Compared with the inhibition assay, the direct detection method provided not only faster and simpler analysis, but also four times the lower limit of detection (LOD 0.091 ng/mL for direct assay on CM5 chip, LOD 0.38 ng/ml for inhibition assay).[71] In a different approach, an SPR immunosensor for ochratoxin A (OTA) was constructed on a nano-size gold hollow ball with a dendritic surface that was used to immobilize anti-OTA monoclonal antibody. OTA detection was reported in the range of 0.05–7.5 ng/mL with a detection limit of 0.01 ng/mL. According to the authors, the three-dimensional network of the gold hallow microspheres provided more space for the protein adsorption and thus improved the sensitivity compared to the SPR sensor with gold nanoparticles.[72] Direct SPR sensor for benzoylecgonine (BZE), a major cocaine metabolite, consisted of high-affinity monoclonal antibody immobilized with high density to a sensor chip which contained a polycarboxylated hydrogel as a three-dimensional immobilization matrix. Detection of BZE in oral fluid could be performed within 180 s with BZE concentrations as low as 4 µg/L in filtered oral fluid-buffer (1:4) samples.[66]

Nonetheless, the majority of antibody-based SPR sensors are based on an inhibition assay format where a target-conjugate is immobilized onto the sensor surface. Although direct assays can be considered more ideal than the competitive inhibition assays, it should be noted that the latter can avoid some of the drawbacks related to antibody immobilization, such as potential changes in the native structure, improper orientation of the immobilized antibody, or a deteriorated affinity, all of which have direct effects on the assay performance. Therefore, immobilization of the target, either directly or conjugated to a carrier molecule, might provide a more robust sensor surface.[73] A variety of different surfaces chemistries have been used with different binding site densities, but probably the most used and the most versatile surface is the Biacore CM5 sensor chip which consists of carboxymethylated dextran covalently attached to a gold surface and can be used to covalently couple molecules *via* amine, thiol, aldehyde, or carboxyl groups.[67] During the last 10 years, a wide range of SPR immunosensors for small molecules have been reported using the inhibition assay, and several of them have presented sub-regulatory detection limits including validation with sample analysis. A specially designed multi-microchannel SPR sensor for the detection of herbicide 2,4-D was based on an array of thin Au-films, and a multi-microchannel plate with a flow-cell and the protein-conjugate was immobilized merely by physical adsorption onto the sensing surface.[74] Majority of reported methods are based on protein-conjugated target which is covalently attached to the sensor surface. For example, contamination of mycotoxins nivalenol (NIV) and deoxynivalenol (DON) in wheat was tested using a sensor chip with DON–bovine serum albumin (BSA)-conjugate immobilized using a conventional amine coupling method. The competitive inhibition assay with a monoclonal antibody that cross-reacts with NIV and DON provided $IC_{50}$ values of 28.8 and 14.9 ng/mL for NIV and DON, respectively.[75] Likewise, SPR immunosensors with BSA-conjugated domoic acid (DA) and cortisol were used to analyze DA contamination in clam extracts[76] or cortisol levels in saliva,[77] respectively, whereas others have reported sensors with ovalbumin (OVA)-conjugated enrofloxacin (ENRO)[78] as well as patulin[79] and benzylpenicillin[80] conjugated to glutamine-binding protein for target immobilization. Alternatively, protein-conjugated small molecules have been immobilized on a sensor surface using self-assembled monolayers (SAMs) to obtain good stability high degree of reproducibility. SPR immunosensors using SAMs or mixed SAMs to immobilized protein-conjugated targets have been reported at least for the detection of atrazine,[81] ractopamine[82] and antibiotics amikacin[73] and fluoroquinolones.[83] Robustness of the SAMs has been proven as the surface could be reused at least 40 times over span of three days[83] or even up to 150 times.[82] In the work of Herranz *et al*.,[84] several assay formats with different immobilization strategies were evaluated for the detection of microcystin-LR (MCLR). Compared to the protein-conjugated or biotinylated target, direct immobilization of MCLR onto an amine-SAM-functionalized chip was concluded to provide the best performance. Alternatively, detection of saxitoxin[85, 86] and HT-2 toxin[87] has been accomplished by directly immobilizing the target to the biosensor chip *via* amino-coupling. Recently, a self-tuning interfacial architecture for estradiol detection was described with a decreased detection limit and widened dynamic range.[46] The novel immobilization strategy was based on a "charged" surface where a flexible and structurally variable architecture was created by a variety of weak electrostatic interactions utilizing the electrostatic levitation phenomenon (**Figure 3B**).

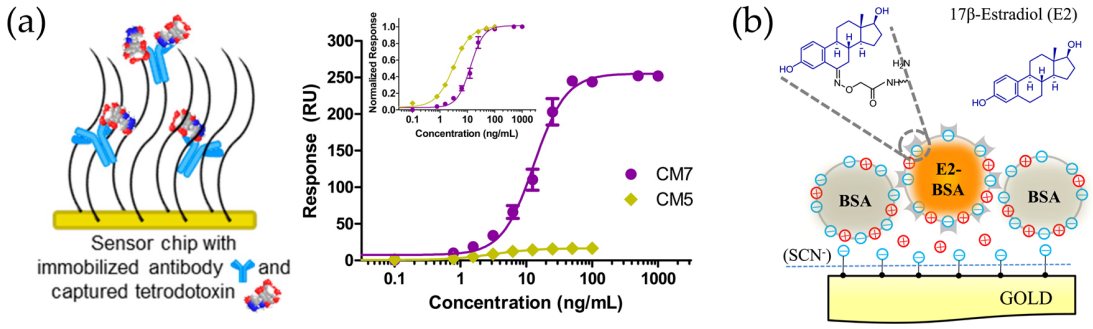


**Figure 3**. (A) For tetrodotoxin detection, the antibody was covalently immobilized onto carboxymethylated (CM) dextran surface (left). A comparison of high-density CM7 and low-density CM5 surfaces for antibody immobilization (right). (B) Schematic representation of the immobilization of estradiol(E2)-BSA conjugate within the BSA matrix utilizing the electrostatic levitation phenomenon for forming a "fluid"-like interfacial membrane with rotation freedom and in-plane mobility of membrane components ((A), reprinted from ref. [71], copyright (2014) American Chemical Society; (B), reprinted from ref. [46] with permission from Elsevier).

Also, a few SPR biosensors using recombinant antibodies have been reported for small molecules, mainly mycotoxins and other biotoxins with sub-regulatory detection limits, but most SPR-based methods in the literature in combination with recombinant antibodies consists of examples where SPR is used as a method to characterize novel antibodies and determine the binding affinities.[88–95] For these applications, the target is immobilized directly,[88] *via* a biotin-linker,[89] or as a protein-conjugate[90–95] to the sensor chip. It has been noted that the structural format of recombinant antibody fragments, as well as chip functionalization, strongly affects the SPR response. Townsend *et al.*[96] concluded that direct coating and the Fab antibody format would be optimal since multimerization of scFvs might result in incomparable SPR sensorgrams. Although recombinant antibodies still often suffer from lower affinity than monoclonal antibodies, which consequently limits the sensitivity levels that can be reached, they offer some intriguing characteristics, including their small size which could provide immobilization at high density, and the possibility to genetically engineer specific tags or reactive groups to facilitate the immobilization.[31, 97, 98]

Finally, numerous examples have demonstrated that nanoparticles can be used to enhance SPR signals and overcome the challenges related to the small molecule detection.[99–104] However, it could be argued that after incorporating a nanoparticle label to the sensor configuration, such a method is no longer genuinely label-free. Also, advanced SPR instrumentation based on microfluidic channels[105–107] or imaging surface plasmon resonance[108–110] have enabled multiplex detection of several targets simultaneously in the inhibition assay format.

## SPR sensors based on aptamers

Aptamers are rarely able to compete with monoclonal antibodies when it comes to affinity, but they show several advantages such as relatively simple synthesis without significant batch differences. Moreover, chemically synthesized aptamers are easily modified or extended from their 3' or 5' end, which allows designing particular immobilization strategies which do not have a negative influence on their recognition activity. Direct binding of thiolated aptamers to the gold

surface is a widely used method, although many other alternatives have been reported as well. As with other recognition elements, the immobilization manner of aptamers is crucial as in some cases immobilization at one end of the aptamer has been seen to abolish the binding.[111]

First aptamer-based SPR sensors were based on the competitive assay-format. For example, after an unsuccessful first trial to directly detect the small molecule target binding with an immobilized aptamer, neomycin B was covalently immobilized onto the sensor surface, and detection of free neomycin B was achieved in the competitive format with a range of quantification between 10 nM and 100 μM.[112] On the other hand, competitive replacement assays which take advantage of aptamers and partially complementary single-stranded DNA (ssDNA) have been reported as an alternative to improve the detection of small molecules. Hybridization of gold nanoparticle (AuNP)-tagged secondary ssDNA with the immobilized aptamer results in a substantial change in SPR signal, whereas upon target binding the secondary ssDNA is not able to hybridize with the target-bound aptamer causing a remarkable decrease in the signal. In this manner, adenosine was detected over the range of $10^{-9}$ to $10^{-6}$ M using an aptamer immobilized on SPR gold film and complementary ssDNA with AuNPs.[113] Alternatively, a double-AuNP system comprising of ATP (adenosine triphosphate) aptamer functionalized 39-nm-AuNPs array chip and a partially complementary ssDNA which was immobilized on 13-nm-AuNPs. A wall-less LSPR array chip was fabricated on a hydrophilic-hydrophobic patterned glass slide, which enabled high throughput detection and the chip fabrication and sample processing could be simplified using the wall-less configuration (**Figure 4A**). The detection limit was reported down to 0.01 μM ATP which was a 5-order-of-magnitude improvement over the non-enhanced setup.[114]

Interestingly, the versatility of aptamers as recognition elements has been elaborated by use of two anti-cocaine aptamer subunits in an aptasensor where one subunit was assembled on gold surface and the second subunit was labeled with AuNPs. In the presence of cocaine, binding of both aptamer subunits resulted in electronic coupling between the localized plasmon of the AuNPs and the surface plasmon wave of the gold surface and a significant shift in the SPR spectrum was observed. The dissociation constant of the aptamer complex was determined to be $(8.9 \pm 0.4) \times 10^{-6}$ M and a detection limit of $10^{-6}$ M for cocaine was reported.[115]

Later, advances in the sensor technology and alternative immobilization methods have also enabled the direct detection of small molecules. For example, Zhu *et al.*[116] reported Biacore aptasensor for the detection of OTA using streptavidin as a cross-linker to immobilize a biotinylated aptamer. Linear detection range from 0.094 to 10 ng/mL of OTA with a lower detection limit of 0.005 ng/mL was reported, and after liquid-liquid sample extraction spiked wine and peanut oil samples were analyzed with recoveries from 86.9% to 116.5%. An alternative immobilization strategy on the Biacore sensor was reported by Chang *et al.*[117] who characterized the affinity and kinetics of a diverse panel of 12 small molecule-binding RNA and DNA aptamers. Instead of direct aptamer immobilization or streptavidin linker, a poly(T) DNA linker was covalently immobilized to a Biacore sensor chip, and the aptamer was captured through hybridization of a poly(A) tail, which enabled simple regeneration of the surface and testing different aptamers or targets on the same chip.

Recently, direct detection of tetracycline was reported with a Biacore sensor where the aptamer was immobilized on the top of a tetrahedron nanostructure to provide better accessibility of the target. The sensor was based on the conformational reorganization of the aptamer which formed G-quadruplex structure upon target binding. The aptasensor was

validated in a real application for tetracycline screening in multiple honey samples, and the detection limit was calculated to be 0.0069 µg/kg, 10-fold lower than that of the aptasensor with the single-stranded aptamer.[68] Also, an LSPR-based aptasensor based on the G-quadruplex structure and gold nanorods (GNRs) enabled detection of OTA in nM-range.[118] Later, an enhancement in a similar approach was achieved using G-quadruplex (GQx) binders to increase the signal change upon target binding (**Figure 4B**). Addition of berberine as GQx binder improved the detection limits for OTA, ATP, aflatoxin $B_1$ ($AFB_1$), and potassium ions 1000-fold.[119] Recently, the same group reported another aptasensor for OTA detection based on an optical fiber coated with aptamer-modified GNRs which enabled in situ detection of OTA by simply dipping the fiber into a solution. Linear range was determined from 10 pM to 100 nM with a detection limit of 12.0 pM, and OTA-spiked samples were analyzed from 50% grape juice with recoveries from 85.5% to 116.9% (1–100 nM OTA).[120]

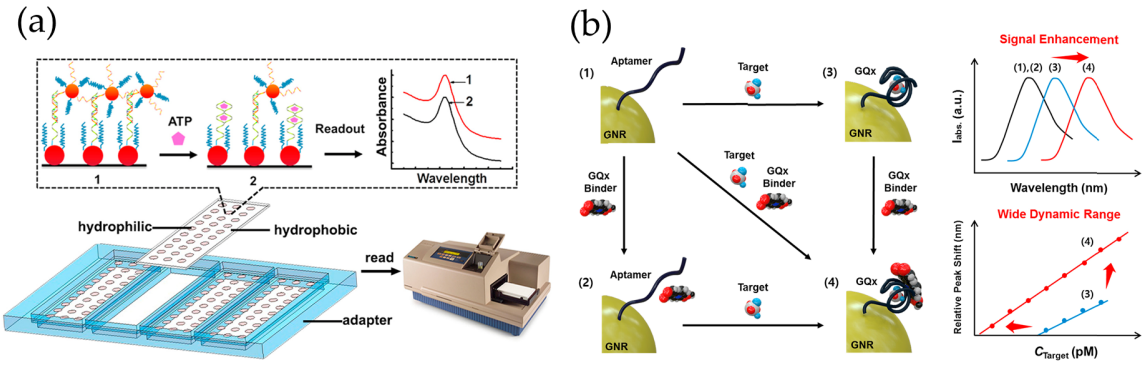


**Figure 4**. (A) Wall-less LSPR array chip for detection of adenosine triphosphate (ATP) using a normal microplate reader. Plasmonic nanoparticles (NPs) are immobilized on hydrophilic–hydrophobic patterned glass slide and a double-gold NPs system constitute a competitive replacement assay for signal amplification. (B) LSPR sensor for small molecule detection based on (1) aptamer-modified gold nanorods (GNRs), (2) addition of the G-quadruplex (GQx) binder, (3) addition of a target that induces GQx structure, and (4) addition of the target and GQx binder; interaction between the GQx binder and GQx occurs. GQx binder provides signal enhancement and enables a broad dynamic range. (A, reprinted from ref. [114]; B, reprinted from ref. [119], both with permission from Elsevier).

Examples of instrumental advances in aptasensors include the development of a lab-made plasmonic sensing platform based on sinusoidal gratings and the azimuthally-controlled SPR under phase interrogation which leads to enhanced refractive index compared to the classic grating-based SPR setup. After optimization of the aptamer immobilization strategy, the biosensor was demonstrated to detect down to 0.2 ng/mL of OTA with a detection limit of 0.005 ng/mL.[121] In a different approach, a portable, palm-sized transmission-localized surface plasmon resonance setup with aptamer-functionalized gold nanoislands deposited on a glass slide was reported for the detection of tobramycin, measuring concentrations down to 0.5 µM in buffer and down to 10 µM in filtered undiluted blood serum with a theoretical detection limit of 3.4 µM.[122]

## SPR sensors using molecularly imprinted polymers

In recent years, MIPs have been rather widely used in SPR sensors for small molecule detection.[32] The interaction of the target molecule with the active sites of the polymer causes a change in the dielectric nature of the sensing layer which can be detected by SPR. Compared to antibodies, MIPs can provide a more robust surface as they can withstand better harsh regeneration conditions and are less susceptible to lose their binding capability.[123] Several methods to prepare a selective MIP layer on SPR sensor chips have been described, and they are either based on physical deposition or covalent coupling of the MIP film or particles onto the chip or, alternatively, involve *in situ* polymerization directly onto the sensor surface. For example, the spin coating has been used to create the recognition layer for SPR sensors with imprinted nanofilms or -gels for the detection amoxicillin,[124] citrinin,[125] and pesticides.[126] A recent report showed that an enhancement in the SPR signals was achieved using a nano-hybrid film for the detection of ractopamine.[127] In this work, MIP particles were synthesized by precipitation polymerization and coated with AuNPs and reduced graphene oxide to improve the SPR signals. The novel SPR sensor with the nano-hybrid film for ractopamine detection had a wide linear range from 20 to 1000 ng/mL with a detection limit of 5 ng/mL. Another recent work reported the use of atrazine imprinted nanoparticles which were deposited and dried onto the SPR chip. Attachment of the nanoparticles was confirmed by scanning electron microscopy, and the SPR measurements showed the linear response from 0.5 ng/mL to 15 ng/mL with a detection limit of 0.7134 ng/mL of atrazine.[128]

Alternatively, imprinting can be performed directly *in situ* on the sensor surface thus avoiding a separate MIP immobilization, which is the approach that the majority of reported SPR sensors for small molecules rely on. Various methods for creating imprinted films have been reported, including thermal-initiated polymerization, photo-initiated polymerization, and electrical polymerization. For example, molecularly imprinted polypyrrole films were prepared *via* electropolymerization onto bare gold chips for the detection of zearalenone[129] and DON.[95] Likewise, π-conjugated MIP with nanopatterns for T-2 toxin was prepared on SPR chip by *in situ* electropolymerizations. Kinetic measurements showed excellent affinity with a $K_D$-value of 12.7 fM, and the sensor had a linear response for T-2 toxin from 2.1 fM to 33.6 fM with a detection limit of 0.1 fM (0.05 pg/mL). Interference was studied with high concentrations of other toxic small molecules which showed less than 10% selectivity efficiencies; however, the response using other toxins with similar structures was not tested.[130] By surface-initiated polymerization, where the initiator is immobilized to the sensor surface prior to the

polymerization, ultrathin MIP films have been prepared, for example, for DA,[123] malachite green,[131] acephate,[132] ametryn,[133] and profenofos[134] detection showing the potential of MIPs for selective and sensitive analysis of small molecules. Another SPR sensor based on nanoscale MIP film as recognition element was developed for selective detection of the antibiotic ciprofloxacin (CIP). The MIP film was prepared by *in situ* photo-initiated polymerization method, and the sensor had good linear relation with CIP concentration over the range $10^{-11}$–$10^{-7}$ M and the detection limit was determined to be ~0.08 μg/L. Furthermore, using the MIP-modified SPR imaging (SPRi) chip with separate sensing spots, the SPR response for two different types of antibiotics (CIP and azithromycin) could be measured simultaneously.[135]

MIPs are also able to provide a three-dimensional binding matrix which can improve the sensitivity due to higher binding capacity. For this purpose, a water-compatible macroporous molecularly imprinted film (MIF) was synthesized by photo copolymerization of monomers, cross-linker and polystyrene nanoparticles in the presence of testosterone as the template molecule.[136] After removal of the template and the polystyrene nanoparticles, a macroporous MIF was formed. By in situ polymerization, the thickness of the film could be observed as the shift in the SPR resonant angle and the UV radiation was stopped when, approximately, 177 nm thick film was observed, a thickness comparable to the penetration depth of SPR. SPR-based MIF sensor was applied to testosterone detection in buffer and artificial urine with a detection limit down to 10−15 g/mL (*i.e.*, 3.5 fM) which is among the lowest values reported for small molecule detection by SPR. Conventional MIF showed 30-fold lower response compared to the macroporous MIF indicating improved accessibility and sensitivity for testosterone due to the high porosity. High stability of the MIF was proved as the sensor chips could be stored at room temperature for 8 months and, approximately, 84% of their affinity was retained, whereas conventional antibody-based biosensors survive storage at room temperature only for days, which highlights one of the most remarkable advantages of MIPs as recognition elements.

Additionally, MIPs have been used to create a sensing layer in fiber optic SPR sensors for which the cladding of a small part of the optical fiber is replaced by a thin metal film on top of which a sensing layer is constructed, and the evanescent waves generated at the core–metal interface are then used to excite surface plasmons at the sensing interface.[63] Application of MIPs to fiber optic SPR sensors has been reported to enhance their sensing ability for the detection of selected small molecules. For example for 2,4,6-trinitrotoluene (TNT) detection, an unclad plastic optical fiber was coated with a thin gold film where the selective MIP film was deposited and based on the changes in the obtained SPR transmission spectra, a detection limit of $5.1 \times 10^{-5}$ M was established.[137] Similarly, a sensing probes for tetracycline,[138] melamine,[139] atrazine,[140] profenofos,[141] and erythromycin[142] detection were fabricated by coating the unclad core of an optical fiber with a 40 nm thick silver film which was further coated with the target-specific MIP by dip coating (**Figure 5**). A red shift in resonance wavelength indicated target recognition, and excellent detection limits for atrazine (LOD = $1.92 \times 10^{-14}$ M), profenofos (LOD = $2.5 \times 10^{-6}$ μg/L) and erythromycin (LOD = $1.62 \times 10^{-3}$ μM) were reported. To improve the sensitivity, a 10 nm thick aluminum layer was added between silver and MIP layer and slightly lower limit of detection for atrazine was measured.[140] Erythromycin sensor was additionally applied to the analysis of spiked milk and honey samples, and excellent recoveries were reported for micromolar erythromycin concentrations.[142]

Alternatively, enhancement in the sensitivity of MIP-based detection has been achieved by incorporating gold nanostars in LSPR sensor for the detection of TNT[143] and L-nicotine.[144]

TNT-specific MIPs, identical to the previously reported,[137] were used with five-branched gold nanostars and three times better sensitivity was obtained (LOD = 2.4 × $10^{-6}$ M). Further enhancement of the sensitivity was achieved using tapered optical fibers (LOD = 7.2 × $10^{-7}$ M), which was attributed to the reduction of incidence angles of the guided rays in the fiber close to the critical angle of the unclad uniform tapered region.[143] For ascorbic acid (vitamin C) detection, enhancement in the sensitivity of a polyaniline MIP-based optical fiber SPR sensor[145] was achieved by employing both SPR and LSPR techniques.[146] *In situ* molecularly imprinted polyaniline-Ag nanocomposite was coated on the Ag layer on the optical fiber core thus combining LSPR of the Ag nanoparticles and SPR of the Ag thin film. Compared to the LSPR probe without the Ag film (LOD = 1.117 × $10^{-10}$ M), lower detection limit could be achieved with the LSPR+SPR probe (LOD = 7.383 × $10^{-11}$ M) and ascorbic acid contents of commercial vitamin C tablets could be analyzed with good recoveries.[146]

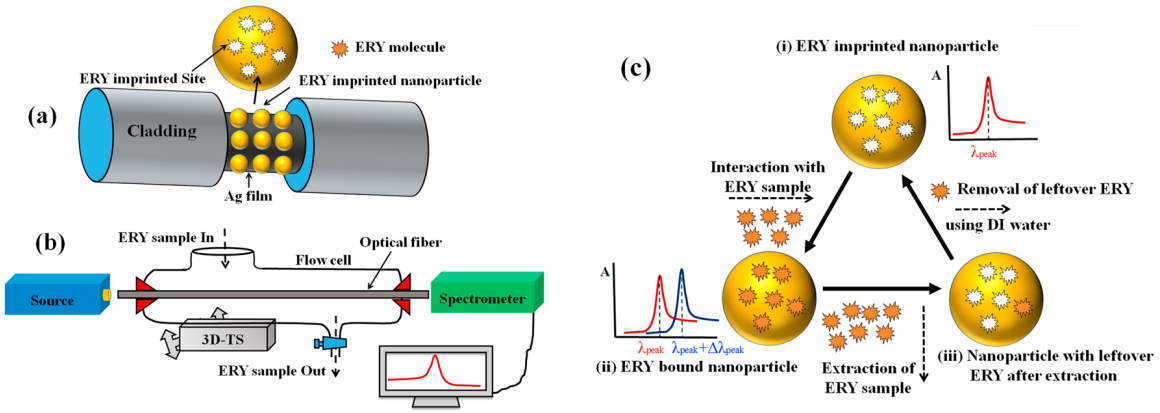


**Figure 5.** Schematic of (A) fabricated sensing probe for the detection of erythromycin (ERY) using the fiber optic core decorated with the coatings of silver and a layer of ERY imprinted nanoparticles (B) experimental set-up and (C) sensing mechanism. Figure reprinted from ref. [142] with permission from Elsevier.

## Enzyme-based SPR sensors

Although for certain sensor applications enzymes are the most extensively studied recognition elements, only a few examples of enzyme-based SPR sensors have been described.[147] In some recent strategies acetylcholinesterase (AchE), a key enzyme in neurotransmission, which is inhibited by organophosphorus compounds such as nerve agents, pesticides and several toxins, has been used in SPR sensors for the detection of these inhibitors.[148] Fiber-based LSPR-sensor for pesticide detection using AChE covalently coupled to AuNPs was based on the change of the light attenuation in the presence of pesticides which inhibited the activity of AChE to hydrolyze acetylcholine chloride (ACh). In optimized conditions, the detection limit of the sensor was 0.234 µg/L and using a powerful nucleophilic agent the sensor surface could be reactivated with 94% recovery rate after six cycles of inhibition.[149] Based on the same principle, AChE was used in a fiber-optic sensor based on silver coated core of a plastic-cladding silica fiber. AChE was immobilized using gel entrapment, and detection of chlorpyrifos pesticide (CPF) was reported in the micromolar range.[150] More recently, Milkani *et al*.[151] reported direct detection of

AChE inhibitors used for Alzheimer's disease therapy by immobilizing AChE covalently to a self-assembled monolayer on the gold surface of a commercial SPR sensor. The reversible carbamate inhibitors, neostigmine and serine, could be detected at micromolar concentrations, and considering the small target size, a relatively large change observed in the refractive index was attributed to the conformational changes in AChE as a result of inhibitor binding to the enzyme's active site. It has also been reported that conjugation of the target molecule to a carrier protein does not significantly alter the AChE recognition but could be used to increase the SPR signals. In the AChE-based SPR sensor by Puiu *et al.*[152] the target $AFB_1$ alone did not give a detectable SPR signal but using $AFB_1$–horseradish peroxidase (HRP)-conjugate in a competitive approach a detection limit of 0.003 µM (0.94 ng/mL) for $AFB_1$ was reported.

Enhancement in AChE-based detection has been achieved using magnetic MIPs with recognition sites for pesticide CPF, which enabled enrichment of the target to the sensor surface. Magnetic MIPs were synthesized by self-polymerization of dopamine on the surface of $Fe_3O_4$ nanoparticles in the presence of the template CPF. Rebinding of the target and analysis of these CPF-imprinted nanoparticles by AChE-based SPR showed a low detection limit of 0.76 nM due to the significant signal amplification caused by the high molecular weight of the MIPs. Compared to direct analysis of CPF, approximately 64 times higher SPR angle shift could be observed with CPF-imprinted nanoparticles (**Figure 6**). Although CPF rebinding to MIPs required 12 h incubation, which can be considered as a limiting aspect, the MIP-based method showed excellent selectivity against other pesticides tested.[153]

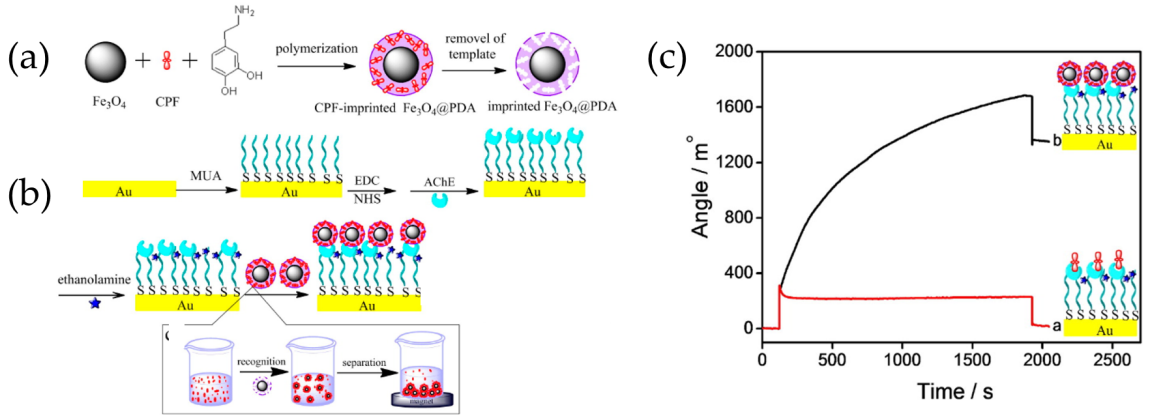


**Figure 6**. (A) Preparation of magnetic MIPs for chlorpyrifos (CPF) recognition and (B) schematic illustration of the stepwise preparation process of the sensor surface with immobilized AChE. (C) SPR response curve with 10 µM CPF using direct detection of free CPF in PBS (red) and amplification with magnetic MIPs (black). Figure reprinted from ref. [153], copyright (2013) American Chemical Society.

**Table 1**. Examples of SPR- and LSPR-based methods using different recognition elements. The limit of detection (LOD), calculated as the blank response plus three times the standard deviation, is reported. Alternatively, the measured concentration range is shown between brackets.

| Analyte | Recognition element | Assay format | Immobilization | LOD | Sample matrix | Ref. |
|---|---|---|---|---|---|---|
| Tetrodotoxin | MAb | Direct | Covalent amine coupling on CM5/CM7 sensor chip | 0.091 ng/mL | – | [71] |
| Benzoylecgonine | MAb | Direct | Covalent amine coupling on a polycarboxylated hydrogel matrix | 6.7 nM (=2 µg/L) | Oral fluid | [66] |
| Estradiol | MAb | Competitive inhibition | E2-BSA on the SCN-modified "charged" Au surface weak electrostatic interactions | [0.1–1000 ng/mL] | – | [46] |
| Tetracycline | Aptamer | Direct | DNA nanostructure | 0.0069 µg/kg | Honey | [68] |
| OTA, $AFB_1$, ATP | Aptamer | Direct, signal enhancement with berberine | Thiol modified aptamer on GNR | 0.56 pM (OTA), 0.63 pM ($AFB_1$), 0.87 pM (ATP) | – | [119] |
| Ractopamine | MIP/GNPs/rGO nano-hybrid | Direct | Deposition by spin-coating | 5 ng/mL (LR 20–1000 ng/mL) | – | [127] |
| T-2 toxin | MIP | Direct | *In situ* electropolymerization | 0.1 fM (=0.05 pg/mL) (LR 2.1–33.6 fM) | – | [130] |
| Testosterone | Macroporous MIF | Direct | *In situ* photo copolymerization | $10^{-15}$ g/mL | Urine | [136] |
| TNT | GNS-MIPs | Direct | Polymerization on exposed POF core | $7.2 \times 10^{-7}$ M | – | [143] |
| Neostigmine Eserine | AChE | Direct | Covalent attachment of AChE to COOH-terminated SAM on Au surface | [10–1000 µM] | – | [151] |
| Chlorpyrifos | AChE/MIP | Direct after MIP capture | Covalent attachment of AChE to COOH-terminated SAM on Au surface | 0.76 nM (LR 0.001–10 µM) | – | [153] |

*Abbreviations: AChE, acetylcholinesterase; $AFB_1$, aflatoxin $B_1$; ATP, adenosine triphosphate; DR, dynamic range; GNP, gold nanoparticle; GNR, gold nanorod; GNS, gold nanostar; LOD, limit of detection; LR, linear range; MAb, monoclonal antibody; MIF, molecularly imprinted film; MIP, molecularly imprinted polymer; OTA, ochratoxin A; POF, plastic optical fiber; rGO, reduced graphene oxide; SAM, self-assembled monolayer; TNT, 2,4,6-trinitrotoluene.*

## Surface-enhanced Raman spectroscopy

Surface-enhanced Raman spectroscopy (SERS) is a powerful vibrational spectroscopy technique that has unique features compared to other sensor devices using various kinds of signal readouts, including colorimetry, fluorescence, surface plasmon resonance, and electrochemistry.[154–156] SERS is a vibrational spectroscopy technique that can be used to identify unknown compounds since it provides structural information of the target molecule as a "fingerprint," similar to that derived from infrared spectroscopy. Also, SERS sensors can be used to analyze aqueous-rich samples and complex matrices, such as food samples, because water does not interfere in SERS signals and it has deep penetration depth.

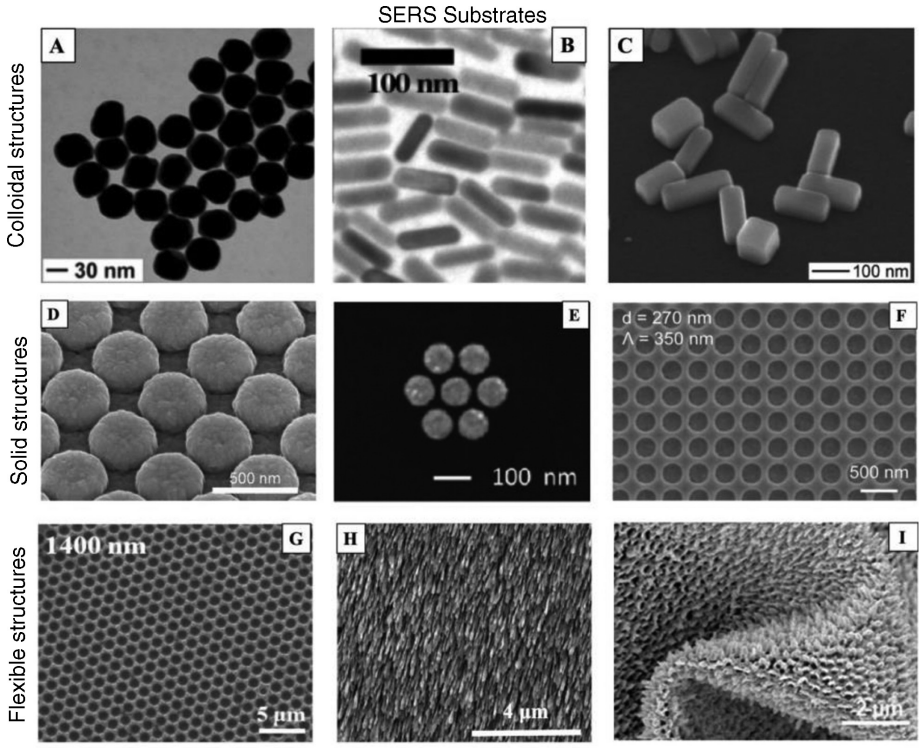


**Figure 7**. SEM images of different types of SERS substrates. (A) Spherical gold nanoparticles, (B) gold nanorods, (C) silver nanobar, (D) silver plasmonic nanodome array, (E) gold nanocluster, (F) gold nanoholes, (G) silver nanovoids, (H) silver nanocolumnar film, and (I) silver nano-pillars. Reprinted with permission from ref. [157], copyright (2017) De Gruyter.

Generally speaking, Raman scattering is tremendously inefficient due to the small scattering cross section of ca. 10–30 $cm^2$/molecule, which is about 14 orders of magnitude lower than the cross sections of fluorescent dye molecules.[158] Therefore, it is fundamental the use of SERS reporters or substrates that, similarly to SPR-based sensors, enhance the Raman signal to improve the sensitivity. Mostly all SERS reporters are plasmonic nanostructures, such as gold, silver, copper, or aluminum nanoparticles with dimensions lower than the wavelength of the incident light (**Figure 7**).

In these particular cases, the electronic oscillations are confined within a small volume, resulting in a specific type of surface plasmon called localized surface plasmon (LSPR). The excitation of LSPR plasmons produces a strongly amplified electromagnetic (EM) field because

of the collectivity oscillation of the conductive electrons on the nanoparticle surface. The basic concept of surface-enhanced Raman spectroscopy is that the Raman scattering signal of molecules at or close to the metallic surface can be enhanced to a factor of $10^{10}$–$10^{11}$.[156] There are at least two enhancement mechanisms in SERS:[159, 160] (1) electromagnetic, referring to the electromagnetic effect that occurs near to the particle surface and is associated with long-range enhancement; (2) chemical effect, induced by the charged transfer between the metal nanoparticle and the molecule chemically adsorbed.

Several factors significantly influence SERS, such as the type and energy of the bond between the molecule and the nanoparticle (NP), the surface roughness of the NP, light excitation wavelength and media conditions (*e.g.*, pH, buffer nature). Interestingly, a significant enhancement has been observed when the analyte molecules are located in the gap between two or more nanoparticles, or are situated at sharp angles or tips of anisotropic plasmonic NPs (*e.g.*, rods, stars, prisms). These areas are known as SERS "hot spots" and maximization of their number is desirable (**Figure 8**). Although aggregation of metal NPs in liquid induces "hot spots", reproducibility during measurements is challenging and a real disadvantage in sensing applications. Thus, some of the current focuses on material science is to create SERS reporters with three-dimensional large-ordered nanostructures to achieve signal uniformity and reproducibility. Some examples include rods, holes, clusters, domes 3D nanostructures which have been successfully fabricated (**Figure 7**).[157] Moreover, the use of coating nanomaterials to improve the chemical stability of the metal structures and to preserve the SERS signal is under investigation. For example, graphene, mesoporous silica, polymers, and even proteins are starting to be widely used in the fabrication of SERS reporters.[161]

Benchtop Raman microscopes have been the gold standard platform for analytical methods based on SERS.[162] However, the large size and high cost restrict their use to the laboratory, although the transition to the field as portable SERS sensors is a reality proved by the arrival of affordable small portable Raman spectrometers with dimensions similar to a smartphone, such as FirstDefender™ RMX (Thermo Fisher Scientific, Inc., Waltham, MA, US).[163] The diversity of SERS-active platforms offers sufficient choices for analyzing proteins, disease biomarkers, ions, toxins, bacteria, viruses, *etc*.

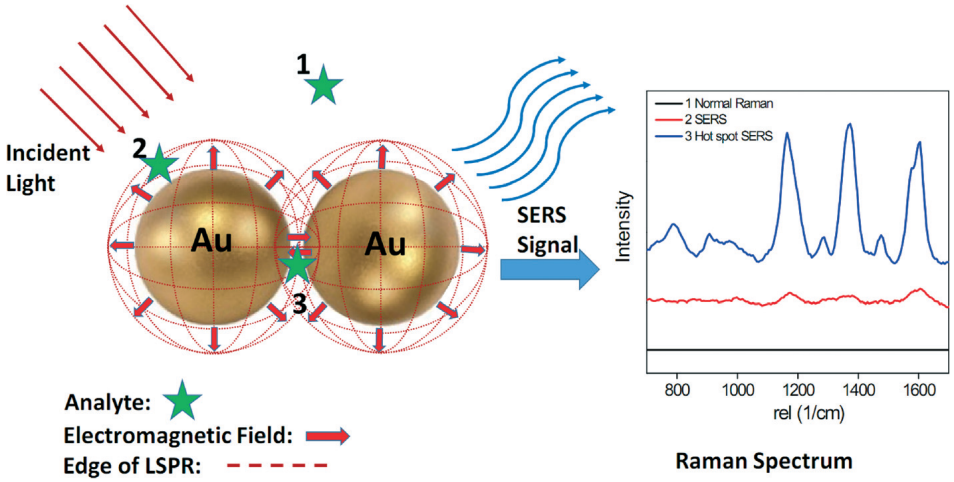


**Figure 8**. Schematic of SERS effect for a small molecule on gold nanoparticles (AuNPs). (1) Analyte outside the enhanced magnetic field (red dotted lines), no Raman signal is observed; (2) analyte located within the enhanced magnetic field but at long-distance, and (3) analyte located within a "hot spot". Reprinted with permission from ref. [159]. Copyright 2015 The Royal Society of Chemistry.

In contrast to label-based SERS devices, in which the accuracy depends on the selective binding of the label to the target analyte, in label-free SERS methods the signal is directly dependent on either the analyte or the recognition element–analyte complex; thus understanding intra- and intermolecular interactions of the analyte is feasible. Direct recognition of the analyte by its characteristic Raman vibration bands when it is adsorbed, chemically or physically, on the SERS reporter surface is the most straightforward approach for detecting and quantifying small molecules. For example, dithiocarbamate pesticides thiram, ferbam, and ziram were detected individually using a gold nanoparticle colloid as SERS reporter.[164, 165] The three organic pollutants were adsorbed firmly on the plasmonic surface through their sulfur groups allowing detection limits as low as 34 nM, 26 nM and 23 nM, respectively. Using a different SERS reporter type, Meng *et al.*[164] prepared a self-assembled layer of silver nanocubes on a flexible polyethylene film. Direct deposition of SERS sensor pieces on contaminated oranges demonstrated the presence of 10 nM of thiram, 1 μM of 3-chlorobiphenyl, and 10 nM of parathion.

A critical factor in label-free detection using SERS sensors is that the analyte should be confined inside the enhanced EM field of the SERS reporter. This issue is a significant challenge for SERS sensing since high non-polar or small hydrophobic molecules present low affinity for hydrophilic SERS reporters (Ag, Au, *etc.*), which prevents their detection at low concentrations. In this context, (bio)recognition elements can provide a set of analytical strengths that add value to SERS sensor platforms. For example, they can provide a degree of selectivity and an increase in the sensitivity by concentrating the analyte at the sensing surface. Most of the (bio)recognition elements used in label-free SERS sensors are antibodies, aptamers, molecularly imprinted polymers, and small molecules affinity agents. The following sections highlight label-free SERS sensor approaches reported for small molecule detection using the aforementioned (bio)recognition elements. **Table 2** summaries some of the most interesting approaches from recent years.

## SERS sensors based on antibodies

The first report that described the use of antibodies as the biorecognition element in SERS was a label-based "sandwich" immunoassay. The target, thyroid stimulating hormone (TSH), was detected using anti-TSH capture antibodies bound to silver surfaces to form SERS probes and a detection antibody labeled with p-dimethylaminoazobencene, a well-known SERS reporter. The intensity of the resultant Raman scattering signal and the TSH concentration had a linear relationship ranging from 4 to 60 μIU/mL.[166]

It is worth noting that, as in the case of SPR sensor platforms, the number of direct SERS methods for small molecule detection using antibodies is limited. This is likely due to the large size of the antibody (*ca*. 150 kDa) that occupies the volume just above of the SERS substrate area and thus, is in the most active region of the enhancing EM field.[167] Antibodies, which are composed of amino acids, produce a significant SERS signal particularly from the side chains of phenylalanine, tyrosine, and tryptophan residues,[168] and thus, a discrepancy between the antibody and small molecule signal is produced. As a consequence, spectral information of the target small molecules can only be obtained under two particular circumstances: (1) binding of the small molecule to the antibody paratope triggers a structural change in the latter, or (2) the small target features a large scattering cross-section.

A representative example of a direct SERS-based immunoassay for the detection of small molecule targets is the work of Sanles-Sobrido *et al.*[169] The authors demonstrated that BZE could be detected and quantified by simple comparison of the antibody-BZE complex Raman spectra, enhanced by the use of silver-coated carbon nanotubes, with the spectrum of the antibody alone. For supporting this strategy, structural information of the anti-BZE antibody was illustrated through the study by single-crystal X-ray diffraction and computational modeling of the modifications in the fragment antigen binding (Fab) region upon binding to BZE (**Figure 9**). The detection limit for BZE was in the range of 1 ng/mL (*ca.* 1 nM), which was in the same order of magnitude than using other immunological methods. Moreover, the reported SERS-sensor could be suitable for *in situ* detection of BZE even in complex biological fluids, similarly as was reported later with the antibody-based SPR-sensor for the same analyte.[66]

An exciting alternative to minimize the strong SERS signal produced by the antibody is the use of recombinant antibody fragments. Up to now, the most used antibody fragment type is scFv (single chain fragment variable, 25 kDa) which consists only of the $V_H$ and $V_L$ domains, joined by a peptide linker. Surprisingly, to the best of our knowledge, no reports have been published based on the combination of label-free SERS-based immunoassays and recombinant antibodies for small molecule detection.

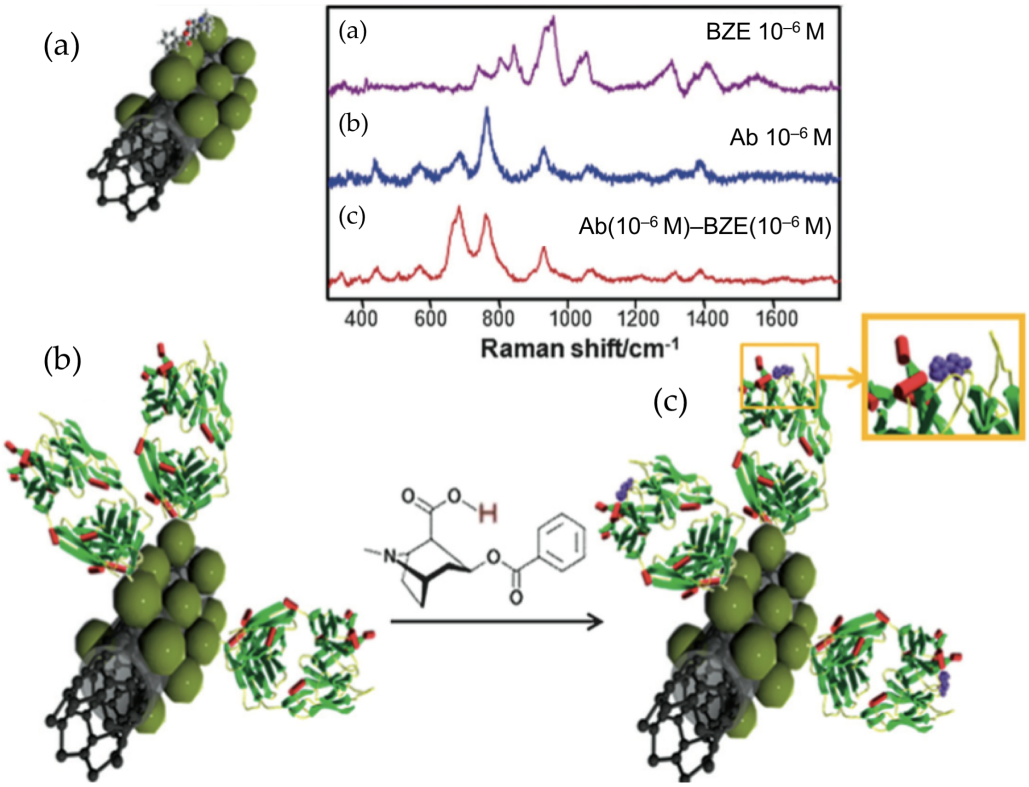


**Figure 9.** Schematic representation of benzoylecgonine (BZE) detection by SERS using silver-coated carbon nanotubes (CNT@Ag). Direct binding of BZE to AgNPs (green spheres) (A), label-free indirect detection of BZE on CNT@Ag coated with BZE-specific antibody fragment alone (B) and in complex with BZE (C). Corresponding SERS spectra are depicted in the graph on top. Figure reprinted from ref. [169] with permission from The Royal Society of Chemistry.

## SERS sensors based on aptamers

Aptamers are small (usually from 15 to 60 nucleotides, or 5–20 kDa) DNA or RNA oligonucleotides that have specific affinity for a target molecule. Since 1996, when the first aptasensors were published, their sensing applications are on the rise with particular emphasis in SERS-based aptasensors.[170] Despite their simplicity, aptamers feature excellent binding constants, resulting from the three-dimensional architecture acquired upon binding to the target molecule through hydrogen bonding, Van der Waals, and/or electrostatic interactions. Aptamer immobilization onto SERS substrates does not result in random orientation since there are only two ends, 5' and 3', in its structure. The most popular immobilization approaches are based on:[171, 172] (1) the use of thiolated aptamers which behave as ligands to form metal-thiolated complexes; (2) adsorption or π-π stacking interactions between the oligonucleotide bases of the aptamer and graphene-modified SERS reporters; (3) covalent linkage of amino-functionalized aptamers to carboxylic acid groups present on a particular substrate.

Mostly all label-free SERS platforms based on aptamers, detect small molecules using either the direct signal from the target or the target/aptamer complex. The latter approach is relatively simple to analyze since the assignment of the SERS vibration peaks of the DNA bases is fully covered in the literature.[173] One of the first reports combining aptamers and SERS detection demonstrated a label-free optical method for monitoring cocaine and platelet-derived grow factor.[174] Similarly to work presented by Sanles-Sobrido *et al.*[169] SERS spectra of the DNA

aptamer, acquired before and after exposure to the target analyte, enabled detection of the conformational changes in the oligonucleotide induced by the formation of the aptamer–analyte complex. This observation was well correlated with circular dichroism spectroscopy. Direct monitoring of the target molecule using a SERS device was described by Barahona *et al.*[175] The approach presented an aptasensor for monitoring the pesticide malathion using polymeric microspheres that were prepared with methacrylic acid and ethylene glycol dimethacrylated. Then, the beads were activated with 2-aminoethanethiol and decorated with AuNPs in which thiolated anti-malathion aptamers were immobilized. Characteristic peaks of malathion were observed in a region of the spectra free of DNA signal, and finally, 495 $cm^{-1}$ (shift assigned to P-S stretching) was selected for quantification of the pesticide. The linear range was established between 3.3–33 μg/mL and the detection limit was 3.3 μg/mL with an RSD < 14%.

## SERS sensors based on molecularly imprinted polymers

To solve some of the problems that prevented the use of molecularly imprinted polymers in SERS sensing platforms,[35] homogeneous MIP films with controlled thickness have been synthesized using methods like atom transfer radical polymerization[133] and reversible addition-fragmentation chain transfer (RAFT).[123] Moreover, the development of core-shell nanocomposite imprinted polymers is of high interest when the material includes additional benefits, such as magnetic, luminescent, or metal core nanoparticles.[176] AuNPs are the most widely used noble metal colloid in the manufacture of sensors based on core-shell structures (Au@MIP) thanks to the advantages it offers, such as optimal electro-optical properties, biocompatibility, and ease of fabrication and functionalization.

Wulff and coworkers reported one of the first approaches of SERS chemosensor based on MIPs.[177] Imprinted polymer layers were prepared on SERS archive surfaces built with either gold or silver deposited films. As a proof of concept, (2S,3S)-(+)-di-*O*-benzoyltartaric acid or *N*-benzyloxy-carbonyl-(L)-aspartic acid were selected as templates. The functional monomer and crosslinker used were *N,N′*-diethyl-4-vinylbenzamidine and ethylenglycol dimethacrylate, respectively. The rebinding of the target molecules was performed with a 10 mM solution of the aspartic acid derivative in 0.1 M HEPES at pH 7.3 during 15 min. Under these conditions, the uptake was followed at 1007 $cm^{-1}$ and normalized with the polymer band at 1615 $cm^{-1}$. As the authors mentioned, this method was not suitable for direct monitoring of the target molecules, pointing out the need for robust methods to anchor MIP layers onto metal surfaces without losing the SERS enhancement. Nevertheless, the work definitively opened the door to the use of MIPs for the development of SERS chemosensors as have been demonstrated in recent years.[178–180]

To circumvent the aforementioned problem, Carrasco *et al*.[181] prepared selective Au@MIPs for ENRO using multibranched AuNPs as cores to act as intrinsic hot spots. The optimized nanostructures were obtained through a multistep synthetic approach that involved: (1) the growth of nanometric mesoporous silica layer, (2) formation of gold branches inside the silica, (3) functionalization with RAFT agent and (4) polymerization of the selective MIP (**Figure 10**). The use of this material resulted in a significant enhancement of the Raman scattering of ENRO upon binding to the selective sites of the MIP and improved sensitivity with a detection limit of 1.5 nM and minimal cross-reactivity toward potential interfering species

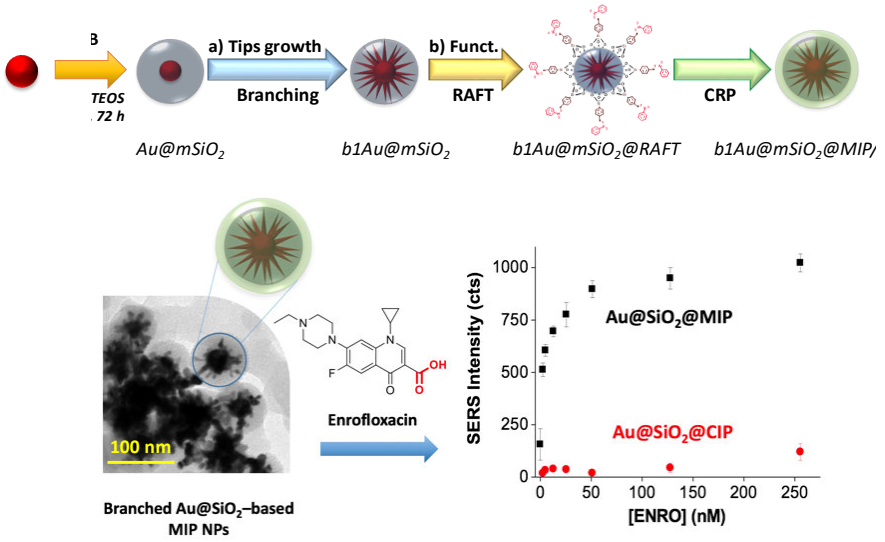


**Figure 10.** (A) Schematic representation of the nanocomposite fabricated in this work for the development of a SERS–MIP sensor, using Au@mSiO$_2$ nanoparticles and a branching–functionalization–polymerization approach to produce branched Au@mSiO$_2$@MIP/CIP (molecularly imprinted/control imprinted polymer) nanoparticles; (B) Schematic overview of the rebinding features towards the target molecule. Reprinted with permission from ref. [181]. Copyright 2016 American Chemical Society.

In contrast to the numerous examples of MIP-metal composites prepared by core–shell approaches, Kamra *et al.*[182] prepared MIP microspheres by RAFT polymerization, templated to the target nicotine and decorated with terminal thiol groups to increase the adsorption to gold-based substrates. Raman signal of nicotine was enhanced by positioning the SERS substrates near the specific sites of the MIP by three different strategies: (1) coating MIP microspheres with gold colloids, (2) sputtering of AuNPs onto the MIP surfaces, and (3) measuring the MIP microspheres trapped on a commercial SERS-active substrate. All the approaches tested transformed the MIP microspheres into SERS-active substrates although gold colloidal coating yielded the strongest signal when nicotine was detected.

In a different strategy, Ashley *et al.*[183] combined the separation properties of magnetic molecularly imprinted polymer (MMIP)-based sample pretreatment with SERS detection for quantitative analysis of cloxacillin in pig serum. Magnetic $FeO_x$ nanospheres were synthesized and coated with mesoporous silica and metacryloxy propyl trimethoxyl silane to allow the polymerization of the MIP layer directly attached to the silica surface. The target antibiotic was then extracted from pig serum using the MMIPs and eluted into a clean solvent. Then, the extract was deposited into the SERS substrates, consisting of vertical silicon nanopillars coated with gold, and quantitative analysis was performed using acetic acid as internal standard. The sensor presented good sensitivity (7.8 pmol) toward the antibiotic with recoveries ranging from 85% to 126%. Although the results were adequate, the strategy followed for measuring rendered SERS redundant because of the MIP specificity and the separation of the target from the matrix by extraction.

The multiplexing ability of SERS sensing in combination with MIPs was demonstrated by Holthoff et al. 184 for the simultaneous analysis of TNT and their derivatives. The MIP against TNT, based on organosilane precursors, contained 3-mercaptopropyl trimethoxysilane to facilitate the adhesion of the spin-coated MIP xerogel to the SERS reporter through thiol-metal interactions. The MIP bound selectively dinitro species that could be differentiated by the molecular "fingerprint" of each analyte afforded by the SERS measurements. Quantification of TNT was performed at 1352 cm−1, the peak corresponding to the asymmetric stretching band for nitrate, presenting a detection limit of 3 μM in solution after 24 h exposure.

### SERS sensors based on molecular traps

Small molecules are exciting alternatives to trap hydrophobic organic targets that have a very low affinity to SERS surfaces. The two most common molecular trap agents are partition layers and functional monolayers of small molecules.[167] For the first type, diffusion enables the transport of a set of analytes that are soluble inside of them. The second interact directly through covalent binding, hydrogen bonding, ionic, polar, nonpolar, *etc*.

For example, polychlorinated biphenyls[185] and polycyclic aromatic hydrocarbons (PAHs)[186] have been detected using partition layer-functionalized SERS substrates. For instance, decanethiol on silver substrates could perform pM sensitivity with multiplexing analysis capability. PAHs are a group of small molecules intensely studied using label-free SERS sensors and multicycle organic compounds, such as calixarenes, viologens, and cyclodextrins, have been broadly used.[187, 188] For example, calix[4]arene dithiocarbamate[189] was able to host pyrene, benzo[c]phenanthrene, triphenylene, and coronene facilitating their SERS detection (LODs from 100 pM to 10 nM) when the calixarene was linked to AgNPs. Viologen dications (VGDs) lucigerin, diquat, and paraquat have also been evaluated as PAHs-molecular traps after their immobilization onto AgNPs.[188] VGDs were able to induce the formation of hot spots to locate the analyte yielding a significant intensification of the Raman emission of the target molecule. Lucigerin provided the most robust VGD–AgNPs sensor due to its bifunctional nature and its large aromatic character and allowed a limit of detection down to $10^{-9}$ M for pyrene detection. Another molecular trap used to determine PAHs (anthracene and pyrene) was reported by Xie *et al*.[187] The designed system (**Figure 11**) used AgNPs modified with per-6-deoxy-(6-thio)-β-cyclodextrin. The SERS signals for each PAH were easy to differentiate and were significantly enhanced thanks to the selective cyclodextrin cavity that hosted the hydrophobic molecules near to the EM field. However, the sensitivity of the sensors was not impressive, reporting a limit of detection for anthracene of 10 μM and 7.5 μM for pyrene.

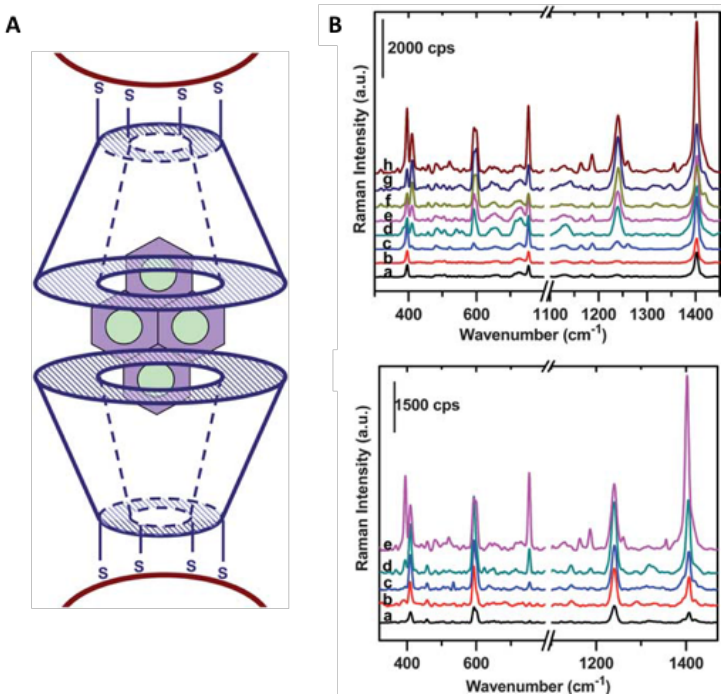


**Figure 11**. (A) Schematic representation of the host-guest complexation mechanism for pyrene. (B) Top graph: SERS spectra of mixtures of 333 mM anthracene with different concentrations of pyrene; a–h (0, 17, 25, 33, 83, 166, 250 and 333 mM). Bottom graph: SERS spectra of mixtures of 333 mM pyrene with different concentrations of anthracene, from a–e (0, 83, 166, 250 and 333 mM). Reprinted with permission from ref. [187]. Copyright 2010 the Royal Society of Chemistry.

## Interferometric biosensors

Interferometric biosensors are based on refractive index changes produced by a biorecognition event which takes place in the sensing area. This change is measured with the aid of two light beams, the sensor, and reference beams, which are combined to produce an interference pattern. The sensor area is functionalized with the recognition element (*e.g.*, antibodies, aptamers, enzymes) which is responsible for the selective recognition of the target analyte, and the immobilization of the recognition element is of crucial importance for the sensor performance.[190–192] On the other hand, a good intrinsic reference channel is necessary to obtain high sensitivity.[190] The reference channel is designed to take into account the background signals derived from thermal drift, the light source stability, mechanical noise, and non-specific binding, *i.e.*, all the processes that also occur in the sensing channel other than the specific binding event.[193]

**Table 2.** Examples of SERS-based methods using different recognition elements. The limit of detection (LOD), calculated as the blank response plus three times the standard deviation, is reported.

| Analyte | Recognition element | Assay format | Immobilization | LOD | Sample matrix | Ref. |
|---|---|---|---|---|---|---|
| PCB-47 | Alkanethiols (C8, C10, C16, C18) | Direct | SAMs of alkanethiols built over AgFON | 5 mM | – | [185] |
| PCB-3<br>PCB-29<br>PCB-77 | β-CD | Direct | β-CD adsorbed over $SiO_2$@Au@AgNPs and immobilized on quartz slides | 1 μM | – | [194] |
| Malathion | Aptamer | Direct | Thiol-modified aptamer on AgNPs@SP | 5–100 × $10^{-7}$ M | tap water | [195] |
| Isocarbophos (1)<br>Omethoate (2)<br>Phorate (3)<br>Profenofos (4) | Aptamer | Direct | Thiolated aptamer on Ag dendrites | 3.4 μM (1)<br>24 μM (2)<br>0.4 μM (3)<br>14 μM (4) | apple juice | [196] |
| s-propanolol | MIP | Direct | MIP attached to the SERS-active klarite® substrate | 7.7 × $10^{-4}$ M | Urine | [197] |
| Ciprofloxacin | MIP | Direct | $Fe_3O_4$ NPs@MIP dispersed on a silver solution | $10^{-9}$ M (1)<br>$10^{-7}$ M (2) | water (1)<br>serum (2) | [198] |

*Abbreviations: β-CD, β-cyclodextrin; AgFON, roughened silver film over nanosphere; AgNPs, silver nanoparticles; AuNPs, gold nanoparticles; C8, n-octane; C10, n-decane; C16, n-hexadecane; C18, n-octadecano; $Fe_3O_4$, iron (II,III) oxide; MIP, molecularly imprinted polymer; PCB-3-chlorobiphenyl; PCB-29, 2,4,5-trichlorobiphenyl; PCB-47, 2,2′,4,4′-tetrachlorobiphenyl; PCB-77, 3,3′,4,4′-tetrachlorobiphenyl; SAM, self assembled monolayer; $SiO_2$, silicon dioxide.*

Numerous interferometric configurations have been reported for measuring small molecules; the most used ones are described hereafter and shown in **Figure 12**. The two most commonly used platforms are the Mach-Zehnder (MZI) and Young's (YI) interferometers which are both formed by a waveguide which splits a laser beam into the sample and reference arms and differ only in the way the two beams are merged to form the interference pattern. YI converges through natural divergence and MZI through a physically forced combination.[191] Dual polarization interferometer (DPI) employs two stacked planar waveguides (sample and reference) that are illuminated by a single laser beam, and the interference pattern is formed in the far field by emerging light.[199] Backscattering interferometry (BSI) differs from other interferometric techniques by its ability to measure interactions in solution within a channel or capillary.[200] Porous sensors use the Fabry-Perot interferometer principle where the interference is produced by reflected light from different surfaces within the sensor.[201] In biolayer interferometry (BLI) the binding event takes place at the end of an optical fiber where the reference is formed by a portion of propagated light that is reflected back towards the light source as it reaches a polymeric layer near the tip. The interference occurs between the reference beam and a small amount of light reflected from the interface between the fiber and the sample.[202] Along with these setups, there are several other interferometric configurations, such as reflectometric interference spectroscopy (RIfS),[203] spectral-phase interferometry (SPI)[204] or spectral-correlation interferometry (SCI), among others. Moreover, some configurations can be found in commercial devices such as ForteBio Octet (BLI) or Optiqua MiniLab (MZI).

Interferometric sensors can be produced in optical fibers or integrated optical waveguides. Generally, optical fibers can avoid problems related to channel blocking[205] and enable manufacturing of compact and economical equipment,[206] but integrated optics offer greater flexibility in the geometry of the design and the combination of materials, allowing greater complexity and ease of access to the optical path in evanescent field sensing.[192] Sensing surfaces are generally prepared by depositing on the surface of a glass substrate an optically transparent thin layer of a high refractive index, such as silicon nitride ($Si_3N_4$)[207, 208] or tantalum pentoxide ($Ta_2O_5$).[209, 210] Light can be coupled into the waveguide either by prism coupling, end firing, or diffraction grating, the latter being the most commonly used in interferometry measurements due to the simple manufacturing in the waveguide by etching the surface or by embossing.[190]

Interferometric biosensors can monitor directly small changes in the optical properties and allow measuring binding and dissociation events in real time. These biosensors generally do not require prior sample treatment or additional steps such as washing. Consequently, they have been used in a broad range of applications such as sensing, determination of biomolecule or protein-ligand interactions,[211] drug discovery,[212] and kinetic measurements,[202, 211] among others. Also, multi-analyte or multi-sample analysis is possible by joining different channel pairs (sensing–reference) into a single waveguide.[207, 213] Detection of small molecules with interferometric biosensors using different recognition elements is discussed in the following sections, and some representative examples are listed in **Table 3**.

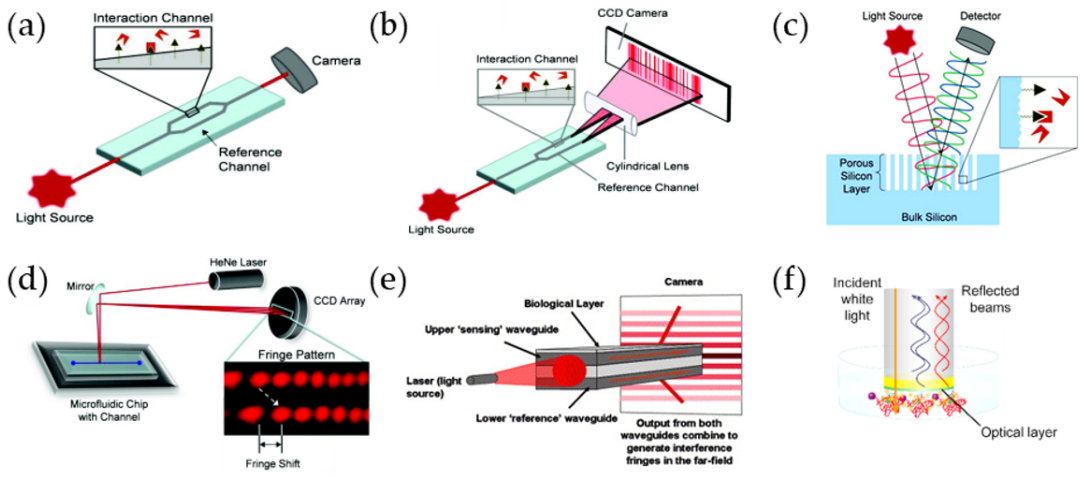


**Figure 12**. Schematic of the most commonly used interferometric configurations: (A) Mach–Zehnder interferometer (MZI), (B) a Young interferometer (YI), (C) porous silicon sensor, (D) backscattering interferometry (BSI), (E) dual-polarization interferometer (DPI), (F) biolayer interferometry. ((A–D), reprinted with permission from ref. [201], copyright (2012) American Chemical Society; (E), reprinted with permission from ref. [214] and (F), reprinted with permission from ref. [215] copyrights 2004 and 2017 Elsevier.

## Antibody-based interferometric sensors

Only a few examples of antibody-based interferometric sensors for small molecules have been reported using the direct assay format. A polarization interferometer biosensor based on a planar waveguide for the detection of mycotoxins $AFB_1$[216] and OTA[217] was able to detect the mycotoxins at concentrations down to ppts in a direct immunoassay format. The operating mode was similar to MZI, but the design was simpler, and the waveguide was not split into two arms. The waveguides consisted of a thin $Si_3O_4$ layer (200 nm) sandwiched between thicker $SiO_2$ layers (3 µm) and the light propagated in the core at an angle of 47 ° and experienced about 3000[216] or 800[217] reflections per mm. For biosensor development, a portion of the $SiO_2$ layer was etched, and a layer of positively charged poly-allylamine hydrochloride was deposited, followed by adsorption of protein A molecules, negatively charged, followed by immobilization of the monoclonal antibodies selective to the analyzed mycotoxin. The liquid sample was placed in contact with the sensing window using a reaction cell that included inlet and outlet tubes. Any changes in the refractive index or in the thickness of adsorbed molecules on the $Si_3O_4$ layer affected the p-component of the polarized light while the s-component was used as a reference. The light was collected with a charge-coupled device (CCD) array, and the phase shift between *p*- and *s*-components of polarized light was converted to variations of light intensity using a polarizer placed in front of the CCD camera. The sensor detected 0.01 ng/mL of $AFB_1$ or OTA in water.

Most commonly antibody-based interferometric sensors use the competitive immunoassay format with an immobilized the antibody,[207] or the binding inhibition assay where the target[218] is attached to the surface (**Figure 1**). In some cases, structural analogs of the target compound are needed for immobilization if the analyte lacks appropriate groups required for covalent coupling,[219–223] or due to the risks associated with the analyte.[224] Alternatively, a protein-conjugate can be immobilized on the surface. For example, Pagkali *et al.*[225] reported

detection OTA in beer with an MZI where the sensing area was functionalized with OTA–OVA conjugate. This 10-channel sensor was based on a binding inhibition assay with signal amplification using a secondary antibody to form another bimolecular layer increasing the effective RI. The assay exhibited a LOD of 2.0 ng/mL and a dynamic range from 4.0 to 100 ng/mL in beer samples. Later, the authors used the same platform and methodology for simultaneously detect $AFB_1$, fumonisin $B_1$, and DON, achieving LODs of 0.8, 5.6 and 24 ng/mL, respectively, in undiluted beer in less than 15 min.[213] In a different approach, Maragos[205] applied the BLI system for the detection of DON in wheat flour with using immobilized DON–BSA obtaining a detection limit of 0.1 mg/kg.[226] To improve the detection limit and assay time, they tested the use of a secondary antibody marked with HRP, as well as a primary antibody conjugated to colloidal gold. After signal amplification using colloidal gold, the detection limit was decreased to 0.09 mg/kg.

Given the importance of the suitable surface for the covalent binding of the analyte, Krieg *et al*.[210] compared the performance of amino-dextran and diamino-polyethylene glycol as biopolymer coatings for sensing purposes. After binding dimethylated amitriptyline, binding inhibitions assays were carried out with RIfS, and better results were obtained with the amino-dextran surface. The most sensitive assay showed a limit of detection of 268 ng/L in buffer and 540 ng/L in diluted (1:10) human serum, making it competitive even with HPLC measurements. Moreover, the platform showed high stability as 80 measurement cycles could be performed on each transducer chip after guanidine hydrochloride regeneration.[220] Recently in a different approach, using bimodal waveguide interferometry (BiMW), Chocarro-Ruiz *et al*.[219] employed several silanization protocols to evaluate the most suitable biofunctionalization procedure for Irgarol 1051 detection.

To improve the analytical characteristics of a porous silicon sensor, Orlov *et al*.[227] described a method for enhancing the reproducibility of the assay using the specific absorption capacity within the sensing area. For this purpose, after obtaining the signal produced by the competitive assay (S), an excess of the monoclonal antibody was put in contact with the surface to saturate the sites not occupied in the previous stage ($\Delta$). The normalized $S/\Delta$-ratio provided a better reproducibility even with non-uniform surface coatings (**Figure 13**). OTA, zearalenone, and $AFB_1$ were detected in white wine with detection limits of 0.25, 0.48 and 1 ng/mL respectively, with CVs less than 5% and 2–3-fold lower detection limit compared a standard competitive assay. Furthermore, Tinsley-Bown *et al*.[224] develop a competitive assay for TNT detection which combined porous silicon interferometry with an Orthogonal Subspace Signal Projection Algorithm (OSPA), reaching a detection limit of 1 µg/mL. The OSPA method used reference reflectivity data before the sensing event to "self-calibrate" and measured any changes between the reference data and the test data overcoming the baseline drift, temperature fluctuation, and some systematic tendency such as the systematic reduction in optical thickness through erosion of the material.

### Interferometric sensors based on aptamers

Since aptamers first emerged in 1990 with the SELEX (systematic evolution of ligands by exponential enrichment) technique,[228] they became an alternative to antibodies. However, they are still consolidating their role as biorecognition elements. SELEX process screens random sequences of a fixed length of a large oligonucleotide library; sequences are exposed to the

target, and those with higher affinity are enriched through successive rounds. Wang's group used this tool to find the aptamers with better affinity and specificity to different marine toxins, such as gonyautoxin 1/4 (GTX1/4),[229] nodularin-R (NOD-R),[230] and palytoxin (PTX),[215] and afterward applied to BLI sensors. Aptamers against GTX1/4 and NOD-R were employed in direct assays with detection limits of 50 pg/mL and 167 pM, respectively. BLI biosensor for PTX detection was based on a binding inhibition assay with immobilized PTX and an HRP-conjugated aptamer. After signal amplification by submerging the sensor tip in a 3,3′-diaminobenzidine solution, which resulted in the formation of a precipitated polymeric product directly on the biosensor surface, a detection limit of 0.04 pg/mL was obtained (**Figure 14**). In a similar approach, marine toxin saxitoxin (STX) was detected with a detection limit of 0.5 ng/mL and a linear range from 100 to 800 ng/mL[231] using a modified aptamer which had been improved via site-directed mutation and truncation and had a 30-fold higher affinity for STX compared with the parent aptamer.[232, 233]

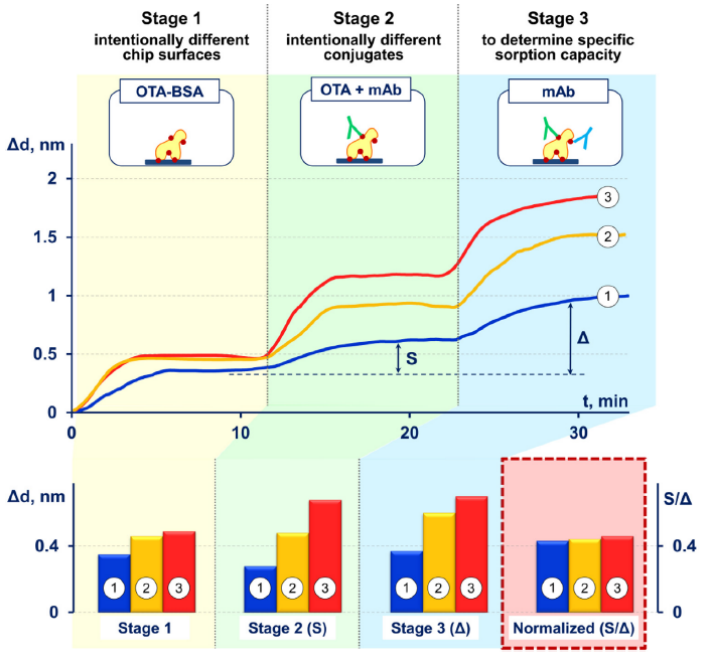


**Figure 13**. Scheme of reproducibility enhancement of label-free detection of small molecules. Spectral-correlation interferometry (SCI) sensograms for detection of ochratoxin A (OTA, 10 ng/mL) using intentionally different chip surfaces with different conjugates (top). Signal variations at each stage and the normalized signal (bottom). Reprinted with permission from ref. [227]. Copyright 2017 Elsevier.

Unlike in SPR where thiolated aptamers are often directly immobilized to the gold surface, interferometric sensors usually require a modified surface for the immobilization. The most widely used method, and perhaps the fastest, is the use of biotinylated aptamers in combination with surfaces modified with streptavidin[229, 230, 234] or avidin.[235, 236] For example, bisphenol A (BPA) -specific aptamer was immobilized on the surface of a DPI sensor chip through biotin-avidin interaction, and detection limits of 2.5 mM on the mass signals and 1.7 mM on the thickness signals were reported.[235] In an alternative approach, adenine-rich ssDNA aptamer was immobilized through a preadsorbed layer of poly(ethylenimine) for the direct detection of Coralyn

on a DPI. The mass, thickness and refractive index parameters were used to establish each calibration equation for the biosensor, achieving detection limits of 0.22 μM, 0.14 μM, and 0.32 μM respectively. Coralyn was detected in the range of 0.5 to 12 μM, with a high selectivity that was confirmed by comparison with three other common intercalators (ethidium bromide, daunomycin, and methylene blue).[237]

An unconventional competitive assay for testosterone was described by Zhang *et al.*[234] who used a BLI sensor with aptamers and testosterone-binding RepA protein. RepA could bind the biotinylated double-stranded DNA aptamers immobilized onto a streptavidin-coated chip in the absence of testosterone, whereas the conformational changes in RepA upon testosterone binding led to the displacement of RepA from the surface-bound aptamers. Testosterone could be determined in 17 min with a linear range of 2.13 to 136.63 ng/mL, exhibiting a sensitivity comparable to that achieved by HPLC.

Alternatively, using BSI which does not depend on surface-immobilization, Kammer *et al.* characterized interactions between small molecule and aptamers, providing $K_D$ values with minimal sample manipulation on small volume sample quantities and at low nanomolar sensitivity. For this propose they measured the aptamer affinity for BPA (20.2 ± 2.1 nM), tenofovir (9.0 ± 1.4 nM) and epirubicin (626 ± 121 nM); showing values reliable with those published previously for the same molecules. In addition, $K_D$ values for aptamers to ampicillin (402 ± 99 nM), tetracycline (2.94 ± 0.28 mM) and norepinephrine (188 ± 64 nM) were determined.[202]

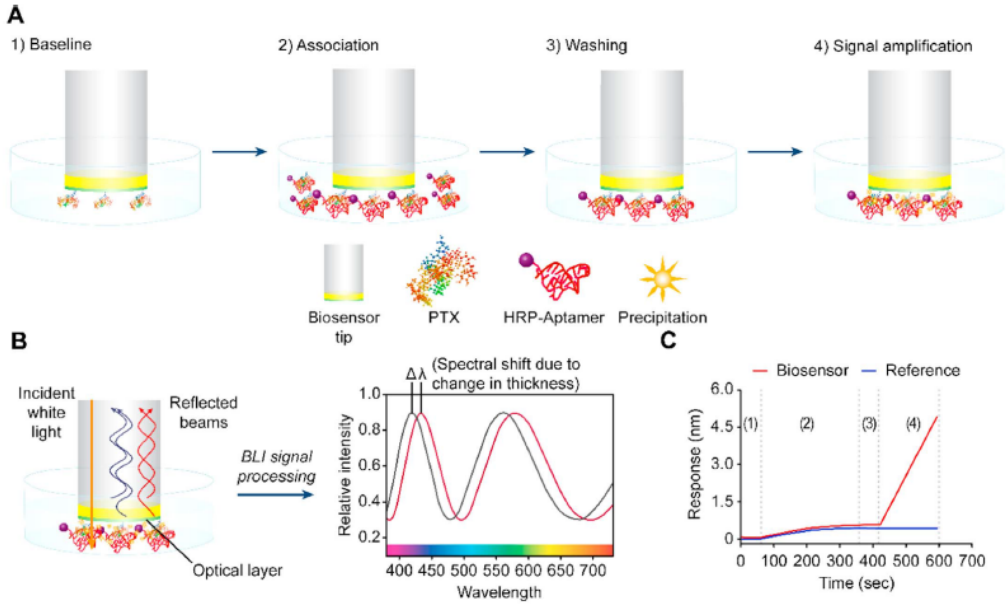


**Figure 14**. (A) Schematic of the working principles of the biosensor with the competitive assay for palytoxin (PTX) detection using horse-radish peroxidase (HRP)-modified aptamer. (B) Schematic of the biolayer interferometry (BLI)-based detection system and (C) the expected sensor response after each step: (1) baseline (1 min), (2) capture of free HRP-aptamer (5 min), (3) washing (1 min), and (4) signal amplification (3 min). Reprinted with permission from ref. [215]. Copyright 2017 Elsevier.

### Polymer-based interferometric sensors

Also, MIPs have been described as bioinspired receptors for interferometric sensors 208. MIPs can be produced directly on sensor surface,[238] by thermal or photochemical initiation, or be integrated later by dip or spin coating.[208, 209] In situ polymerization circumvents a separate immobilization step but sometimes has the disadvantage of long response times, low reproducibility and long-term stability, and regeneration problems.

Belmont *et al.*[208] applied two different methods for the deposition of MIPs, selective to atrazine, on the RIfS transducer surface. The first method consisted of in situ polymerizations of a thin film produced after spin-coating of monomers and template. In the second method, MIP nanoparticles produced by mini-emulsion polymerization were auto-assembled with the aid of polyethyleneimine. Using the autoassembled particle film in a RIfS platform, atrazine detection was established at concentrations as low as 1.7 ppm which was several orders of magnitude lower than previously reported with the same surface using a chiral chemosensor[238] for (*R,R*)- or (*S,S*)-2,3-di-*O*-benzoyltartraric acid. RIfS has also been used for the detection of L-Boc-phenylalanine anilide through miniemulsion polymerized imprinted nanospheres which provided a detection limit of 60 μM, good reproducibility, and selectivity, as well as long-term stability for up to 1 year.[209]

Also, non-imprinted polymers have been used as recognition elements in interferometric sensors. Porous silicon (pSi) films, which can be fabricated with the desired morphological structures, allows the design of a porous matrix to optimize the access of the target analyte, making it suitable for sensing applications.[239] These surfaces can be combined with polymers to carry out selective recognition, as in the glucose sensor described by Krismastuti *et al*.[240] using phenylboronic acid polymers. Thiol-terminated poly(4-vinylphenylboronic acid) was covalently bound to the pores of succinimidyl 4-(p-maleimidophenyl)butyrate modified pSi. In the presence of glucose, the properties of the polymer changed as cyclic boronate esters were formed. Surface behavior was monitored by interferometric reflectance spectroscopy (IRS) which could detect as low as 0.15 mM glucose at physiological pH, and no interferences were found when measuring in wound fluid samples.

A less common form of detection is based on measuring the decrease in surface thickness caused by polymer degradation. Wu et al. prepared a dithiothreitol (DTT) sensor based on an optical fiber Fabry-Perot interferometer (FPI). When DTT solution was in contact with the sensor, a cleavage in the disulfide-crosslinked PAAm hydrogel on the optical fiber was produced and monitored in real time as changes in the refractive index. A concentration of 50 μM DTT was successfully detected within 36 min,[241] improving the sensitivity 2000 times compared to previous work.[242]

Finally, there is no clear difference between interferometry and diffraction because of the similarity between their principles from a physical point of view.[243] For example, antimicrobial ENRO could be detected via optical diffraction using a selective MIP on a $Si_3N_4/SiO_2$ strip waveguide sensor. ENRO produced large signal response, saturating at 70 M and selectivity was evaluated with the temple analog flumequine.[208] Optical diffraction in combination with MIPs has also been used for testosterone detection. This approximation used a holographic structure (diffraction grating) obtained via photopolymerization of photoinitiators and monomers with interfering laser beams and was able to detect testosterone between 1 and 100 μM.[244]

### Protein-based interferometric sensors

Although enzymes are used in numerous bioassay formats, there are hardly any examples in the case of interferometry.[208] Instead, certain models of interaction between small molecules and proteins have been used, such as glucose and mannose with lectin concanavalin A (ConA). An interferometric sensor developed by Paek *et al*.[245] used a semi-continuous determination of glucose in human serum by placing an optic fiber in the hollow of a syringe needle. The BLI glucose sensor measured glucose levels by quantifying the wavelength shifts caused by the binding of glucose to ConA immobilized on the tip. Direct glucose measurement was limited by the signal-to-noise ratios and to overcome this problem authors used a sugar-protein conjugate enclosed inside the needle by a semi-permeable membrane to competitively bind to the immobilized ConA and satisfy the clinical range of interest (70–200 mg/dL). Recently, the same group described a modification to the previous sensor because of considerable migration distance of the ligand to the sensor surface and the limited pore size of the membrane due to the artificial conjugates. Authors addressed these limitations by placing the sugar-protein conjugate outside of the membrane (**Figure 15**) and increasing the pore size. Results obtained with this platform were compared with the ideal BLI, showing high reproducibility and good stability over time, ascribed to the fact that the sensing zone was not directly exposed to serum and thereby avoided non-specific binding of other compounds.[246]

BSI has also been used to study the binding affinity of mannose and glucose to ConA under significantly different physical conditions (tethered ConA on the surface and free solution). When comparing the results of the free solution with those obtained by having the ConA anchored at different distances from the surface, they observed that the binding affinity increased when the distance from the ConA to the surface decreased; thereby understanding how protein immobilization affects binding.[211]

Alternatively, optical coherence tomography (OCT) has been used to study the viability of semi-noninvasive continuous monitoring sensors. The OCT sensor described by Ballerstadt *et al*.[247] for glucose measurement in interstitial fluid (ISF) was established using a porous membrane with a suspension of macroporous hydrogel particles and ConA within. A reference compartment, containing buffer or ISF, was added next to the glucose-sensitive compartment for signal normalization. Performance of the sensor was demonstrated *in vitro* for 160 days with excellent reversibility, stability and good response over the physiological concentration range (2.5–20 mM glucose). Additionally, to mimic in vivo conditions and evaluate the possibility of using the sensor as an implant under the skin, they covered the sensor with a tissue phantom and were able to measure glucose changes of 10 mM.

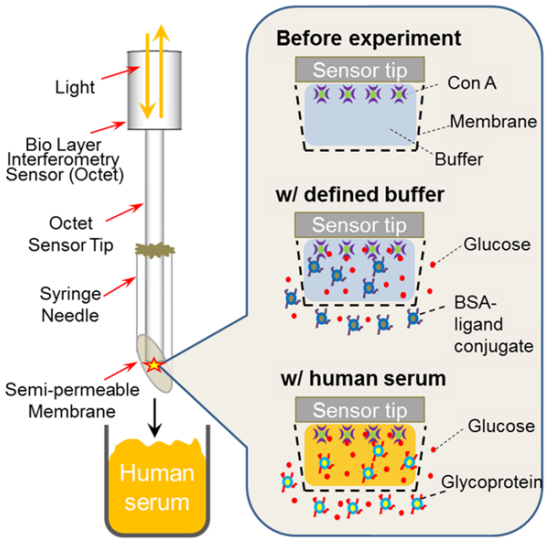


**Figure 15**. Schematic of the needle-type sensor. A syringe needle was modified and covered with a semi-permeable membrane to fabricate the needle-type sensor. Sensor tip was modified with concanavalin A (ConA) and bovine serum albumin (BSA)-ligand conjugate was kept outside of the semi-permeable membrane. Reprinted with permission from ref. [246]. Copyright 2016 MDPI.

**Table 3.** Examples of interferometric-based methods using different recognition elements. The limit of detection (LOD), calculated as the blank response plus three times the standard deviation, is reported. Alternatively, the measured concentration range is shown between brackets.

| Analyte | Recognition element | Assay format | Immobilization | Sensitivity | Sample matrix | Interf. type | Ref. |
|---|---|---|---|---|---|---|---|
| Domoic acid | PAb | Inhibition | Covalent binding of domoic acid by active ester chemistry | 2.0 ng/mL ($IC_{50}$) | Mussel tissue extracts | BLI | [218] |
| Irgarol 1051 | PAb | Binding inhibition | Covalent binding of a derivative onto an APTES functionalized surface | 3 ng/L | Sea water | BiMW | [219] |
| DON | MAb | Competitive | Adsorption of DON–OVA on the sensor chip | 128 µg/kg<br>737 µg/kg | Wheat<br>Wheat dust | BLI | [248] |
| Testosterone | MAb | Binding inhibition | Covalent binding by active ester chemistry of a derivative onto a DAPEG coated surface | 94.4 ng/L | Milk | RIfS | [223] |
| $AFM_1$ | Fab′ | Competitive | Fab′ binding to a mercaptosilane functionalized surface | $5 \times 10^{-7}$ RIU | Milk | aMZI | [207] |
| Vancomycin | Peptide | Direct | Covalent binding of the peptide to a pSi surface via a carboxy-linker | $K_D = 1.09 \times 10^{-5}$ mol/L | – | RIFTS | [249] |
| Testosterone | Aptamer | Competitive | Biotinylated aptamer on streptavidin-coated chip | [2.13–136.63 ng/mL] | – | BLI | [234] |
| Argininamide | Aptamer | Direct | Biotinylated aptamer on avidin-coated chip | 5 µM | – | DPI | [236] |
| Microcystin-LR (MC-LR) | MIP | Direct | Dip coating of the sol–gel matrix | [0.3–1.4 g/L] | Environmental water | FP | [250] |
| Melamine | MIP | Direct | Spin coating | 1251 rad/RIU | – | YI | [251] |
| Methyl-parathion | AChE | Direct | Covalent attachment to a APTES-GLU-functionalized surface | $2.4 \times 10^{-10}$ M<br>(2.1 nM–47 µM) | – | ITFS | [252] |

*Abbreviations: AChE, acetylcholinesterase; $AFM_1$, aflatoxin $M_1$; aMZI, asymmetric Mach-Zehnder interferometer; APTES-GLU, 3-aminopropyltriethoxysilane-glutaraldehyde; BiMW, bimodal waveguide interferometer; BLI, biolayer interferometry; DAPEG, diamino-poly(ethylene glycol); DON, deoxynivalenol; DPI, dual polarization interferometer; Fab′, antibody fragments; FP, Fabry-Perot interferometer; $IC_{50}$, half maximal inhibitory concentration; ITFS, interferometric tapered fiber sensor; $K_D$, equilibrium dissociation constant; mAb, monoclonal antibody; MIP, molecularly imprinted polymer; OVA, ovalbumin; PAb, polyclonal antibody; pSi, porous silicon; RIFTS, reflective interferometric Fourier transform spectroscopy; RIU, refractive index unit; YI, Young's interferometer*

**Table 4.** Comparative table of different optical label-free biosensors for the detection of ochratoxin A (OTA) as an example of a small molecule.

| Method | Recognition element | Assay format | Immobilization | Sensitivity | Measurement | Regeneration | Assay time | Sample | Ref. |
|---|---|---|---|---|---|---|---|---|---|
| SPR | MAb | Direct | GHBs on electropolymerized thionine (PTh) film | LOD 0.01 ng/mL | ESPR with SPR sensor in a flow cell | Up to eight times with glycine-HCl solution (pH 2.8) | <30 min | Milk | [72] |
| iSPR | MAb | Inhibition | Covalently immobilized toxins on CMD surface | LOD 3 ng/mL | iSPR instrument with nanostructured gold chips | More than 450 times with 10 mM HCl | ≈15 min | Beer | [109] |
| LSPR | Aptamer | Direct | Aptamer with 5′ thiol on Au surface | <1 nM (=0.4 ng/mL) | Microplate reader with 96-well plate | Seven times with 10% methanol at +70°C | ≈15 min | Corn | [118] |
| OWLS | MAb | Direct and competitive | Covalently immobilized MAb (direct) or OTA–BSA (competitive) | DR 5–10 ng/mL for direct, 0.5–10 ng/mL for competitive | Integrated OWLS sensor chips | n.d. | <10 min | Barley and wheat | [41] |
| PW (PI principle) | MAb | Direct | Antibody *via* protein A | DR 0.01–100 ng/mL | PW structures on silicon wafers, CCD array and a polarizer | n.d. | n.d. | – | [217] |
| SERS | Aptamer | Direct | Aptamer with 5′ thiol on Au surface | DR 0.05–4 μM | SERS platform with microfluidic channel | n.d. | n.d. | – | [253] |

*Abbreviations: BSA; bovine serum albumin, CCD; charge-coupled device (CCD), CMD; 3-dimensional carboxymethylated dextran, DON; deoxynivalenol, DR; detection range, ESPR; electrochemical surface plasmon resonance, GHB; gold hollow balls, LOD; limit of detection, MAb; monoclonal antibody, iSPR; imaging surface plasmon resonance, OWLS; optical waveguide lightmode spectroscopy, PI; polarization interferometry, PW; planar waveguide.*

## Conclusions

During the last decades, biosensors have become an essential tool for small molecule analysis in different disciplines, such as drug discovery, environmental security, and food safety, complementing and, in some cases, even replacing the existing analytical methodologies. Biosensors can provide not only selective and sensitive detection but can be also portable and offer a rapid response in real time, which makes them ideal for many applications. The performance of biosensors depends on many factors including, the bioreceptor layer, the transducer, and the instrumentation. Therefore all these different parameters must be taken into account in the design of the device.

SPR continues its reign as the most used label-free sensor configuration for small molecule analysis, partly due to the availability and simple use of advanced commercial devices. Nevertheless, significant advances in other transduction schemes have made important contributions to the field of label-free sensing. On the other hand, although antibodies are probably the most common biorecognition elements, during the last decade also several exciting applications using, for example, aptamers or MIPs as recognition elements have been reported. **Table 4** collects examples of different optical label-free methods for the detection of OTA which has been one of the most widely used targets in the papers revised for this review.

Nevertheless, it should also be noted that the research in many label-free methods is still their infancy and many reports in the literature, particularly those related to instrumental or material improvements, are rather fundamental including only proof-of-concept bioassays and are thus yet to encompass the challenges associated with the real analyte analysis. For example, many of the most recent biosensors reviewed here have shown excellent characteristics for synthetic samples, but still, lack characterization in complex matrices which better resemble the real applications. Moreover, many designs based on nanostructures could be able to overcome some of the optical and biological limitations of sensors but the inherent nanofabrication procedures, such as electron beam lithography and focused ion-beam milling, might limit their widespread application.[62] In any case, as discussed in this paper, recent advances in the field of optical label-free methods are impressive, and new technologies and materials for improved detection are reported every year.

### Funding

This research was funded by the Spanish Ministry of Economy and Competitiveness grant number CTQ2015-69278-C2-1-R/AIE

### Acknowledgments

RP thanks Complutense University for a predoctoral contract.

### Conflicts of Interest

The authors declare no conflict of interest.

## References


1. *Lehninger Principles of Biochemistry*, 4th ed.; Nelson, D. L., Cox, M. M., Eds.; Freeman: New York, US, **2005**.
2. Breitling, R.; Takano, E. Synthetic biology advances for pharmaceutical production. *Curr. Opin. Biotechnol.* **2015**, *35*, 46–51.
3. Stein, R. A.; Bulboacă, A. E. Mycotoxins. In *Foodborne Diseases*; Elsevier, **2017**; pp 407–446.
4. Wu, F.; Groopman, J. D.; Pestka, J. J. Public health impacts of foodborne mycotoxins. *Annu. Rev. Food Sci. Technol.* **2014**, *5*, 351–372.
5. Johnson, E. A.; Schantz, E. J. Seafood toxins. In *Foodborne Diseases*; Elsevier, 2017; pp 345–366.
6. Vilariño, N.; Louzao, M. C.; Fraga, M.; Rodríguez, L. P.; Botana, L. M. Innovative detection methods for aquatic algal toxins and their presence in the food chain. *Anal. Bioanal. Chem.* **2013**, *405*, 7719–7732.
7. Kim, K.; Tsay, O. G.; Atwood, D. A.; Churchill, D. G. Destruction and detection of chemical warfare agents. *Chem. Rev.* **2011**, *111*, 5345–5403.
8. Uniyal, S.; Sharma, R. K. Technological advancement in electrochemical biosensor based detection of organophosphate pesticide chlorpyrifos in the environment: a review of status and prospects. *Biosens. Bioelectron.* **2018**, *116*, 37–50.
9. Verma, N.; Bhardwaj, A. Biosensor technology for pesticides – A review. *Appl. Biochem. Biotechnol.* **2015**, *175*, 3093–3119.
10. Fechner, P.; Bleher, O.; Ewald, M.; Freudenberger, K.; Furin, D.; Hilbig, U.; *et al*. Size does matter! Label-free detection of small molecule–protein interaction. *Anal. Bioanal. Chem.* **2014**, *406*, 4033–4051.
11. Dasgupta, A. *Therapeutic Drug Monitoring: Newer Drugs and Biomarkers*; Academic Press, **2012**.
12. aus der Beek, T.; Weber, F. A.; Bergmann, A.; Hickmann, S.; Ebert, I.; Hein, A.; Küster, A. Pharmaceuticals in the environment – Global occurrences and perspectives. *Env. Toxicol Chem* **2016**, *25*, 823–835.
13. Mompelat, S.; Le Bot, B.; Thomas, O. Occurrence and fate of pharmaceutical products and by-products, from resource to drinking water. *Environ. Int.* **2009**, *35*, 803–814.
14. Kümmerer, K. Drugs in the environment: emission of drugs, diagnostic aids and disinfectants into wastewater by hospitals in relation to other sources – A review. *Chemosphere* **2001**, *45*, 957–969.
15. Kabir, E. R.; Rahman, M. S.; Rahman, I. A review on endocrine disruptors and their possible impacts on human health. *Environ. Toxicol. Pharmacol.* **2015**, *40*, 241–250.
16. World Health Organization. Endocrine Disrupting Chemicals www.who.int/ceh/risks/cehemerging2/ (accessed Oct 12, 2018).
17. Yu, X.; Zhang, X.; Wang, Z.; Jiang, H.; Lv, Z.; Shen, J.; Xia, G.; Wen, K. Universal simultaneous multiplex ELISA of small molecules in milk based on dual luciferases. *Anal. Chim. Acta* **2018**, *1001*, 125–133.
18. Zhang, D.; Tao, X.; Jiang, H.; Wen, K.; Shen, J.; Cao, X. Simultaneous detection of forbidden chemical residues in milk using dual-label time-resolved reverse competitive chemiluminescent immunoassay based on amine group functionalized surface. *PLOS One* **2014**, *9*, e109509.
19. Jawaid, W.; Campbell, K.; Melville, K.; Holmes, S. J.; Rice, J.; Elliott, C. T. Development and validation of a novel lateral flow immunoassay (LFIA) for the rapid screening of paralytic shellfish toxins (PSTs) from shellfish extracts. *Anal. Chem.* **2015**, *87*, 5324–5332.
20. Hu, W.; Li, X.; He, G.; Zhang, Z.; Zheng, X.; Li, P.; Li, C. M. Sensitive competitive immunoassay of multiple mycotoxins with non-fouling antigen microarray. *Biosens. Bioelectron.* **2013**, *50*, 338–344.
21. Käppel, N. D.; Pröll, F.; Gauglitz, G. Development of a TIRF-based biosensor for sensitive detection of progesterone in bovine milk. *Biosens. Bioelectron.* **2007**, *22*, 2295–2300.
22. Nie, J.; Yuan, L.; Jin, K.; Han, X.; Tian, Y.; Zhou, N. Electrochemical detection of tobramycin based on enzymes-assisted dual signal amplification by using a novel truncated aptamer with high affinity. *Biosens. Bioelectron.* **2018**, *122*, 254–262.
23. Ligler, F. S. Perspective on optical biosensors and integrated sensor systems. *Anal. Chem.* **2009**, *81*, 519–526.
24. *Biosensors: Fundamentals and Applications*; Turner, A. P. F., Karube, I., Wilson, G. S., Eds.; Oxford University Press: Oxford; New York, US, **1987**.

25. Borisov, S. M.; Wolfbeis, O. S. Optical biosensors. *Chem. Rev.* **2008**, *108*, 423–461.
26. Fan, X.; White, I. M.; Shopova, S. I.; Zhu, H.; Suter, J. D.; Sun, Y. Sensitive optical biosensors for unlabeled targets: A review. *Anal. Chim. Acta* **2008**, *620*, 8–26.
27. Khansili, N.; Rattu, G.; Krishna, P. M. Label-free optical biosensors for food and biological sensor applications. *Sens. Actuators B Chem.* **2018**, *265*, 35–49.
28. *The Immunoassay handbook: Theory and applications of ligand* binding ELISA and related techniques, 4th ed.; Wild, D., (Editor); Elsevier Science, Oxford, UK, **2013.**
29. Holliger, P.; Hudson, P. J. Engineered antibody fragments and the rise of single domains. *Nat. Biotechnol.* **2005**, *23*, 1126–1136.
30. Bradbury, A. R. M.; Sidhu, S.; Dübel, S.; McCafferty, J. Beyond natural antibodies: The power of *in vitro* display technologies. *Nat. Biotechnol.* **2011**, *29*, 245–254.
31. Kavanagh, O.; Elliott, C. T.; Campbell, K. Progress in the development of immunoanalytical methods incorporating recombinant antibodies to small molecular weight biotoxins. *Anal. Bioanal. Chem.* **2015**, *407*, 2749–2770.
32. Fodey, T.; Leonard, P.; O'Mahony, J.; O'Kennedy, R.; Danaher, M. Developments in the production of biological and synthetic binders for immunoassay and sensor-based detection of small molecules. *TrAC Trends Anal. Chem.* **2011**, *30*, 254–269.
33. Rhouati, A.; Catanante, G.; Nunes, G.; Hayat, A.; Marty, J.-L. Label-free aptasensors for the detection of mycotoxins. *Sensors* **2016**, *16*, 2178.
34. Wanekaya, A. K.; Chen, W.; Mulchandani, A. Recent biosensing developments in environmental security. *J. Environ. Monit.* **2008**, *10*, 703.
35. Moreno-Bondi, M. C.; Navarro-Villoslada, F.; Benito-Peña, E.; Urraca, J. L. Molecularly imprinted polymers as selective recognition elements in optical sensing. *Curr. Anal. Chem.* **2008**, *4*, 316–340.
36. Homola, J. Surface plasmon resonance sensors for detection of chemical and biological species. *Chem. Rev.* **2008**, *108*, 462–493.
37. Xiao-hong, Z.; Lan-hua, L.; Wei-qi, X.; Bao-dong, S.; Jian-wu, S.; Miao, H.; Han-chang, S. A reusable evanescent wave immunosensor for highly sensitive detection of bisphenol A in water samples. *Sci. Rep.* **2015**, *4*.
38. *Optochemical Nanosensors*; Cusano, A., Arregui, F. J., Giordano, M., Cutolo, A., Eds.; Series in Sensors; CRC Press, Boca Raton, FL, US, **2013**.
39. Benito-Peña, E.; Valdés, M. G.; Glahn-Martínez, B.; Moreno-Bondi, M. C. Fluorescence based fiber optic and planar waveguide biosensors. a review. *Anal. Chim. Acta* **2016**, *943*, 17–40.
40. Taitt, C. R.; Anderson, G. P.; Ligler, F. S. Evanescent wave fluorescence biosensors: advances of the last decade. *Biosens. Bioelectron.* **2016**, *76*, 103–112.
41. Adányi, N.; Levkovets, I. A.; Rodriguez-Gil, S.; Ronald, A.; Váradi, M.; Szendrő, I. Development of immunosensor based on OWLS technique for determining aflatoxin $B_1$ and ochratoxin A. *Biosens. Bioelectron.* **2007**, *22*, 797–802.
42. Székács, A.; Adányi, N.; Székács, I.; Majer-Baranyi, K.; Szendrő, I. Optical waveguide light-mode spectroscopy immunosensors for environmental monitoring. *Appl. Opt.* **2009**, *48*, B151.
43. Majer-Baranyi, K.; Székács, A.; Szendrő, I.; Kiss, A.; Adányi, N. Optical waveguide lightmode spectroscopy technique–based immunosensor development for deoxynivalenol determination in wheat samples. *Eur. Food Res. Technol.* **2011**, *233*, 1041–1047.
44. Majer-Baranyi, K.; Zalán, Z.; Mörtl, M.; Juracsek, J.; Szendrő, I.; Székács, A.; Adányi, N. Optical waveguide lightmode spectroscopy technique-based immunosensor development for aflatoxin $B_1$ determination in spice paprika samples. *Food Chem.* **2016**, *211*, 972–977.
45. Ton, X. A.; Acha, V.; Bonomi, P.; Tse Sum Bui, B.; Haupt, K. A disposable evanescent wave fiber optic sensor coated with a molecularly imprinted polymer as a selective fluorescence probe. *Biosens. Bioelectron.* **2015**, *64*, 359–366.
46. Boltovets, P.; Shinkaruk, S.; Vellutini, L.; Snopok, B. Self-tuning interfacial architecture for estradiol detection by surface plasmon resonance biosensor. *Biosens. Bioelectron.* **2017**, *90*, 91–95.
47. Barrios, C.A.; Canalejas-Tejero, V.; Herranz, S.; Urraca, J.L.; Moreno-Bondi, M. C.; Avella-Oliver, M.; Maquieira, A.; Puchades, R. Aluminum nanoholes for optical biosensing. *Biosens.* **2015**, *5*, 417–431.

48. Canalejas-Tejero, V.; Herranz, S.; Bellingham, A.; Bondi, M. C. M.; Barrios, C. A. Passivated aluminum nanohole arrays for label-free biosensing applications. *ACS Appl Mater Interfaces* **2014**, *144*, 1005–1010.
49. Margheri, G.; Giorgetti, E.; Marsili, P.; Zoppi, A.; Lascialfari, L.; Cicchi, S. Metal-clad optical waveguide fluorescence device for the detection of heavy metal ions. *Opt. Eng.* **2014**, *53*, 071816/1-071816/8.
50. Gui, Q.; Lawson, T.; Shan, S.; Yan, L.; Liu, Y. The application of whole cell-based biosensors for use in environmental analysis and in medical diagnostics. *Sensors* **2017**, *17*, 1623–1640.
51. Kuncová, G.; Ishizaki, T.; Solovyev, A.; Trögl, J.; Ripp, S. The repetitive detection of toluene with bioluminescence bioreporter *Pseudomonas putida* TVA8 encapsulated in silica hydrogel on an optical fiber. *Materials* **2016**, *6*, 467–477.
52. Kalabova, H; Pospisilova, M; Siroka, R; Kuncova, G. A biosensor with encapsuled bioreporters – Optical fiber element for enhanced detectection of bioluminescence. *Meas. Sci. Technol.* **2018**, *29*, 075104.
53. Pospíšilová, M.; Kuncová, G.; Trögl, J. Fiber-optic chemical sensors and fiber-optic bio-sensors. *Sensors* **2015**, *15*, 25208–25259.
54. Plotnikova, E. G.; Shumkova, E. S.; Shumkov, M. S. Whole-cell bacterial biosensors for the detection of aromatic hydrocarbons and their chlorinated derivatives (review). *Appl. Biochem. Microbiol.* **2016**, *52*, 347–357.
55. Roda, A.; Cevenini, L; Michelini, E.; Branchini, B. R. A portable bioluminescence engineered cell-based biosensor for on-site applications. *Biosens. Bioelectron.* **2011**, *26*, 3647–3653.
56. Wang, Q.; Tang, S.-Y.; Yang, S. Genetic biosensors for small-molecule products: design and applications in high-throughput screening. *Front. Chem. Sci. Eng. 2* **2017**, *11*, 15–26.
57. Peña-Vazquez, E.; C.P. Conde; Costas, E.; Moreno-Bondi, M. C. Development of a microalgal pam test method for Cu(II) in waters: comparison of using spectrofluorometry. *Ecotoxicology* **2010**, *19*, 1059–1065.
58. Peña-Vázquez, E.; Maneiro, E.; Pérez-Conde, C.; Moreno-Bondi, M.C.; Costas, E. Microalgae fiber optic biosensors for herbicide monitoring using sol–gel technology. *Biosens. Bioelectron.* **2009**, *24*, 3538–3543.
59. Haigh-Flórez, D.; Hera, C.; Costas, E.; Orellana, G. Microalgae dual-head biosensors for selective detection of herbicides with fiber-optic luminescent O2 transduction. *Biosens. Bioelectron.* **2014**, *54*, 484–491.
60. Estevez, M.-C.; Otte, M. A.; Sepulveda, B.; Lechuga, L. M. Trends and challenges of refractometric nanoplasmonic biosensors: A review. *Anal. Chim. Acta* **2014**, *806*, 55–73.
61. Hunt, H. K.; Armani, A. M. Label-free biological and chemical sensors. *Nanoscale* **2010**, *2*, 1544.
62. Abbas, A.; Linman, M. J.; Cheng, Q. New trends in instrumental design for surface plasmon resonance-based biosensors. *Biosens. Bioelectron.* **2011**, *26*, 1815–1824.
63. Gupta, B. D.; Shrivastav, A. M.; Usha, S. P. Surface plasmon resonance-based fiber optic sensors utilizing molecular imprinting. *Sensors* **2016**, *16*.
64. Guo, T.; González-Vila, Á.; Loyez, M.; Caucheteur, C. Plasmonic optical fiber-grating immunosensing: A review. *Sensors* **2017**, *17*, 2732.
65. Yakes, B. J.; Prezioso, S.; Haughey, S. A.; Campbell, K.; Elliott, C. T.; DeGrasse, S. L. An improved immunoassay for detection of saxitoxin by surface plasmon resonance biosensors. *Sens. Actuators B Chem.* **2011**, *156*, 805–811.
66. Munoz, E. M.; Lorenzo-Abalde, S.; González-Fernández, Á.; Quintela, O.; Lopez-Rivadulla, M.; Riguera, R. Direct surface plasmon resonance immunosensor for *in situ* detection of benzoylecgonine, the major cocaine metabolite. *Biosens. Bioelectron.* **2011**, *26*, 4423–4428.
67. GE Healthcare Life Sciences. Biacore™ Assay Handbook. www.gelifesciences.com (accessed Jun 1, 2018).
68. Wang, S.; Dong, Y.; Liang, X. Development of a SPR aptasensor containing oriented aptamer for direct capture and detection of tetracycline in multiple honey samples. *Biosens. Bioelectron.* **2018**, *109*, 1–7.
69. Tomassetti, M.; Merola, G.; Martini, E.; Campanella, L.; Sanzò, G.; Favero, G.; Mazzei, F. Comparison between a direct-flow SPR immunosensor for ampicillin and a competitive conventional amperometric device: analytical features and possible applications to real samples. *Sensors* **2017**, *17*.

70. Yang, S.; Wu, T.; Zhao, X.; Li, X.; Tan, W. The optical property of core-shell nanosensors and detection of atrazine based on localized surface plasmon resonance (LSPR) sensing. *Sensors* **2014**, *14*, 13273–13284.
71. Yakes, B. J.; Kanyuck, K. M.; DeGrasse, S. L. First report of a direct surface plasmon resonance immunosensor for a small molecule seafood toxin. *Anal. Chem.* **2014**, *86*, 9251–9255.
72. Fu, X. Surface plasmon resonance immunoassay for ochratoxin A based on nanogold hollow balls with dendritic surface. *Anal. Lett.* **2007**, *40*, 2641–2652.
73. Losoya-Leal, A.; Estevez, M.-C.; Martínez-Chapa, S. O.; Lechuga, L. M. Design of a surface plasmon resonance immunoassay for therapeutic drug monitoring of amikacin. *Talanta* **2015**, *141*, 253–258.
74. Kim, S. J.; Gobi, K. V.; Iwasaka, H.; Tanaka, H.; Miura, N. Novel miniature SPR immunosensor equipped with all-in-one multi-microchannel sensor chip for detecting low-molecular-weight analytes. *Biosens. Bioelectron.* **2007**, *23*, 701–707.
75. Kadota, T.; Takezawa, Y.; Hirano, S.; Tajima, O.; Maragos, C. M.; Nakajima, T.; Tanaka, T.; Kamata, Y.; Sugita-Konishi, Y. Rapid detection of nivalenol and deoxynivalenol in wheat using surface plasmon resonance immunoassay. *Anal. Chim. Acta* **2010**, *673*, 173–178.
76. Stevens, R. C.; Soelberg, S. D.; Eberhart, B.-T. L.; Spencer, S.; Wekell, J. C.; Chinowsky, T. M.; Trainer, V. L.; Furlong, C. E. Detection of the toxin domoic acid from clam extracts using a portable surface plasmon resonance biosensor. *Harmful Algae* **2007**, *6*, 166–174.
77. Stevens, R. C.; Soelberg, S. D.; Near, S.; Furlong, C. E. Detection of cortisol in saliva with a flow-filtered, portable surface plasmon resonance biosensor system. *Anal. Chem.* **2008**, *80*, 6747–6751.
78. Pan, M.; Li, S.; Wang, J.; Sheng, W.; Wang, S. Development and validation of a reproducible and label-free surface plasmon resonance immunosensor for enrofloxacin detection in animal-derived foods. *Sensors* **2017**, *17*, 1984.
79. Pennacchio, A.; Ruggiero, G.; Staiano, M.; Piccialli, G.; Oliviero, G.; Lewkowicz, A.; Synak, A.; Bojarski, P.; D'Auria, S. A surface plasmon resonance based biochip for the detection of patulin toxin. *Opt. Mater.* **2014**, *36*, 1670–1675.
80. Pennacchio, A.; Varriale, A.; Esposito, M. G.; Scala, A.; Marzullo, V. M.; Staiano, M.; D'Auria, S. A rapid and sensitive assay for the detection of benzylpenicillin (PenG) in milk. *PLoS One* **2015**, *10*.
81. Farré, M.; Martínez, E.; Ramón, J.; Navarro, A.; Radjenovic, J.; Mauriz, E.; Lechuga, L.; Marco, M. P.; Barceló, D. Part per trillion determination of atrazine in natural water samples by a surface plasmon resonance immunosensor. *Anal. Bioanal. Chem.* **2007**, *388*, 207–214.
82. Liu, M.; Ning, B.; Qu, L.; Peng, Y.; Dong, J.; Gao, N.; Liu, L.; Gao, Z. Development of indirect competitive immunoassay for highly sensitive determination of ractopamine in pork liver samples based on surface plasmon resonance sensor. *Sens. Actuators B Chem.* **2012**, *161*, 124–130.
83. Fernández, F.; Pinacho, D. G.; Sánchez-Baeza, F.; Marco, M. P. Portable surface plasmon resonance immunosensor for the detection of fluoroquinolone antibiotic residues in milk. *J. Agric. Food Chem.* **2011**, *59*, 5036–5043.
84. Herranz, S.; Bocková, M.; Marazuela, M. D.; Homola, J.; Moreno-Bondi, M. C. An SPR biosensor for the detection of microcystins in drinking water. *Anal. Bioanal. Chem.* **2010**, *398*, 2625–2634.
85. Campbell, K.; Stewart, L. D.; Doucette, G. J.; Fodey, T. L.; Haughey, S. A.; Vilariño, N.; Kawatsu, K.; Elliott, C. T. Assessment of specific binding proteins suitable for the detection of paralytic shellfish poisons using optical biosensor technology. *Anal. Chem.* **2007**, *79*, 5906–5914.
86. Fonfría, E. S.; Vilariño, N.; Campbell, K.; Elliott, C.; Haughey, S. A.; Ben-Gigirey, B.; Vieites, J. M.; Kawatsu, K.; Botana, L. M. Paralytic shellfish poisoning detection by surface plasmon resonance-based biosensors in shellfish matrixes. *Anal. Chem.* **2007**, *79*, 6303–6311.
87. Meneely, J. P.; Sulyok, M.; Baumgartner, S.; Krska, R.; Elliott, C. T. A rapid optical immunoassay for the screening of T-2 and HT-2 toxin in cereals and maize-based baby food. *Talanta* **2010**, *81*, 630–636.
88. Yang, L.; Ding, H.; Gu, Z.; Zhao, J.; Chen, H.; Tian, F.; Chen, Y. Q.; Zhang, H.; Chen, W. Selection of single chain fragment variables with direct coating of aflatoxin $B_1$ to enzyme-linked immunosorbent assay plates. *J. Agric. Food Chem.* **2009**, *57*, 8927–8932.

89. Lauer, B.; Ottleben, I.; Jacobsen, H.-J.; Reinard, T. Production of a single-chain variable fragment antibody against fumonisin $B_1$. *J. Agric. Food Chem.* **2005**, *53*, 899–904.

90. Alvarez-Rueda, N.; Behar, G.; Ferré, V.; Pugnière, M.; Roquet, F.; Gastinel, L.; *et al*. Generation of llama single-domain antibodies against methotrexate, a prototypical hapten. *Mol. Immunol.* **2007**, *44*, 1680–1690.

91. Moghaddam, A.; Løbersli, I.; Gebhardt, K.; Braunagel, M.; Marvik, O. J. Selection and characterisation of recombinant single-chain antibodies to the hapten aflatoxin $B_1$ from naive recombinant antibody libraries. *J. Immunol. Methods* **2001**, *254*, 169–181.

92. Sun, Y.; Ning, B.; Liu, M.; Gao, X.; Fan, X.; Liu, J.; Gao, Z. Selection of diethylstilbestrol-specific single-chain antibodies from a non-immunized mouse ribosome display library. *PLoS One* **2012**, *7*.

93. Zhao, L.; Ning, B.; Bai, J.; Chen, X.; Peng, Y.; Sun, S.; *et al*. Selection of bisphenol A – single-chain antibodies from a non-immunized mouse library by ribosome display. *Anal. Biochem.* **2015**, *488*, 59–64.

94. Daly, S.; Dillon, P.; Manning, B.; Dunne, L.; Killard, A.; O'Kennedy, R. Production and characterization of murine single chain fv antibodies to aflatoxin $B_1$ derived from a pre-immunized antibody phage display library system. *Food Agric. Immunol.* **2002**, *14*, 255–274.

95. Choi, S.-W.; Chang, H.-J.; Lee, N.; Chun, H. S. A surface plasmon resonance sensor for the detection of deoxynivalenol using a molecularly imprinted polymer. *Sensors* **2011**, *11*, 8654–8664.

96. Townsend, S.; Finlay, W. J. J.; Hearty, S.; O'Kennedy, R. Optimizing recombinant antibody function in SPR immunosensing: the influence of antibody structural format and chip surface chemistry on assay sensitivity. *Biosens. Bioelectron.* **2006**, *22*, 268–274.

97. Ta, D. T.; Guedens, W.; Vranken, T.; Vanschoenbeek, K.; Steen Redeker, E.; Michiels, L.; Adriaensens, P. Enhanced biosensor platforms for detecting the atherosclerotic biomarker VCAM1 based on bioconjugation with uniformly oriented VCAM1-targeting nanobodies. *Biosensors* **2016**, *6*, 34.

98. Steen Redeker, E.; Ta, D. T.; Cortens, D.; Billen, B.; Guedens, W.; Adriaensens, P. Protein engineering for directed immobilization. *Bioconjug. Chem.* **2013**, *24*, 1761–1777.

99. Jia, Y.; Peng, Y.; Bai, J.; Zhang, X.; Cui, Y.; Ning, B.; *et al*. Magnetic nanoparticle enhanced surface plasmon resonance sensor for estradiol analysis. *Sens. Actuators B Chem.* **2018**, *254*, 629–635.

100. Kawaguchi, T.; Shankaran, D. R.; Kim, S. J.; Matsumoto, K.; Toko, K.; Miura, N. Surface plasmon resonance immunosensor using Au nanoparticle for detection of TNT. *Sens. Actuators B Chem.* **2008**, *133*, 467–472.

101. Karczmarczyk, A.; Reiner-Rozman, C.; Hageneder, S.; Dubiak-Szepietowska, M.; Dostálek, J.; Feller, K.-H. Fast and sensitive detection of ochratoxin a in red wine by nanoparticle-enhanced SPR. *Anal. Chim. Acta* **2016**, *937*, 143–150.

102. Yuan, J.; Deng, D.; Lauren, D. R.; Aguilar, M.-I.; Wu, Y. Surface plasmon resonance biosensor for the detection of ochratoxin A in cereals and beverages. *Anal. Chim. Acta* **2009**, *656*, 63–71.

103. Mitchell, J. S.; Lowe, T. E. Ultrasensitive detection of testosterone using conjugate linker technology in a nanoparticle-enhanced surface plasmon resonance biosensor. *Biosens. Bioelectron.* **2009**, *24*, 2177–2183.

104. Mitchell, J. S.; Wu, Y.; Cook, C. J.; Main, L. Sensitivity enhancement of surface plasmon resonance biosensing of small molecules. *Anal. Biochem.* **2005**, *343*, 125–135.

105. Campbell, K.; McGrath, T.; Sjölander, S.; Hanson, T.; Tidare, M.; Jansson, Ö.; Moberg, A.; Mooney, M.; Elliott, C.; Buijs, J. Use of a novel micro-fluidic device to create arrays for multiplex analysis of large and small molecular weight compounds by surface plasmon resonance. *Biosens. Bioelectron.* **2011**, *26*, 3029–3036.

106. Fernández, F.; Hegnerová, K.; Piliarik, M.; Sanchez-Baeza, F.; Homola, J.; Marco, M.-P. A label-free and portable multichannel surface plasmon resonance immunosensor for on site analysis of antibiotics in milk samples. *Biosens. Bioelectron.* **2010**, *26*, 1231–1238.

107. Mauriz, E.; Calle, A.; Manclús, J. J.; Montoya, A.; Lechuga, L. M. Multi-analyte SPR immunoassays for environmental biosensing of pesticides. *Anal. Bioanal. Chem.* **2007**, *387*, 1449–1458.

108. Dorokhin, D.; Haasnoot, W.; Franssen, M. C. R.; Zuilhof, H.; Nielen, M. W. F. Imaging surface plasmon resonance for multiplex microassay sensing of mycotoxins. *Anal. Bioanal. Chem.* **2011**, *400*, 3005–3011.

109. Joshi, S.; Annida, R. M.; Zuilhof, H.; van Beek, T. A.; Nielen, M. W. F. Analysis of mycotoxins in beer using a portable nanostructured imaging surface plasmon resonance biosensor. *J. Agric. Food Chem.* **2016**, *64*, 8263–8271.

110. Joshi, S.; Segarra-Fas, A.; Peters, J.; Zuilhof, H.; van Beek, T. A.; Nielen, M. W. F. Multiplex surface plasmon resonance biosensing and its transferability towards imaging nanoplasmonics for detection of mycotoxins in barley. *Analyst* **2016**, *141*, 1307–1318.

111. McKeague, M.; De Girolamo, A.; Valenzano, S.; Pascale, M.; Ruscito, A.; Velu, R.; *et al*. Comprehensive analytical comparison of strategies used for small molecule aptamer evaluation. *Anal. Chem.* **2015**, *87*, 8608–8612.

112. de-los-Santos-Álvarez, N.; Lobo-Castañón, M. J.; Miranda-Ordieres, A. J.; Tuñón-Blanco, P. SPR sensing of small molecules with modified RNA aptamers: detection of neomycin B. *Biosens. Bioelectron.* **2009**, *24*, 2547–2553.

113. Wang, J.; Zhou, H. S. Aptamer-based Au nanoparticles-enhanced surface plasmon resonance detection of small molecules. *Anal. Chem.* **2008**, *80*, 7174–7178.

114. Xie, L.; Yan, X.; Du, Y. An aptamer based wall-less LSPR array chip for label-free and high throughput detection of biomolecules. *Biosens. Bioelectron.* **2014**, *53*, 58–64.

115. Golub, E.; Pelossof, G.; Freeman, R.; Zhang, H.; Willner, I. Electrochemical, photoelectrochemical, and surface plasmon resonance detection of cocaine using supramolecular aptamer complexes and metallic or semiconductor nanoparticles. *Anal. Chem.* **2009**, *81*, 9291–9298.

116. Zhu, Z.; Feng, M.; Zuo, L.; Zhu, Z.; Wang, F.; Chen, L.; Li, J.; Shan, G.; Luo, S.-Z. An aptamer based surface plasmon resonance biosensor for the detection of ochratoxin A in wine and peanut oil. *Biosens. Bioelectron.* **2015**, *65*, 320–326.

117. Chang, A. L.; McKeague, M.; Liang, J. C.; Smolke, C. D. Kinetic and equilibrium binding characterization of aptamers to small molecules using a label-free, sensitive, and scalable platform. *Anal. Chem.* **2014**, *86*, 3273–3278.

118. Park, J.-H.; Byun, J.-Y.; Mun, H.; Shim, W.-B.; Shin, Y.-B.; Li, T.; Kim, M.-G. A regeneratable, label-free, localized surface plasmon resonance (LSPR) aptasensor for the detection of ochratoxin A. *Biosens. Bioelectron.* **2014**, *59*, 321–327.

119. Park, J.-H.; Byun, J.-Y.; Jang, H.; Hong, D.; Kim, M.-G. A highly sensitive and widely adaptable plasmonic aptasensor using berberine for small-molecule detection. *Biosens. Bioelectron.* **2017**, *97*, 292–298.

120. Lee, B.; Park, J.-H.; Byun, J.-Y.; Kim, J. H.; Kim, M.-G. An optical fiber-based LSPR aptasensor for simple and rapid *in-situ* detection of ochratoxin A. *Biosens. Bioelectron.* **2018**, *102*, 504–509.

121. Bianco, M.; Sonato, A.; De Girolamo, A.; Pascale, M.; Romanato, F.; Rinaldi, R.; Arima, V. An aptamer-based SPR-polarization platform for high sensitive OTA detection. *Sens. Actuators B Chem.* **2017**, *241*, 314–320.

122. Cappi, G.; Spiga, F. M.; Moncada, Y.; Ferretti, A.; Beyeler, M.; Bianchessi, M.; Decosterd, L.; Buclin, T.; Guiducci, C. Label-free detection of tobramycin in serum by transmission-localized surface plasmon resonance. *Anal. Chem.* **2015**, *87*, 5278–5285.

123. Lotierzo, M.; Henry, O. Y. F.; Piletsky, S.; Tothill, I.; Cullen, D.; Kania, M.; Hock, B.; Turner, A. P. F. Surface plasmon resonance sensor for domoic acid based on grafted imprinted polymer. *Biosens. Bioelectron.* **2004**, *20*, 145–152.

124. Yola, M. L.; Eren, T.; Atar, N. Molecular imprinted nanosensor based on surface plasmon resonance: application to the sensitive determination of amoxicillin. *Sens. Actuators B Chem.* **2014**, *195*, 28–35.

125. Atar, N.; Eren, T.; Yola, M. L. A molecular imprinted SPR biosensor for sensitive determination of citrinin in red yeast rice. *Food Chem.* **2015**, *184*, 7–11.

126. Saylan, Y.; Akgönüllü, S.; Çimen, D.; Derazshamshir, A.; Bereli, N.; Yılmaz, F.; Denizli, A. Development of surface plasmon resonance sensors based on molecularly imprinted nanofilms for sensitive and selective detection of pesticides. *Sens. Actuators B Chem.* **2017**, *241*, 446–454.

127. Yao, T.; Gu, X.; Li, T.; Li, J.; Li, J.; Zhao, Z.; Wang, J.; Qin, Y.; She, Y. Enhancement of surface plasmon resonance signals using a MIP/GNPs/rGO nano-hybrid film for the rapid detection of ractopamine. *Biosens. Bioelectron.* **2016**, *75*, 96–100.

128. Yılmaz, E.; Özgür, E.; Bereli, N.; Türkmen, D.; Denizli, A. Plastic antibody based surface plasmon resonance nanosensors for selective atrazine detection. *Mater. Sci. Eng. C* **2017**, *73*, 603–610.

129. Choi, S.-W.; Chang, H.-J.; Lee, N.; Kim, J.-H.; Chun, H. S. Detection of mycoestrogen zearalenone by a molecularly imprinted polypyrrole-based surface plasmon resonance (SPR) sensor. *J. Agric. Food Chem.* **2009**, *57*, 1113–1118.

130. Gupta, G.; Bhaskar, A. S. B.; Tripathi, B. K.; Pandey, P.; Boopathi, M.; Rao, P. V. L.; Singh, B.; Vijayaraghavan, R. Supersensitive detection of T-2 toxin by the in situ synthesized π-conjugated molecularly imprinted nanopatterns. an *in situ* investigation by surface plasmon resonance combined with electrochemistry. *Biosens. Bioelectron.* **2011**, *26*, 2534–2540.

131. Dong, J.; Peng, Y.; Gao, N.; Bai, J.; Ning, B.; Liu, M.; Gao, Z. A novel polymerization of ultrathin sensitive imprinted film on surface plasmon resonance sensor. *Analyst* **2012**, *137*, 4571.

132. Wei, C.; Zhou, H.; Zhou, J. Ultrasensitively sensing acephate using molecular imprinting techniques on a surface plasmon resonance sensor. *Talanta* **2011**, *83*, 1422–1427.

133. Zhao, N.; Chen, C.; Zhou, J. Surface plasmon resonance detection of ametryn using a molecularly imprinted sensing film prepared by surface-initiated atom transfer radical polymerization. *Sens. Actuators B Chem.* **2012**, *166–167*, 473–479.

134. Dong, J.; Gao, N.; Peng, Y.; Guo, C.; Lv, Z.; Wang, Y.; Zhou, C.; Ning, B.; Liu, M.; Gao, Z. Surface plasmon resonance sensor for profenofos detection using molecularly imprinted thin film as recognition element. *Food Control* **2012**, *25*, 543–549.

135. Luo, Q.; Yu, N.; Shi, C.; Wang, X.; Wu, J. Surface plasmon resonance sensor for antibiotics detection based on photo-initiated polymerization molecularly imprinted array. *Talanta* **2016**, *161*, 797–803.

136. Zhang, Q.; Jing, L.; Zhang, J.; Ren, Y.; Wang, Y.; Wang, Y.; Wei, T.; Liedberg, B. Surface plasmon resonance sensor for femtomolar detection of testosterone with water-compatible macroporous molecularly imprinted film. *Anal. Biochem.* **2014**, *463*, 7–14.

137. Cennamo, N.; D'Agostino, G.; Galatus, R.; Bibbò, L.; Pesavento, M.; Zeni, L. Sensors based on surface plasmon resonance in a plastic optical fiber for the detection of trinitrotoluene. *Sens. Actuators B Chem.* **2013**, *188*, 221–226.

138. Verma, R.; Gupta, B. D. Optical fiber sensor for the detection of tetracycline using surface plasmon resonance and molecular imprinting. *Analyst* **2013**, *138*, 7254.

139. Shrivastav, A. M.; Mishra, S. K.; Gupta, B. D. Fiber optic SPR sensor for the detection of melamine using molecular imprinting. *Sens. Actuators B Chem.* **2015**, *212*, 404–410.

140. Agrawal, H.; Shrivastav, A. M.; Gupta, B. D. Surface plasmon resonance based optical fiber sensor for atrazine detection using molecular imprinting technique. *Sens. Actuators B Chem.* **2016**, *227*, 204–211.

141. Shrivastav, A. M.; Usha, S. P.; Gupta, B. D. Fiber optic profenofos sensor based on surface plasmon resonance technique and molecular imprinting. *Biosens. Bioelectron.* **2016**, *79*, 150–157.

142. Shrivastav, A. M.; Usha, S. P.; Gupta, B. D. Highly sensitive and selective erythromycin nanosensor employing fiber optic SPR/ERY imprinted nanostructure: application in milk and honey. *Biosens. Bioelectron.* **2017**, *90*, 516–524.

143. Cennamo, N.; Donà, A.; Pallavicini, P.; D'Agostino, G.; Dacarro, G.; Zeni, L.; Pesavento, M. Sensitive detection of 2,4,6-trinitrotoluene by tridimensional monitoring of molecularly imprinted polymer with optical fiber and five-branched gold nanostars. *Sens. Actuators B Chem.* **2015**, *208*, 291–298.

144. Cennamo, N.; D'Agostino, G.; Pesavento, M.; Zeni, L. High selectivity and sensitivity sensor based on MIP and SPR in tapered plastic optical fibers for the detection of L-nicotine. *Sens. Actuators B Chem.* **2014**, *191*, 529–536.

145. Shrivastav, A. M.; Mishra, S. K.; Gupta, B. D. Surface plasmon resonance-based fiber optic sensor for the detection of ascorbic acid utilizing molecularly imprinted polyaniline film. *Plasmonics* **2015**, *10*, 1853–1861.

146. Shrivastav, A. M.; Usha, S. P.; Gupta, B. D. A localized and propagating SPR, and molecular imprinting based fiber-optic ascorbic acid sensor using an *in situ* polymerized polyaniline–Ag nanocomposite. *Nanotechnology* **2016**, *27*, 345501.

147. Leca-Bouvier, B. D.; Blum, L. J. Enzyme for biosensing applications. In *Recognition receptors in biosensors*; Springer: New York, US, **2010**.

148. Xia, N.; Wang, Q.; Liu, L. Nanomaterials-based optical techniques for the detection of acetylcholinesterase and pesticides. *Sensors* **2014**, *15*, 499–514.

149. Lin, T.-J.; Huang, K.-T.; Liu, C.-Y. Determination of organophosphorous pesticides by a novel biosensor based on localized surface plasmon resonance. *Biosens. Bioelectron.* **2006**, *22*, 513–518.

150. Rajan; Chand, S.; Gupta, B. D. Surface plasmon resonance based fiber-optic sensor for the detection of pesticide. *Sens. Actuators B Chem.* **2007**, *123*, 661–666.

151. Milkani, E.; Lambert, C. R.; McGimpsey, W. G. Direct detection of acetylcholinesterase inhibitor binding with an enzyme-based surface plasmon resonance sensor. *Anal. Biochem.* **2011**, *408*, 212–219.

152. Puiu, M.; Istrate, O.; Rotariu, L.; Bala, C. Kinetic approach of aflatoxin $B_1$–acetylcholinesterase interaction: a tool for developing surface plasmon resonance biosensors. *Anal. Biochem.* **2012**, *421*, 587–594.

153. Yao, G.-H.; Liang, R.-P.; Huang, C.-F.; Wang, Y.; Qiu, J.-D. Surface plasmon resonance sensor based on magnetic molecularly imprinted polymers amplification for pesticide recognition. *Anal. Chem.* **2013**, *85*, 11944–11951.

154. Wang, Z.; Zong, S.; Wu, L.; Zhu, D.; Cui, Y. SERS-activated platforms for immunoassay: probes, encoding methods, and applications. *Chem. Rev.* **2017**, *117*, 7910–7963.

155. Kearns, H.; Goodacre, R.; Jamieson, L. E.; Graham, D.; Faulds, K. SERS detection of multiple antimicrobial-resistant pathogens using nanosensors. *Anal. Chem.* **2017**, *89*, 12666–12673.

156. Zeng, Z.; Liu, Y.; Wei, J. Recent advances in surface-enhanced Raman spectroscopy (SERS): Finite-difference time-domain (FDTD) method for SERS and sensing applications. *TrAC Trends Anal. Chem.* **2016**, *75*, 162–173.

157. Kahraman, M.; Mullen, E. R.; Korkmaz, A.; Wachsmann-Hogiu, S. Fundamentals and applications of SERS-based bioanalytical sensing. *Nanophotonics* **2017**, *6*, 831–852.

158. Tang, H.; Zhu, C.; Meng, G.; Wu, N. Review – Surface-enhanced Raman scattering sensors for food safety and environmental monitoring. *J. Electrochem. Soc.* **2018**, *165*, B3098–B3118.

159. Wei, H.; Hossein Abtahi, S. M.; Vikesland, P. J. Plasmonic colorimetric and SERS sensors for environmental analysis. *Environ. Sci. Nano* **2015**, *2*, 120–135.

160. Vo-Dinh, T. SERS chemical sensors and biosensors: new tools for environmental and biological analysis. *Sens. Actuators B Chem.* **1995**, *29*, 183–189.

161. Jiang, T.; Wang, X.; Tang, S.; Zhou, J.; Gu, C.; Tang, J. Seed-mediated synthesis and SERS performance of graphene oxide-wrapped Ag nanomushroom. *Sci. Rep.* **2017**, *7*, 9795.

162. Kotanen, C. N.; Martinez, L.; Alvarez, R.; Simecek, J. W. Surface enhanced Raman scattering spectroscopy for detection and identification of microbial pathogens isolated from human serum. *Sens. Bio-Sens. Res.* **2016**, *8*, 20–26.

163. Sharma, B.; Frontiera, R. R.; Henry, A.-I.; Ringe, E.; Van Duyne, R. P. SERS: materials, applications, and the future. *Mater. Today* **2012**, *15*, 16–25.

164. Zhou, X.; Zhou, F.; Liu, H.; Yang, L.; Liu, J. Assembly of polymer–gold nanostructures with high reproducibility into a monolayer film SERS substrate with 5 nm gaps for pesticide trace detection. *Analyst* **2013**, *138*, 5832–5838.

165. Saute, B.; Premasiri, R.; Ziegler, L.; Narayanan, R. Gold nanorods as surface enhanced Raman spectroscopy substrates for sensitive and selective detection of ultra-low levels of dithiocarbamate pesticides. *Analyst* **2012**, *137*, 5082–5087.

166. Rohr, T. E.; Cotton, T.; Fan, N.; Tarcha, P. J. Immunoassay employing surface-enhanced Raman spectroscopy. *Anal. Biochem.* **1989**, *182*, 388–398.

167. Szlag, V. M.; Rodriguez, R. S.; He, J.; Hudson-Smith, N.; Kang, H.; Le, N.; Reineke, T. M.; Haynes, C. L. Molecular affinity agents for intrinsic surface-enhanced Raman scattering (SERS) sensors. *ACS Appl. Mater. Interfaces* **2018**, *10*, 31825–31844.

168. Gelder, J. D.; Gussem, K. D.; Vandenabeele, P.; Moens, L. Reference database of Raman spectra of biological molecules. *J. Raman Spectrosc.* **2007**, *38*, 1133–1147.

169. Sanles-Sobrido, M.; Rodríguez-Lorenzo, L.; Lorenzo-Abalde, S.; González-Fernández, Á.; A. Correa-Duarte, M.; A. Alvarez-Puebla, R.; M. Liz-Marzán, L. Label-free SERS detection of relevant bioanalytes on silver-coated carbon nanotubes : The case of cocaine. *Nanoscale* **2009**, *1*, 153–158.

170. Peltomaa, R.; Benito-Peña, E.; Moreno-Bondi, M. C. Bioinspired recognition elements for mycotoxin sensors. *Anal. Bioanal. Chem.* **2018**, *410*, 747–771.

171. Zhou, L.; Wang, M.-H.; Wang, J.-P.; Ye, Z.-Z. Application of biosensor surface immobilization methods for aptamer. *Chin. J. Anal. Chem.* **2011**, *39*, 432–438.

172. Zhang, X.; Yadavalli, V. K. Surface immobilization of DNA aptamers for biosensing and protein interaction analysis. *Biosens. Bioelectron.* **2011**, *26*, 3142–3147.

173. Cottat, M.; D'Andrea, C.; Yasukuni, R.; Malashikhina, N.; Grinyte, R.; Lidgi-Guigui, N.; *et al*. High sensitivity, high selectivity SERS detection of MnSOD using optical nanoantennas functionalized with aptamers. *J. Phys. Chem. C* **2015**, *119*, 15532–15540.

174. Neumann, O.; Zhang, D.; Tam, F.; Lal, S.; Wittung-Stafshede, P.; Halas, N. J. Direct optical detection of aptamer conformational changes induced by target molecules. *Anal. Chem.* **2009**, *81*, 10002–10006.

175. Barahona, F.; Bardliving, C. L.; Phifer, A.; Bruno, J. G.; Batt, C. A. An aptasensor based on polymer-gold nanoparticle composite microspheres for the detection of malathion using surface-enhanced Raman spectroscopy. *Ind. Biotechnol.* **2013**, *9*, 42–50.

176. Carter, S. R.; Rimmer, S. Surface molecularly imprinted polymer core–shell particles. *Adv. Funct. Mater.* **2004**, *14*, 553–561.

177. Kostrewa, S.; Emgenbroich, M.; Klockow, D.; Wulff, G. Surface-enhanced Raman scattering on molecularly imprinted polymers in water. *Macromol. Chem. Phys.* **2003**, *204*, 481–487.

178. Wackerlig, J.; Lieberzeit, P. A. Molecularly imprinted polymer nanoparticles in chemical sensing – Synthesis, characterisation and application. *Sens. Actuators B Chem.* **2015**, *207*, 144–157.

179. Uzun, L.; Turner, A. P. F. Molecularly-imprinted polymer sensors: Realising their potential. *Biosens. Bioelectron.* **2016**, *76*, 131–144.

180. Dabrowski, M.; Lach, P.; Cieplak, M.; Kutner, W. Nanostructured molecularly imprinted polymers for protein chemosensing. *Biosens. Bioelectron.* **2018**, *102*, 17–26.

181. Carrasco, S.; Benito-Peña, E.; Navarro-Villoslada, F.; Langer, J.; Sanz-Ortiz, M. N.; *et al*. Multibranched gold–mesoporous silica nanoparticles coated with a molecularly imprinted polymer for label-free antibiotic surface-enhanced Raman scattering analysis. *Chem. Mater.* **2016**, *28*, 7947–7954.

182. Kamra, T.; Zhou, T.; Montelius, L.; Schnadt, J.; Ye, L. Implementation of molecularly imprinted polymer beads for surface enhanced Raman detection. *Anal. Chem.* **2015**, *87*, 5056–5061.

183. Ashley, J.; Wu, K.; Hansen, M. F.; Schmidt, M. S.; Boisen, A.; Sun, Y. Quantitative detection of trace level cloxacillin in food samples using magnetic molecularly imprinted polymer extraction and surface-enhanced Raman spectroscopy nanopillars. *Anal. Chem.* **2017**, *89*, 11484–11490.

184. Holthoff, E. L.; Stratis-Cullum, D. N.; Hankus, M. E.; Holthoff, E. L.; Stratis-Cullum, D. N.; Hankus, M. E. A nanosensor for TNT detection based on molecularly imprinted polymers and surface enhanced Raman scattering. *Sensors* **2011**, *11*, 2700–2714.

185. Bantz, K. C.; Nelson, H. D.; Haynes, C. L. Plasmon-enabled study of self-assembled alkanethiol ordering on roughened Ag substrates. *J. Phys. Chem. C* **2012**, *116*, 3585–3593.

186. Jones, C. L.; Bantz, K. C.; Haynes, C. L. Partition layer-modified substrates for reversible surface-enhanced Raman scattering detection of polycyclic aromatic hydrocarbons. *Anal. Bioanal. Chem.* **2009**, *394*, 303–311.

187. Xie, Y.; Wang, X.; Han, X.; Xue, X.; Ji, W.; Qi, Z.; Liu, J.; Zhao, B.; Ozaki, Y. Sensing of polycyclic aromatic hydrocarbons with cyclodextrin inclusion complexes on silver nanoparticles by surface-enhanced Raman scattering. *Analyst* **2010**, *135*, 1389–1394.

188. Guerrini, L.; Garcia-Ramos, J. V.; Domingo, C.; Sanchez-Cortes, S. Nanosensors based on viologen functionalized silver nanoparticles: Few molecules surface-enhanced Raman spectroscopy detection of polycyclic aromatic hydrocarbons in interparticle hot spots. *Anal. Chem.* **2009**, *81*, 1418–1425.

189. Leyton, P.; Sanchez-Cortes, S.; Garcia-Ramos, J. V.; Domingo, C.; Campos-Vallette, M.; Saitz, C.; Clavijo, R. E. Selective molecular recognition of polycyclic aromatic hydrocarbons (PAHs) on calix[4]arene-functionalized Ag nanoparticles by surface-enhanced Raman scattering. *J. Phys. Chem. B* **2004**, *108*, 17484–17490.

190. Sapsford, K. E.; Ligler, F. S. TIRF array biosensor for environmental monitoring. In *Optical Sensors: Industrial Environmental and Diagnostic Applications*; Narayanaswamy, R., Wolfbeis, O. S., Eds.; Springer Series on Chemical Sensors and Biosensors; Springer, Berlin, Heidelberg, Germany, **2004**; pp 359–390.

191. Campbell, D. P. Interferometric biosensors. In *Principles of bacterial detection: Biosensors, recognition receptors and Mmicrosystems*; Zourob, M., Elwary, S., Turner, A., Eds.; Springer, New York, NY, US, **2008**; pp 169–211.

192. Lechuga, L. M.; Prieto, F.; Sepúlveda, B. Interferometric biosensors for environmental pollution detection. In *Optical sensors: Industrial environmental and diagnostic applications*; Narayanaswamy, R., Wolfbeis, O. S., Eds.; Springer Series on Chemical Sensors and Biosensors; Springer, Heidelberg, Berlin, Germnay, **2004**; pp 227–250.

193. *Optical Sensors: Industrial Environmental and Diagnostic Applications*; Narayanaswamy, R., Wolfbeis, O. S., Eds.; Springer Series on Chemical Sensors and Biosensors; Springer-Verlag: Berlin Heidelberg, Germany, **2004**.

194. Lu, Y.; Yao, G.; Sun, K.; Huang, Q. β-cyclodextrin coated $SiO_2$@Au@Ag core–shell nanoparticles for SERS detection of PCBs. *Phys. Chem. Chem. Phys.* **2015**, *17*, 21149–21157.

195. Nie, Y.; Teng, Y.; Li, P.; Liu, W.; Shi, Q.; Zhang, Y. Label-free aptamer-based sensor for specific detection of malathion residues by surface-enhanced Raman scattering. *Spectrochim. Acta. A. Mol. Biomol. Spectrosc.* **2018**, *191*, 271–276.

196. Pang, S.; Yang, T.; He, L. Review of surface enhanced Raman spectroscopic (SERS) detection of synthetic chemical pesticides. *TrAC Trends Anal. Chem.* **2016**, *85*, 73–82.

197. Kamra, T.; Xu, C.; Montelius, L.; Schnadt, J.; Wijesundera, S. A.; Yan, M.; Ye, L. Photoconjugation of molecularly imprinted polymer nanoparticles for surface-enhanced Raman detection of propranolol. *ACS Appl. Mater. Interfaces* **2015**, *7*, 27479–27485.

198. Guo, Z.; Chen, L.; Lv, H.; Yu, Z.; Zhao, B. Magnetic imprinted surface enhanced Raman scattering (MI-SERS) based ultrasensitive detection of ciprofloxacin from a mixed sample. *Anal. Methods* **2014**, *6*, 1627–1632.

199. Escorihuela, J.; González-Martínez, M. Á.; López-Paz, J. L.; Puchades, R.; Maquieira, Á.; Gimenez-Romero, D. Dual-polarization interferometry: a novel technique to light up the nanomolecular world. *Chem. Rev.* **2015**, *115*, 265–294.

200. Jørgensen, T. M.; Jepsen, S. T.; Sørensen, H. S.; di Gennaro, A. K.; Kristensen, S. R. Back scattering interferometry revisited – A theoretical and experimental investigation. *Sens. Actuators B Chem.* **2015**, *220*, 1328–1337.

201. Kussrow, A.; Enders, C. S.; Bornhop, D. J. Interferometric methods for label-free molecular interaction studies. *Anal. Chem.* **2012**, *84*, 779–792.

202. Kammer, M. N.; Olmsted, I. R.; Kussrow, A. K.; Morris, M. J.; Jackson, G. W.; Bornhop, D. J. Characterizing aptamer small molecule interactions with backscattering interferometry. *The Analyst* **2014**, *139*, 5879–5884.

203. Proll, G.; Markovic, G.; Steinle, L.; Gauglitz, G. Reflectometric interference spectroscopy. In *Biosensors and biodetection*; Rasooly, A., Herold, K. E., Eds.; Methods in Molecular Biology™; Humana Press: Totowa, NJ, US, **2009**; pp 167–178.

204. Nikitin, P. I.; Gorshkov, B. G.; Valeiko, M. V.; Rogov, S. I. Spectral-phase interference method for detecting biochemical reactions on a surface. *Quantum Electron.* **2000**, *30*, 1099.

205. Maragos, C. M. Signal amplification using colloidal gold in a biolayer interferometry-based immunosensor for the mycotoxin deoxynivalenol. *Food Addit. Contam. Part A* **2012**, *29*, 1108–1117.

206. Reza, A.; Tofighi, S.; Bathaee, M.; Farm, F. Optical fiber interferometers and their applications. In *Interferometry - Research and Applications in Science and Technology*; Padron, I., Ed.; InTech, **2012**.

207. Chalyan, T.; Guider, R.; Pasquardini, L.; Zanetti, M.; Falke, F.; Schreuder, E.; Heideman, R. G.; Pederzolli, C.; Pavesi, L. Asymmetric Mach–Zehnder interferometer based biosensors for aflatoxin $M_1$ detection. *Biosensors* **2016**, *6*, 1.

208. Barrios, C. A.; Carrasco, S.; Francesca, M.; Yurrita, P.; Navarro-Villoslada, F.; Moreno-Bondi, M. C. Molecularly imprinted polymer for label-free integrated optical waveguide bio(mimetic)sensors. *Sens. Actuators B Chem*. **2012**, *161*, 607–614.

209. Kolarov, F.; Niedergall, K.; Bach, M.; Tovar, G. E. M.; Gauglitz, G. Optical sensors with molecularly imprinted nanospheres: A promising approach for robust and label-free detection of small molecules. *Anal. Bioanal. Chem.* **2012**, *402*, 3245–3252.

210. Krieg, A. K.; Hess, S.; Gauglitz, G. Optical sensors for therapeutic drug monitoring of antidepressants for a better medication adjustment; Baldini, F., Homola, J., Lieberman, R. A., Eds.; Prague, Czech Republic, **2013**; p 87740H.

211. Olmsted, I. R.; Kussrow, A.; Bornhop, D. J. Comparison of free-solution and surface-immobilized molecular interactions using a single platform. *Anal. Chem.* **2012**, *84*, 10817–10822.

212. Wartchow, C. A.; Podlaski, F.; Li, S.; Rowan, K.; Zhang, X.; Mark, D.; Huang, K.-S. Biosensor-based small molecule fragment screening with biolayer interferometry. *J. Comput. Aided Mol. Des.* **2011**, *25*, 669–676.

213. Pagkali, V.; Petrou, P. S.; Makarona, E.; Peters, J.; Haasnoot, W.; Jobst, G.; *et al*. Simultaneous determination of aflatoxin $B_1$, fumonisin $B_1$ and deoxynivalenol in beer samples with a label-free monolithically integrated optoelectronic biosensor. *J. Hazard. Mater.* **2018**, *359*, 445–453.

214. Swann, M. J.; Peel, L. L.; Carrington, S.; Freeman, N. J. Dual-polarization interferometry: an analytical technique to measure changes in protein structure in real time, to determine the stoichiometry of binding events, and to differentiate between specific and nonspecific interactions. *Anal. Biochem.* **2004**, *329*, 190–198.

215. Gao, S.; Zheng, X.; Hu, B.; Sun, M.; Wu, J.; Jiao, B.; Wang, L. Enzyme-linked, aptamer-based, competitive biolayer interferometry biosensor for palytoxin. *Biosens. Bioelectron.* **2017**, *89*, 952–958.

216. A. Nabok; A.M. Al-Jawdah; A. Tsargorodska. Development of planar waveguide-based immunosensor for detection of low molecular weight molecules such as mycotoxins. *Sens. Actuators B Chem* **2017**, *247*, 975–980.

217. Al-Jawdah, A.; Nabok, A.; Jarrah, R.; Holloway, A.; Tsargorodska, A.; Takacs, E.; Szekacs, A. Mycotoxin biosensor based on optical planar waveguide. *Toxins* **2018**, *10*, 272.

218. McGrath, T. F.; Campbell, K.; Fodey, T. L.; O'Kennedy, R.; Elliott, C. T. An evaluation of the capability of a biolayer interferometry biosensor to detect low-molecular-weight food contaminants. *Anal. Bioanal. Chem.* **2013**, *405*, 2535–2544.

219. Chocarro-Ruiz, B.; Herranz, S.; Fernández Gavela, A.; Sanchís, J.; Farré, M.; Marco, M. P.; Lechuga, L. M. Interferometric nanoimmunosensor for label-free and real-time monitoring of Irgarol 1051 in seawater. *Biosens. Bioelectron.* **2018**, *117*, 47–52.

220. Krieg, A. K.; Gauglitz, G. Ultrasensitive label-free immunoassay for optical determination of amitriptyline and related tricyclic antidepressants in human serum. *Anal. Chem.* **2015**, *87*, 8845–8850.

221. Ma, K.; Ekblad, T.; Koerkamp, M. K.; Kelderman, H.; Wijlen, M. van; Duarah, A.; Yue, J.; Zhang, L.; Wong, M. V.-M.; Lim, M. H. Contaminant detection in treated water using Optiqua's MiniLab™ biosensing system: a case study for bisphenol A. *Int. J. Environ. Anal. Chem.* **2015**, *95*, 366–378.

222. Rau, S.; Hilbig, U.; Gauglitz, G. Label-free optical biosensor for detection and quantification of the non-steroidal anti-inflammatory drug diclofenac in milk without any sample pretreatment. *Anal. Bioanal. Chem.* **2014**, *406*, 3377–3386.

223. Rau, S.; Gauglitz, G. Reflectometric interference spectroscopy (RIfS) as a new tool to measure in the complex matrix milk at low analyte concentration. *Anal. Bioanal. Chem.* **2012**, *402*, 529–536.

224. Tinsley-Bown, A.; Smith, R. G.; Hayward, S.; Anderson, M. H.; Koker, L.; Green, A.; *et al*. Immunoassays in a porous silicon interferometric biosensor combined with sensitive signal processing. *Phys. Status Solidi A* **2005**, *202*, 1347–1356.

225. Pagkali, V.; Petrou, P. S.; Salapatas, A.; Makarona, E.; Peters, J.; Haasnoot, W.; *et al*. Detection of ochratoxin A in beer samples with a label-free monolithically integrated optoelectronic biosensor. *J. Hazard. Mater.* **2017**, *323*, 75–83.

226. Maragos, C. M. Detection of deoxynivalenol using biolayer interferometry. *Mycotoxin Res.* **2011**, *27*, 157–165.

227. Orlov, A. V.; Burenin, A. G.; Massarskaya, N. G.; Betin, A. V.; Nikitin, M. P.; Nikitin, P. I. Highly reproducible and sensitive detection of mycotoxins by label-free biosensors. *Sens. Actuators B Chem.* **2017**, *246*, 1080–1084.

228. Tuerk, C.; Gold, L. Systematic evolution of ligands by exponential enrichment: rna ligands to bacteriophage T4 DNA polymerase. *Science* **1990**, *249*, 505–510.

229. Gao, S.; Hu, B.; Zheng, X.; Cao, Y.; Liu, D.; Sun, M.; Jiao, B.; Wang, L. Gonyautoxin 1/4 aptamers with high-affinity and high-specificity: from efficient selection to aptasensor application. *Biosens. Bioelectron.* **2016**, *79*, 938–944.

230. Ouyang, S.; Hu, B.; Zhou, R.; Liu, D.; Peng, D.; Li, Z.; Li, Z.; Jiao, B.; Wang, L. Rapid and sensitive detection of nodularin-R in water by a label-free BLI aptasensor. *Analyst* **2018**, *143*, 4316–4322.

231. Gao, S.; Zheng, X.; Wu, J. A biolayer interferometry-based competitive biosensor for rapid and sensitive detection of saxitoxin. *Sens. Actuators B Chem.* **2017**, *246*, 169–174.

232. Zheng, X.; Hu, B.; Gao, S. X.; Liu, D. J.; Sun, M. J.; Jiao, B. H.; Wang, L. H. A saxitoxin-binding aptamer with higher affinity and inhibitory activity optimized by rational site-directed mutagenesis and truncation. *Toxicon* **2015**, *101*, 41–47.

233. Handy, S. M.; Yakes, B. J.; DeGrasse, J. A.; Campbell, K.; Elliott, C. T.; Kanyuck, K. M.; DeGrasse, S. L. First report of the use of a saxitoxin–protein conjugate to develop a DNA aptamer to a small molecule toxin. *Toxicon* **2013**, *61*, 30–37.

234. Zhang, H.; Li, W.; Luo, H.; Xiong, G.; Yu, Y. Quantitative determination of testosterone levels with biolayer interferometry. *Chem. Biol. Interact.* **2017**, *276*, 141–148.

235. Su, Y.; Xu, H.; Chen, Y.; Qi, J.; Zhou, X.; Ge, R.; Lin, Z. Real-time and label-free detection of bisphenol a by an ssDNA aptamer sensor combined with dual polarization interferometry. *New J. Chem.* **2018**, *42*, 2850–2856.

236. Özalp, V. C. Dual-polarization interferometry for quantification of small molecules using aptamers. *Anal. Bioanal. Chem.* **2012**, *402*, 799–804.

237. Wang, Y.; Wang, J.; Yang, F.; Yang, X. Probing biomolecular interactions with dual polarization interferometry: real-time and label-free coralyne detection by use of homoadenine DNA oligonucleotide. *Anal. Chem.* **2012**, *84*, 924–930.

238. Nopper, D.; Lammershop, O.; Wulff, G.; Gauglitz, G. Amidine-based molecularly imprinted polymers – New sensitive elements for chiral chemosensors. *Anal. Bioanal. Chem.* **2003**, *377*, 608–613.

239. Jane, A.; Dronov, R.; Hodges, A.; Voelcker, N. H. Porous silicon biosensors on the advance. *Trends Biotechnol.* **2009**, *27*, 230–239.

240. Krismastuti, F. S. H.; Brooks, W. L. A.; Sweetman, M. J.; Sumerlin, B. S.; Voelcker, N. H. A photonic glucose biosensor for chronic wound prognostics. *J Mater Chem B* **2014**, *2*, 3972–3983.

241. Wu, X.; Liu, H.; Wang, X.; Jiang, H. Fiber-optic biological/chemical sensing system based on degradable hydrogel. *IEEE Sens. J.* **2018**, *18*, 45–52.

242. S. Sridharamurthy, S.; K. Agarwal, A.; J. Beebe, D.; Jiang, H. Dissolvable membranes as sensing elements for microfluidics based biological/chemical sensors. *Lab. Chip* **2006**, *6*, 840–842.

243. Sommerfeld, A. *Mathematical Theory of Diffraction*; Progress in Mathematical Physics; Birkhäuser Basel, **2004**.

244. Fuchs, Y.; Soppera, O.; Mayes, A. G.; Haupt, K. Holographic molecularly imprinted polymers for label-free chemical sensing. *Adv. Mater.* **2013**, *25*, 566–570.

245. Paek, S.-H.; Cho, I.-H.; Kim, D.-H.; Jeon, J.-W.; Lim, G.-S.; Paek, S.-H. Label-free, needle-type biosensor for continuous glucose monitoring based on competitive binding. *Biosens. Bioelectron.* **2013**, *40*, 38–44.

246. Seo, D.; Paek, S.-H.; Oh, S.; Seo, S.; Paek, S.-H. A human serum-based enzyme-free continuous glucose monitoring technique using a needle-type bio-layer interference sensor. *Sensors* **2016**, *16*, 1581.

247. Ballerstadt, R.; Kholodnykh, A.; Evans, C.; Boretsky, A.; Motamedi, M.; Gowda, A.; McNichols, R. Affinity-based turbidity sensor for glucose monitoring by optical coherence tomography: toward the development of an implantable sensor. *Anal. Chem.* **2007**, *79*, 6965–6974.

248. Sanders, M.; McPartlin, D.; Moran, K.; Guo, Y.; Eeckhout, M.; O'Kennedy, R.; De Saeger, S.; Maragos, C. Comparison of enzyme-linked immunosorbent assay, surface plasmon resonance and biolayer interferometry for screening of deoxynivalenol in wheat and wheat dust. *Toxins* **2016**, *8*, 103.

249. Pacholski, C.; Perelman, L. A.; VanNieuwenhze, M. S.; Sailor, M. J. Small molecule detection by reflective interferometric fourier transform spectroscopy (RIfTS). *Phys. Status Solidi A* **2009**, *206*, 1318–1321.

250. Queirós, R. B.; Silva, S. O.; Noronha, J. P.; Frazão, O.; Jorge, P.; Aguilar, G.; Marques, P. V. S.; Sales, M. G. F. Microcystin-LR detection in water by the Fabry–Pérot interferometer using an optical fibre coated with a sol–gel imprinted sensing membrane. *Biosens. Bioelectron.* **2011**, *26*, 3932–3937.

251. Aikio, S.; Zeilinger, M.; Hiltunen, J.; Hakalahti, L.; Hiitola-Keinänen, J.; Hiltunen, M.; *et al*. Disposable (bio)chemical integrated optical waveguide sensors implemented on roll-to-roll produced platforms. *RSC Adv.* **2016**, *6*, 50414–50422.

252. Arjmand, M.; Saghafifar, H.; Alijanianzadeh, M.; Soltanolkotabi, M. A sensitive tapered-fiber optic biosensor for the label-free detection of organophosphate pesticides. *Sens. Actuators B Chem.* **2017**, *C*, 523–532.

253. Galarreta, B. C.; Tabatabaei, M.; Guieu, V.; Peyrin, E.; Lagugné-Labarthet, F. Microfluidic channel with embedded SERS 2D platform for the aptamer detection of ochratoxin A. *Anal. Bioanal. Chem.* **2013**, *405*, 1613–1621.